NTIA REPORT 79-25

SPECTRUM RESOURCE ASSESSMENT IN THE 2.7-2.9 GHz BAND PHASE II: RADAR SIGNAL PROCESSING (REPORT NO.2)

Robert L. Hinkle
Robert M. Pratt
Jay S. Levy

U.S. DEPARTMENT OF COMMERCE
Juanita M. Kreps, Secretary

Henry Geller, Assistant Secretary
for Communications and Information

AUGUST 1979

ACKNOWLEDGEMENT

The completion of this general investigation into the signal processing properties of the primary radars in the 2.7 to 2.9 GHz band and the Automated Radar Terminal System (ARTS-IIIA) required the contributions of many individuals. In particular, the ASR-8 measurements made at Stapleton Airport, Denver, Colorado, were coordinated by Gerald J. Markey, Chief Frequency Engineering Branch, Federal Aviation Administration; and Larry Scofield, Supervisory Electronic Technician, Federal Aviation Administration. In addition, Robert B. Steves, Air Traffic Control (ATC) Systems Engineer, Texas Instruments Incorporated, contributed extensively to the completion of this investigation by providing both analytical and hardware experience in the signal processing properties of the ASR-7 and ASR-8 radars. Also, the generosity of Dr. Gerard V. Trunk, Naval Research Laboratory, Department of Defense, in technically reviewing the report was greatly appreciated.

TABLE OF CONTENTS

SECTION 3

PRIMARY RADAR SIGNAL PROCESSING

SECTION 4

ARTS-IIIA SIGNAL PROCESSING

APPENDIX A

MIXER TRANSFER PROPERTIES

APPENDIX B

IF FILTER TRANSFER PROPERTIES

APPENDIX C

MTI CHANNEL TRANSFER PROPERTIES

APPENDIX D

INTEGRATOR TRANSFER PROPERTIES

APPENDIX E

RADAR SIMULATION

APPENDIX F

APPENDIX G

SYSTEM CHARACTERISTICS

APPENDIX H

LIST OF ILLUSTRATIONS

LIST OF TABLES

ABSTRACT

The National Telecommunications and Information Administration (NTIA) in the Department of Commerce undertook a detailed program to investigate the signal processing properties of the primary radars in the 2.7 to 2.9 GHz band, and the Automated Radar Terminal System (ARTS-IIIA) post processor planned for use by the Federal Aviation Administration on the Airport Surveillance Radars (ASRs). This investigation was the second investigation in a series of tasks undertaken by NTIA as part of a spectrum resource assessment of the 2.7 to 2.9 GHz band. The overall objective of the spectrum resource assessment was to assess the degree of congestion in the band in designated areas in the United States, and to promote more effective utilization of the band.

The investigation into the signal processing properties of the primary radars and ARTS-IIIA included the transfer properties of noise, desired signal, and asynchronous interference along with a detailed parametric analysis of the trade-offs to the desired signal performance in suppressing asynchronous interference. As a result of the investigation, it was concluded that all radars in the 2.7 to 2.9 GHz band have a very low duty cycle (less than 0.2%) thus permitting the use of signal processing techniques in the radars and post processors for suppression of interference to obtain more efficient utilization of the 2.7 to 2.9 GHz band. The use of integrators (enhancers) and other digital signal processing techniques along with the trend of displaying synthetic video on the Plan Position Indicator (PPI) display provides the capability of suppressing asynchronous interference, while also permitting the enhancement of weak desired targets that are below the radar receiver system noise level. Also, with properly designed signal processing techniques, the trade-offs in suppressing the asynchronous interference (target azimuth shift, angular resolution, and desired signal sensitivity) in low duty cycle radars are minimal.

In summary, some spectrum conservation techniques can be used by the radiodetermination services in the 2.7 to 2.9 GHz band to obtain more efficient utilization of the spectrum. Also, the current hardware in the later model primary radars and the ARTS-IIIA will suppress asynchronous interference with trade-offs to the desired signal performance.

KEY WORDS

Primary Radar
ARTS-IIIA
Interference Suppression
Signal Processing
Simulation

SECTION 1

INTRODUCTION

BACKGROUND

During the period of August 1971 through April 1973, the Interdepartment Radio Advisory Committee (IRAC) had under study the accommodation of Department of Defense (DoD), Federal Aviation Administration (FAA), and Department of Commerce (DoC) radar operations in the band 2.7-2.9 GHz. A series of meetings was held between the agencies (Summary Minutes of the First (October 1972) and Second (December 1972) OTP Meetings) to determine if new FAA air traffic control radars could be accommodated in this band without degrading their performance, and what impact these radars would have on the performance of existing radars in the band. An initial assessment of the problem (Maiuzzo, 1972) determined that the addition of new radars to the band could create a potential problem. To resolve the immediate problem of accommodating the new FAA Air Traffic Control Radars, the following actions were taken:

a. The band 3.5-3.7 GHz was reallocated by footnote to provide for co-equal primary Government use by both the Aeronautical Radionavigation and Radiolocation Services. The footnote reads as follows:

> G110 - Government ground-based stations in the aeronautical radionavigation service may be authorized between 3.5-3.7 GHz where accommodation in the 2.7-2.9 GHz band is not technically and/or economically feasible.

Agencies were requested to cooperate to the maximum extent practicable to ensure on an area-by-area, case-by-case basis that the band 2.7-2.9 GHz is employed effectively.

b. The Spectrum Planning Subcommittee was tasked to develop a long-range plan for fixed radars with emphasis on the 2.7-2.9 GHz and 3.5-3.7 GHz bands. The SPS plan (SPS Ad Hoc Committee, 1974) was completed and approved by the IRAC.

The Office of Telecommunications Policy (OTP)* subsequently tasked the Office of Telecommunications (OT)* to perform a spectrum resource assessment of the 2.7-2.9 GHz band. The intent of this assessment was to provide a quantitative understanding of potential problems in the band of concern as well as to identify options available to spectrum managers for dealing with

---

* OTP and OT have been reorganized into the National Telecommunications and Information Administration (NTIA) within the Department of Commerce.

these problems. One of the primary reasons for initiating the assessment was to ensure identification of problems during the early phases of design and planning rather than after-the-fact, i.e., after a system has been designed and hardware fabricated. By making these band assessments early, necessary actions can be taken to assure that appropriate communication channels are established between agencies whose systems are in potential conflict. This will enhance the early identification of solutions which are mutually satisfactory to all parties involved.

A multiphase program to the solution of the 2.7-2.9 GHz Spectrum Resource Assessment task was undertaken by NTIA.

Phase I - The first phase involved the identification of systems existing in and planned for the band in question, determination of available technical and operational data for each system, identification of the potential interactions between systems, and the generation of a plan that leads to an overall assessment of the band's potential congestion. A Phase I report (Hinkle and Mayher, 1975) for the 2.7-2.9 GHz Spectrum Resource Assessment was completed.

Phase II - The second phase encompasses several tasks:

1. A detailed measurement and model validation program in the Los Angeles and San Francisco areas. The objective of this task was to validate models and procedures used to predict radar-to-radar interference, and assess the capability of predicting band congestion. This task was completed and the findings are given in a report by Hinkle, Pratt, and Matheson (1976).

2. Investigation of the signal processing properties of primary radars in the 2.7-2.9 GHz band and the Automated Radar Terminal System (ARTS-IIIA) to assess the capability of the radars to suppress asynchronous interference and the trade-offs in suppressing asynchronous signals.

3. Investigation of the potential band congestion and band efficiency in eight designated congested areas (New York, Philadelphia, Atlanta, Miami, Chicago, Dallas, Los Angeles, and San Francisco) based on the technical findings of Tasks 1 and 2.

4. Development of engineering and management aids to assist the frequency manager in determining if new radars can be accommodated in the 2.7 - 2.9 GHz band, and a methodology for assessing how efficiently the band is being utilized.

This report is the second Phase II report in a series of reports related to the Spectrum Resource Assessment of the 2.7-2.9 GHz band. The nature of the 2.7-2.9 GHz spectrum resource problem requires a rigorous analytical and measurement investigation into the signal processing properties of the radars presently in and planned for the 2.7-2.9 GHz band as well as the ARTS-IIIA

post processor used in the FAA Terminal radars. This report contains the investigation of the signal processing properties of the radars and post processors to noise, desired signal, and interfering signals to access the capability of the equipment to suppress asynchronous signals and the trade-offs to the desired signal in suppressing asynchronous signals. This investigation was necessary to assure that the investigation of potential band congestion will be based on sound technical procedures.

OBJECTIVE

In order to promote effective use of the band, it is necessary to determine the electromagnetic compatibility of present and future radars planned for deployment in the 2.7-2.9 GHz band. The second task of the Phase II program encompassed a detailed investigation into the signal processing properties of the primary radars and ARTS-IIIA post processor. The objectives of this extensive signal processing investigation were to:

1. Determine the signal processing properties of radars presently operating or planned for the 2.7-2.9 GHz band and the terminal radar ARTS-IIIA Radar Data Acquisition System (RDAS).

2. Investigate the trade-offs to desired signal detection in suppressing asynchronous interfering signals, and determine methods to minimize these trade-offs.

3. Determine methods of obtaining more efficient utilization of the band by using interference suppression techniques.

APPROACH

In order to accomplish the objectives related to the radar signal processing task, the following approach was taken:

1. Conduct a preliminary investigation to determine the radar nomenclatures presently operating in the band, and the new radars and post processors planned to be used in the band.

2. Perform a cursory investigation into the operating modes (i.e., normal, log-normal, Moving Target Indicator (MTI), weather background, etc.), types of circuitry and processing techniques (analog or digital) used by radars in the band to determine the representative radars to be analyzed in detail.

3. Perform a detailed signal processing investigation of the transfer properties of the representative radars to noise, desired signal, and interfering signals using analytical techniques, measurements, and simulation.

SECTION 2

CONCLUSIONS AND RECOMMENDATIONS

GENERAL

The following is a summary of the conclusions and recommendations as a result of a detailed investigation into the signal processing properties of the primary radars in the 2.7 to 2.9 GHz band, and the Automated Radar Terminal System (ARTS-IIIA) post processor planned for use by the Federal Aviation Administration (FAA) on the Airport Surveillance Radars (ASRs). The investigation included the signal processing properties of the primary radars and the ARTS-IIIA to noise, desired signal, and asynchronous interference along with a detailed parametric analysis of the trade-offs to the desired signal in suppressing asynchronous interference.

The signal processing of the primary radars was based primarily on the ASR-7 (AN/GPN-12) and ASR-8 radars which are late model digital processing type radars. However, the analysis is in general applicable to the older analog processing type radars in the 2.7 to 2.9 GHz band. The signal processing properties of the primary radars are discussed in Section 3 and Appendices A, B, C, D and E.

The signal processing investigation of the ARTS-IIIA included only the Radar Data Acquisition Subsystem (RDAS) since it is the portion of the ARTS-IIIA which processes the 2.7 to 2.9 GHz radar signals. The signal processing properties of the ARTS-IIIA are discussed in Section 4 and Appendix F.

GENERAL CONCLUSIONS

The following is a summary of general conclusions as a result of the signal processing investigation:

1. Radar signal processing techniques can be used to obtain more efficient spectrum utilization. These techniques may include the elimination of processing in the range-azimuth bin containing interference, the use of integration techniques, or variable thresholding techniques. With properly designed signal processing techniques, the suppression of asynchronous interference in low duty cycle radars will have minimal effects on target azimuth shift, angular resolution, and desired signal sensitivity.

2. Since a complete redesign of existing hardware would be required to obtain the full advantage of signal processing techniques for interference elimination, emphasis must be placed upon design standards for new equipment.

3. The cost of realignment or retrofit of existing systems to

eliminate interference must be weighed against the problems created by interference and the cost of other interference reduction techniques such as waveguide filtering.

PRIMARY RADAR CONCLUSIONS

The following conclusions on the signal processing properties of the primary radars in the 2.7 to 2.9 GHz band are based on a combination of measurements, analytical analysis, and simulation:

1. The investigation showed that the ASR-7 binary integrator and ASR-8 feedback integrators can suppress asynchronous interference in the Normal, Moving Target Indicator (MTI), and log-FTC channels with minimal trade-offs in target azimuth shift, angular resolution, and desired signal sensitivity.

2. The desired signal trade-offs in suppressing asynchronous interference are less for the FAA modified binary integrator than for the feedback integrator.

3. In theory the feedback integrators in the analog radars (ASR-4, 5, 6, etc.) should also be capable of suppressing asynchronous interference.

4. The primary radar MTI canceller circuitry produces several synchronous interfering pulses for each interfering asynchronous pulse. Therefore, asynchronous interference in the MTI channel has the potential to be enhanced by the feedback or binary integrator. Thus, if the integrator (enhancer) is not adjusted properly, the level of interference can be greater with the integrator on than with it off.

5. When operating in the log-FTC mode with weather background displayed, interference could potentially be displayed on the PPI since the weather background channel does not have an integrator (enhancer). Since only the master channel of the frequency diversity radars provides the weather background video, proper choice of the master channel may eliminate the potential interference.

ARTS-IIIA POST PROCESSING CONCLUSIONS

The following conclusions are based on a combination of analytical analysis and simulation. Worst-case interference and desired signal level assumptions were made, and consequently, the conclusions may be slightly pessimistic in regard to the impact of interference. The investigation considered the interference effect on a per antenna rotation basis (as opposed to multiple antenna rotation tracking ability) with the ARTS-IIIA interfaced with an ASR-7 or ASR-8 radar. A parametric range of interfering pulse widths

between 0.5 usec and 4.0 usec were considered in the investigation. Conclusions 1 through 7 are based on the Radar Data Acquisition Subsystem (RDAS) detection parameter combinations that FAA National Aviation Facility Experimental Center (NAFEC) recommended for operational use (rank quantizer threshold 23, hit count threshold 9, miss count threshold 3).

1. For interference levels in currently congested U.S. terminal areas, the reduction in the probability of a target being detected in one antenna rotation would typically be less than 2.5 percent. A congested area interference level is considered to consist of one radar interfering at a given time and interference coupling over 50 percent of the victim radar antenna rotation.

2. If the level of congestion increases in the future to the point where a victim radar receives interference from three radars simultaneously over its entire antenna rotation, the probability of detection would be significantly decreased. The analysis indicated that for a worst-case combination of interfering and victim radars, the probability of target detection could be decreased by as much as 15 percent, and the false alarm probability from 4.6×10^{-7} to 11.7×10^{-7}.

3. Interference has a greater impact on the probability of detection and false alarm when the ARTS-IIIA is connected to the radar MTI channel than when connected to the normal channel because the MTI circuits generate several synchronous interfering pulses for each asynchronous interference pulse at its input. For example, the worse-case (three continually interfering radars), reduction in probability of detection for the MTI channel was 15 percent while that for the normal channel was 5 percent.

4. In general, the impact of interference on the probability of target detection depends on the victim radar's range bin characteristics (width, hold, and sample time), and the interfering radar pulse width and PRF. For the case in which the interfering pulse width is less than the sum of the victim radar range bin width and hold time, the level of interference increases as a function of the interfering radar duty cycle. For the case in which the interfering pulse width is greater than the sum of the victim radar range bin width and hold time, the impact of interference is independent of the interfering radar pulse width and increases only with interfering radar PRF.

5. Asynchronous pulse interference will not significantly affect the RDAS automatic video select (Normal or MTI channel) control function. The probability of an incorrect video channel select decision due to worst-case continual interference from three radars was found to be much less than 0.002.

6. Asynchronous pulse interference will not significantly affect the RDAS's automatic MTI hit count threshold control. The probability of an MTI hit count threshold change due to worst-case continual interference from three radars was found to be insignificant.

7. A rank quantizer threshold of 23 gives superior desired signal detector performance and interference suppression performance over a rank quantizer threshold of 24. For a rank quantizer threshold setting of 23, the analysis indicated the optimum hit/miss count threshold which gives the maximum desired signal detection probabilities with or without interference is (9,4).

GENERAL RECOMMENDATIONS

1. An Ad Hoc committee consisting of Government agencies using radiodetermination services should be established to determine what standards should be adopted in regard to radar interference suppression techniques and the trade-offs in their utilization. The committee findings should then be incorporated in the technical standards of the NTIA Manual of Regulations and Procedures for Radio Frequency Management, and implemented at the systems review level and frequency assignment review level.

2. All new radar systems and post processing systems include during the conceptual design stage of development, a performance evaluation in the presence of asynchronous interference, in addition to clutter and noise, in all designed modes of operation.

3. All technical manuals used in the field on radars and post processors include instructions on how to suppress asynchronous interference while minimizing the trade-offs of the desired signal performance.

PRIMARY RADAR RECOMMENDATIONS

1. In order to ensure that an investigation into the accommodation of future planned radar systems in the 2.7 to 2.9 GHz band is based on sound technical procedures, a measurement program should be undertaken to:

    a. Investigate the operational capability of the feedback and binary integrators (enhancers) to suppress asynchronous interference.

    b. Accurately determine the frequency/distance separation requirements necessary for the new radars using filtered magnetrons, klystrons, or Traveling Wave Tube (TWT) transmitter output devices.

2. The accommodation of projected future radar deployments in congested areas should then be investigated using the measurement results and findings in this report.

3. In congested areas consideration should be given to equipping ASR-8 radars with the FAA modified binary integrator used in the ASR-7 radars. The binary integrator provides superior performance over the feedback integrator in minimizing the desired signal trade-offs while suppressing asynchronous interference.

ARTS-IIIA POST PROCESSING RECOMMENDATIONS

1. Since a rank quantizer threshold setting of 23 provides significantly more interference suppression than a threshold setting of 24 without sacrificing over-all radar performance, it is recommended that a rank quantizer threshold setting of 23 be employed on operational ARTS-IIIAs. NAFEC has also recommended a rank quantizer threshold of 23 based on measurements on desired signal performance.

2. Measurements should be performed on the ARTS-IIIA in congested U.S. areas to determine the particular hit/miss count threshold setting combinations that provide an optimum trade-off between target detection and interference suppression.

SECTION 3

PRIMARY RADAR SIGNAL PROCESSING

INTRODUCTION

This section discusses the signal processing properties of radar receivers in the 2.7 to 2.9 GHz band. A detailed discussion of the receiver signal processing properties to noise, desired signal, and asychronous interfering signals is given. Because of the types of services (aeronautical, radionavigation, meteorological, and radiolocation) provided by radars in the 2.7 to 2.9 GHz band, and number of nomenclatures, it was necessary to limit the signal processing investigation to the ASR-7 and ASR-8 radars which are FAA radars used for aeronautical radionavigation.

The ASR-7 and ASR-8 are later model radars which use digital signal processing after signal detection. Both radars have the capability of selecting several modes of operation for display of the received video information.

Normal Channel:

- Normal Video
- Enhanced Normal Video
- Normal Log-FTC Video
- Enhanced Normal Log-FTC Video
- Normal LOG-FTC with Weather Background Video
- Enhanced Normal LOG-FTC with Weather Background Video

MTI Channel:

- MTI Video
- Enhanced MTI Video
- MTI Log-FTC Video
- Enhanced MTI Log-FTC Video
- MTI Log-FTC with Weather Background Video
- Enhanced MTI Log-FTC with Weather Background Video

The weather background channel of the ASR-7 and ASR-8 is very similar to the circuitry of the meteorological radars (WSR-57 and WSR-74S) in the 2.7 to 2.9 GHz band. Therefore, an investigation of the ASR-7 and ASR-8 radar signal processing characteristics is also applicable to the meteorological radars in the band. Also both the normal and MTI channels of the ASR-7 and ASR-8 are very similar to the radiolocation height finding radar in the 2.7 to 2.9 GHz band. Therefore, an analysis of the ASR-7 and ASR-8 radars is generally applicable to all radars in the 2.7 to 2.9 GHz band. Also since the trend in new radar systems is toward digital signal processing, the analysis of the ASR-7 and ASR-8 radars will be more applicable to other new radar systems

coming in the band.

GENERAL SYSTEM DESCRIPTION

Radar system characteristics of major aeronautical radionavigation, meteorological, and radiolocation radars in the 2.7 to 2.9 GHz band is given in Appendix G. As stated previously, this section will only investigate the signal processing properties of the ASR-7 and ASR-8. However, the analysis is applicable to other aeronautical radionavigation, meteorological, and radiolocation radars in the 2.7 to 2.9 GHz band as well as radars in other bands.

In general, all radar receivers in the 2.7 to 2.9 GHz band can be divided into three sections: antenna and RF waveguide, receiver unit, and processor unit. Figure 3-1 shows a typical radar system block diagram of a radar which only operates one channel at a time (non-diversity mode). Figure 3-2 shows a typical radar system block diagram of a radar which has frequency diversity capability (simultaneous dual channel operation). Radars operating in the frequency diversity mode use one of the channels as a master channel for timing information to the slave channel. The two reflected signals from a target are separated in the diplexer and applied to the two receivers. Each signal is processed in its receiver and the two signals are realigned in time and additively combined in the video processor unit of the master channel before being displayed. The following is a general description of antenna and RF waveguide, receiver unit, and processor units of radars in the 2.7 to 2.9 GHz band.

Antenna and RF Waveguide

Several different types of antennas are used by radars in the 2.7 to 2.9 GHz band. All the aeronautical radionavigation radars use a shaped beam reflector which produces a cosecant-squared elevation pattern. The antenna gain of the aeronautical radionavigation radars range between 31 and 34 dBi. The meteorological radars have parabolic dish antennas with a gain of 32 to 38 dBi. The type of radiolocation radar antennas is varied with antenna gains between 32 and 39 dBi. Some of the later model radars have antennas with several horns.

The RF waveguide system generally consists of rotary-joint, several couplers, waveguide switches, circulators, and Transmit-Receiver (TR) limiters. Radars with frequency diversity capability also have RF diplexers. In general, the RF waveguide characteristics of all radars in the 2.7 to 2.9 GHz band are similar, and therefore, the signal processing properties can be generalized.

Receiver Unit

The radar receiver unit includes all the analog circuitry between the receiver RF input and the detector output of the normal, MTI, and log normal radar channels. The receiver unit generally includes a parametric amplifier,

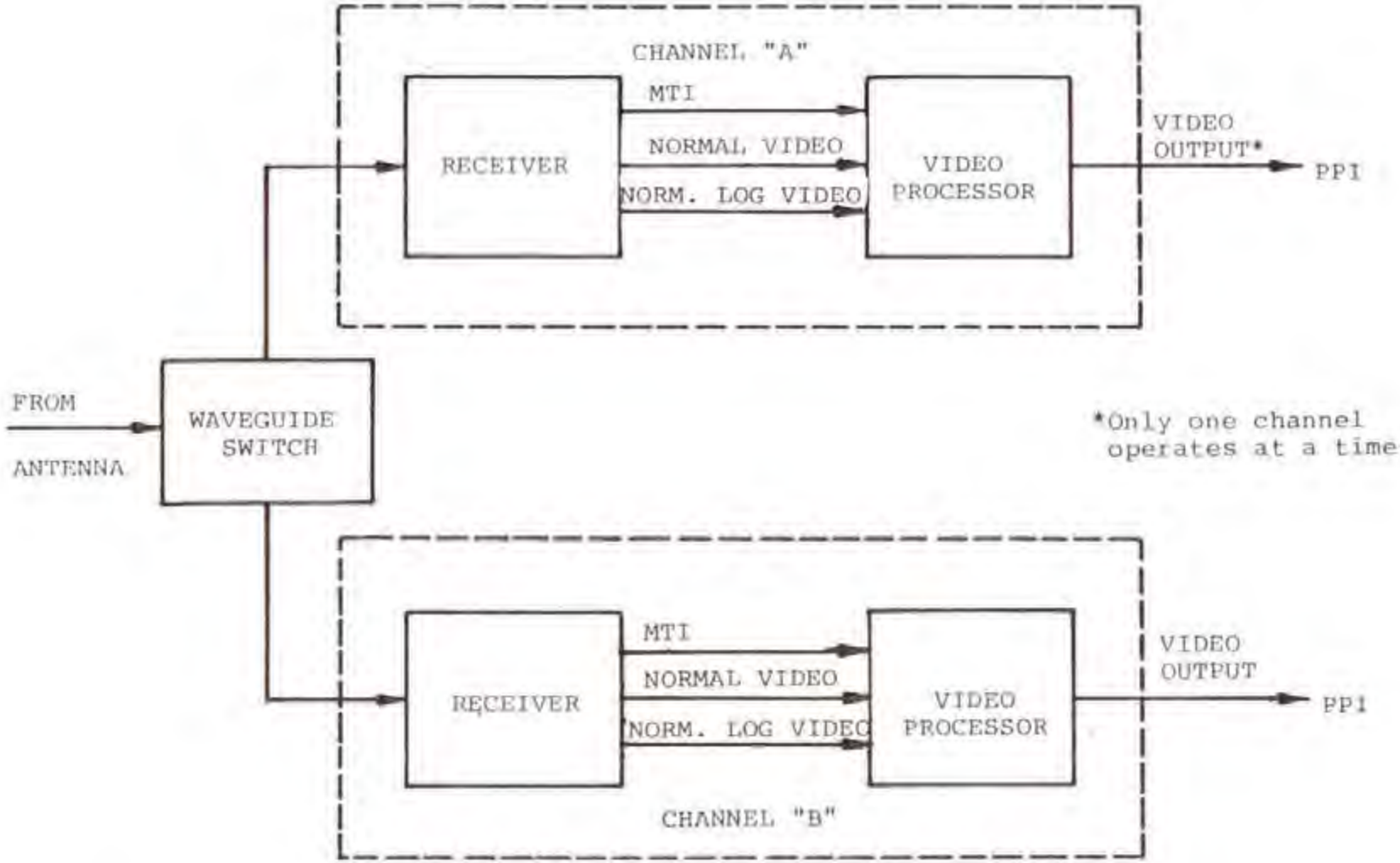

Figure 3-1. Block Diagram of Non-Diversity Radar Receivers

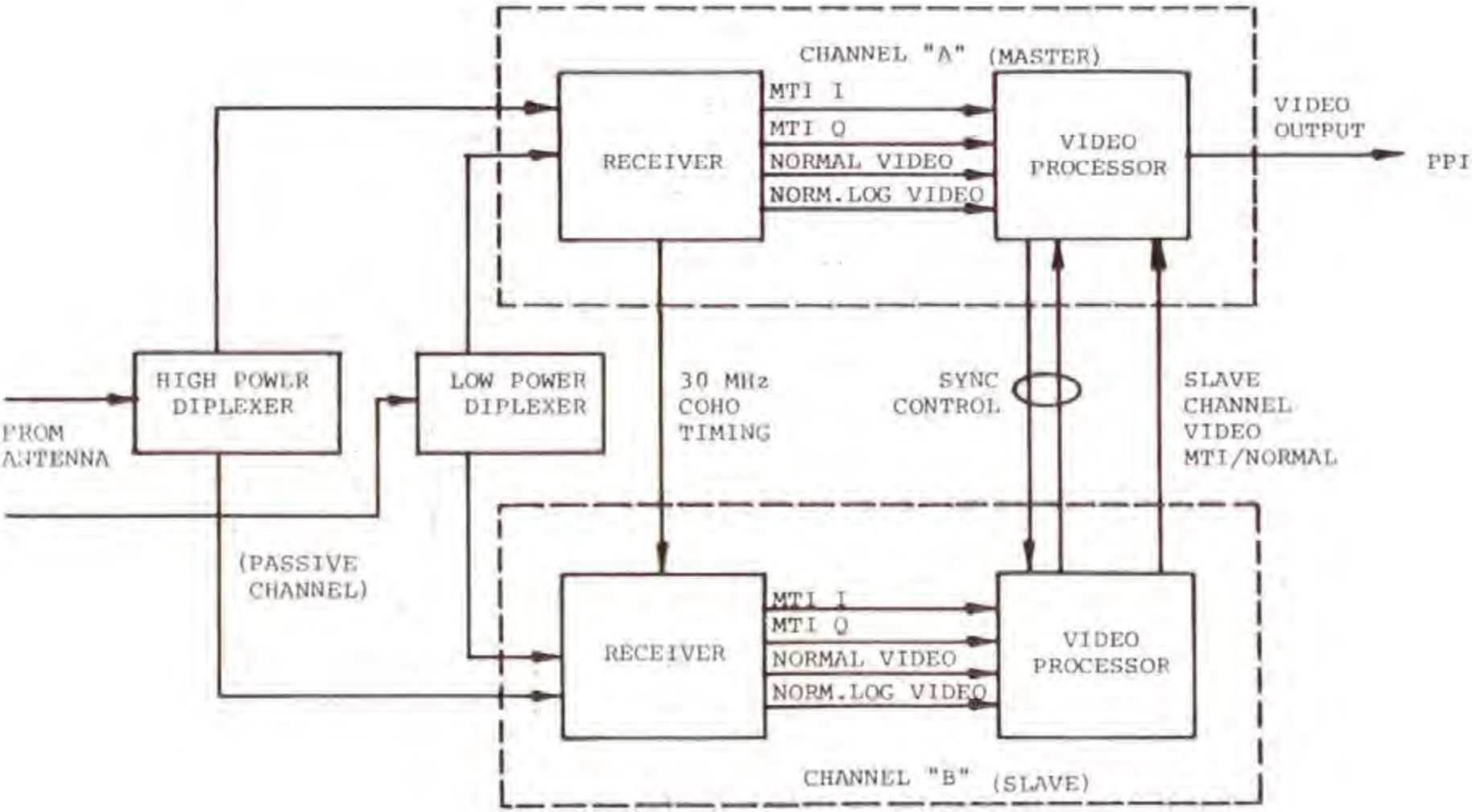

Figure 3-2. Block Diagram of Frequency Diversity Radar Receivers

mixer, IF amplifier, and detectors. The newer radars have solid-state receiver units with the older radars being tube-type. The signal processing properties of the solid-state and tube-type radar receiver units are essentially the same. Since the ASR-7 and ASR-8 have normal, MTI, and log normal channels, the signal processing properties of the ASR-7 and ASR-8 receiver units are generally applicable to all radars in the band.

Processor Unit

The radar processor unit includes all the circuitry between the detector outputs and the display unit. The processor unit generally includes the MTI cancellers, integrator (enhancer), Log Fast-Time-Constant (Log-FTC), and weather background circuitry. The newer radars have digital processor units where the detector output is A/D (analog-to-digital) converted, the signal processing done, and then D/A (digital-to-analog) converted for display. The older radars have analog processor units. The transfer properties of the analog and digital processor units can be treated identically with the exception of the quantization noise due to A/D conversion and roundoff and truncation inherent in digital processing. Therefore, the signal processing properties of the ASR-7 and ASR-8 (digital processor units) is generally applicable to all radars in the 2.7 to 2.9 GHz band.

ANTENNA AND RF WAVEGUIDE SYSTEM

The following is a discussion of the signal processing properties of the antenna and RF waveguide system of typical radars in the 2.7 to 2.9 GHz band. The discussion includes the hardware from the antenna feed horn output to the receiver unit input. The analysis does not include antenna gain, antenna patterns, or polorization discrimination. The antenna types and antenna gains of radars in the 2.7 to 2.9 GHz band are given in Appendix G. Antenna pattern measurement of several radars in the band are contained in a report by Hinkle, Pratt, and Matheson (1976).

Several of the new radars in the band (ASR-8, AN/GPN-20, and AN/TPN-24) have multiple feedhorn antennas and diplexers in the waveguide to permit frequency diversity operation. These new radars have the more complex RF waveguide systems, and have all the waveguide components as the single-horn non-frequency diversity radars. Therefore, the ASR-8 RF waveguide system, which has a normal and passive channel, and frequency diversity capability, was selected as being representative of radars in the 2.7 to 2.9 GHz band.

Figure 3-3 shows a block diagram of the ASR-8 RF waveguide system. The passive channel is used to receive reflected target energy during the first part of the receive period and consists of a rotary-joint, low-power diplexer, TR tube, and waveguide couplers. The normal channel is used to transmit pulses and receive reflected target energy during the remainder of the receive period and consists of a rotary-joint, high-power diplexer, high-power waveguide switch, circulator, and waveguide couplers. Interfering signal power loss in the RF system may occur from insertion loss and, attenuation from the diplexer filter due to frequency separation between the

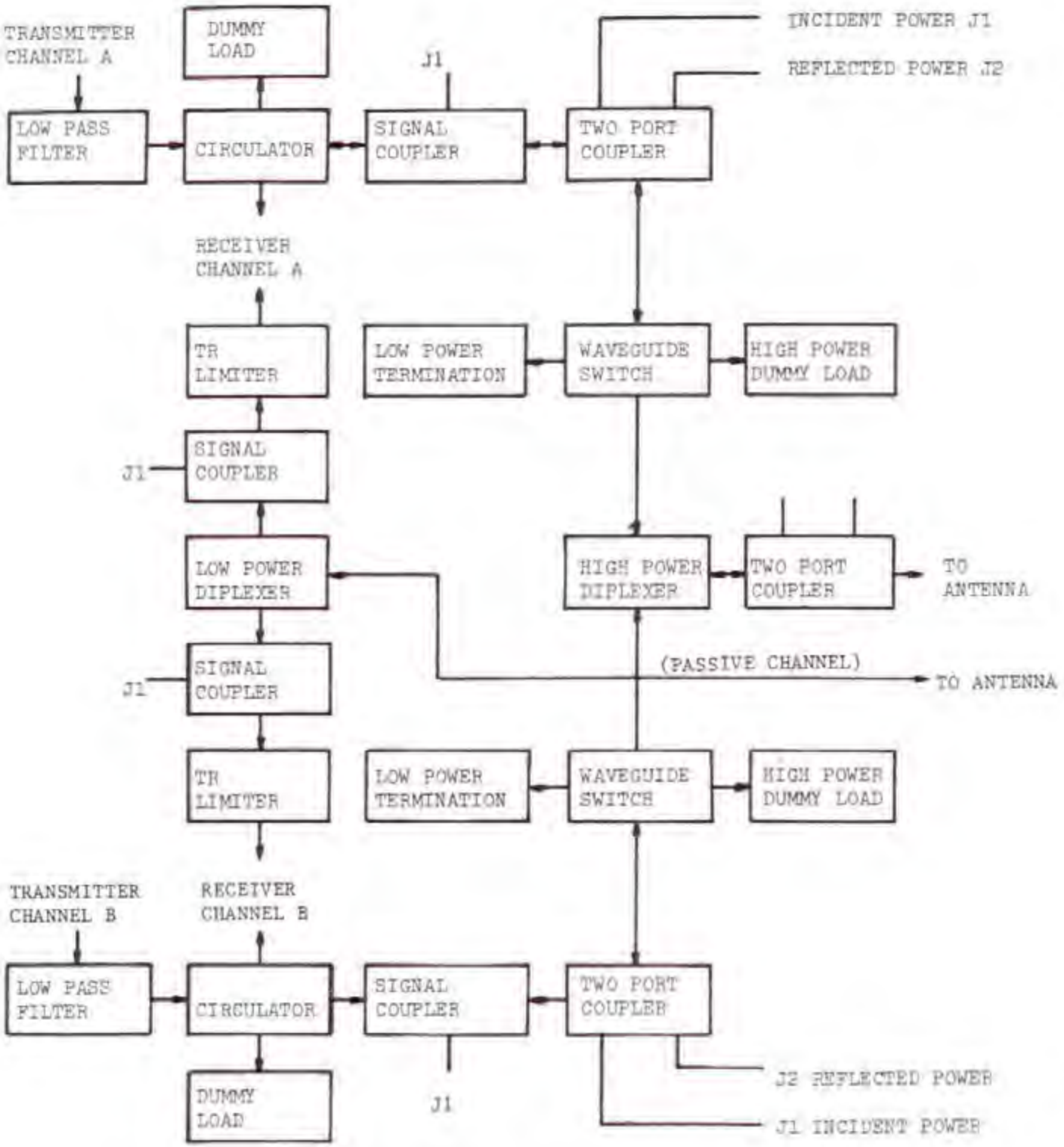

Figure 3-3. ASR-8 RF System Simplified Block Diagram

interfering signal and victim receiver channel tuned frequency. The insertion loss is approximately 2 dB for both the passive and normal channel. Since the low- and high-power diplexer filter bandwidth is much wider than the interference spectrum bandwidth of radars in the 2.7 to 2.9 GHz band, the interfering signal peak power loss for a symetrical emission is given by:

$$\text{For: } \Delta f \leq 1/\pi\tau_I + B_d/2$$

$$P_{I_{OUT}} = P_{I_{IN}} \qquad (3\text{-}1)$$

$$\text{For: } \Delta f > \frac{1}{\pi\tau_I} + B_d/2 \qquad (3\text{-}2)$$

$$P_{I_{OUT}} = \frac{P_{I_{IN}} \; (B_d\tau_I)^2 \; F_{\Delta F}}{4}$$

where:

$P_{I_{IN}}$ = Interfering signal peak power level at diplexer input, in watts

$P_{I_{OUT}}$ = Interfering signal peak power level at diplexer output, in watts

Δf = Frequency separation between interferer carrier and victim receiver tuned frequency, in MHz

B_d = Diplexer 3 dB bandwidth, in MHz

τ_I = Interferer transmitter pulse width, in usec

$F_{\Delta F}$ = Interfering signal emission spectrum level at ΔF relative to level at carrier, in dB

Figure 3-4 shows the selectivity of the ARS-8 diplexer. The frequency selectivity characteristics of diplexer of radars in the 2.7 to 2.9 GHz band varies depending on the radar nomenclature. However, the peak power loss of an interfering signal due to frequency separation is essentially determined by the victim receiver IF selectivity characteristics since the IF bandwidth is much smaller than the RF waveguide diplexer bandwidth.

RECEIVER UNIT

The following is a discussion of the signal processing properties of the receiver unit of the ASR-7 and ASR-8 radars. All the radars in the 2.7 to 2.9 GHz band have a receiver unit very similar to either the normal, log normal, or Moving Target Indicator (MTI) channel of the ASR-7 or ASR-8. Also the signal processing properties of the older tube-type receiver unit radars

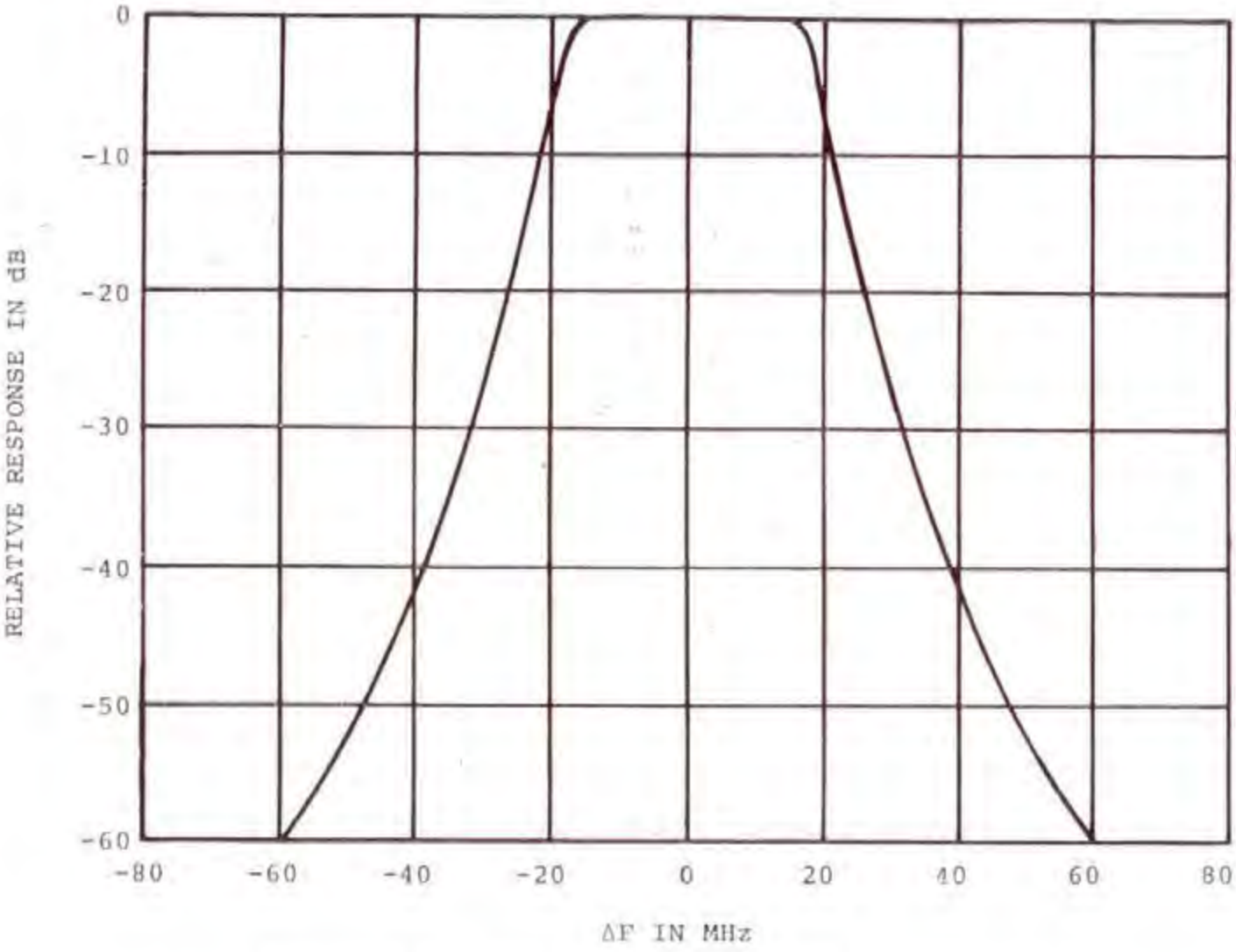

Figure 3-4. ASR-8 Diplexer Filter Characteristics

and the newer solid-state receiver unit radars can be treated identically. In those cases where the ASR-7 or ASR-8 circuitry is significantly different from the other radars in the band, a discussion of the signal processing properties of other types of circuitry will be given.

Figure 3-5 shows a block diagram of the receiver unit of the ASR-8 radar. The radar receiver unit accepts either normal channel or passive channel S-band radar signals from the antenna and waveguide subsystems and provides either normal video, log-normal video, or MTI video to the processor unit.

Receiver Front End

Normal channel RF energy entering the receiver is first applied to the TR-limiter through the waveguide system. The TR-limiter is a passive device. Two diode limiters are used within the TR-limiter for reduction of spike leakage. Output from the TR-limiter is applied through a waveguide-to-coax adapter to the Sensitivity Time Control (STC) attenuator. The attenuator uses bias voltage-controlled RF attenuation of PIN diodes to provide a continuously variable 40 dB range of attenuation at frequencies of 2.7 to 2.9 GHz. STC control voltages are provided to the attenuator from the processor unit. Using control voltages in steps 0 and +10 volts the attenuation provides linear attenuation throughout the input frequency band. Insertion loss is less than 0.6 dB at zero control voltage. Bias voltages of +15 and -15 Vdc are supplied to the attenuator from the respective power supplies located in the module rack. RF energy from the STC attenuator is sent to the antenna pattern switch. The antenna pattern switch is a solid-state device using PIN diodes to switch RF from the normal beam to the passive beam. Switch control logic signals from the processor unit are converted to normal and passive drive signals in the switch driver assembly. The switch drive signals are used by the antenna pattern switch to perform the switching. Either normal or passive beam RF energy is coupled out to the parametric amplifier.

TR Limiter

The TR limiter protects the receiver from high level RF energy during the transmitter pulse. Lower level energy which might not have sufficient amplitude to ionize the TR tube directly is reflected by the limiter portion of the assembly. The effect of the TR limiter on an interfering signal would be to attenuate the interfering signal if it coincided with the transmitted "on" period. During the receive period the TR limiter has approximately a 0.3 dB insertion loss.

Sensitivity Time Control (STC) Attenuators

High levels of reflected energy from ground clutter will saturate the receiver if not reduced in level before entering the parametric amplifier and the following receiver elements. The STC attenuators reduce this clutter as required at any particular site. The attenuators are controlled by signals from the processor unit. Two separate but identical function generators in

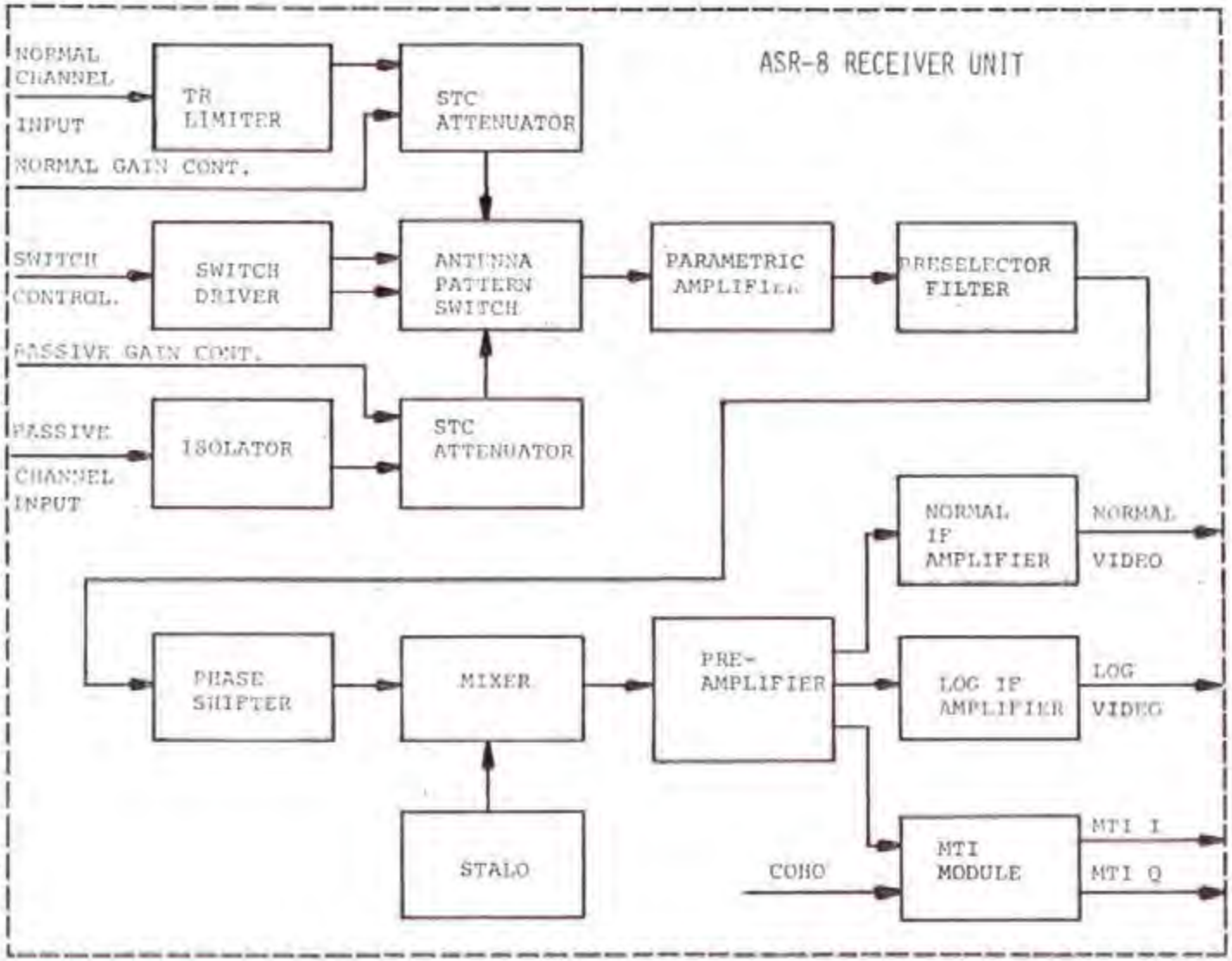

Figure 3-5. ASR-8 Receiver Unit Block Diagram

the processor are provided, one for the normal antenna beam and one for the passive antenna beam. Board-mounted switches permit selection of the initial attenuation (up to 40 dB), delay of initiation of the STC curve after the transmitter pulse up to 100 microseconds, and selection of the STC curve exponent from $1/R$ to $1/R^5$. Receiver sensitivity control, using the RF attenuator, is digitally added to the STC function. Five values of preset receiver sensitivity can be selected by the radar control panel; the individual levels are preset using board-mounted switches. A digital-to-analog converter changes the composite digital STC and sensitivity control signal to an analog voltage to control the RF attenuator. Figure 3-6 shows the STC characteristics of the ASR-8.

The STC function in some radars in the 2.7 to 2.9 GHz band is achieved by varying the IF amplifier gain as a function of time. However, the affect of STC circuitry on a desired or interfering signal is the same. That is, the STC attenuators will attenuate the signal level as a function of the radar receiver period in which the pulse arrives, generally eliminating low level interference in the center of the PPI scope.

Antenna Pattern Switch

The antenna pattern switch accepts signal drive current from the switch driver and connects the receiver to either the normal or passive channels. The switch uses fast-acting PIN diodes which allow channel switching to occur within 100 ns. The antenna pattern switch will reduce the interfering signal power level when the interference is coupled in through the passive horn which has a higher tilt antle than the normal horn. The reduction in interfering signal power can be determined from the mainbeam antenna elevation patterns of the passive and normal horns. The affect of the antenna pattern switch in the interference is that from mainbeam antenna coupling of the victim receiver, the level of interference will be reduced in the center of the PPI display. When the interference is coupled in through the backlobe of the victim radar, the switching between passive and normal horn will not have a significant effect on the median interfering signal level.

Passive Channel

Passive channel RF energy enters the receiver unit from an externally-connected TR-limiter. The energy passes through a two-port isolator to the STC attenuator. Operation of the passive STC attenuator is identical to the normal STC attenuator.

Parametric Amplifier

The antenna pattern switch feeds the signals from the passive and normal channel to the parametric amplifier. The parametric amplifier provides low-noise amplification of RF energy prior to down conversion. The amplifier covers the entire radar frequency range of 2.7 to 2.9 GHz, and has a minimum gain of 15 dB. Noise figure of the parametric amplifier is 1.25 dB maximum.

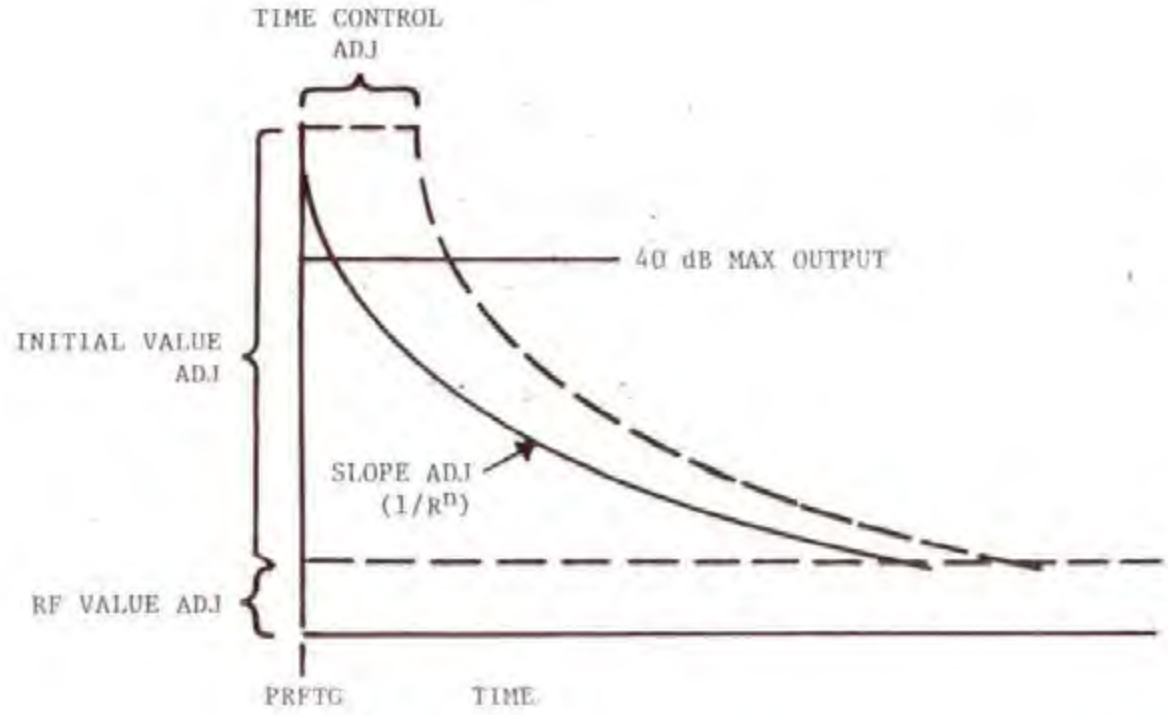

Figure 3-6. STC Waveform Generation

Saturation, the signal level at which the gain decreases 1.0 dB, occurs at an input power level of -30 dBm.

Since this investigation only covers interference from radars in the 2.7 to 2.9 GHz band, the parametric amplifier will not provide any Frequency-Dependent-Rejection to radars in the 2.7 to 2.9 GHz band. For analytical reasons, the parametric amplifier is assumed to be a linear amplifier with 0 dB gain. This assumption of linearity and 0 dB gain allows signal and noise to be treated separately.

Preselector Filter

The preselector filter prevents external signals not in the receiver passband from interfering with receiver operation. The preselector filter is composed of four direct-coupled cavities and has a 10 MHz passband at any selected frequency between 2.7 and 2.9 GHz. The filter has 60 dB rejection at frequencies 50 MHz from the center of its passband. Four micrometer tuners are used to set the filter to any desired frequency from 2.7 to 2.9 GHz. The insertion loss of the filter is approximately 0.6 dB. The effect of the preselector filter on an interfering signal will be to attenuate those signals which fall outside the receiver passband. Since the interfering signal peak power loss as a function of frequency separation (ΔF) is mainly determined by the IF filter selectivity, the analysis of interfering signal peak power loss as a function of interfering signal frequency separation will be discussed in the IF filter section.

Phase Shifter

The phase shifter is used to vary the electrical length of the line between the preselector filter and mixer. Some power from the incoming signal is converted to the image frequency in the mixing process. This power propagates out the mixer input port toward the preselector. It is reflected from the preselector back to the mixer. The phase shifter adjusts the phase of the reflected image so that the IF signal voltage resulting from it is in phase with the IF voltage from the signal frequency. Mixer conversion loss is improved in this manner. The insertion loss of the phase shifter is approximately 0.3 dB. The phase shifter will change the phase of the interfering signal.

Mixer

RF to IF signal conversion of received signals is accomplished by mixing the stable local oscillator (STALO) output signal with the amplified RF return signal. Mixing takes place in the crossbar mixer while the preselector filter and phase shifter are also employed to improve conversion efficiency. The echo signal at frequency ω_o or an interfering signal at frequency $\omega_o+\Delta\omega$ mixes in the mixer with the STALO signal ($\omega_o+\beta_o$) where β_o is equal to 30 MHz. The main signal component produced is the difference between the two inputs, which is the IF frequency β_o. In addition to the IF frequency, harmonics of the STALO frequency and harmonics of the sum of the

STALO and input signal frequencies are produced.

The STALO provides a reference RF signal between 2.67 and 2.93 GHz for the receiver signal mixer to down or up convert received signals to the 30 MHz IF. A three-cavity tunable bandpass filter selects the desired STALO frequency and attenuates the adjacent frequencies by 30 dB or greater applying the output to a RF network. The RF network is a two-stage S-band transistor amplifier which provides +11 dBm gain to the output. The noise 30 MHz away from the carrier is suppressed to near thermal noise. This precludes the STALO signal in the receiver mixer from having appreciable noise or spurious products at the intermediate frequency.

It is shown in Appendix A that the signal-to-noise ratio (SNR) and interference-to-noise ratio (INR) at the mixer output is the same as at the mixer input. Thus the signal transfer properties of the mixer can be expressed as:

$$SNR_{mo} = SNR_{mI} \qquad (3\text{-}3)$$

Preamplifier

The preamplifier model provides low noise amplification of the IF signal. Outputs from the preamplifier are coupled to the normal, log normal, and MTI radar channels. The bandwidth of the preamplifier is approximately 10 MHz, same as the preselector. Therefore the interfering signal time waveform at the preamplifier output will be similar to that at the preselector output (if saturation does not occur) with the exception of the frequency conversion produced by the mixer. As previously mentioned the effect of the preamplifer 10 MHz bandwidth on an interfering signal will be to attenuate those signals which fall outside the receiver passband. Since the interfering signal peak power loss as a function of frequency separation (ΔF) is mainly determined by the IF filter selectivity, the analysis of interfering signal peak power loss as a function of interfering signal frequency separation will be discussed in the IF filter section.

Normal Channel

The normal channel IF subassembly accepts the 30 MHz IF signal from the preamplifier module and provides IF amplification, video detection, and video amplification. The normal channel video amplifier output is a low-noise high-gain video signal supplied to the processor unit.

IF Amplifiers

The normal channel IF amplifiers consist of four wide-band symetrical limiter amplifiers followed by five IF passband filter stages. The overall

bandwidth of the IF stages is 1.2 MHz. Appendix B contains a detailed analysis of the ASR-8 IF selectivity and signal transfer properties.

The relative IF filter selectivity response $A_{dB}(F)$ is derived in Appendix B, Equation B-19, and can be expressed as:

$$A_{dB} = -20 \log (1 + X^2)^{5/2} \qquad (3\text{-}4)$$

where:

$$X = \frac{2\Delta F'}{B_S}$$

and:

$\Delta F'$ = Frequency relative to the receiver IF tuned frequency B_{OF} in Hz

B_S = IF amplifier stage 3 dB bandwidth, in Hz

Since the normal channel IF amplifier stages have a narrower bandwidth and sharper selectivity characteristics than the preceding receiver unit stages, a desired signal or interfering time response at the IF amplifier output is essentially governed by the normal channel IF selectivity characteristics.

For an interfering signal, the peak power and time waveform response at the IF filter output is determined by the receiver IF selectivity characteristics, interfering signal emission spectrum, and frequency separation between the interfering signal carrier and the victim receiver tuned frequency. In general, the receiver front end prior to the receiver normal channel input can be modeled as a linear receiver with 0 dB gain allowing the IF input interference-to-noise ratio, $(INR)_{IF_i}$, to be expressed as (Equation B-37a):

$$INR_{IF_i} = I_{i_{dbm}} - N_{i_{dBm}} \qquad (3\text{-}5)$$

where:

$I_{i_{dBm}}$ = Interfering signal peak power level at the receiver input, in dBm

$N_{i_{dBm}}$ = Receiver noise level, in dBm

The amplitude distribution of the noise at the IF input and output is

Gaussian. The IF output interference-to-noise ratio, INR_{IF_o} can be expressed as (Equation B-38):

$$INR_{IF_o} = INR_{IF_i} - FDR \qquad (3\text{-}6)$$

where:

FDR = Receiver Frequency Dependent Rejection, in dB

The Frequency-Dependent-Rejection (FDR) of the interfering signal is determined by Equation B-21 and is discussed in detail in Appendix B.

The interfering signal IF output time waveform can be expressed as an amplitude and phase modulated pulse given by:

$$V_{IF_o}(t) = Bp(t') \cos [\beta_o t + \phi_o + \phi(t')] \qquad (3\text{-}7)$$

where:

B = Interfering signal voltage amplitude

p(t') = Interfering signal amplitude modulation after IF filtering, value between 0 and 1

β_o = Receiver tuned IF frequency, in radians per second

ϕ_o = Interfering signal carrier phase angle

t' = $t - t_o$ where t_o is the delay time of the IF filter

$\phi(t')$ = Interfering signal phase modulation after IF filtering

The interfering signal IF output time response is a function of the interfering signal pulse width (τ), frequency separation between the interfering signal carrier and the victim receiver tuned frequency (ΔF), and the receiver IF bandwidth (B_{IF}). A detailed discussion of an interfering signal IF output time response as a function of these parameters is given in Appendix B. Figure 3-7 summarizes typical IF output time waveforms for different τB_{IF} products and ΔF's.

Envelope Detector

The envelope detectors used in the normal channel of radars in the 2.7 to 2.9 GHz band generally consists of a full-wave detector followed by a low pass filter and a video amplifier. The IF signal level at the detector input

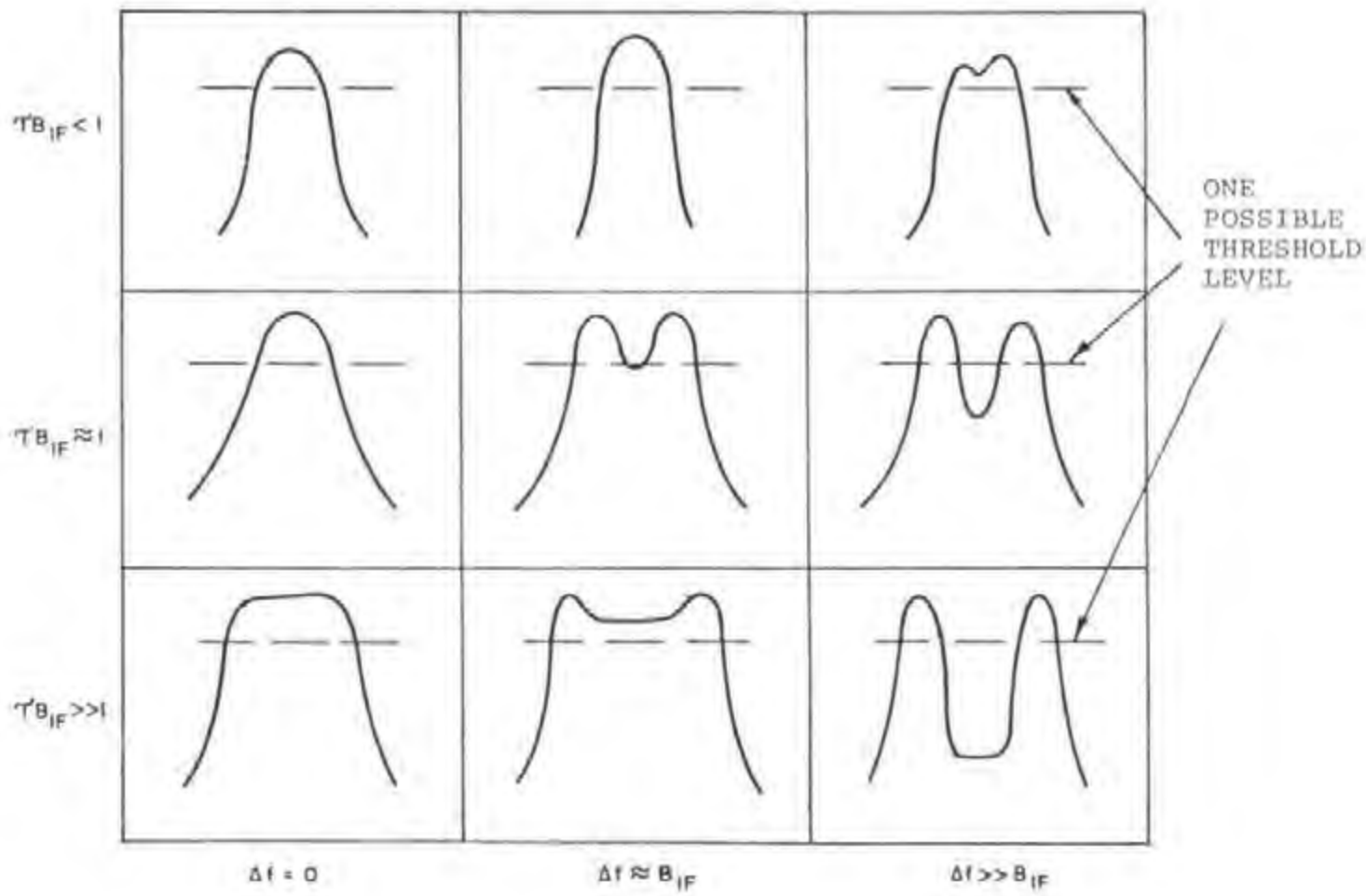

Figure 3-7. Typical IF Output Time Waveform Responses for On-Tune and Off-Tune Pulses

is generally large enough for operation in the linear portion of the diode detectors. However, for completeness both the signal-to-noise transfer properties of a linear and square law detectors are given.

Figure 3-8 shows the signal-to-noise (SNR) transfer characteristics of a linear detector (R. Gannaway, 1965). The signal-to-noise (SNR) transfer characteristics of the square-law detector are shown in Figure 3-9, and are given by (R. Gannaway, 1965 and Davenport and Root, 1958):

$$SNR_o = \frac{(SNR)_i^2}{1 + 2\,(SNR)_i} \qquad (3\text{-}8)$$

For small input signal-to-noise ratios (SNR; <10 dB), the linear and square-law detectors have similar transfer properties. For large input signal-to-noise ratios (SNR; >10), the linear detector performance is better than the square-law detector. However, the collapsing loss for a linear detector is much greater than the collapsing loss for a square-law detector. Thus the difference between the linear and square-law detector performance in the required detector input signal-to-noise ratio is less than a dB (Trunk, 1972). The collapsing loss is the additional signal required to maintain the same probability of detection (P_d) and probability of false alarm (P_{fA}) when noise along with the desired signal-plus-noise are integrated. Figures 3-8 and 3-9 can also be used for the interference-to-noise (INR) transfer properties of a linear and square-law envelope detector, respectively.

The noise amplitude distribution at the linear detector output is Rayleigh distributed. The signal-plus-noise probability density function (PDF) at the envelope detector output for a non-fluctuating target (Marcum Case 0) has a Rice distribution (1954) given by:

$$p(v,A) = \frac{ve}{\sigma^2}\,\frac{-(v^2+A^2)}{2\sigma^2}\,I_o\left(\frac{vA}{\sigma^2}\right) \qquad (3\text{-}9)$$

where:

$I_o(\cdot)$ = Modified Bessel function of the first kind of order zero

A = Peak signal amplitude, in volts

σ = rms noise level, in volts

The normal channel envelope detector output signal-plus-noise was simulated to investigate trade-offs in suppressing asychronous interfering signals. The simulation of the radar normal channel is discussed in Appendix E. Figure 3-10 shows the Rice PDF given by Equation 3-9 as a function of the signal-to-noise ratio.

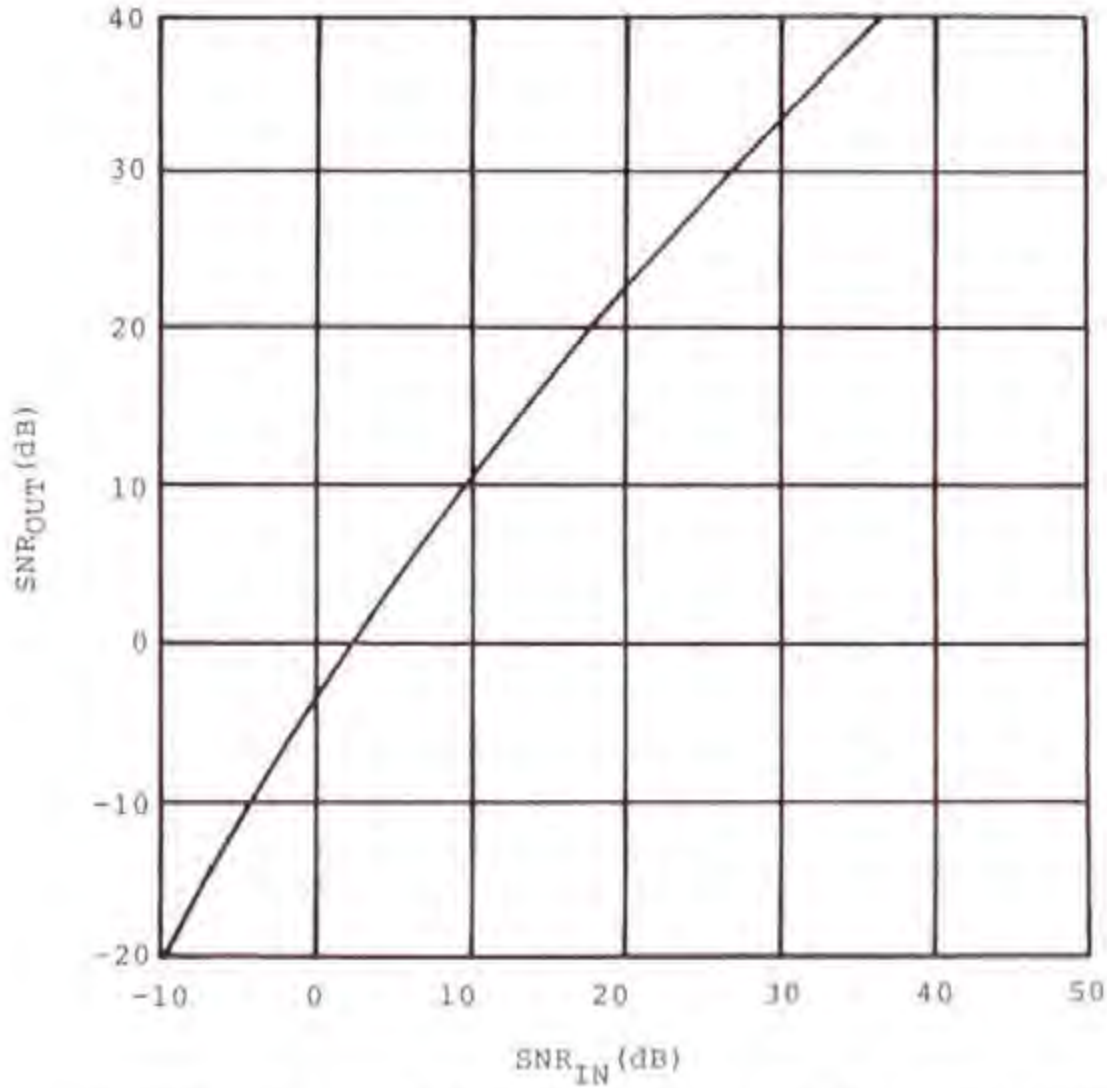

Figure 3-8. Signal-To-Noise Ratio Transfer Properties of a Linear Detector

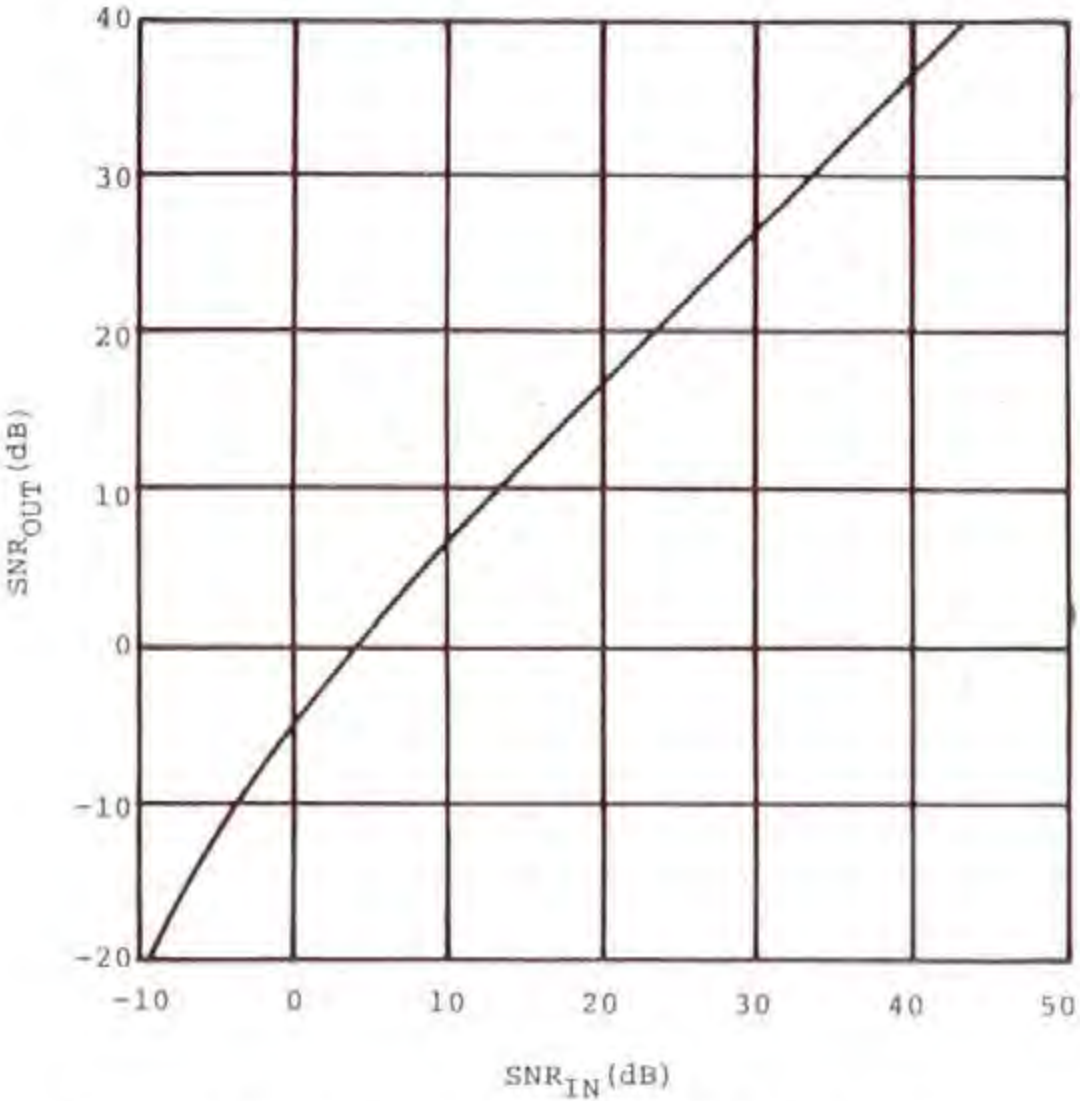

Figure 3-9. Signal-to-Noise Ratio Transfer Properties of a Square-Law Detector

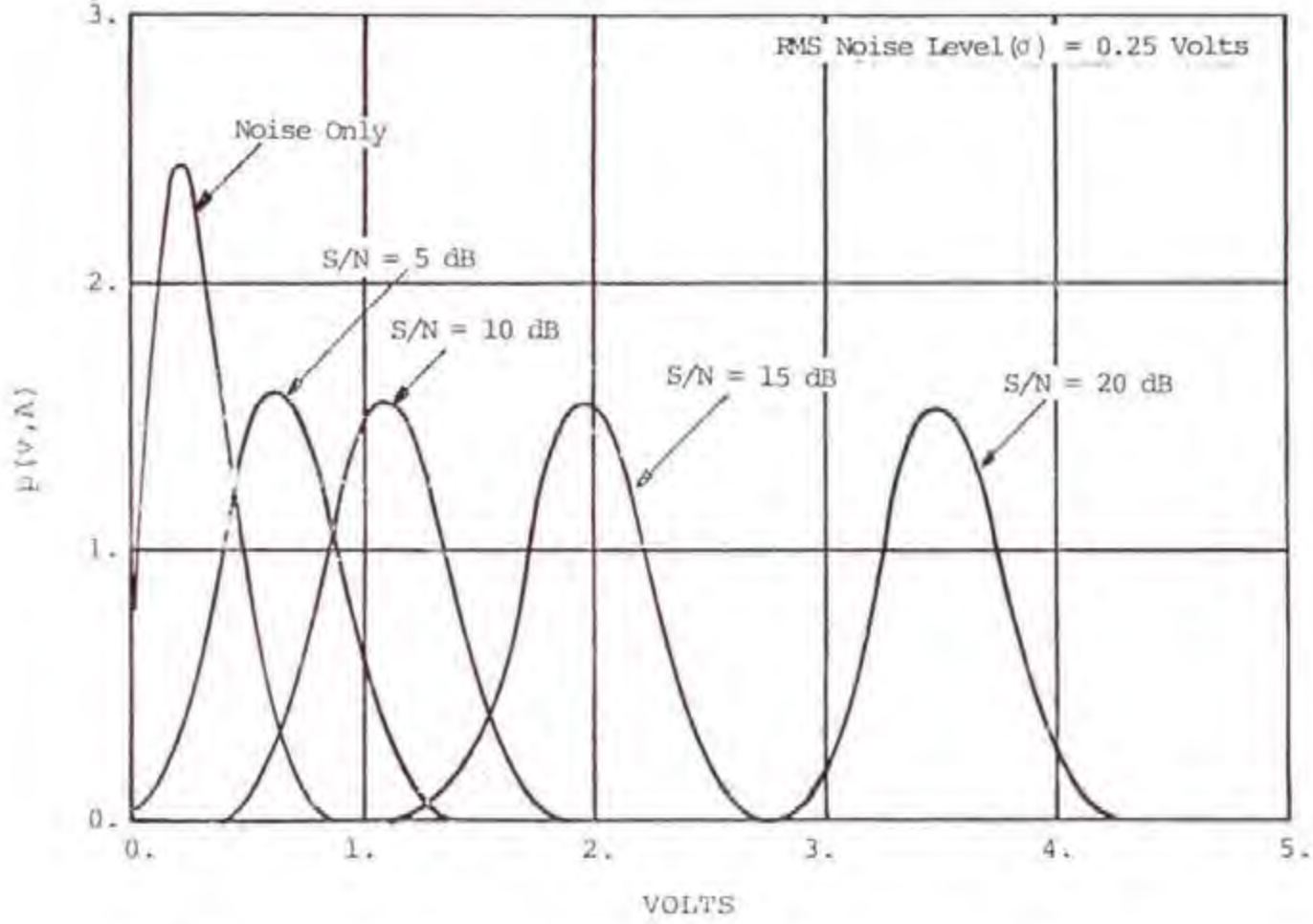

Figure 3-10. Probability-Density Function for Noise Only and for Signal-Plus-Noise at the Normal Channel Envelope Detector Output.

The envelope detector video output is low-pass filtered and amplified. For the normal channel the low-pass filter bandwidth is usually matched to the receiver normal channel IF bandwidth. Therefore, there is no improvement in the signal-to-noise ratio between the input and output of the normal channel low-pass filter. The low-pass filter output is amplified and sent to the video processor unit.

Log-Normal Channel

The log-normal channel IF subassembly accepts the 30 MHz IF signal from the preamplifier module and provides log IF amplification, video detection, and video amplification. The function of the log amplifier is to normalize the variances in precipitation clutter. The circuits operate on the principle that precipitation clutter, after being passed through a logarithmic response, has a noise variation about the average value that is independent of the average value. Filter circuits subtract out the average, leaving only the constant residue level. This level is adjusted to be equal to the receiver noise, thus totally eliminating precipitation clutter from the display. In the radar normal channel, the log function is performed by the log IF subassembly in the receiver unit. The filtering and subtraction is performed by the normal/LOG-FTC assembly in the processor unit. In general, the normal log IF channel amplifies IF signals logarithmically so that small target amplitudes are amplified more than large target amplitudes, and suppresses precipitation clutter; thus allowing for possible detection of small targets in precipitation clutter.

The log IF amplifier also permits a large radar receiver dynamic range in excess of 80 dB in some radars. Log IF amplifiers are also used in the WSR-57 and WSR-74S weather radars for the purpose of achieving a large dynamic range.

The ASR-7 and ASR-8 have a log IF bandpass filter followed by a chain of untuned amplifier-video detectors and a video amplifier (see Figure 3-11). The gain of the string of amplifier-video detectors is such that the last stage in the string becomes overdriven with inherent noise signals and limiting commences. As the 30 MHz signal amplitude increases, successive stages toward the first stage becomes overdriven and further limiting occurs. The net effect is that the video output increases as a function of the log of the input signal. The resultant video output is sent to both the weather channel and the subtractor antilog circuitry in the processor unit. The log-function begins at signal levels 20 dB below the rms noise level for the ASR-7 and ASR-8. Some radars (WSR-57 and WSR-74S) include the tuned bandpass filter circuits in the amplifier-video detector chain. Therefore, the log IF amplifier bandwidth becomes a function of the signal level.

Log IF Bandpass Filter

As with the normal channel IF bandpass filter, this log IF bandpass filter has a much narrower bandwidth and a sharper selectivity characteristic

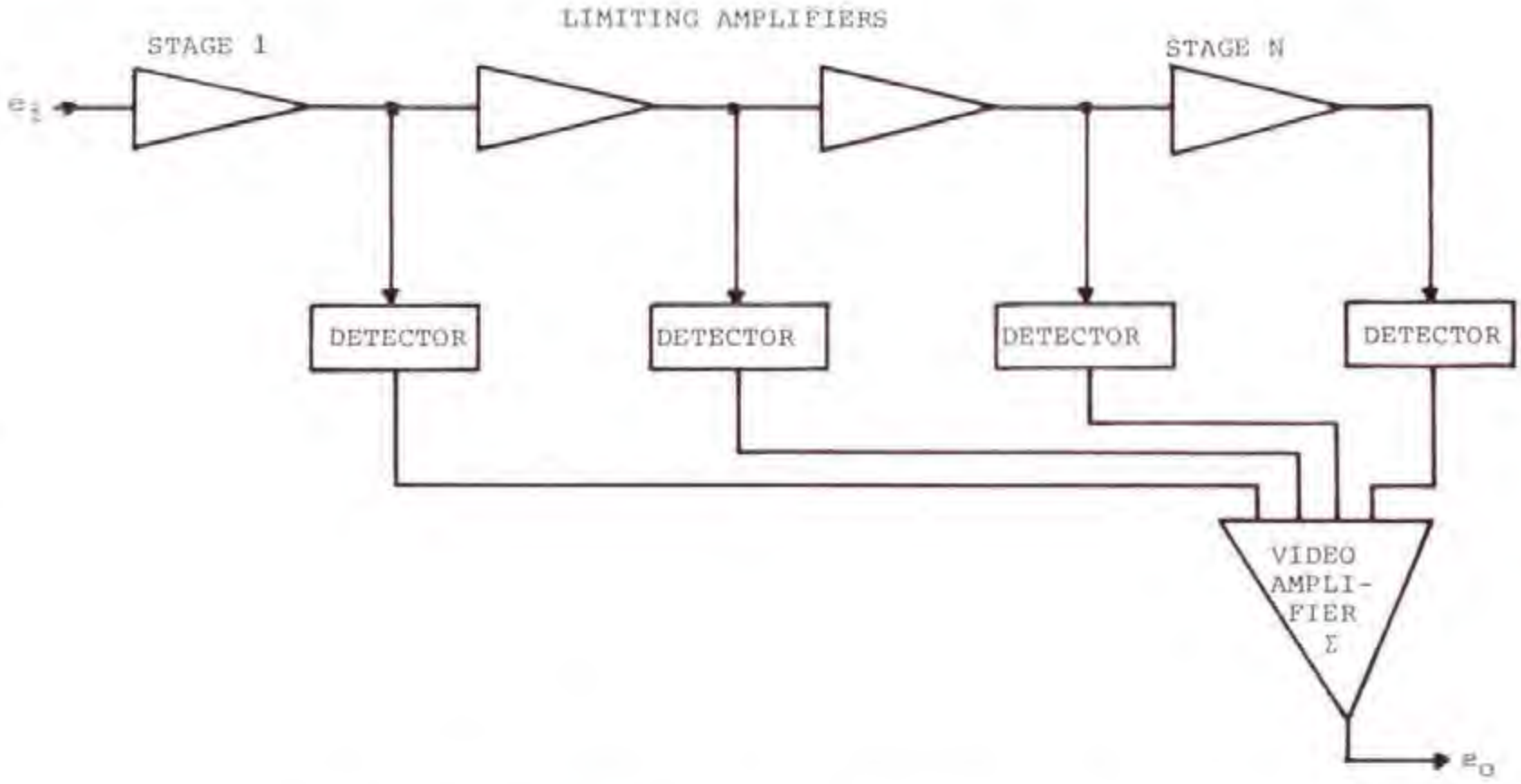

Figure 3-11. Logarithmic Amplifier-Detector Block Diagram.

than the preceding receiver unit stages. Therefore, the desired signal or interfering signal time response at the log IF bandpass filter output is essentially governed by the log IF bandpass filter characteristics.

The desired and interfering signal transfer properties of the log IF bandpass filter are identical to the normal channel IF bandpass filter, and are discussed in detail in Appendix B and previously discussed in the radar normal channel section (Equations 3-5 through 3-7 and Figure 3-7).

Log IF Amplifier-Video Detector

Figure 3-11 shows a typical block diagram of the log IF amplifier and video detector hardware of the ASR-7 and ASR-8 radars. The response of a log amplifier can be expressed as:

$$e_o = a \ln [1 + be_i] \qquad (3\text{-}10)$$

Where the break point between the linear region and logarithmic region occurs approximately where $be_i=1$. The signal-to-noise ratio (SNR) transfer properties have been derived (Atlantic Research Corporation, 1974), and are given by:

$$(S/N)_o = (\eta_{S+N} - \eta_N)^2/\sigma_N^2 \qquad (3\text{-}11)$$

where:

$$\eta_{S+N} = \ln(1 + 0.885\ kF) - 1/2 \left(\frac{0.215\ K^2 B}{(1 + 0.885\ kF)^2}\right)$$

$$\eta_N = \ln(1 + 0.885\ K) - 1/2 \left(\frac{0.215\ K^2}{(1 + 0.885K)^2}\right)$$

$$\sigma_N^2 = \frac{0.215\ K^2}{(1 + 0.885\ K)^2}$$

$$F(-1/2;\ 1;\ -z) = e^{-z/2}\ [(1 + z)\ I_o\ (z/2) + zI_1\ (z/2)]$$

$$B = \left(\frac{1 + 2.33\ (S/N)_i}{1 + (S/N)_i}\right)$$

$$z = (S/N)_i$$

Figure 3-12 shows the signal-to-noise transfer characteristics for various Break Points (BP) in a logarithmic amplifier relative to the RMS noise input level. As previously mentioned the ASR-7 and ASR-8 have a BP = -20 dB.

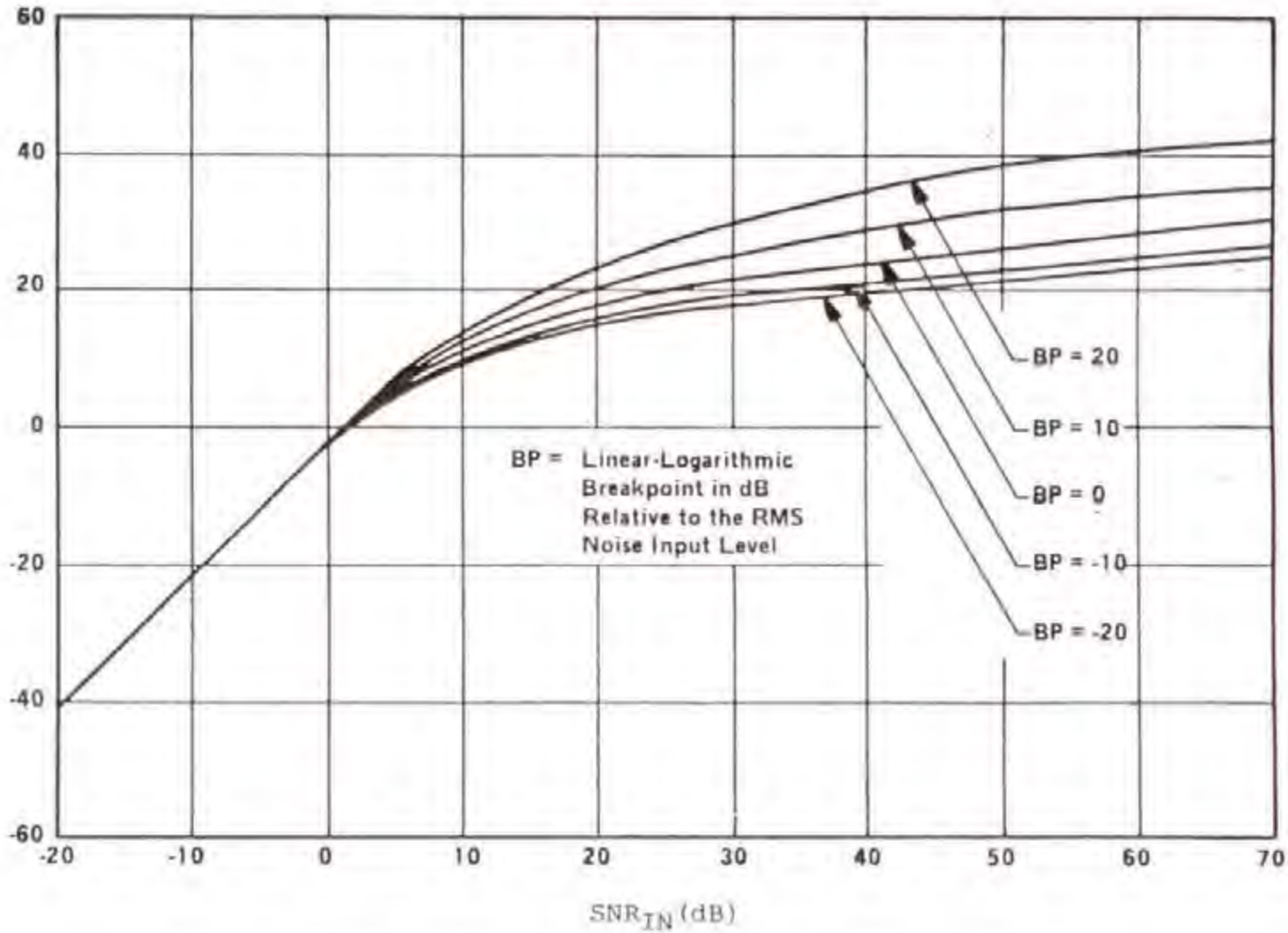

Figure 3-12. Log Amplifier Transfer Characteristics

The signal-to-noise ratio (SNR) transfer characteristics shown in Figure 3-12 are also applicable to interfering signal transfer characteristics.

The detectors in the log-normal channel are linear envelope detectors. Therefore, the signal-to-noise ratio (SNR) transfer curve shown in Figure 3-8 can be used.

Moving Target Indicator (MTI) Channel

The ASR-8 MTI receiver unit channel consists of IF filter, linear limiting amplifier, quadrature phase detector, and low pass filter amplifier circuits (Figure 3-13). The receiver unit MTI channel output feeds the digital cancelling circuits and other processing circuits in the processor unit. The function of the MTI receiver unit channel and processor unit is to reduce ground clutter return and stationary target echoes to system noise level and to enhance moving target echoes on the PPI display. This is accomplished by using the phase difference between the transmitted pulse and reflected pulse. The COHO provides the basic timing and phase reference. One output from the COHO is mixed with an output from the STALO to produce the RF signal used to drive the transmitter amplifier. Another output from the COHO is applied to the phase detector in the MTI circuit. This output retains the phase of the transmitted signal. After down conversion to IF, the returned signal is amplified and applied to the phase detector. The phase detector output voltage is proportional to the phase difference between the transmitted (reference) signal and the returned signal. For stationary targets, the phase difference from pulse to pulse is always the same, causing the output voltage from the phase detector to be constant. For moving targets, the changing range from pulse to pulse causes a pulse-to-pulse change in phase. The output voltage from the phase detector varies from pulse-to-pulse rather than remaining constant as it does for stationary targets. The output from the phase detector, consisting of the return from both stationary and moving targets, is sent to the processor unit where the constant voltage is removed leaving only the fluctuating voltage caused by moving target echoes. The fluctuating voltage is applied to the PPI to provide the visual presentation of moving targets. In a MTI system employing a single phase detector and canceller the voltage fluctuations cause fading of parts of the visual display as the antenna scans past the moving target. To overcome this undesirable fading, the ASR-8 employs an "inphase" (I) and "quadrature" (Q) phase detector and digital canceller for each of these MTI channels. Because the phase detector output varies from a plus voltage through zero to a minus voltage as the relative phase between transmitted and received signals varies through 180 degrees, there are times when the return from a target produces a zero or near-zero output from the phase detector. If a second phase detector is used and supplied with a reference voltage delayed in phase 90 degrees from the reference voltage supplied to the first detector and the reflected voltage is divided and applied in phase to the signal inputs of each of the phase detectors, there is always a non-zero output from one of the detectors. If after cancellation, the two phase detector outputs are combined with the appropriate format, very little fluctuation will be present in the moving target voltage applied to the PPI.

A block diagram of the ASR-8 receiver unit MTI I and MTI Q channel is shown in Figure 3-13.

IF Filter

The ASR-8 MTI channel IF filter consists of eight cascaded synchronous single tuned stages with a 3 dB bandwidth of 5.0 MHz. The relative IF filter amplitude response $A_{dB}(F)$ is derived in Appendix B, and can be expressed as (Equation B-19):

$$A_{dB}(F) = -20 \log (1 + X^2)^{8/2} \qquad (3\text{-}12)$$

where:

$$X = \frac{2\Delta F}{B_S}$$

and:

ΔF = Frequency relative to the receiver IF tuned frequency , in Hz

B_S = IF amplifier stage 3 dB bandwidth, in Hz

Since the MTI IF filter has the narrowest bandwidth and sharpest selectivity characteristics, the interfering signal peak power loss as a funtion of off-tuning (Frequency-Dependent-Rejection, FDR) is essentially governed by the receiver IF selectivity characteristics, interfering signal emission spectrum and the frequency separation between the interfering signal and victim radar tuned frequency. Appendix B discusses in detail the signal transfer properties of an IF filter. In summary, the MTI channel IF filter transfer properties can be treated the same as the normal channel. That is the interference-to-noise ratio (INR) at the MTI channel IF input is given by Equation 3-5, and the transfer properties of the MTI IF filter are given by Equation 3-6. Also the MTI channel IF output time waveform is given by Equation 3.7.

Since the MTI channel uses a phase detector which is amplitude and phase sensitive, both amplitude and phase modulation of the interfering signal IF output time waveform are important. Appendix B discusses in detail both the amplitude and phase response of an IF filter to an interfering signal as a function of off-tuning. It is shown in Appendix B that when the interfering signal is off-tuned, the IF filter causes a beat tone phase modulation during the steady state portion of the pulse equal to the off-tuning (Figure B-15). The affect of this beat tone phase modulation in relation to the MTI channel interfering signal processing properties will be discussed later. The

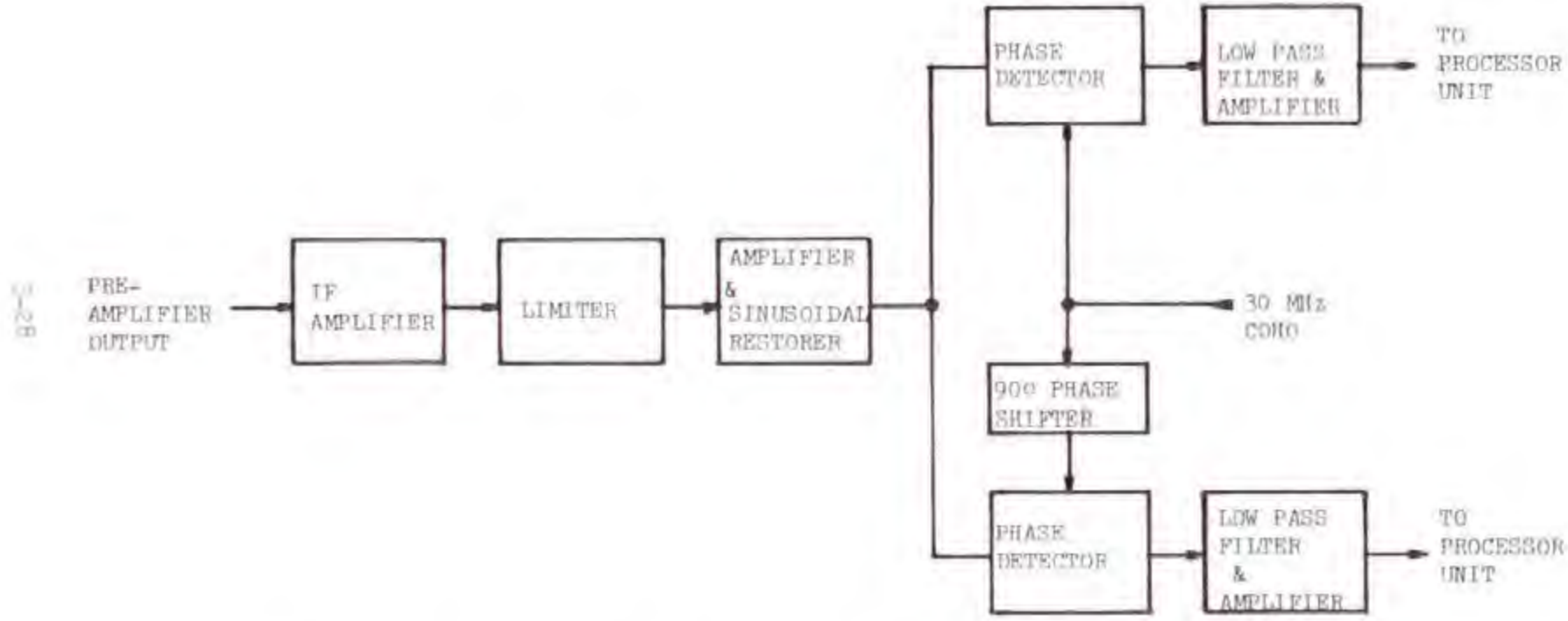

Figure 3-13. Receiver Unit MTI I and MTI Q Channel

narrowband white noise at the IF filter output has a Gaussian amplitude distribution and a uniform phase angle distribution.

Linear-Limiting Amplifier

The output of the IF amplifier is amplified and limited by series-diode limiters. The setting of the limit level is adjustable (L = 35 to 42 dB SNR) by setting the bias voltage level on the diodes. When the signal at the limiter input exceeds the bias level the signal is limited. The MTI linear-limiting amplifier signal processing properties can be expressed as:

$$SNR_o = SNR_i \text{ for } SNR_i < LNR \qquad (3\text{-}13)$$

$$LNR \text{ for } SNR_i > LNR$$

Equation 3-13 also applies to the interference-to-noise (INR) transfer properties of the linear-limiting amplifer.

MTI Quadrature Phase Detector

The ASR-8 has a quadrature phase detector. Most of the radars in the 2.7-2.9 GHz band only have a single channel MTI phase detector. The quadrature MTI channel uses two phase detectors with the COHO signal into the two phase detectors being shifted by 90 degrees (see Figure 3-13). Both the single channel and quadrature channel MTI signal processing properties are discussed in detail in Appendix C. Since the inphase (I) and quadrature (Q) channel are identical except for the COHO being shifted by 90 degrees, it is sufficient to analyze the signal processing properties of only one phase detector.

The phase detector output is a function of the phase difference between the amplified and limited received signal and the reference COHO signal. The output is a video pulse of polarity and amplitude which is a function of the received signal amplitude and the phase difference between the applied input signals. Appendix C contains a derivation of the signal-to-noise ratio (SNR) and the interference-to-noise ratio (INR) transfer properties of the MTI phase detector. The transfer properties of the phase detector can be expressed as (Equation C-15):

$$SNR_{pdo} = SNR_{pdi} \qquad (3\text{-}14)$$

Equation 3-14 also applies to the interference-to-noise ratio transfer properties. That is the SNR or INR at the phase detector output is equal to the SNR or INR at the phase detector input.

The noise probability density function at the phase detector output is Gaussian. This is due to the fact that the phase detector is amplitude as well as phase sensitive. The noise amplitude PDF at the input to the phase detector is Gaussian distributed, and the noise phase PDF is uniform distributed. Therefore, the noise amplitude PDF at the phase detector output is Gaussian. If one considers a fixed amplitude (non-fluctuating) desired or interfering signal at the phase detector input, the signal-plus-noise at the phase detector output is given by:

$$v_{pdo}(t) = N(t) + A\cos\phi \qquad (3\text{-}15)$$

where:

$N(t)$ = Noise amplitude which is Gaussian distributed, in volts

A = Desired or interfering signal amplitude, in volts

ϕ = Phase difference between received signal and COHO which is uniformly distributed

Popoulis (1965) derives the probability density function for Equation 3-15 which can be expressed as:

$$p(v,A) = \frac{1}{\pi\sigma\sqrt{2\pi}} \int_0^{\pi} e^{\frac{-(v-A\cos\phi)^2}{2\sigma^2}} d\phi \qquad (3\text{-}16)$$

where:

σ = rms noise level, in volts

Equation 3-16 can not be written in closed form. The MTI channel phase detector output was simulated to investigate trade-offs in suppressing asychronous interfering signals. The simulation of the radar MTI channel is discussed in Appendix E. Figure 3-14 shows the PDF given by Equation 3-16 as a function of the signal-to-noise ratio. The PDF was obtained by simulation.

Low Pass Filter

The low pass filter in the MTI channel is used to reduce the MTI channel video noise level. The low pass filter bandwidth (B_{lpf}) is approximately equal to $1/\tau$ where τ is the desired signal pulse width. The MTI channel IF bandwidth is always much greater than $1/\tau$ (generally 5.0 MHz) to produce a constant phase characteristic across the desired pulse. Therefore, a narrower low pass filter bandwidth will improve the video signal-to-noise ratio. The MTI channel low pass filters are usually several stages. The low pass filter frequency response can be expressed as:

$$A_{LP}(F) = \frac{1}{[1 + j\,(\frac{F}{F_L})\gamma]^n} \qquad (3\text{-}17)$$

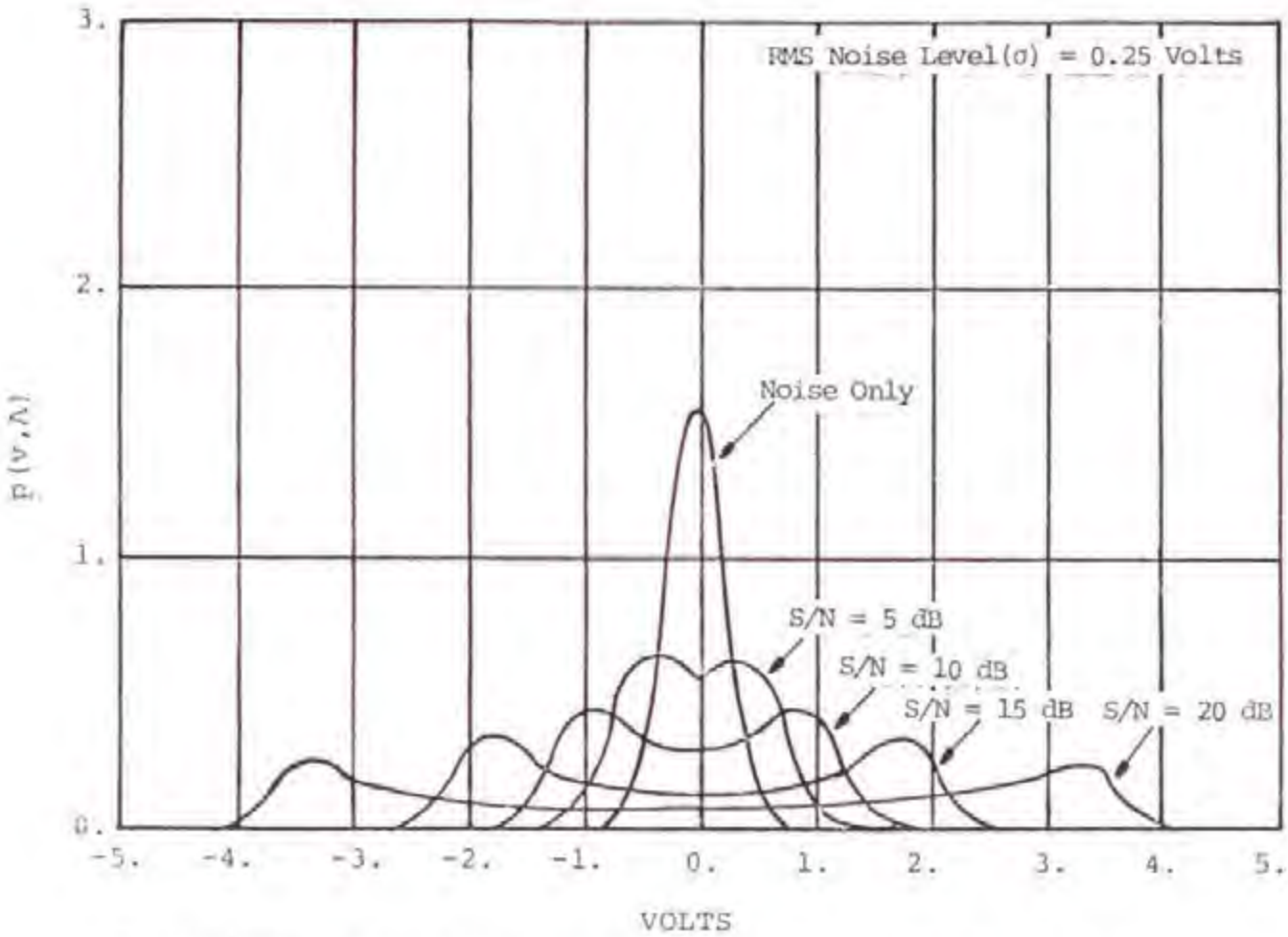

Figure 3-14. Probability Density Function for Noise Only and for Signal-Plus-Noise at the MTI Phase Detector Output.

where:

F_L = Low pass filter 3 dB cutoff frequency, in Hz

n = Number of low pass filter stages

$\gamma = \sqrt{2^{1/n}-1}$

The interfering signal low pass filter output time response, $V_{lpo}(t)$, can be obtained by multiplying in the frequency domain the low pass filter frequency response with the phase detector output interfering signal frequency spectrum, $V_{pdo}(F)$, and taking the Fourier transform. That is:

$$V_{lpo}(t) = \mathcal{F}^{-1}\left[V_{pdo}(F) \cdot A_{LP}(F)\right] \qquad (3\text{-}18)$$

Measurements made on an ASR-8 showed that as the interfering signal is off-tuned (ΔF), the signal level followed the low pass filter selectivity due to the sinusoidal modulation during the steady state portion of the pulse. However, for ΔF greater than 3 MHz, the off-tuned interfering signal response started to follow the interfering signal RF frequency spectrum, and the low pass filter interfering signal output response was caused by the phase modulation that occurs during the transient part (rabbit ear response occurring at the leading and trailing edge of the IF filter output response, see Figures B-10, B-11, B-13, and B-14) of the interfering signal time waveform. Figure C-5 shows a photograph of the phase detector output time waveform of a 60 µs pulse signal off-tuned 200 kHz. The measurement was made on an ASR-8 radar. The pulse width was set at 60 µs to demonstrate the 200 kHz sinusoidal modulation during the steady state portion of the pulse which is caused by the phase modulation produced by the IF filter transfer properties, and is equal to the off-tuned frequency (ΔF). Figure C-6 shows a photograph of an ASR-8 low pass filter output of a .83 µs pulse off-tuned 5.0 MHz. Since the low pass filter interfering signal output response for off-tuned interference is due to the phase modulation which occurs during the transient portion of the IF filter response, the low pass filter output interfering signal time response changes from pulse-to-pulse. However, the average pulse amplitude appears to follow the interfering signal RF spectrum envelope as the interfering signal is off-tuned. Figure C-7 shows a photograph of the low pass filter output for the same interfering signal parameters as in Figure C-6. However, the phase modulation during the transient portion of the interfering signal did not cause a low pass filter output response.

The signal-to-noise (SNR) transfer properties of the MTI low pass filter can be expressed as:

$$SNR_{lpo} = SNR_{lpi} + 10 \log \frac{B_{IF}}{B_{lpf}} \qquad (3\text{-}19)$$

For a radar with a 5.0 MHz IF bandwidth and a 1.2 MHz low pass filter bandwidth, the noise power at the low pass filter output is given by:

$$SNR_{lpo} = SNR_{lpi} + 6.2 \text{ dB} \qquad (3\text{-}20)$$

Therefore, the low pass filter increases the MTI channel signal-to-noise ratio by 6.2 dB. Equations 3-19 and 3-20 also apply to the interference-to-noise transfer properties of the MTI channel low pass filter. The affect of the MTI channel low pass filter on off-tuned interference is discussed in detail in Appendix C.

PROCESSOR UNIT

The following is a discussion of the signal processing properties of the processor units of the ASR-7 and ASR-8 radars. The function of the processor unit is to accept raw video from the receiver unit, condition the video depending on the operating mode desired, and present the video to a Plan Position Indicator (PPI) display for Air Traffic Control (ATC) purposes. The processor unit accepts as inputs normal, log-normal, and bipolar MTI video. Both the ASR-7 and ASR-8 have digital processor units. Some of the radars in the 2.7 to 2.9 GHz band have analog processing units. In general, the signal processing properties of the analog radars can in most cases, and for analytical simplicity, be modeled by the same operations as the digital signal processing units. The digital processing units will introduce some quantization, roundoff and truncation error. However, the error due to quantization, roundoff and truncation is generally very small and can be neglected in most cases. The following is a discussion of the signal processing properties of the processor unit normal, log-normal, and MTI channels to noise, desired signal, and asynchronous interference.

Processor Unit Normal Channel

A simplified block diagram of the processor unit normal channel is shown in Figure 3-15. The following types of normal video can be provided at the processor unit output for display on the PPI:

Normal Video
Enhanced Normal Video

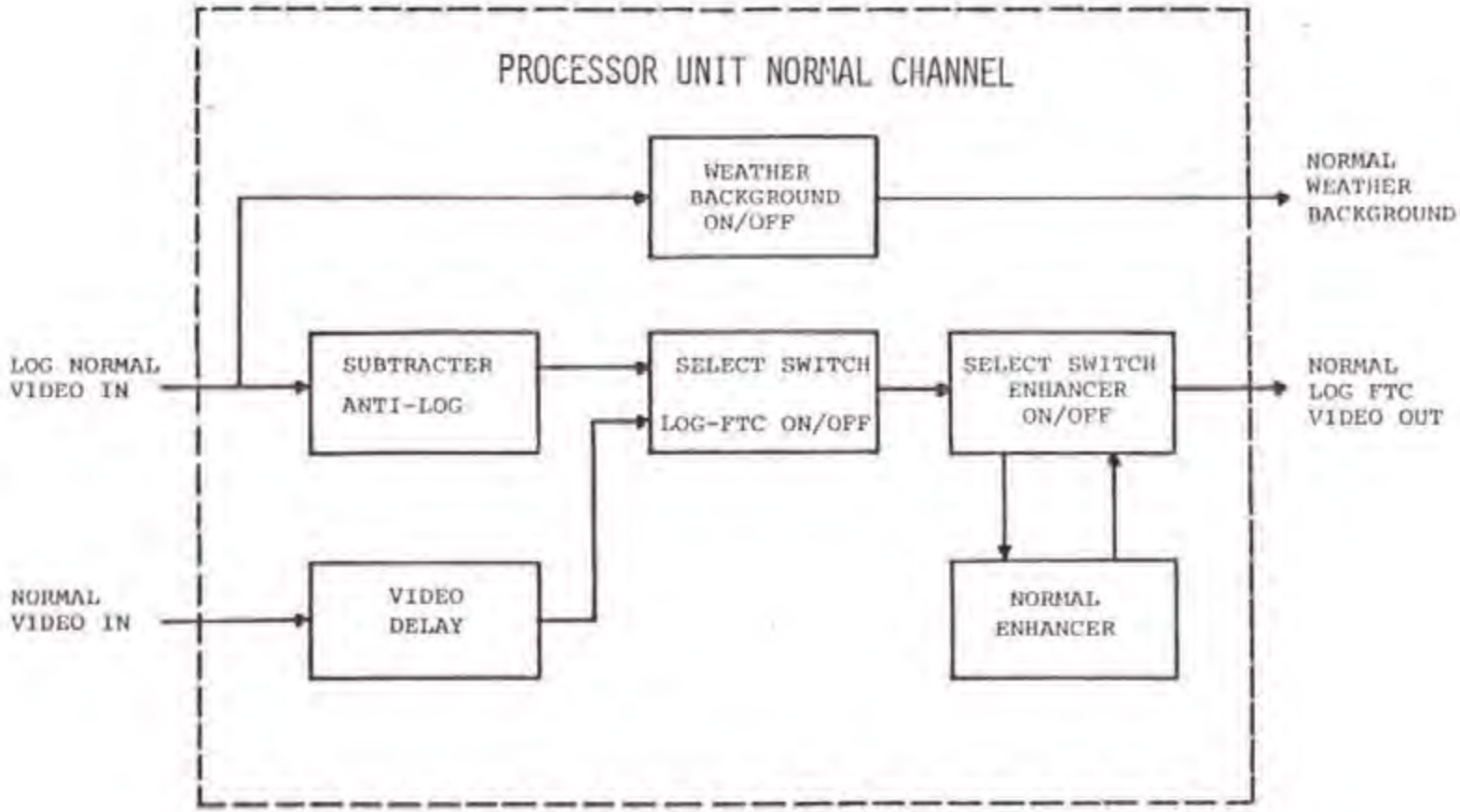

Figure 3-15. Processor Unit Normal Channel Block Diagram

Normal Log-FTC Video
Enhanced Normal Log-FTC Video
Normal LOG-FTC with Weather Background Video
Enhanced Normal LOG-FTC with Weather Background Video

The various normal channel modes are obtained by switching the Log-FTC and enhancer selection switches on or off.

Subtractor Anti-Log

Radars in the 2.7 to 2.9 GHz band use Logarithmic Fast Time Constant (Log-FTC) or Logarithmic Constant False-Alarm Rate (Log-CFAR) circuits to remove precipitation clutter or residue. The circuits operate on the principle that precipitation clutter, after being passed through a logarithmic response, has a noise variation about the average value that is independent of the average value. Filter circuits subtract out the average, leaving only the constant residue level. This level is adjusted to be equal to the receiver noise, thus totally eliminating precipitation clutter from the display.

Figure 3-16 shows a block diagram of the normal Log-FTC channel. In the radar normal channel, the log function is performed by the log IF module in the receiver unit. The filtering subtraction and anti-log functions are performed by the normal/Log-FTC assembly in the processor unit. The filter averages the log video over a certain time interval (8 to 12 range bins) to form an average value. The delay line delays the video signal of interest (one range-bin) so as to maintain coincidence with the averaging filter. The average video signal is then subtracted from the delayed video signal. A DC bias is then added to produce a positive mean and eliminate negative signals. The signal is then applied to an anti-log amplifier to return the signal to a linear function and eliminate the loss in detectability caused by logarithmic compression.

Noise - The DC bias in the Log-FTC circuitry is adjusted so that the noise amplitude distribution after the logarithmic detection, subtraction and anti-log function are performed is approximately Raleigh at the Log-FTC circuitry output.

Desired Signal - For the desired signal in the presence of noise only (no clutter), the detectability of the desired signal is only slightly degraded (1 or 2 dB) due to a small amount of the target energy falling in the adjacent range bins. In the presence of clutter, the desired signal level must be greater than the clutter in order for the signal to be detected. This is due to the fact that the signal must be greater than the average clutter signal in order to appear at the subtractor output.

Interference - The Log-FTC circuitry acts as a pulse width discriminator for interfering signals with a pulse width greater than the system designed pulse width. Long pulse interference which covers several range bins increases the average energy in the filter since the filter

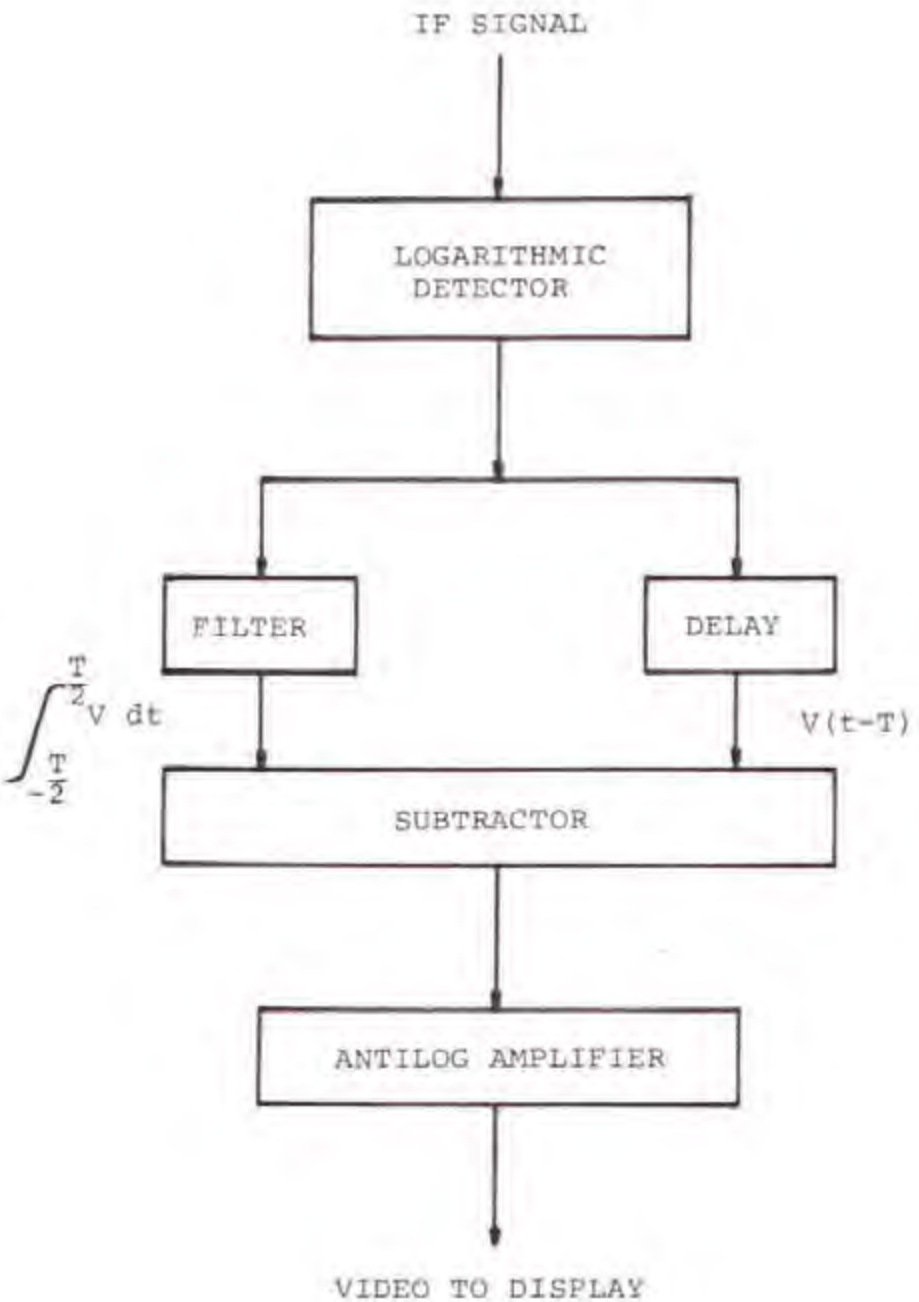

Figure 3-16. Log-FTC Block Diagram

averages over several range bins. Therefore, long pulse interference acts somewhat like clutter, and the interfering signal level at the subtractor output is reduced. Measurements made on an ASR-8 radar showed that for interfering pulse widths greater than 2.0 μsecs the interference was suppressed. Thus, interference from height finding radars (AN/FPS-6, 90), and weather radars operating in the 4.0 μsec mode can be suppressed by operating in the Log-FTC mode. For CW type interference, the Log-FTC circuit reduces the interference down to the receiver noise level since the CW interference appears somewhat like clutter. However, the desired signal will not be detected unless the signal is above the CW interference. Therefore, for every dB the CW interference is above the receiver noise level the desired signal sensitivity will be reduced by that number of dB.

Normal Enhancer

The process of summing the echo pulses from a target is called integration. The following is a discussion of the transfer properties of integrators (enhancers) used by radars in the 2.7 to 2.9 GHz band. The discussion includes the integrator transfer properties of noise, desired signal, and asynchronous interfering signals. Also discussed are the trade-offs in the desired signal transfer properties of the enhancers in suppressing asynchronous interfering signals.

Integrators are generally used in the primary radars for two reasons:

1. To enhance weak desired targets for PPI display.

2. To suppress asynchronous pulsed interference.

The principle of the radar video integrator is that radar signal returns from a point target consist of a series of pulses generated as the radar antenna beam scans past the target, all the pulses from the target will occur in the same range bins in successive radar periods. It is this series of pulses from a target which permits integration of target returns to enhance the weak signals. The number of pulse returns (N) from a target depends upon the radar antenna beamwidth (BW), the rate of antenna rotation (RPM), the radar pulse repetition rate (PRF), and the target characteristics. The equation for the number of pulses from a point target is given by (Skolnik, 1962):

$$N = \frac{PRF \cdot BW}{6 \cdot RPM} \qquad (3\text{-}21)$$

where:

PRF = Radar pulse repetition frequency, in PPS

BW = Antenna 3 dB beamwidth, in degrees

RPM = Antenna scan rate, in rpm

A range value of N for radars in the 2.7 to 2.9 GHz band is 12 to 20. The integrator will suppress asynchronous interference since the interfering pulses will not be separated in time by the radar period, and thus will not occur in the same range bin in successive periods (asynchronous with the system). Therefore, the asynchronous interference will not add-up, and can be suppressed.

All radars in the 2.7 to 2.9 GHz band employ post detection or noncoherent integrators. The types of post detection integrator employed in radars in the 2.7 to 2.9 GHz band can be categorized either as a feedback integrator or a binary integrator. Radars employing feedback integrators may be of analog (delay line) or digital (shift register) type. Only digital binary integrators are used. Appendix D contains a detailed discussion of the feedback and binary integrator transfer properties and the trade-offs in suppressing asynchronous interference. The transfer properties were investigated analytically and by simulating the noise, desired signal, interfering signals, and the feedback and binary integrator hardware. Appendix E contains a detailed discussion of the methods used to simulate the noise, desired signal, interfering signal, and the actual radar hardware simulated.

Feedback Integrator Figure 3-17 shows a block diagram of a typical feedback integrator used by radars in the 2.7 to 2.9 GHz band. The feedback integrator consists of an input limiter, an adder, and a feedback loop with an output limiter and a delay equal to the time between transmitter pulses (1/PRF). The radar period delay for digital radars is achieved by clocking a shift register, and the actual integrator hardware is essentially represented in Figure 3-17. Analog radars in the 2.7 to 2.9 GHz band generally use quartz delay lines, thus accomplishing the delay accoustically to reduce the size of the delay line. However, the inherent loss of quartz delay lines requires use of additional hardware, such as, modulators, attenuators, amplifiers, detectors, and balancing circuits (AGC) to achieve integration. If the analog integrator balancing circuitry is aligned properly, the transfer properties of an analog integrator can, for analytical simplicity, be modeled by the operations shown in Figure 3-17. Digital integrators will also introduce some quantization, roundoff and truncation error. However, the error due to quantization, roundoff and truncation is generally very small and can be neglected in most cases.

Prior to the input of the feedback integrator, signal processing circuitry is used to reduce the mean noise level at the input to the feedback integrator. This circuitry generally consists of an attenuator, subtractor, and bottom clipper so that the noise at the input to the feedback integrator will be positive. The function of this circuitry is to reduce the mean level of the noise at the integrator input to reduce the noise gain of the feedback integrator. Since the noise is being continually added by the feedback integrator, the noise amplitude probability density function at the feedback integrator output by the central limit theorem is approximately Gaussian with

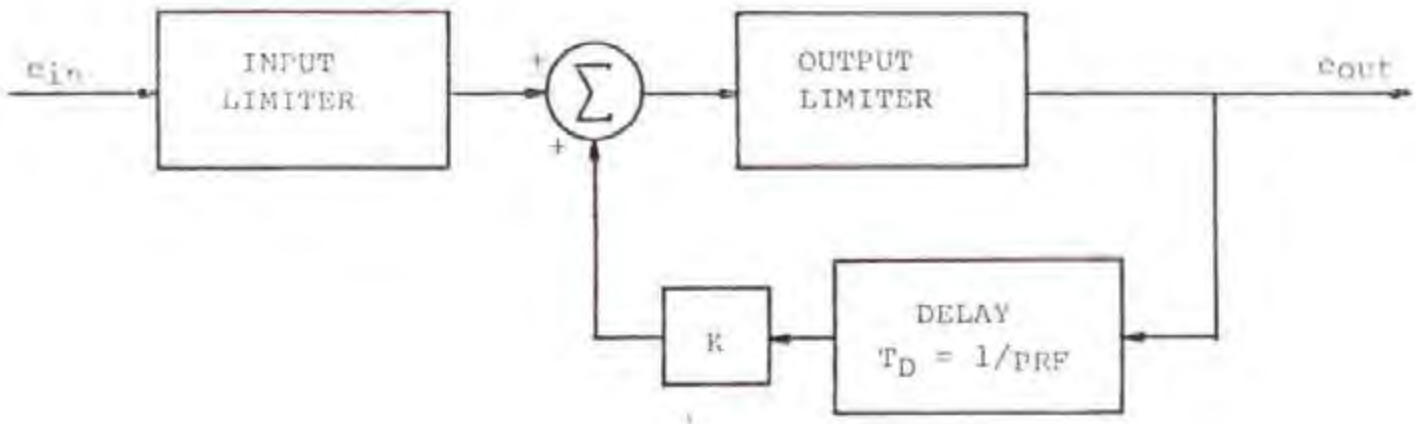

Figure 3-17. Feedback Integrator Block Diagram

non-zero mean.

It is shown in Appendix D (Equation D-10) that the signal-to-noise-ratio enhancement (SNR_E) of the desired signal is given by:

$$SNR_E = 20 \log_{10} \left[\left(\frac{1-K^N}{1-K} \right) (1-K^2)^{1/2} \right] \qquad (3-22)$$

where:

N = Number of target return pulses

K = Integrator feedback constant

Equation 3-22 is only a first order approximation of the signal-to-noise ratio enhancement of a feedback integrator since it assumes zero mean noise amplitude distribution and a constant desired signal level. The desired signal level actually varies from pulse-to-pulse due to fluctuations in target returns (scintillation and antenna pattern modulation). Studies (Trunk, 1970) have been made which take into account pulse amplitude variations due to the antenna pattern modulation. Trunk concluded that the SNR enhancement of a feedback integrator could be reduced by as much as 1.6 dB due to antenna beam shape pulse amplitude variations. The actual reduction in SNR enhancement due to the radar antenna pattern is between 0 and 1.6 dB, and is also a function of the integrator input limiter limit level setting. It is shown in Appendix D using Equation 3-22 and measurement results that the optimum value of the feedback constant (K) is between .92 and .94 for 20 pulses from a target (N = 20), and the signal-to-noise-ratio enhancement (SNR_E) due to integration is approximately 10 to 12 dB.

Figure 3-18 shows a simulated unintegrated target return pulse train for target azimuth shift and angular resolution reference. Figures 3-19 through 3-21 show a simulated feedback integrator output of a target return pulse train for 20 pulses for an input limiter limit level setting of 1.0, 0.5, and 0.34 volts. A detailed discussion of the radar simulation model is given in Appendix E. When a feedback integrator is used there are trade-offs in target azimuth shift and angular resolution. A comparison of Figure 3-18 with Figures 3-19 through 3-21 shows that the center of the target return pulse train has shifted in time. This shift in time is related to a target azimuth shift on the Plan Position Indicator (PPI) display. Also a comparison of Figure 3-18 with Figures 3-19 through 3-21 shows that the number of pulses above 1.0 volts (peak noise level) increases when the feedback integrator is used. This increase in number of pulses results in a decrease in angular resolution. (The property of the radar to distinguish between two targets.) Appendix D contains a detailed investigation of the trade-offs in target azimuth shift and angular resolution when an integrator is used. In summary, it was shown that a feedback integrator causes a target azimuth shift of approximately 0.90 degrees, and an angular resolution loss

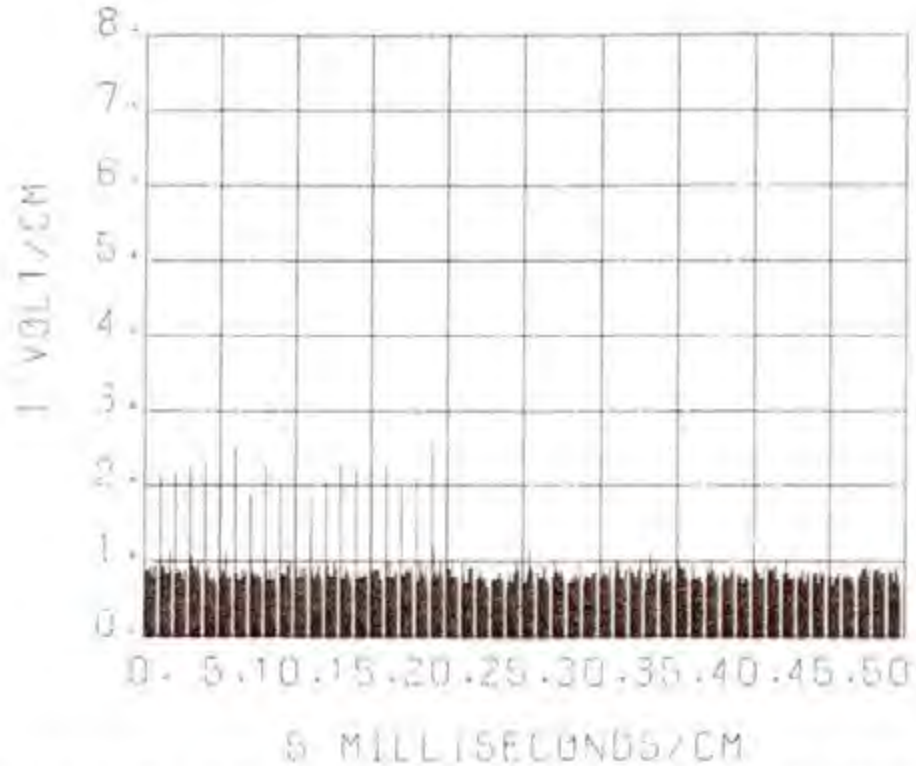

Figure 3-18. Simulated Normal Channel Unintegrated Target Return Pulse Train for a SNR = 15 dB

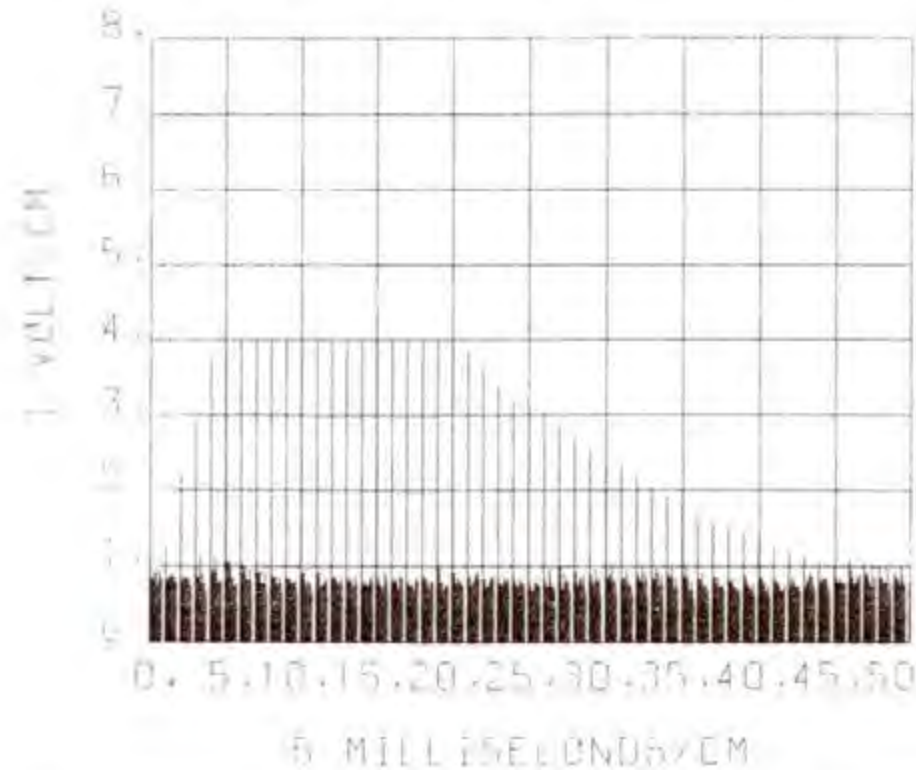

Figure 3-19. Simulated Normal Channel Integrated Target Return Pulse Train for the Input Limiter Set at 1.0 Volts and a SNR = 15 dB

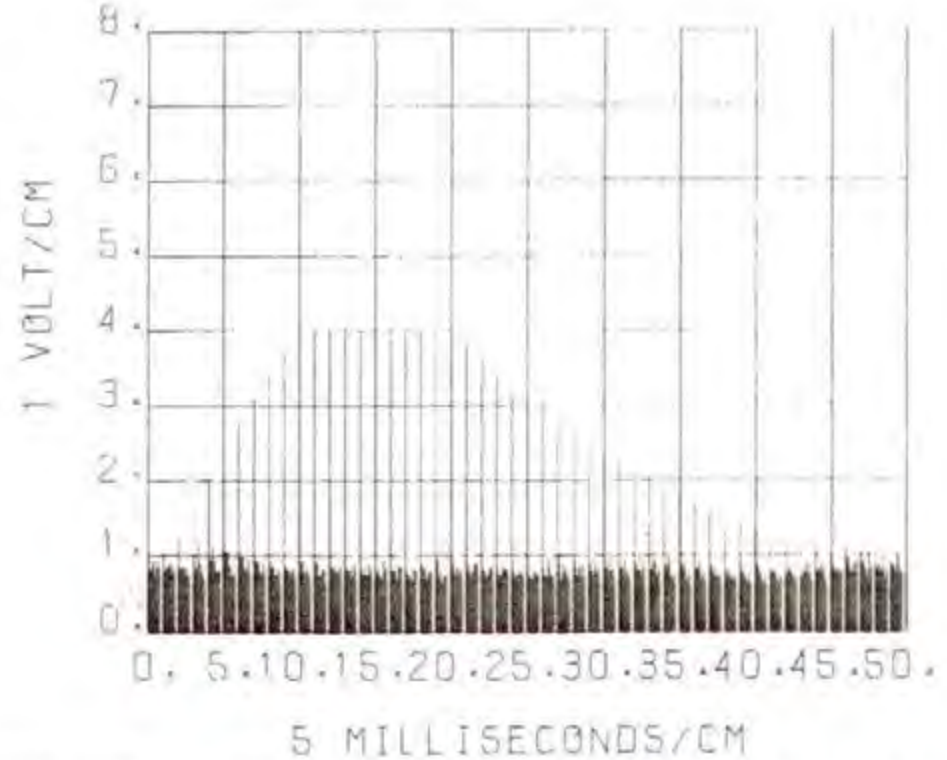

Figure 3-20. Simulated Normal Channel Integrated Target Return Pulse Train for the Input Limiter Set at 0.5 Volts and a SNR = 15 dB

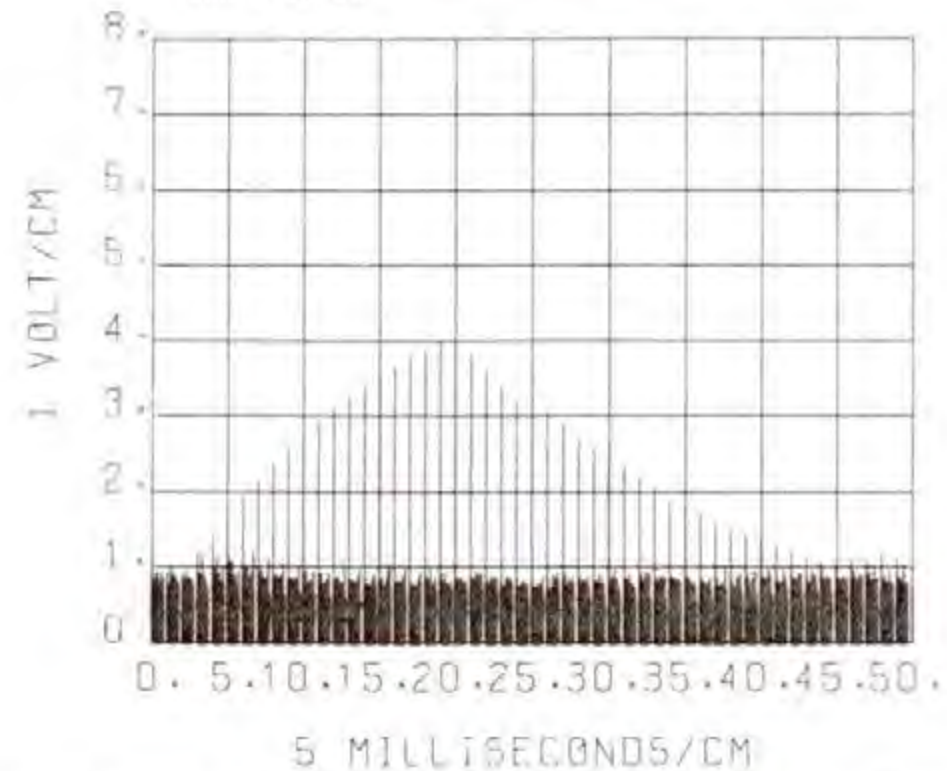

Figure 3-21. Simulated Normal Channel Integrated Target Return Pulse Train for the Input Limiter Set at 0.34 Volts and a SNR = 15 dB

of approximately 1.2 to 1.5 degrees relative to an unintegrated target return pulse train.

In congested areas when there is potential for asynchronous interference from other radars in the 2.7 to 2.9 GHz band, adjustments to the feedback integrator input limiter are required to suppress the asynchronous interference. By adjusting the integrator input limiter limit level the peak interference level can be suppressed to the one volt noise level at the integrator output. Suppression of asynchronous interference in the radar normal channel and the trade-offs to the desired signal are discussed in detail in Appendix D. The analysis showed that the suppression of asynchronous interference does not significantly increase the target azimuth shift or decrease the target angular resolution given the integrator is going to be used. Figure 3-22 shows a simulated normal channel radar unintegrated output for three interference sources (ASR-5, INR = 10 dB; ASR-8, INR = 15 dB; and AN/FPS-90, INR = 20 dB), and a desired target signal-to-noise ratio of 15 dB. Figure 3-23 shows for the same interference condition the radar output after feedback integration for an input limit level setting of 0.34 volts. The asynchronous interference has been suppressed (compare Figure 3-21 with 3-23) by the feedback integrator. Measurements made on the Stapelton Airport ASR-8 radar in Denver, Colorado, showed that on-tune pulsed interference levels of 50 dB above the receiver noise level (approximately -60 dBm) could be suppressed by the feedback integrator so that they did not appear on the PPI display. The measured change in target detection sensitivity in suppressing the asynchronous interference was 1 dB or less. In summary, feedback integrators can suppress asynchronous interference, in the normal channel, by adjusting the feedback integrator input limiter limit level, and the trade-offs in target azimuth shift, angular resolution, and target detection sensitivity appear to be minimal.

Binary Integrator The ASR-7 and AN/GPN-12 radars are made by the same manufacturer, and the enhancer used in the two radars are electronically identical. The integrator (enhancer) used in the two radars can be represented by the block diagram shown in Figure 3-24. The binary integrator consists of a threshold detector or comparator, binary counter (adder/subcontractor circuit), a five bit shift register memory, and a digital-to-analog (D/A) converter. Each PRF period is divided into range bins of .625 usec. If a pulse of a target return pulse train exceeds the comparator threshold level, the enhancer stores a one level digital signal in the shift register memory for that range bin. If the successive pulses of the target return pulse train continue above the comparator threshold in the given range bin, the binary counter will add one level to the stored digital signal in the shift register memory in each PRF period until a maximum integrator level of 31 is reached. If in any PRF period the signal fails to exceed the comparator threshold, the binary counter subtracts one from the stored integrator state in the given range bin until a digital signal level of zero is reached. The subtraction provides the target return pulse train signal decay required after the antenna beam has passed the target, and also enables the suppression of asynchronous interfering signals. The voltage amplitude at the enhancer D/A converter output is determined by the binary

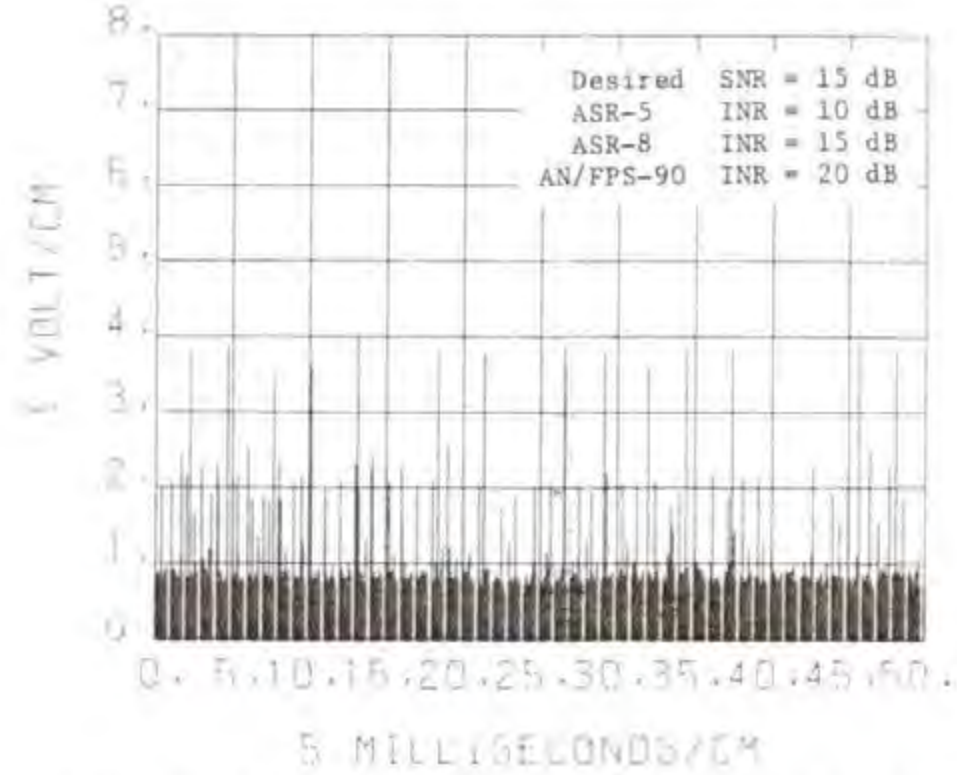

Figure 3-22. Simulated Normal Channel Unintegrated Radar Output with Interference

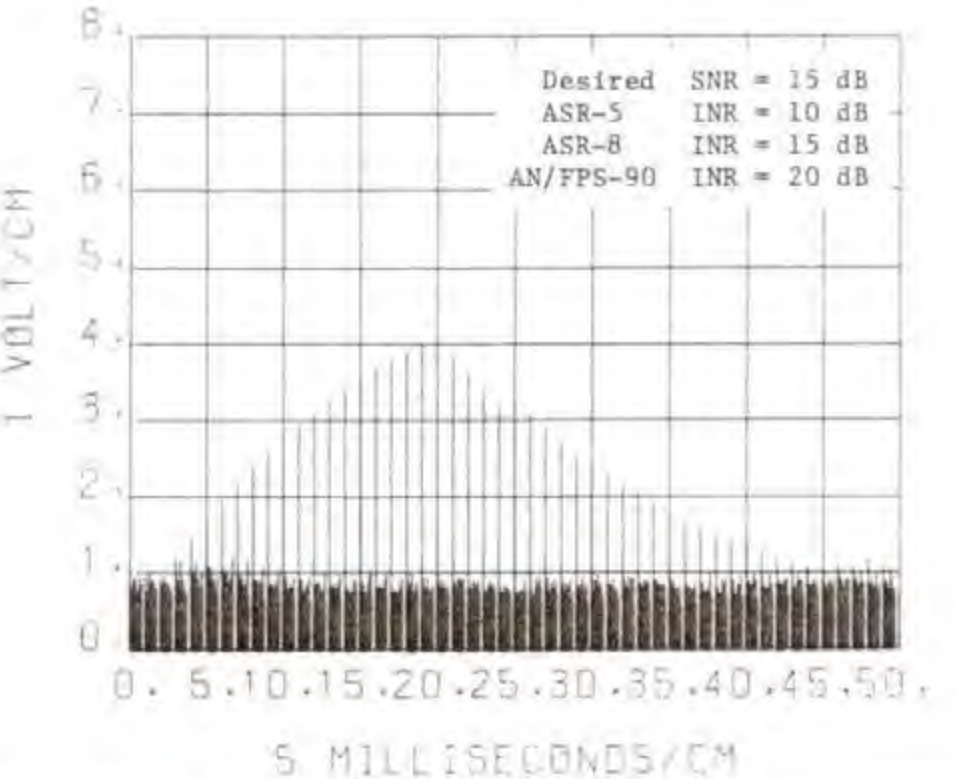

Figure 3-23. Simulated Normal Channel Integrated Radar Output with Interference

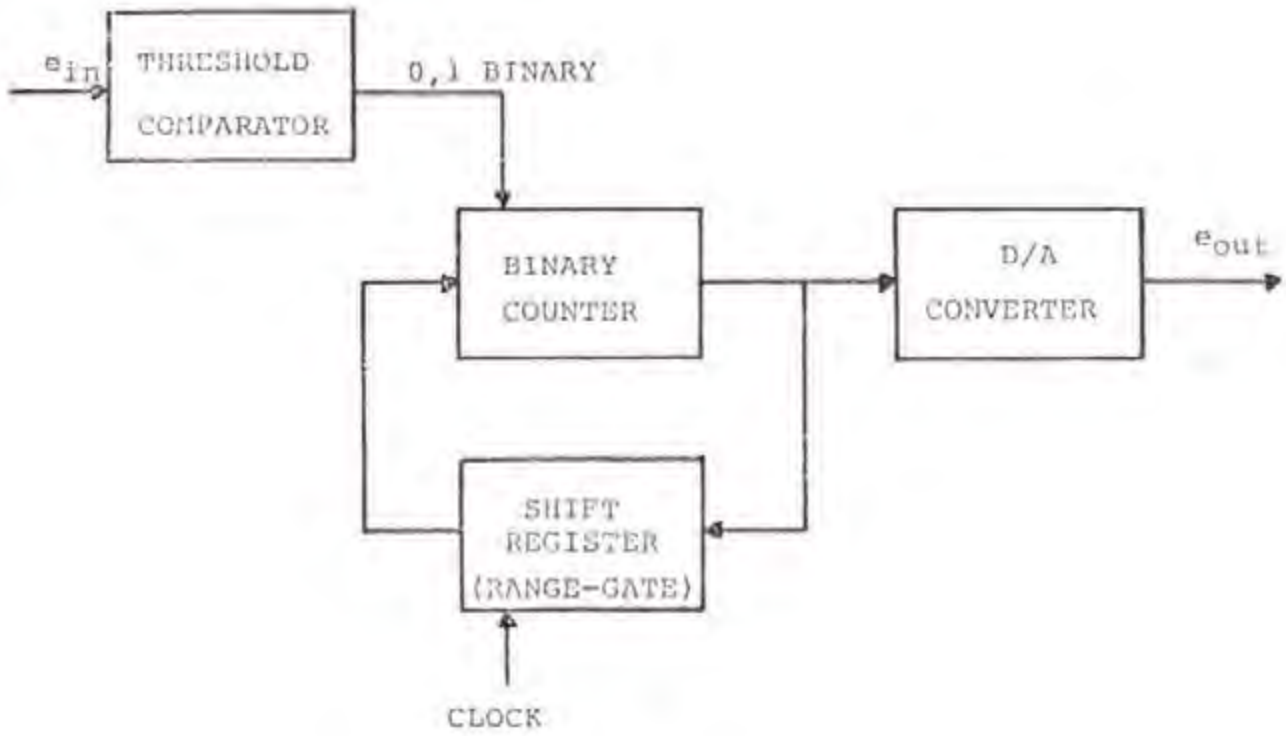

Figure 3-24. ASR-7 (AN/GPN-12) Binary Integrator Block Diagram

counter level (0 to 31) for the particular range bin times .125 volts. Therefore, for a binary counter level of 31, the maximum enhancer output voltage would be 3.875 volts (31 x .125).

FAA Integrator Modification

The FAA made modifications to the manufacturer's integrator (enhancer) printed circuit board due to deficiencies that were observed on the ASR-7 video enhancer at operational field sites. Deficiencies that were observed were: (1) loss of weak targets due to design of the enhancer integrators, and (2) excessive azimuth shift of the target (NAFEC Letter Report, FAA-MA-76-39-LR, 1976). The major modification made by the FAA was the replacement of the binary counter (IC's) with a programmable read-only-memory (PROM) logic. The PROMs permit the bypassing of some of the intermediate levels (0 to 31), depending on the PROM programming. Figure 3-25 shows the FAA standard hit/miss characteristic curve which is programmed into the PROMs. The figure shows that the enhancer state is a nonlinear function of the target hits above the comparator threshold level. It only takes four hits to get to level 8 (one volt noise level), and six hits to get to level 31 (3.875 volts). This results in a strong target enhancement with only a few hits. The primary advantage of the PROM enhancer is that, due to its programmable feature, it permits a radar site flexibility in selecting a hit-count sequence based on the radar site environment (interference and clutter). Similarly, the miss-count sequence can be precisely controlled to minimize the target azimuth shift and loss in angular resolution. In this way, the video enhancer performance can be optimized to give improved performance in a variety of environmental conditions.

The following discussion will center on the particular signal processing characteristics of the conventional integrator deployed in the ASR-7 and AN/GPN-12 and the modified ASR-7 integrator to noise, desired target return pulse train, and asynchronous interference. Also discussed are the trade-offs in the desired signal transfer properties of the enhancer in suppressing asynchronous interfering signals. Appendix D contains a detailed discussion of the binary integrator transfer properties and the trade-offs in suppressing asynchronous interference.

The normal channel noise amplitude distribution at the binary integrator input is Raleigh distributed. It is shown in Appendix D (Equation D-20b) that the probability of the binary counter being in state E_j due to noise (P_{nj}) can be modeled by a one-dimentional random walk with reflecting barriers where levels 0 and 31 are the reflecting barriers. Since the noise is continually summed in the binary integrator the number of steps (k) in the random walk is infinite. It can be shown that a one-dimentional random walk with reflecting barriers model for an infinite number of steps is identical to a truncated single channel queue model where the probability of being in state E_j due to noise (P_{nj}) can be expressed as (Saaty, 1968):

$$P_{nj} = \frac{(P_{N1}/P_{NO})^{j-1}}{\sum_{j=1}^{D} (P_{N1}/P_{NO})^{j-1}} \qquad (3\text{-}23)$$

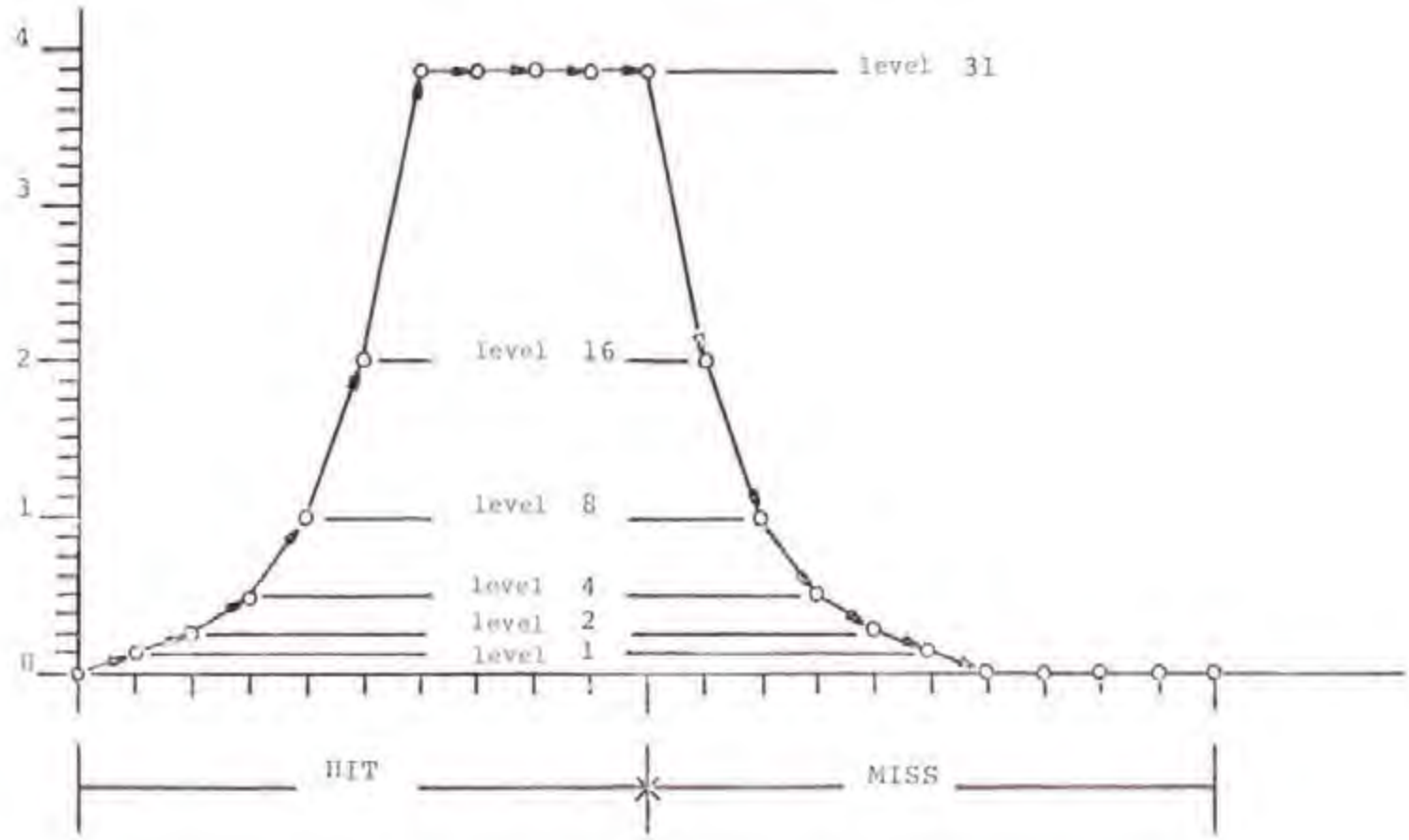

Figure 3-25. Hit/Miss Characteristic Curve for FAA Modified ASR-7 Enhancer

where:

$P_{N\emptyset}$ = Probability of the noise causing a 0 at the threshold comparator output

P_{N1} = Probability of the noise causing a 1 at the threshold comparator output

ρ = Number of states (function of counter level sequence)

The probability distribution given by Equation 3-23 is a geometric distribution, and is independent of the noise amplitude distribution at the enhancer input. The threshold comparator threshold level is normally adjusted to give a peak noise level of one volt (enhancer level 8, 8 x .125) with a certain probability of false alarm (probability of exceeding level 8). A detailed discussion of the setting of the threshold comparator threshold level for noise is given in Appendix D.

The normal channel signal-plus-noise amplitude distribtuion at the binary integrator input is Rice distributed (see Equation 3-9, and Figure 3-10). It is shown in Appendix D (Equation D-25a) that the probability of a desired target return pulse train of 20 pulses causing the binary integrator to be in state E_j can be determined by using a one-dimensional random walk with reflecting barriers model where levels 0 and 31 are the reflecting barriers. The probability of the desired target return pulse train causing the binary integrator to be in state E_j for a given signal-to-noise ratio is given by:

$$P_{sj} = \frac{\sum_{k=1}^{N} P_{1j}^{(k)}}{\sum_{j=1}^{\rho} \sum_{k=1}^{N} P_{ij}^{(k)}} \qquad (3\text{-}24)$$

where:

$$P_{ij}^{(k)} = \frac{(p/q)-1}{(p/q)^{\rho}-1}\left(\frac{p}{q}\right)^{j-1} + \frac{2p}{\rho}\sum_{r=1}^{\rho-1} \frac{x_i^{(r)} y_j^{(r)} \left[2\sqrt{pq}\cos \pi r/\rho\right]^k}{1 - 2\sqrt{pq}\cos \pi r/\rho} \qquad (3\text{-}24a)$$

and:

$$x_i^{(r)} = \left(\frac{q}{p}\right)^{i/2} \sin \frac{\pi r i}{\rho} - \left(\frac{q}{p}\right)^{(i+1)/2} \sin \frac{\pi r (i-1)}{\rho} \qquad (3\text{-}24b)$$

$$y_j^{(r)} = \left(\frac{p}{q}\right)^{j/2} \sin \frac{\pi r j}{\rho} - \left(\frac{p}{q}\right)^{(j-1)/2} \sin \frac{\pi r (j-1)}{\rho} \qquad (3\text{-}24c)$$

ℓ = Number of states (function of counter level sequence)

$q = P_{s\emptyset}$ = Probability of 0 at threshold comparator output

$p = P_{s1}$ = Probability of 1 at threshold comparator output

N = Number of desired signal pulses in target return pulse train

The values of P_{sj} as a function of the signal-to-noise ratio are discussed in detail in Appendix D. Also the probability of the desired signal being in state E_j as a function of the signal-to-noise ratio is also discussed in detail in Appendix D (see TABLE D-6).

The signal processing of the ASR-7 binary integrator was simulated to investigate the trade-offs to the desired signal in suppressing asynchronous interference. A simulated ASR-7 enhancer output for a desired target return pulse train of 20 pulses without noise present is shown in Figures 3-26 and 3-27 for the conventional ASR-7 enhancer, and the FAA modified ASR-7 enhancer, respectively. A comparison of Figures 3-26 and 3-27 shows that the FAA Modified ASR-7 enhancer provides a significant improvement in signal enhancement, target azimuth shift, and angular resolution. Figure 3-28 shows the simulated radar output of the normal channel for a Signal-to-Noise-Ratio (SNR) of 15 dB with the binary integrator off (unintegrated). Figure 3-29 shows the radar output with the enhancer on (integrated) for the same SNR. Appendix D contains a detailed discussion of the desired signal transfer properties of the binary integrator as a function of the signal-to-noise-ratio.

It is shown in Appendix D that the FAA modified binary integrator causes a target azimuth shift of approximately .179 degrees. However, the feedback integrator causes a target azimuth shift of approximately 0.90 degrees. Therefore, the FAA modified binary integrator results in a significant improvement in target azimuth shift over the feedback integrator. Also the FAA modified integrator does not cause any loss in target angular resolution while the feedback integrator results in a loss in angular resolution of 1.2 to 1.5 degeees.

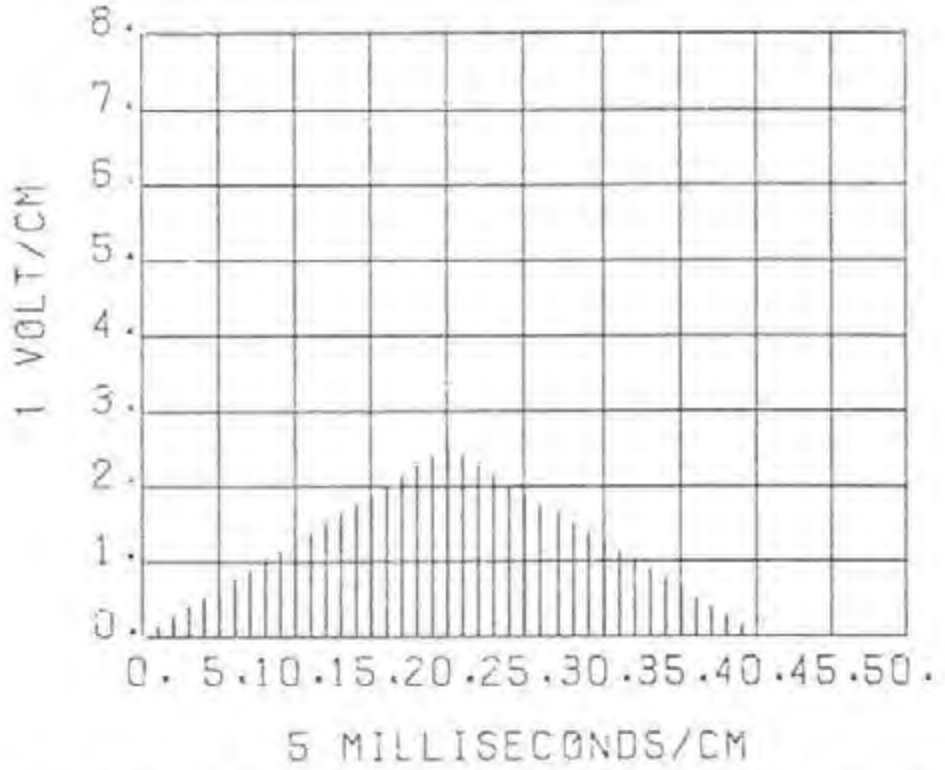

Figure 3-26. Simulated Binary Integrator Output for Target Return Pulse Train (ASR-7, AN/GPN-12)

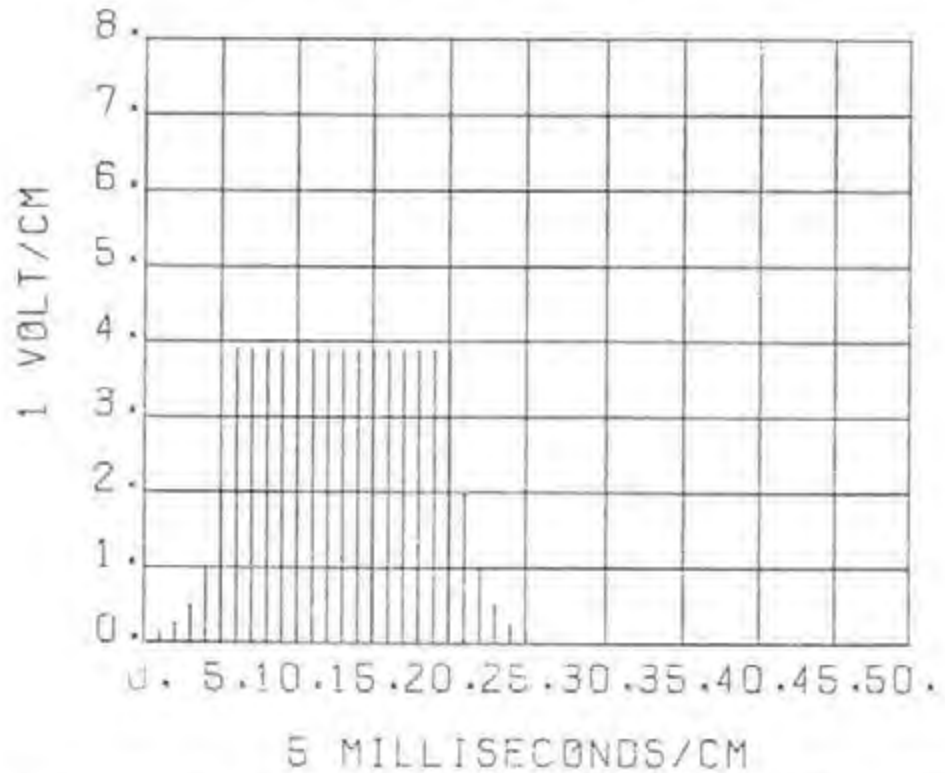

Figure 3-27. Simulated FAA Modified Binary Integrator Output for Target Return Pulse Train (ASR-7)

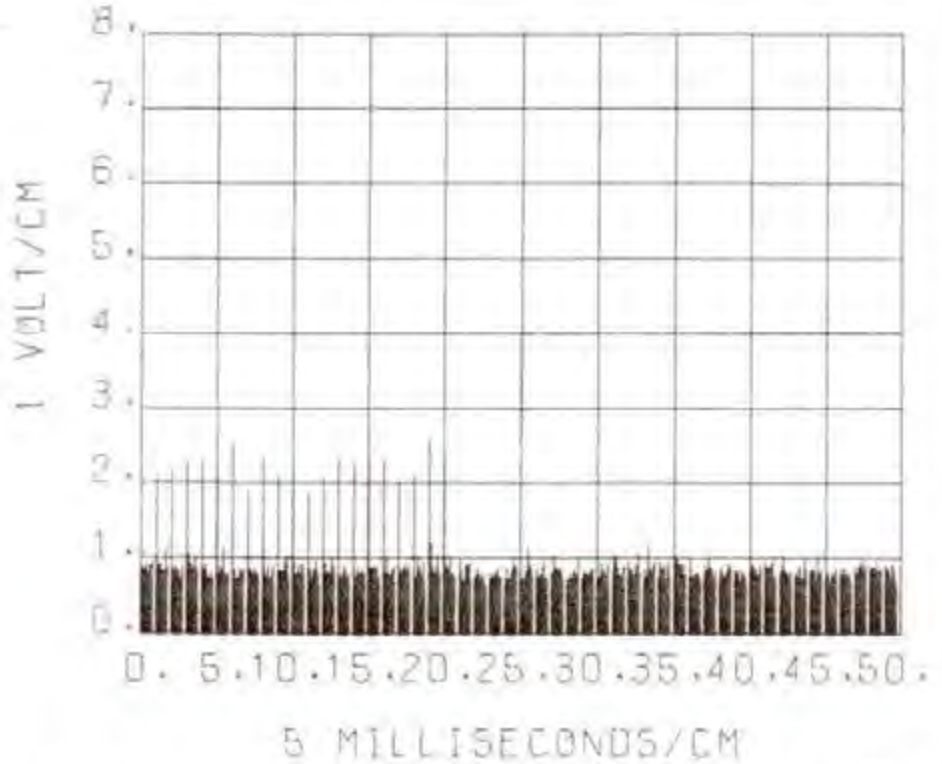

Figure 3-28. Simulated Normal Channel Unintegrated Target Return Pulse Train for a SNR = 15dB

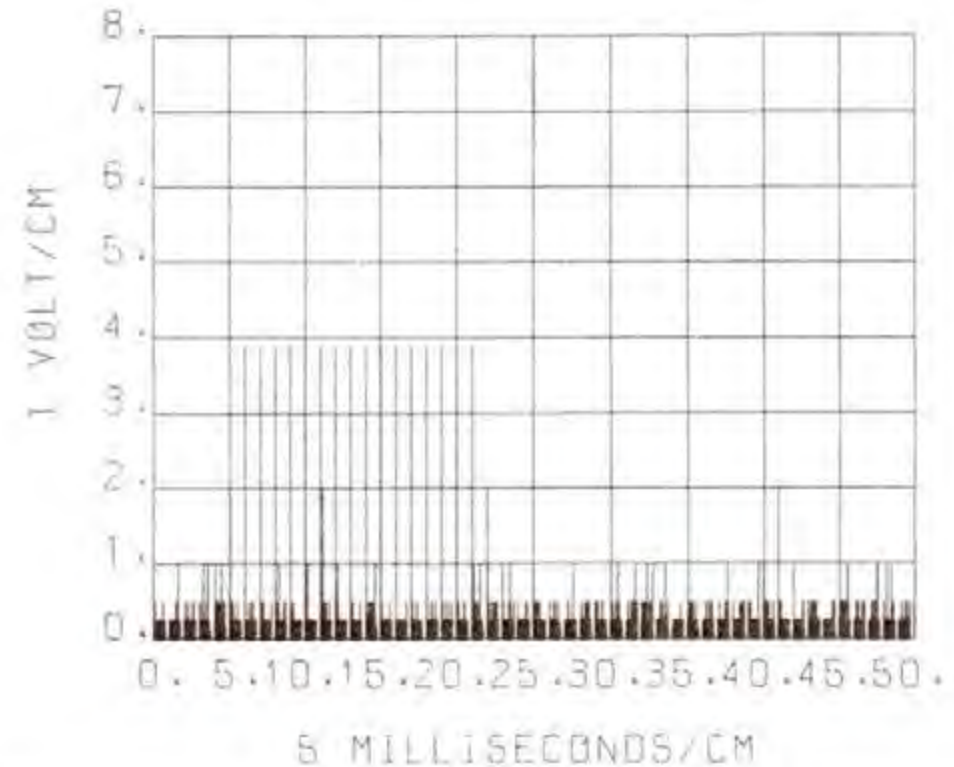

Figure 3-29. Simulated Normal Channel Integrated Target Return Pulse Train for a SNR = 15dB

The capability of the binary integrator in the ASR-7 to suppress normal channel asynchronous interference was also investigated using the radar simulation model (see Appendix E). Three interfering radar sources were simulated: ASR-5, ASR-8, and the AN/FPS-90. Figures E-3 through E-5 in Appendix E show the respective time waveforms simulated for each of the radar interfering sources. Figure 3-30 shows a simulated normal channel radar unintegrated output for three interference sources (ASR-5, INR = 10 dB; ASR-8, INR = 15dB; and AN/FPS-90, INR = 20 dB), and a desired target signal-to-noise ratio of 15 dB. Figure 3-31 shows for the same interference condition the radar output after binary integration. The asynchronous interference has been suppressed (compare Figure 3-29 with 3-31) by the binary integrator.

In summary, the FAA modified binary enhancer has the capability of suppressing normal channel asynchronous interference with very little trade-offs in target azimuth shift, target angular resolution, and desired target probability of detection. Asynchronous interference can be suppressed by the FAA modified enhancer by either adjusting the threshold comparator level setting, or by programming a hit/miss state sequence that will suppress the interference. Thus the FAA modified ASR-7 enhancer can be adjusted to optimize the radar desired signal performance in a variety of environmental conditions.

Normal Channel Weather Background

Both the ASR-7 and ASR-8 have weather background circuits which can be selected to add a weather outline to the processor output video when the normal Log-FTC video is selected. The weather background video is adjustable in amplitude relative to the Log-FTC video to provide the operator with the proper contrast between operating video and background video. The ASR-8 has two display modes for the weather background. The first is merely a limited and adjustable display of the entire detected weather area. In this mode, the operator views the complete weather video pattern at a reduced brightness. The second mode is an adjustable brightness contour or outline of the storm or weather video area. In this mode the operator views the outline of the weather video pattern but is not distracted by the complete weather video pattern which can compete with aircraft returns.

In the normal video channel, the background is generated from the receiver logarithmic video, which is low pass filtered to reduce the noise variation amplitudes. The filtering reduces the possibility of weather background false-alarm signals which would clutter the display, yet does not degrade the detection of the extended weather blocks themselves. The filter is designed with a time constant which matches the Log-FTC delay in the normal channel. The filtered weather background video is presented to variable threshold circuits and the threshold output signals are converted to a binary-coded signal. The threshold circuits are voltage comparators with adjustable reference voltages. The upper threshold, which is adjustable from 10 dB above rms noise to the maximum input amplitude, is used for blanking.

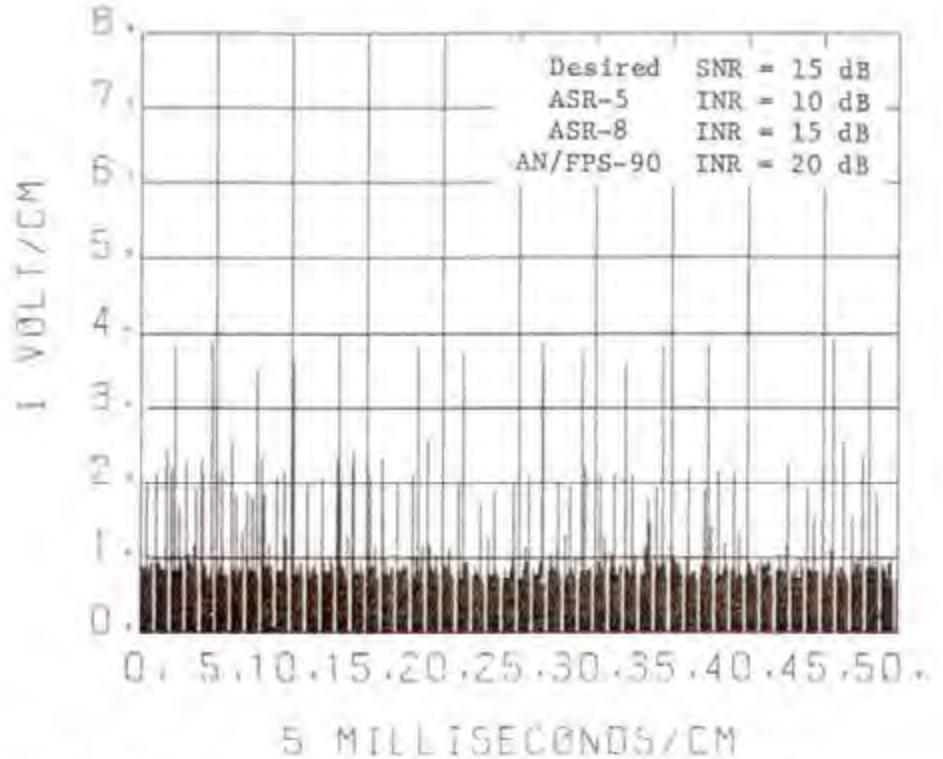

Figure 3-30. Simulated Normal Channel Unintegrated Radar Output with Interference

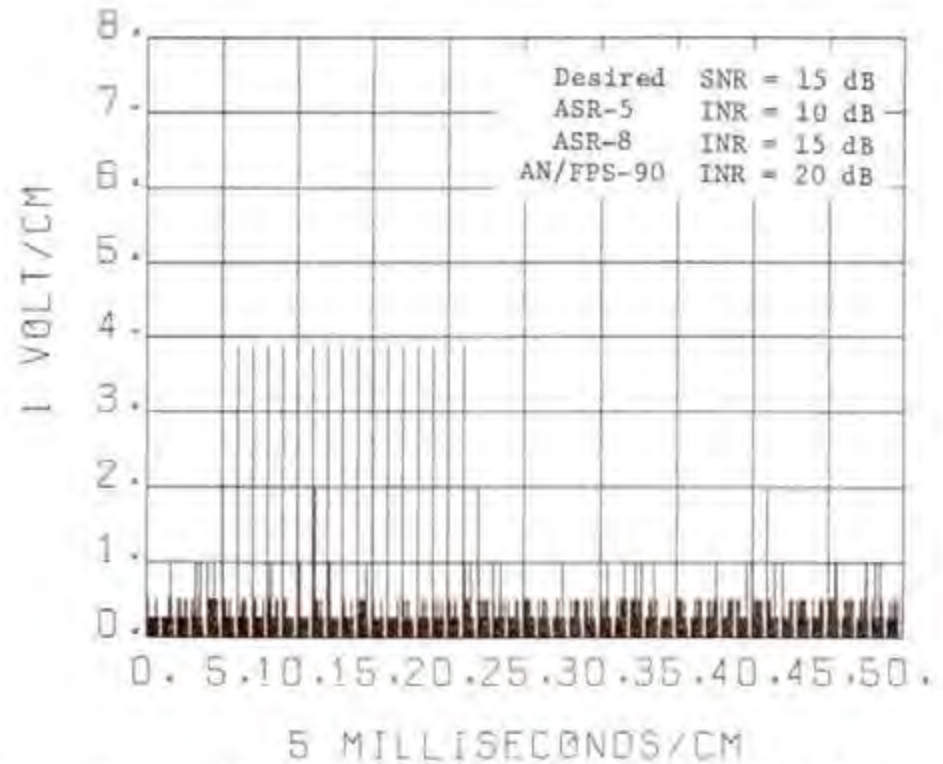

Figure 3-31. Simulated Normal Channel Integrated Radar Output with Interference

The other two independently adjustable thresholds are for top clipping and bottom clipping. They are adjustable over the range from 0 to 15 dB above rms noise. The fourth threshold is an intermediate threshold between the top-clip and bottom-clip thresholds and is used when the weather video output is reconstructed in a multiple level form. The four possible modes of weather background are:

Mode 1 - No blanking, quantize with bottom clipping
Mode 2 - Blanking, quantize with bottom clipping
Mode 3 - No blanking, top and bottom clipping
Mode 4 - Blanking, top and bottom clipping

One of the four operating modes can be selected. Input video, before and after filtering, as well as representative output waveforms for these four modes, are shown in Figure 3-32. The normal weather background video is routed to the weather background/diversity combiner where it is added to the combined or single channel video.

The weather background channel does not have an integrator (enhancer). (See Figure 3-15.) However, asynchronous pulsed interference in the weather background channel will be reduced by the low pass filter since the filter essentially averages over six to eight range bins. Also if the interference appears above the blanking threshold level (approximately 10 dB INR), it will be suppressed by the blanking circuit. Since the master channel weather background video is used for display on the PPI, the channel that minimizes interference can be chosen as the master channel.

Processor Unit MTI Channel

A simplified block diagram of the processor unit Moving Target Indicator (MTI) channel is shown in Figure 3-33. The following types of MTI video can be provided at the processor unit output for display on the PPI:

MTI Video
Enhanced MTI Video
MTI Log-FTC Video
Enhanced MTI Log-FTC Video
MTI Log-FTC with Weather Background Video
Enhanced MTI Log-FTC with Weather Background Video

The various MTI channel modes are obtained by switching the Log-FTC and enhancer selection switches on or off.

MTI Cancellers

The target return signals after phase detection are processed in the MTI cancellers. The MTI canceller circuits provide for cancelling fixed target signals (clutter), such as buildings, hills, and trees and allowing only moving targets, such as aircraft to be displayed on the PPI. The action of the MTI cancellers is that of a linear filter. In the ideal case, the

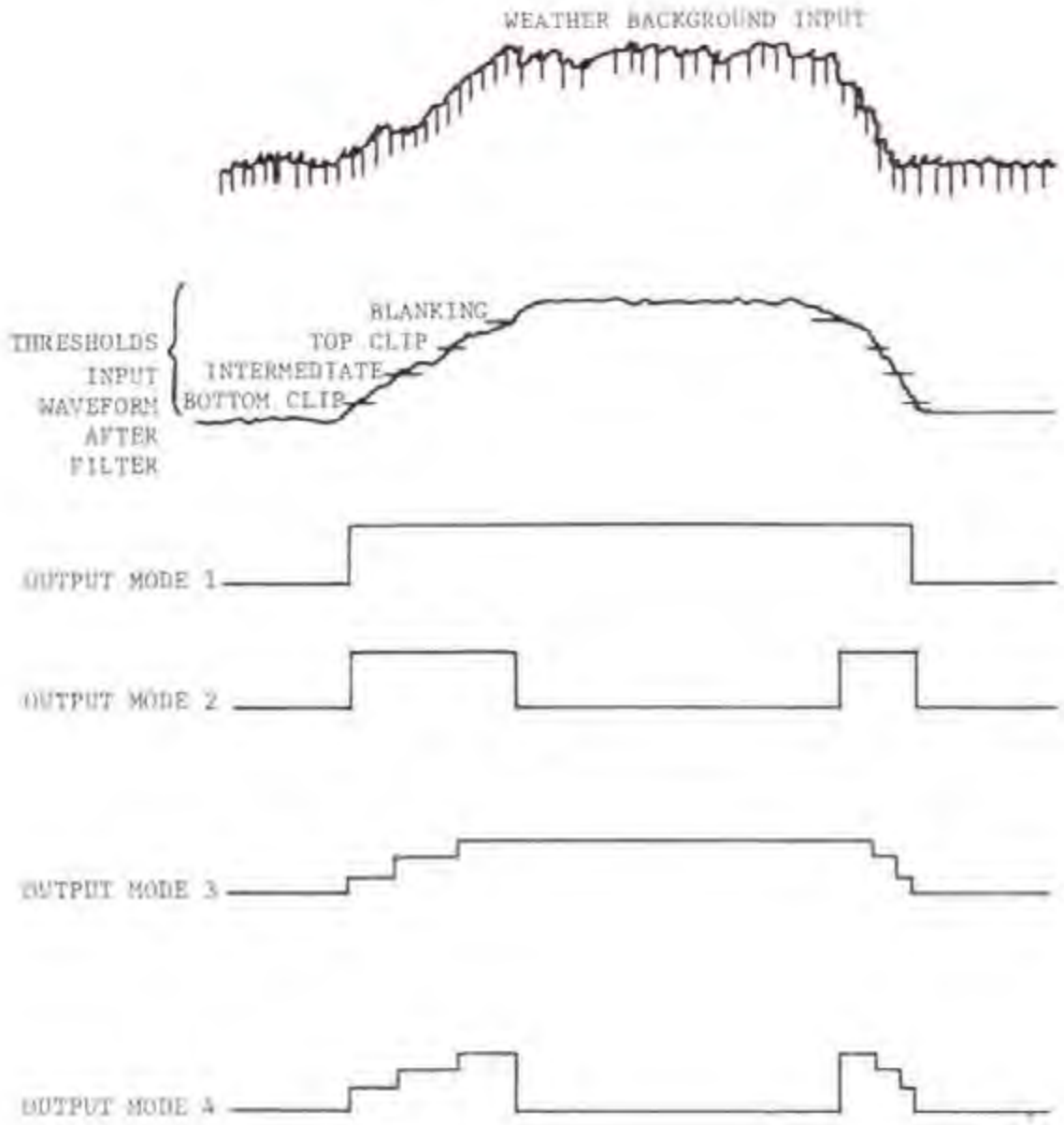

Figure 3-32. Weather Background Modes.

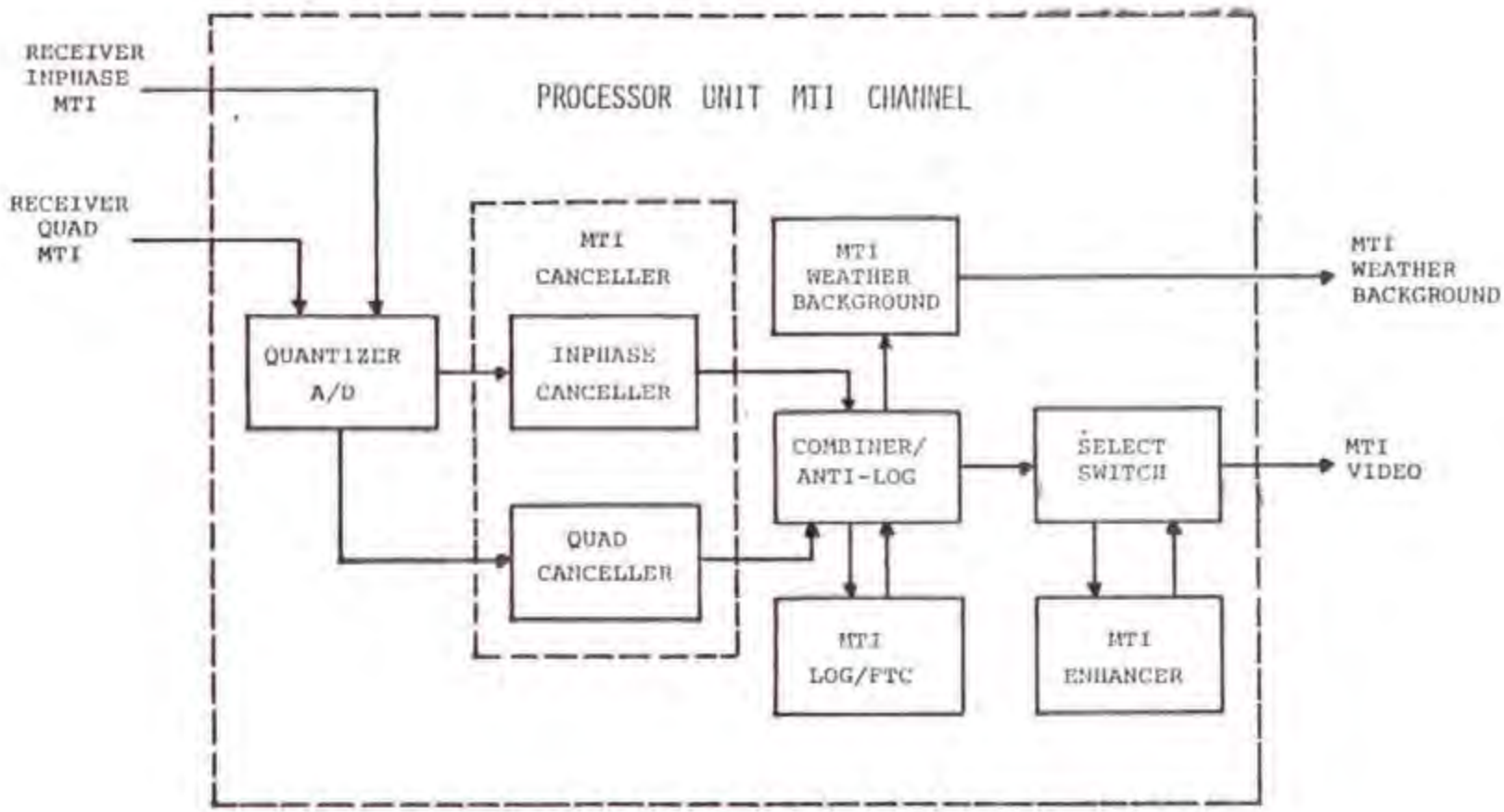

Figure 3-33. Processor Unit MTI Channel Block Diagram

clutter components will appear at zero frequency and at integral multiples of the radar Pulse Repetition Frequency (PRF), and will be suppressed.

Staggered PRF is generally employed by radars in the 2.7 to 2.9 GHz band to extend the blind speed of the radars. Analog radars typically have two or three staggers, while digital radars with their greater stability may have more than three staggers. The ASR-8 has a four-stagger system, and the ASR-7 has a six-stagger system. The analog MTI processors do not have Analog-to-Digital (A/D) converters and use delay line cancellers, while digital MTI processors have A/D converters and use shift register cancellers. The digital shift register cancellers have a much higher stability and do not decay in time. The transfer properties of analog and digital MTI cancellers can be treated identically with the exception of the quantization noise due to A/D conversion, roundoff, and truncation inherent in digital processing. In general, the error due to quantization, roundoff and truncation is very small, and can be neglected in most cases.

Both single channel and dual channel (inphase, I; and quadrature, Q) MTI processing is employed by radars in the 2.7 to 2.9 GHz band. The single channel MTI processors have either analog or digital cancellers, while the dual channel MTI processors are all digital. For dual MTI channel processing, it is only necessary to analyze one channel since both the I and Q channels are identical with the exception of the COHO signal being shifted 90 degrees and to take into account the transfer properties of the combiner.

Most radars in the 2.7 to 2.9 GHz band employ both single and double stage cancellers. Generally, the radars are operated in the double stage canceller mode which provides broader clutter-rejection nulls than the single cancellers. Some of the radars in the band also have the capability of introducing feedback in the double-canceller mode to improve the velocity response of the MTI filter, and thus have several Subclutter Visibility (SCV) modes of operation. The various operating modes of MTI cancellers are obtained by using the feed-forward coefficients (a_0, a_1, a_2) and feedback coefficients (b_1 and b_2) in the canceller hardware. For analytical purposes the single stage and double stage MTI cancellers with and without feedback can be represented in a canonical form as shown in Figure 3-34. TABLE 3-1 shows the equivalent canonical coefficients for the different modes of operation of the MTI cancellers in the ASR-7 and ASR-8 radars. The single stage MTI canceller mode is CANC1, and the double stage canceller mode without feedback is 1 & 2 CASC. The feedback modes are SCV-25, SCV-30, SCV-35, and SCV-40.

The following is a discussion of the MTI canceller transfer properties for the various modes for noise, desired signal, and asynchronous interference. A more detailed discussion of the MTI channel transfer properties and filter frequency response is given in Appendix C.

Noise - The noise amplitude at the MTI canceller input is Gaussian with zero mean. In all pulse radars, the inter pulse period (1/PRF) is much greater than 1/system bandwidth. Thus the sample of noise taken from the

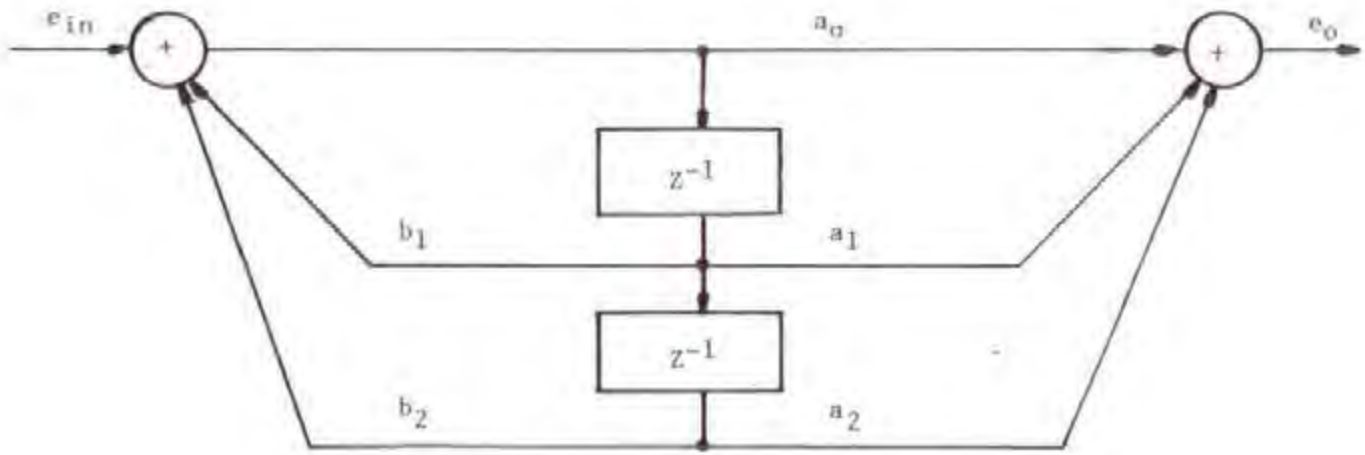

Figure 3-34. Canonical Form of Simulated ASR-7 MTI Canceller

TABLE 3-1

MTI CANCELLER TRANSFER PROPERTIES

MTI MODE	FEED-FORWARD COEFFICIENTS			FEEDBACK COEFFICIENTS		NOISE GAIN		PEAK INTERFERENCE GAIN		PEAK INR (dB)
	a_0	a_1	a_2	b_1	b_2	VOLTS	dB	VOLTS	dB	
CANC 1	1	-1	0	0	0	$\sqrt{2}$	3	1.0	0	-3
1&2 CASC	1/2	-1	1/2	0	0	$\sqrt{1.5}$	1.76	1.0	0	-1.76
SCV-25	1/2	-1	1/2	1 1/4	-1/2	$\sqrt{0.454}$	-3.42	0.50	-6.0	-2.58
SCV-30	1/2	-1	1/2	1	-1/2	$\sqrt{0.6}$	-2.21	0.50	-6.0	-3.79
SCV-35	1/2	-1	1/2	3/4	-1/2	$\sqrt{0.777}$	-1.09	0.625	-4.08	-2.99
SCV-40	1/2	-1	1/2	1/2	-1/2	1.0	0	0.75	-2.49	-2.49

same source at intervals of 1/PRF apart are essentially uncorrelated. Zero mean uncorrelated sources add rms. The noise gain of the MTI canceller is a function of the feed-forward and feedback coefficients, and therefore is a function of the MTI canceller mode. Appendix C contains an analytical derivation of the MTI canceller noise gains. TABLE 3-1 shows the MTI canceller noise gain for each of the operating modes of the ASR-7 and ASR-8 radars.

Since the MTI canceller sums the noise at the input to the canceller which has a Gaussian amplitude distribution, the canceller output noise amplitude distribution is also Gaussian. Therefore, the noise amplitude distribution at the MTI canceller input and output are Gaussian distributed with zero mean.

Desired Signal - For the desired signal (synchronous signal), the signal power transfer gain of the MTI canceller without feedback or with feedback when averaged over all possible Doppler frequencies is the same as the noise power transfer gain (see noise gain in TABLE 3-1). Since the noise power density is uniform over the MTI filter, the filter treats both noise and signal (on the average) alike. Thus the signal-to-noise ratio (SNR) at the MTI canceller output is the same as at the input to the canceller when averaged over all doppler frequencies.

Interfering Signal - For an asynchronous interfering signal, the MTI canceller will produce several interfering pulses at the canceller output for each asynchronous interfering pulse at the MTI canceller input. These interfering pulses at the MTI canceller output are synchronous with the radar system (i.e., fall in the same range bin in successive azimuth change pulses). The amplitude and number of pulses produced by each interfering pulse are a function of the feed-forward coefficients (a_0, a_1, a_2) and the feedback coefficients (b_1 and b_2), and therefore are a function of the MTI canceller mode the radar is operating in.

For a single stage canceller (mode CANC 1), each interfering pulse produces two synchronous interfering pulses. For a double stage canceller without feedback (mode 1 & 2 CASC), each interfering pulse produces three synchronous interfering pulses. When operating in the feedback mode, there are more than three pulses out for each interfering pulse. However, by the third or fourth pulse, the interfering signal is down below the receiver noise level (1 volt) depending on the feedback constants and interfering signal level. Appendix C Figure C-11 and Figures C-15 through C-20 show measured and simulated responses of a MTI canceller to asynchronous interference for the various modes of MTI canceller operation.

The peak interfering signal transfer properties were obtained using a combination of analytical and simulation techniques, and are discussed in Appendix C. TABLE 3-1 summarizes the peak interfering signal and peak Interference-to-Noise Ratio (INR) transfer properties for each of the MTI canceller modes after rectification.

Rectifier

The output of single channel MTI canceller circuits are fed to a full-wave rectifier in analog radars or a magnitude and scale algorithm in digital radars to convert the bipolar video at the canceller output to unipolar. The signal-to-noise ratio (SNR) or interference-to-noise ratio (INR) at the rectifier or magnitude and scale output is the same as at the input. The noise amplitude distribution at the full-wave rectifier output will be one-sided Gaussian since the noise amplitude at the MTI canceller output was Gaussian. The noise amplitude PDF at the rectifier output is given by:

$$p(v) = \frac{2}{\sqrt{2\pi}\sigma} e^{-v^2/2\sigma^2} \quad ; \; 0 \leq v \leq \infty \qquad (3\text{-}25)$$

where:

σ = rms noise level, in volts

The desired signal-plus-noise amplitude distribution PDF at the single channel MTI rectifier output for a double stage MTI canceller is shown in Figure 3-35. It should be noted that the rectifier output signal-plus-noise amplitude distribution PDF shown in Figure 3-35 is for the radar operating in the staggered mode and the signal averaged over all possible doppler frequencies. The PDF shown in Figure 3-35 was obtained by simulation. Although the desired signal-plus-noise amplitude distribution PDF is not of the nature of a one-sided Gaussian distribution, it is shown in Appendix C that the desired signal-plus-noise amplitude distribution PDF at the single channel MTI rectifier output for a double stage MTI canceller can be approximated by a one-sided Gaussian distribution.

Combiner

The output of dual channel (inphase and quadrature) MTI canceller circuits are fed to a combiner. The signal transfer properties of the inphase and quadrature channels are identical to the single channel transfer properties previously discussed. The output of each channel is combined in the following manner:

$$R = \sqrt{(I)^2 + (Q)^2} \qquad (3\text{-}26)$$

Circuit implementation to achieve Equation 3-26 in the combiner is complex. Often a simplified approximation to Equation 3-26 is implemented by summing the larger vector amplitude with one-half the smaller vector amplitude as

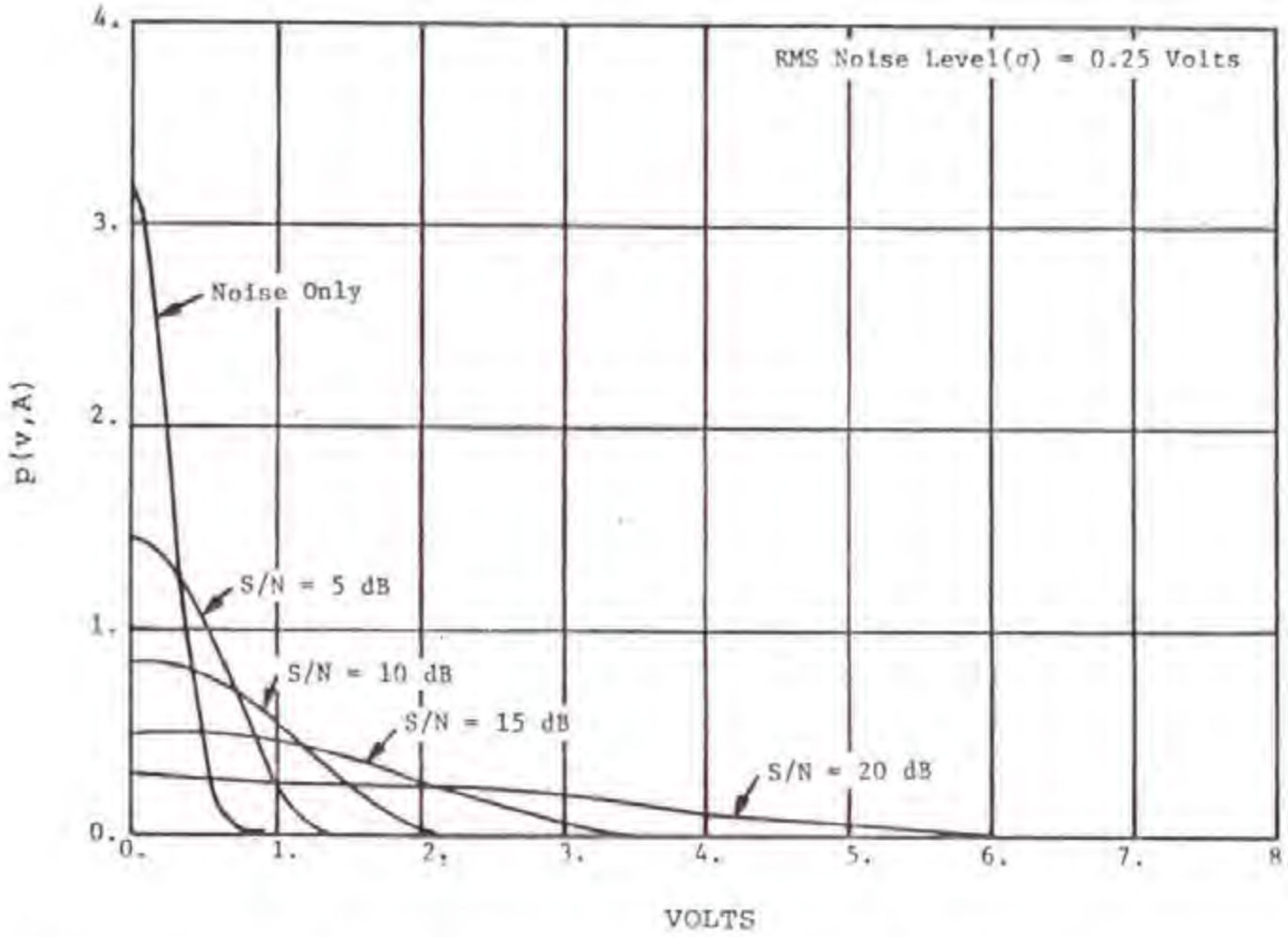

Figure 3-35. Probability Density Function for Noise Only and for Signal-Plus-Noise at the MTI Canceller Output for a Single Channel Double Stage Canceller (Simulated).

shown below:

$$R = |I| + |Q/2| \text{ if } |I| > |Q| \qquad (3\text{-}27)$$
$$R = |Q| + |I/2| \text{ if } |I| < |Q|$$

The noise amplitude distribution at the combiner output of a dual MTI canceller is Rayleigh since the transfer properties of the combiner (Equation 3-26) are similar to an envelope detector. The desired signal-plus-noise amplitude distribution PDF at the dual channel MTI combiner output for a double stage MTI canceller is shown in Figure 3-36. It should be noted that the combiner output signal-plus-noise amplitude ditribution PDF shown in Figure 3-36 is for the radar operating in the staggered mode and the signal averaged over all possible doppler frequencies. The PDF shown in Figure 3-36 was obtained by simulation. Although the desired signal-plus-noise amplitude distribution PDF is not of the nature of a Rayleigh distribution, it is shown in Appendix C that the desired signal-plus-noise amplitude distribution PDF at the dual channel MTI combiner output for a double stage MTI canceller can be approximated by a Rayleigh distribution.

The fact that dual MTI cancellers have the COHO reference signal of the inphase and quadrature channels phase shifted by 90 degrees, and the method in which the two channels are combined, a signal-to-noise ratio (SNR) improvement is achieved over a single MTI channel. The SNR improvement of dual MTI channels over a single MTI channel was investigated by Nathanson and Luke (1972). The SNR improvement of dual channel MTI over a single channel MTI for a single pulse is a function of the probability of detection and probability of false alarm. Nathanson and Luke show the SNR improvement to be between 3 and 13 dB for a single pulse. However, for a desired signal target return pulse train of 20 pulses the SNR improvement of a dual MTI channel is only about 1.5 dB. For asynchronous interfering signals, the INR enhancement of a dual MTI channel over a single MTI channel is approximately 1 to 2 dB at MDS.

MTI Log-FTC

Both the ASR-7 and ASR-8 have digital MTI log circuits. The log circuit converts the MTI digital video from a linear value to a base two logarithmic equivalent value, when Log-FTC is selected, the video is averaged over several range bins and subtraction takes place to eliminate weather clutter from the MTI video. In the ASR-8 the averaging, subtraction, and anti-log functions are done digitally, and in the ASR-7 the averaging, subtraction, and anti-log functions are done analog. The MTI Log-FTC circuit performs the same functions as the normal channel Log-FTC circuits, and therefore, the hardware can be represented by the same operations as the normal channel Log-FTC circuit (see Figure 3-16). The signal processing properties of the MTI Log-FTC circuit are also identical to the normal channel, and are discussed in the processor unit normal channel section.

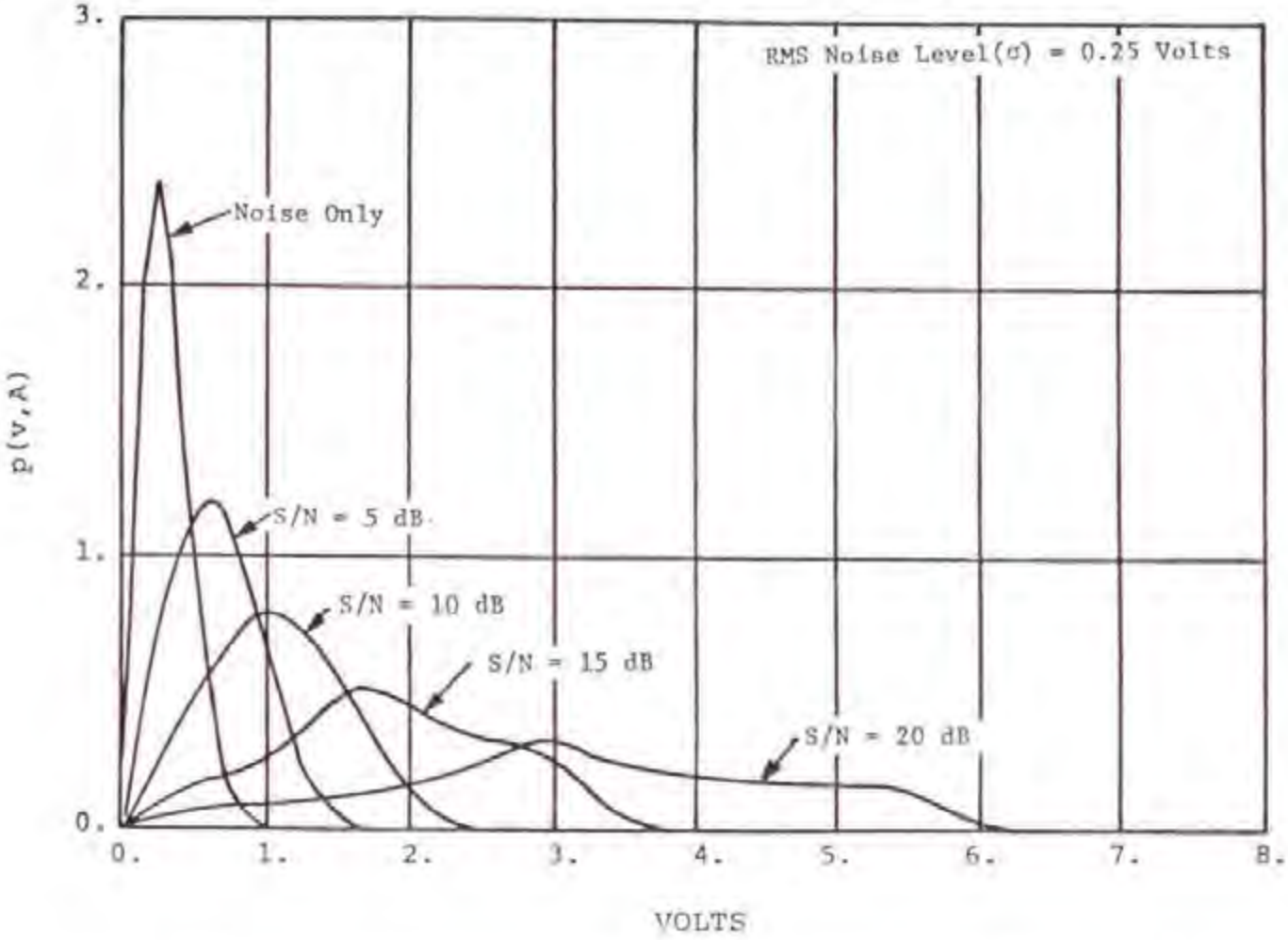

Figure 3-36. Probability Density Function for Noise Only and for Signal-Plus-Noise at the MTI Canceller Output for a Dual Channel Double Stage Canceller (Simulated).

In the ASR-8 the log-anti-log circuits are also used to introduce a bias for each of the various MTI operating modes so that the MTI channel output video noise level remains constant and independent of the operating mode. Noise normalization is achieved by scaling the video data by some factor. In the MTI channel this is implemented by adding the bias to the video data. The video data at this point in the processing is logarithmic; therefore, multiplication is accomplished by adding the logarithm of the two numbers. Since the scaling involves both adding to and subtracting from the video data, the bias values are positive or negative, respectively.

In the ASR-7 a rms noise compensation network is used to normalize the noise. The rms-noise compensation network consists of a resister divider network. Both methods of normalizing the noise will not change the signal-to-noise ratio (SNR) or interference-to-noise ratio (INR) at the output of the noise normalization networks.

MTI Enhancer

The MTI channel integrator (enhancer) circuits are separate but electronically identical to the normal channel enhancer circuitry. Therefore, the MTI channel enhancer hardware and functions are identical to the normal channel enhancer which has been previously described in the processor unit normal channel. (See Figures 3-17 and 3-24 for feedback and binary integrator block diagrams, respectively.) The major difference in the signal processing properties of the MTI channel enhancer and the normal channel enhancer are due to the difference in the statistical characteristics of the noise, desired signal, and interference signal at the input of the normal and MTI enhancer. The following is a summary of the MTI channel enhancer transfer properties for both the feedback and binary integrators which are discussed in detail in Appendix D.

Noise - The noise at the output of a single channel MTI canceller has a one-sided Gaussian amplitude distribution, while the noise at the output of a dual channel MTI canceller has a Rayleigh amplitude distribution like the normal channel. For the feedback integrator, the signal processing of the noise (attenuation, subtraction, and bottom-clipping) will result in a slightly different noise gain of the feedback integrator for a radar with a single channel MTI canceller than for a dual channel MTI canceller. However, this difference can be made small by adjusting the attenuation, subtraction, and bottom clipping circuits prior to the enhancer input. For the binary integrator the noise level at the integrator output for a single or dual channel MTI canceller can be made equal by adjusting the threshold comparator level at the input to the binary integrator. The adjustment of the threshold comparator as a function of the noise amplitude statistical characteristics is discussed in detail in Appendix D.

Another factor which affects the noise gain of the MTI channel enhancers is that the noise is correlated from range/azimuth cell to range/azimuth cell due to the MTI cancellers. This correlation of the noise is discussed in

detail in Appendix D. The MTI channel noise correlation affect for a feedback integrator was simulated by Trunk (1977), and found to be approximately 1 dB for a single stage MTI canceller and 1.8 dB for a double stage MTI canceller. Therefore, the feedback integrator signal-to-noise ratio enhancement (SNR_E, see Equation 3-22) would be reduced by 1 dB for a single stage MTI canceller and 1.8 dB for a double stage MTI canceller over the normal channel SNR_E due to MTI noise correlation.

Desired Signal - The desired signal-plus-noise amplitude distribution when averaged over all possible Doppler frequencies is shown in Figure 3-35 for a single channel MTI canceller, and Figure 3-36 for a dual channel MTI canceller. The desired signal enhancement of a feedback or binary integrator for a single MTI channel will be significantly less than a dual MTI channel. This should be expected when comparing the signal-plus-noise amplitude distribution at the MTI canceller output as a function of the signal-to-noise ratio (SNR) for the single and dual MTI channels. Compare Figure 3-35 (single MTI channel signal-plus-noise amplitude distribution) with Figure 3-36 (dual MTI channel signal-plus-noise distribution).

Interference - As discussed previously in the MTI canceller signal processing properties of interference, and in Appendix C, each interfering pulse at the MTI canceller input produces several synchronous interfering pulses (i.e., fall in the same range bin in successive azimuth change pulses) at the MTI canceller output. The number of interfering synchronous pulses at the MTI canceller output is a function of the MTI canceller operating mode. Because the interference at the MTI canceller output consists of several synchronous pulses which occur in the same range bin in successive azimuth change pulses, there is potential for the interference to be integrated like the desired signal. That is, the peak interference-to-noise ratio (INR) at the MTI channel enhancer output will be greater than the peak (INR) at the MTI channel enhancer input. However, since the synchronous interference at the MTI canceller output only consists of two or three pulses that are above the receiver system noise level (one volt), the interference can be suppressed by both the feedback and binary integrators if adjusted properly.

The capability of the feedback and binary integrators to suppress MTI channel asynchronous interference was investigated using a radar simulation model (see Appendix E). Three interfering radar sources were simulated: ASR-5, ASR-8, and the AN/FPS-90. Figures E-3 through E-5 in Appendix E show the respective time waveforms simulated for each of the radar interfering sources. Figure 3-37 shows a simulated single channel MTI canceller radar unintegrated output for three interfering sources (ASR-5, INR = 10dB; ASR-8, INR = 15 dB; and AN/FPS-90, INR = 20 dB), and a desired target signal-to-noise ratio (SNR) of 20 dB. Figure 3-38 shows a simulated output of a feedback integrator for the feedback integrator input limit level adjusted improperly (2.0 volts) for the same interference condition shown in Figure 3-37. As discussed previously the asynchronous MTI channel interference can be enhanced if the feedback enhancer is not adjusted properly. Figure 3-39 shows a simulated output of a feedback integrator for the feedback integrator input limit level adjusted at .34 volts for the same

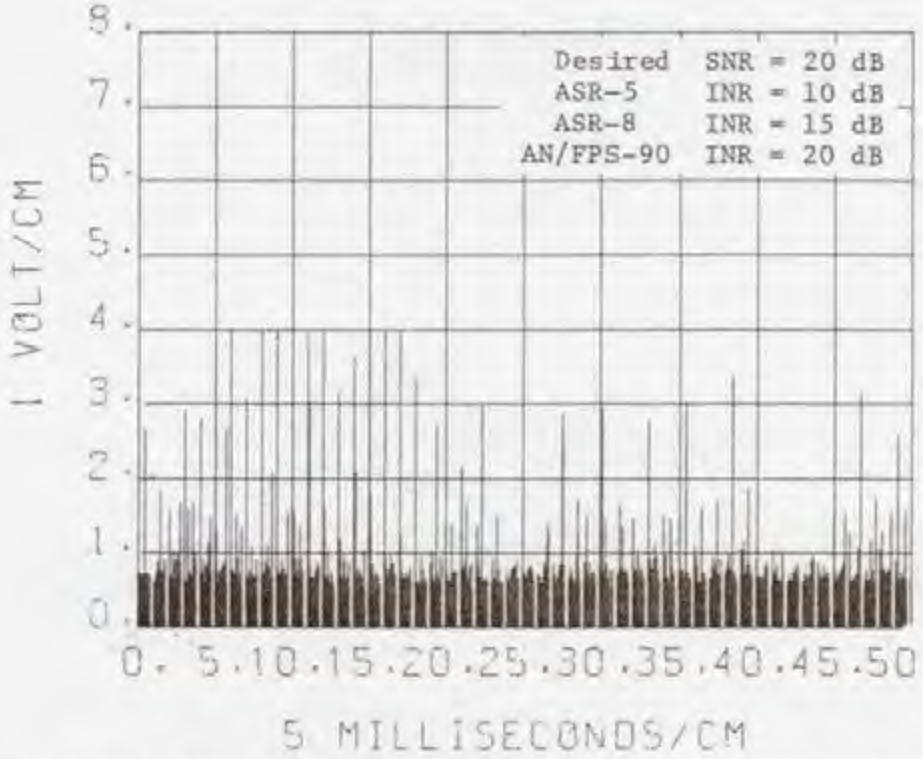

Figure 3-37. Simulated MTI Channel (Mode 1 & 2 CASC) Unintegrated Radar Output with Interference

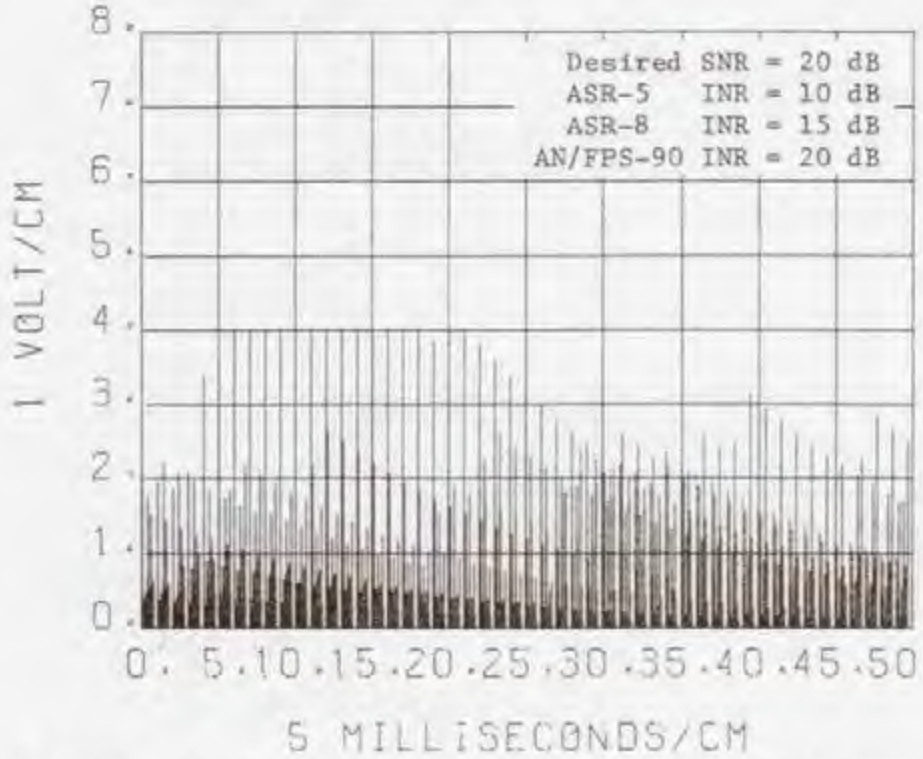

Figure 3-38. Simulated MTI Channel (Mode 1 & 2 CASC) Radar Feedback Integrator Output with Interference for the Input Limiter Set at 2.0 Volts

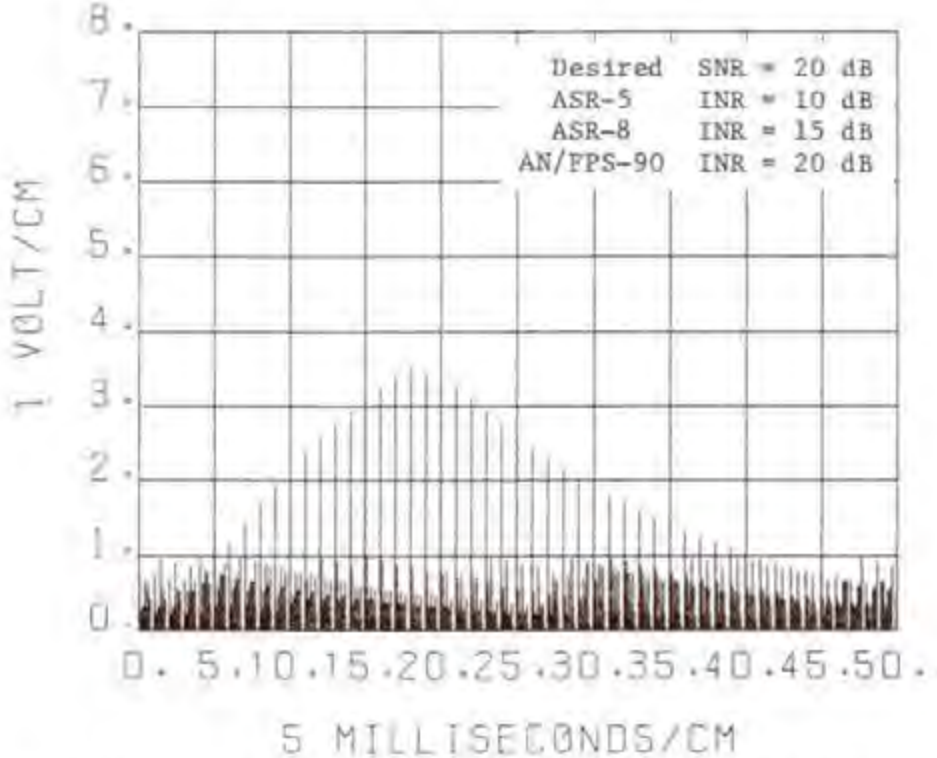

Figure 3-39. Simulated MTI Channel (Mode 1 & 2 CASC) Radar Feedback Integrator Output with Interference for the Input Limiter Set at 0.34 Volts

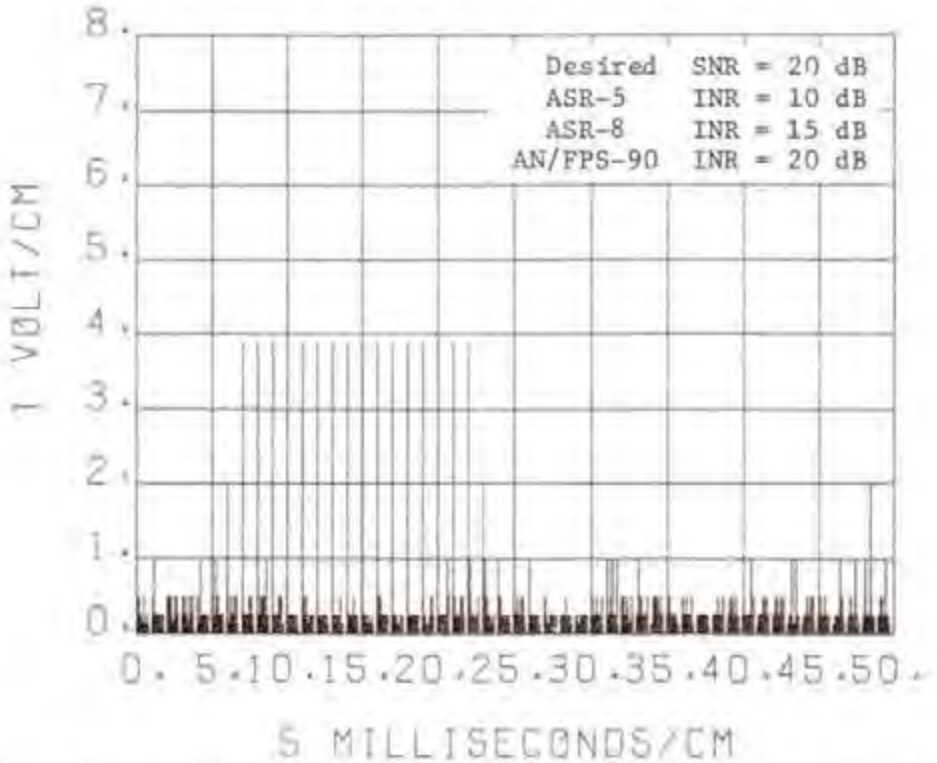

Figure 3-40. Simulated MTI Channel (Mode 1 & 2 CASC) Radar Binary Integrator Output with Interference

interference condition shown in Figure 3-37. The asynchronous interference has been suppressed by the feedback integrator. Measurements made on the Stapelton Airport ASR-8 radar in Denver, Colorado, showed that on-tune interference levels of 50 dB above the receiver noise level (approximately -60 dBm) could be suppressed in the MTI channel so that they did not appear on the PPI display. The ASR-8 radar has a feedback integrator (enhancer) and dual channel (Inphase and Quadrature) MTI channel processing. Figure 3-40 shows a simulated output of a binary integrator for the same interference condition shown in Figure 3-37. The asynchronous interference has also been suppressed by the binary integrator.

In summary, both the feedback and binary integrators will suppress asynchronous interference in the MTI channel. However, if the integrators are not adjusted properly, the integrators will enhance the interfering signals due to the synchronous interfering pulse transfer properties of the MTI cancellers. Therefore, if the integrators are not adjusted properly, the interference level will be greater with the integrators on than with the integrators off.

Processor Unit Alignment/Diversity Combiner

Figure 3-41 shows a block diagram of the processor unit Alignment/Diversity Combiner hardware in the ASR-8. Similar operations are performed in the ASR-7. The FAA is modifying the ASR-7 radars for frequency diversity. Therefore, the operations shown in Figure 3-41 should also be representative of the ASR-7 when modified for frequency diversity. The output of the Alignment/Diversity Combiner is sent to the Normal/MTI gating circuits then to the line drivers for distribution to the PPI displays.

MTI/Normal Alignment

The MTI and Normal Alignment circuits provide the delay required during STAGGER PRF operation to insure that a specific range bin in each PRF period occurs at the average PRF. During Non-STAGGER PRF operation, the alignment circuits are bypassed and the video has zero delay through the circuits. The circuit provides for the alignment of the MTI and Normal video as well as the weather background video associated with the MTI and normal channels.

The MTI/Normal Alignment circuitry does not have any affect on the desired signal-to-noise ratio or interference-to-noise ratio transfer properties since the circuitry only realigns the video information in time.

Output D/A Converter

The Digital-to-Analog (D/A) converter circuit follows the MTI/Normal Alignment processed to convert the realigned MTI and Normal video words to an analog voltage.

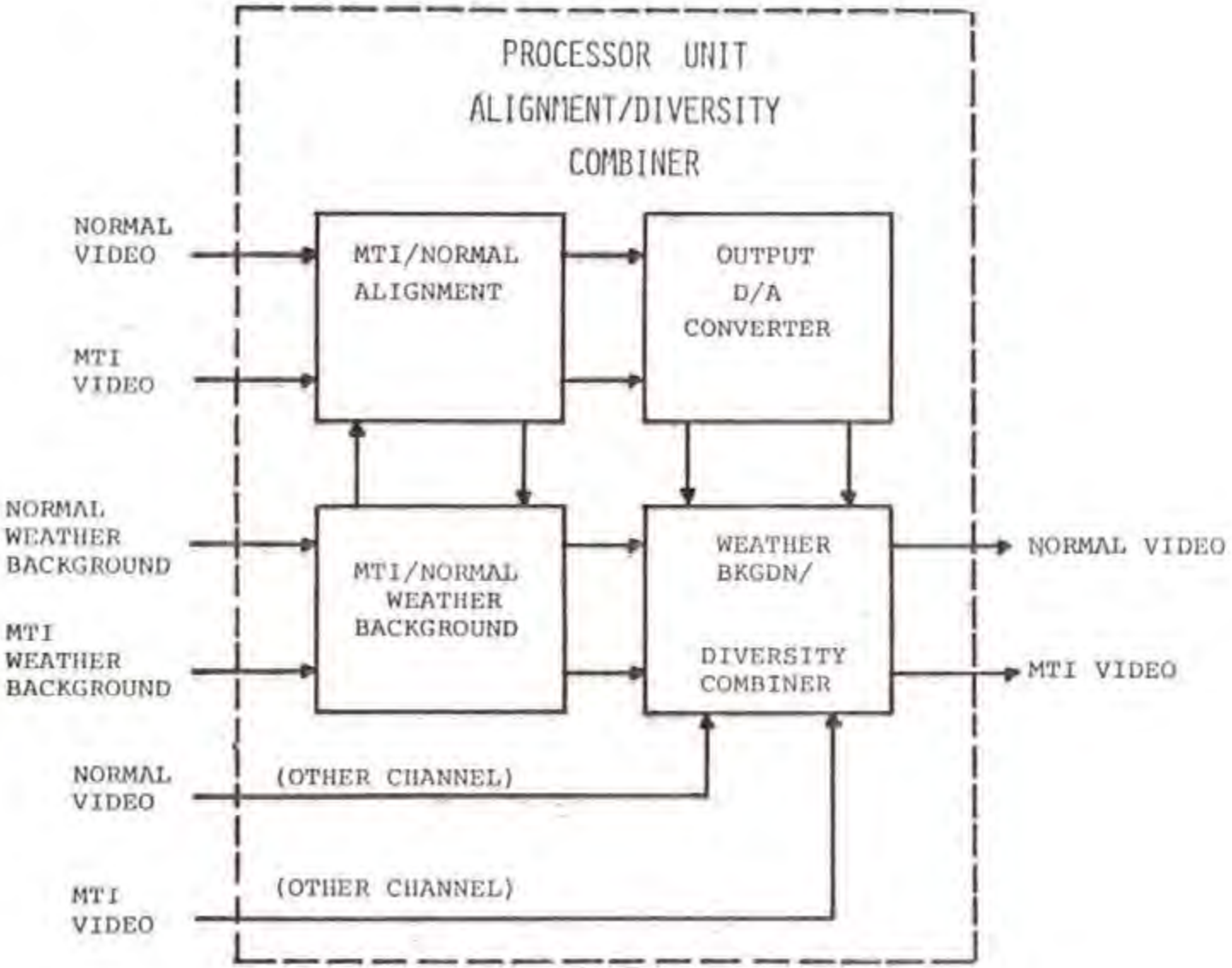

Figure 3-41. Processor Unit Alignment/Diversity Combiner Block Diagram

Weather Background/Diversity Combiner

The weather background/diversity combiner includes both MTI and normal combining circuits. After the MTI and Normal video is converted to an analog form in the output D/A converter it is routed to both the master and slave channel diversity combiners. Diversity operation involves the simultaneous operation of both radar channels to increase the effective transmittal power and improve the probability of detection. To prevent waveguide breakdown problems, the two transmitted outputs are separated in time by 1.4 μsec. To sum the signals from the two channels corresponding to the same target, this offset is realigned. A compensating delay line is, therefore, placed in the channel pulsed first, which is the master channel, thus making the two channels coincident. When two noise signals are summed, the output rms noise voltage increases by the square root of two. To maintain a constant output noise level from the radar, whether operating in diversity or single channel mode, a compensating attenuator is also included in the combiner circuit. When operating single channel, this attenuator is bypassed. After the combined or single channel video signal leaves the attenuator, it is applied to the output amplifier. The video output amplifier sums the weather background video and combined (single channel) video from the master channel when the weather background is enabled. Only the master channel weather background video is used, and it is mixed in after diversity combining since only one channel is needed to provide weather contour information. The output amplifier gain can be adjusted, however, the nominal gain is 1.4 for the combined video and 0.5 for the weather background video. A balance adjustment is also included in the summing amplifier and output amplifier.

The desired signal-to-noise ratio (SNR) improvement when operating in the frequency diversity mode is between 3 and 5 dB (Offi, 1969). The interference-to-noise ratio (INR) transfer properties of the diversity combiner when operating in the frequency diversity mode are a function of the operating frequency of the interfering radar relative to the victim radar, and the interfering signal pulse width. For the case where the interfering signal pulse width is less than 1.4 μsec, the interfering signal will not fall in the same range bin of both channels due to the 1.4 μsec separation of the transmitted pulses of the two channels, and there will be approximately a 3 dB loss in the INR. For the case where the interfering pulse is longer than 1.4 μsec (AN/FPS-6, 90; 2 μsec; WSR-57, 74S; 4.0 μsec), the interfering signal will fall in the same range bin of both channels, and there will be an increase in the INR. The maximum increase in the INR for this case is 3 dB which would only occur if the interference level was equal in both channels. When operating in the frequency diversity mode if there is interference above the noise level in either channel, the interference will appear on the PPI display.

SECTION 4

ARTS-IIIA SIGNAL PROCESSING

INTRODUCTION

This section considers the effects of asynchronous pulse interference on the FAA ARTS-III Enhancement signal processing and its impact on the radar's probability of detection and false alarm. The Automated Radar Terminal System (ARTS) III processor presently employed at terminal radar control facilities utilizes flight plan information from Air Route Traffic Control Centers (ARTCC) and Air Traffic Control Beacon Interrogator (ATCBI) video. In addition to providing target reports on transponder aircraft, alphanumeric data blocks available for display are continually associated with the appropriate aircraft targets by a tracking program. The primary or radar video is not processed by the present ARTS-III system. The ARTS-III enhancement, referred to as the ARTS-IIIA, processes the video target information from both the Airport Surveillance Radars (ASR) and the ATCRBS. The ARTS-IIIA consists of a Radar Data Acquisition Subsystem (RDAS), Beacon Data Acquisition Subsystem (BDAS), and a Common Processor Subsystem (CPS). Primary radar inputs are processed by the RDAS to produce radar reports and weather map data, and the beacon inputs are processed by the BDAS to produce beacon reports. The CPS correlates radar and beacon reports and transmits target and weather reports. Interference effects on the RDAS only are considered in this report since it is the portion of the ARTS-IIIA which processes the 2.7 to 2.9 GHz radar signals.

The ARTS-IIIA is currently scheduled to be operationally deployed at 60 airports throughout the United States. This is a substantial deployment since it involves over 25 percent of the FAA Radar equipped airports in the U.S. The first ARTS-IIIA operational deployment is scheduled for July 1979 at Minneapolis, Minnesota. The deployment at each of the remaining 59 locations is scheduled at every two-month interval after this initial date.

RADAR DATA ACQUISITION SUBSYSTEM DESCRIPTION

The RDAS is designed to receive analog video signals from the ASR-4, 5, 6, 7, and ARSR-2 radar or digital signals from the ASR-8 or ARSR-3. Provisions are made in the RDAS design for processing analog or digital video input by a printed circuit board insertion. The function of the RDAS is to detect and report aircraft and clutter derived from the search radar. The RDAS, as illustrated in Figure 4-1, consists of two functional units, referred to as the Radar Extractor (REX) and the Radar Microcontroller (RMC). The RDAS/REX simultaneously accepts normal, MTI, and synchronizing signals from the radar receiver.

The REX performs target detection and clutter monitor functions, and provides target reports and clutter counts to the RMC. The RMC employs these

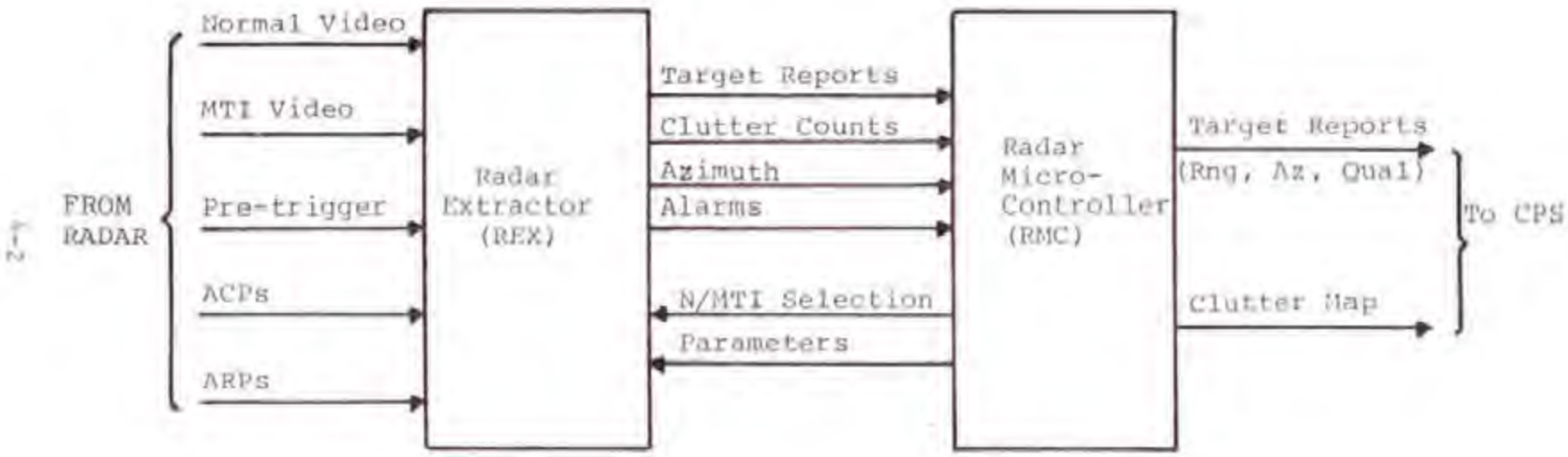

Figure 4-1. Block Diagram of Radar Data Acquisition Subsystem

clutter counts to determine the type video (normal or MTI) and MTI target detection threshold for optimum target detection performance. The video select and MTI threshold control signals from the RMC are fed back to the REX. The RDAS/RMC output provides target reports, including target range, azimuth, and report quality, to the Common Processing Subsystem (CPS). A two level clutter map is also provided to the CPS for indication of weather conditions.

A functional description of the REX and RMC follows. Only those control functions will be discussed that have a bearing on the interference analysis.

Radar Extractor

A simplified block diagram of the Radar Extractor (REX) is shown in Figure 4-2. The function of each unit in the signal flow path will be briefly described in this subsection.

Video Multiplexer Converter

The video multiplexer converter transforms the MTI and normal video received from the radar into a multiplexed serial digital bit stream. The multiplexer converter includes analog to digital converters when the RDAS is interfaced with ASR-4, 5, 6 and 7 analog video radars. When the RDAS is interfaced with the frequency diversity ASR-8 radar, in which both frequency channels are simultaneously operated, one sample per range bin from each channel are received by the REX multiplexer converter.

Rank Order Detection Process

The ARTS-IIIA employs a rank order detection process to detect target hits or pulse returns. The rank order detection process is performed by the Rank Quantizer and Hit Processor (see Figure 4-2). Rank order detection is a binary detection concept that utilizes a nonparametrical statistical decision process. That is, the rank order detector has a distribution free property in which the probability of a 1 being generated when no target is present (probability of false target hit) is independent of the noise or clutter distribution if the samples are from an identical probability distribution and statistically independent. Under these conditions the rank order detector yields a constant false alarm rate regardless of the environmental clutter level. The operation of the rank order detector involves comparing the amplitude sample of the range or target bin of interest with the sampled noise and clutter levels in adjacent range bins over each Azimuth Change Pulse (ACP). The number of cases that the amplitude of the target sample exceeds adjacent range samples is defined as the rank of the target sample. If this rank exceeds or equals a rank threshold, a target hit (logical 1) is generated, otherwise a miss (logical 0) is generated.

Rank Quantizer. The rank quantizer portion of the REX (see Figure 4-2) computes the rank of the range bin, and the hit processor unit compares this rank with a threshold to determine if a target hit has occurred. A

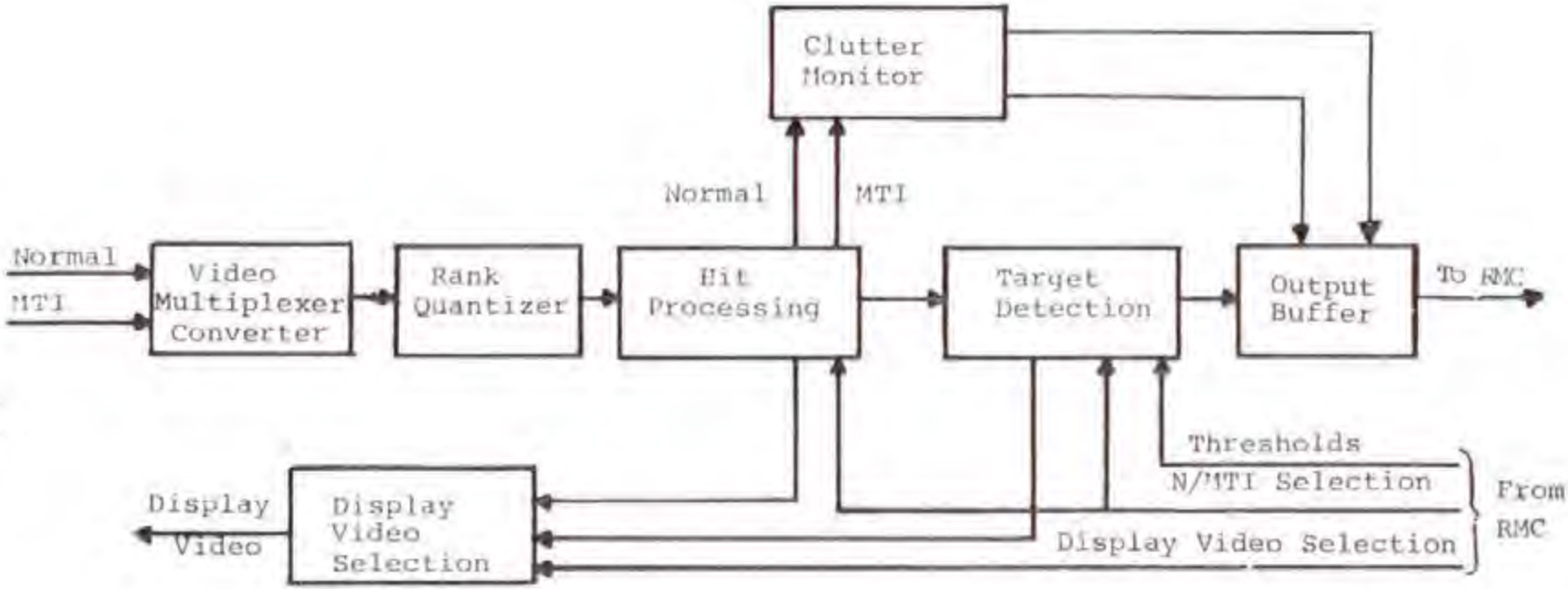

Figure 4-2. Block Diagram of Radar Extractor

simplified block diagram of the rank quantizer portion of the rank order detector is shown in Figure 4-3. The digital range bin samples enter a 27 stage shift register, in which delays between adjacent shift register stage taps correspond to the time resolution of the range bins. The signal amplitude in the range bin of interest (S14) from the center tap of the shift register is compared with the signal amplitude (usually noise) in the range bins before (S1-S12) and after (S16-S27) the range bin of interest. Signal samples from range bins S13 and S15 immediately adjacent to the range bin of interest are not compared with the range bin of interest to prevent long target pulses from overlapping both target and adjacent range bins and being interpreted as noise samples. The comparators (C_i) associated with each range bin outputs a one if the signal in the bin of interest (S14) is greater than the compared to range bin (S1-S12 and S16-S27). The comparator outputs are summed to obtain a rank (0-24) of the range bin of interest. It should be pointed out that the actual rank quantizer utilized in the REX is slightly more complicated than that indicated in Figure 4-3, because the rank quantizing processing is performed on a serial stream of interlaced normal and MTI bits. However, the logic depicted in Figure 4-3 is identical for both the normal and MTI channels.

Hit Processor. The block diagram of the hit processing logic is shown in Figure 4-4. The input consists of a five bit rank value from the rank quantizer. The rank data is processed simultaneously in two paths to produce target and clutter hits respectively. If the rank value in the upper path equals or exceeds a rank quantizer threshold (typically 23 or 24) a target hit is generated and a logical 1 assigned to the range bin of interest. That is, if the signal amplitude in the range bin of interest has exceeded the voltage level in all but one of the 24 adjacent reference range bins or all 24 of the adjacent reference range bins, depending on which rank quantizer threshold setting is used, a target hit is generated. If the rank does not exceed the rank quantizer threshold, a miss is generated and a logical 0 assigned to the range bin of interest. In the lower path (see Figure 4-4), if the rank exceeds or equals a rank quantizer threshold of 17, a clutter hit is generated and a logical 1 assigned to the range bin of interest. In other words, for a clutter hit to be declared the signal amplitude in the range bin of interest has to exceed 17 of the 24 adjacent sample range bins. This rank quantizer threshold testing in the upper and lower channel of the hit processor provides the last phase in the rank order detection process. Both the target and clutter hit paths include demultiplexers after the rank quantizer threshold comparators to separate out the normal and MTI digital signals. The normal or MTI target hits are selected for further target detection processing by a feedback control signal from the RMC. The selection is based on the normal clutter hit data provided by the hit processing logic. Basically, normal is selected in light clutter and MTI in heavy clutter conditions. A normal or MTI video selection is made for each 32 azimuth change pulse (ACP) by 32 range bin (RB) zone. This represents approximately a 2.8 degree by 2 nmi zone. The normal and MTI clutter hit information used for the normal/MTI target hit selection is routed to the RMC through the clutter monitor unit and output buffer (see Figure 4-2).

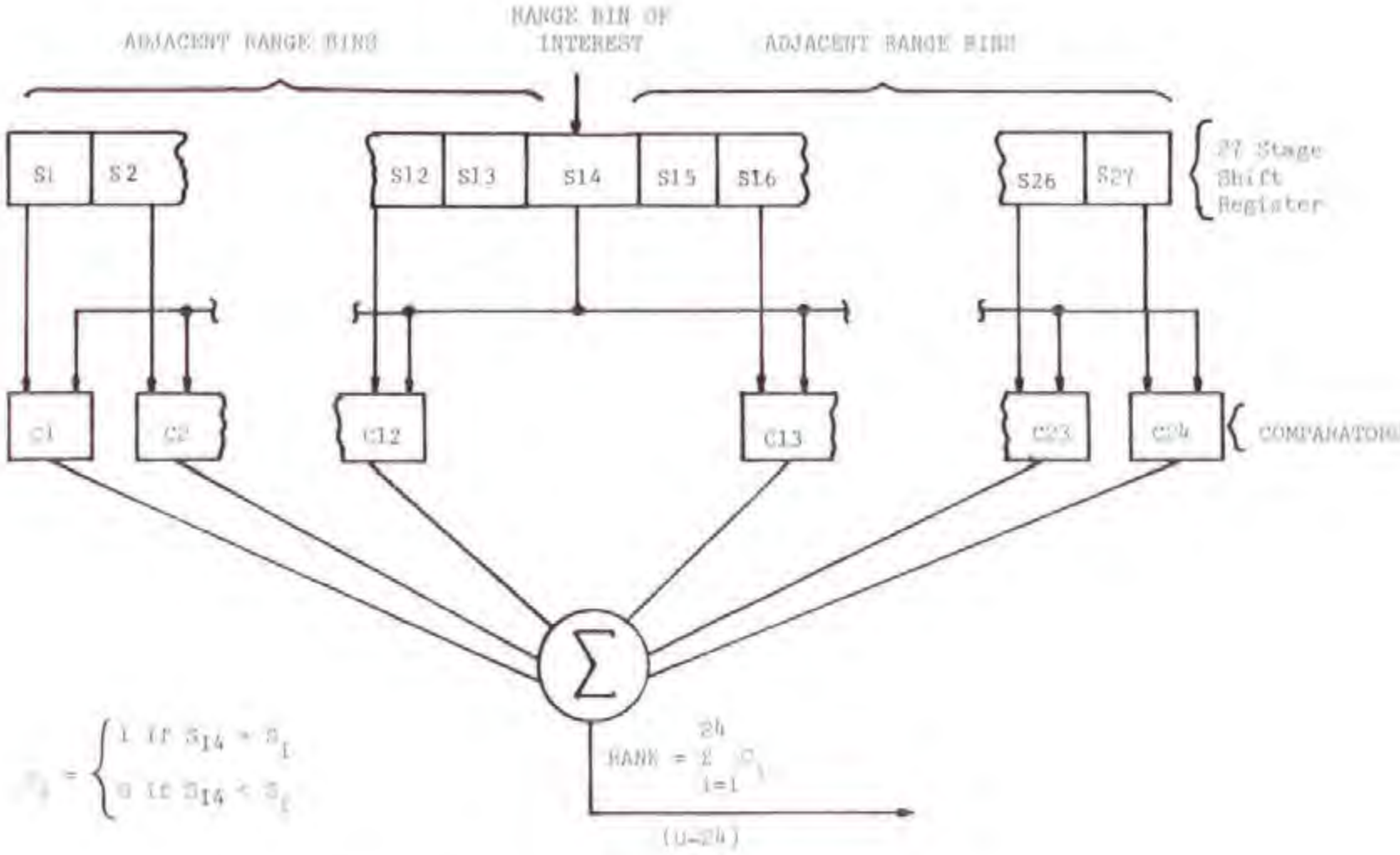

Figure 4-3. Block Diagram of Rank Quantizer Logic

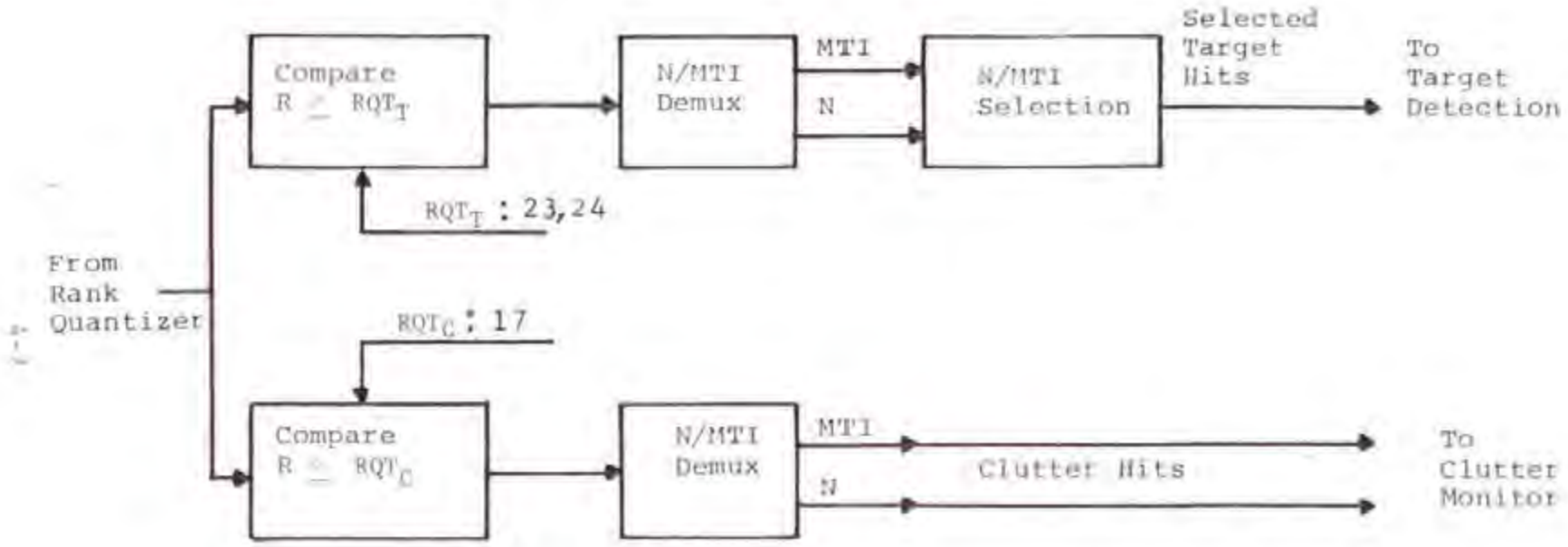

Figure 4-4. Block Diagram of Hit Processing Logic

Target Detection

The target detection stage in the REX is shown in Figure 4-2 and the details of the software functions in Figure 4-5. The target detection software logic first correlates the hit and miss data received from the hit processor unit with the appropriate range bins. A record of the target hits (1) and misses (0) in azimuth for a given range bin is initialized and maintained when a target hit is generated. When the consecutive misses (zeros) in the record equals or exceeds a miss count threshold (typically 3 or 4), the accumulated sum of the target hits since the beginning of the record is examined. If the target hit count equals or exceeds the hit count threshold, a target is declared. For the normal radar channel the target hit count threshold is fixed (typically at 8 or 9) and the MTI channel is variable. The MTI hit target count threshold is increased from the normal channel threshold value up to 20 depending on the degree of pulse-to-pulse correlation of the clutter. When a target is declared, the hit/miss record is terminated. The record is also terminated under the following two conditions:

(1) The miss count threshold is exceeded but the hit count threshold is not.

(2) The record length (number of ACPs) reaches 30 and the consecutive miss count and hit count threshold are not satisfied.

The target hit/miss record is extended beyond 30 ACPs if the hit count threshold is satisfied, but the miss count threshold is not. In this case, the hit and consecutive miss count is continued until the target detection or record termination criteria is met.

Clutter Monitor Logic

The function of the clutter monitor logic, shown in Figures 4-2 and 4-6, is to count "isolated hits" over 32 range bin (RB) blocks in both the normal and MTI channel, and output these counts to the RMC. Isolated hits are those preceded and followed by a miss (010 pattern) over a 3 ACP (pulse transmission) sequence in azimuth at a fixed range. The "isolated hits" (010 hit/miss pattern) are detected by the 3 stage shift register, inverters, and "and gate" logic shown in each video channel in Figure 4-6. The counters following the "and gate" count the number of isolated hits that occur over the 32 RB's. If more than 15 isolated hits occur in a 32 RB interval, a maximum count of 15 is outputted.

Radar Micro Controller

The Radar Micro Controller (RMC) is a digital data processing device that uses a microprogrammed control structure, involving microinstructions and control data stored in a read only memory (ROM). This RMC firmware controls the data flow between the REX and RMC and formats the RDAS output data. The RMC receives normal and MTI channel Isolated Hit Sum (IHS) data

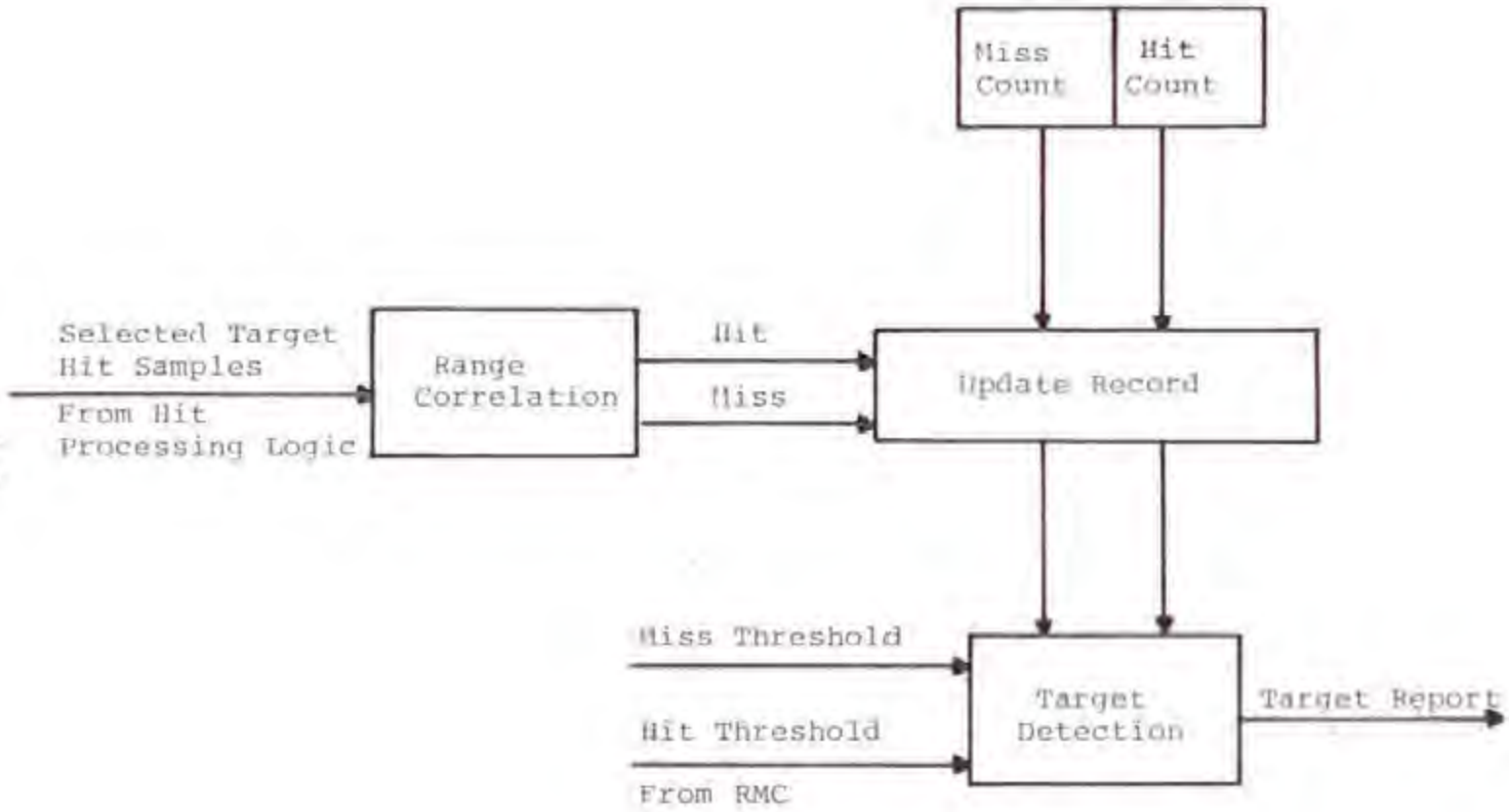

Figure 4-5 Block Diagram of Target Detection

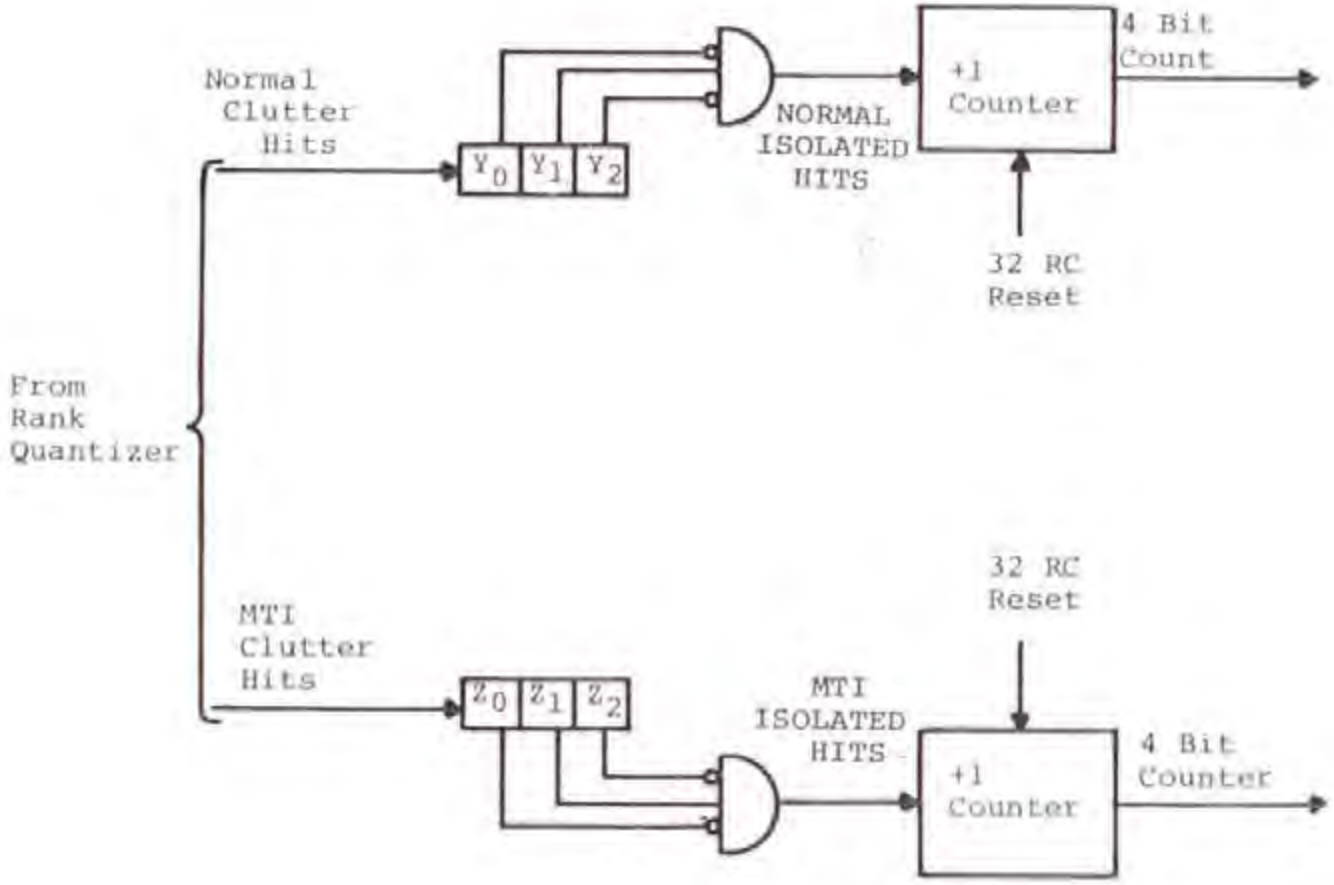

Figure 4-6 Block Diagram of Clutter Monitor Logic

from the REX clutter monitor. The normal channel IHS clutter data is used by the RMC to select the optimum video (normal or MTI) for target detection processing, and the MTI channel IHS clutter data to adjust the MTI target detection criteria (target hit count threshold). The first paragraph below discusses the RMC control processing associated with the video selection, and the second paragraph the RMC control processing associated with the MTI target detection threshold control.

The RMC receives normal channel IHS clutter data in 32 RB blocks and forms a clutter map of IHS's in 32 RB by 32 ACP zones. The sum of the normal video isolated hits for the zone on the previous antenna scan is used to update a clutter zone on the current antenna scan. The magnitude of the updated clutter count represents the level of clutter returns and is used to derive the video select command for the zone. The following criteria is used to update the zone clutter count and arrive at a video select decision. If the IHS for the 32 RB x 32 ACP zone on the previous antenna scan is greater than a variable clutter count threshold (typically 166), the clutter count shall be incremented by 1. If the IHS is less than or equal to this threshold value, the clutter count is decremented by 1. If the resulting clutter count exceeds 7, the MTI channel is selected. Conversely, if the clutter count is less than or equal to 7, the normal channel is selected. Basically normal video is selected in light or zero clutter zones, and MTI video is selected in heavy clutter zones.

When MTI video has been selected, the RMC controls the MTI video target hit threshold to maintain a constant false alarm rate. Unlike noise hits, the amplitude of pulse-to-pulse clutter returns are often correlated which results in a higher probability of false alarm. The rank order detection process is only partially effective in maintaining a constant false alarm rate for these conditions, since it only accounts for first order statistics (average number of independent hits) of the clutter distribution. The RMC uses the MTI channel clutter IHS measured by the clutter monitor logic to determine the degree of pulse-to-pulse correlation. The RMC maintains a 32 RB (2 nmi) by 32 ACP (2.8 degrees) sliding window of MTI cumulative IHS. The 32 RB blocks of MTI channel IHS received from the clutter monitor logic are added to the sliding window's cumulative sum, and the 32 RB block IHS received 32 ACPs before subtracted. The current sliding window cumulative sum is used to derive the MTI channel target hit count threshold. The target hit count threshold is linearly increased from the normal channel threshold value with decreasing values of sliding window IHS's in the manner indicated in Figure 4-7. This type of functional control tends to maintain a constant false alarm by increasing the hit count threshold for a high pulse-to-pulse amplitude correlated clutter or equivalently a low IHS count.

ARTS-IIIA RDAS INTERFERENCE ANALYSIS

The ARTS-IIIA RDAS interference analysis involved determining the effect of radar asynchronous interference on the victim radar's probability of false alarm and target detection. This involved applying a combination of analytical and simulation techniques.

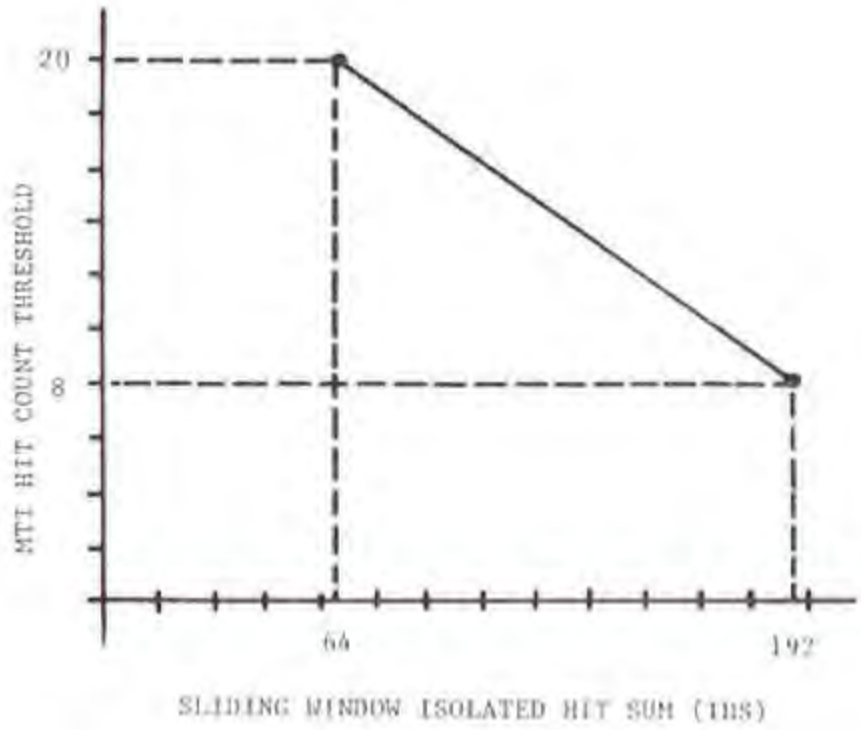

Figure 4-7. ARTS-IIIA/RDAS MTI Channel Hit Count Threshold Control for Maintaining a Constant False Alarm Rate

In particular, the effect of interference on the probability of a false target hit and target hit detection was defined analytically for worst-case interference signal level conditions, and then related to probability of false alarm and target detection by simulation of the processors target detection criteria. This method of analysis was performed for all combinations of ARTS-IIIA/RDAS target detection parameters so that trade-offs between interference suppression and radar performance could be investigated. The effect of interference on the ARTS-IIIA/RDAS automatic video selection and MTI hit count threshold control was analyzed using statistical and probability theory. Those interference and target signal level conditions which maximized the effect of interference were assumed in the analysis. This worst-case approach allowed analytical techniques to be employed instead of the more time consuming complete ARTS-IIIA/RDAS hardware simulation. The rationale for this decision was that if a worst-case analysis indicated that asynchronous interference would not significantly affect the ARTS-IIIA/RDAS performance a complete hardware simulation would not be necessary.

The two victim radars considered were the ASR-7 and ASR-8 interfaced with the ARTS-IIIA/RDAS processor. The interfering type radars considered included the ASR-7, ASR-8, AN/CPN-4, AN/FPS-90, and WSR-57. However, the analysis results are applicable to other type interfering radars in the 2.7 to 2.9 GHz band that have the same pulse width and pulse repetition frequency range.

Effect of Interference on the Probability of a Hit

The following is a discussion of the impact of interference on the RDAS rank order detection process which includes the rank quantizer and hit processor. A general equation is presented to determine the effect of interference on the probability of a hit (logical 1) when noise, desired signal, or clutter are in the range bin of interest. The effect of interference on the probability of a hit when noise, desired signal, or clutter is present in the range bin of interest is a function of the probability of a hit (logical 1) when noise only is present (P_{n1}), probability of a hit when noise and desired signal only are present (P_{s1}), and the probability of a hit when noise and clutter only are present (P_{c1}), respectively. For purposes of deriving a general equation for all the above conditions, a general term (P_1) will be used to represent a hit for P_{n1}, P_{s1}, and P_{c1}. The specific equation for P_{n1}, P_{s1}, and P_{c1} will then be derived in later subsections.

Asynchronous interfering radar video pulses can affect the probability of a hit at the hit processor output in two ways. First, an interfering radar pulse falling in the rank quantizer range bin of interest increases the probability of a hit (logical 1) being generated. Second, an interfering pulse falling in the rank quantizer comparison range bins decreases the probability of a hit. This is because an interference pulse falling in one or more of the comparison range bins lowers the probability of the voltage level in the range bin of interest exceeding the comparison range bin levels.

Both the above described interference mechanisms can be accounted for in a simple equation if it is assumed that the interfering signal-plus-noise level at the input to the RDAS is always greater than the target return signal-plus-noise level. If it is also assumed that the random arrival of interfering radar pulses in time can be described by a Poisson probability distribution, the effect of interference on the probability of a hit occurring is given by:

$$P_{I1} = [N(1-P_1)(1-e^{-X_1\nu})+P_1]e^{-NX_2\nu} \qquad (4\text{-}1)$$

where

P_{I1} = Probability of a logical 1 or hit being generated with interference present

P_1 = Probability of a logical 1 or hit being generated with no interference present

N = Indicator variable which takes into account the radar channel connected to the ARTS-IIIA/RDAS (N = 1 for Normal and N = 3 for MTI channel)

X_1 = Time interval that interfering radar pulse overlaps sample time of the rank quantizer range bin of interest, in seconds

X_2 = Time interval that interfering radar pulse overlaps the sample time of the rank quantizer comparison range bins, in seconds

ν = interfering pulse arrival rate, in pulses per second

The first factor in Equation 4-1 accounts for the probability of the interfering pulse falling in the rank quantizer range bin of interest. The second factor ($e^{-NX_2\nu}$) in the equation gives the probability of no interfering pulses falling in the comparison range bins since this is a necessary requirement for a logical 1 or hit to be generated. A detailed derivation of Equation 4-1 and justification of the assumptions is given in Appendix F.

The variable N in Equation 4-1 is set equal to 3 for the MTI channel because there is a high probability that one interfering pulse at the input of the double MTI canceller circuit (feed forward mode) input will produce three synchronous interfering pulses at its output. This implies that the probability of an interfering pulse falling into a given rank quantizer range bin is actually equal to the probability of it falling in that range bin for any one of three ACPs (present and two previous ACPs).

The values of X_1, and X_2, in Equation 4-1 depends on the interfering radar pulse width (τ_i) and victim radar range bin characteristics. In particular, the victim radar range bin width in time (RB_w), range bin sample

time (RB_g), and range bin hold time (RB_H), have to be considered. The value of X_1 for a given range of interfering radar pulse widths is defined by:

$$X_1 = \begin{cases} \tau_i + RB_g & \text{for } \tau_i < (3RB_w + RB_H) \\ 0 & \text{for } \tau_i > (3RB_w + RB_H) \end{cases} \qquad (4\text{-}2)$$

for the indicated interfering pulse width ranges. The value of X_2 also depends on the rank quantizer threshold setting. The value X_2 for a rank quantizer threshold (RQT) of 23 is given by:

$$X_{23} = \begin{cases} 22(\tau_i - RB_H) & \text{for } RB_g < \tau_i < (RB_w + RB_H) \\ 24RB_w & \text{for } \tau_i > (RB_w + RB_H) \end{cases} \qquad (4\text{-}3)$$

and for a RQT of 24 by:

$$X_{24} = \begin{cases} 24RB_w + 2(\tau_i - RB_H) & \text{for } RB_H < \tau_i < (RB_w + RB_H) \\ 26RB_w & \text{for } \tau_i > (RB_w + RB_H) \end{cases} \qquad (4\text{-}4)$$

Equations 4-2, 4-3, and 4-4 were derived graphically by assuming the interfering pulses to be perfectly square shaped and of constant amplitude.

Effect of Interference on Probability of False Alarm

A false alarm is defined as the declaration of a target when a target is not actually present. For a false target to be declared, a sequence of false hits (logical 1) due to noise or interference must first be generated by the hit processor in the same range bin in adjacent ACPs, and the target declaration hit and miss count threshold in the target detection software equaled or exceeded. Therefore, to analytically determine the probability of a false alarm, the probability of a false hit at the hit processor output for noise and interference must first be addressed and then be applied to the target declaration hit and miss count threshold. The last portion of this subsection discusses the operational interpretation of the probability of false alarm caused by noise and interference on the ARTS-IIIA.

Probability of False Target Hit Caused by Noise

The effects of noise (no interference present) on the probability of a false target hit (logical 1) at the hit processor output can be expressed as:

$$P_{n1} = \frac{J - RQT + 1}{J + 1} \qquad (4\text{-}5)$$

where

J = The number of rank quantizer comparison range bins (24)

RQT = Possible rank quantizer threshold settings (23 or 24)

For RQT=24, Equation 4-5 indicates a 0.04 probability that the noise level in the range bin of interest will exceed the noise level in all 24 comparison range bins. Similarly, for RQT=23, the equation gives a 0.08 probability that the noise level in the range bin of interest will exceed at least 23 of the 24 bins. Sufficient conditions for Equation 4-5 to hold are that the probability distributions for all of the bin samples be identical and independent. Under these statistical conditions, the rank order detection technique maintains a constant probability of false target hit for varying levels of noise and clutter. Equation 4-5 indicates this fact by being only a function of hardware parameters.

Probability of False Target Hits Caused by Interference

In order to determine the effect of interference on the probability of false target hit, the probability of a false target hit due to noise only must also be considered since the noise is always present in the RDAS. Therefore, the probability of a false target hit (logical 1) at the hit processor output due to interference (P_{i1}) is obtained by substituting Equation 4-5 (probability of target hit due to noise, P_{n1}) in Equation 4-1, which after algebraic simplification gives:

$$P_{i1} = \left\{ \frac{RQT}{J+1} \left[N(1-e^{-X_1 v}) - 1 \right] + 1 \right\} e^{-NX_2 v} \qquad (4\text{-}6)$$

For a rank quantizer threshold (RQT) of 23 Equation 4-6 becomes:

$$P_{i1}(23) = \left\{ 0.92 \left[N(1-e^{-X_1 v}) - 1 \right] + 1 \right\} e^{-NX_{23} v} \qquad (4\text{-}7)$$

and for RQT 24

$$P_{i1}(24) = \left\{ 0.96 \left[N(1-e^{-X_1 v}) - 1 \right] + 1 \right\} e^{-NX_{24} v} \qquad (4\text{-}8)$$

The X_1, X_{23}, and X_{24} are defined by Equations 4-2, 4-3, and 4-4, respectively, and evaluated for various interfering and victim radar combinations in TABLE 4-1. The probability of a false target hit as a function of the interfering signal pulse arrival rate (v) was computed for each interfering and victim radar combination, using Equations 4-7 and 4-8, and the X_1, X_{23}, X_{24} values indicated in TABLE 4-1. The results of these calculations are indicated in Figures 4-8 through 4-15. The graphs in

TABLE 4-1

TIME INTERVALS THAT INTERFERING RADAR PULSES OVERLAP
THE RANK QUANTIZER RANGE BIN SAMPLE TIMES FOR
VARIOUS COMBINATIONS OF INTERFERING AND VICTIM RADARS

INTERFERING RADAR TYPE	INTERFERING PULSE WIDTH (τ_I) IN μs	VICTIM RADAR	X_1 IN μs (RQT = 23, 24)	X_{23} IN μs (RQT = 23)	X_{24} IN μs (RQT = 24)
ASR-7	0.833	ASR-7	0.989	8.030	15.730
ASR-8	0.600	ASR-7	0.756	7.904	15.264
AN/CPN-4	0.500	ASR-7	0.656	0.704	15.064
AN/FPS-90	2.000	ASR-7	2.156	15.000	16.250
WSR-57	4.000	ASR-7	0.000	15.000	16.250
ASR-7	0.833	ASR-8	0.999	11.726	12.142
ASR-8	0.600	ASR-8	0.766	6.600	11.808
AN/CPN-4	0.500	ASR-8	0.666	4.400	11.608
AN/FPS-90	2.000	ASR-8	0.000	11.208	12.142
WSR-57	4.000	ASR-8	0.000	11.208	12.142

NOTE: 1. VICTIM RADAR RANGE BIN CHARACTERISTICS
ASR-7 : RB_W = 0.625 μs, RB_S = 0.156 μs, RB_H = 0.468 μs
ASR-8 : RB_W = 0.467 μs, RB_S = 0.166 μs, RB_H = 0.300 μs

2. RQT = RANK QUANTIZER THRESHOLD

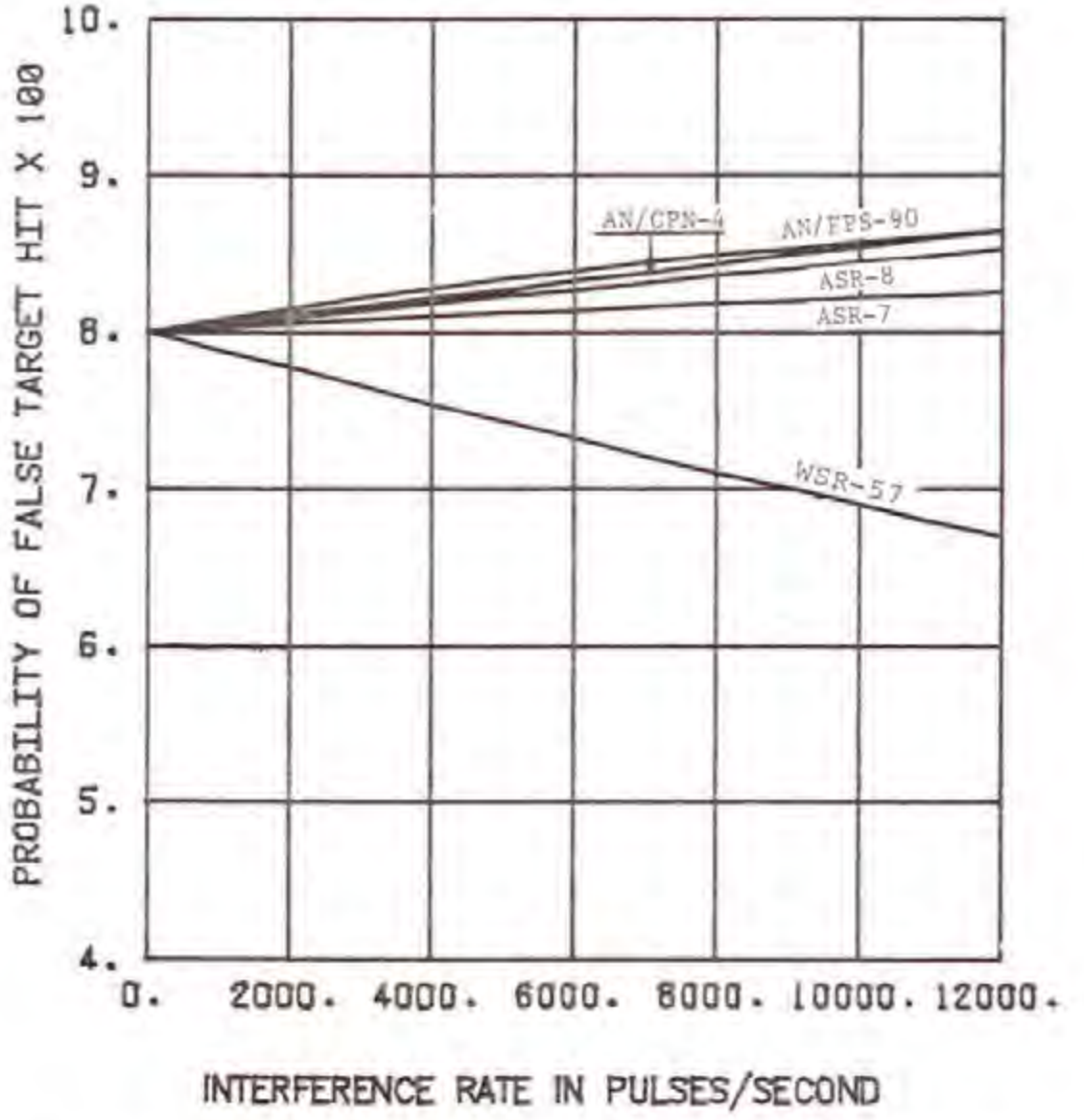

Figure 4-8. ARTS-IIIA/RDAS Probability of False Target Hit Versus Rate of Received Interference (ASR-7 Victim Radar, Normal Channel, Rank Quantizer Threshold 23)

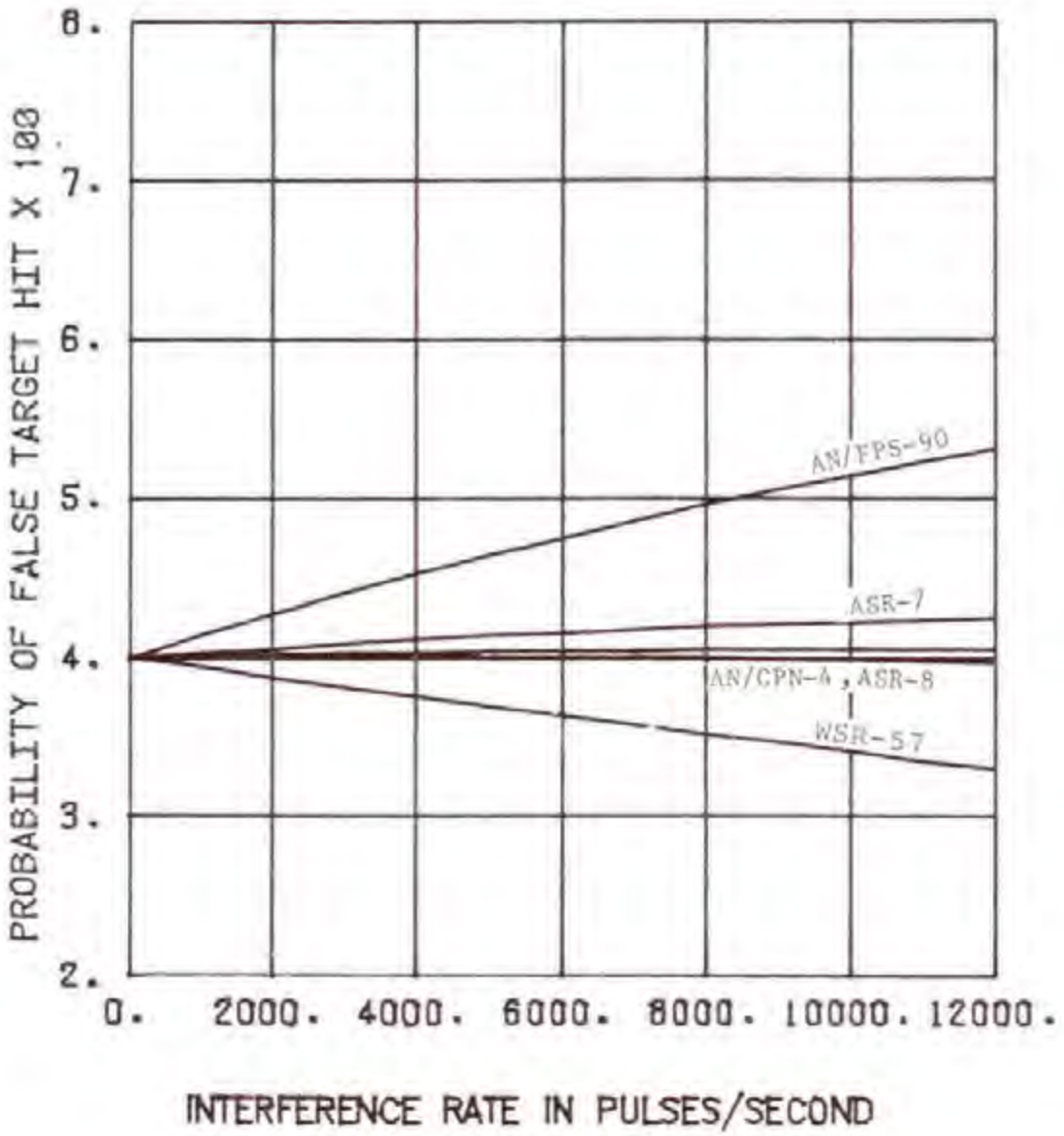

Figure 4-9. ARTS-IIIA/RDAS Probability of False Target Hit Versus Rate of Received Interference (ASR-7 Victim Radar, Normal Channel, Rank Quantizer Threshold 24)

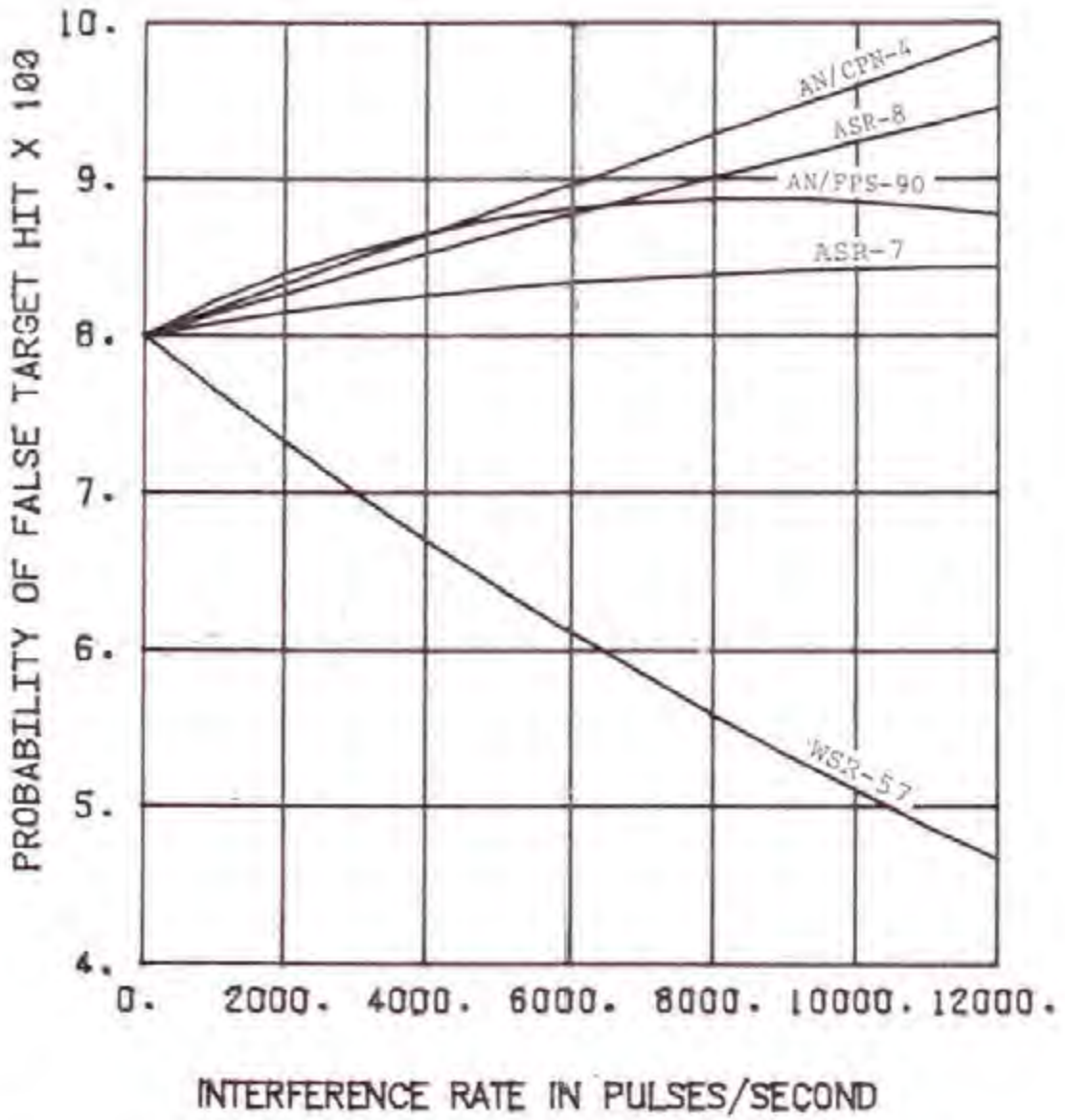

Figure 4-10. ARTS-IIIA/RDAS Probability of False Target Hit Versus Rate of Received Interference (ASR-7 Victim Radar, MTI Channel, Rank Quantizer Threshold 23)

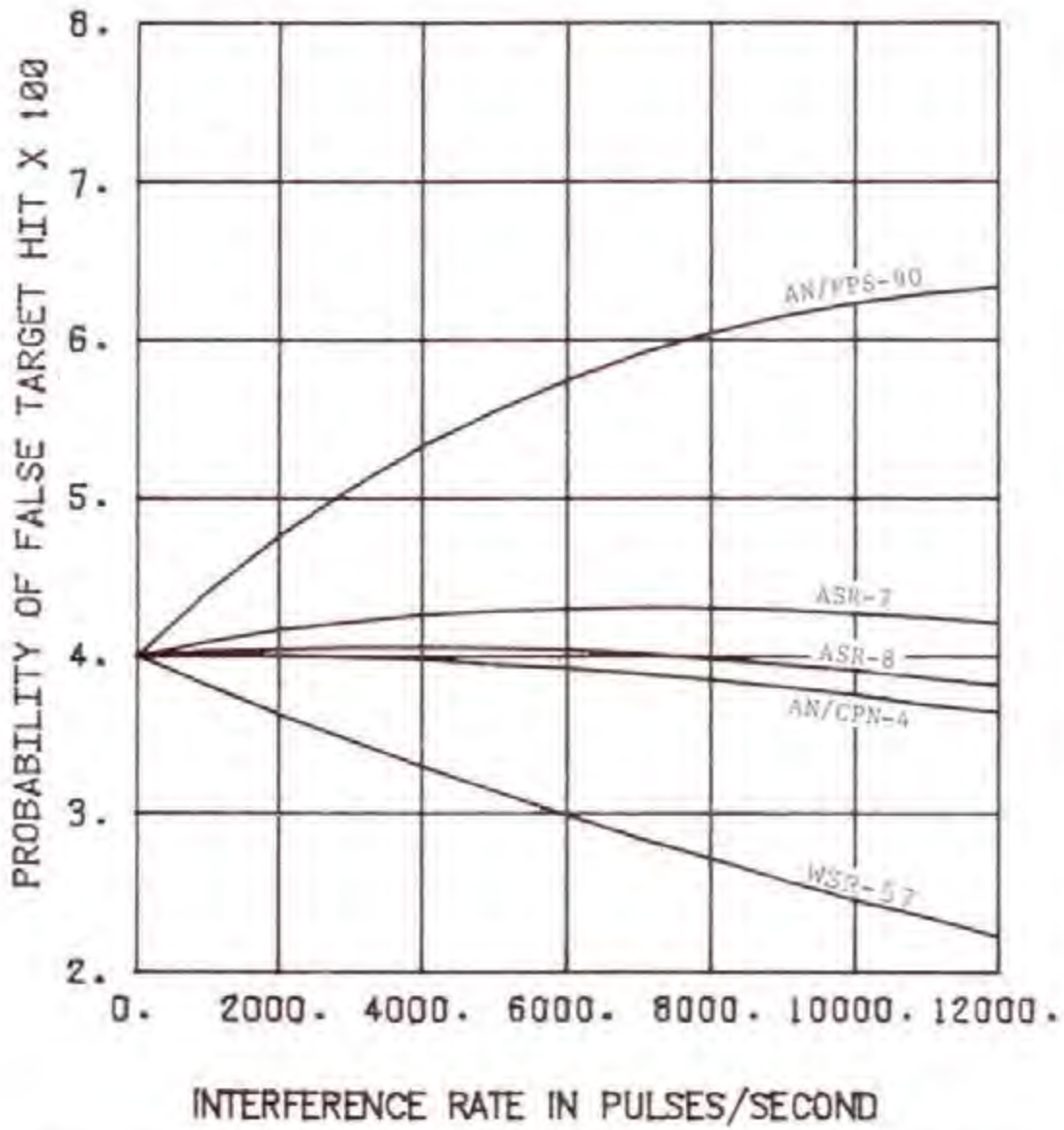

Figure 4-11. ARTS-IIIA/RDAS Probability of False Target Hit Versus Rate of Received Interference (ASR-7 Victim Radar, MTI Channel, Rank Quantizer Threshold 24)

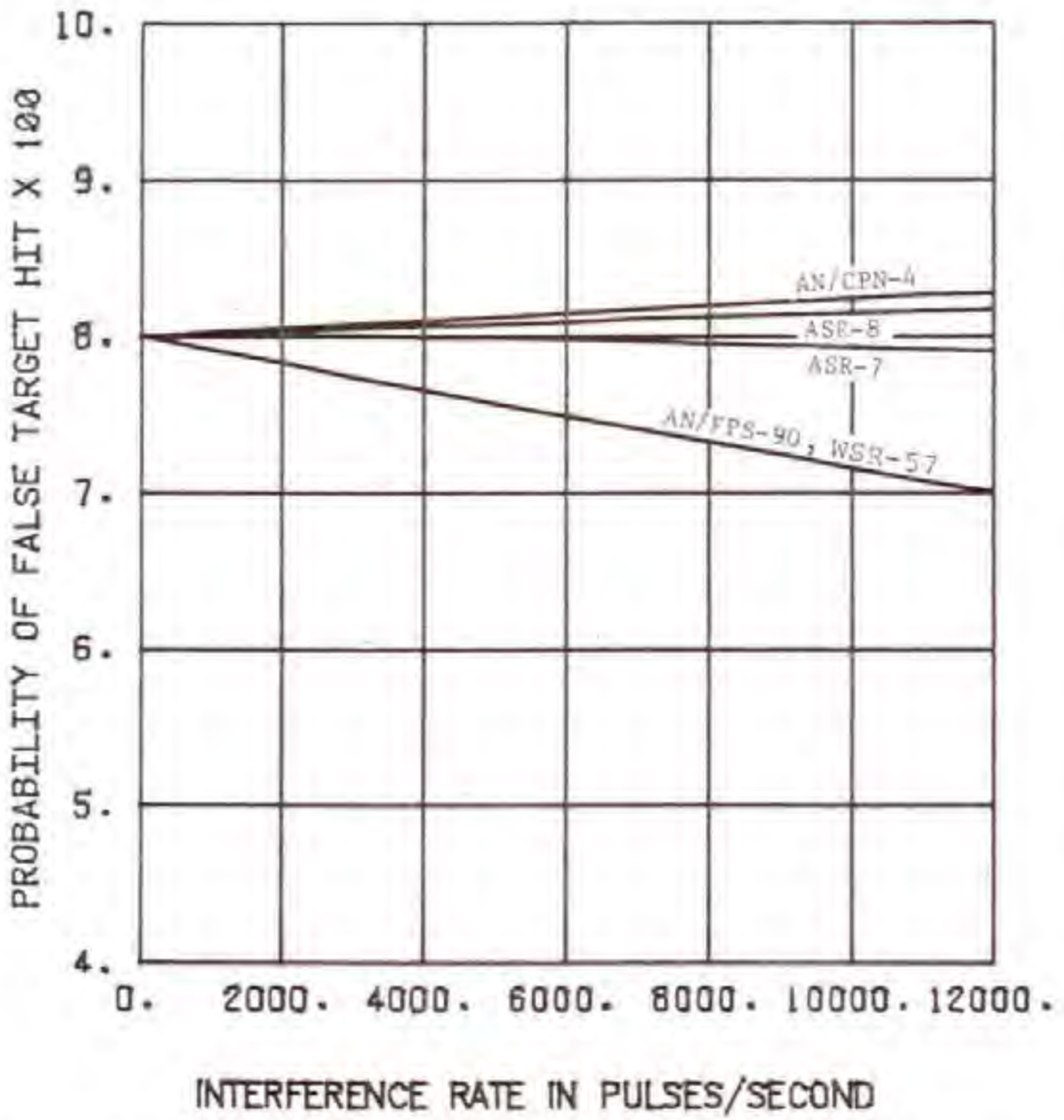

Figure 4-12. ARTS-IIIA/RDAS Probability of False Target Hit Versus Rate of Received Interference (ASR-8 Victim Radar, Normal Channel, Rank Quantizer Threshold 23)

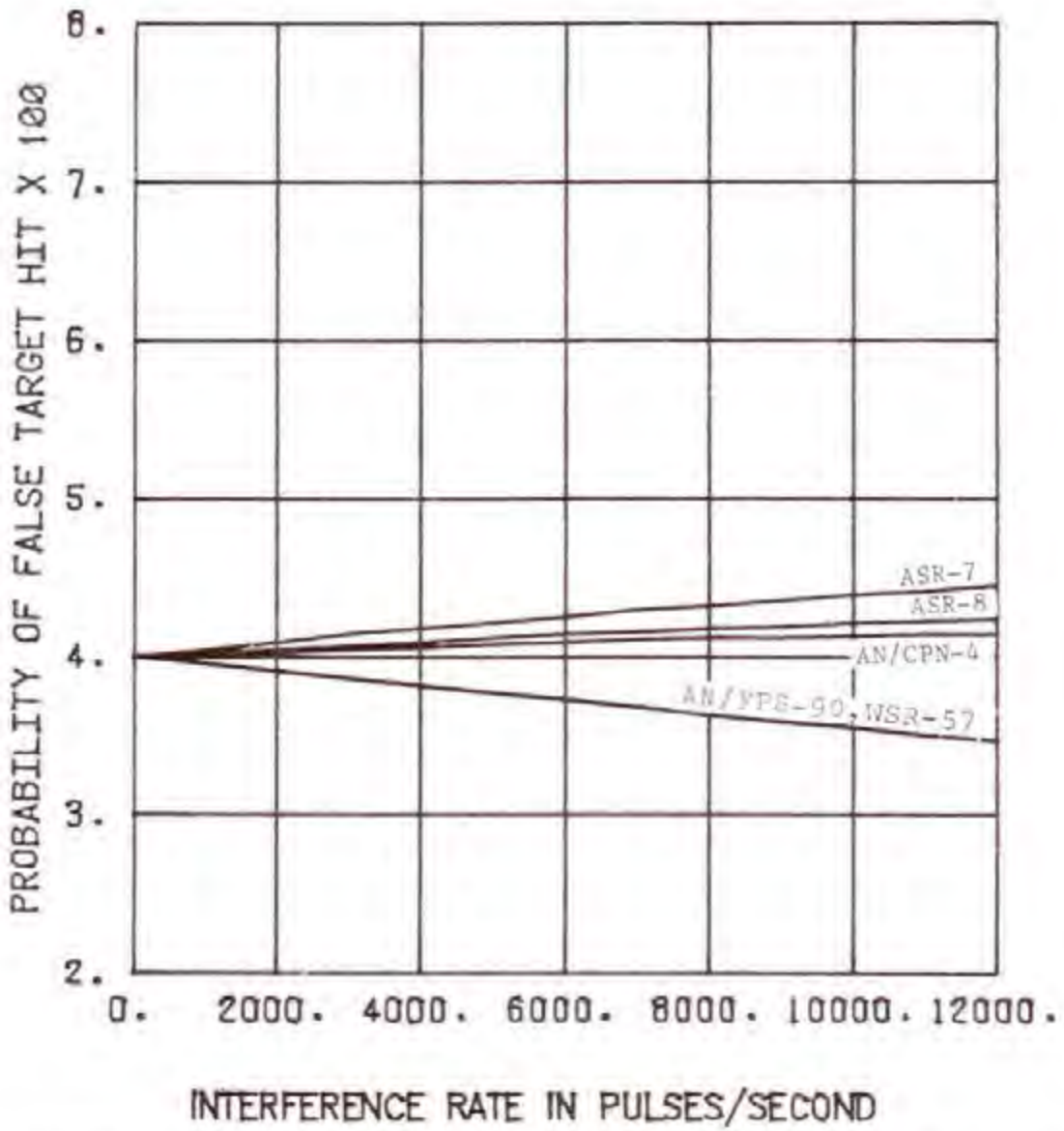

Figure 4-13. ARTS-IIIA/RDAS Probability of False Target Hit Versus Rate of Received Interference (ASR-8 Victim Radar, Normal Channel, Rank Quantizer Threshold 24)

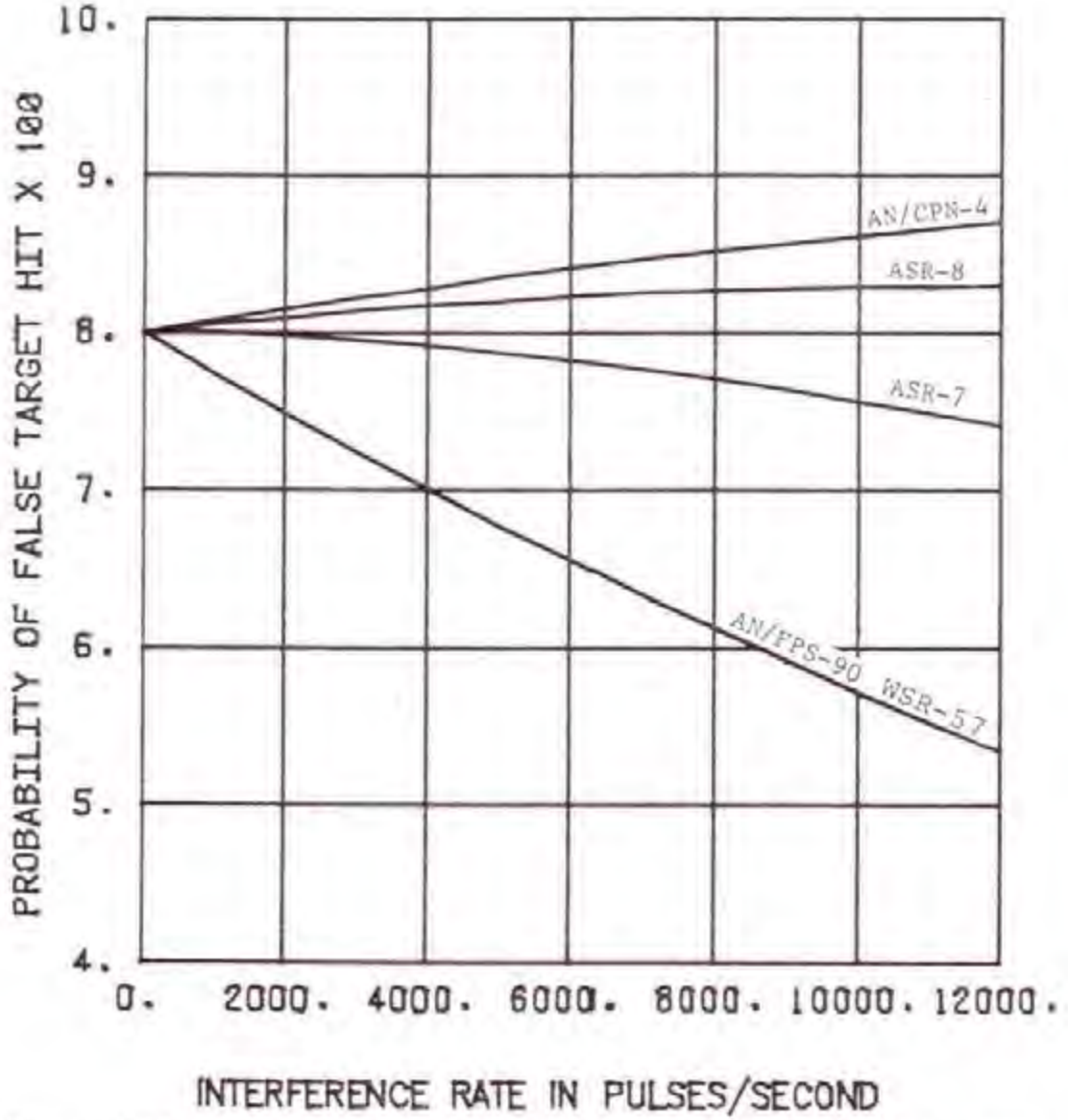

Figure 4-14. ARTS-IIIA/RDAS Probability of False Target Hit Versus Rate of Received Interference (ASR-8 Victim Radar, MTI Channel, Rank Quantizer Threshold 23)

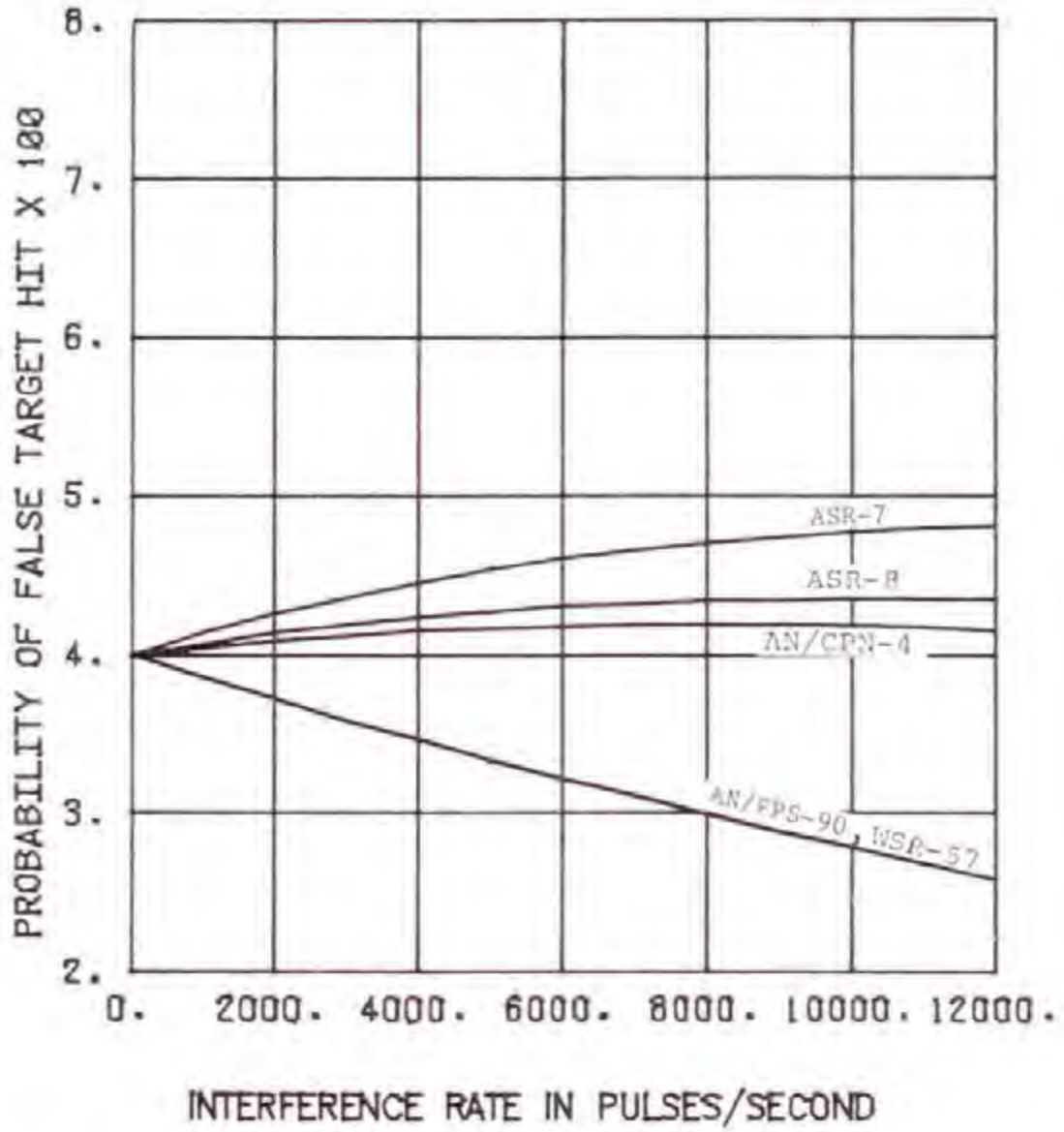

Figure 4-15. ARTS-IIIA/RDAS Probability of False Target Hit Versus Rate of Received Interference (ASR-8 Victim Radar, MTI Channel, Rank Quantizer Threshold 24)

Figures 4-8 through 4-11 are for the ARTS-IIIA/RDAS interfaced to the ASR-7, and Figures 4-12 through 4-15 the ARTS-IIIA interfaced to the ASR-8. In addition, the graphs consider the ARTS-IIIA/RDAS connected to both the normal and MTI channel. The family of curves on each graph represent various interfering radar types. However, the curves are applicable to other interfering radar types in the 2.7-2.9 GHz band that have the same pulse widths. The interfering radar pulse widths corresponding to the various radar types is given in Appendix G. The 4.0 us pulse width mode of the WSR-57 was used for calculation of the curves. The even numbered figures are for RQT=23 and the odd number for a RQT=24. The interference rate of zero value on each curve represents the probability of a false target hit due to only noise. It is evident from the graphs that the probability of false target hit is more affected for a rank quantizer threshold setting of 24 than 23. In addition, interference has a greater impact on the RDAS when connected to the MTI than the normal channel. This is due to the generation of several synchronous interfering pulses by the MTI cancellers in the primary radar (see Section 3 and Appendix C).

The data represented by the curves in Figures 4-8 through 4-15 were reduced to the form shown in TABLES 4-2 through 4-5 to indicate the effect of a particular number and type of interfering radars on the probability of false target hit. TABLES 4-2 and 4-3 represent data for the ARTS-IIIA/RDAS interfaced to an ARS-7 radar that is receiving interference from one and three radars, respectively. Similarly, TABLES 4-4 and 4-5 give the probability of false target hit when the ARTS-IIIA/RDAS is connected to an ASR-8 victim radar. The interfering pulse arrival rate (v) in TABLES 4-2 and 4-4 are simply equal to the interfering radar average pulse repetition frequency (PRF), and in TABLES 4-3 and 4-5, 3 times the interfering radar PRF.

Probability of False Alarm Caused by Interference

The decision in regard to the presence of a target is accomplished by the target detection software functions shown in Figure 4-5. The details of this target detection processing is given in the RDAS description section of this report. Basically, a count of hits (logical 1's) and consecutive misses (logical 0's) are maintained in azimuth for a given range bin. If the consecutive miss count equals or exceeds a miss count threshold and the hit count equals or exceeds a hit count threshold, a target is declared.

A computer program was written to calculate the probability of false alarm as a function of false target hit probability . The program employs a combination of simulation and analytical methods. The details of this program are given in Appendix F, and the results of the calculations are shown in Figure 4-16. The probability of false alarm versus probability of false target hit for various combinations of detection parameters is shown. It is evident from the curves in Figure 4-16 that holding the miss count threshold constant and decreasing the hit count threshold increases the probability of false alarm. This result is reasonable when one considers that a sequence of hits and misses is a set of Bernoulli trials. Since the

TABLE 4-2

ARTS-IIIA/RDAS PROBABILITY OF FALSE TARGET HIT WHEN CONNECTED TO ASR-7 RADAR THAT IS RECEIVING INTERFERENCE FROM ONE RADAR

VICTIM RADAR CHANNEL	INTERFERING RADAR	INTERFERING RATE ν PULSES/SEC	PROBABILITY OF FALSE TARGET HIT (RQT=23)	PROBABILITY OF FALSE TARGET HIT (RQT=24)
NORMAL	ASR-7	1002	0.08026	0.04031
NORMAL	ASR-8	1040	0.08048	0.04011
NORMAL	AN/CPN-4	1192	0.08065	0.04002
NORMAL	AN/FPS-90	356	0.08027	0.04049
NORMAL	WSR-57	166	0.07980	0.03989
MTI	ASR-7	1002	0.08076	0.04087
MTI	ASR-8	1040	0.08143	0.04030
MTI	AN/CPN-4	1192	0.08195	0.04003
MTI	AN/FPS-90	356	0.08077	0.04143
MTI	WSR-57	166	0.07942	0.03932

NOTE: RQT = RANK QUANTIZER THRESHOLD
PROBABILITY OF FALSE TARGET HIT FOR RQT 23 AND NO INTERFERENCE = 0.08
PROBABILITY OF FALSE TARGET HIT FOR RQT 24 AND NO INTERFERENCE = 0.04

TABLE 4-3

ARTS-IIIA/RDAS PROBABILITY OF FALSE TARGET HIT WHEN CONNECTED TO ASR-7 RADAR THAT IS RECEIVING INTERFERENCE FROM THREE RADARS OF THE SAME TYPE

VICTIM RADAR CHANNEL	INTERFERING RADAR	INTERFERING RATE ν PULSES/SEC	PROBABILITY OF FALSE TARGET HIT (RQT=23)	PROBABILITY OF FALSE TARGET HIT (RQT=24)
NORMAL	ASR-7	3006	0.08076	0.04087
NORMAL	ASR-8	3120	0.08143	0.04030
NORMAL	AN/CPN-4	3576	0.08194	0.04003
NORMAL	AN/FPS-90	1068	0.08081	0.04148
NORMAL	WSR-57	498	0.07941	0.03968
MTI	ASR-7	3006	0.08203	0.04213
MTI	ASR-8	3120	0.08418	0.04055
MTI	AN/CPN-4	3576	0.08582	0.03976
MTI	AN/FPS-90	1068	0.08229	0.04424
MTI	WSR-57	498	0.07824	0.03905

NOTE: RQT = RANK QUANTIZER THRESHOLD
PROBABILITY OF FALSE TARGET HIT FOR RQT 23 AND NO INTERFERENCE = 0.08
PROBABILITY OF FALSE TARGET HIT FOR RQT 24 AND NO INTERFERENCE = 0.04

TABLE 4-4

ARTS-IIIA/RDAS PROBABILITY OF FALSE TARGET HIT WHEN CONNECTED TO ASR-8 RADAR THAT IS RECEIVING INTERFERENCE FROM ONE RADAR

VICTIM RADAR CHANNEL	INTERFERING RADAR	INTERFERING RATE ν PULSES/SEC	PROBABILITY OF FALSE TARGET HIT (RQT=23)	PROBABILITY OF FALSE TARGET HIT (RQT=24)
NORMAL	ASR-7	1002	0.07998	0.04046
NORMAL	ASR-8	1040	0.08018	0.04027
NORMAL	AN/CPN-4	1192	0.08031	0.04144
NORMAL	AN/FPS-90	356	0.07968	0.03983
NORMAL	WSR-57	166	0.07985	0.03989
MTI	ASR-7	1002	0.07990	0.04134
MTI	ASR-8	1040	0.08052	0.04076
MTI	AN/CPN-4	1192	0.08090	0.04056
MTI	AN/FPS-90	356	0.07906	0.03949
MTI	WSR-57	166	0.07956	0.03976

NOTE: RQT = RANK QUANTIZER THRESHOLD
PROBABILITY OF FALSE TARGET HIT FOR RQT 23 AND NO INTERFERENCE = 0.08
PROBABILITY OF FALSE TARGET HIT FOR RQT 24 AND NO INTERFERENCE = 0.04

TABLE 4-5

ARTS-IIIA/RDAS PROBABILITY OF FALSE TARGET HIT
WHEN CONNECTED TO ASR-8 RADAR THAT IS RECEIVING
INTERFERENCE FROM THREE RADARS OF THE SAME TYPE

VICTIM RADAR CHANNEL	INTERFERING RADAR	INTERFERING RATE ν PULSES/SEC	PROBABILITY OF FALSE TARGET HIT (RQT=23)	PROBABILITY OF FALSE TARGET HIT (RQT=24)
NORMAL	ASR-7	3006	0.07989	0.04134
NORMAL	ASR-8	3120	0.08052	0.04076
NORMAL	AN/CPN-4	3576	0.08090	0.04056
NORMAL	AN/FPS-90	1068	0.07904	0.03948
NORMAL	WSR-57	498	0.07956	0.03976
MTI	ASR-7	3006	0.07942	0.04359
MTI	ASR-8	3120	0.08140	0.04200
MTI	AN/CPN-4	3576	0.08244	0.04136
MTI	AN/FPS-90	1068	0.07718	0.03848
MTI	WSR-57	498	0.07868	0.03929

NOTE: RQT = RANK QUANTIZER THRESHOLD
PROBABILITY OF FALSE TARGET HIT FOR RQT 23 AND NO INTERFERENCE = 0.08
PROBABILITY OF FALSE TARGET HIT FOR RQT 24 AND NO INTERFERENCE = 0.04

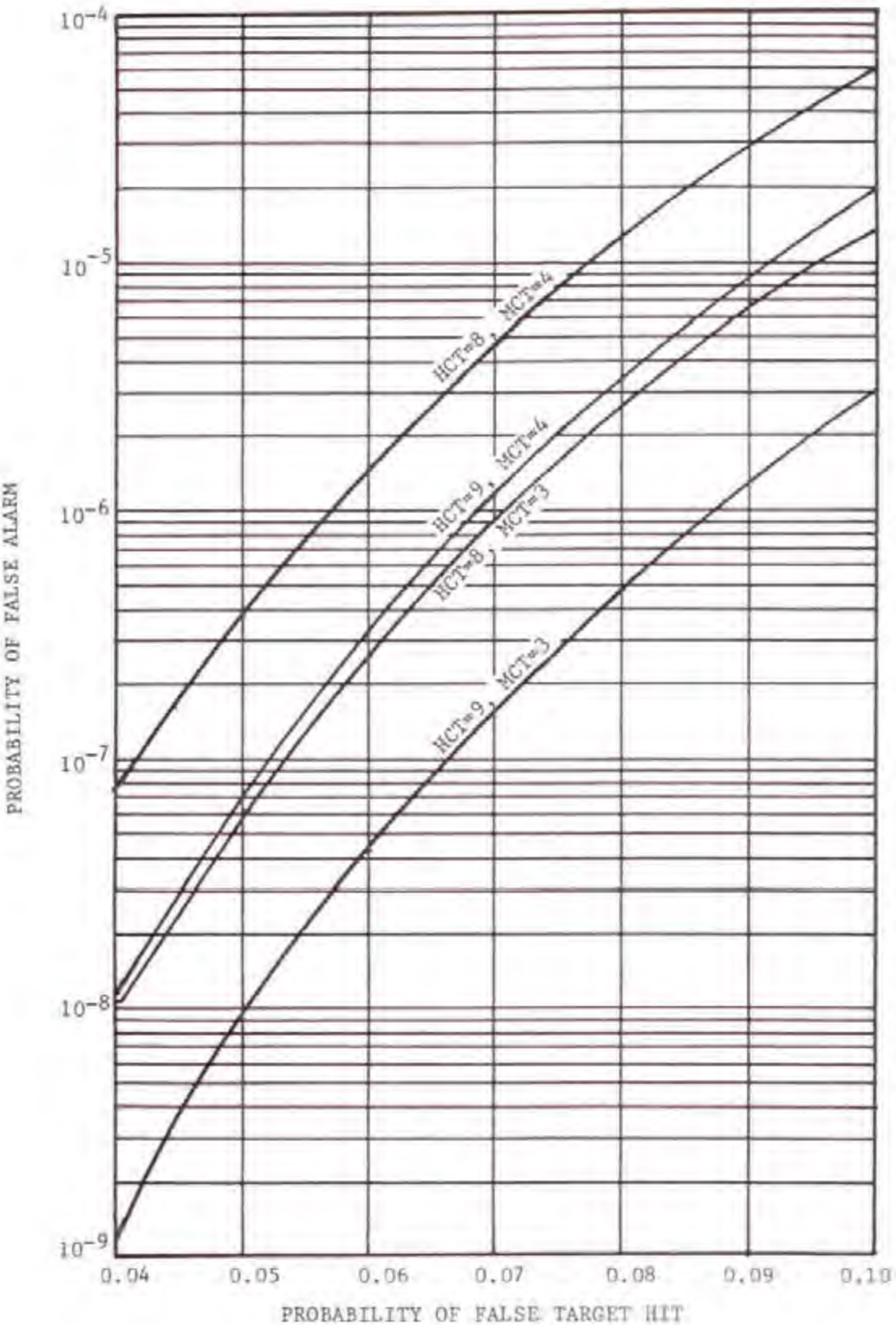

Figure 4-16. ARTS-IIIA/RDAS Probability of False Alarm Versus Probability of False Target Hit for Various Hit/Miss Count Threshold Parameter Combinations

probability of a given sequence is the product of the individual event probabilities, there is a higher probability that the number of noise hits in the sequence will satisfy a lower hit count threshold than a high one.

It is also evident from the curves in Figure 4-16 that raising the consecutive miss count threshold, while maintaining a constant hit count threshold increases the probability of false alarm. Since there is a higher probability of a miss occurring than a hit, due to noise, it is more likely that 4 consecutive misses will occur than 3 consecutive misses and one hit.

The probability of false target hits due to interference shown in TABLES 4-2 through 4-5 were related to the probability of false alarm for a particular hit and miss count threshold by the curves in Figure 4-16. The resulting probability of false alarm values are shown in TABLE 4-6. The probability of false alarms are for the most likely ARTS-IIIA/RDAS parameter settings that will be used in the field:

1. Rank Quantizer Threshold (RQT) = 23

2. Hit Count Threshold (HCT) = 9

3. Miss Count Threshold (MCT) = 3

FAA personnel at NAFEC who have thoroughly tested the ARTS-IIIA are recommending these detection parameter settings be used for optimum performance. In addition, this parameter combination was found in this study (see section on Trade-Off between Interference Suppression and ARTS-IIIA/RDAS Performance) to be near optimum for interference suppression.

The probability of false alarm without interference (4.596×10^{-7}) is shown at the bottom of TABLE 4-6. This number corresponds to a probability of false target hit (0.08) for no interference and a rank quantizer threshold of 23. It is evident from TABLE 4-6 that interfacing the ARTS-IIIA/RDAS to the ASR-7 radar usually results in a higher probability of false alarm than when interfaced to an ASR-8. A higher probability of false alarm also results when the ARTS-IIIA is connected to the MTI channel than the normal channel. The highest probability of false alarm for interfering and victim radar combinations occurred for the AN/CPN-4 and ASR-7. This is because the AN/CPN-4 radar has a higher PRF than any other interfering radar considered. In addition, the probability of an AN/CPN-4 radar pulse falling into a rank quantizer comparison range bin and preventing a hit (logical 1) from being generated by the hit processor is low. This is because the difference between the AN/CPN-4 pulse width (τ_i = 0.5μs) and victim radar range bin hold time (RB_H=0.468μs for ASR-7 versus 0.300μs for ASR-8) is small. It can be seen from Equation 4-3 that a small ($\tau i - RB_H$) results in a low value of X_{23} and therefore from Equation 4-6 a high probability of false alarm.

All probability of false alarms for the WSR-57 (τ_i=4.0 μs mode) in TABLE 4-6 are less than for no interference. This is because the WSR-57 wide pulse width cannot overlap the rank quantizer range bin of interest without

TABLE 4-6

ARTS-IIIA/RDAS PROBABILITY OF FALSE ALARM FOR TYPICAL DETECTION PARAMETERS AND VARIOUS COMBINATIONS OF INTERFERING AND VICTIM RADARS

VICTIM RADAR	VICTIM RADAR CHANNEL	NUMBER INTERFERING RADARS OF SAME TYPE	INTERFERING RADAR TYPE				
			ASR-7 τ_1=0.83μs PRF=1002	ASR-8 τ_1=0.60μs PRF=1040	AN/CPN-4 τ_1=0.5μs PRF=1192	AN/CPN-4 τ_1=2.0μs PRF=356	WSR-57 τ_1=4.0μs PRF=166
ASR-7	NORMAL	1	4.914×10^{-7}	5.182×10^{-7}	5.390×10^{-7}	4.926×10^{-7}	4.534×10^{-7}
ASR-7	NORMAL	3	5.524×10^{-7}	6.347×10^{-7}	6.965×10^{-7}	5.585×10^{-7}	4.413×10^{-7}
ASR-7	MTI	1	5.524×10^{-7}	5.182×10^{-7}	6.977×10^{-7}	5.536×10^{-7}	4.417×10^{-7}
ASR-7	MTI	3	7.075×10^{-7}	9.699×10^{-7}	11.702×10^{-7}	7.382×10^{-7}	4.051×10^{-7}
ASR-8	NORMAL	1	4.589×10^{-7}	4.816×10^{-7}	4.975×10^{-7}	4.497×10^{-7}	4.550×10^{-7}
ASR-8	NORMAL	3	4.362×10^{-7}	5.231×10^{-7}	5.695×10^{-7}	4.299×10^{-7}	4.460×10^{-7}
ASR-8	MTI	1	4.565×10^{-7}	5.231×10^{-7}	5.695×10^{-7}	4.305×10^{-7}	4.460×10^{-7}
ASR-8	MTI	3	4.417×10^{-7}	6.305×10^{-7}	7.575×10^{-7}	3.723×10^{-7}	4.187×10^{-7}

NOTE: 1. ARTS-IIIA/RDAS TYPICAL TARGET DETECTION PARAMETERS
RANK QUANTIZER THRESHOLD = 23
HIT COUNT THRESHOLD = 9
MISS COUNT THRESHOLD = 3
2. PROBABILITY OF FALSE ALARM WITHOUT INTERFERENCE = 4.596×10^{-7}

overlapping many comparison range bins. Consequently, there is a very low probability of the range bin of interest having a higher interference signal level than the comparison range bins, which precludes generation of a hit.

Interpretation of Interference Effects on False Alarms

The probability of false alarms shown in TABLE 4-6 can be related to the approximate number of false alarms (false target detection indication on the PPI) per antenna rotation by:

$$FA = PFA \times M \times \frac{PRF \times T}{K} \qquad (4\text{-}9)$$

where

PFA = Probability of false alarm

M = Number of range bins in victim radars radial coverage (1200 for ASR-7 and 1607 for ASR-8)

PRF = Victim Radar Pulse Repetition Frequency (1002 for ASR-7 and 1040 for ASR-8), in pulses per second

T = Victim Radar Antenna Rotation Time (5 seconds assumed for ASR-7 and ASR-8)

K = The average number of azimuth change pulses (ACPs) since initial hit for a probability of false alarm to occur

The average number of ACPs (K) for a false alarm to occur was determined from the program used to compute the probability of false alarm as a function of the probability of a false target hit. The resulting values of K for possible hit and miss count thresholds are given in TABLE 4-7. The probability of false alarms listed in TABLE 4-6 are for a hit and miss count threshold of 9 and 3, respectively. Therefore K=17 was used in Equation 4-9 to relate TABLE 4-6 false alarm probabilities to false alarms per antenna rotation. Evaluating Equation 4-9 for the false alarm probability without interference (4.596×10^{-7}) and the maximum false alarm probability listed in TABLE 7-6 for interference (11.702×10^{-7}) for an ASR-7 victim radar indicates that the number of false alarms per antenna rotation can increase from 0.1625 to 0.41383. This corresponds to an approximate increase from 2 to 5 false alarms every 12 antenna rotations, or 1 additional false alarm every 4 antenna rotations. It should be pointed out that this result reflects extreme worst-case interference conditions. That is, three radars simultaneously and continually interfering over the entire antenna rotation period, and a worst-case interfering radar and victim radar channel combination.

NTIA noted in its 1975 Los Angeles area radar interference measurements (Hinkle, 1976) that FAA radars did not receive interference from more than

TABLE 4-7

AVERAGE NUMBER OF AZIMUTH CHANGE PULSE SINCE INITIAL HIT FOR A FALSE ALARM TO OCCUR

HIT COUNT THRESHOLD (HCT)	MISS COUNT THRESHOLD (MCT)	AVERAGE NO. OF ACPS FOR PFA TO OCCUR (K)
8	3	15
8	4	18
9	3	17
9	4	21

one radar at a given time. In addition, interference coupling in all measurement cases were caused by antenna mainbeam-to-mainbeam or antenna mainbeam-to-backlobe coupling and resulted in interference occurring only over small sectors of the PPI. The maximum false alarm probability listed in TABLE 4-6 for one interfering radar and the ARTS-IIIA connected to the MTI channel is 6.977×10^{-7}.

From Equation 4-9, this corresponds to an increase in false alarms per antenna rotation from 0.1625 to 0.2463, or one additional false alarm every 12 antenna rotations. If interference is received over less than 50 percent of the antenna rotation, due to a single radar or combination of radars interfering one at a time, only one additional false alarm would occur every 24 antenna rotations. It is therefore concluded that present radar interference conditions in congested terminal areas of the U.S. would not significantly affect the ASR-7 or ASR-8 probability of false alarm when these radars are interfaced to the ARTS-IIIA/RDAS.

The hit count threshold of 9 used in the false alarm analysis corresponds to only the lowest hit count threshold value that the MTI channel can have at any given time. As discussed in a previous section and described in Figure 4-7, the MTI channel hit count threshold is increased from 8 to a maximum of 20 depending on the degree of clutter correlation. The probability of false alarm versus probability of false target hit curves in Figure 4-16 have nearly the same slope regardless of the hit count threshold. Therefore, it is reasonable to assume that an increase in the MTI target hit count threshold would not result in interference having any greater impact than indicated in TABLE 4-6.

Effect of Interference on Probability of Target Detection

The following discusses the impact of interference on the RDAS probability of target detection. The probability of target detection is defined as the probability of declaring a target when the target is actually present. For a target to be declared, a sequence of hits (logical 1) due to target return pulses must be generated by the hit processor in the same range bin for adjacent ACPs, and the target declaration hit and miss count threshold in the target detection software satisfied. Therefore, to analytically determine the probability of target detection, the probability of a target hit at the hit processor output for the target and interference signal are first determined, and then related to probability of target detection through simulation of the target detection criteria. The last portion of this subsection discusses the interpretation of the results.

Probability of Target Hit Caused by a Target

The probability of a logical 1 occurring at the Hit Processor output when a target is present is defined as the probability of a target hit and derived in Appendix F to be:

$$P_{sl}(J,RQT) = \int_{-\infty}^{+\infty} \sum_{K=RQT}^{J} \binom{J}{K} [F(v)]^K [1-F(v)]^{J-K} d[G(v)] \qquad (4\text{-}10)$$

where

v = Voltage level, in volts

J = Number of rank quantizer comparison range bins (24)

RQT = Rank quantizer threshold (23 or 24)

F(v) = Statistical cumulative distribution for noise

G(v) = Statistical cumulative distribution for signal-plus-noise

The probability of target hit (PTH), unlike the probability of false target hit, is dependent not only on the distribution of noise but also the signal-plus-noise distribution. Equation 4-10 gives the probability of the target range bin (range bin of interest with target in it) having a voltage level greater than at least RQT of the surrounding J comparison range bin noise samples. These noise range bins are assumed to each have the same cumulative distribution F(v). The particular distributions for F(v) and G(v) depends on the radar channel (normal or MTI) connected to the ARTS-IIIA/RDAS.

Normal Channel. The noise distribution at the radar normal channel output (before integrator) is Rayleigh distributed (Skolnik, 1962) and given by:

$$F(v) = 1-e^{-v^2/2} \qquad (4\text{-}11)$$

Where v is a sample of the voltage amplitude. The cumulative distribution for signal-plus-noise at the radar normal channel output is given by the Rice distribution (Skolnik, 1962):

$$G(v) = \int_0^v t\, e^{-\frac{t^2+2\cdot SNR}{2}} I_0(t\sqrt{2\cdot SNR})\, dt \qquad (4\text{-}12)$$

t = Dummy variable of integration

SNR = Signal-to-noise voltage ratio

I_0 = Modified Bessel function of the first kind and of zero order

Substituting F(v) and G(v) into Equation 4-10 gives:

$$P_{sl}(J,RQT) = \int_0^{+\infty} \sum_{K=RQT}^{J} \binom{J}{K} \left(1-e^{-\frac{v^2}{2}}\right)^K \left(e^{-\frac{v^2}{2}}\right)^{J-K} v\, e^{-\frac{v^2+2\cdot SNR}{2}} I_0(v\sqrt{2\cdot SNR})\, dv \qquad (4\text{-}13)$$

For a rank quantizer threshold (RQT=23) and range bin sample number (J=24), Equation 4-13 becomes:

$$P_{s1}(24,23) = 24\int_0^{\infty}(1-e^{-\frac{v^2}{2}})^{23}(e^{-\frac{v^2}{2}})v\,e^{-\frac{v^2+2\cdot SNR}{2}}I_o(v\sqrt{2\cdot SNR})\,dv + \int_0^{\infty}(1-e^{-\frac{v^2}{2}})^{24}v\,e^{-\frac{v^2+2\cdot SNR}{2}}I_o(v\sqrt{2\cdot SNR})\,dv \qquad (4\text{-}14)$$

Evaluation of Equation 4-13 for a rank quantizer threshold of 24 gives:

$$P_{s1}(24,24) = \int_0^{\infty}(1-e^{-\frac{v^2}{2}})^{24}v\,e^{-\frac{v^2+2\cdot SNR}{2}}I_o(v\sqrt{2\cdot SNR})\,dv \qquad (4\text{-}15)$$

The two above integral equations were evaluated for various signal-to-noise ratios (SNRs) using a Fortran numerical integration routine. The resulting curves are shown plotted on probability paper in Figure 4-17. The probability of target hit curves for RQT=23 is higher than for RQT=24 because there is a higher probability of the signal-plus-noise level in the target range bin exceeding 23 range bin noise samples than 24. Since the distribution of noise and signal-plus-noise out of the ASR-7 and ASR-8 radar normal channel are identical, the curves in Figure 4-17 apply to an ARTS-IIIA/RDAS connected to either an ASR-7 or ASR-8 radar normal channel.

MTI Channel. The ASR-7 has a single channel MTI canceller, and the ASR-8 has a dual (Inphase and Quadrature) MTI canceller. The probability of a target hit with the ARTS-IIIA/RDAS connected to these circuits was computed by the following form of Equation 4-10.

$$P_{s1}(J,RQT) = \int_{-\infty}^{+\infty}\sum_{K=RQT}^{J}\binom{J}{K}[F(v)]^K[1-F(v)]^{J-K}\frac{d[G(v)]}{dv}dv \qquad (4\text{-}16)$$

where d[G(v)]/dv is the signal-plus-noise amplitude distribution PDF.

The noise only amplitude distribution PDF at the output of the ASR-7 MTI channel is a one-sided Gaussian and described by Equation C-40. Therefore, the noise only cumulative distribution is given by:

$$F(v) = \frac{2}{\sqrt{2\pi}\,\sigma}\int_0^{V} e^{-v^2/2\sigma^2}dv = 2nBr(v) \qquad (4\text{-}17)$$

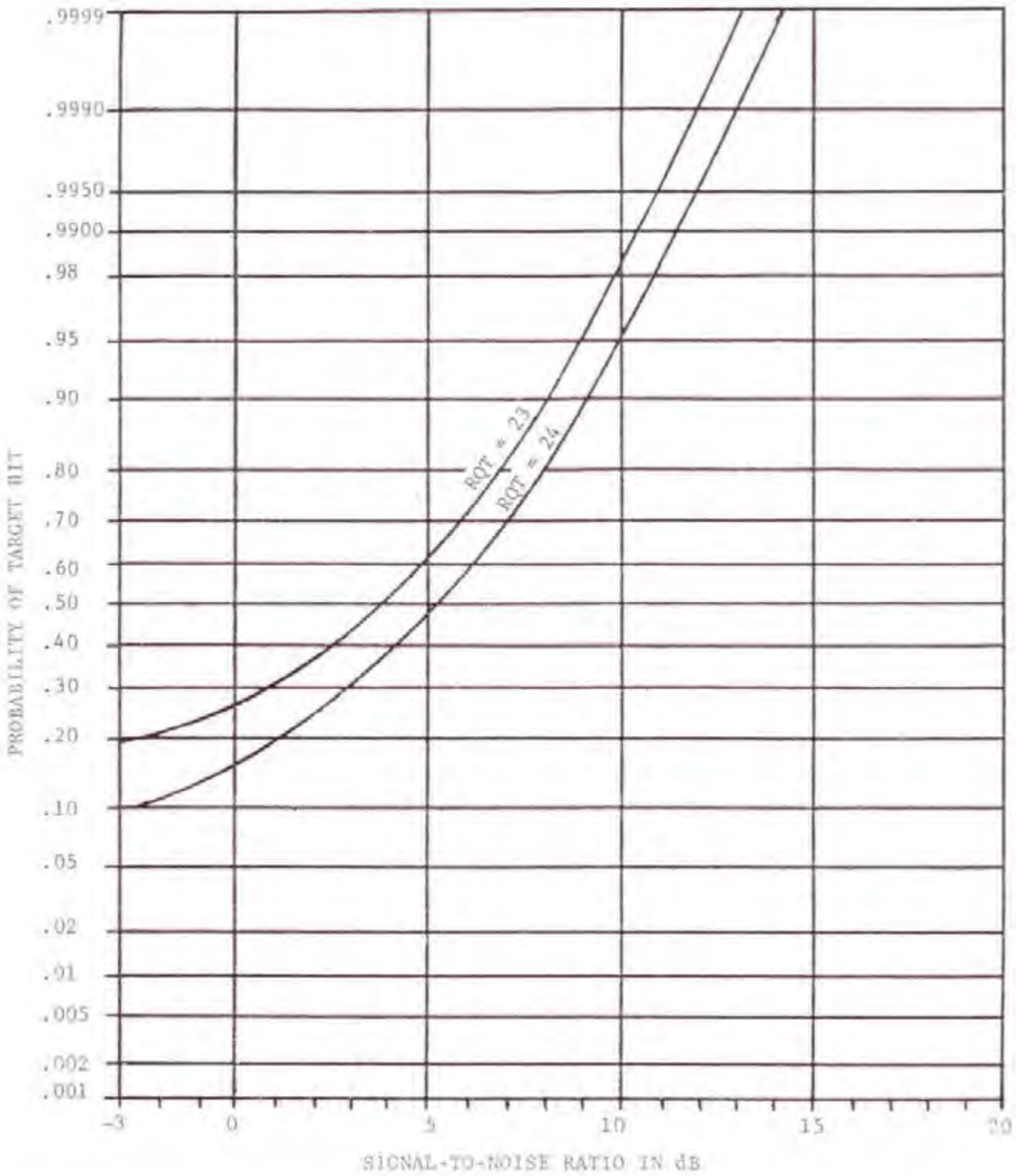

Figure 4-17. Probability of Target Hit Versus Signal-to-Noise Ratio for the ARTS-IIIA/RDAS Connected to the ASR-7 or ASR-8 Radar Normal Channel (Rank Quantizer Threshold 23 and 24)

where ERF(v) is the mathematical error function. The signal-plus-noise amplitude distribution PDF was determined from actual ASR-7 radar MTI channel simulations and is shown in Figure C-21. The probability of a target hit occurring was computed by substituting Equation 4-17 for F(v) in Equation 4-16, and the density distribution data obtained from simulations for d[G(v)]/dv in Equation 4-16. Equation 4-16 was then evaluated for various signal-to-noise ratios (SNR's) using Fortran error function and numerical integration routines. The resulting probability of target hit versus signal-to-noise ratios are shown plotted on probability paper in Figure 4-18.

The noise only amplitude distribution PDF at the ASR-8 MTI Channel output is Rayleigh distributed and given by Equation D-15. Therefore, the noise only cumulative distribution is given by:

$$P(v) = 1 - e^{-v^2/2\sigma^2} \qquad (4-18)$$

As in the case of the ASR-7 MTI channel, the ASR-8 MTI channel was simulated to determine its output signal-plus-noise amplitude distribution PDF. The resulting density function, shown in Figure C-23, was substituted for d[G(v)]/dv in Equation 4-16. Similarly, Equation 4-18 was substituted for F(v) in Equation 4-16. Equation 4-16 was then evaluated for various signal-to-noise ratios (SNR's) by a numerical integration routine. The resulting probability of target hit versus signal-to-noise ratios are shown plotted in Figure 4-19. The RMS noise voltage level (σ) was set at 0.25 volts for the calculation, since this corresponds to the one volt peak noise level usually set at the radar receiver output.

Interference Effect on Target Hit

A 0.7 probability of target hit was chosen for a zero interference reference base in the analysis. It will be shown later in this section that this probability of target hit results in a worst-case interference effect on probability of target detection. It is evident from Figures 4-17, 4-18, and 4-19 that a 0.7 probability of target hit and RQT=23 corresponds to a signal-to-noise ratio of approximately 6 dB for the ARTS-III/RDAS connected to the normal channel, 12 dB for the ASR-7 MTI channel, and 7 dB for the ASR-8 MTI channel. The effect of interference on the probability of false target hit can be determined from Equation 4-1. As discussed earlier, for worst-case interfering signal level assumptions Equation 4-1 defines the effect of interference on a hit (logical 1) caused by either noise or signal-plus-noise. Substituting 0.7 for P_1 in Equation 4-1 and evaluating it for various interfering pulse arrival rates (υ), gives the curves shown in Figures 4-20 through 4-27. The graphs in Figures 4-20 through 4-23 are for

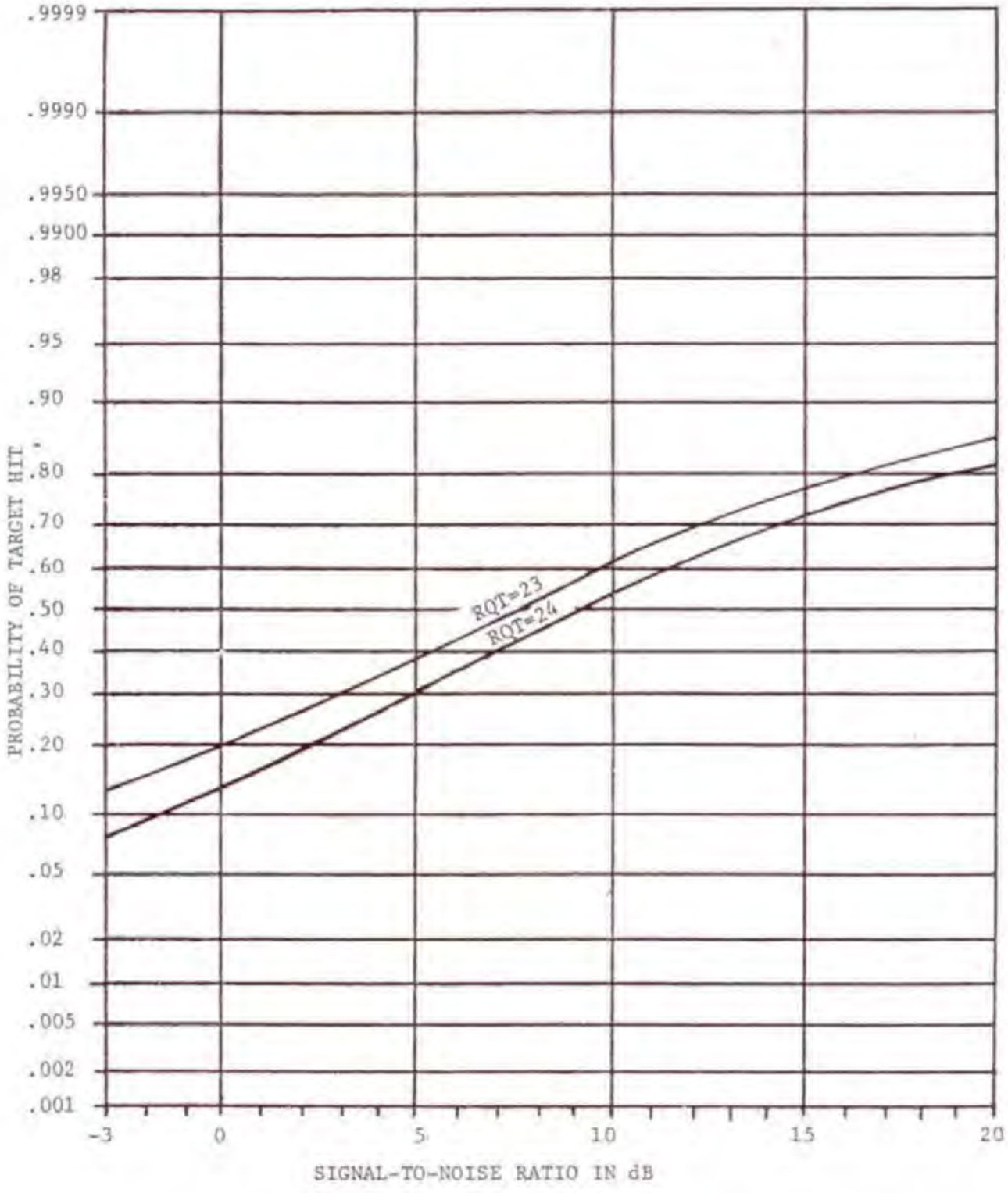

Figure 4-18. Probability of Target Hit Versus Signal-to-Noise Ratio for the ARTS-IIIA/RDAS Connected to the ASR-7 Radar MTI Channel (Rank Quantizer Threshold 23 and 24)

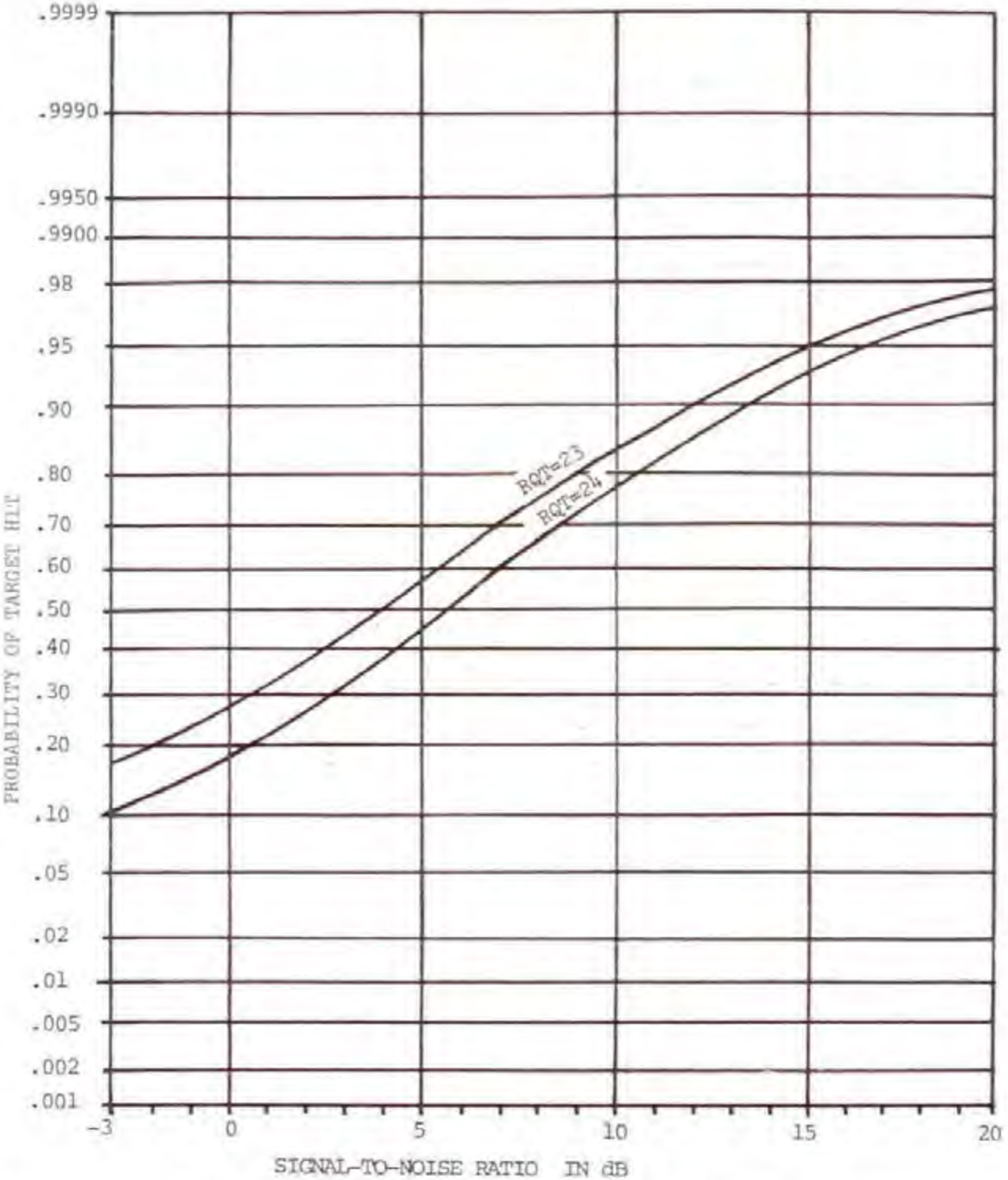

Figure 4-19. Probability of Target Hit Versus Signal-to-Noise Ratio for the ARTS-IIIA/RDAS Connected to the ASR-8 Radar MTI Channel (Rank Quantizer Threshold 23 and 24)

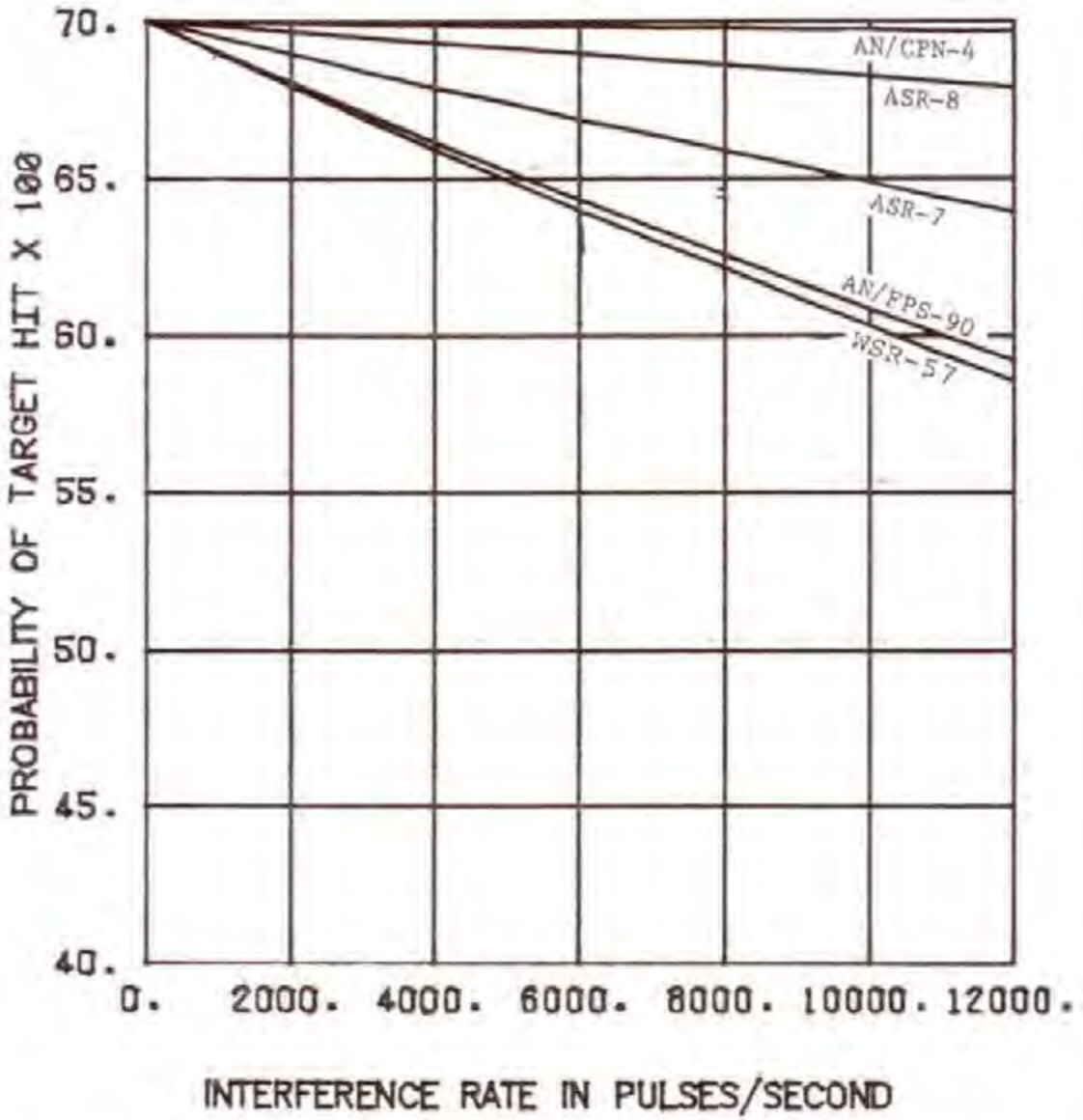

Figure 4-20. ARTS-IIIA/RDAS Probability of Target Hit Versus Rate of Received Interference (ASR-7 Victim Radar, Normal Channel, Rank Quantizer Threshold 23)

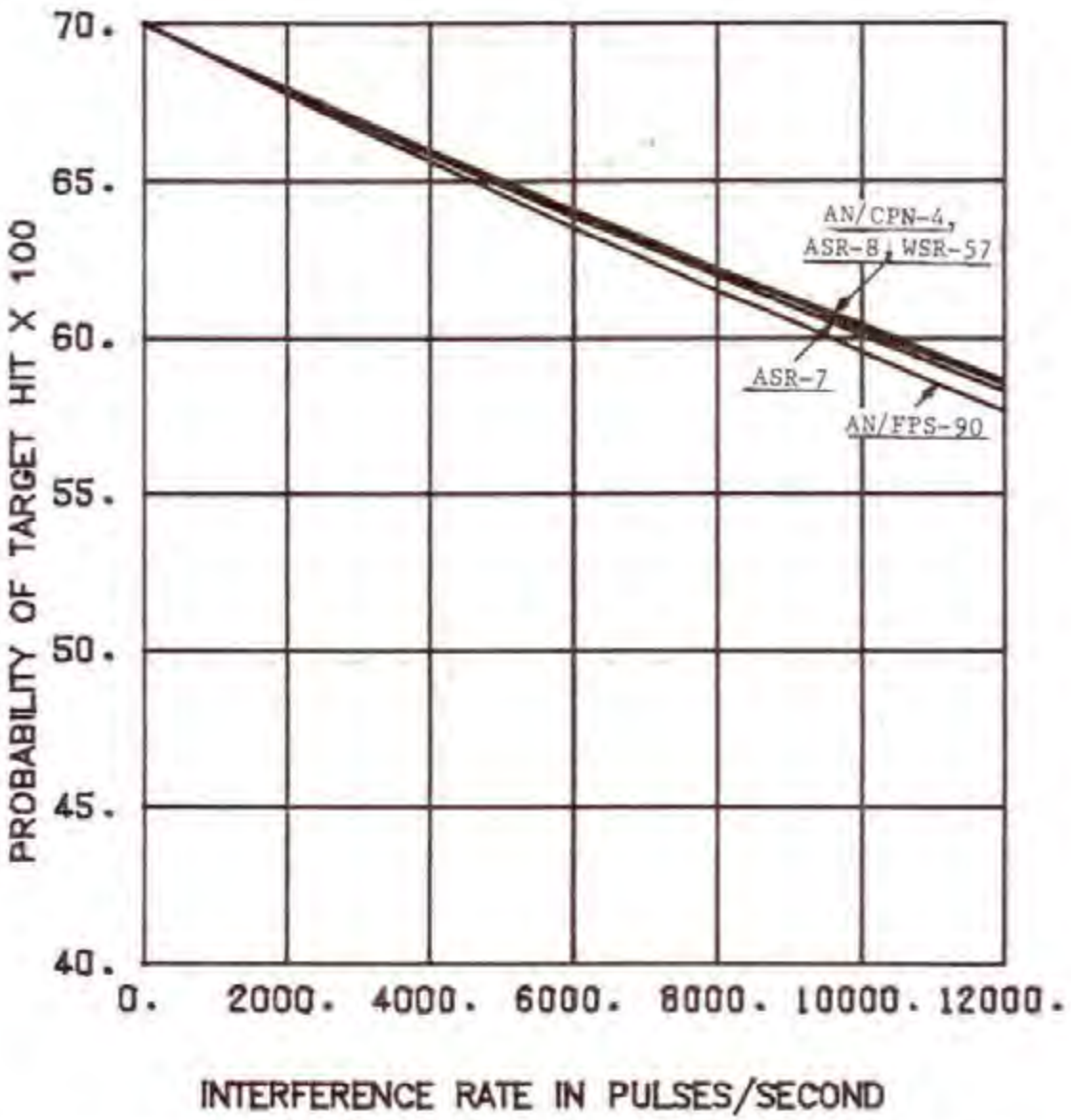

Figure 4-21. ARTS-IIIA/RDAS Probability of Target Hit Versus Rate of Received Interference (ASR-7 Victim Radar, Normal Channel, Rank Quantizer Threshold 24)

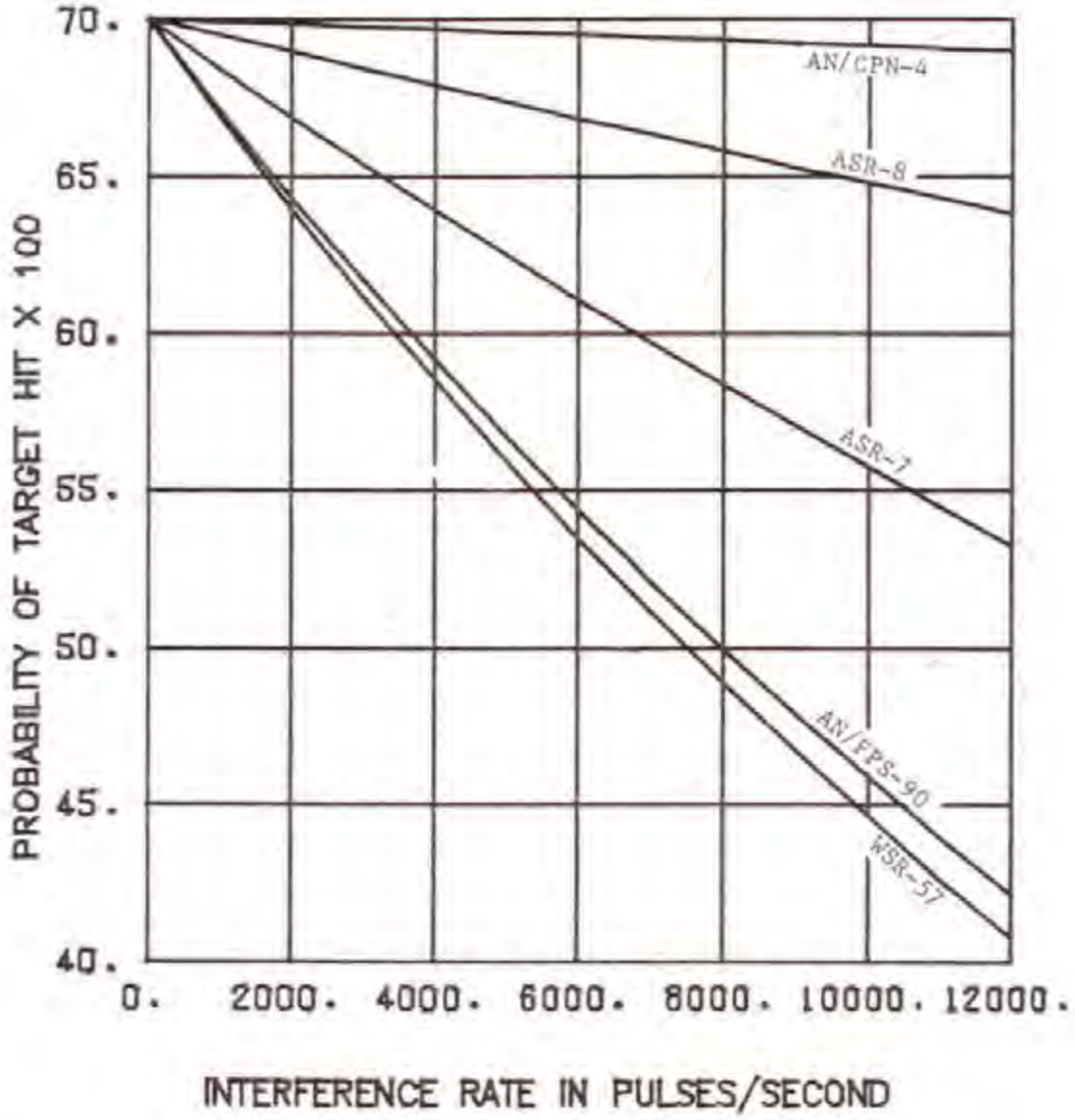

Figure 4-22. ARTS-IIIA/RDAS Probability of Target Hit Versus Rate of Received Interference (ASR-7 Victim Radar, MTI Channel, Rank Quantizer Threshold 23)

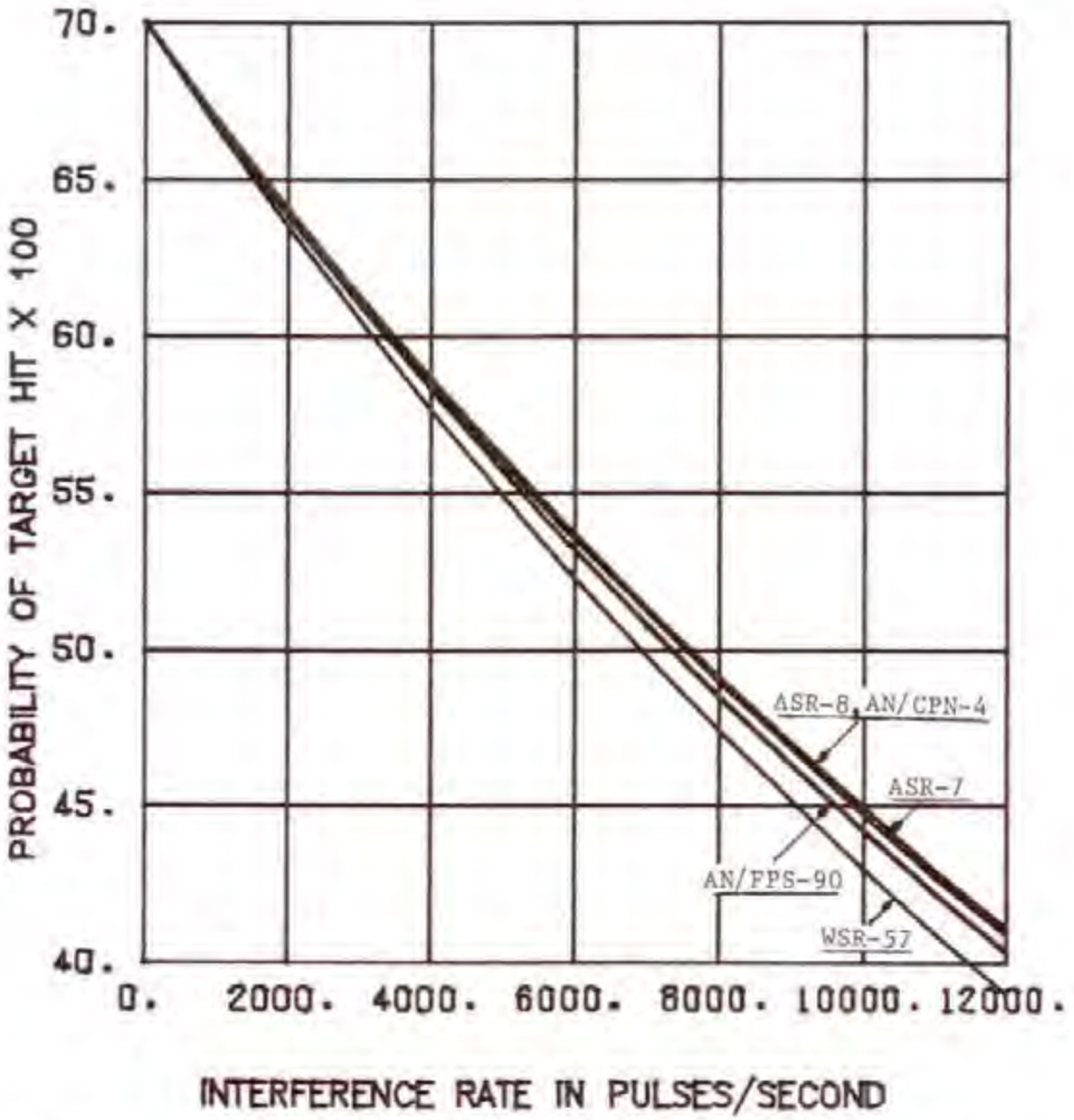

Figure 4-23. ARTS-IIIA/RDAS Probability of Target Hit Versus Rate of Received Interference (ASR-7 Victim Radar, MTI Channel, Rank Quantizer Threshold 24)

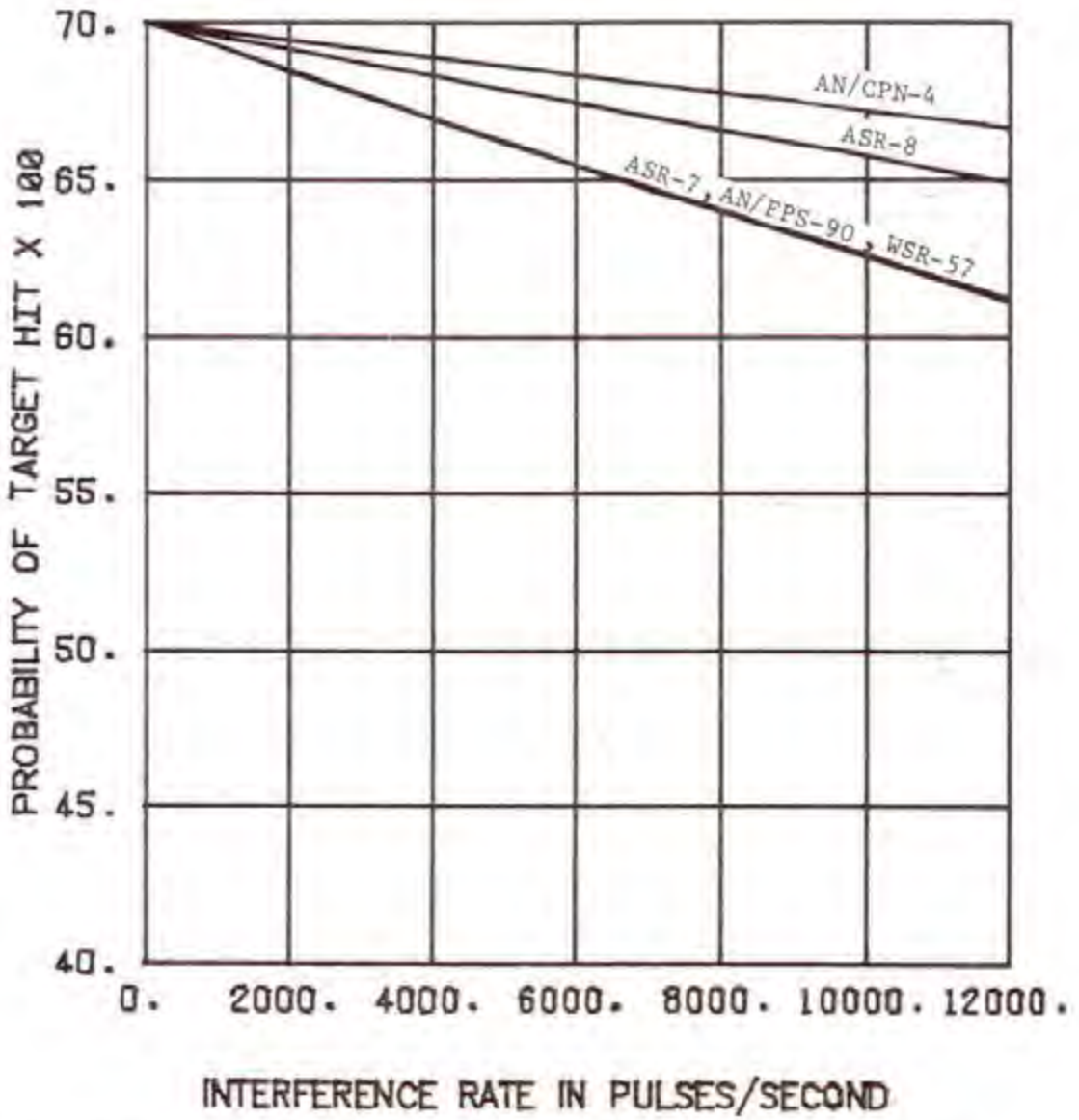

Figure 4-24. ARTS-IIIA/RDAS Probability of Target Hit Versus Rate of Received Interference (ASR-8 Victim Radar, Normal Channel, Rank Quantizer Threshold 23)

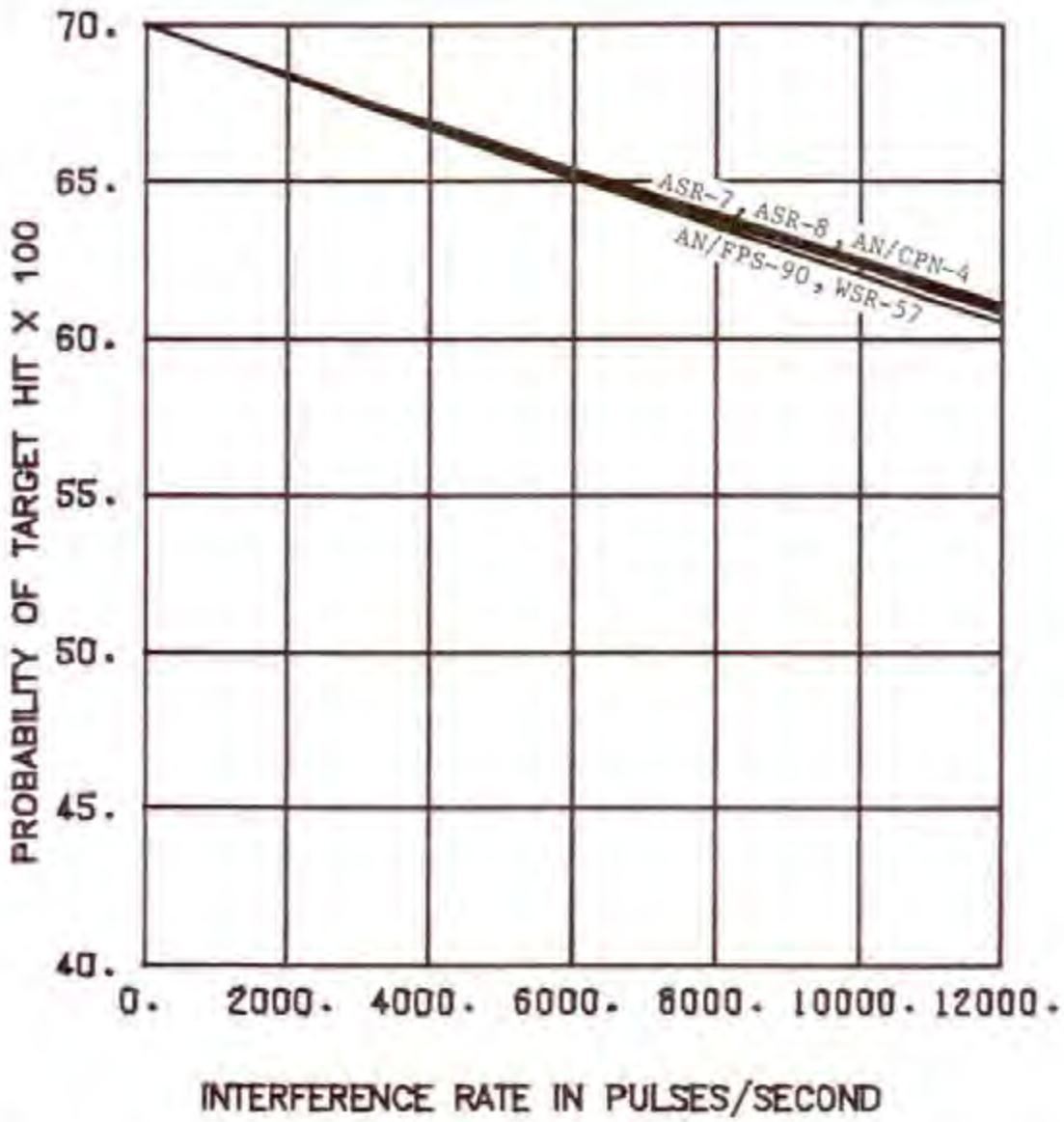

Figure 4-25. ARTS-IIIA/RDAS Probability of Target Hit Versus Rate of Received Interference (ASR-8 Victim Radar, Normal Channel, Rank Quantizer Threshold 24)

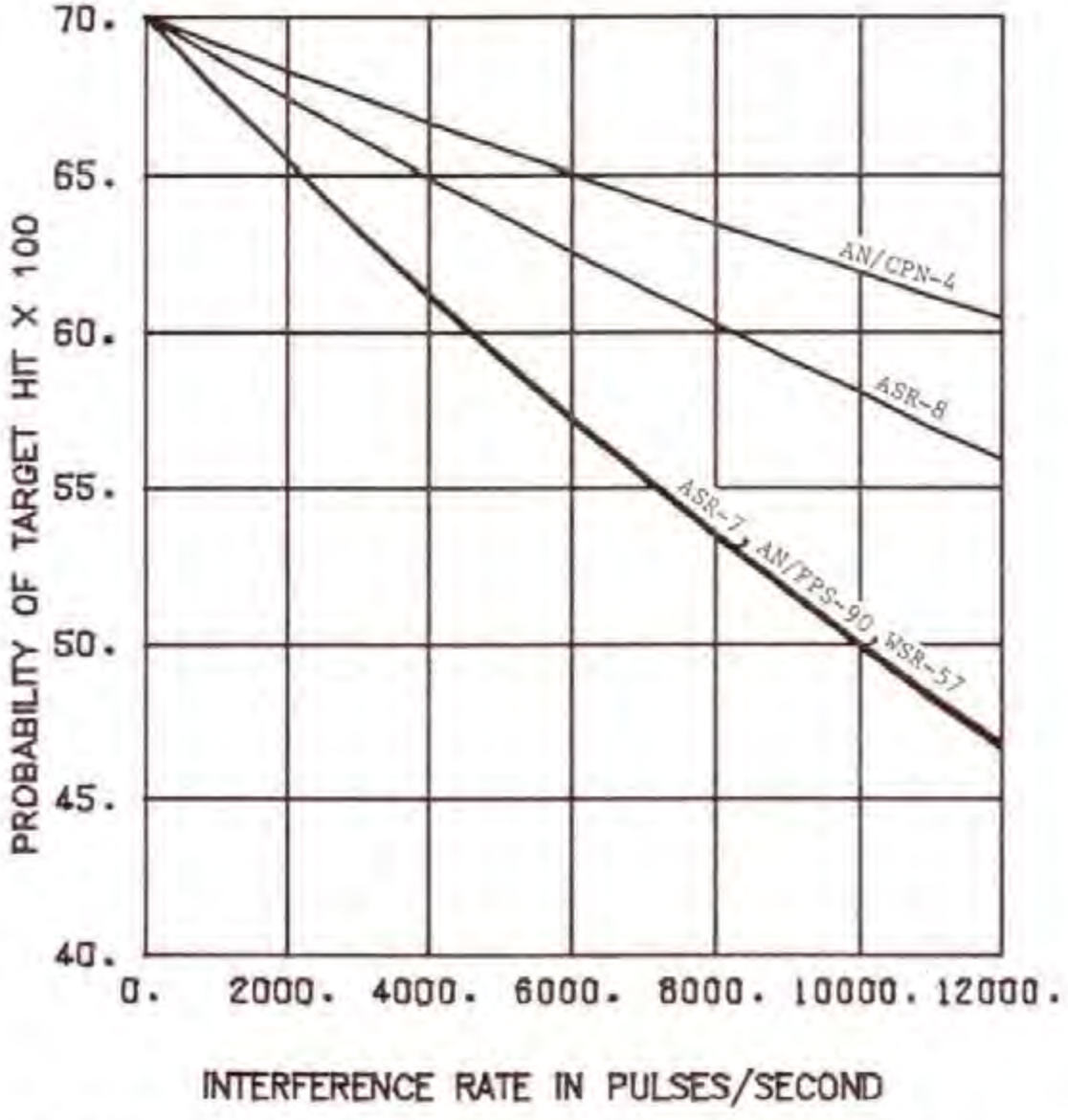

Figure 4-26. ARTS-IIIA/RDAS Probability of Target Hit Versus Rate of Received Interference (ASR-8 Victim Radar, MTI Channel, Rank Quantizer Threshold 23)

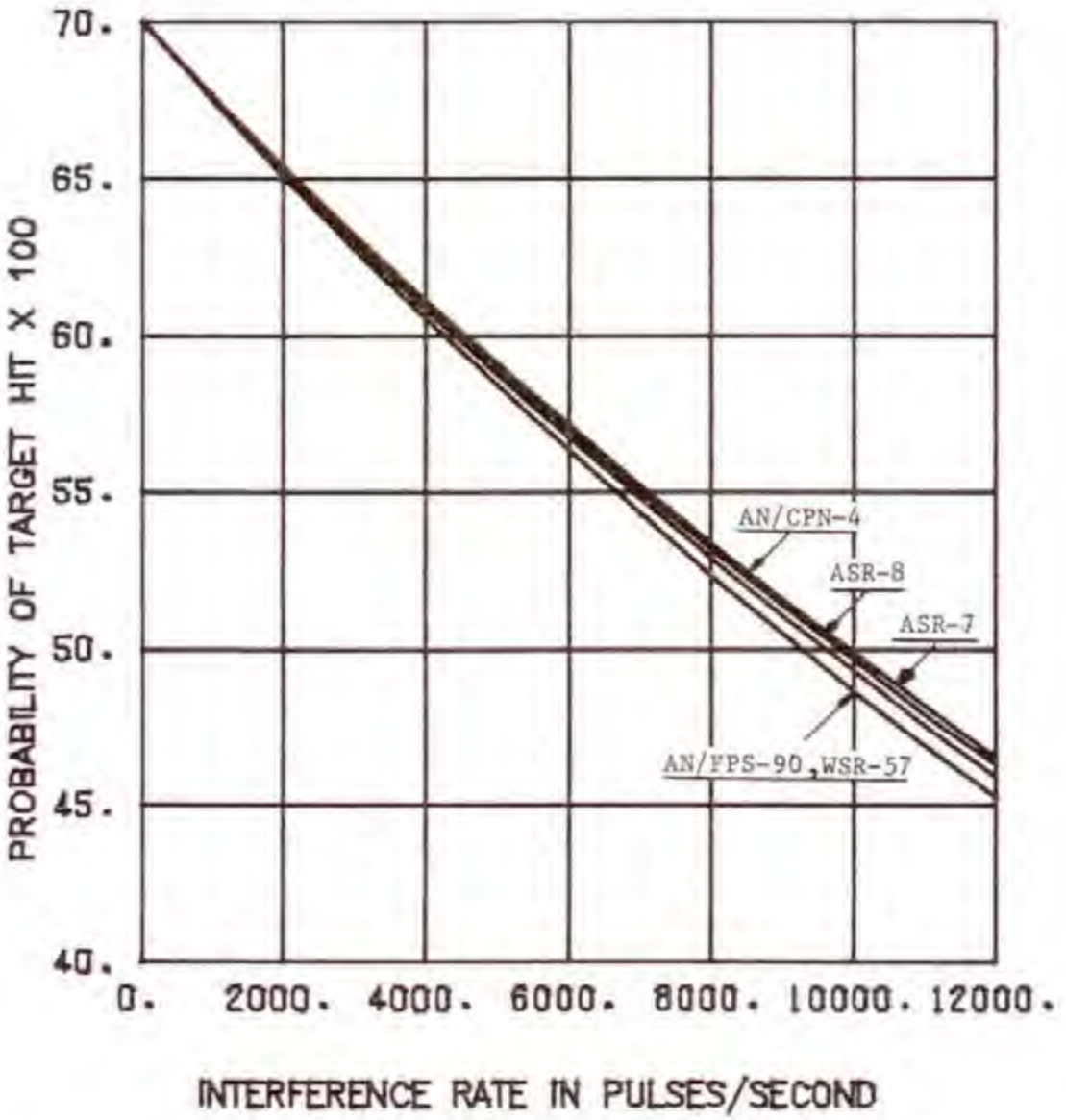

Figure 4-27. ARTS-IIIA/RDAS Probability of Target Hit Versus Rate of Received Interference (ASR-8 Victim Radar, MTI Channel, Rank Quantizer Threshold 24)

the ARTS-IIIA/RDAS interfaced to the ASR-7, and Figures 4-24 through 4-27 interfaced to the ASR-8. The graphs also account for the radar channel (normal or MTI) that is connected to the ARTS-IIIA/RDAS. The family of curves on each graph represent various interfering radar types. The even numbered graphs are for RQT=23 and the odd number graphs for RQT=24. The ν=0 value on each curve gives the probability of a target hit (0.7) without interference present. The same factors (interfering radar pulse width and PRF, and victim radar range bin characteristics) which affected the degree of interference impact on the probability of false target hit also applies to the probability of target hit. However, the probability of target hit decreased with interference, while in most cases the probability of a false target hit increased. This is because the probability of target hit (P_1 in Equation 4-1) is much greater than the probability of an interference pulse falling in the range bin of interest ($1-e^{-X_1\nu}$ in Equation 4-1). Under these conditions, Equation 4-1 can be approximated by:

$$P_{11} = P_1 e^{-NX_2\nu} \qquad (4\text{-}19)$$

It is evident from this expression that the probability of hit can only decrease with increasing values of ν.

The data representing the curves in Figures 4-20 through 4-27 were reduced to the form shown in TABLES 4-8 through 4-11 to indicate the effect of a particular number and type of interfering radars on the probability of target hit. TABLES 4-8 and 4-9 represent data for an ARTS-IIIA/RDAS interfaced to an ASR-7 radar that is receiving interference from one and three radars, respectively. Similarly, TABLES 4-10 and 4-11 gives the probability of target hit when the ARTS-IIIA/RDAS is interfaced to an ASR-8 radar that is receiving interference. The interfering pulse arrival rate (ν) in TABLES 4-8 and 4-10 are simply equal to the average PRF of the interfering radar. In TABLES 4-9 and 4-11, ν is equal to three times the PRF of the interfering radar. The probability of target hit values listed in TABLES 4-8 through 4-11 indicate that connecting the ARTS-IIIA/RDAS to the MTI channel results in a lower probability of target hit than when connected to the normal channel. This is because N in Equation 4-19 is 3 for MTI and only 1 for normal channel. In other words, the probability of an interference pulse falling in a rank quantizer comparison range bin and precluding generation of a hit (logical 1) is greater for the MTI channel.

Interference Effect on Target Detection

The decision to declare a target is accomplished by the target detection software functions shown in Figure 4-5. The details of this target detection processing is given in the RDAS Subsystem Description section of this report. A computer program was written to determine the probability of target detection as a function of probability of target hit. The program involves

TABLE 4-8

ARTS-IIIA/3DAS PROBABILITY OF TARGET HIT WHEN CONNECTED TO ASR-7 RADAR THAT IS RECEIVING INTERFERENCE FORM ONE RADAR

VICTIM RADAR CHANNEL	INTERFERING RADAR	INTERFERING RATE ν PULSES/SEC	PROBABILITY OF TARGET HIT (RQT = 23)	PROBABILITY OF TARGET HIT (RQT = 24)
NORMAL	ASR-7	1002	0.6947	0.6893
NORMAL	ASR-8	1040	0.6981	0.6892
NORMAL	AN/CPN-4	1192	0.6996	0.6878
NORMAL	AN/FPS-90	356	0.6965	0.6962
NORMAL	WSR-57	166	0.6983	0.6981
MTI	ASR-7	1002	0.6842	0.6686
MTI	ASR-8	1040	0.6944	0.6681
MTI	AN/CPN-4	1192	0.6989	0.6641
MTI	AN/FPS-90	356	0.6897	0.6888
MTI	WSR-57	166	0.6949	0.6945

NOTE: RQT = RANK QUANTIZER THRESHOLD
PROBABILITY OF TARGET HIT WITHOUT INTERFERENCE = 0.7

TABLE 4-9

ARTS-IIIA/RDAS PROBABILITY OF TARGET HIT WHEN CONNECTED TO ASR-7 RADAR THAT IS RECEIVING INTERFERENCE FROM THREE RADARS OF THE SAME TYPE

VICTIM RADAR CHANNEL	INTERFERING RADAR	INTERFERING RATE ν PULSES/SEC	PROBABILITY OF TARGET HIT (RQT = 23)	PROBABILITY OF TARGET HIT (RQT = 24)
NORMAL	ASR-7	3006	0.6842	0.6686
NORMAL	ASR-8	3120	0.6944	0.6681
NORMAL	AN/GPN-4	3576	0.6989	0.6639
NORMAL	AN/FPS-90	1068	0.6895	0.6886
NORMAL	WSR-57	498	0.6948	0.6944
MTI	ASR-7	3006	0.6536	0.6097
MTI	ASR-8	3120	0.6832	0.6087
MTI	AN/GPN-4	3576	0.6968	0.5975
MTI	AN/FPS-90	1068	0.6692	0.6665
MTI	WSR-57	498	0.6842	0.6834

NOTE: RQT = RANK QUANTIZER THRESHOLD
PROBABILITY OF TARGET HIT WITHOUT INTERFERENCE = 0.7

TABLE 4-10

ARTS-IIIA/RDAS PROBABILITY OF TARGET HIT WHEN CONNECTED TO ASR-8 RADAR THAT IS RECEIVING INTERFERENCE FROM ONE RADAR

VICTIM RADAR CHANNEL	INTERFERING RADAR	INTERFERING RATE ν PULSES/SEC	PROBABILITY OF TARGET HIT (RQT = 23)	PROBABILITY OF TARGET HIT (RQT = 24)
NORMAL	ASR-7	1002	0.6921	0.6918
NORMAL	ASR-8	1040	0.6954	0.6916
NORMAL	AN/CPN-4	1192	0.6965	0.6906
NORMAL	AN/FPS-90	356	0.6972	0.6970
NORMAL	WSR-57	166	0.6987	0.6985
MTI	ASR-7	1002	0.6767	0.6758
MTI	ASR-8	1040	0.6864	0.6753
MTI	AN/CPN-4	1192	0.6898	0.6723
MTI	AN/FPS-90	356	0.6918	0.6911
MTI	WSR-57	166	0.6961	0.6958

NOTE: RQT = RANK QUANTIZER THRESHOLD
PROBABILITY OF TARGET HIT WITHOUT INTERFERENCE = 0.7

TABLE 4-11

ARTS-IIIA/RDAS PROBABILITY OF TARGET HIT WHEN CONNECTED TO ASR-8 RADAR THAT IS RECEIVING INTERFERENCE FROM THREE RADARS OF THE SAME TYPE

VICTIM RADAR CHANNEL	INTERFERING RADAR	INTERFERING RATE v PULSES/SEC	PROBABILITY OF TARGET HIT (RQT = 23)	PROBABILITY OF TARGET HIT (RQT = 24)
NORMAL	ASR-7	3006	0.6767	0.6758
NORMAL	ASR-8	3120	0.6870	0.6753
NORMAL	AN/CPN-4	3576	0.6898	0.6722
NORMAL	AN/FPS-90	1068	0.6917	0.6910
NORMAL	WSR-57	498	0.6961	0.6958
MTI	ASR-7	3006	0.6323	0.6300
MTI	ASR-8	3120	0.6601	0.6287
MTI	AN/CPN-4	3576	0.6698	0.6200
MTI	AN/FPS-90	1068	0.6753	0.6733
MTI	WSR-57	498	0.6885	0.6875

NOTE: RQT = RANK QUANTIZER THRESHOLD
PROBABILITY OF TARGET HIT WITHOUT INTERFERENCE = 0.7

Monte-Carlo simulating a series of target hits and misses and comparing this binary sequence to the target detection criteria. The details of this program are given in Appendix F, and the results of the calculations plotted on probability paper in Figures 4-28 and 4-29. The probability of target detection versus probability of target hit curves in Figure 4-28 are for a rank quantizer threshold of 23 and those in Figure 4-29 for a rank quantizer threshold 24. The family of curves on each graph represent combinations of hit and miss count threshold detection parameters. From the graphs, it is evident that for a given hit and miss count threshold, a rank quantizer threshold setting of 23 results in a slightly higher probability of target detection than 24. This is because a rank quantizer threshold setting of 23 results in a greater probability of hit due to noise alone (probability of false target hit), which in effect increases the probability of the hit count satisfying the target detection criteria (hit count threshold). That is, the noise hits in azimuth for a given range bin can cause an initial non-zero hit count before radar return pulses from the target are received. The probability of this occurring is greater for a rank quantizer threshold setting of 23 than 24.

The curves in Figures 4-28 and 4-29 were used to relate the interference effect on probability of target hit to probability of target detection. This procedure was followed to relate the probability of target hits in TABLES 4-8 through 4-11 for various interfering conditions to the probability of target detection values shown in TABLE 4-12. The values are for the most likely ARTS-IIIA/RDAS detection parameters that will be used in the field (hit count threshold of 9, miss count threshold of 3, and rank quantizer threshold setting 23). The probability of detection without interference (0.8892) is shown at the bottom of TABLE 4-12. It is evident from TABLE 4-12 that interfacing the ARTS-IIIA/RDAS to the ASR-8 results in, except for the AN/FPS-90 and WSR-57 interfering radar types, a lower probability of target detection than when interfaced to an ASR-7. A lower probability of detection also results when the ARTS-IIIA is connected to a single MTI channel than to a normal or dual MTI channel. The lowest probability of detections occurred for the interferer and victim radar combinations involving the ASR-7 and ASR-8, because this combination resulted in the greatest decrease in probability of target hit due to interference. The impact of interference on the probability of target hit detection was defined for rank quantizer threshold 23 by Equations 4-3 and 4-19. For the case in which the interfering pulse width is less than the sum of the victim radar range bin width and hold time, radars with the largest duty cycles (τ_I x PRF) have the greatest interference effect on ARTS-IIIA/RDAS performance. For the case in which the interfering radar pulse width is greater than the sum of the victim radar range bin width and hold time, the impact of interference is independent of the interfering radar pulse width and increases only with interfering radar PRF.

Interpretation of Interference Effects on Target Detection

It is evident from TABLE 4-12 that the difference between the lowest probability of target detection (0.7581) and that for no interference

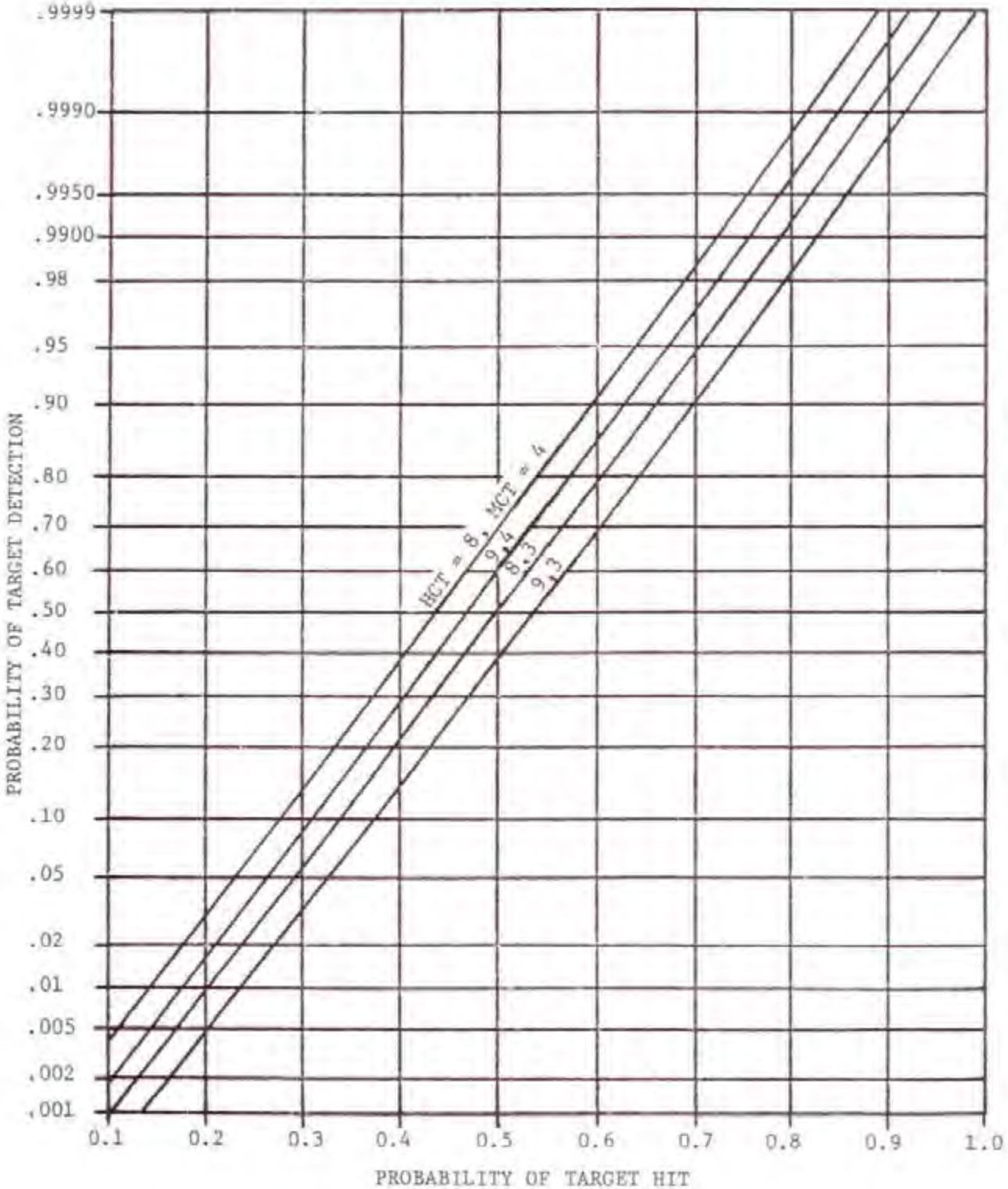

Figure 4-28. ARTS-IIIA/RDAS Probability of Target Detection Versus Probability of Target Hit for Rank Quantizer Threshold 23 and Various Hit/Miss Count Threshold Parameters Combinations (Probability Scale)

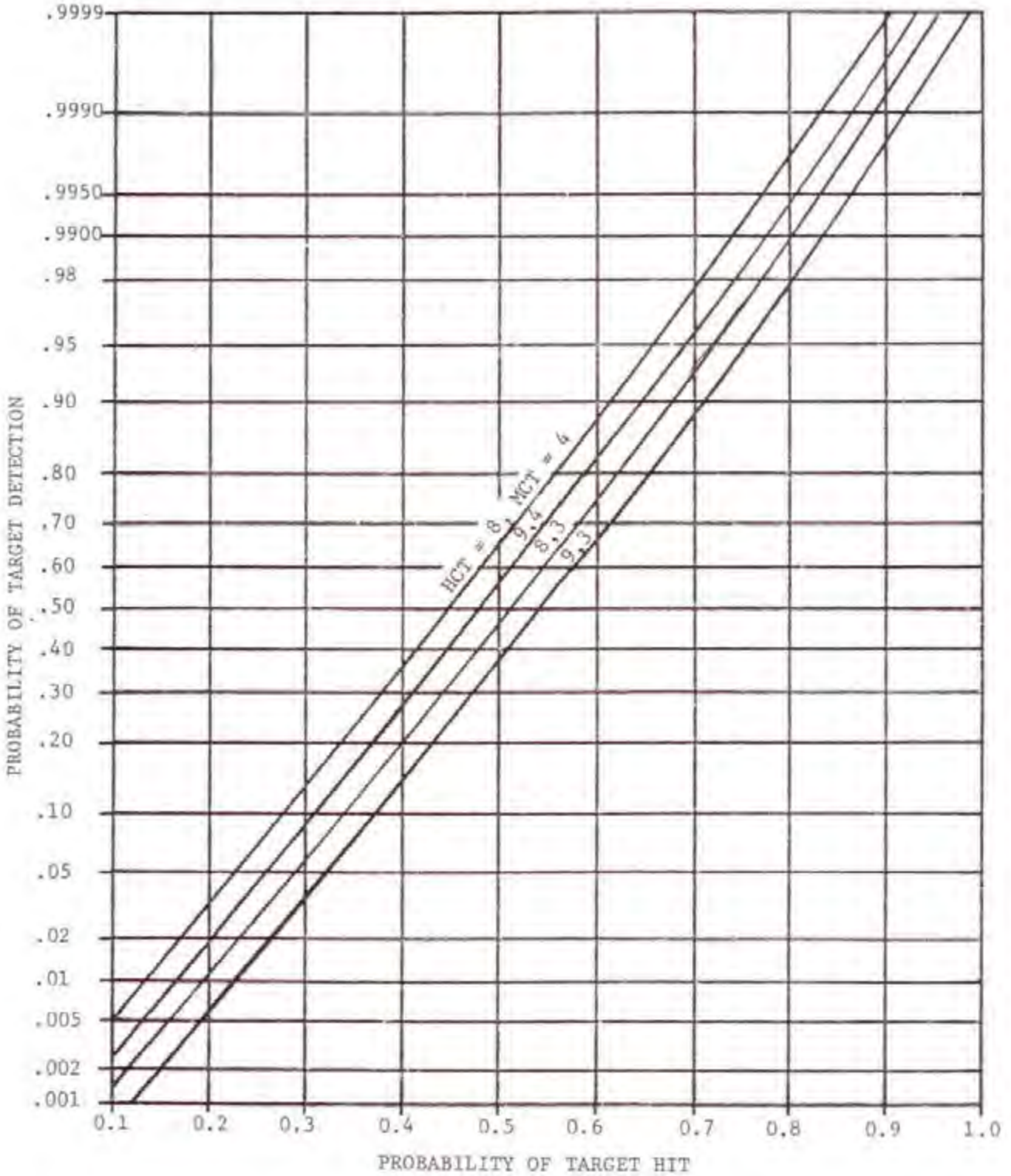

Figure 4-29. ARTS-IIIA/RDAS Probability of Target Detection Versus Probability of Target Hit for Rank Quantizer Threshold 24 and Various Hit/Miss Count Threshold Parameter Combinations (Probability Scale)

TABLE 4-12

ARTS-IIIA/RDAS PROBABILITY OF TARGET DETECTION FOR TYPICAL DETECTION PARAMETERS AND VARIOUS COMBINATIONS OF INTERFERING AND VICTIM RADARS

VICTIM RADAR	VICTIM RADAR CHANNEL	NUMBER INTERFERING RADARS OF SAME TYPE	INTERFERING RADAR TYPE				
			ASR-7 τ_1 = 0.83 µs PRF = 1002	ASR-8 τ_1 = 0.60 µs PRF = 1040	AN/CPN-4 τ_1 = 0.5 µs PRF = 1192	AN/FPS-90 τ_1 = 2.0 µs PRF = 356	WSR-57 τ_1 = 4.0 µs PRF = 166
ASR-7	NORMAL	1	0.8789	0.8855	0.8884	0.8824	0.8859
ASR-7	NORMAL	3	0.8586	0.8784	0.8871	0.8689	0.8791
ASR-7	MTI	1	0.8586	0.8784	0.8871	0.8693	0.8793
ASR-7	MTI	3	0.7994	0.8567	0.8830	0.8296	0.8596
ASR-8	NORMAL	1	0.8739	0.8803	0.8824	0.8838	0.8867
ASR-8	NORMAL	3	0.8441	0.8640	0.8695	0.8731	0.8816
ASR-8	MTI	1	0.8441	0.8628	0.8695	0.8733	0.8816
ASR-8	MTI	3	0.7581	0.8119	0.8307	0.8414	0.8669

NOTE: 1. ARTS IIIA/RDAS TYPICAL TARGET DECTECTION PARAMETERS
RANK QUANTIZER THRESHOLD = 23
HIT COUNT THRESHOLD = 9
MISS COUNT THRESHOLD = 3

2. PROBABILITY OF TARGET DETECTION WITHOUT INTERFERENCE = 0.8892

(0.8892) is 0.13. This reduction in probability of target detection is for the MTI channel of the victim radar receiving continual and simultaneous interference from three radars. A 0.13 reduction in target detection probability implies that if 350 targets per antenna rotations are detected without interference, only about 305 would be detected with interference. This degree of target detection degradation due to interference would be unacceptable. However, it should be pointed out that this number represents extremely worst-case interference conditions which do not currently exist in congested U.S. terminal areas. Recent measurements by NTIA (Hinkle, 1976) in the Los Angeles and San Francisco area indicated that for those FAA radars which received interference, interference was usually received from one radar at a time over only small sectors of the PPI. The lowest probability of target detection listed in TABLE 4-12 for one interfering radar is 0.8441, and represents a 0.045 decrease due to interference. This implies that if 350 targets are detected without interference, only 334 targets would be detected with interference. If it is assumed that interference is received over only 50 percent of the antenna rotation and that aircraft targets are uniformly distributed in azimuth, the number of targets detected per antenna rotation would be decreased by interference from 350 to 342. This is equivalent to a 0.02 decrease in the probability of a target being detected in one antenna rotation. The decrease corresponds to one radar interfering over 50 percent of the antenna rotation, or multiple interfering radars which do not interfere simultaneously but in combination, interfere over 50 percent of the antenna rotation.

The above estimated reduction in detection probability (0.02) due to present interference levels in congested terminal areas, and in general those detection probabilities listed in TABLE 4-12, are pessimistic. In addition to worst-case interference signal level assumptions, the 0.7 target hit probability chosen for a zero interference reference base results in a worst-case interference impact on target detection probability. This can be seen from the linear plot of target detection probability versus target hit probability shown in Figure 4-30. The slope of the (9/3) curve (used in the analysis) in the 0.7 target hit probability region is very steep. Consequently, a decrease in probability of target hit from 0.7 due to interference results in a significant decrease in probability of target detection. For interference reference target hit probabilities greater than 0.7 the slope of the curve approaches zero. Therefore, interference has considerably less impact on target detection probability for these target hit probability ranges.

It is evident from Figures 4-17, 4-18, and 4-19 that a 0.7 probability of target hit and rank quantizer threshold of 23 chosen for the analysis corresponds to a signal-to-noise ratio of approximately 6 dB, 12 dB, and 7 dB for the ARTS-IIIA/RDAS connected to the ASR-7 or ASR-8 normal channel, ASR-7 MTI channel, and ASR-8 MTI channel, respectively. The 12 dB signal-to-noise ratio for the single MTI channel is fairly typical; however, the 6 dB and 7 dB signal-to-noise ratio for the normal and dual MTI channel is considerably less than typical. For this reason, the interference effects on target detection indicated in TABLE 4-12 are more pessimistic for the normal and

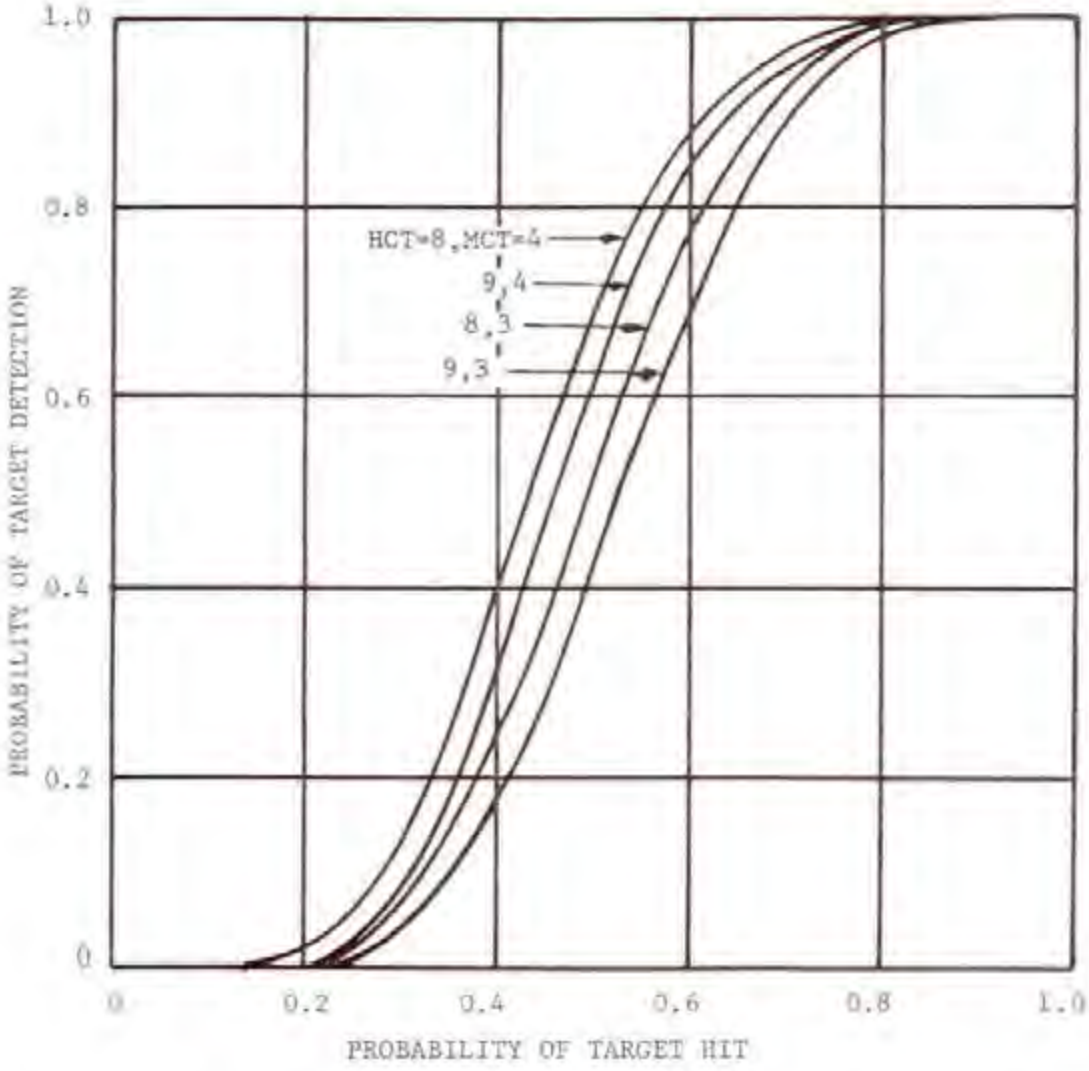

Figure 4-30. ARTS-IIIA/RDAS Probability of Target Detection Versus Probability of Target Hit for Rank Quantizer Threshold 23 and Various Hit/Miss Count Threshold Parameter Combinations (Linear Scale)

dual MTI channel than the single MTI channel.

The hit count threshold of 9 used in the target detection analysis corresponds to only the lowest hit count threshold value that the MTI channel can have at any given time. As discussed in a previous section and described in Figure 4-7, the MTI channel hit count threshold is automatically increased from 9 to a maximum of 20 depending on the degree of clutter correlation. From comparison of the target detection probability curves in Figure 4-30, it is evident that the slope of the curves for hit count thresholds greater than 9, in the 0.7 target hit probability region, would be approximately the same as for the (9, 3) hit/miss count threshold curve. Since the (9, 3) curve and a 0.7 target hit probability (zero interference reference base) was used to determine the interference impact on detection probability, the analysis results should at least typify ASR-7 MTI channel performance for a 12 dB signal-to-noise ratio, and 7 dB signal-to-noise ratio for the ASR-8 MTI channel, in the lower portion of the automatically varied hit count threshold range of 9 to 20.

Trade-Off Between Interference Suppression and ARTS-IIIA/RDAS Performance

This subsection addresses the trade-offs between interference suppression and radar performance for various ARTS-IIIA/RDAS detection parameter settings. The interference case chosen for the trade-off analysis included three continually interfering radars and the ARTS-IIIA/RDAS connected to the victim radar MTI channel. This combination was chosen for the trade-off analysis because it results in the greatest impact of interference on target detection probability.

TABLES 4-13 through 4-16 indicates the effect of interference on the probability of detection and false alarm for various interfering radar types and ARTS-IIIA/RDAS detection parameter combinations. In particular, TABLES 4-13 and 4-14 indicate the affect of interference on false alarm and TABLES 4-15 and 4-16 the interference effect on target detection. The first column of the table gives the ARTS-IIIA/RDAS rank quantizer, hit count, and miss count threshold combinations. The probability of false alarm or target detection for no interference and a particular combination of detection parameters is given in the last column of the tables. From the tables and detection theory, it is evident that increasing probability of target detection also increases probability of false alarm. An optimum set of detection parameters involve maximizing the probability of detection while maintaining an acceptable false alarm rate (probability of false alarm). FAA considers probability of false alarms that exceed approximately 10^{-6} to be unacceptable. Therefore, the false alarm probability (1.164×10^{-5}) listed in TABLES 4-13 and 4-14 for no interference and the (23, 8, 4) rank/hit/miss detection threshold parameter combination would likely be unacceptable.

Rank Quantizer Threshold Trade-Off

It is evident from TABLES 4-13 and 4-14 that, with the exception of the

TABLE 4-13

ARTS-IIIA/RDAS PROBABILITY OF FALSE ALARM WHEN CONNECTED TO ASR-7 RADAR (MTI CHANNEL) THAT IS RECEIVING INTERFERENCE FROM THREE RADARS OF THE SAME TYPE

ARTS-IIIA PARAMETERS			INTERFERING RADAR TYPE					PROBABILITY OF FALSE ALARM WITHOUT INTERFERENCE
RQT	HCT	MCT	ASR-7 PW = 0.83 μs PRF = 1002	ASR-8 PW = 0.60 μs PRF = 1040	AN/CPN-4 PW = 0.5 μs PRF = 1192	AN/FPS-90 PW = 2.0 μs PRF = 356	WSR-57 PW = 4.0 μs PRF = 166	
23	8	3	3.176×10^{-6}	3.893×10^{-6}	4.440×10^{-6}	3.263×10^{-6}	2.195×10^{-6}	2.500×10^{-5}
23	8	4	1.505×10^{-5}	1.869×10^{-5}	2.145×10^{-5}	1.550×10^{-5}	2.408×10^{-5}	1.164×10^{-3}
23	9	3	7.075×10^{-7}	9.699×10^{-7}	11.702×10^{-7}	7.392×10^{-7}	4.051×10^{-7}	4.596×10^{-7}
23	9	4	4.085×10^{-6}	4.956×10^{-6}	5.622×10^{-6}	4.190×10^{-6}	2.881×10^{-6}	3.262×10^{-6}
24	8	3	2.129×10^{-8}	1.352×10^{-8}	1.038×10^{-8}	3.168×10^{-8}	0.909×10^{-8}	1.081×10^{-8}
24	8	4	10.839×10^{-8}	7.997×10^{-8}	6.766×10^{-8}	14.633×10^{-8}	6.050×10^{-8}	7.008×10^{-8}
24	9	3	2.688×10^{-9}	1.621×10^{-9}	1.230×10^{-9}	4.112×10^{-9}	1.203×10^{-9}	1.250×10^{-9}
24	9	4	2.323×10^{-8}	1.384×10^{-8}	1.043×10^{-8}	3.577×10^{-8}	1.003×10^{-8}	1.057×10^{-8}

NOTE: RQT = RANK QUANTIZER THRESHOLD
HCT = HIT COUNT THRESHOLD
MCT = MISS COUNT THRESHOLD

TABLE 4-14

ARTS-IIIA/RDAS PROBABILITY OF FALSE ALARM WHEN CONNECTED TO ASR-8 RADAR (MTI CHANNEL) THAT IS RECEIVING INTERFERENCE FROM THREE RADARS OF THE SAME TYPE

ARTS-IIIA PARAMETERS			INTERFERING RADAR TYPE					PROBABILITY OF FALSE ALARM WITHOUT INTERFERENCE
RQT	HCT	MCT	ASR-7 PW = 0.83 μs PRF = 1002	ASR-8 PW = 0.60 μs PRF = 1040	AN/GPN-4 PW = 0.5 μs PRF = 1192	AN/FPS-90 PW = 2.0 μs PRF = 356	WSR-57 PW = 4.0 μs PRF = 166	
23	8	3	2.400×10^{-6}	2.966×10^{-6}	3.313×10^{-6}	2.011×10^{-6}	2.271×10^{-6}	2.500×10^{-6}
23	8	4	1.116×10^{-5}	1.400×10^{-5}	1.575×10^{-5}	0.931×10^{-5}	1.055×10^{-5}	1.164×10^{-5}
23	9	3	4.417×10^{-7}	6.305×10^{-7}	7.575×10^{-7}	3.723×10^{-7}	4.187×10^{-7}	4.596×10^{-7}
23	9	4	3.136×10^{-6}	4.364×10^{-6}	5.183×10^{-6}	2.652×10^{-6}	2.976×10^{-6}	3.262×10^{-6}
24	8	3	2.848×10^{-8}	2.065×10^{-8}	1.175×10^{-8}	0.872×10^{-8}	0.887×10^{-8}	1.081×10^{-8}
24	8	4	13.464×10^{-8}	10.606×10^{-8}	9.454×10^{-8}	5.997×10^{-8}	6.292×10^{-8}	7.008×10^{-8}
24	9	3	3.673×10^{-9}	2.600×10^{-9}	2.168×10^{-9}	1.174×10^{-9}	1.215×10^{-9}	1.250×10^{-9}
24	9	4	3.190×10^{-8}	2.245×10^{-8}	1.865×10^{-8}	0.938×10^{-8}	1.001×10^{-8}	1.057×10^{-8}

NOTE: RQT = RANK QUANTIZER THRESHOLD
HCT = HIT COUNT THRESHOLD
MCT = MISS COUNT THRESHOLD

TABLE 4-15

ARTS-IIIA/RDAS PROBABILITY OF TARGET DETECTION WHEN CONNECTED TO ASR-7 RADAR (MTI CHANNEL) THAT IS RECEIVING INTERFERENCE FROM THREE RADARS

ARTS-IIIA PARAMETERS			INTERFERING RADAR TYPE					PROBABILITY OF DETECTION WITHOUT INTERFERENCE
RQT	HCT	MCT	ASR-7 PW = 0.83 μs PRF = 1002	ASR-8 PW = 0.60 μs PRF = 1040	AN/GPN-4 PW = 0.5 μs PRF = 1192	AN/FPS-90 PW = 2.0 μs PRF = 356	WSR-57 PW = 4.0 μs PRF = 166	
23	8	3	0.8559	0.9028	0.9242	0.8806	0.9051	0.9293
23	8	4	0.9352	0.9619	0.9741	0.9492	0.9633	0.9770
23	9	3	0.7994	0.8567	0.8830	0.8295	0.8596	0.8892
23	9	4	0.9068	0.9418	0.9579	0.9253	0.9436	0.9617
24	8	3	0.7786	0.7770	0.7568	0.8688	0.8956	0.9219
24	8	4	0.8924	0.8915	0.8788	0.9426	0.9576	0.9723
24	9	3	0.7025	0.7006	0.6752	0.8160	0.8497	0.8829
24	9	4	0.8513	0.8506	0.8338	0.9176	0.9373	0.9567

NOTE: RQT = RANK QUANTIZER THRESHOLD
HCT = HIT COUNT THRESHOLD
MCT = MISS COUNT THRESHOLD

TABLE 4-16

ARTS-IIIA/RDAS PROBABILITY OF TARGET DETECTION WHEN CONNECTED TO ASR-8 RADAR (MTI CHANNEL) THAT IS RECEIVING INTERFERENCE FROM THREE RADARS OF THE SAME TYPE

ARTS-IIIA PARAMETERS			INTERFERING RADAR TYPE					PROBABILITY OF DETECTION WITHOUT INTERFERENCE
RQT	HCT	MCT	ASR-7 PW = 0.83 μs PRF = 1002	ASR-8 PW = 0.60 μs PRF = 1040	AN/CPN-4 PW = 0.5 μs PRF = 1192	AN/FPS-90 PW = 2.0 μs PRF = 356	WSR-57 PW =4.0 μs PRF = 166	
23	8	3	0.8223	0.8663	0.8816	0.8903	0.9111	0.9293
23	8	4	0.9160	0.9411	0.9498	0.9547	0.9666	0.9770
23	9	3	0.7581	0.8120	0.8307	0.8414	0.8669	0.8892
23	9	4	0.8816	0.9145	0.9620	0.9325	0.9481	0.9617
24	8	3	0.8109	0.8088	0.7950	0.8796	0.9021	0.9219
24	8	4	0.9104	0.9092	0.9015	0.9487	0.9612	0.9723
24	9	3	0.7431	0.7405	0.7232	0.8296	0.8579	0.8829
24	9	4	0.8750	0.8735	0.8633	0.9255	0.9421	0.9567

NOTE: RQT = RAMP QUANTIZER THRESHOLD
HCT = HIT COUNT THRESHOLD
MCT = MISS COUNT THRESHOLD

(23, 8, 4) detection parameters combination, either a rank quantizer threshold setting of 23 or 24 would yield an acceptable false alarm probability. Even for heavy interfering conditions, the probability of false alarm is not increased up to an unacceptable level for these two parameter settings.

The probability of target detection values listed in the right column of TABLES 4-15 and 4-16 for no interference indicates that for a given hit and miss count threshold, and target hit probability, that detection performance is slightly greater for a rank quantizer threshold 23 than 24. However, the probability of detecting a target without interference is actually larger for a rank quantizer threshold setting of 23 than indicated. It is evident from Figures 4-17, 4-18, and 4-19 that approximately 1 to 2 dB greater signal-to-noise ratio is required for a rank quantizer threshold of 24 than 23 to achieve a given probability of target hit. This implies that for a given signal-to-noise ratio, a rank quantizer threshold setting of 23 results in a higher probability of target detection. Therefore, a rank quantizer threshold setting of 23 is optimum for radar detection performance without interference.

It is evident from TABLES 4-15 and 4-16 that a rank quantizer threshold setting of 23 is also more desirable than 24 for interference suppression. For a given interfering radar and hit/miss threshold combination, the decrease in probability of detection caused by interference is significantly less for a rank quantizer threshold setting of 23 than 24. This is because there is a lower probability of interfering pulses falling in two rank quantizer comparison range bins than one. As discussed previously, a rank quantizer threshold setting of 24 implies that the signal level in the target range bin of interest has to exceed all 24 comparison range bin signal levels before a target hit (logical 1) is generated. However, the signal level in the target range bin of interest for rank quantizer threshold setting 23 only has to exceed 23 of the 24 comparison range bins for a target hit to be generated.

It is evident from this logic and the results of the analysis that rank quantizer thresholds lower than 23 would further reduce the impact of interference on target detection probability. However, lowering the rank quantizer threshold below 23 would begin to adversely affect the rank order detection processor's capability to maintain a constant false alarm rate (probability of false alarm) in varying levels of clutter.

Hit and Miss Count Threshold Trade-Off

It was shown in the previous section that a rank quantizer threshold setting of 23 is superior to 24 for ARTS-IIIA performance, with or without interference. This section considers the hit and miss count threshold detection parameter combinations associated with this rank quantizer threshold which yields optimum ARTS-IIIA performance. As previously discussed, the (23, 8, 4) rank/hit/miss detection threshold parameter

combination yields an unacceptably high false alarm probability. Therefore, only the (23, 8, 3), (23, 9, 3), and (23, 9, 4) parameter combinations will be considered.

It is evident from TABLES 4-13 and 4-14 that for a rank quantizer threshold of 23, the probability of false alarm increased the most for the (9, 3) hit/miss count threshold combination and the least for the (8, 3) combination. The probability of false alarm increase for the (9, 4) combination was between that for the (8, 3) and (9, 3) combination. However, the increase in false alarm probability is not significant enough to warrant recommendation of a particular hit/miss count threshold combination.

From TABLES 4-15 and 4-16, it is evident that the probability of target detection decreased the most for the (9, 3) hit/miss count threshold parameter combination and the least for the (9, 4) combination. For example, the probability of detection for an ASR-7 radar interfering with an ASR-8 and (9, 3) hit/miss count threshold combination decreased from 0.8892 to 0.7581 (14.7 percent decrease). On the other hand, for a (9, 4) hit/miss count threshold parameter combination, the probability of detection decreased from 0.9617 to 0.8816 (8.3 percent decrease). The target detection probability decreased for the (8, 3) hit/miss count threshold parameter combination from 0.9293 to 0.8223 represents a 11.5 percent decrease.

The reason that the (23, 9, 4) rank/hit/miss detection threshold parameter combination results in the probability of detection being less affected by interference than other parameter combinations can be seen from Figure 4-30. The graph indicates a linear scale plot of target detection probability versus target hit probability for various hit/miss count threshold parameter combinations. The tangential slope of the (9, 4) curve for a 0.7 target hit probability (value used as zero interference reference) is less than that for the (8, 3) and (9, 3) hit/miss parameter curves. This implies that a smaller reduction in probability of detection occurs on the (9, 4) curves, for a given reduction in probability of target hit due to interference, than for the (8, 3) and (9, 3) curves. In general the tangential slope of the (9, 4) curve is less than the (8, 3) and (9, 3) curve for target hit probabilities greater than 0.5. From Figures 4-17, 4-18, and 4-19, a 0.5 probability of target hit corresponds to a 4 dB signal-to-noise ratio for the ARTS-IIIA/RDAS connected to the normal (ASR-7 or ASR-8) and ASR-8 MTI channel, and 7.5 dB when connected to the ASR-7 MTI channel. Since typical signal-to-noise ratios are greater than these values, the (9,4) hit/miss count parameter combination will result in suppression of interference most of the time.

The previous analysis indicated that the (9, 4) hit/miss count threshold parameter combination yields a maximum probability of target detection with and without interference while yielding an acceptable probability of false alarm. It should be pointed out that the analysis was based on the MTI channel with uncorrelated noise and clutter. As discussed previously, the MTI hit count threshold is automatically varied from 9 to 20 depending on the degree of pulse-to-pulse clutter correlation. However, comparison of the

curves in Figure 4-30 for a given miss count threshold indicate that the interference suppression benefits of the (9, 4) hit/miss count threshold parameter combination should at least be realized over the lower hit count threshold values in the 9 to 20 range. If the tangential slope of the curve that represents the initial hit count threshold is low, the tangential slope of the curves which represent higher hit count thresholds will also be low.

FAA's NAFEC (National Aviation Facility Experimental Center) completed an evaluation of the ARTS-IIIA/RDAS performance at the end of 1978. Based on their measurements, they are recommending (23, 9, 3) rank/hit/miss detection threshold RDAS parameter settings for operational ARTS-IIIA's in the field.

Second Order Interference Effects

This section addresses the possible interference effects on the ARTS-IIIA/RDAS channel (normal or MTI) video select and MTI channel target hit count threshold controls. As discussed previously, the ARTS-IIIA/RDAS automatically selects normal radar channel video in zero or light clutter conditions, and MTI radar video in heavy clutter conditions. In addition, the MTI hit count threshold is adjusted to maintain a constant false alarm rate in pulse-to-pulse correlated clutter. The RDAS estimates the level of clutter by counting the normal channel isolated hits and the clutter correlation by counting the MTI channel isolated hits. An isolated clutter hit is defined as a clutter hit (logical 1) preceded and followed by a miss (logical 0) on adjacent ACP's.

Interference Effect on Clutter Hit Probability

A rank quantizer threshold of 17 is employed in the RDAS hit processing logic (see Figure 4-4) for generation of a clutter hit. This implies that the clutter level in the rank quantizer cell of interest must equal or exceed 17 or more of the 24 comparison range bins before a clutter hit is generated. Substituting 17 for RQT in Equation 4-5 gives a clutter hit probability of 0.32. Equation 4-6 can be used to determine the effect of interference on clutter hit probability by substituting 17 for RQT:

$$P_{11}(17) = \left\{0.68\left[N(1-e^{-X_1 v})-1\right]+1\right\} e^{-NX_{17} v} \qquad (4\text{-}20)$$

The variable X_{23} in Equation 4-6 was changed to X_{17} in Equation 4-20 to indicate that the equation is for a rank quantizer threshold of 17. The variable X_{17} in Equation 4-20 is given by:

$$X_{17} = \begin{cases} 0 & \text{for } \tau_1 \leq 6\ RB_w \\ 2(\tau_1 - RB_H) & \text{for } \tau_1 > 6\ RB_w \end{cases} \qquad (4\text{-}21)$$

where

τ_I = Interfering radar pulse width, in μs

RB_H = Victim radar range bin hold time (0.468 μs for ASR-7 and 0.300 μs for ASR-8)

RB_W = Victim radar range bin width (0.625 μs for ASR-7 and 0.467 μs for the ASR-8)

It is evident from Equation 4-21 that X_{17} is zero for an ASR-7 victim radar if the interfering radar pulse width is less than 3.75 μs. Similarly, X_{17} is zero for the ASR-8 as a victim radar if the interfering radar pulse width is less than 2.8 μs. The only radar considered in the analysis that has a pulse width greater than these two values is the WSR-57 (4.0 μs pulse width mode). Therefore, all interfering radars considered in the analysis have a zero X_{17} value except the WSR-57. From Equation 4-21, the value of X_{17} for the WSR-57 interfering with the ASR-7 is 7.064×10^{-6} and for the ASR-8, 7.40×10^{-6}. The variable X_1 in Equation 4-20 is independent of rank quantizer threshold and is given by Equation 4-2. The value of X_1 for various interfering and victim radar combinations is shown in TABLE 4-1. Equation 4-20 with appropriate values of X_1 and X_{17} substituted was used to compute the effect of interference on clutter hit probability for various interfering and victim radar combinations. The results of these calculations are shown in TABLE 4-17. The probability of clutter hit for normal and MTI channel are shown for three continually interfering radars of the same type. Therefore, a V value equal to three times the interfering radar PRF was used in Equation 4-20 for the calculations. A value of 3 for N was used in Equation 4-20 to compute MTI channel clutter hit probability and a value of 1 for normal channel clutter hit probability.

Interference Effect on Video Selection Control

The RDAS radar micro controller maintains a count of the normal channel isolated clutter hits in each 32 Range Bins (RB) by 32 Azimuth Change Pulse (ACP) zone, and compares this sum with a clutter map threshold (typically 166). If the Isolated Hit Sum (IHS) for the zone exceeds the map threshold, the clutter count parameter is incremented by 1. If the IHS for the zone is less than the clutter map threshold, the clutter count parameter is decremented by 1. Normal channel is selected if the clutter count parameter is less than or equal to 7; otherwise the MTI channel is selected.

The probability of a normal channel isolated clutter hit (010 hit/miss sequence) occurring is given by:

$$P_N(ICH) = P_{11}(1-P_{11})^2 \qquad (4\text{-}22)$$

TABLE 4-17

ARTS-IIIA/TOAS PROBABILITY OF CLUTTER HIT WHEN CONNECTED TO VICTIM RADAR THAT IS RECEIVING INTERFERENCE FROM THREE RADARS OF THE SAME TYPE

VICTIM RADAR	INTERFERING RADAR	INTERFERING PULSE ARRIVAL RATE (PULSES/SEC)	PROBABILITY OF CLUTTER HIT P_{cl} (NORMAL CHANNEL)	PROBABILITY OF CLUTTER HIT P_{cl} (MTI CHANNEL)
ASR-7	ASR-7	3006	0.32192	0.32575
ASR-7	ASR-8	3120	0.32160	0.32481
ASR-7	AN/CPN-4	3576	0.32159	0.32478
ASR-7	AN/FPS-90	1068	0.32156	0.32469
ASR-7	WSR-57	498	0.31888	0.31664
ASR-8	ASR-7	3006	0.32204	0.32612
ASR-8	ASR-8	3120	0.32162	0.32487
ASR-8	AN/CPN-4	3576	0.32162	0.32485
ASR-8	AN/FPS-90	1068	0.32000	0.32000
ASR-8	WSR-57	498	0.31882	0.31648

NOTE: PROBABILITY OF CLUTTER HIT WITHOUT INTERFERENCE = 0.32000

where P_{il} is the probability of a clutter hit caused by interference and defined by Equation 4-20. Each of the 1024 range-azimuth bins in the 32 RB by 32 ACP clutter zone has an isolated clutter hit probability given by Equation 4-22. The isolated hit sum for the zone is the sum of 1024 (32^2) binary random variables and therefore has a binomial distribution given by:

$$P_N(IHS=K) = \binom{1024}{K} [P_N(ICH)]^K [1-P_N(ICH)]^{1024-K} \qquad (4-23)$$

where K is the sum of isolated hits in the clutter zone. Substituting Equation 4-22 for $P_N(ICH)$ in Equation 4-23 gives:

$$P_N(IHS=K) = \binom{1024}{K} [P_{il}(1-P_{il})][1-P_{il}(1-P_{il})]^{1024-K} \qquad (4-24)$$

The probability of the zone IHS equaling or exceeding the clutter map threshold (166) and causing the clutter count parameter to be incremented by 1 is therefore given by:

$$P_{UP} = \sum_{K=166}^{1024} \binom{1024}{K} [P_{il}(1-P_{il})]^K [1-P_{il}(1-P_{il})]^{1024-K} \qquad (4-25)$$

The probability of the zone IHS being less than the clutter map threshold, and causing the clutter count parameter to be decremented by 1 is:

$$P_{DOWN} = \sum_{K=0}^{165} \binom{1024}{K} [P_{il}(1-P_{il})]^K [1-P_{il}(1-P_{il})]^{1024-K} \qquad (4-26)$$

Since the number of samples (1024) is large, $1024 \times [1-P_{il}(1-P_{il})] >> 5$, the binomial distribution can be closely approximated by a normal distribution with a standardized variable given by:

$$Z = \frac{IHS-\overline{IHS}_N}{\sigma_N} \qquad (4-27)$$

The symbol IHS is the mean isolated clutter hit sum for the binomial distribution and is given by:

$$\overline{IHS}_N = 1024[P_{11}(1-P_{11})^2] \tag{4-28}$$

The σ_N in Equation 4-27 is the standard deviation of the normal distribution and given by:

$$\sigma_N = 1024[P_{11}(1-P_{11})^2][1-P_{11}(1-P_{11})^2] \tag{4-29}$$

The approximation of Equations 4-25 and 4-26 by the normal distribution with standardized variable Z is:

$$P_{UP} = \frac{1}{\sqrt{2\pi}} \int_{Z_1}^{Z_2} e^{-Z^2/2} = ERF(Z_2)-ERF(Z_1) \tag{4-30}$$

$$P_{DOWN} = \frac{1}{\sqrt{2\pi}} \int_{0}^{Z_3} e^{-Z^2/2} dZ = ERF(Z_3) \tag{4-31}$$

where $Z_1 = (166-\overline{IHS}_N)/\sigma_N$, $Z_2 = (1024-\overline{IHS}_N)/\sigma_N$, and $Z_3 = (165-\overline{IHS}_N)/\sigma_N$. The ERF symbol in Equations 4-30 and 4-31 represents the mathematical error function associated with the normal distribution and can readily be evaluated from probability tables (Ng, 1977).

The maximum (0.32204) and minimum (0.31882) clutter hit probability for interference and clutter hit probability for no interference (0.3200) listed in TABLE 4-17 were related to the probability of clutter parameter change by Equations 4-30 through 4-31. The results of these calculations are shown in TABLE 4-18. The first two columns of the table describes the probability of clutter hits extracted from TABLE 4-17. The last four columns, from left to right, indicate the results of evaluating Equations 4-28, 4-29, 4-30, and 4-31. From the last two columns, it is evident that the difference in the

TABLE 4-18

ARTS-IIIA/RDAS PROBABILITY OF CLUTTER PARAMETER DECREMENT AND INCREMENT DUE TO INTERFERENCE EFFECT ON NORMAL CHANNEL CLUTTER HITS

TABLE 4-13 CLUTTER HIT CHARACTERISTICS	PROBABILITY OF NORMAL CHANNEL CLUTTER HIT (P_{11})	MEAN ISOLATED CLUTTER HIT SUM ($\overline{TES}_M$)	STD. DEV. OF ISOLATED CLUTTER HIT SUM (σ_S)	PROBABILITY OF CLUTTER PARAMETER DECREMENT (P_{DOWN})	PROBABILITY OF CLUTTER PARAMETER INCREMENT (P_{UP})
NO INTERFERENCE	0.32000	151.51923	11.36218	0.3830	0.6170
MAXIMUM DUE TO INTERFERENCE	0.32204	151.56879	11.36372	0.3810	0.6190
MINIMUM DUE TO INTERFERENCE	0.31882	151.48488	11.36112	0.3815	0.6185

TABLE 4-19

ARTS-IIIA/RDAS PROBABILITY OF MTI HIT COUNT THRESHOLD AND SLIDING WINDOW ISOLATED HIT SUM CHANGE DUE TO INTERFERENCE

TABLE 4-J CLUTTER HIT CHARACTERISTICS	PROBABILITY OF MTI CHANNEL CLUTTER HIT (P_{11})	MEAN ISOLATED CLUTTER HIT SUM ($\overline{THS}_M$)	STD. DEV. OF ISOLATED CLUTTER HIT SUM (σ_M)	PROBATILITY OF HIT COUNT THRESH. CHANGE BY 1 OR MORE	PROBARILITY OF ISOLATED HIT SUM CHANGE BY 1 OR MORE
NO INTERFERENCE	0.32000	96.97231	9.36958	———	———
MAXIMUM DUE TO INTERFERENCE	0.32617	97.05650	9.37322	$< 10^{-18}$	0.01351
MINIMUM DUE TO INTERFERENCE	0.31648	96.90109	9.36650	$< 10^{-18}$	0.01243

probability of a clutter parameter being changed (incremented or decremented) due to interference is no greater than 0.002. This implies that 500 antenna rotations would occur before a clutter parameter is changed in a particular clutter zone due to interference. It is therefore concluded that continuous interference from three radars would not have a significant degradation effect on automatic video selection control.

Interference Effect on MTI Channel Hit Count Threshold Control

The RDAS radar micro controller maintains a count of radar MTI channel isolated clutter hits in a sliding 32 RB by 32 ACP window. The MTI channel target hit count threshold is adjusted every ACP based on the current isolated hit count sum of the sliding window. The adjusted value of the MTI hit count threshold as a function of the sliding window isolated clutter hit sum is shown in Figure 4-7. Basically, the MTI hit count threshold is increased for high pulse-to-pulse correlation which is characterized by low isolated clutter hit sums.

The probability of a MTI channel isolated clutter hit (010 hit/miss sequence) occurring for correlated clutter can be derived using Discrete Time Markov Chain probability theory (Barnes, 1975). The resulting equation is given by:

$$P_M(ICH) = P_{i1}(1-P_{i1})^2(1-r)^2 \qquad (4-32)$$

where P_{i1} is the probability of a single clutter hit caused by interference, and defined by Equation 4-20. The symbol r in Equation 4-32 depicts the pulse-to-pulse correlation of the clutter. There is a probability of an isolated clutter hit occurring in each of the 1024 range-azimuth bins in the 32 RB by 32 ACP sliding window. Therefore, the isolated clutter hit sum for the sliding window is the sum of 1024 binary random variables, and is defined by the binomial distribution:

$$P_M(IHS=K) = \binom{1024}{K} [P_M(ICH)]^K [1-P_M(ICH)]^{1024-K} \qquad (4-33)$$

where K is the sum of the isolated hits in the sliding window. Substituting Equation 4-32 for $P_M(ICH)$ in Equation 4-33 gives

$$P_M(IHS=K) = \binom{1024}{K} [P_{i1}(1-P_{i1})^2(1-r)^2]^K [1-P_{i1}(1-P_{i1})^2(1-r)^2]^{1024-K} \qquad (4-34)$$

The mean isolated hit sum for the binomial distribution is:

$$\overline{IHS}_M = 1024[P_{i1}(1-P_{i1})^2(1-r)^2] \qquad (4\text{-}35)$$

and standard deviation:

$$\sigma_M = 1024[P_{i1}(1-P_{i1})^2(1-r)^2][1-P_{i1}(1-P_{i1})^2(1-r)^2] \qquad (4\text{-}36)$$

Since the number of trials (1024) is large, $1024 \times P_{i1}(1-P_{i1})^2(1-r)^2 >> 5$, and $1024 \times [1-P_{i1}(1-P_{i1})^2(1-r)^2] >> 5$, the binomial distribution can be approximated by a normal distribution.

The normal distribution approximation to the binomial distribution can be employed to determine the probability of interference increasing the IHS by a sufficient amount to result in a MTI hit count threshold change. If IHS_i and IHS_o represent sample sliding window isolated hit sums with and without interference, respectively, the distribution of their difference can be closely approximated by a normal distribution. This is possible because the IHS_i and IHS_o samples are normally distributed and their population standard deviations are known exactly (computed from Equation 4-36). The standard variable for the normal distribution which describes the IHS sample difference is given by (Natrella, 1963):

$$Z = \frac{(IHS_i - IHS_o) - (\overline{IHS}_{Mi} - \overline{IHS}_{Mo})}{\frac{1}{N}(\sigma_{Mi}^2 + \sigma_{Mo}^2)^{1/2}} \qquad (4\text{-}37)$$

where

IHS_i = the sample isolated hit sum with interference

IHS_o = the sample isolated hit sum mean without interference

IHS_{Mi} = the actual isolated hit sum mean with interference computed from Equation 4-35

IHS_{Mo} = the actual isolated hit sum mean without interference computed by Equation 4-35

σ_{MI} = the actual isolated hit sum standard deviation with interference computed by Equation 4-36

σ_{Mo} = the actual isolated hit sum standard deviation without interference computed by Equation 4-36

N = the number of samples (1024 in this analysis)

The probability of the difference, between the isolated hit sum with and without interference, exceeding a particular value Z is given by the integral:

$$P(\Delta IHS > Z_1) = \frac{1}{\sqrt{2\pi}} \int_{Z_1}^{\infty} e^{-Z^2/2}\, dZ = 0.5 - ERF(Z_1) \qquad (4\text{-}38)$$

where

Δ IHS = difference between isolated hit sums in sliding window ($IHS_i - IHS_o$) with and without interference

ERF(Z) = mathematical error function that can be readily evaluated from probability tables

Z_1 = value of standard normal variable (Z) from evaluation of Equation 4-37

Similarly, the probability of the difference (ΔIHS) being less than a particular value Z_2 is given by:

$$P(\Delta IHS < Z_2) = \frac{1}{\sqrt{2\pi}} \int_{-\infty}^{Z_2} e^{-Z^2/2}\, dZ = 0.5 + ERF(Z_2) \qquad (4\text{-}39)$$

The maximum (0.32617) and minimum (0.31648) clutter hit probability for interference and clutter hit probability for no interference (listed in TABLE 4-17 for the MTI channel) were related to the mean and standard deviation of the isolated clutter hit sum by Equations 4-35 and 4-36. The results of these calculations are indicated in the third and fourth columns of TABLE 4-19. A clutter correlation coefficient (r) of 0.2 was assumed for the calculation because this value gives a typical isolated hit sum of 96.97 (see Figure 4-7). The probability of worst-case interference increasing the

isolated hit sum enough to cause a hit count threshold decrease was computed from Equations 4-37 and 4-38, and the result is indicated in TABLE 4-19 (second row, fifth column). The isolated hit sum mean and standard deviation listed in the third and fourth columns of TABLE 4-19 were used in this calculation. In particular, the mean and standard deviation associated with no interference and maximum clutter hit probabilities due to interference, were used to calculate Z_1 in Equation 4-37. This combination resulted in the greatest (worst-case) probability of interference decreasing the MTI hit count threshold.

The probability of worst-case interference decreasing the isolated hit sum enough to cause a hit count threshold increase was computed from Equations 4-37 and 4-39, and the result is indicated in the bottom of the fifth column of TABLE 4-19. The isolated hit sum statistical parameters (mean and standard deviation listed in columns three and four of TABLE 4-19) that correspond to no interference, and minimum clutter hit probabilities due to interference, were used to calculate Z in Equation 4-37. This combination of values resulted in the greatest (worst-case) probability of interference increasing the MTI hit count thereshold.

An isolated hit sum difference (IHS_1-IHS_0) value of 5.333 was used in the above calculations (Equation 4-37) to represent a MTI channel hit count threshold change of 1. It is evident from Figure 4-7 that the MTI hit count threshold changes by 1 for each sliding window isolated hit sum change of 10.66. However, it is likely that the hit sum sample value without interference is closer to the point required for a hit count threshold change than 10.66. For this reason, a median value of 5.333 was chosen for the analysis.

The probability of interference causing the sliding window isolated hit sum to change by 1 was also computed from Equations 4-35, 4-36, 4-37, 4-38, and 4-39 by setting (IHS_1-IHS_0) in Equation 4-37 to 1. The results of these calculations are indicated in the last column of TABLE 4-19. It is evident from the above probability calculations and TABLE 4-19 that continual interference from three radars will not have a significant degradation effect on RDAS automatic MTI hit count threshold control. The probability of interference causing the MTI hit count threshold to change by 1 or more is less then 10^{-18}. In addition, the probability of interference causing the sliding window isolated hit sum count to change by only 1 or more is less than 0.01243.

APPENDIX A

MIXER TRANSFER PROPERTIES

INTRODUCTION

The RF to IF conversion of received signals in radars is accomplished by the radar mixer which mixes the stable local oscillator (STALO) output signal with the amplified RF received signal. Figure A-1 shows a simplified block diagram of a radar mixer. The following is a discussion of the Noise, Signal-to-Noise (SNR), and Interference-to-Noise (INR) transfer properties of a typical radar mixer.

MIXER TRANSFER PROPERTIES

The radar STALO signal time waveform, $v_s(t)$, can be expressed as:

$$v_s(t) = \cos\left[(\omega_0 + \beta_0)\tau + \phi_s\right] \qquad (A\text{-}1)$$

where:

β_0 = Receiver tuned IF frequency, in radians per second

ϕ_s = Phase of STALO signal

Assuming linear transfer properties for a radar mixer, the noise and signal can be treated separately.

Noise

To calculate N_{mi} and N_{mo}, the noise power at the input and output of the mixer, the bandpass noise model is used, and the mixer input noise signal, $n_{mi}(t)$, is given by:

$$n_{mi}(t) = n_c(t)\cos\omega_0 t + n_s(t)\sin\omega_0 t \qquad (A\text{-}2)$$

Where $n_{mi}(t)$ is the RF bandpass noise at the input of the mixer, and the mixer input noise power (mean square of $n_{mi}(t)$ is given by:

$$N_{mi} = \overline{n_{mi}^2(t)} \qquad (A\text{-}3)$$

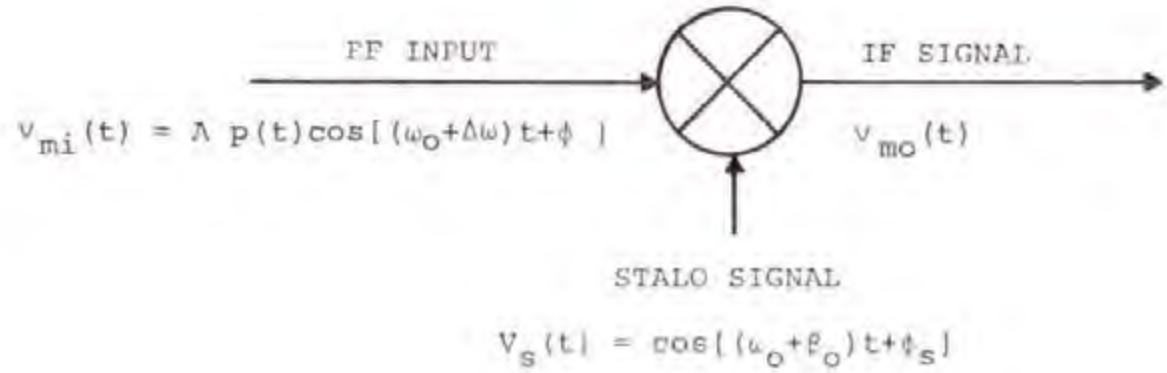

Figure A-1. Radar Mixer Block Diagram

Generally, the STALO signal power level is greater than 0 dBm. Therefore, the mixer noise figure (conversion loss) is very small and can be neglected. Also, the STALO signal is usually filtered and the noise suppressed, thus permitting the STALO signal noise level to be neglected.

If $n_{mi}(t)$ is applied at the input of the mixer (which multiplies the incoming noise signal, $n_{mi}(t)$ by $v_s(t)$, then $n_{mo}(t)$, the output noise of the mixer, is given by:

$$n_{mo}(t) = n_c(t) \cos \omega_o t \cdot \cos [(\omega_o + \beta_o)t + \phi_s] + n_s(t) \sin \omega_o t \cdot \cos [(\omega_o + \beta_o)t + \phi_s] \quad (A\text{-}4a)$$

$$= \frac{n_c(t)}{2} [\cos[(2\omega_o + \beta_o)t + \phi_s] + \cos [\beta_o t + \phi_s]] + \frac{n_s(t)}{2} [\sin[(2\omega_o + \beta_o)t + \phi_s] - \sin[\beta_o t + \phi_s]] \quad (A\text{-}4b)$$

The terms $\cos [(2\omega_o+\beta_o)t+\phi_s]$ and $\sin [(2\omega_o+\beta_o)t+\phi_s]$ represents the spectra of $n_c(t)$ and $n_s(t)$, respectively, shifted at $(2\omega_o \pm \beta_o)$ and are filtered out by the IF filter at the mixer output. Hence, $n_{mo}(t)$ is given by:

$$n_{mo}(t) = \frac{n_c(t)}{2} \cos (\beta_o t + \phi_s) - \frac{n_s(t)}{2} \sin (\beta_o t + \phi_s) \quad (A\text{-}5)$$

The mixer output noise power (mean square of $n_{mo}(t)$ can be related to the mixer input noise power, Equation A-3, and the mixer noise power transfer properties expressed as:

$$N_{mo} = \overline{n_{mo}^2(t)} = \overline{\tfrac{1}{2} n_{mi}^2(t)} \quad (A\text{-}6a)$$

$$= \tfrac{1}{2} N_{mi} \quad (A\text{-}6b)$$

Desired/Interfering Signal

The desired and interfering signal voltage waveform at the mixer input, $v_{mi}(t)$, can be expressed as:

$$v_{mi}(t) = Ap(t) \cos [(\omega_o + \Delta\omega)t + \phi] \quad (A\text{-}7)$$

where:

A = Signal voltage amplitude

$p(t)$ = Signal amplitude modulation, value between 0 and 1

ω_o = Receiver tuned RF frequency, in radians per second

$\Delta\omega$ = Frequency separation between interfering signal carrier frequency and receiver tuned frequency ($\Delta\omega$ = 0 for desired signal), in radians per second

ϕ = Phase of signal

Since we are only concerned with the peak power of the desired or interfering signal, $p(t)$ equals 1, and the signal power at the input to the mixer (the mean square of $v_{mi}(t)$ is:

$$S_{mi} = \overline{v_{mi}^2(t)} = \frac{A^2}{2} \qquad (A\text{-}8)$$

The signal voltage time waveform at the mixer output, $v_{mo}(t)$, can be found by performing the operation shown in Figure A-1 and is given by:

$$v_{mo}(t) = v_{mi}(t) \cdot v_s(t) \qquad (A\text{-}9a)$$

$$= A \cos[(\omega_o + \Delta\omega)t + \phi] \cdot \cos[(\omega_o + \beta_o)t + \phi_s] \qquad (A\text{-}9b)$$

$$= \frac{A}{2}[\cos[(2\omega_o + \Delta\omega + \beta_o)t + \phi + \phi_s] + \cos[(\beta_o - \Delta\omega)t + \phi_s - \phi]] \qquad (A\text{-}9c)$$

The first term of Equation A-9c is filtered out by the IF filter, resulting in a signal with a frequency $(\beta_o - \Delta\omega)$ where $\Delta\omega$ = 0 for the desired signal, and a mixer output power (the mean square of $v_{mo}(t)$ of:

$$S_{mo} = \overline{v_{mo}^2(t)} = \frac{A^2}{8} \qquad (A\text{-}10a)$$

$$= \tfrac{1}{4} S_{mi} \qquad (A\text{-}10b)$$

Therefore, the signal peak power is reduced 6 dB by the mixer.

SNR Transfer Properties

Using Equations A-6b and A-10b, the mixer signal-to-noise (SNR) transfer properties of the mixer are given by:

$$SNR_{mo} = SNR_{mi} \qquad (A\text{-}11)$$

Therefore, the SNR at the mixer output is equal to the SNR at the mixer input. Equation A-11 is also applicable to the interference-to-noise (INR) transfer properties of the mixer.

IMAGE RESPONSE

For the case when the interfering signal frequency separation, $\Delta\omega$, is equal to $2\beta_0$, the interfering signal frequency at the mixer output will equal the IF tuned frequency. However, in most radars in the 2.7 to 2.9 GHz band, the preselector filter attenuates the interfering signal image response by approximately 50 to 60 dB.

APPENDIX B

IF FILTER TRANSFER PROPERTIES

INTRODUCTION

The interfering signal peak power level and time waveform at the radar receiver IF output is a function of the interfering signal emission spectrum, victim receiver IF selectivity characteristics, and the frequency separation between the interfering and victim radars. This appendix discusses the techniques and models used to compute the victim radar receiver IF selectivity characteristics, Frequency-Dependent-Rejection (FDR), interfering signal IF output time waveform, receiver equivalent noise level, and IF filter interference-to-noise ratio (INR) transfer properties.

IF SELECTIVITY

Since a victim radar receiver's IF selectivity characteristic is the principal means by which the receiver discriminates against undesired signals, the receiver's IF selectivity characteristic is required to determine a receiver's Frequency-Dependent-Rejection (FDR) of an undesired signal and IF output undesired signal time waveform.

Receiver spurious responses must also be considered when determining the FDR of a victim radar to an undesired signal. Spurious responses occur when the undesired signal is at a frequency such that it mixes with the local oscillator to produce an output at the receiver IF frequency. Since most radars have relatively clean local oscillator signals or employ balanced mixers, only image responses were investigated. The local oscillator frequency of most radars are tuned to 30 MHz above the receiver RF tuned frequencies in order to obtain an IF frequency of 30 MHz. An RF undesired signal that is 30 MHz above the local oscillator frequency (60 MHz above RF receiver center tuned frequency) will also be down-converted to the 30 MHz IF frequency. Modern radars normally employ an image-rejection mixer or a notch filter at the radar input to suppress image responses. The image response of the AN/CPN-4 and AN/MPN-13 radars are generally only 15 dB down from their center-tuned response, the ASR-4 through ASR-8 have an image response greater than 50 dB down. Reduced FDR due to receiver image response was not incorporated in the FDR model, but was considered in an independent FDR calculation.

The selectivity of a receiver is the composite selectivity of all the tuned circuitry in the receiver prior to detection; however, in a superheterodyne receiver, the selectivity is determined by the IF stages because the preceding mixer and RF circuits are relatively broader band. This is because the required filter characteristics are more physically realizable and less expensive to build at the lower IF frequency.

IF Selectivity Modeling

The radars in the 2.7 to 2.9 GHz band generally employ a combination of synchronously-tuned, staggered-tuned doublet, and stagger-tuned triplet stages of IF amplification. Figure B-1 shows a few stages of the ASR-8 normal channel IF amplifier. Neglecting the bias resistors, since they are usually larger than the source resistor, and also the coupling and bypass capacitors, the equivalent "Y" parameter circuit for one ASR-8 normal channel IF amplifier stage is shown in Figure B-2.

The gain of the equivalent circuit shown in Figure B-2 is:

$$A = \frac{V_2}{V_1} = \frac{Y_{fe}}{Y_{oe}+G+G'} \qquad \text{(B-1)}$$

Where: $Y_{oe} = g_{oe} + j\beta C_{oe}$

Letting: $C = C_{oe} + C_1$

The equivalent impedance of the parallel combination of capacitor ($-j/\beta C$) and inductor ($R+j\beta L$) can be expressed as:

$$Z' = \frac{\frac{L}{C}\left(1 - j\,\frac{R}{\beta L}\right)}{R\left[1 + j\,\frac{\beta L}{R}\left(1 - \frac{1}{\beta^2 LC}\right)\right]} \qquad \text{(B-2)}$$

Letting: $\beta_o = 1/\sqrt{LC}$ (B-3)

$$\delta = \frac{\beta}{\beta_o} - 1 = \frac{F - F_o}{F_o} \qquad \text{(B-4)}$$

$$Q = \frac{\beta_o L}{R} = \frac{1}{\beta_o CR} \qquad \text{(B-5)}$$

Where: β_o = Receiver tuned IF frequency, in radians per second

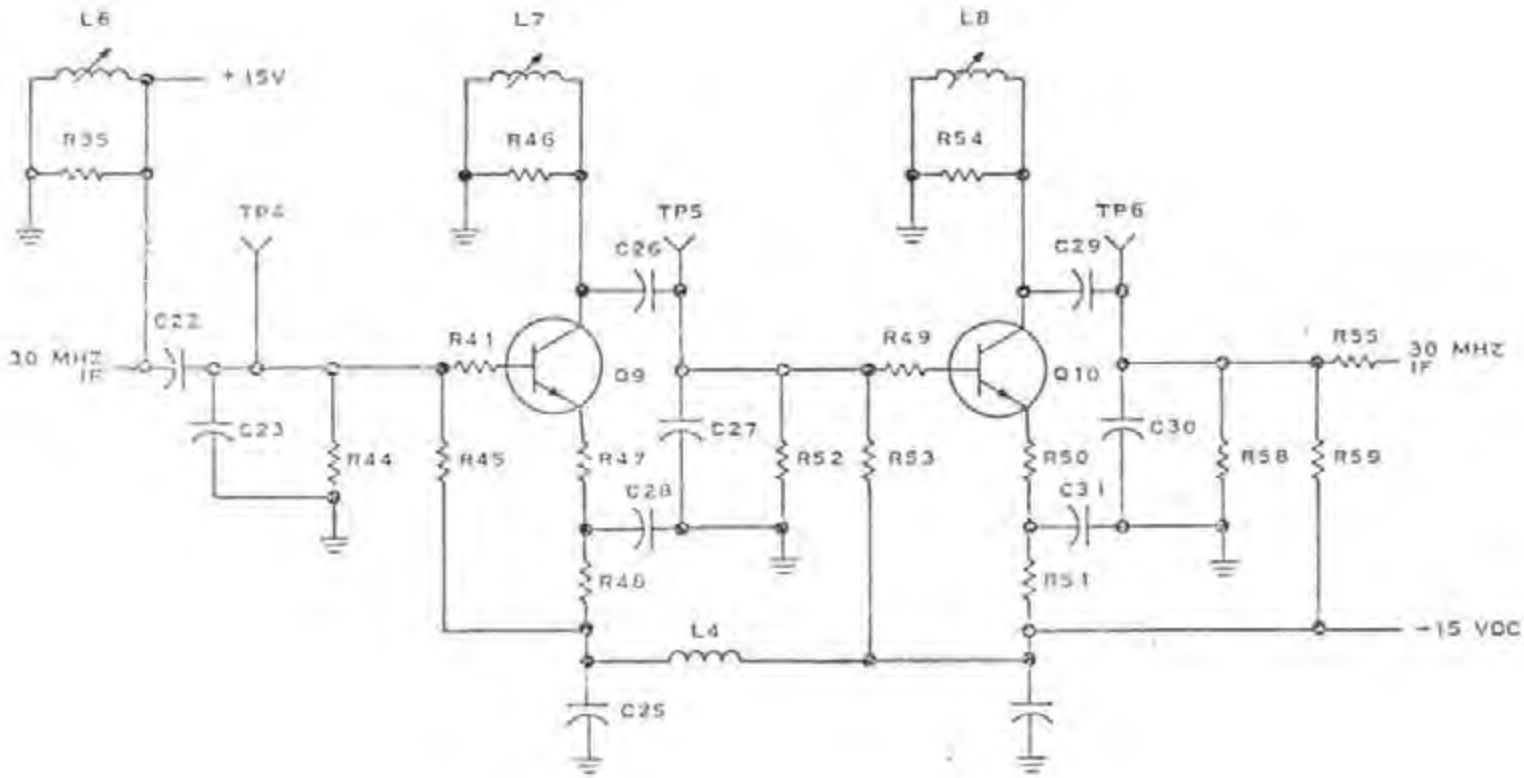

Figure B-1. ASR-8 Normal IF Bandpass Filter Schematic

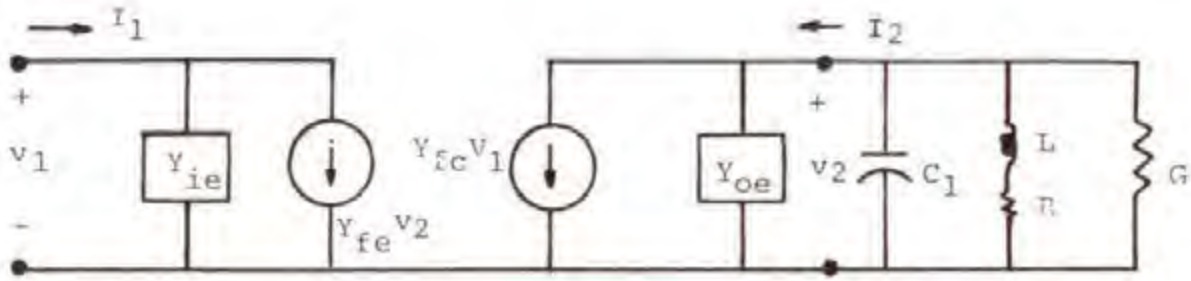

Figure B-2. "Y" Parameter Equivalent Circuit for One IF Amplifier Stage Shown in Figure B-1.

Using Equations B-3 through B-5, Equation B-2 becomes:

$$Z' = \frac{RQ^2 \left(1 - j\frac{1}{Q}\frac{\beta_o}{\beta}\right)}{1 + jQ\left(\frac{\beta}{\beta_o} - \frac{\beta_o}{\beta}\right)} \qquad \text{(B-6a)}$$

$$= RQ^2 \left[\frac{(1 + \delta) - j(1/Q)}{(1 + \delta) + jQ\delta(2 + \delta)}\right] \qquad \text{(B-6b)}$$

At resonance $\beta = \beta_o$, and $\delta = 0$, then

$$Z' = RQ^2 \left(1 - j\frac{1}{Q}\right) \qquad \text{(B-7)}$$

Since the Q for the circuit used is usually high, $Q \geq 10$, then with good approximation

$$Z' = RQ^2 \qquad \text{(B-8)}$$

Therefore, the gain at resonance combining Equations B-1 and B-8 is:

$$A_{RES} = \frac{Y_{fe}}{g_{oe} + G + \frac{1}{RQ^2}} \qquad \text{(B-9a)}$$

$$A_{RES} \quad \frac{-Y_{fe}\,\beta_o LQ}{\beta_o LQg_{oe} + \beta_o LQG + 1} \qquad \text{(B-9b)}$$

Equation B-9b may be written as:

$$A_{RES} = -Y_{fe}\,\beta_o LQ_e \qquad \text{(B-10)}$$

Where Q_e, the effective "Q" of the amplifier, is:

$$Q_e = \frac{Q}{1 + \beta_o LQg_{oe} + \beta_o LQG} \qquad \text{(B-11a)}$$

$$= \frac{F_o}{B_s} \qquad \text{(B-11b)}$$

Where: B_s = The amplifier stage 3 dB bandwidth, in Hz

The impedance, Z', of the single-tuned amplifier at some off-tuned frequency, B, where $B = B_0$ and δ is small is:

$$Z' = \frac{RQ^2}{1 + j2\delta Q} \qquad (B-12)$$

Therefore, the off-tuned gain is:

$$A = \frac{-Y_{fe}}{g_{oe} + G + \dfrac{1 + j2\delta Q}{RLQ^2}} \qquad (B-13)$$

$$= \frac{-Y_{fe}B_0{}^2LQ_e}{1 + j2\delta Q} \qquad (B-13a)$$

Thus the gain ratio can be obtained from Equations B-10 and B-13a as:

$$\frac{A}{A_{RES}} = A(F) = \frac{1}{1 + j2\delta Q} \qquad (B-14)$$

For "m" cascaded synchronous single-tuned stages, the gain ratio becomes:

$$A(F) = \frac{1}{[1 + j2\delta Q]^m} \qquad (B-15)$$

The gain ratio for a single-tune stage using an electron tube is identical to Equation B-14, and is derived by Seeley (1958).

The IF bandwidth of "m" cascaded synchronous-tuned stages is given by:

$$B_{IF} = B_S \sqrt{2^{1/m} - 1} \qquad (B-16)$$

Where: B_{IF} = Receiver IF 3 dB bandwidth, in Hz

Substituting Equations B-4 and B-11a into Equation B-14, the amplitude characteristic in dB form of a single-tuned stage is:

$$A_{dB}(F) = -20 \log_{10}(1 + X^2)^{1/2} \qquad (B-17)$$

Where:

$$X = \frac{2(F - F_0)}{B_S} \qquad (B-18)$$

The IF selectivity characteristics, $A_{dB}(F)$ for "m" cascaded synchronous single-tuned stages is given by:

$$A_{dB}(F) = -20 \log_{10}(1 + X^2)^{m/2} \quad \text{(B-19)}$$

For "m" cascaded amplifiers consisting of "n" staggered-tuned stages, the IF filter amplitude characteristics are given by Seeley (1958).

$$A_{dB}(F) = -20 \log_{10}(1 + X^{2n})^{m/2} \quad \text{(B-20)}$$

RECEIVER FREQUENCY-DEPENDENT-REJECTION CHARACTERISTICS

A necessary component in predicting radar to radar interference is the victim radar receiver's Frequency Dependent Rejection (FDR) characteristic to cochannel and adjacent channel undesired signals. The victim receiver's IF selectivity characteristic and undesired signal emission spectrum characteristic determine the victim receiver's rejection (peak power loss) of the undesired signal which is dependent on the frequency separation (ΔF) between the victim receiver RF tuned frequency (ω_o), and the undesired signal RF carrier frequency. The following is a discussion of the technique and model used to determine a radar receiver's FDR of an undesired signal.

FDR Model

FDR is the sum of attenuation of the undesired signal due to Off-Frequency Rejection (OFR) and the On-Tune Rejection (OTR) in dB.

$$FDR(dB) = OFR(dB) + OTR(dB) \quad \text{(B-21)}$$

Off-Frequency Rejection (OFR) is defined by Fleck (1967) as:

$$OFR = \frac{\int \frac{P(F)}{A(F + \Delta F)} \, dF}{\int \frac{P(F)}{A(F)} \, dF} \quad \text{(B-22)}$$

Where:

P(F) = Transmitter relative power density

A(F) = Relative receiver selectivity

ΔF = Frequency separation between interfering signal carrier frequency and receiver tuned frequency, in Hz

Absolute transmitter power and receiver sensitivity does not enter into the calculation because FDR depends only on the shape of the victim receiver IF

selectivity and undesired signal emission spectrum.

Since the undesired signal emission spectrum and victim receiver selectivity curves are usually given in dB units, a more practical form of Equation B-22 in dB is:

$$OFR = 10 \log \int 10^{[P_{dB}(F) - A_{dB}(F + \Delta F)]/10} dF - 10 \log \int 10^{[P_{dB}(F) - A_{dB}(F)]/10} dF \qquad (B\text{-}23)$$

Where:

$P_{dB}(F)$ = Emission spectrum, in dB

$A_{dB}(F)$ = Receiver IF selectivity curve, from Equations B-17 through B-20, in dB.

Approximations to Equation B-23 can be obtained using the following equations (Newhouse):

$$\text{Case I, } TB_{IF} > 1 \text{ and } \Delta F = \text{any value}$$

$$OFR = 20 \log TB_{IF} + (F_{\Delta F}) \qquad (B\text{-}24)$$

$$\text{Case II, } TB_{IF} > 1 \text{ and } \Delta F \leq \frac{1}{\pi\tau} + \frac{B_{IF}}{2}$$

$$OFR = 0 \text{ dB} \qquad (B\text{-}25)$$

$$\text{Case III, } TB_{IF} > 1 \text{ and } \Delta F > \frac{1}{\pi\tau} + \frac{B_{IF}}{2}$$

$$OFR = 20 \log TB_{IF} + (F_{\Delta F}) - 6_{dB} \qquad (B\text{-}26)$$

Where:

τ = Interfering signal pulsewidth, in seconds

$F_{\Delta F}$ = Interfering signal emission spectrum level relative to fundamental frequency, in dB.

The victim receiver On-Tuned Rejection (OTR) factor is derived by White

(1972). In summary, the OTR factor can be obtained by considering the Laplace transforms of a single pulse of amplitude "A" and width T:

$$\mathcal{L}\begin{bmatrix}\text{SINGLE}\\ \text{PULSE}\end{bmatrix} = AT\left(\frac{\sin \pi FT}{\pi FT}\right)e^{-j\pi FT} \qquad (B\text{-}27)$$

Where the Laplace transform parameter, s, has been replaced by $j2\pi F$. The phase given by the exponential factor indicates that when the receiver bandwidth B_{IF} is less than the emission bandwidth $B_T = 1/\tau$, the phase variation over the receiver bandwidth is small. This means that the voltage must be summed first and then squared instead of summing the square of the voltages as many documents imply. For a relatively constant emission spectrum over the IF pass band, the received peak power is therefore proportional to the ratio of the receiver to transmitter bandwidths and the OTR factor in dB is given by:

$$OTR = \begin{cases} 20 \log_{10} B_{IF}/B_T & B_{IF} < B_T \\ 0 & B_{IF} > B_T \end{cases} \qquad (B\text{-}28)$$

Where:

B_{IF} = Receiver IF 3 dB bandwidth, in Hz

B_T = Emission 3 dB bandwidth, in Hz

IF OUTPUT TIME WAVEFORM

The following analysis considers the tranformation of pulsed signals through an effective linear IF filter. In general, the IF amplifier output for a pulsed input signal can be expressed as the sum of a steady state term and a transient term. The transient term represents a distortion term and includes the amplitude and phase modulation produced in the IF amplifier. The transient term arises because the system response is unable to build up and decay as fast as the input signal.

It is necessary to have an IF filter model to predict these transient and steady state terms. One method of modeling the IF filter function is in terms of cascaded tuned amplifiers. Both single-tuned and stagger-tuned amplifiers are used in radar receivers. For this analysis, eight cascaded single-tuned amplifier stages were used to model the radar receiver IF filter characteristics. The transfer function for eight cascaded synchronous tuned amplifiers is given by Equation B-15 as:

$$A(F) = \frac{1}{[1 + j2\delta Q]^8} \qquad (B\text{-}29)$$

If the IF filter has an impulse response a(t), the IF filter output response to an input signal, x(τ), is given by the convolution integral:

$$h(t) = \int_{-\infty}^{\infty} x(T)a(t-T)dT \qquad \text{(B-30)}$$

Since convolution in the time domain is equivalent to multiplication in the frequency domain, it will be more convenient to use the frequency domain expressions. If the input signal, x(τ), has a Fourier transform, X(F), and the transfer function of the IF filter is A(F), then the output spectrum is given by:

$$H(F) = X(F)A(F) \qquad \text{(B-31)}$$

The interfering signal spectrum for a periodic trapezoidal pulse is given by Meyers (1971).

$$X(F) = \frac{1}{T d \pi^2 \tau F_x^2} \sin\left[\pi \tau F_x (1 + d)\right] \sin\left(\pi \tau d F_x\right) \qquad \text{(B-32)}$$

Where:

T = Radar pulse period, 1/PRF

τ = Interfering signal pulse width, in seconds

d = Rise time/τ = Fall time/ τ

$F_x = F_o - \Delta F$

The interfering signal output spectrum H(F), after being band limited by the IF filter, is the product of the filter transfer function and the pulse spectrum. The inverse Fourier Transform of H(F) will be the IF filter output time waveform h(t). For modeling purposes, the carrier frequency can, without loss of generality, be assigned the value of the center frequency, β_o, of the IF filter. The interfering signal at the IF output can then be expressed as:

$$v_{IFo}(t) = B p(t') \cos[\beta_o t + \phi_o + \phi(t')] \qquad \text{(B-33)}$$

Where:

B = Interfering signal voltage amplitude

p(t') = Interfering signal amplitude modulation after IF filtering, value between 0 and 1

ϕ_o = Interfering signal carrier phase angle

t' = t - t_o where t_o is the delay time of the IF

filter

$\phi(t')$ = Interfering signal phase modulation after IF filtering

Typical IF filter bandwidths of radars in the 2.7 to 2.9 GHz band are 1.2 MHz to 5.0 MHz. The following is a discussion of the IF output time waveform as a function of the interfering signal pulsewidth, τ, and off-tuning (ΔF). The simulated output time waveforms were obtained using the RWS Model, Meyers (1971).

When the pulse bandwidth is much greater than the bandwidth of the IF filter, $\tau B_{IF} \ll 1$, the spectrum of the pulse within the IF passband for the on-tune, $\Delta F = 0$, case is approximately flat and has even symmetry about the carrier frequency. The Fourier transform of the resulting spectrum will approximate the impulse response of the network with some ringing on the trailing edge. The output time waveform will be much longer than the input pulse time waveform with the peak amplitude of the output pulse reduced approximately by the ratio of the pulse bandwidth to the filter bandwidth. Since the bandwidth of the pulse is much greater than the IF bandwidth, the shape of the spectrum within the IF passband as the pulse is off-tuned will be approximately the same except near the nulls of the input spectrum. Therefore, as the pulse spectrum is off-tuned the IF output time waveform will remain approximately the same as the on-tune case with the inband power determining the peak level of the output pulse. In the vicinity of the null point the spectrum will no longer be flat and it will approach odd symmetry when centered about the null point. The Fourier transform of an unsymmetrical spectrum will produce both amplitude and phase modulation as shown in Equation B-33. Simulated IF output time waveforms for an IF bandwidth of 1.2 MHz and a 5 μs pulse ($\tau B_{IF} \ll 1$) for ΔF = 0, 5.0 MHz and 20.0 MHz off-tune are shown in Figures B-3, B-4 and B-5. The input pulse of width τ and unity amplitude is assumed to be symmetrical about time t = 0. This is true for all pulses discussed in this section.

When the pulse bandwidth is approximately equal to the IF bandwidth $\tau B_{IF} = 1$, the spectrum of the pulse within the IF passband for the on-tune, $\Delta F = 0$, case will be symmetrical and even. The sidelobes will be attenuated by the filter function causing a more rapid fall-off of the pulse spectrum. The Fourier transform of the resulting spectrum will approximate the impulse response, with the amount of energy within the passband again determining the peak level of the output pulse. As the pulse is off-tuned the pulse spectrum out of the IF filter will be unsymmetrical, thereby producing both amplitude and phase modulation as shown in Equation B-33. The Fourier transform of the output pulse spectrum produces time waveforms that appear to contain a separate response for the leading and trailing edge of the IF input pulse. As the off-tuning is increased the double response becomes more pronounced due to the attenuation of the steady state portion of the pulse by the filter characteristics. Simulated IF output time waveforms for an IF bandwidth of 2.7 MHz and a .83 μs pulse for ($\tau B_{IF} = 1$) for ΔF = 0, 5.0 MHz and 20.0 MHz are shown in Figures B-6, B-7, and B-8, respectively.

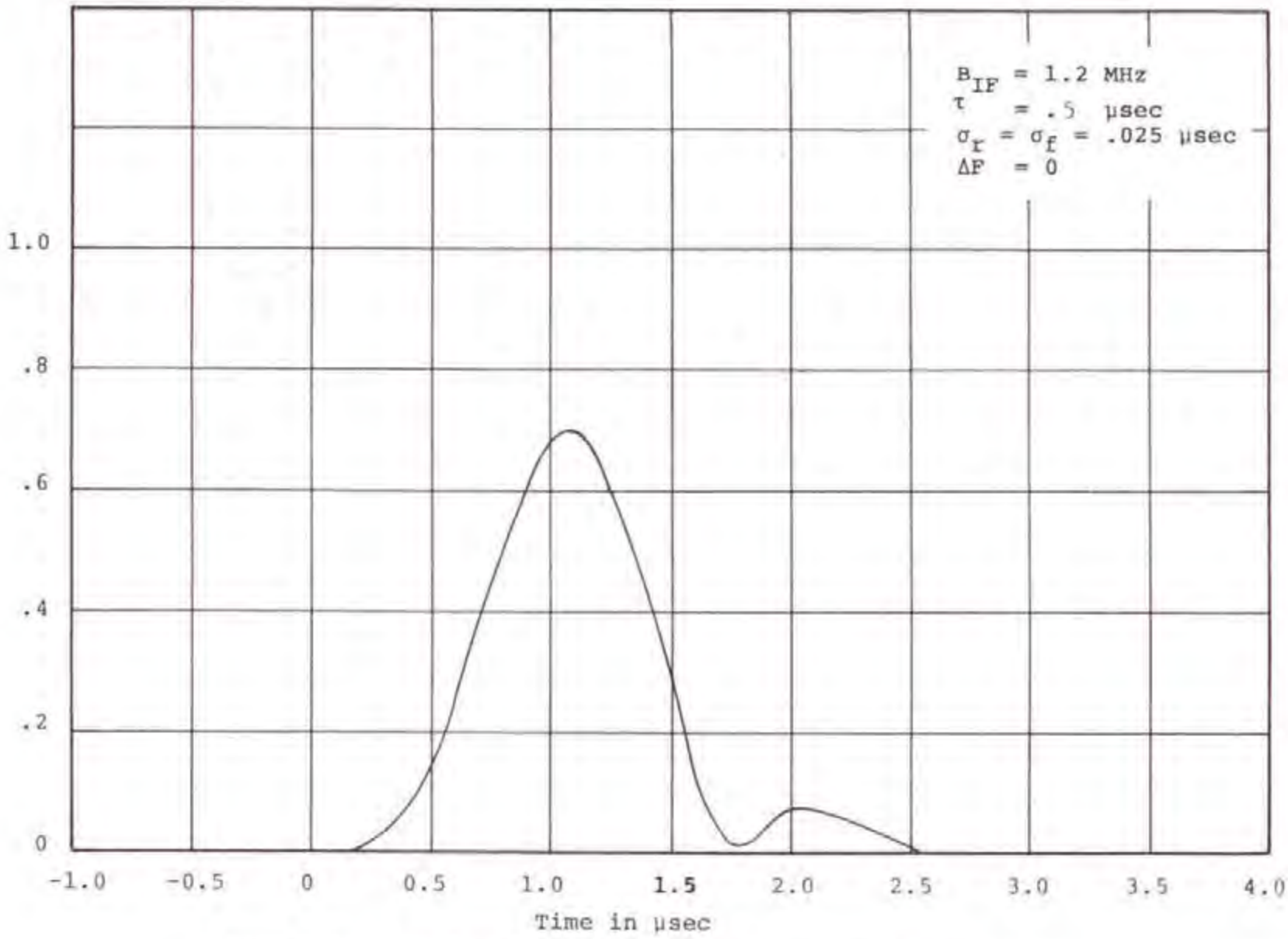

Figure B-3. Simulated IF Output Time Waveform Envelope

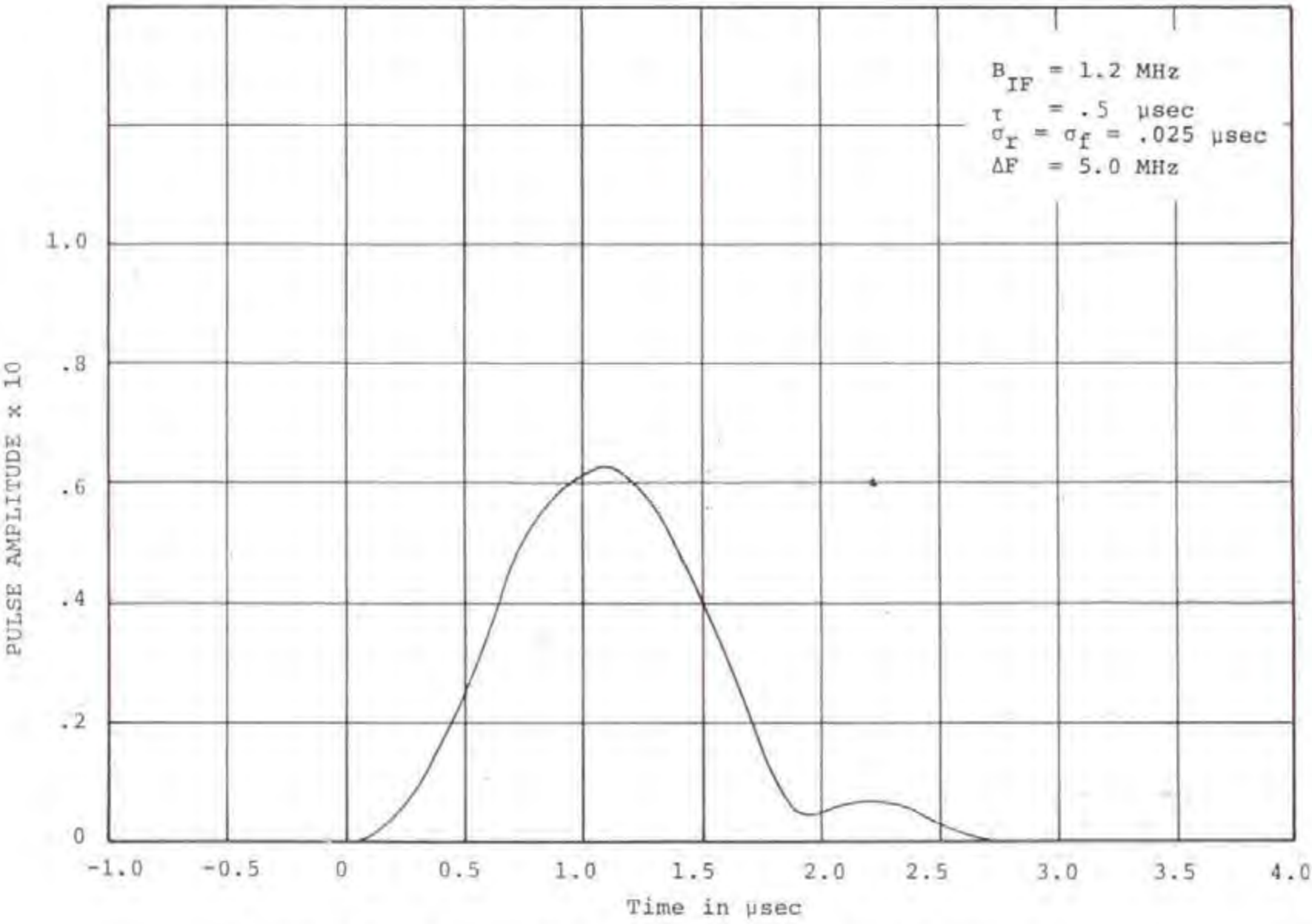

Figure B-4. Simulated IF Output Time Waveform Envelope

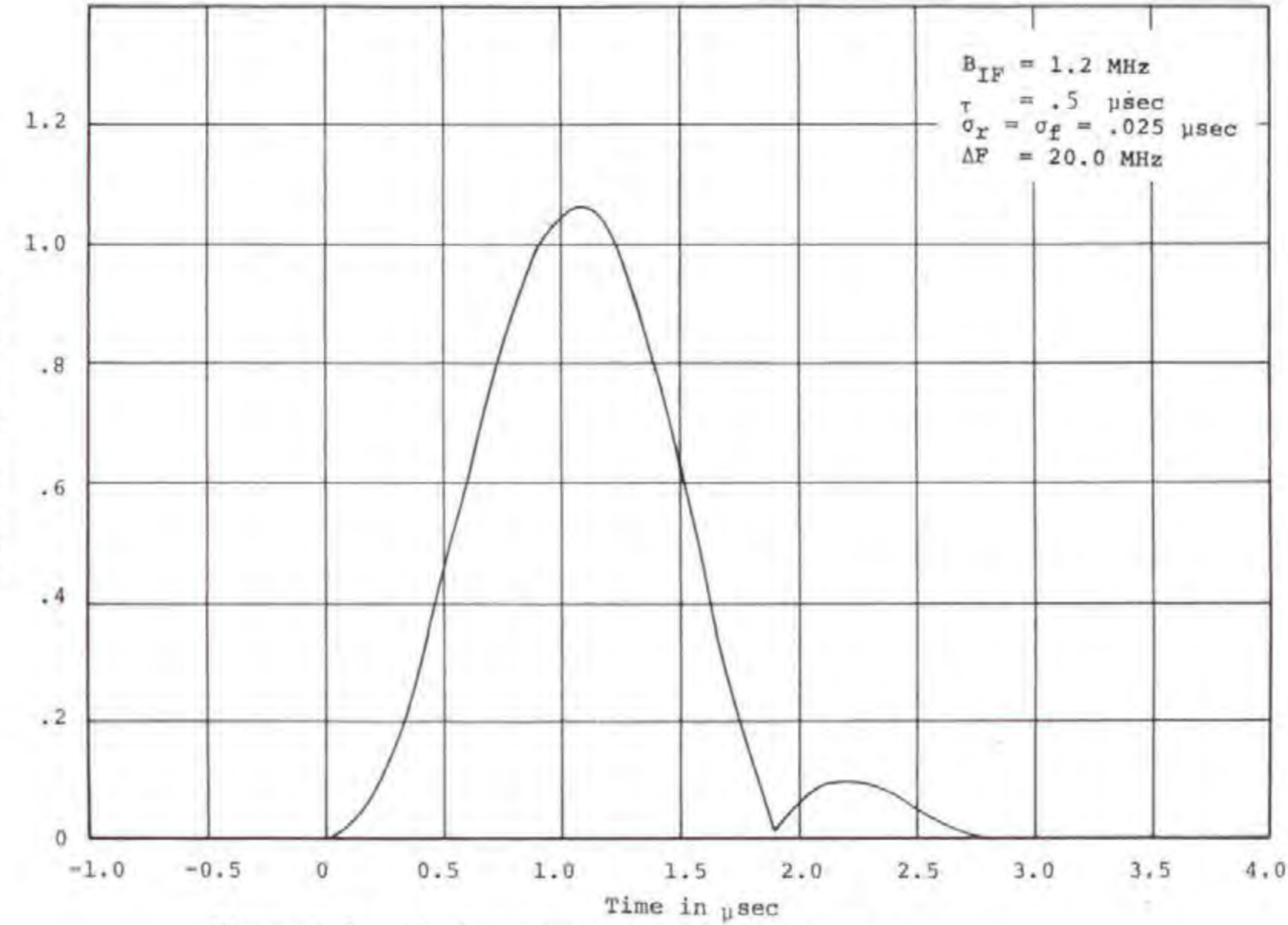

Figure B-5. Simulated IF Output Time Waveform Envelope

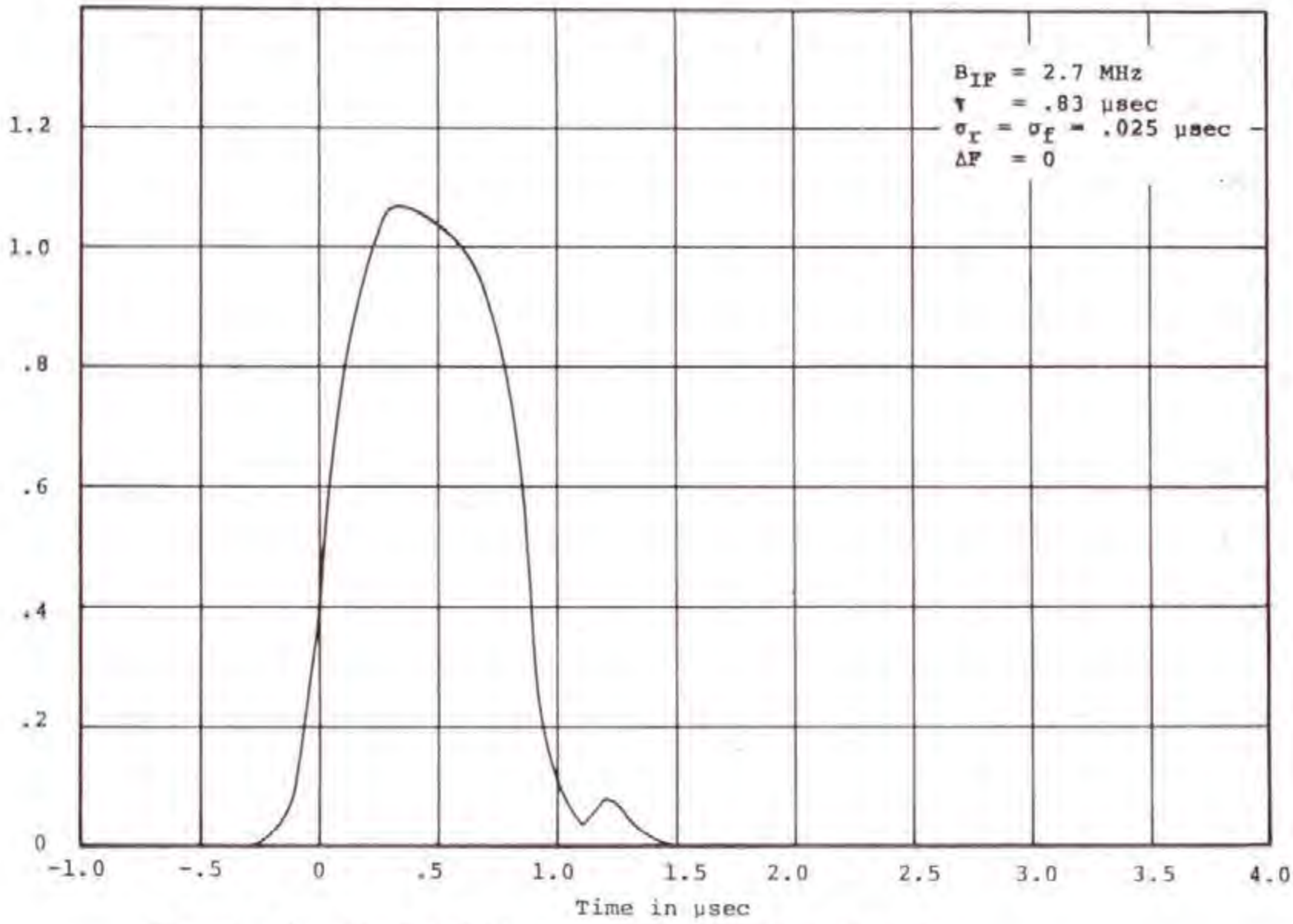

Figure B-6. Simulated IF Output Time Waveform Envelope

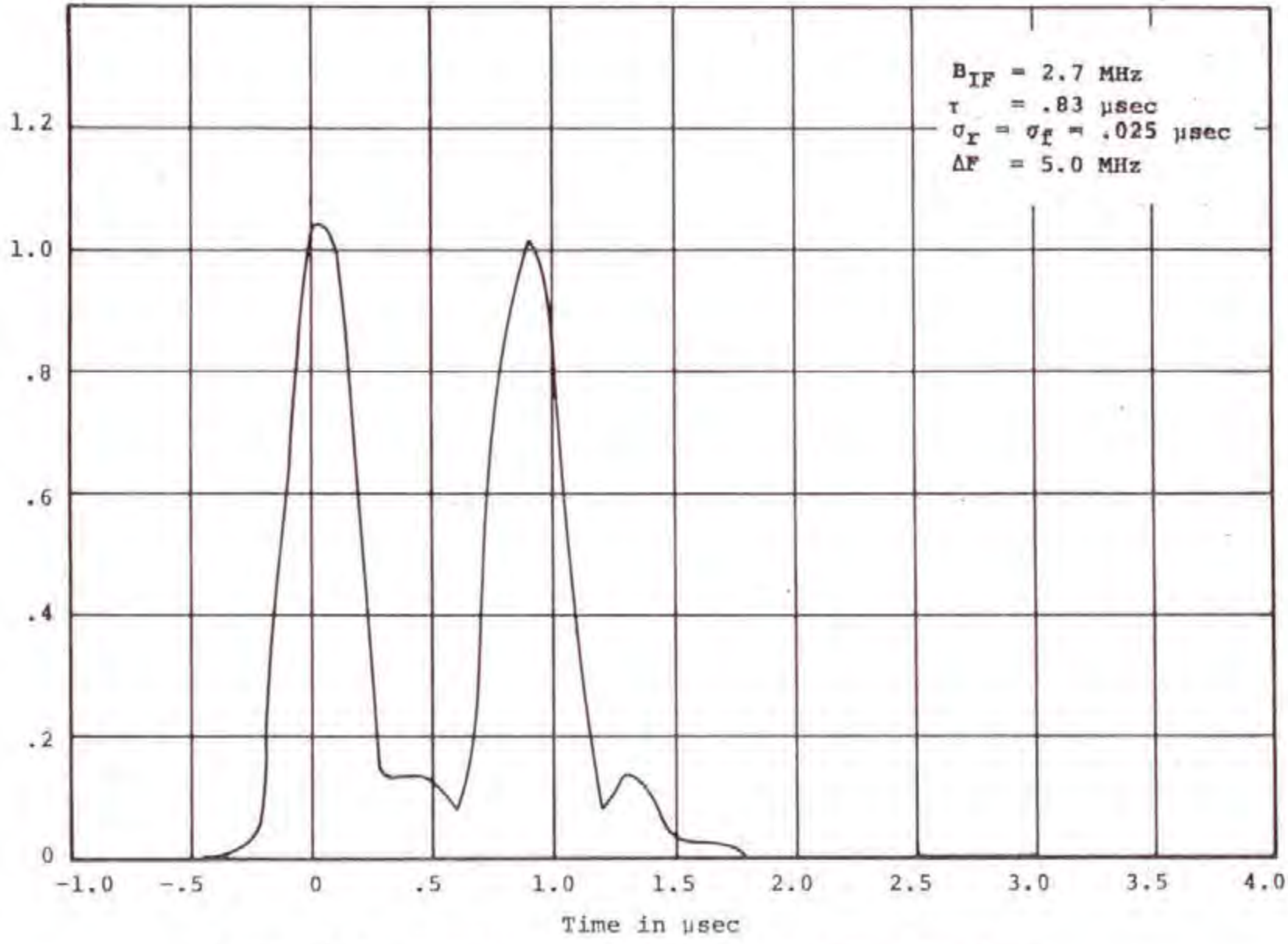

Figure B-7. Simulated IF Output Time Waveform Envelope

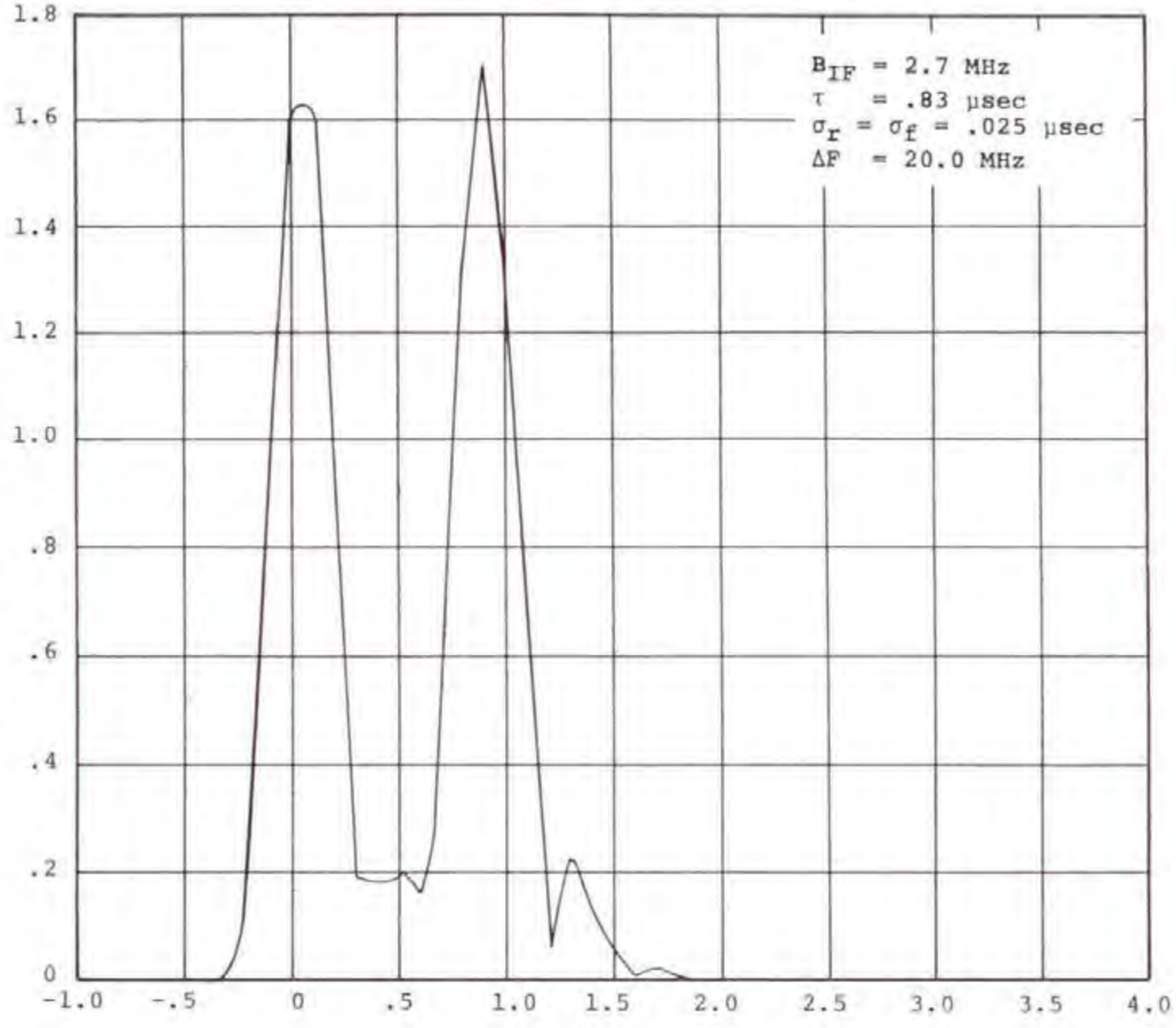

Figure B-8. Simulated IF Output Time Waveform Envelope

When the pulse bandwidth is much narrower than the IF filter bandwidth, $\tau B_{IF} >> 1$, and ΔF less than one half the IF bandwidth, the input time characteristics are produced at the filter output along with some ringing or overshoot on the leading and trailing edges. As the pulse is further off-tuned, the pulse spectrum out of the filter will be unsymmetrical, thereby producing amplitude and phase modulation. The steady state portion of the output pulse will again be attenuated by the off-tuned characteristics of the filter and, therefore, the shape and magnitude of the output pulses will be determined by the power and shape of the spectrum within the filter passband. Simulated IF out time waveform for an IF bandwidth of 5.0 MHz and a .83 μs pulse ($\tau B >> 1$) for ΔF = 0, 5.0 MHz and 20.0 MHz are shown in Figures B-9, B-10, and B-11, respectively. Photographs of measured IF output time waveforms on an ASR-8 (Figures B-12 through B-14) are shown for identical parameter conditions as the simulated waveforms shown in Figures B-9 through B-11, respectively.

Figure B-15 is a plot of phase angle as a function of time at the output of a 5.0 MHz bandwidth IF filter for a .83 μs pulse off-tuned 5.0 MHz. The plot shows the phase modulation produced by an off-tuned pulse during the leading edge, steady state and trailing edge of the pulse. The 5.0 MHz beat tone phase modulation during the steady state portion of the pulse is equal to the 5.0 MHz off-tuning of the pulse. The effect of this phase modulation produced by off-tuned pulsed interference on the MTI channel phase detector is discussed in Appendix C.

In summary, the transformation of pulsed signals through a radar linear IF filter has been discussed in terms of τB_{IF} categories and off-tuning. An understanding of the transfer properties of radar IF filters is required since the IF output time waveform determines the waveform at the normal channel detector output, and the phase modulation produced by the IF filter determines the MTI channel phase detector output waveform.

IF OUTPUT NOISE LEVEL

The receiver equivalent noise level at the radar input is essentially determined by the radar receiver RF stages since the noise contribution due to the IF stages is small because of the high gain of the IF and previous receiver stages. Since the radar receiver can be modeled as a linear receiver with 0 dB gain up to the receiver IF output, which allows the signal and noise to be treated separately, the noise level at the radar IF output can be treated as being equal to the receiver RF input equivalent noise level N_I. Thus, the receiver equivalent noise level at the receiver input is given by:

$$N_I = kT_O B_{IF} F \qquad \text{(B-34)}$$

Where:

N_I = Receiver noise (referenced to RF input)

T_O = Reference Temperature = 290°K

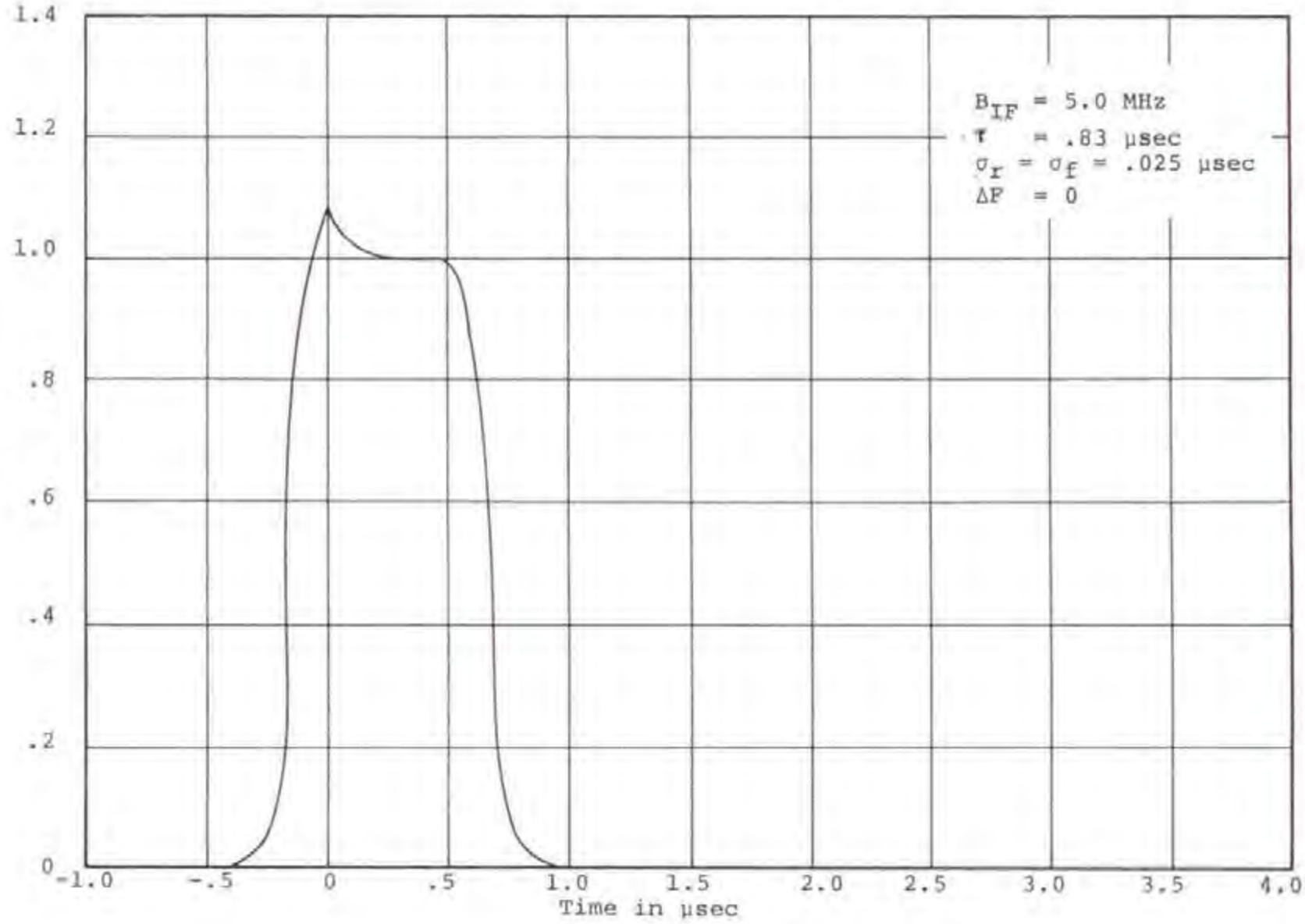

Figure B-9. Simulated IF Output Time Waveform Envelope

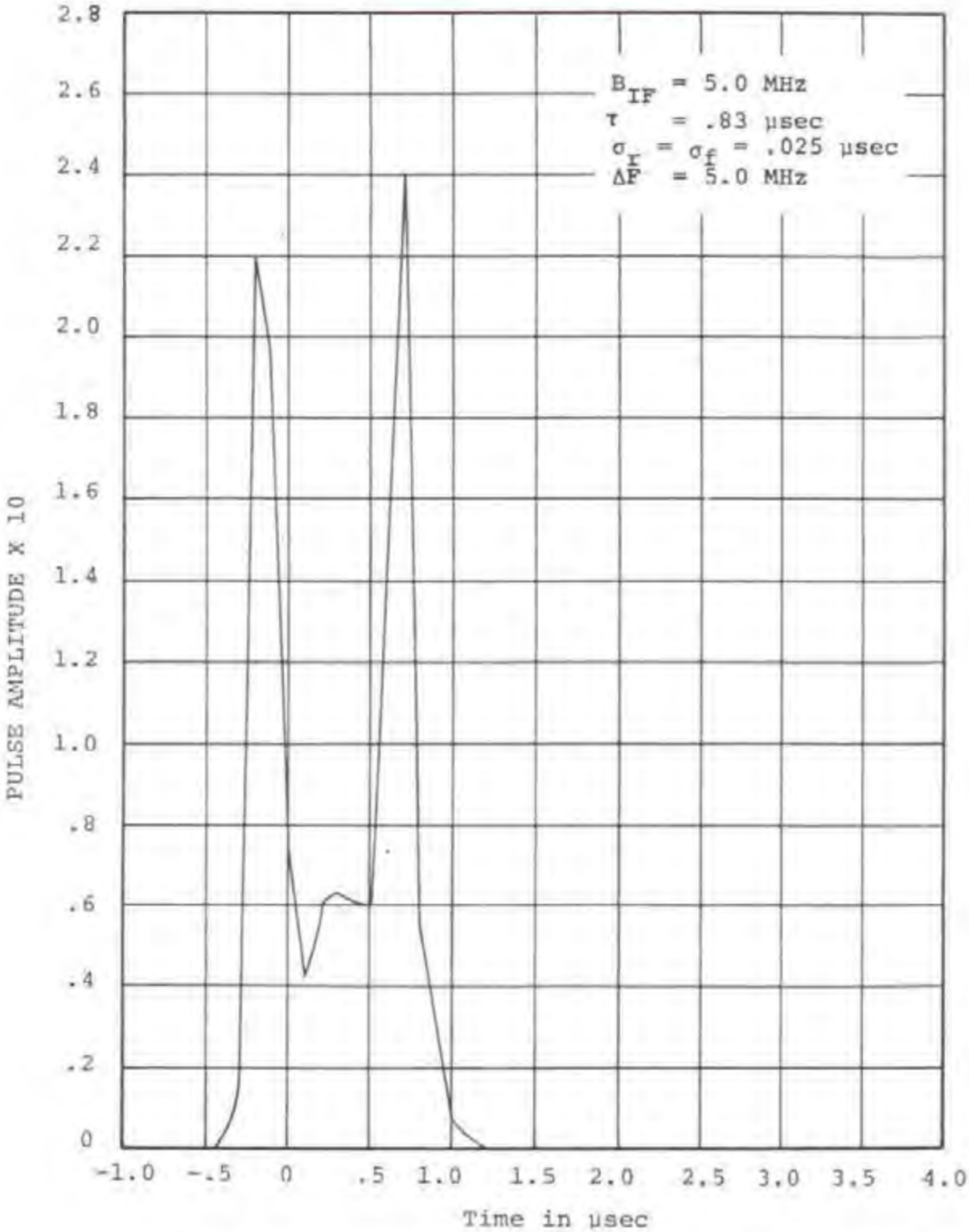

Figure B-10. Simulated IF Output Time Waveform Envelope

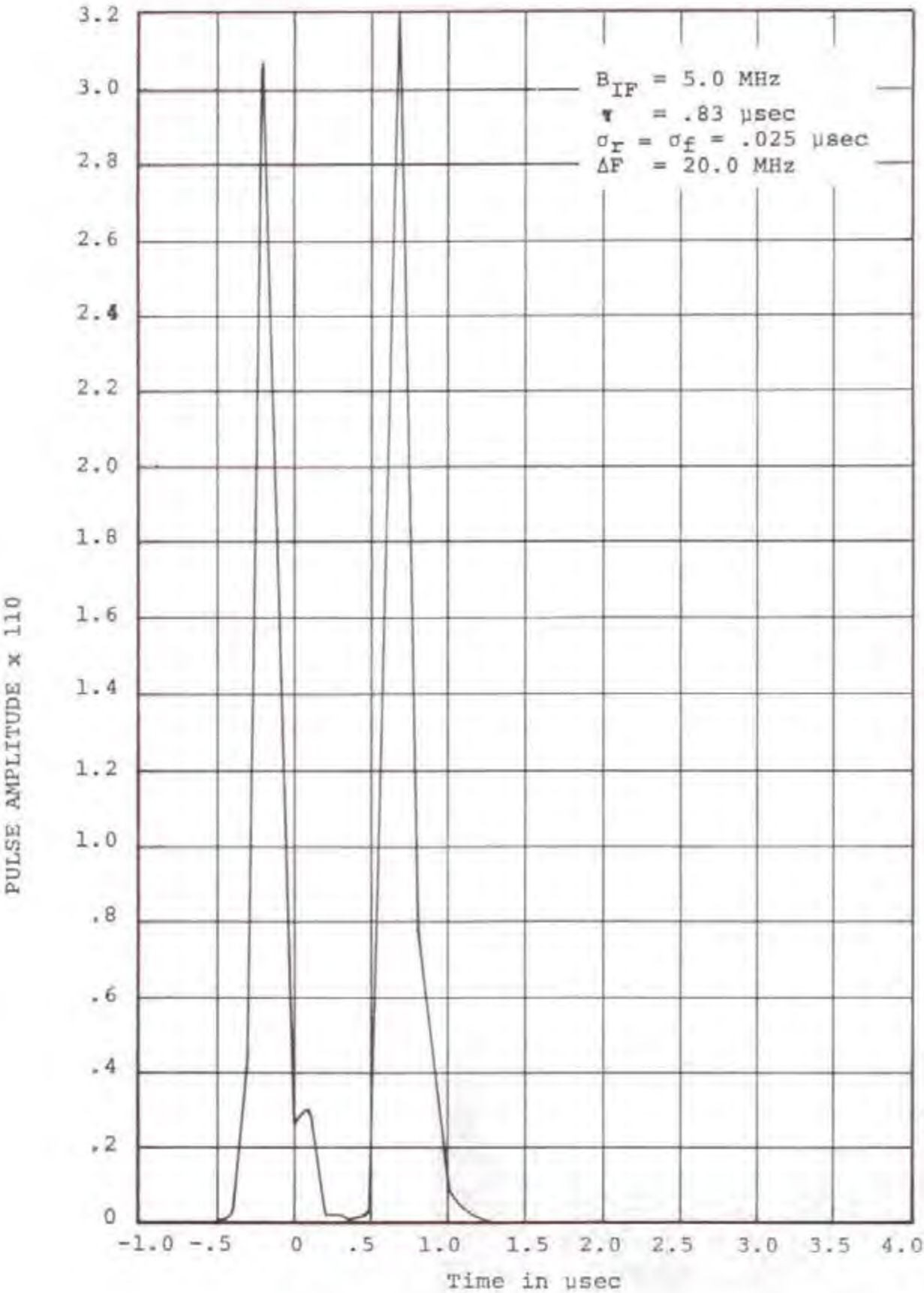

Figure B-11. Simulated IF Output Time Waveform Envelope

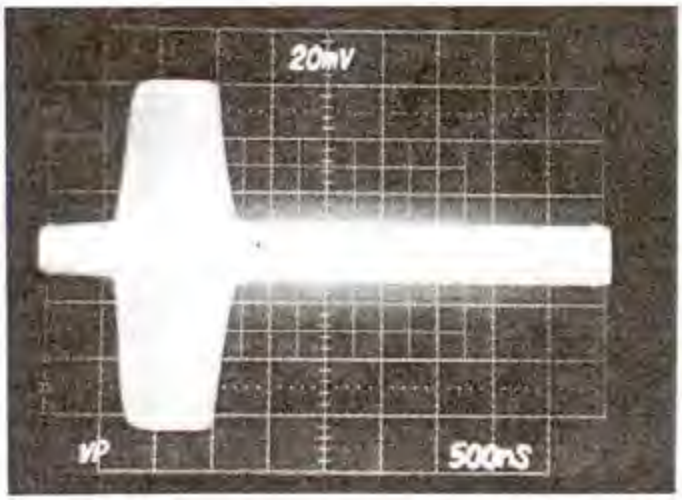

Figure B-12. Measured IF Output Time Waveform

B_{IF} = 5.0 MHz

τ = .83 μsec

ΔF = 0

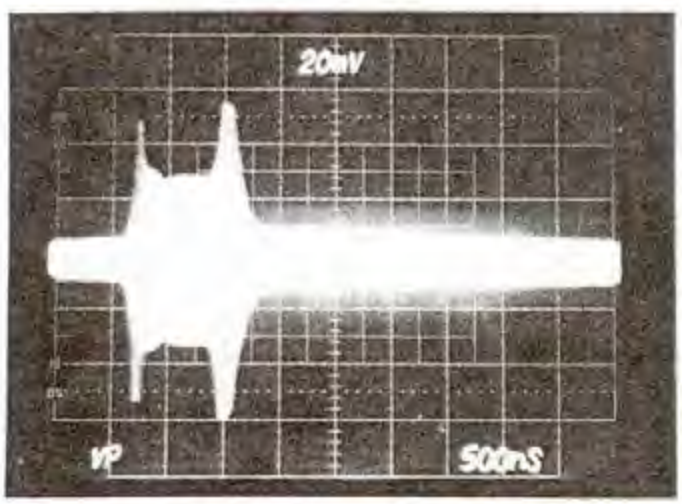

Figure B-13. Measured IF Output Time Waveform

B_{IF} = 5.0 MHz

τ = .83 μsec

ΔF = 5.0 MHz

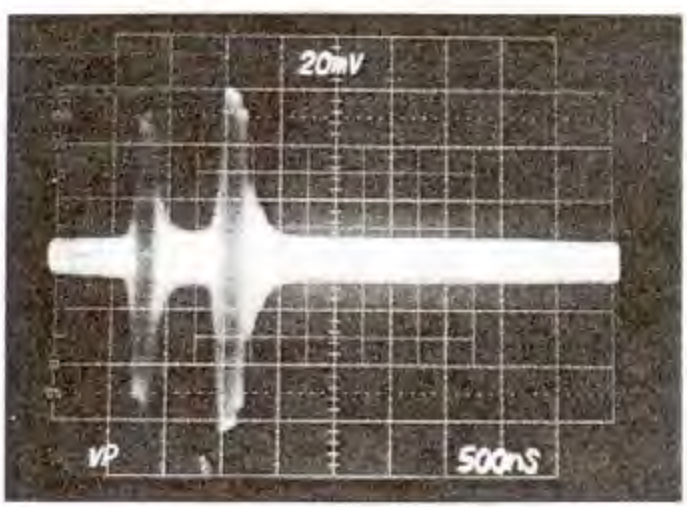

Figure B-14. Measured IF Output Time Waveform

B_{IF} = 5.0 MHz

τ = .83 μsec

ΔF = 20.0 MHz

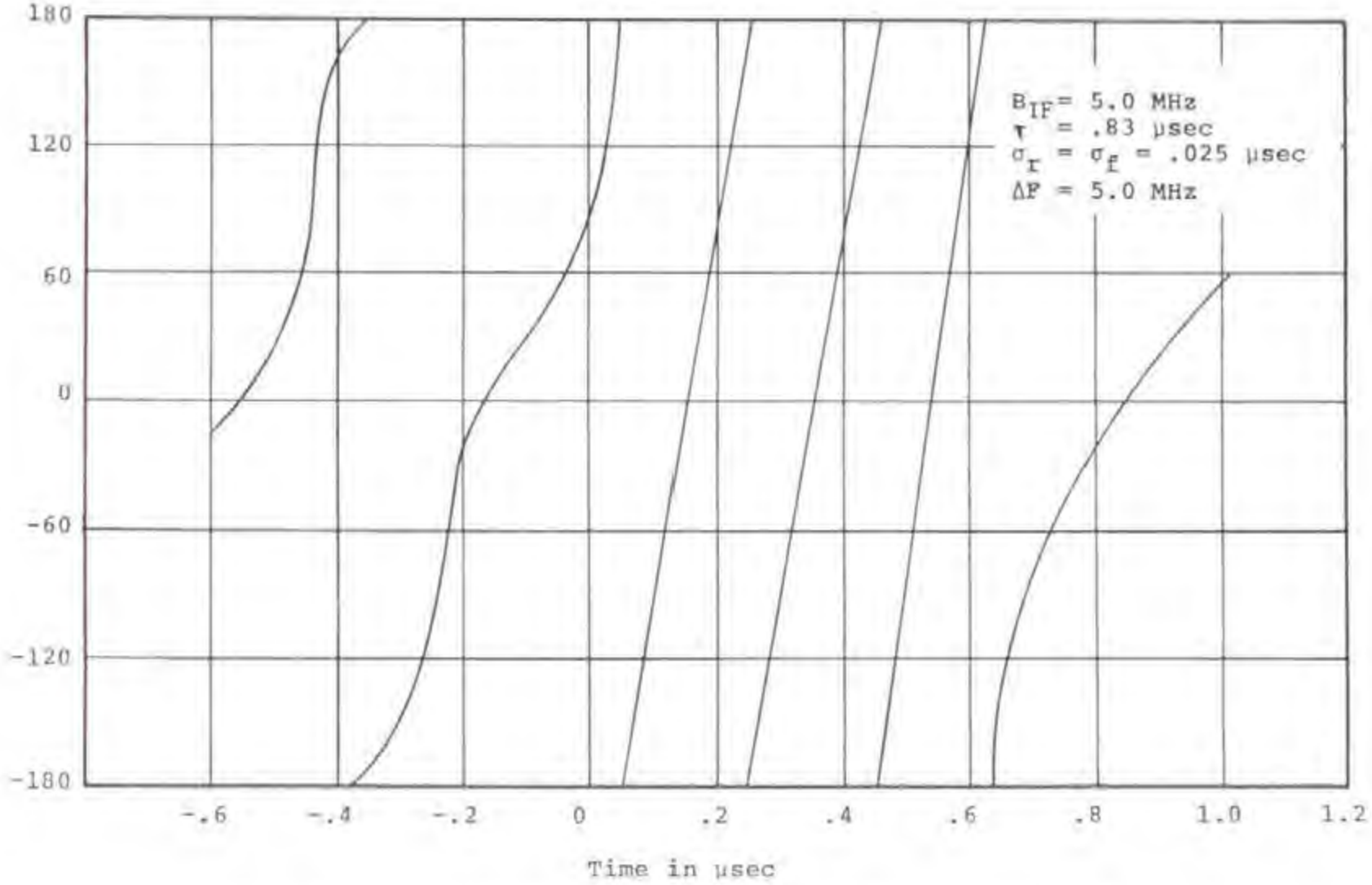

Figure B-15. Simulated IF Output Phase Modulation for an off-tuned Pulse Signal

k = Boltzmann's constant = 1.38×10^{-23} $\frac{\text{Watt-sec}}{°K}$

F = Receiver noise figure = 4 dB

B_{IF} = Receiver IF 3 dB bandwidth, in Hz

Expressing Equation B-34 in dBm

$$N_{IdBm} = -174 \text{ dBm} + 10 \log B_{IF} + F \qquad \text{(B-35)}$$

The interference-to-noise ratio at the receiver RF input can be expressed as:

$$INR_I = I_{IdBm} - N_{IdBm} \qquad \text{(B-36)}$$

Where:

$I_{I_{dBm}}$ = Interfering signal peak power level at the receiver input, in dBm

IF FILTER INR TRANSFER PROPERTIES

Since the IF filter has the narrowest bandwidth and sharpest selectivity characteristics in the radar receiver front end, the filtering prior to the receiver IF filter can be neglected for analytical simplicity, and the interference to noise ratio at the IF filters input (INR_{IFi}) can be treated as being equal to the receiver input interference to noise ratio. Thus:

$$INR_{IFi} = INR_I \qquad \text{(B-37)}$$

$$= I_{I_{dBm}} - N_{I_{dBm}} \qquad \text{(B-37a)}$$

The receiver IF output interference to noise ratio, INR_{IFo}, is determined by the receiver FDR, and can be expressed as:

$$INR_{IFo} = INR_I - FDR \qquad \text{(B-38)}$$

Where the FDR factor is given by Equation B-21.

APPENDIX C

MTI CHANNEL TRANSFER PROPERTIES

INTRODUCTION

Radars in the 2.7 to 2.9 GHz band generally employ coherent Moving Target Indicator (MTI) phase detector. Coherent MTI radars make use of the phase fluctuations in the target return signal to recognize the doppler component produced by a moving target. In these systems, the amplitude fluctuations are removed by the phase detector. A 30 MHz signal coherent with the transmitted pulse signal is mixed with the 30 MHz target IF output response to produce a signal proportional to the phase difference between the target return and the coherent reference signal. The video signal out of the phase detector is then low pass filtered and fed to the cancellers which suppress stationary targets since their phase difference is the same from pulse-to-pulse.

Both single channel and dual channel (inphase and quadrature) MTI processing is employed by radars in the 2.7 to 2.9 GHz band. The single channel MTI processors are either analog or digital types. The analog MTI processors do not have A-D converters and use delay line cancellers, while digital MTI processors have A-D converters and use shift register cancellers. The digital shift register cancellers have a much higher stability and do not decay in time. Figure C-1 shows a block diagram of a typical single channel digital MTI processor. Figure C-2 shows the block diagram of a dual channel, inphase (I) and quadrature (Q), digital MTI processor.

This appendix discusses the noise, desired signal, and interfering signal transfer properties of the MTI phase detector, low pass filter, and cancellers. The transfer properties of analog and digital MTI cancellers can be treated identically with the exception of the quantization noise due to A-D conversion, roundoff, and truncation inherent in digital processing. For dual MTI channel processing, it is only necessary to analyze one channel since both the I and Q channels are identical with the exception of the COHO signal being shifted 90 degrees and to take into account the transfer properties of the combiner. The signal processing properties of the IF linear-limiting amplifier are discussed in Section 3 and Appendix B.

PHASE DETECTOR TRANSFER PROPERTIES

Figure C-3 shows a simplified block diagram of a coherent MTI radar phase detector. The analysis of the signal transfer properties of the MTI phase detector is very similar to the radar mixer (Appendix A). Assuming linear transfer properties for the phase detector, the noise and signal can be treated separately.

Noise

To calculate the noise power at the input and output of the phase

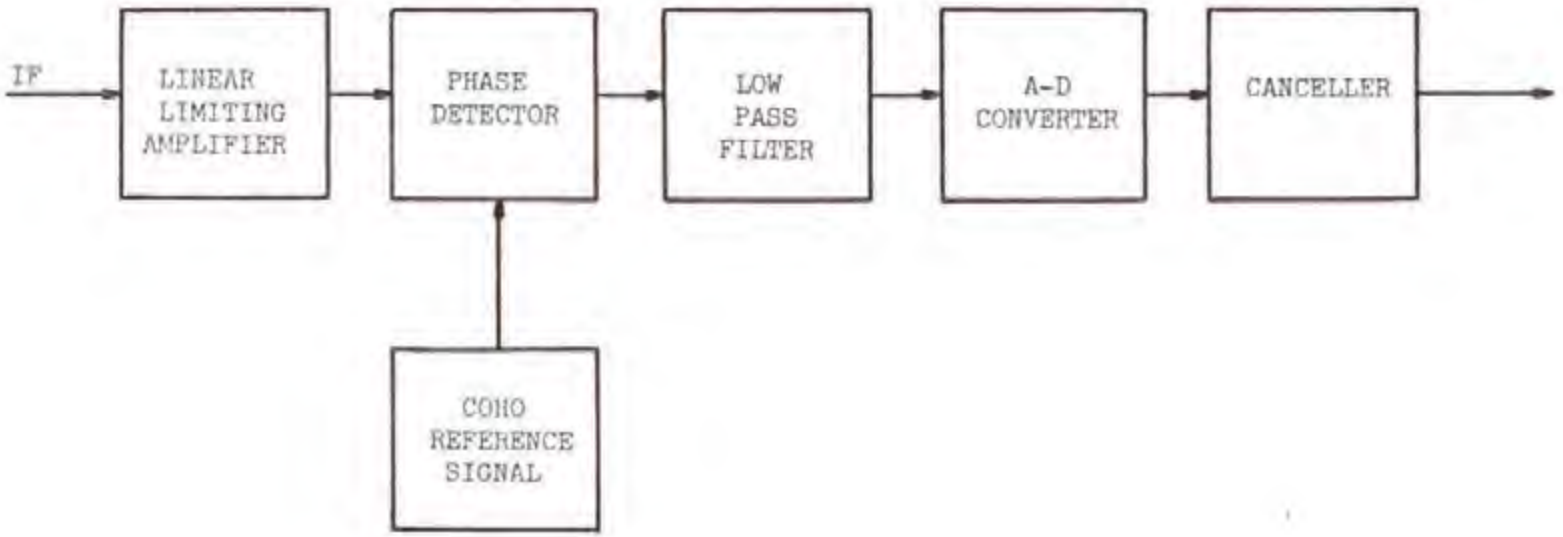

Figure C-1. Digital MTI Channel Block Diagram

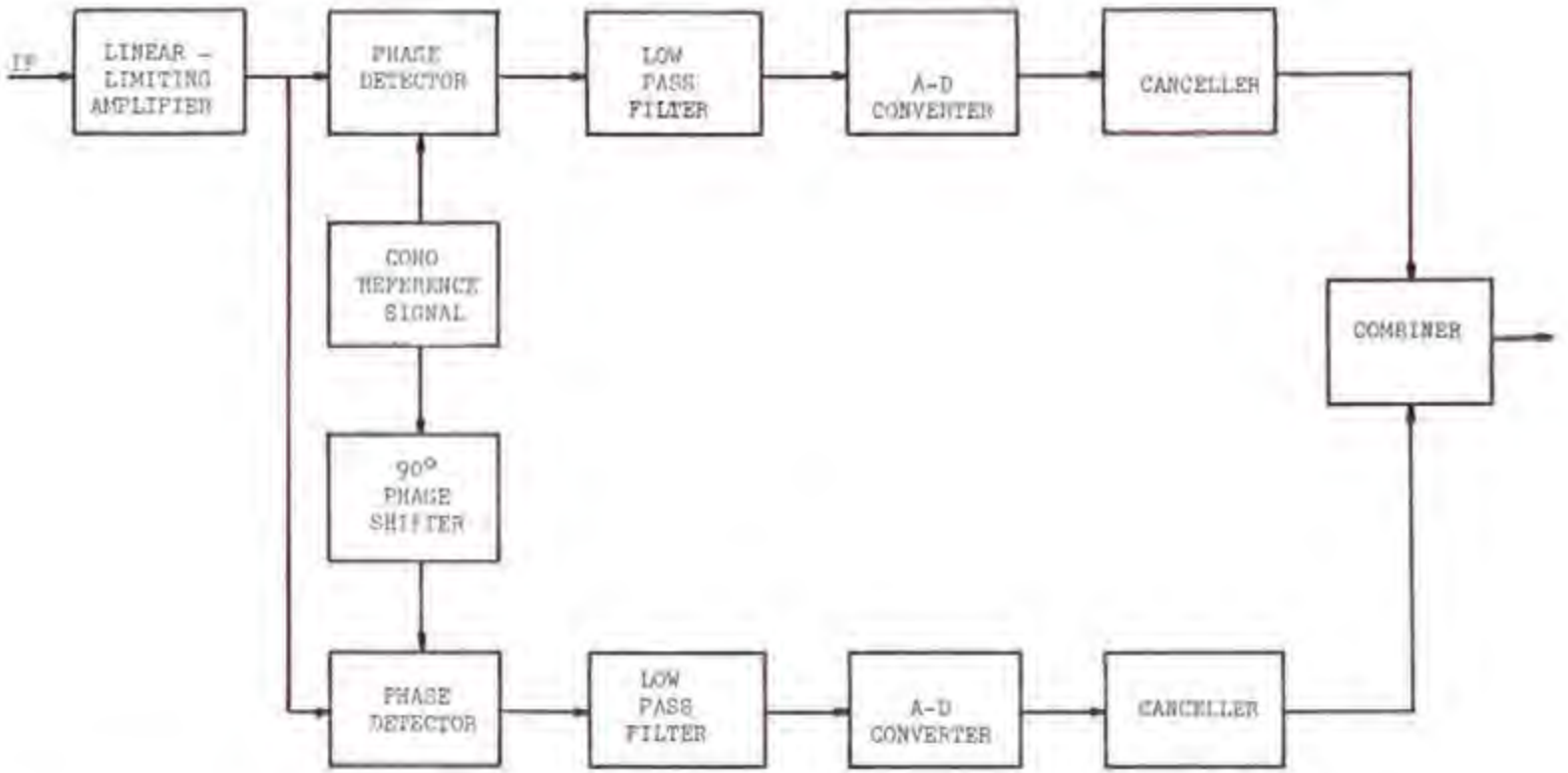

Figure C-2. Inphase and Quadrature Digital MTI Channel Block Diagram

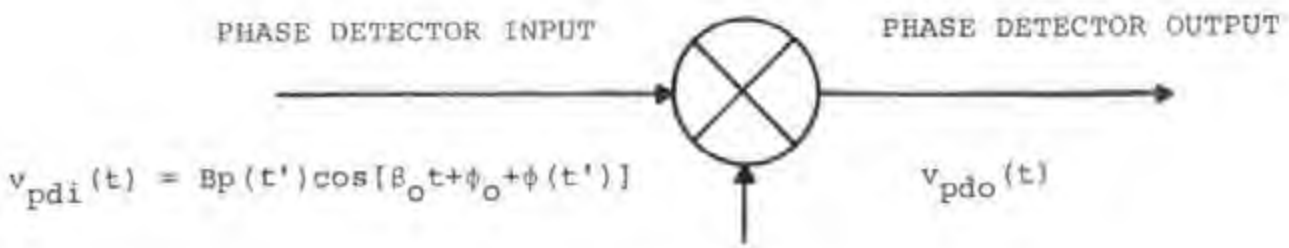

Figure C-3. Radar Coherent MTI Phase Detector

detector (N_{pdo} and N_{pdi}), the bandpass noise model is used, and the input noise signal, $n_{pdi}(t)$, is given by:

$$n_{pdi}(t) = n_c(t) \cos \beta_o t + n_s(t) \sin \beta_o t \qquad (C\text{-}1)$$

Where $n_{pdi}(t)$ is the IF bandpass noise at the input of the MTI phase detector, and the noise power of $N_{pdi}(t)$ is given by:

$$N_{pdi} = \overline{n_{pdi}^2(t)} \qquad (C\text{-}2)$$

Generally, the COHO signal power level is greater than 0 dBm. Therefore, the COHO noise figure (conversion loss) is very small and can be neglected. Also, the COHO signal is usually filtered and the noise suppressed, thus permitting the COHO signal noise level to be neglected. If $n_{pdi}(t)$ is applied at the input of the phase detector (which multiplies the incoming noise signal, $n_{pdi}(t)$, by $v_c(t)$, then $n_{pdo}(t)$, the output noise of the MTI phase detector is given by:

$$n_{pdo}(t) = n_c(t) \cos \beta_o t . \cos (\beta_o t + \phi_c) + n_s(t) \sin \beta_o t . \cos (\beta_o t + \phi_c) \qquad (C\text{-}3a)$$

$$= \frac{n_c(t)}{2} [\cos (2\beta_o t + \phi_c) + \cos (\phi_c)] + \frac{n_s(t)}{2} [\sin (2\beta_o t + \phi_c) - \sin (\phi_c)] \qquad (C\text{-}3b)$$

The terms $\cos (2\beta_o t + \phi_c)$ and $\sin (2\beta_o t + \phi_c)$ represent the spectra of $n_c(t)$ and $n_s(t)$, respectively, shifted at $(2\beta_o t)$ and are filtered out by the low pass video filter at the phase detector output. Hence, $n_{pdo}(t)$ is given by:

$$n_{pdo}(t) = \frac{n_c(t)}{2} \cos (\phi_c) - \frac{n_s(t)}{2} \sin (\phi_c) \qquad (C\text{-}4)$$

and the MTI phase detector output noise power is:

$$N_{pdo} = \overline{n^2_{pdo}(t)} = \overline{\tfrac{1}{2}n^2_{pdi}(t)} \qquad \text{(C-5a)}$$

$$= \tfrac{1}{2}N_{pdi} \qquad \text{(C-5b)}$$

Since the phase detector is sensitive to both the amplitude and phase of the detector input, the noise amplitude distribution at the phase detector output is Gaussian since the phase detector input noise amplitude distribution is Gaussian.

Desired/Interfering Signal

It is shown in Appendix B that the desired and interfering signal IF output time waveform ($V_{IFo}(t)$, Equation B-33), MTI phase detector input time waveform, can be expressed as:

$$V_{pdi}(t) = Bp(t') \cos\left[\beta_o t + \phi_o + \phi(t')\right] \qquad \text{(C-6)}$$

Since we are only concerned with the peak power of the signal, p(t') equals 1, and phase detector input signal peak power (the mean square of $v_{pdi}(t)$) is:

$$S_{pdi} = \overline{V^2_{pdi}(t)} = \frac{B^2}{2} \qquad \text{(C-7)}$$

The radar COHO signal can be defined as:

$$V_c(t) = \cos\left[\beta_o t + \phi_c\right] \qquad \text{(C-8)}$$

Where:

β_o = Receiver tuned IF frequency, in radians per second

ϕ_c = Phase of COHO signal, in radians

The signal voltage time waveform at the phase detector output can be found by performing the operation shown in Figure C-3, and is given by:

$$v_{pdo}(t) = v_{pdi}(t) \cdot v_c(t) \qquad \text{(C-9a)}$$

$$= Bp(t') \cos [\beta_o t + \phi_o + \phi(t')] \cdot \cos [\beta_o t + \phi_c] \qquad \text{(C-9b)}$$

$$= \frac{Bp(t')}{2} [\cos[2\beta_o t + \phi_o + \phi(t') + \phi_c] + \cos [\phi(t') + \phi_o - \phi_c]] \qquad \text{(C-9c)}$$

The first term of Equation C-9c is filtered out by the low pass video filter at the phase detector output, resulting in a signal at the phase detector output of:

$$v_{pdo}(t') = \frac{Bp(t')}{2} \cos [\phi(t') + \phi_o - \phi_c] \qquad \text{(C-10)}$$

and a signal output peak power (the mean square of $v_{pdo}(t)$) of:

$$S_{pdo} = \overline{[v_{pdo}^2(t)]} = \frac{B^2}{8} \qquad \text{(C-11a)}$$

$$= \tfrac{1}{4} S_{pdi} \qquad \text{(C-11b)}$$

The term $\phi(t')$ in Equation C-5 is the phase modulation produced by the radar IF filter transfer properties when the pulsed interfering signal is off-tuned. $\phi(t')$ consists of a steady state term which is a function of the frequency separation (ΔF) between the interfering signal and victim radar tuned frequency, and a transient term. A detailed discussion of this phase modulation on the interfering signal is given in Appendix B (see Figure B-15). A further discussion of the steady state and transient phase modulation properties of off-tuned pulsed interference will follow in the MTI video low pass filter transfer properties.

In the case where the signal is on-tune, $\Delta F=0$, the term $\phi(t')$ equals zero for the steady state portion of the pulse. For this case the signal at the phase detector output is given by:

$$v_{pdo}(t) = \frac{Bp(t')}{2} \cos(\phi_o - \phi_c) \quad \text{(C-12)}$$

and the signal phase detector output peak power is given by:

$$V_{pdo} = \overline{[v_{pdo}^2(t)]} = \frac{B^2}{4} \cos^2(\phi_o - \phi_c) \quad \text{(C-13)}$$

The term $(\phi_o - \phi_c)$ is the phase difference between the signal and the reference COHO signal. Therefore, the signal voltage waveform at the phase detector output will vary between $\pm B/2$. The signal at the phase detector input can be assumed to have a uniform phase difference distribution between 0 to 360 degrees with the reference COHO signal. Thus, if the signal power at the phase detector output is averaged over all phase angles, the signal power is given by:

$$S_{pdo} = \frac{1}{\pi} \int_{o}^{\pi} V_{pdo}(\phi) d\phi = \frac{B^2}{8} \quad \text{(C-14a)}$$

$$S_{pdo} = \frac{1}{2} S_{pdi} \quad \text{(C-14b)}$$

Using Equations C-5b, C-11b, and C-14b, the MTI phase detector SNR and INR transfer properties are given by:

$$SNR_{pdo} = SNR_{pdi} \quad \text{(C-15)}$$

Signal-Plus-Noise Distribution

The noise probability density function at the phase detector output is Gaussian. This is due to the fact that the phase detector is amplitude as well as phase sensitive. The noise amplitude Probability Density Function (PDF) at the input to the phase detector is Gaussian distributed, and the noise phase PDF is uniform distributed. Therefore, the noise amplitude PDF at the phase detector output is Gaussian. If one considers a fixed amplitude (non-fluctuating) desired or interfering signal at the phase detector input, the signal-plus-noise at the phase detector output is given by:

$$v_{pdo}(t) = N(t) + A \cos \phi \quad \text{(C-16)}$$

Where:

N(t) = Noise amplitude which is Gaussian distributed, in volts

A = Desired or interfering signal amplitude, in volts

ϕ = Phase difference between received signal and COHO which is uniform distributed

Papoulis (1965) derives the probability density function for Equation C-16 which can be expressed as:

$$p(v,A) = \frac{1}{\sigma\sqrt{2\pi}} \int_0^{2\pi} e^{\frac{-(v-A\cos\phi)^2}{2\sigma^2}} d\phi \qquad (C-17)$$

where:

σ = rms noise level, in volts

Equation C-17 can not be written in closed form. The MTI channel phase detector output was simulated to investigate trade-offs in suppressing asynchronous interfering signals. The simulation of the radar MTI channel is discussed in Appendix E. Figure C-4 shows the PDF given by Equation C-17 as a function of the signal-to-noise ratio. The PDF was obtained by simulation.

MTI LOW PASS FILTER TRANSFER PROPERTIES

The low-pass filter in the MTI channel is used to reduce the MTI channel video noise level. The low- pass filter bandwidth (B_{lpf}) is approximately equal to $1/\tau$ where τ is the desired signal pulse width. The MTI channel IF bandwidth is always much greater than $1/\tau$ (generally 5.0 MHz) to produce a constant phase characteristic across the desired pulse. Therefore, a narrower low-pass filter bandwidth will improve the video signal-to-noise ratio. The MTI channel low pass filters are usually several stages. The low-pass filter frequency response can be expressed as:

$$A_{LP}(F) = \frac{1}{[1 + j\,(\frac{F}{F_L})\gamma]^n} \qquad (C-18)$$

where:

F_L = Low pass filter 3 dB cutoff frequency, in Hz

n = Number of low pass filter stages

$\gamma = \sqrt{2^{1/n} - 1}$

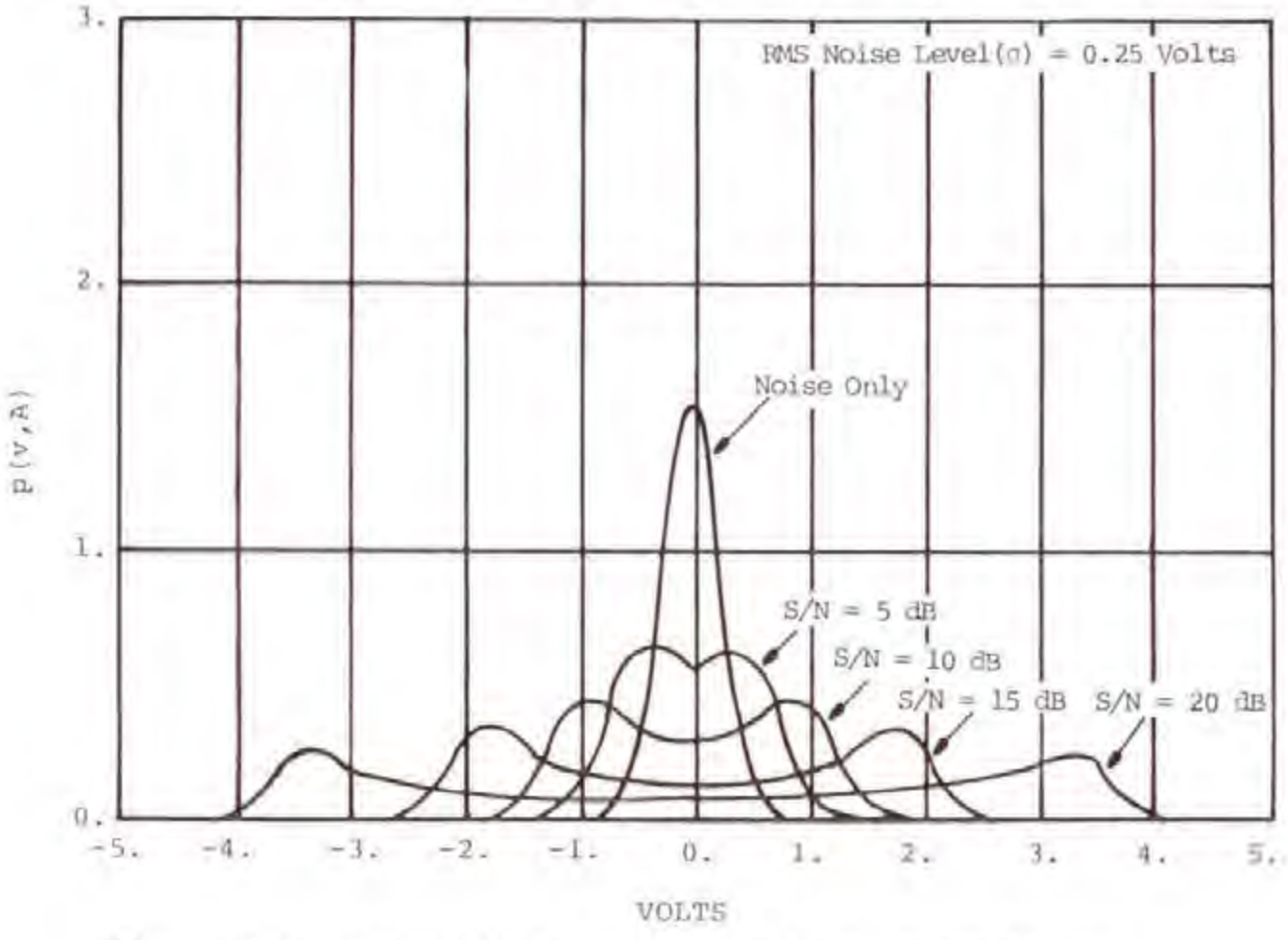

Figure C-4. Probability Density Function for Noise Only and for Signal-Plus-Noise at the MTI Phase Detector Output.

Noise

The noise transfer properties of the MTI low pass filter can be expressed as:

$$N_{lpo} = N_{lpi} + 10 \log \frac{B_{lpf}}{B_{IF}} \qquad (C\text{-}19)$$

For a radar with a 5.0 MHz IF bandwidth and a 1.2 MHz low pass filter bandwidth, the noise power at the low pass filter output is given by:

$$N_{lpo} = N_{lpi} - 6.2 \text{ dB} \qquad (C\text{-}20)$$

Therefore, the low pass filter reduces the MTI channel noise level by 6.2 dB.

Desired/Interfering Signal

The desired and interfering signal low pass filter output time response, $V_{lpo}(t)$, can be obtained by multiplying in the frequency domain the low pass filter frequency response with the phase detector output signal frequency spectrum, $V_{pdo}(F)$, and taking the Fourier transform. That is:

$$V_{lpo}(t) = \mathcal{F}^{-1}\left[V_{pdo}(F) \cdot A_{LP}(F)\right] \qquad (C\text{-}21)$$

Measurements made on an ASR-8 showed that as an interfering signal is off-tuned (ΔF), the signal level followed the low pass filter selectivity due to the sinusoidal modulation during the steady state portion of the pulse. However, for ΔF greater than 3 MHz, the off-tuned interfering signal response started to follow the interfering signal RF frequency spectrum, and the low pass filter interfering signal output response was caused by the phase modulation that occurs during the transient part (rabbit ear response occurring at the leading and trailing edge of the IF filter output response, see Figures B-10, B-11, B-13, and B-14) of the interfering signal time waveform. Figure C-5 shows a photograph of the phase detector output time waveform of a 60 μs pulse signal off-tuned 200 KHz. The measurement was made on an ASR-8 radar. The pulse width was set at 60 μs to demonstrate the 200 KHz sinusoidal modulation during the steady state portion of the pulse which is caused by the phase modulation produced by the IF filter transfer

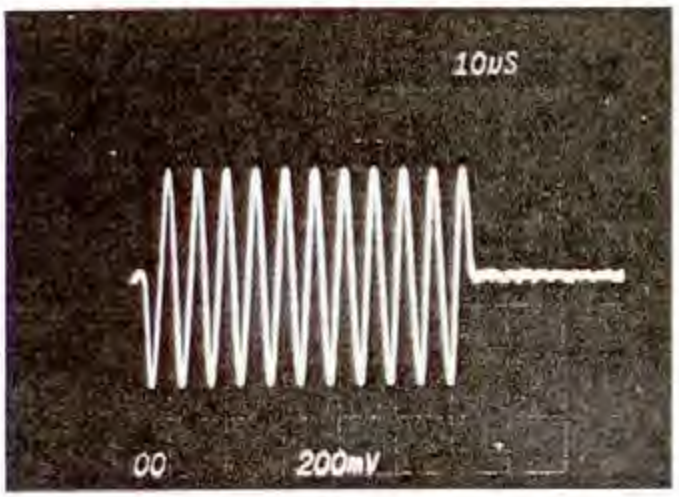

Figure C-5. Measured MTI Low Pass Filter Output Time Waveform

τ = 60 μsec

ΔF = 200 kHz

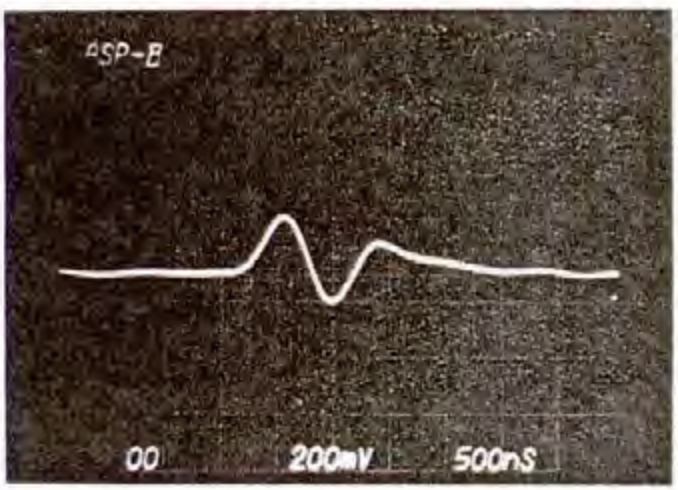

Figure C-6. Measured MTI Low Pass Filter Output Time Waveform

τ = .83 μsec

ΔF = 5.0 MHz

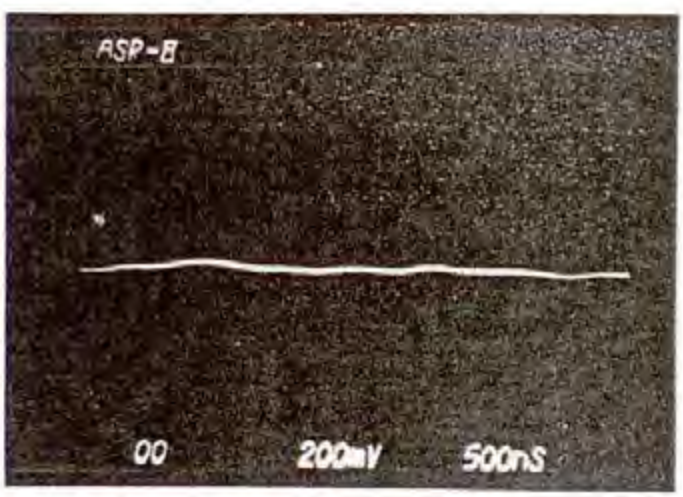

Figure C-7. Measured MTI Low Pass Filter Output Time Waveform

τ = .83 μsec

ΔF = 5.0 MHz

properties, and is equal to the off-tuned frequency (ΔF). Figure C-6 shows a photograph of an ASR-8 low pass filter output of a .83 μs pulse off-tuned 5.0 MHz. Since the low pass filter interfering signal output response for off-tuned interference is due to the phase modulation which occurs during the transient portion of the IF filter response, the low pass filter output interfering signal time response changes from pulse-to-pulse. However, the average pulse amplitude appears to follow the interfering signal RF spectrum envelope. Figure C-7 shows a photograph of the low pass filter output for the same interfering signal parameters as in Figure C-6. However, the phase modulation during the transient portion of the interfering signal did not cause a low pass filter output response.

MTI CANCELLER TRANSFER PROPERTIES

The target return signals after phase detection are processed in the MTI cancellers. The MTI canceller circuits provide for cancelling fixed target signals (clutter), such as buildings, hills, and trees and allowing only moving targets, such as aircraft to be displayed on the PPI. The action of the MTI cancellers is that of a linear filter. In the ideal case, the clutter components will appear at zero frequency and at integral multiples of the radar Pulse Repetition Frequency (PRF), and will be suppressed.

Most radars in the 2.7 to 2.9 GHz band employ both single and double cancellers. Generally, the radars are operated in the double canceller mode which provides broader clutter-rejection nulls than the single cancellers. Some of the radars in the band also have the capability of introducing feedback in the double-canceller mode to improve the velocity response of the MTI filter.

Both analog and digital filtering is used by the radars in the 2.7 to 2.9 MHz band. Radars using analog filters (delay lines) have the capability of continuously variable feedback control, while the digital filter (shift registers) radars generally have several modes of fixed feedback.

Staggered PRF is also generally employed by radars in the 2.7 to 2.9 GHz band to extend the blind speed of the radars. Analog radars typically have two or three staggers, while digital radars with their greater stability may have more than three staggers. The ASR-8 has a four-stagger system, and the ASR-7 has a six-stagger system. A radar operating in the staggered mode affects the range bins in which the interfering pulses may occur. However, the peak interfering signal transfer properties through the MTI canceller are not affected when operating in the staggered mode. Therefore, the staggered PRF modes of the radars can be neglected for analytical simplicity in determining the interfering signal peak power transfer properties of MTI cancellers.

Single Stage Canceller Transfer Properties

Figure C-8 shows a block diagram of a single stage canceller (first-order nonrecursive filter). The canonical form of the single stage

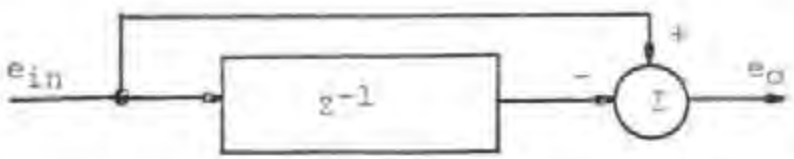

Figure C-8. First-Order Nonrecursive Filter

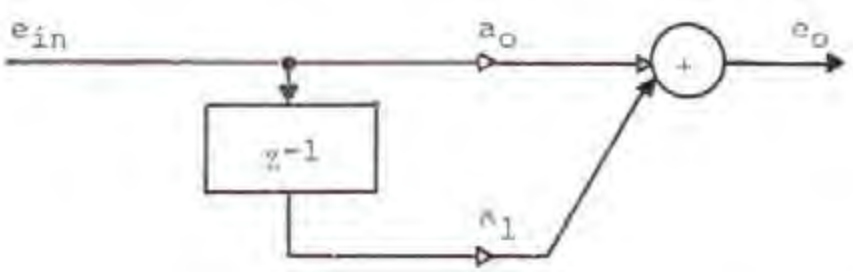

Figure C-9. Canonical Form of First-Order Nonrecursive Filter

canceller is shown in Figure C-9. The Z-Transfer function of the first-order nonrecursive filter is given by:

$$H(Z) = \frac{e_o}{e_{in}} = 1 - Z^{-1}$$

$$= a_0 + a_1 Z^{-1} \qquad \text{(C-22)}$$

where:

Z^{-1} = Unit delay (t - T)

T = Radar pulse period, in seconds

a_i = Binomial weighting factors, $(-1)^i \binom{n}{i}$

n = Filter order, 1

The frequency response magnitude of the first-order nonrecursive filter transfer function is determined by letting $Z^{-1}=e^{-j\omega_d T}$, and is given by:

$$|H(e^{j\omega_d T})| = |1 - (\cos\omega_d T - j \sin \omega_d T)| \qquad \text{(C-23a)}$$

$$= \left|2 \sin \frac{\omega_d T}{2}\right| \qquad \text{(C-23b)}$$

where:

ω_d = Doppler frequency of return signal, in radians per second

Figure C-10 shows the frequency response characteristics for a first-order nonrecursive filter. The improvement factor (I) is 21.3 dB. The improvement factors are defined as the signal-to-clutter ratio at the output of the MTI system compared with that at the input, where the signal is understood as that averaged uniformly over all radial velocities, that is:

$$I = 10 \log \frac{\bar{S}_o/C_o}{S_i/C_i} \qquad \text{(C-24)}$$

Equation C-22 can be expressed in canonical form (Figure C-9) as a n-order difference equation relating the input signal, e_{in}, to the output signal, e_o, by:

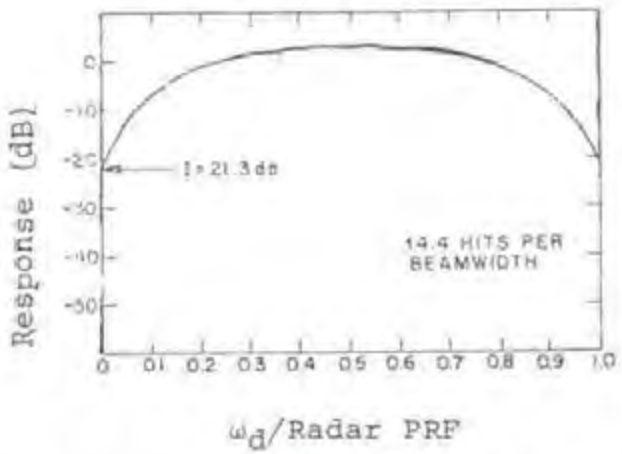

Figure C-10. Frequency Response for a Single Stage MTI Canceller

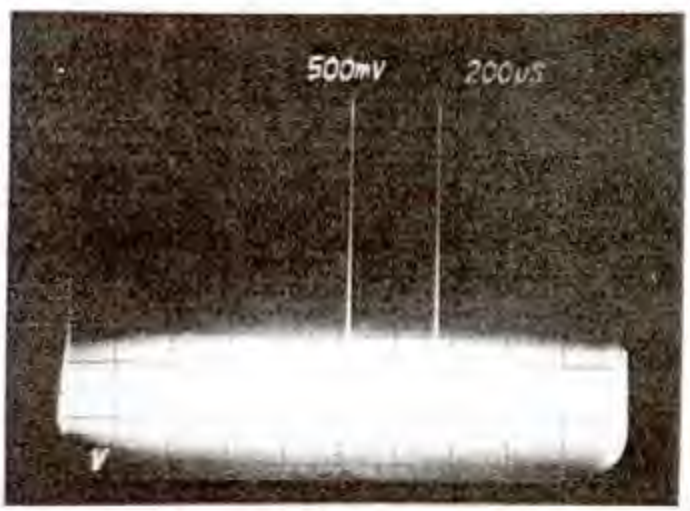

τ = .83 usec

PRF_I = 800

Figure C-11 Measured Single Stage MTI Canceller Output Time Waveform

$$e_o = \sum_{i=0}^{n} a_i e_{in}(t-iT) \qquad (C\text{-}25)$$

$$i=0,1,\ldots n$$

where:

a_i = Binomial weighting factors, $(-1)^i \binom{n}{i}$

Therefore, the impulse response of a first-order nonrecursive filter to a single pulse is given by:

$$e_o = e_{in}(t) - e_{in}(t-T) \qquad (C\text{-}26)$$

Noise

The rms noise transfer properties of a single stage MTI canceller is:

$$n_{MTI_{lo}} = \sqrt{a_o^2 n_{MTI_{li}}^2 + a_i^2 n_{MTI_{li}}^2} \qquad (C\text{-}27a)$$

$$= \sqrt{2}\, n_{MTI_{li}} \qquad (C\text{-}27b)$$

Thus, the noise power transfer function of a single stage MTI canceller is:

$$N_{MTI_{lo}} = N_{MTI_{li}} + 3 \text{ dB} \qquad (C\text{-}28)$$

Desired Signal

For a desired signal (synchronous signal), the signal power transfer gain for a single stage MTI canceller when averaged over all possible doppler frequencies is 3 dB (Nathanson, 1969). Since the noise power density is uniform over the MTI filter, the filter treats both noise and signal (on the average) alike. Thus, there is also a 3 dB power transfer gain in both noise and desired signal in a first-order MTI filter. Hence, the signal-to-noise ratio (SNR) at the MTI canceller output is the same as at the input to the MTI canceller.

Interfering Signal

For an asynchronous interfering signal, the number of interfering pulses is increased by a factor of two for a single stage MTI canceller, resulting in an increase in the interfering signal average power. The asynchronous interfering signal bipolar output is converted back to unipolar resulting in two positive output pulses for each asynchronous input pulse. Figure C-11 shows an aysnchronous interfering signal output measured on an ASR-8 operating in the CANC 1 mode. Equation C-26 indicates that the interfering signal peak power transfer properties of a single stage MTI canceller is given by:

$$I_{MTI_{1o}} = I_{MTI_{1i}} \qquad \text{(C-29)}$$

Using Equations C-28 and C-29, the INR transfer properties of a single stage MTI canceller for asynchronous interference are given by:

$$INR_{MTI_{1o}} = INR_{MTI_{1i}} - 3 \text{ dB} \qquad \text{(C-30)}$$

Double Stage Canceller Transfer Properties

Figure C-12 shows a block diagram of a double stage MTI canceller with feedback (second-order recursive filter). The canonical form of the double stage canceller with feedback is shown in Figure C-13. Different modes of MTI canceller operation are obtained by varying the feedback coefficients (b_1 and b_2). By changing the feedback coefficients, the doppler frequency response of the MTI filter is shaped to permit improvement in the subclutter visibility (SCV). TABLE C-1 shows the canonical feed-forward coefficients (a_o, a_1, a_2) and feedback coefficients (b_1 and b_2) for the different modes of operation of the double stage cancellers in the ASR-7 and ASR-8. The Z-Transfer function of the second-order recursive filter is given by:

$$H(Z) = \frac{e_o}{e_{in}} = \frac{a_o + a_1 Z^{-1} + a_2 Z^{-2}}{b_1 Z^{-1} + b_2 Z^{-2}} \qquad \text{(C-31)}$$

where:

Z^{-1} = Unit delay, (t- T)

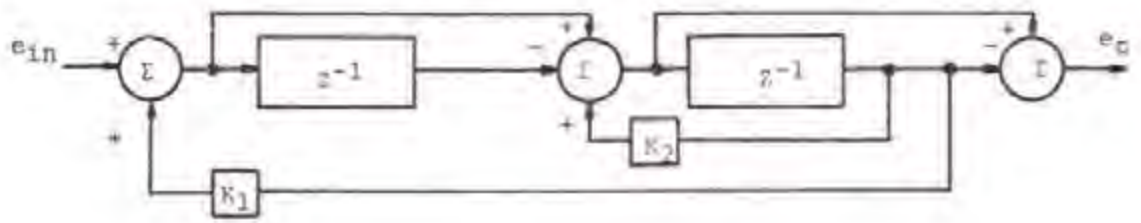

Figure C-12. Second-Order MTI Filter with Feedback for Velocity Shaping

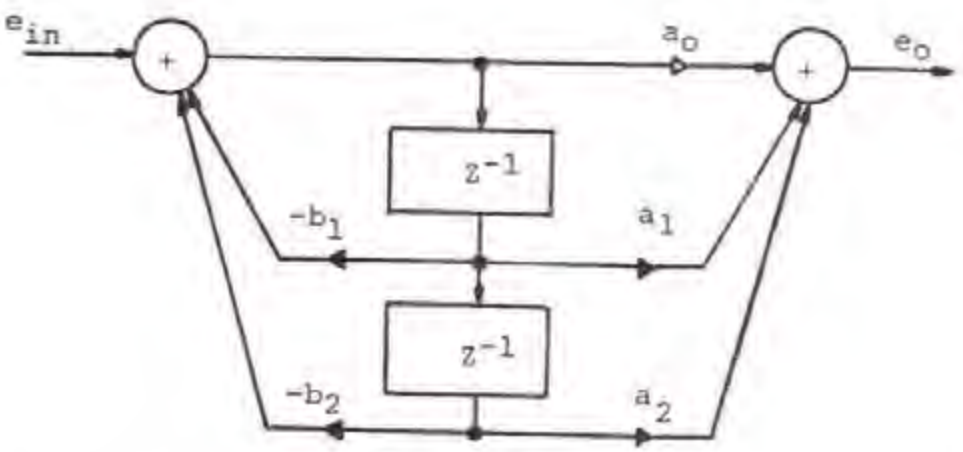

Figure C-13. Canonical Form of Second-Order Recursive Filter

TABLE C-1

MTI CANCELLER TRANSFER PROPERTIES

MTI MODE	FEED-FORWARD COEFFICIENTS			FEEDBACK COEFFICIENTS		NOISE GAIN		PEAK INTERFERENCE GAIN		PEAK INR (dB)
	a_o	a_1	a_2	b_1	b_2	VOLTS	dB	VOLTS	dB	
CANC 1	1	-1	0	0	0	$\sqrt{2}$	3	1.0	0	-3
1&2 CASC	1/2	-1	1/2	0	0	$\sqrt{1.5}$	1.76	1.0	0	-1.76
SCV-25	1/2	-1	1/2	1 1/4	-1/2	$\sqrt{0.454}$	-3.42	0.50	-6.0	-2.58
SCV-30	1/2	-1	1/2	1	-1/2	$\sqrt{0.6}$	-2.21	0.50	-6.0	-3.79
SCV-35	1/2	-1	1/2	3/4	-1/2	$\sqrt{0.777}$	-1.09	0.625	-4.08	-2.99
SCV-40	1/2	-1	1/2	1/2	-1/2	1.0	0	0.75	-2.49	-2.49

T = Radar pulse period, in seconds

a_i = Binomial weighting factors, $(-1)^i \binom{n}{i}$

n = filter order, 2

b_i = Canonic feedback factors

The binomial weighting factors are 1, -2, and 1 for a second order filter. However, on some of the new digital radars binomial weighting factors (feed-forward coefficients) of 1/2, -1, and 1/2 are used to reduce word size. Equation C-21 can be rewritten using the non-canonic feedback coefficient (K_1 and K_2):

$$H(Z) = \frac{e_o}{e_{in}} = \frac{a_0 + a_1 Z^{-1} + a_2 Z^{-2}}{1-(K_1 + K_2)Z^{-1} + K_1 Z^{-2}} \qquad \text{(C-32)}$$

The frequency response magnitude of the second-order recursive filter transfer function is determined by letting $Z^{-1} = e^{-j\omega_d T}$ and is given by:

$$|H(e^{j\omega T})| = \frac{\sin^4 \frac{(\omega_d T)}{2}}{[1+(K_1+K_2)+K_1^2]-2(1+K_1)(K_1+K_2)\cos \omega_d T + 2K_1 \cos 2\omega_d T} \qquad \text{(C-33)}$$

where:

ω_d = Doppler frequency of return signal, in radians per second

K_1 and K_2 = Feedback constants

Figure C-14 shows the frequency response characteristics and improvement factor for several feedback constants for a second-order recursive filter.

For the non-feedback MTI canceller mode (1 and 2 CASC, b_1 and $b_2 = 0$) the MTI filter has no poles, and Equation C-31 reduces to:

$$H(Z) = \frac{e_o}{e_{in}} = a_0 + a_1 Z^{-1} + a_2 Z^{-2} \qquad \text{(C-34)}$$

Therefore, the MTI canceller output response becomes:

$$e_o = a_0 e_{in}(t) + a_1 e_{in}(t-T) + a_2 e_{in}(t-2T) \qquad \text{(C-35)}$$

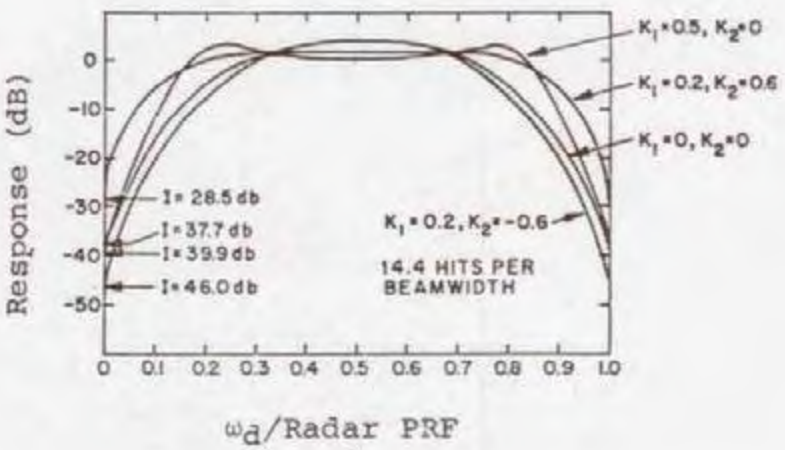

Figure C-14. Frequency Response for a Double Stage Canceller with Feedback

Noise

The rms noise transfer properties of a double stage MTI canceller for the non-feedback mode (b_1 and b_2 = 0) is given by:

$$n_{MTI_{2o}} = \sqrt{a_o^2 n_{MTI_{2i}}^2 + a_1^2 n_{MTI_{2i}}^2 + a_2^2 n_{MTI_{2i}}^2} \qquad (C\text{-}36a)$$

$$= \sqrt{1.5}\, n_{MTI_{2i}}; \quad \text{for } a_i = \tfrac{1}{2}, -1, \text{ and } \tfrac{1}{2} \qquad (C\text{-}36b)$$

$$= \sqrt{6}\, n_{MTI_{2i}}; \quad \text{for } a_i = 1, -2, \text{ and } 1 \qquad (C\text{-}36c)$$

Thus, the noise power transfer function of a double stage MTI canceller is:

$$N_{MTI_{2o}} = N_{MTI_{2i}} + 1.8 \text{ dB}; \text{ for } a_i = \tfrac{1}{2}, -1, \text{ and } \tfrac{1}{2} \qquad (C\text{-}37a)$$

$$N_{MTI_{2o}} = N_{MTI_{2i}} + 7.8 \text{ dB}; \text{ for } a_i = 1, -2, \text{ and } 1 \qquad (C\text{-}37b)$$

For the MTI canceller feedback modes of operation the rms noise transfer properties are determined using a recursive algorithm. The noise power transfer properties for the different feedback modes were obtained by simulation (see Appendix E), and are shown in TABLE C-1.

The noise amplitude distribution at the canceller output is Gaussian distributed with a zero mean. Since the MTI canceller sums the noise at the input to the canceller which has a Gaussian amplitude distribution, the output noise amplitude distribution is also Gaussian.

Desired Signal

For desired signal (synchronous signal), the signal power transfer gain for a double stage MTI canceller without feedback or with feedback when averaged over all possible doppler frequencies is the same as the noise power transfer gain (see noise gain in TABLE C-1). Since the noise power density is uniform over the MTI filter, the filter treats both noise and signal (on the average) alike. Thus the signal-to-noise ratio (SNR) at the MTI canceller output is the same as at the input to the canceller when averaged over all possible doppler frequencies.

Interfering Signal

For an asynchronous interfering signal, a double stage MTI canceller will produce several interfering signal pulses at the canceller output for each interfering pulse at the MTI canceller input. These interfering pulses at the MTI canceller output are synchronous with the radar system (i.e., fall in the same range bin in successive azimuth change pulses). The amplitude of these pulses produced by a single interfering pulse are a function of the feed-forward coefficients (a_0, a_1, a_2) and the feedback coefficients (b_1 and b_2).

For the non-feedback MTI canceller mode (1 and 2 CASC, b_1 and $b_2 = 0$), the response of a double stage MTI canceller to a single interfering pulse is given in Equation C-35. Therefore, each interfering pulse produces three synchronous interfering pulses. Equation C-35 indicates that the interfering signal peak power transfer properties of a double stage MTI canceller due to the binomial weighting factors (feed-forward coefficients) is given by:

$$I_{MTI_{2o}} = I_{MTI_{2i}} \quad \text{; for } a_i = \tfrac{1}{2}, -1, \text{ and } \tfrac{1}{2} \qquad \text{(C-38a)}$$

$$I_{MTI_{2o}} = I_{MTI_{2i}} + 6 \text{ dB; for } a_i = 1, -2, \text{ and } 1 \qquad \text{(C-38b)}$$

Figure C-15 shows a photograph of a MTI canceller output measured on an ASR-8 operating in the 1 and 2 CASC mode. The center pulse in Figure C-15 is twice the amplitude of the first and third pulses due to the binomial weighting factors of 1/2, -1, and 1/2. Figure C-16 shows a simulated MTI canceller output for the 1 and 2 CASC mode, and a four volt interfering pulse. The two additional pulses generated by the MTI canceller are synchronous with the radar PRF.

Using Equations C-37 and C-38, the INR transfer properties of a double stage MTI canceller in non-feedback mode for $a_i = 1/2, -1$, and $1/2$ or $1, -2$, and 1 are given by:

$$INR_{MTI_{2o}} = INR_{MTI_{2i}} - 1.8 \text{ dB} \qquad \text{(C-39)}$$

The double stage MTI canceller output response after rectification to an interfering pulse for various feedback modes of operation were simulated and are shown in Figures C-17 through C-20. The simulated responses are for a four volt interfering signal at the MTI canceller input. The figures show that when operating in the feedback mode, there are more than three pulses out for each interfering pulse. However, by the third or fourth pulse, the interfering signal is down below noise level (1 volt) depending on the feedback constants and interfering signal level. The interfering signal peak

Figure C-15. Measured Double Stage MTI Canceller Response to an Interfering Pulse (1&2 CASC Mode)

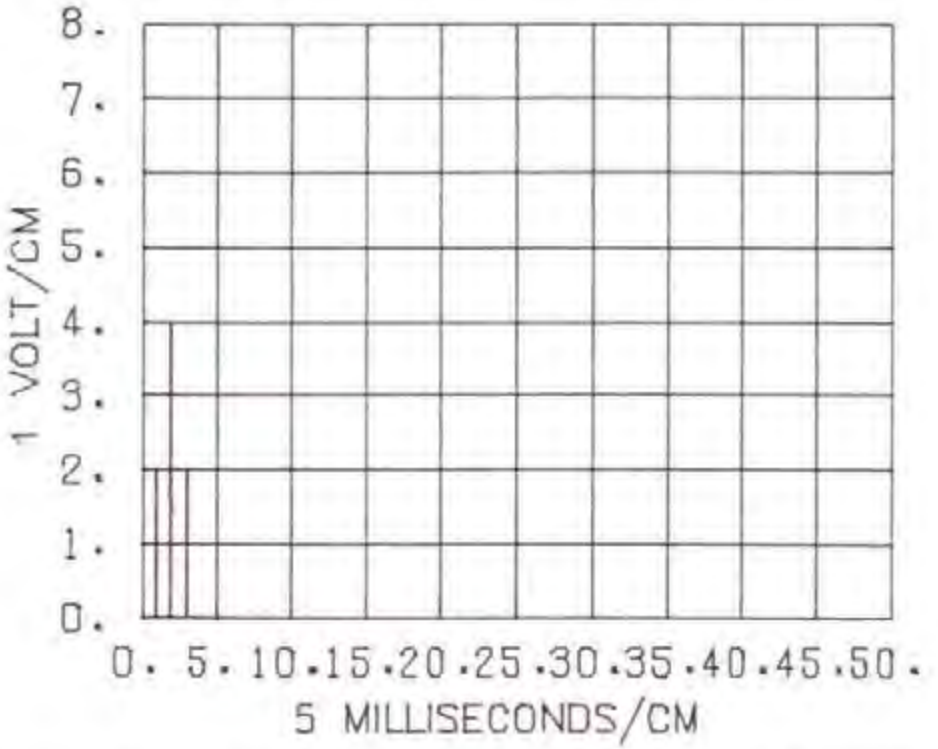

Figure C-16. Simulated Double Stage MTI Canceller Response to an Interfering Pulse (1&2 CASC Mode)

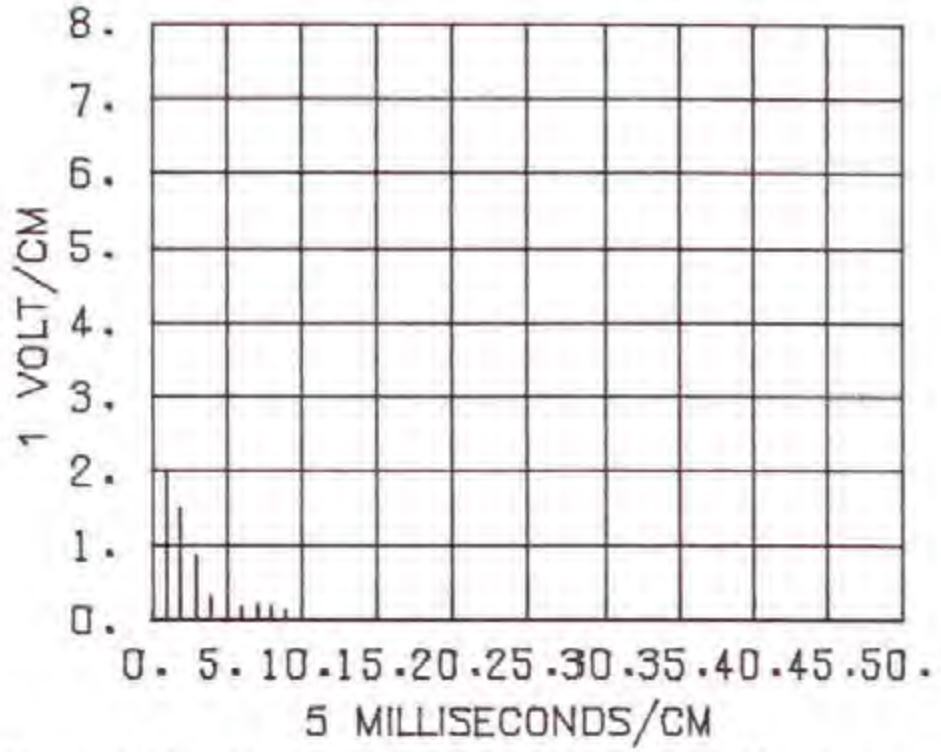

Figure C-17. Simulated Double Stage MTI Canceller Response to an Interfering Pulse (SCV-25 Mode)

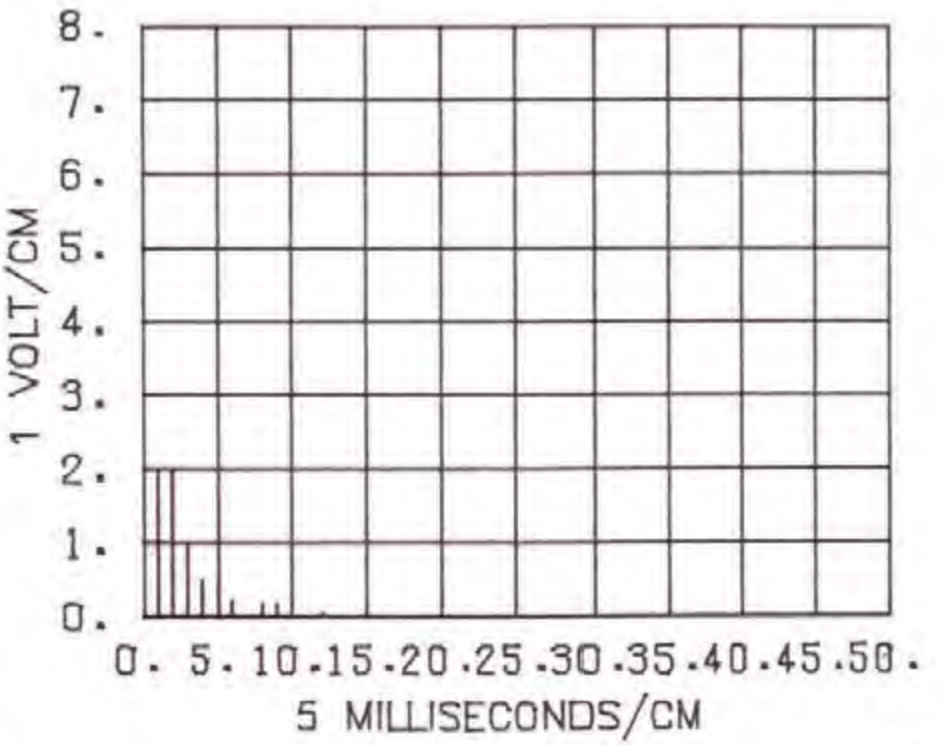

Figure C-18. Simulated Double Stage MTI Canceller Response to an Interfering Pulse (SCV-30 Mode)

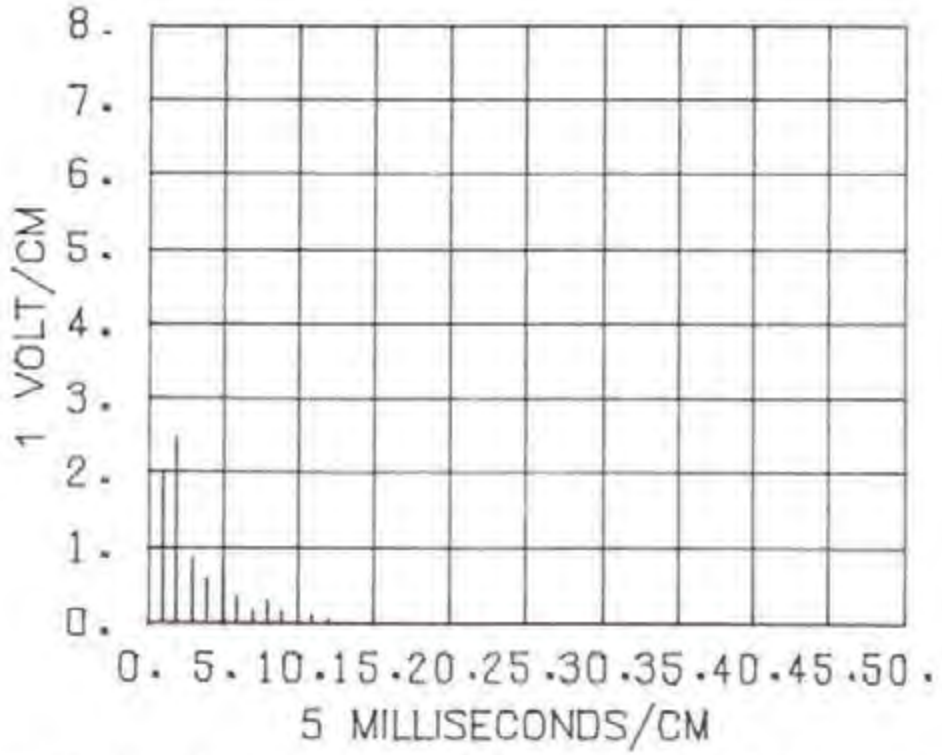

Figure C-19. Simulated Double Stage MTI Canceller Response to an Interfering Pulse (SCV-35 Mode)

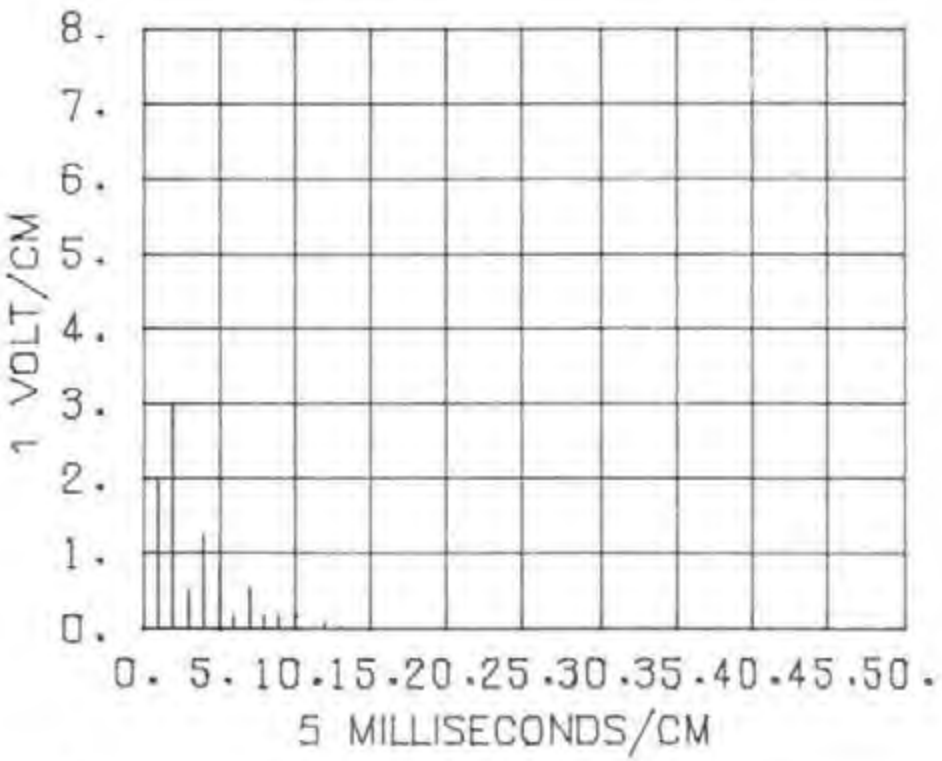

Figure C-20. Simulated Double Stage MTI Canceller Response to an Interfering Pulse (SCV-40 Mode)

power transfer properties for each of the MTI canceller modes are shown in TABLE C-1 along with the INR transfer properties of the various MTI canceller feedback modes.

RECTIFIER

The output of the MTI canceller circuits are fed to a full-wave rectifier in analog radars or an absolute value algorithm in digital radars to convert the bipolar video at the canceller output to unipolar. The rectifier output signal-to-noise ratio (SNR) is the same as at the rectifier input. The noise amplitude distribution at the full-wave rectifier output will be one-sided Gaussian since the noise amplitude at the MTI canceller output was Gaussian. The noise amplitude PDF at the rectifier output is given by:

$$p(v) = \frac{2}{\sqrt{2\pi}\sigma} e^{-v^2/2\sigma^2} \quad ; \; o \leq v \leq \infty \qquad \text{(C-40)}$$

Where:

σ = rms noise level, in volts

The desired signal-plus-noise amplitude distribution PDF at the single channel MTI rectifier output for a double stage MTI canceller is shown in Figure C-21. It should be noted that the rectifier output signal-plus-noise amplitude distribution PDF shown in Figure C-21 is for the radar operating in the staggered mode and the signal averaged over all possible doppler frequencies. The PDF shown in Figure C-21 was obtained by simulation. Although the signal-plus-noise amplitude distribution PDF at the rectifier output is not of the nature of a one-sided Gaussian distribution, it can be approximated by:

$$p(v,A) = \frac{2}{\sqrt{2\pi(\sigma^2+A^2/2)}} e^{-v^2/2(\sigma^2+A^2/2)} \quad ; \; o \leq v \leq +\infty \qquad \text{(C-41)}$$

where:

σ = rms noise level, in volts

A = Desired signal amplitude, in volts

Figure C-22 shows a plot of Equation C-41 for comparison with the

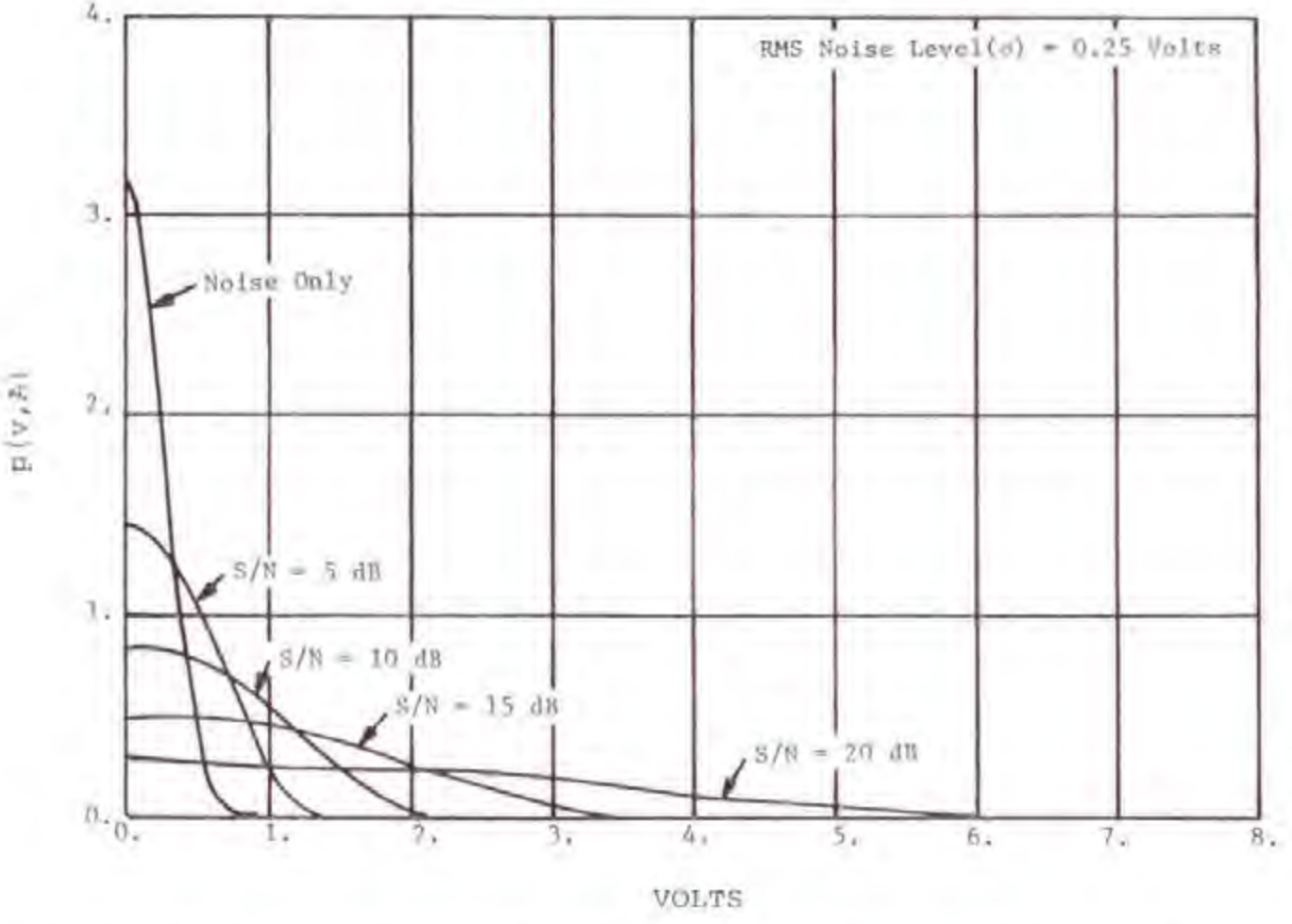

Figure C-21. Probability Density Function for Noise Only and for Signal-Plus-Noise at the MTI Canceller Output for a Single Channel Double Stage Canceller (Simulated).

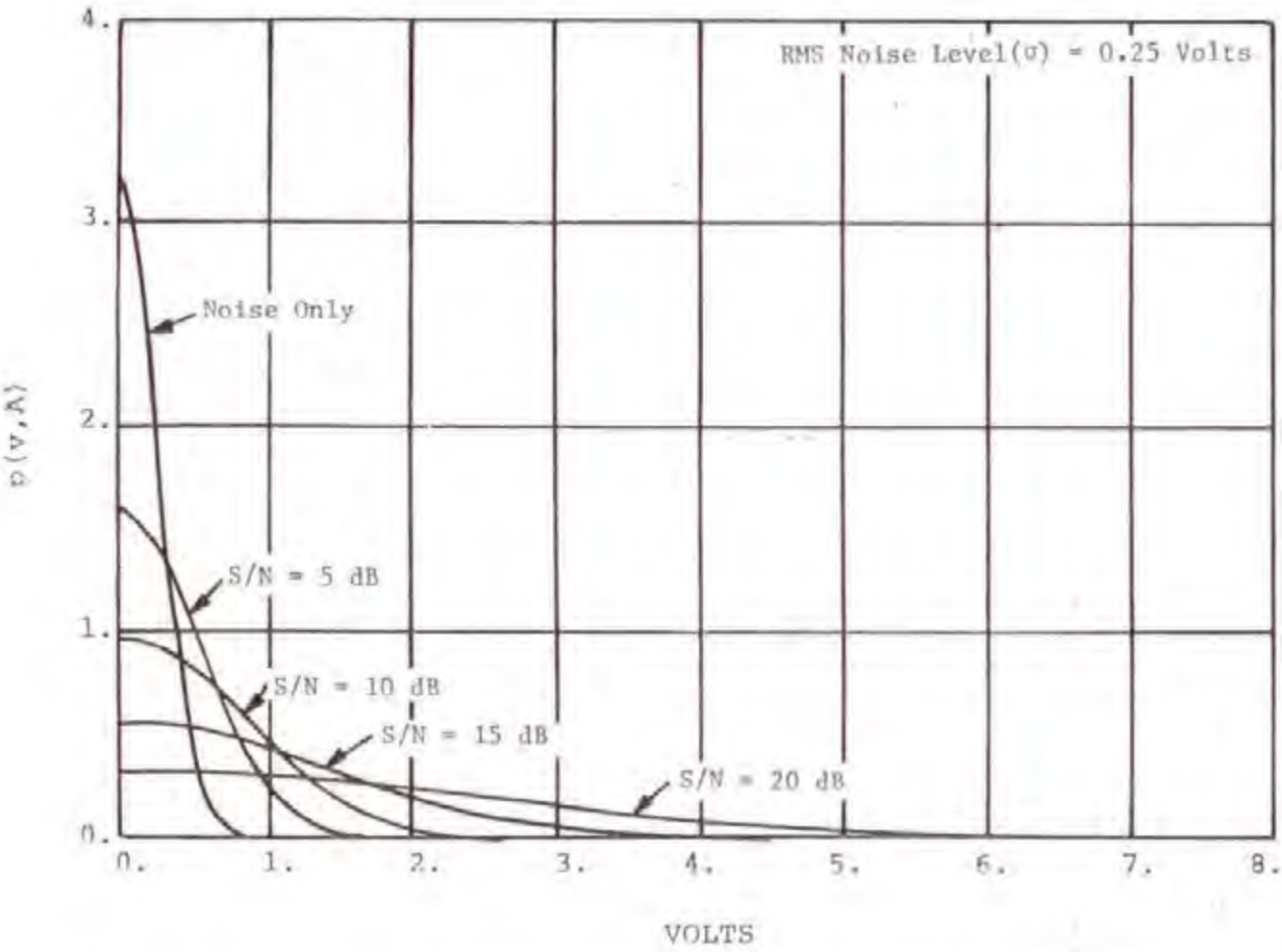

Figure C-22. Probability Density Function of One-Sided Gaussian Distribution (Equation C-41).

simulated single channel MTI rectifier output signal-plus-noise amplitude distribution PDF shown in Figure C-21.

DUAL MTI CHANNEL TRANSFER PROPERTIES

Figure C-2 shows a block diagram of a dual channel (inphase and quadrature) MTI radar. The signal transfer properties of the inphase and quadrature channels are identical to the single channel transfer properties previously discussed. The output of each channel is combined in the following manner:

$$R = \sqrt{(I)^2 + (Q)^2} \qquad \text{(C-42)}$$

Circuit implementation to achieve Equation C-42 in the combiner is complex. Often a simplified approximation to Equation C-42 is implemented by summing the larger vector amplitude with one-half the smaller vector amplitude as shown below:

$$\begin{aligned} R &= |I| + |Q/2| \text{ if } |I| > |Q| \\ R &= |Q| + |I/2| \text{ if } |I| \leq |Q| \end{aligned} \qquad \text{(C-43)}$$

The noise amplitude distribution at the output of a dual MTI canceller is Rayleigh since the transfer properties of the combiner (Equation C-42) are similar to an envelope detector. The desired signal-plus-noise amplitude distribution PDF at the dual channel MTI combiner output for a double stage MTI canceller is shown in Figure C-23. It should be noted that the combiner output signal-plus-noise amplitude distribution PDF shown in Figure C-23 is for the radar operating in the staggered mode and the signal averaged over all possible doppler frequencies. The PDF shown in Figure C-23 was obtained by simulation. Although the signal-plus-noise amplitude distribution PDF at the combiner output is not of the nature of a Rayleigh distribution, it can be approximated by:

$$p(v,A) = \frac{v}{(\sigma^2 + A^2/2)} e^{-v^2/2(\sigma^2 + A^2/2)} \quad ; \quad 0 \leq v \leq +\infty \qquad \text{(C-44)}$$

where:

σ = rms noise level, in volts

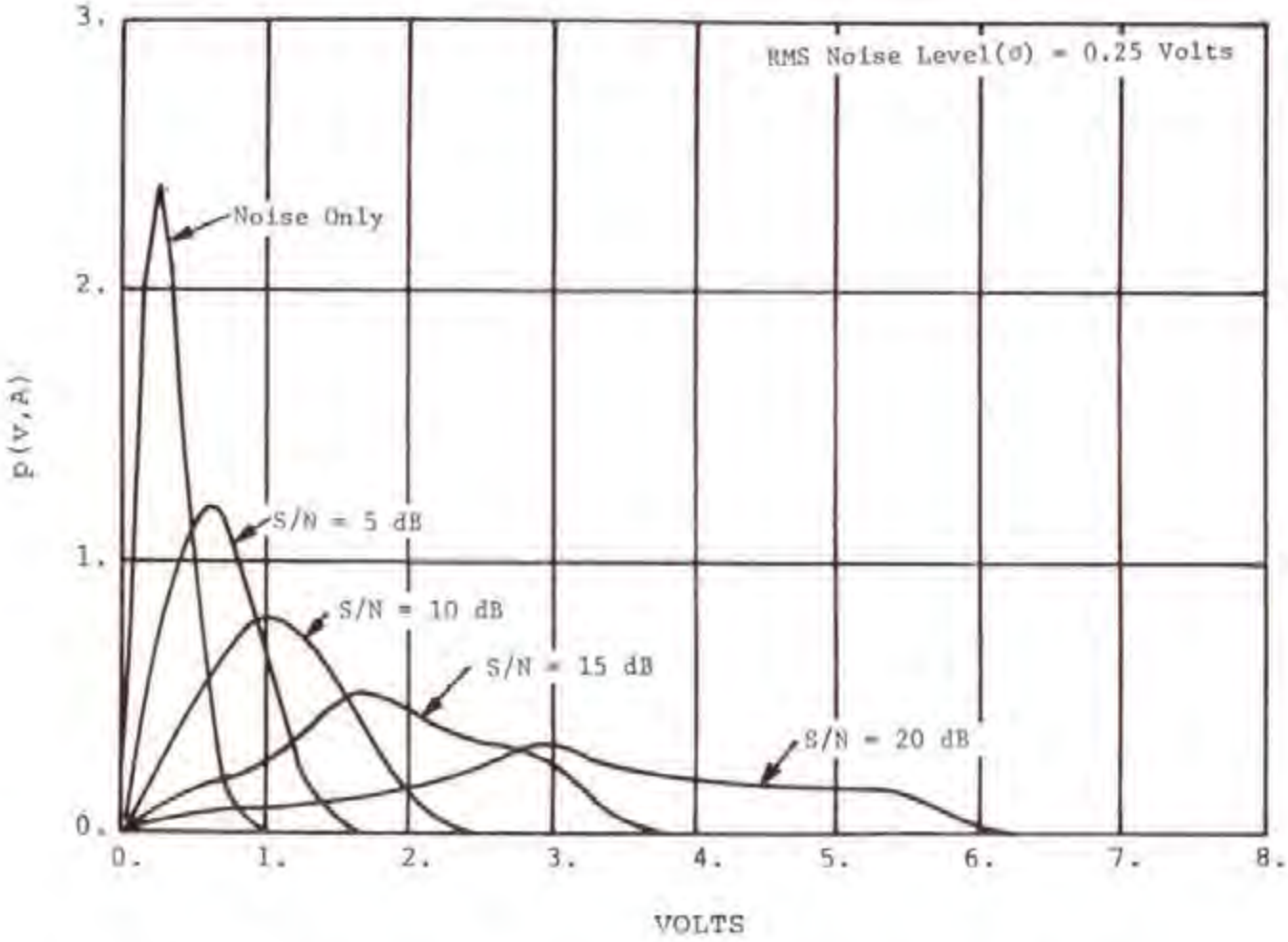

Figure C-23. Probability Density Function for Noise Only and for Signal-Plus-Noise at the MTI Canceller Output for a Dual Channel Double Stage Canceller (Simulated).

A = Desired signal amplitude, in volts

Figure C-24 shows a plot of Equation C-44 for comparison with the simulated dual channel MTI combiner output signal-plus-noise amplitude distribution PDF shown in Figure C-23.

The fact that dual MTI cancellers have the COHO reference signal of the inphase and quadrature channels phase shifted by 90 degrees, and the method in which the two channels are combined, a signal-to-noise ratio (SNR) improvement is achieved over a single MTI channel. The SNR improvement of dual MTI channels over a single MTI channel was investigated (Nathanson and Luke, 1972), and is shown in TABLE C-2. The table shows the SNR improvement for a single pulse (unintegrated pulse train) as a function of probability of false alarm (P_f) and probability of detection (P_d). For an asynchronous interfering signal, the INR enhancement of a dual MTI channel over a single MTI channel is approximately 1 to 2 dB at MDS.

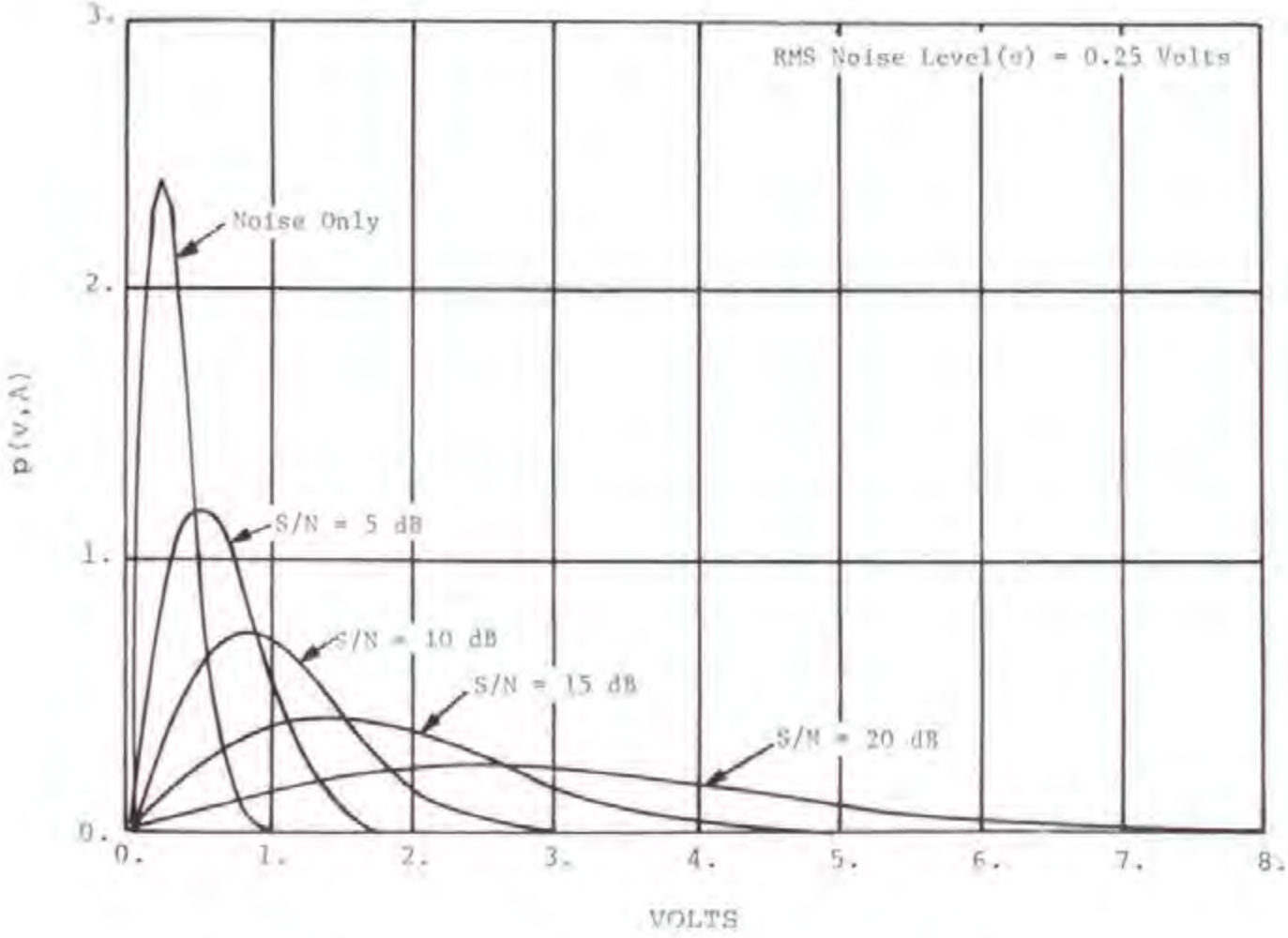

Figure C-24. Probability Density Function of Rayleigh Distribution (Equation C-44).

TABLE C-2

SIGNAL-TO-NOISE IMPROVEMENT (IN DECIBELS) RELATIVE TO DETECTION OF $I^2 + Q^2$ (FLUCTUATING SIGNAL), SINGLE PULSE

	|I| Only or |Q| Only						
P_f / P_a	10^{-1}	10^{-2}	10^{-3}	10^{-4}	10^{-6}	10^{-8}	10^{-10}
0.5	3.29	3.81	4.05	4.19	4.35	4.45	4.51
0.8	6.45	7.17	7.48	7.66	7.80	7.97	8.04
0.9	9.12	9.92	10.26	10.45	10.66	10.78	10.85
0.95	11.95	12.79	13.14	13.34	13.56	13.68	13.76

APPENDIX D

INTEGRATOR TRANSFER PROPERTIES

INTRODUCTION

The process of summing the echo pulses from a target is called integration. This appendix discusses the transfer properties of integrators (enhancers) used by radars in the 2.7 to 2.9 GHz band. The discussion includes the integrator transfer properties of noise, desired signal, and asynchronous interfering signals. It should be noted that this appendix does not discuss the cathode ray tube display integration, or the integration properties of the eye and brain of the radar operator, but is limited to the discussion of electronic device integrators only.

Integrators are generally used in the primary radars for two reasons:

1. To enhance weak desired targets for PPI display.

2. To suppress asynchronous pulsed interference.

The principle of the radar video integrator is that radar signal returns from a point target consist of a series of pulses generated as the radar antenna beam scans past the target, all of which fall in the same range bin in successive periods (synchronous with the system). It is this series of synchronous pulses from a target which permits integration of target returns to enhance the weak signals. The number of pulse returns (N) from a target depends upon the radar antenna beamwidth (BW), the rate of antenna rotation (RPM), the radar pulse repetition rate (PRF) and the target characteristics. The equation for the number of pulses from a point target is given by (Skolnik, 1962):

$$N = \frac{PRF \cdot BW}{6 \cdot RPM} \qquad (D-1)$$

Where:

PRF = Radar pulse repetition frequency, in PPS

BW = Antenna 3 dB beamwidth, in degrees

RPM = Antenna scan rate, in rpm

A range value of N for radars in the 2.7 to 2.9 GHz band is 12 to 20. The integrator will suppress asynchronous interference since the interfering pulses will not be separated in time by the radar period, and thus will not occur in the same range bin in successive periods (asynchronous with the system). Therefore, the asynchronous interference will not add-up, and can be suppressed.

All radars in the 2.7 to 2.9 GHz band employ post detection or noncoherent integrators. The types of post detection integrator employed in radars in the 2.7 to 2.9 GHz band can be categorized either as a feedback integrator or a binary integrator. Radars employing feedback integrators may be of analog (delay line) or digital (shift register) type. Only digital binary integrators are used.

The following is a discussion of the transfer properties of the feedback and binary integrators. The noise, desired signal and asynchronous interfering signal transfer properties are discussed along with the tradeoffs of the desired signal transfer properties in suppressing asynchronous interference. The transfer properties were investigated by measurements, analytically and by simulating the noise, desired signal, interfering signals, and the feedback and binary integrator hardware. Appendix E contains a detailed discussion of the methods used to simulate the noise, desired signal, interfering signal, and the actual radar hardware simulated.

FEEDBACK INTEGRATOR

Figure D-1 shows a block diagram of a typical feedback integrator. The radar period delay (1/PRF) for digital radars is achieved by clocking a shift register, and the actual integrator hardware is essentially represented in Figure D-1. Analog radars in the 2.7 to 2.9 GHz band generally use quartz delay lines, thus accomplishing the delay acoustically to reduce the size of the delay line. However, the inherent loss of quartz delay lines requires use of additional hardware, such as, modulators, attenuators, amplifiers, detectors, and balancing circuits (AGC) to achieve integration. If the analog integrator balancing circuitry is aligned properly, the transfer properties of an analog integrator can, for analytical simplicity, be modeled by the operations shown in Figure D-1. Digital integrators will also introduce some roundoff or truncation error. However, the error due to roundoff and truncation is generally very small and can be neglected in most cases.

The feedback integrator depicted in Figure D-1 consists of an input limiter, an adder, and a feedback loop with an output limiter and a delay equal to the time between transmitter pulses (1/PRF). The following is a discussion of the transfer properties of these feedback integrator elements to noise, desired signal and asynchronous interference.

Input Limiter Transfer Properties

The integrator input limiter serves as a video clipping circuit to provide constant level input pulses to the feedback integrator, and is a necessary integrator circuit element to suppress asynchronous interference. The input limiter limit level is always adjustable, and controls the transfer properties of the feedback integrator. The effect of the limiter limit level setting on the desired signal, interfering signal, and noise transfer properties of the integrator are discussed in detail in latter sections of this appendix. The desired signal-to-noise (SNR) transfer properties of the

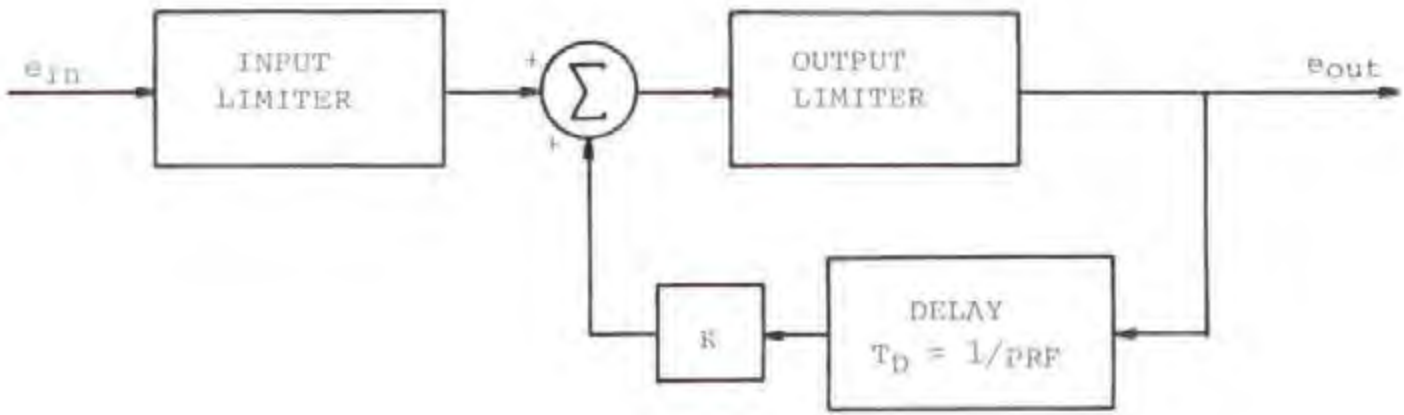

Figure D-1. Feedback Integrator Block Diagram

limiter are given by:

$$SNR_o = \begin{cases} SNR_i ; \text{for } SNR_i < LNR \\ LNR ; \text{for } SNR_i \geq LNR \end{cases} \qquad (D\text{-}2)$$

Where:

SNR_o = Limiter output peak signal-to-rms noise ratio, in dB

SNR_i = Limiter input peak signal-to-rms noise ratio, in dB

LNR = Limiter limit-to-*rms* noise ratio, in dB

The interference-to-noise (INR) transfer properties of the input limiter can also be expressed by Equation D-2. Also Equation D-2 represents the transfer properties of the output limiter. Generally the output limiter limit level is set at 4.0 volts.

Feedback Integrator Loop Transfer Properties

The feedback integrator loop consists of an adder, an output limiter, a feedback loop with a delay equal to the time between transmitter pulses (1/PRF) and a loop gain of K. The overall gain, K, of the feedback loop is less than unity to prevent instability.

The signal transfer properties of the integrator feedback loop to noise, desired signal, and asynchronous interference will be treated separately. This is possible since the integrator feedback loop is a linear device. First consider noise.

Noise

The noise voltage amplitude distribution at the feedback integrator input is either Rayleigh distributed (normal channel or inphase and quadrature MTI channel) or a one-sided Gaussian distributed (single channel MTI). Both the Rayleigh and one-sided Gaussian distributions have a non-zero mean. To minimize the noise gain through the feedback integrator, prior to the feedback integrator circuitry shown in Figure D-1, the radar receivers generally have an attenuator, subtractor and bottom clipper. The noise transfer properties of a non-zero mean distribution can be expressed as:

$$n_{I_o} = \left[\sum_{j=0}^{n} K^{2j} \sigma_{n_{I_j}}^2 + \left(\sum_{j=0}^{n} K^j \mu_{n_{I_j}} \right)^2 \right]^{\frac{1}{2}} \qquad (D\text{-}3)$$

Where:

$\sigma_{n_{Ii}}$ = The input noise amplitude distribution rms level, in volts

$\mu_{n_{Ii}}$ = The input noise amplitude distribution mean level, in volts

K = Integrator feedback factor.

The sum series in the above equation are a geometric series, and the equation can be rewritten as:

$$n_{Io} = \left[\sigma^2_{n_{Ii}} \left(\frac{1}{1 - K^2} \right) + \mu^2_{n_{Ii}} \left(\frac{1}{1 - K} \right)^2 \right]^{\frac{1}{2}} \qquad \text{(D-4a)}$$

The affect of the attenuator, subtractor, and bottom clipper is to reduce the mean level of the noise amplitude distribution. Alignment procedures of this circuitry generally result in the rms noise level being much greater than the mean noise level. In this case, the second term of Equation D-4a can be neglected for analytical simplicity, and the noise treated as an uncorrelated zero mean amplitude distribution. Making this assumption, Equation D-4a becomes:

$$n_{Io} = \sigma_{n_{Ii}} \left[\frac{1}{1-K^2} \right]^{\frac{1}{2}} \qquad \text{(D-4b)}$$

Therefore, the noise power transfer function of a feedback integrator loop for the radar normal channel is:

$$n_{Io} = N_{Ii} - 10 \log_{10} (1-K^2) \qquad \text{(D-5)}$$

In digital radars such as the ASR-8, the analog-to-digital (A/D) converter causes quantization errors due to truncation. The truncation at low signal levels (less than one volt) has an effect of causing a non-linear feedback constant, K. For low signal levels the feedback signal can vary between K and approximately 1/2. This has an overall affect of reducing the feedback integrator noise gain given by Equation D-4b.

Since the feedback integrator sums or convolves the noise distribution at the input of the feedback loop with itself continuously, the central limit theorem applies which states that the noise distribution at the integrator feedback loop output will be Gaussian distributed even though the input noise distribution was Rayleigh (normal or dual MTI channel).

The noise out of the MTI channel is correlated from range/azimuth cell to range/azimuth cell. Figure D-2 shows how the noise becomes correlated by the transfer properties of a second-order MTI filter. The figure shows the input noise samples (N_1 through N_5) for a specific instant in time (T_1 through T_5). The noise level at the canceller output as a function of time (T_1 through T_5) is also shown. The figure shows that at time T_5, the noise output consists of noise samples N_3, N_4, and N_5. At time T_4, the noise output consists of noise samples N_2, N_3, and N_4. Since noise samples N_3 and N_4 contribute to the noise level at time T_4 and T_5, the noise at the MTI canceller output is correlated. The increase in noise amplitude caused by the integration of the correlated MTI channel noise, is a function of the MTI canceller Type (single stage canceller, double stage canceller, etc.). The MTI channel noise level increase was simulated by Trunk, 1977, and found to be approximately 1 dB for a single stage canceller and 1.8 dB for a double stage canceller. Therefore, the feedback integrator noise transfer properties for the MTI channel can be obtained using Equation D-5 and adding 1 dB for a single stage MTI canceller and 1.8 dB for a double stage MTI canceller.

Desired Signal

The desired signal phases at the input of the feedback loop integrator are coherent and add directly since the feedback loop delay is equal to the desired signal pulse period. For the feedback loop shown in Figure D-1, the general output response (Y_N) at the Nth input pulse (X_N) is given by:

$$Y_N = X_N + Y_{N-1} \tag{D-6}$$

Equation D-6 is a first order constant coefficient linear difference equation with a solution

$$Y_N = \left(\frac{1-K^N}{1-K}\right) X_N \tag{D-7}$$

Recognizing the transfer function in Equation D-7 as the geometric progression for a series, Equation D-7 becomes:

$$Y_N = \left[1+K+K^2+\ldots+K^{N-1}\right] \cdot X_N \tag{D-8a}$$

$$Y_N = \sum_{i=1}^{N} K^{(i-1)} \cdot X_N \tag{D-8b}$$

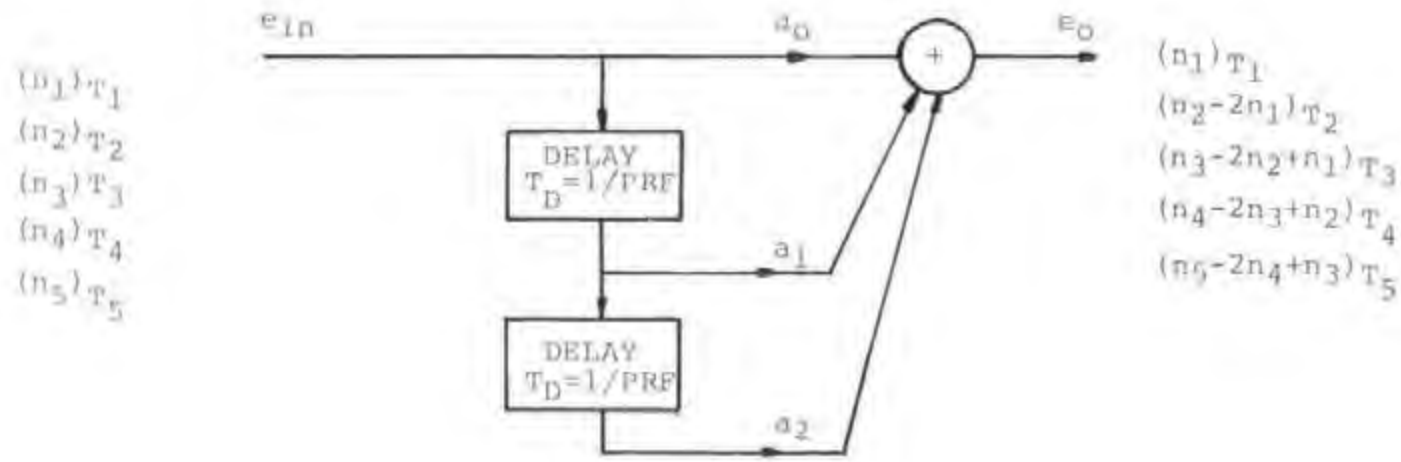

Figure D-2. Canonical Form of Second-Order MTI Canceller Filter Showing Noise Correlation at MTI Channel Output

Thus, for N equal amplitude voltage input pulses (S_{Ii}), the Nth pulse amplitude at the integrator output (S_{Io}) can be expressed as:

$$S_{Io} = S_{Ii} \sum_{i=1}^{N} K^{(i-1)} \qquad (D-9)$$

The series expressed in Equation D-8a can be intuitively obtained using Figure D-1 (feedback loop), and recursively applying a series of N equal voltage amplitude pulses to the input.

The signal-to-noise ratio enhancement (SNR_E) factor for the integrator feedback loop for the normal channel can be obtained from Equations D-4b and D-7, and is given by:

$$SNR_E = 20 \log_{10} \left[\left(\frac{1-K^N}{1-K} \right) (1-K^2)^{1/2} \right] \qquad (D-10)$$

It should be noted that Equation D-10 is only a first order approximation of the actual signal-to-noise ratio enhancement of a feedback integrator since it assumes a zero mean noise amplitude distribution, and a constant desired signal level. For the MTI channel the signal-to-noise ratio enhancement given by Equation D-10 should be reduced by 1.0 dB for a single stage canceller and 1.8 dB for a double stage MTI canceller due to the correlation of noise by the MTI cancellers.

Equation D-10 can be used to approximate the optimum feedback factor K for the radar design by maximizing the signal-to-noise ratio enhancement (SNR_E). TABLE D-1 shows the SNR_E as a function of the integrator feedback factor (K) for a range of number of pulses integrated (N) between 12 and 20, which is a typical range of N for radionavigation radars in the 2.7 to 2.9 GHz band. The asterisks in each column of the table indicate the maximum SNR_E and optimum integrator feedback factor (K) for that particular value of N. For the range of number of pulses integrated (N) between 12 and 20, the optimum feedback factor (K) ranges from .90 to .94. The table also shows that if an integrator feedback factor of .92 is used for radars with a range of N between 12 and 20, the loss in actual SNR_E and maximum SNR_E is less than .1 dB. Therefore, the design of the integrator feedback factor (K) for a range of number of pulses integrated is not that critical.

Actually, the optimum value of K is difficult to obtain due to fluctuations in target returns (scintillation) and antenna pattern amplitude modulation, and thus requires a complicated Monte Carlo model to determine. Skolnik (1970) gives an empirical value of K as:

$$K = 1 - \frac{1.56}{N} \qquad (D-11)$$

TABLE D-1

FEEDBACK INTEGRATOR PEAK SIGNAL-TO-NOISE ENHANCEMENT
FOR NORMAL CHANNEL **

Feedback Factor K	Peak Signal-to-Noise Enhancement (SNR_E)				
	N=12	N=14	N-16	N=18	N=20
.70	7.41	7.47	7.50	7.52	7.53
.71	7.56	7.63	7.67	7.69	7.70
.72	7.71	7.80	7.84	7.86	7.87
.73	7.87	7.96	8.01	8.04	8.05
.74	8.02	8.13	8.19	8.22	8.23
.75	8.17	8.29	8.36	8.40	8.42
.76	8.32	8.46	8.54	8.59	8.62
.77	8.48	8.64	8.73	8.78	8.82
.78	8.63	8.81	8.92	8.98	9.02
.79	8.78	8.98	9.10	9.18	9.23
.80	8.92	9.15	9.29	9.38	9.44
.81	9.07	9.32	9.49	9.59	9.66
.82	9.21	9.49	9.68	9.80	9.88
.83	9.34	9.66	9.87	10.01	10.11
.84	9.46	9.82	10.06	10.22	10.34
.85	9.58	9.97	10.24	10.43	10.57
.86	9.68	10.11	10.42	10.64	10.80
.87	9.77	10.25	10.59	10.84	11.03
.88	9.84	10.36	10.75	11.03	11.25
.89	9.89	10.46	10.89	11.21	11.46
.90	9.90*	10.53	11.01	11.37	11.66
.91	9.89	10.57*	11.10	11.51	11.84
.92	9.82	10.56	11.15*	11.61	11.99
.93	9.69	10.50	11.14	11.66*	12.09
.94	9.48	10.36	11.06	11.64	12.12*
.95	9.16	10.10	10.87	11.51	12.05
.96	8.66	9.68	10.52	11.23	11.83
.97	7.89	8.98	9.90	10.68	11.36
.98	6.62	7.79	8.78	9.64	10.39
.99	4.10	5.35	6.43	7.36	8.19

*Maximum signal-to-noise ratio enhancement
**For MTI channel signal-to-noise ratio enhancement reduce the values in the table by 1.0 dB for a single stage canceler and 1.8 dB for a double stage canceler.

For N = 20, the value for K from Equation D-11 is .92, which is close to the value of K obtained using Equation D-10 (see TABLE D-1).

Studies (Trunk, 1970) have been made which take into account pulse amplitude variations due to the antenna beam shape. Trunk concluded that the SNR_E could be reduced by as much as 1.6 dB due to the antenna beam shape pulse amplitude variations. The actual reduction in SNR_E due to the radar antenna pattern is between 0 and 1.6 dB, and is also a function of the integrator input limiter limit level setting.

In congested areas where there is potential for asynchronous interference, adjustments to the integrator input limit level setting are required to suppress the asynchronous interference. However, adjustments of the limiter level setting affect the desired signal pulse train processing characteristics of the feedback integrator. Desired signal pulse train characteristics which are effected include: target azimuth shift, angular resolution and probability of detection. The following is a discussion of the desired signal transfer properties of a feedback integrator loop as a function of the input signal-to-noise ratio (SNR) and input limiter level setting.

Figures D-3 through D-6 show a simulated radar performance of a feedback enhancer for the normal channel as a function of the signal-to-noise ratio (SNR). The enhancer input limiter limit level (V_L) was set at 2.0 volts, and the feedback factor (K) was set at 0.94. The desired target return pulse train consists of 20 pulses. Each figure shows the simulated radar output with the enhancer off (unintegrated) and enhancer on (integrated). Figures D-3 (SNR = 3 dB) and D-4 (SNR = 5 dB)show that with the enhancer off the desired signal is down in the noise. However, when the enhancer is on the signal is pulled out of the noise by the feedback enhancer. Figures D-7 through D-10 show the affect on the desired signal of adjusting the input limiter limit level (V_L) of the feedback enhancer. The SNR for Figures D-7 through D-10 was 15 dB. For comparison with the simulated integrator model (Figures D-7 through D-10), Figures D-11 through D-13 show actual measured ASR-8 normal channel integrated output for input limiter switch settings of 15, 9, and 7, respectively. The receiver input desired signal level was set at -84 dBm.

The target azimuth shift (ω_s) due to integration can be calculated by:

$$\omega_s = \Delta C_p \cdot \theta_s \qquad \text{(D-12)}$$

Where:

ΔC_p = Shift of the center pulse position of an integrated video pulse train relative to an unintegrated pulse train (Figure D-6a).

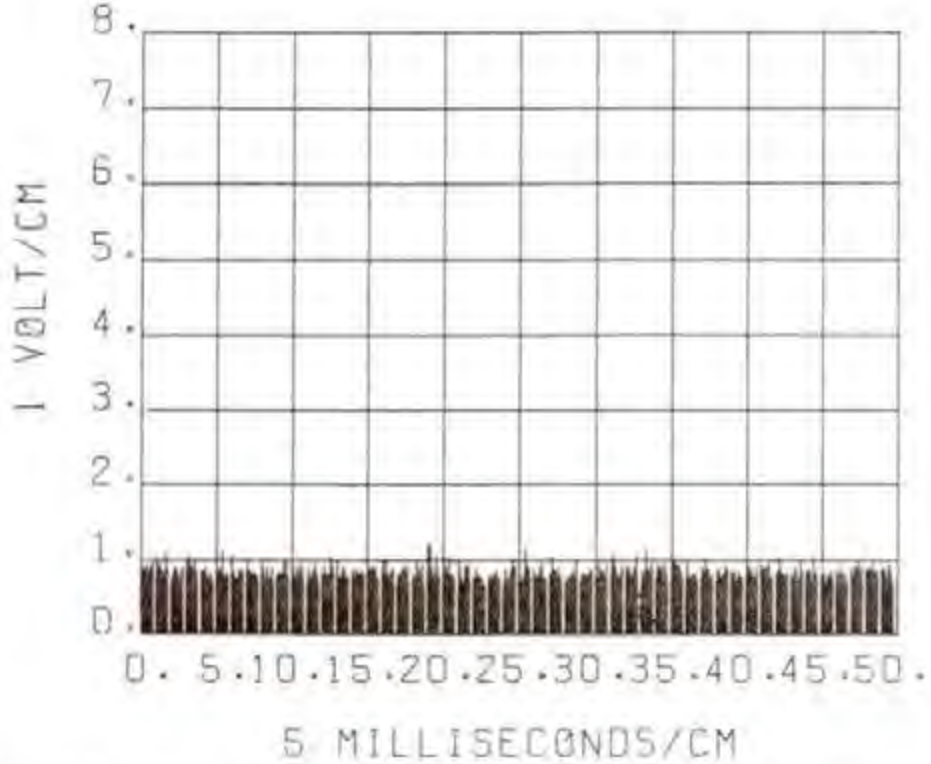

Figure D-3a. Simulated Normal Channel Unintegrated Target Return Pulse Train for a SNR = 3dB

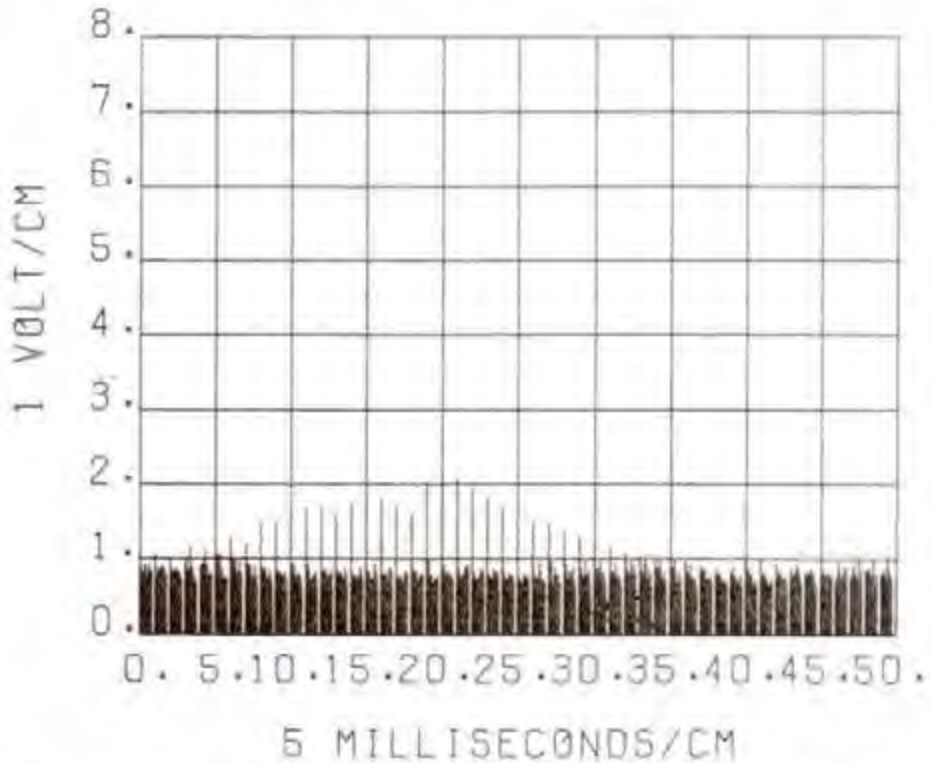

Figure D-3b. Simulated Normal Channel Integrated Target Return Pulse Train for a SNR = 3dB (V_L = 2.0)

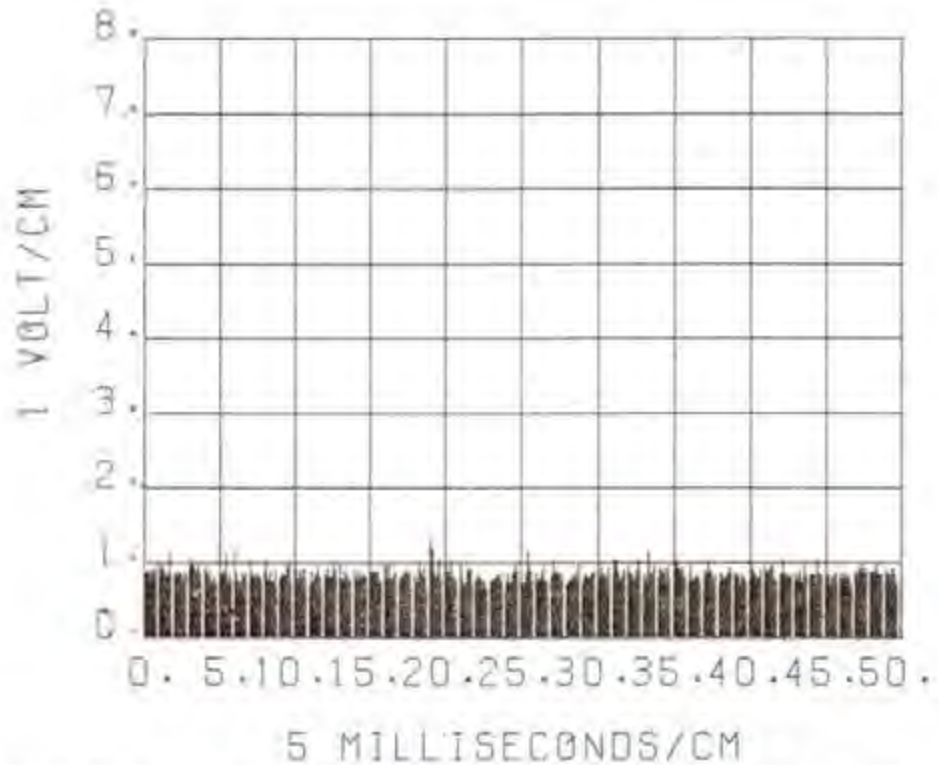

Figure D-4a. Simulated Normal Channel Unintegrated Target Return Pulse Train for a SNR = 5dB

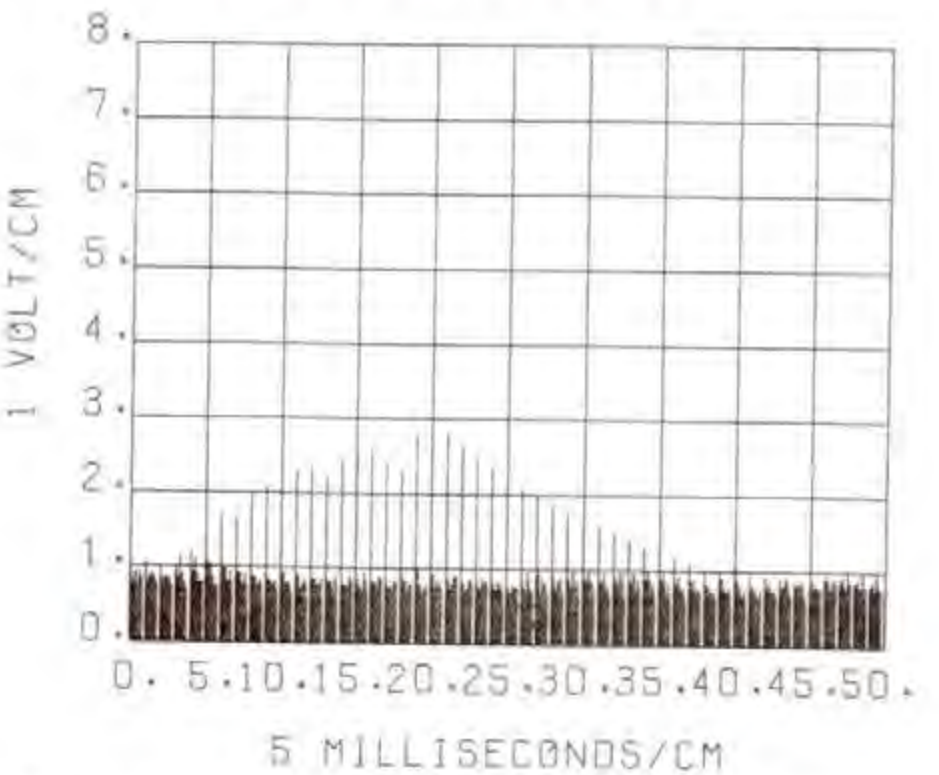

Figure D-4b. Simulated Normal Channel Integrated Target Return Pulse Train for a SNR = 5dB (V_L = 2.0)

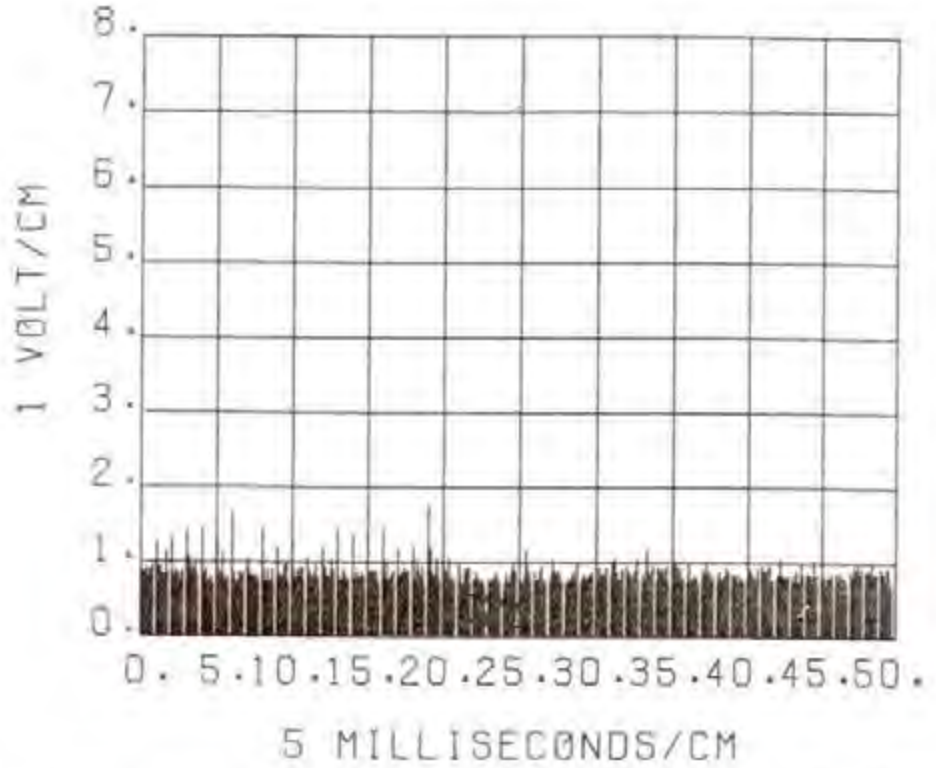

Figure D-5a. Simulated Normal Channel Unintegrated Target Return Pulse Train for a SNR = 10dB

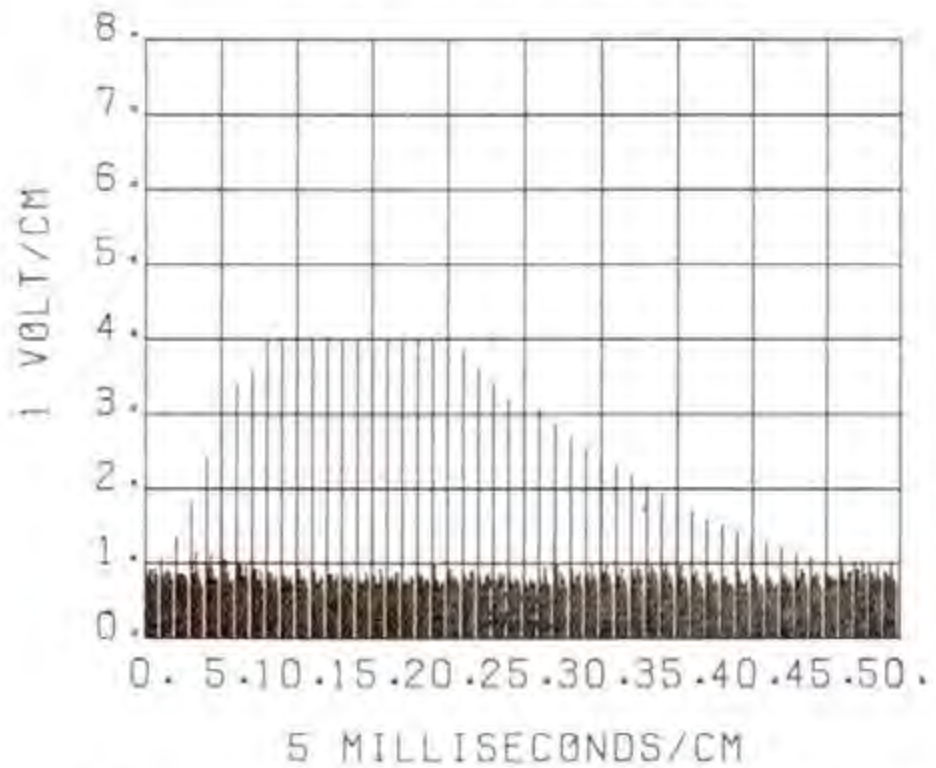

Figure D-5b. Simulated Normal Channel Integrated Target Return Pulse Train for a SNR = 10dB (V_L = 2.0)

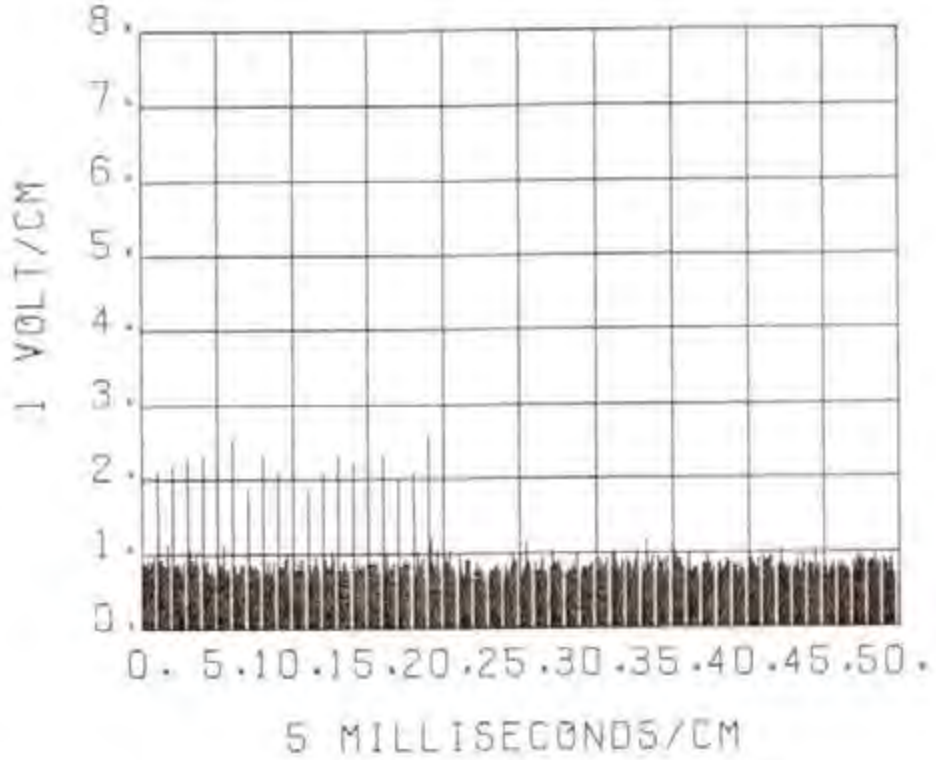

Figure D-6a. Simulated Normal Channel Unintegrated Target Return Pulse Train for a SNR = 15dB

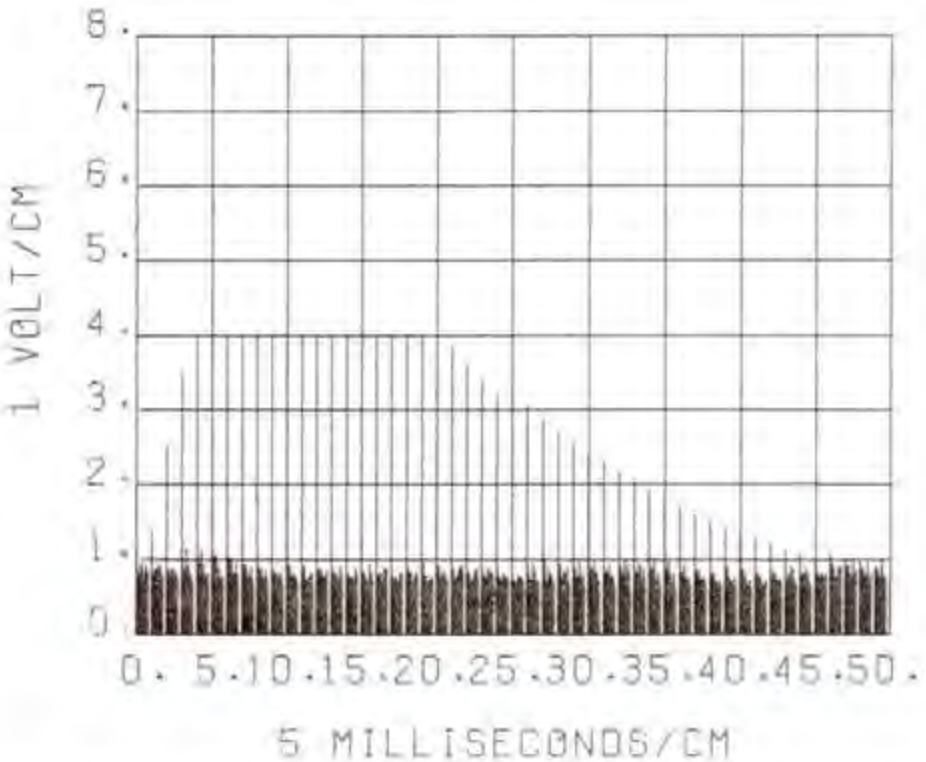

Figure D-6b. Simulated Normal Channel Integrated Target Return Pulse Train for a SNR = 15dB (V_L = 2.0)

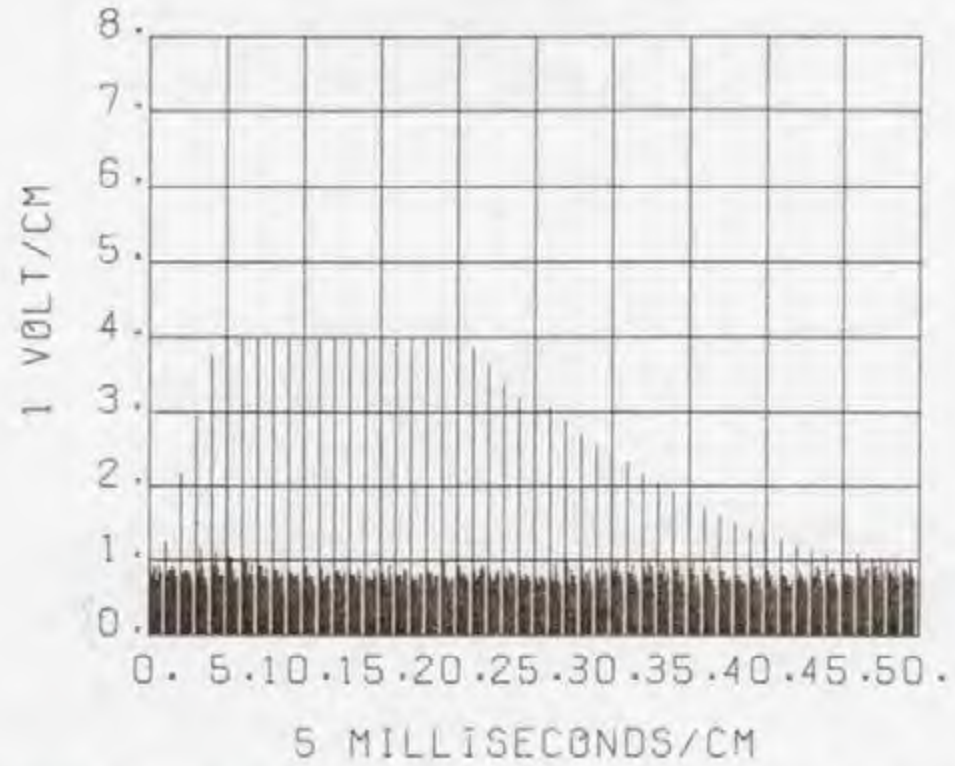

Figure D-7. Simulated Normal Channel Integrated Target Return Pulse Train for a SNR = 15 (V_L = 1.0)

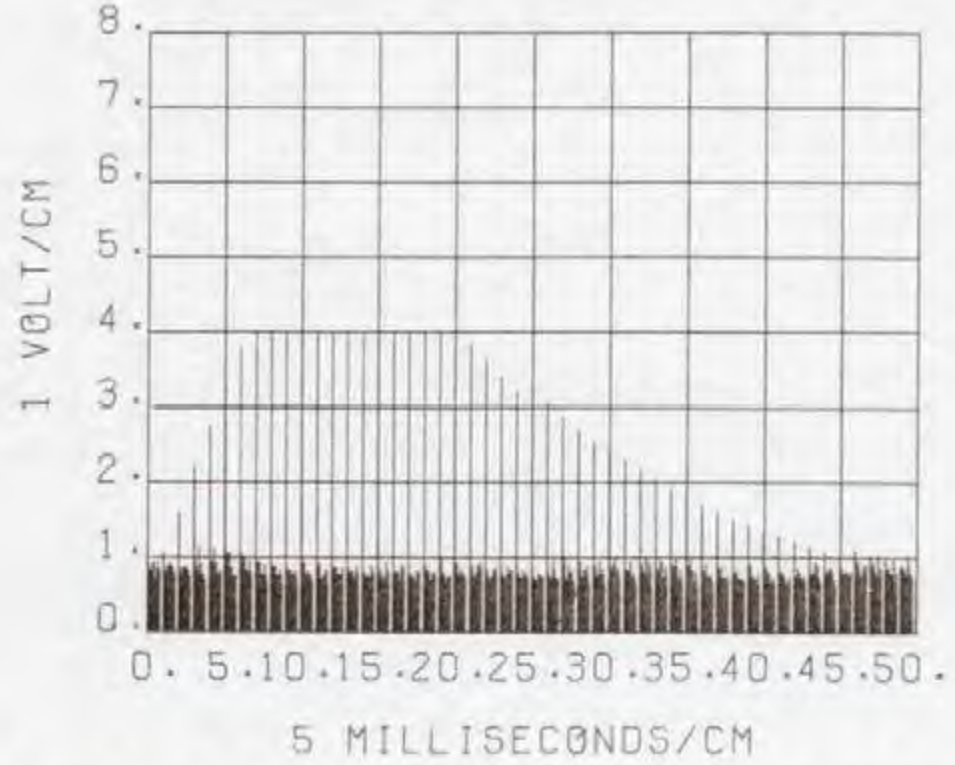

Figure D-8. Simulated Normal Channel Integrated Target Return Train for a SNR = 15 (V_L = 0.7)

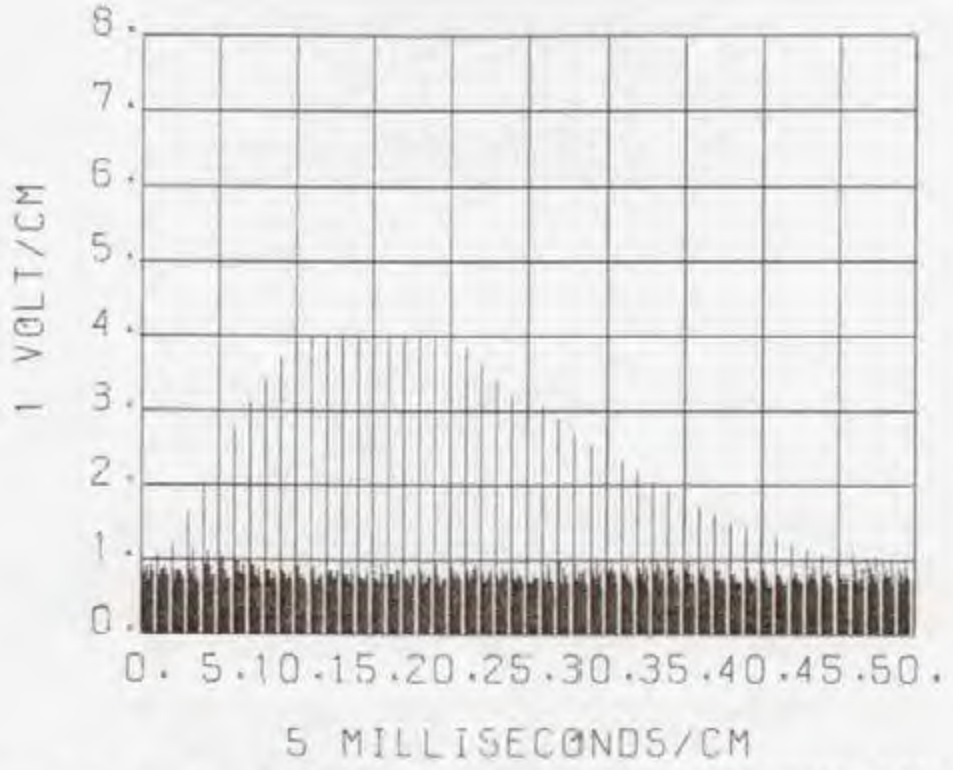

Figure D-9. Simulated Normal Channel Integrated Target Return Pulse Train for a SNR = 15 (V_L = 0.5)

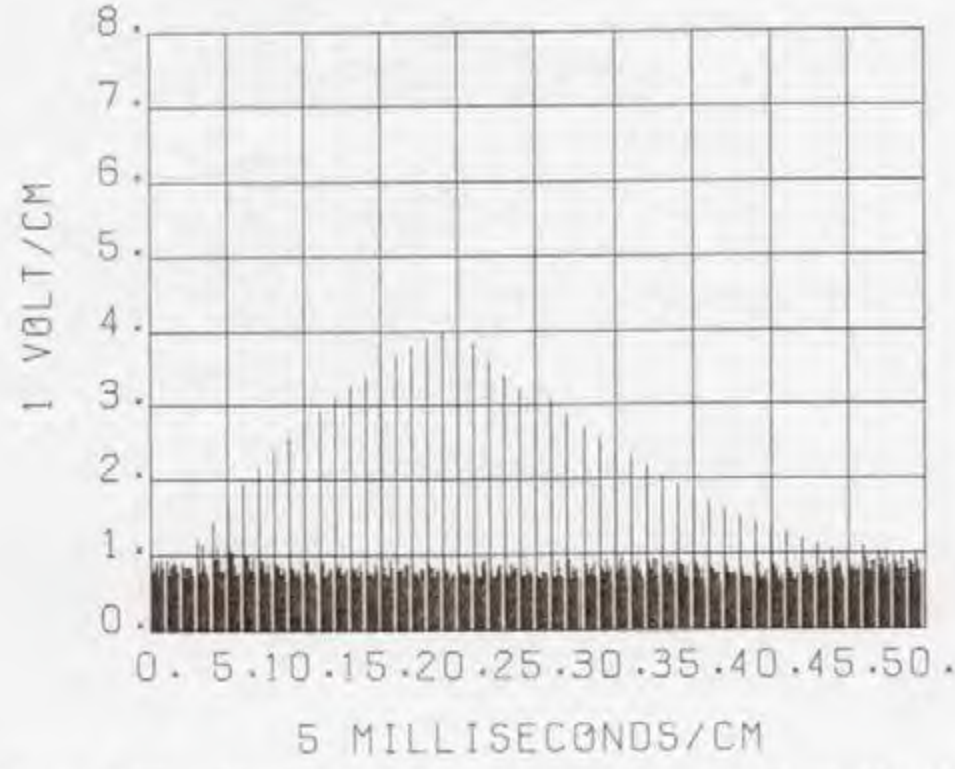

Figure D-10. Simulated Normal Channel Integrated Target Return Pulse Train for a SNR = 15 (V_L = 0.34)

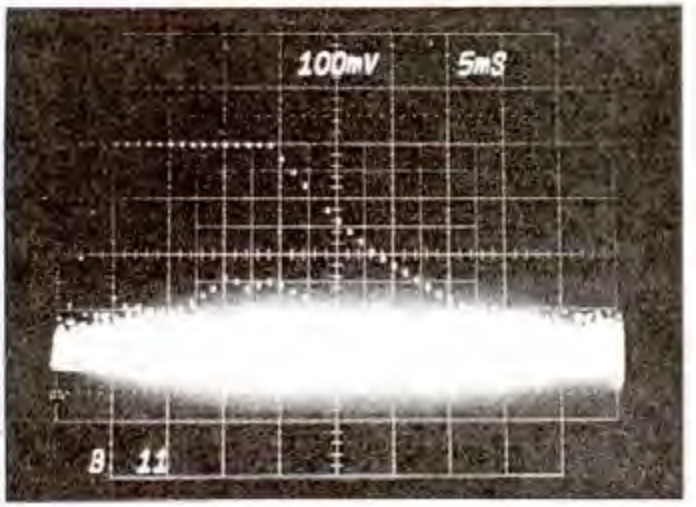

Figure D-11. Measured ASR-8 Normal Channel Integrated Output

Limit Adjust = 15
S =-84 dBm

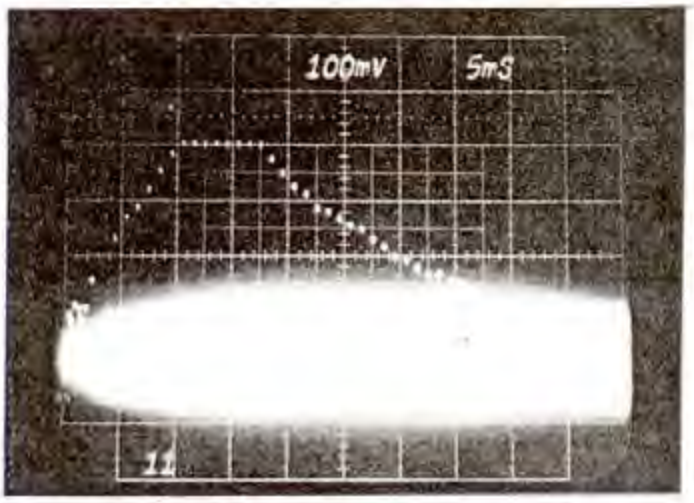

Figure D-12. Measured ASR-8 Normal Channel Integrated Output

Limit Adjust = 9
S = -84 dBm

Figure D-13. Measured ASR-8 Normal Channel Integrated Output

Limit Adjust = 7
S = -84 dBm

ϕ_s = Degrees of antenna rotation per pulse

$$\phi_s = \frac{6 \cdot RPM}{PRF}$$

For an ASR-8 with an antenna RPM of 12.5 and PRF equal to 1000, ϕ_s equals 0.075 degrees per pulse. TABLE D-2 shows the target azimuth shift (Equation D-12) due to target integration for various SNRs and feedback integrator input limiter limit level settings. The table shows a target azimuth shift due to integration of approximately .900 degrees relative to an unintegrated target return pulse train. Also shown in TABLE D-2 is the fact that the target azimuth shift due to integration is essentially independent of the integrator input limit level setting. Therefore, hard limiting in the integrator input limiter to suppress asynchronous interference does not cause a significant increase in target azimuth shift. However, the feedback integrator causes a target azimuth shift of .900 degrees over an unintegrated target return pulse train.

The property of the radar to distinguish between targets is called resolution. A comparison of Figure D-6a (unintegrated target return pulse train) with Figures D-6b through D-10 (integrated target return pulse train) shows a decrease in target angular resolution when the feedback enhancer is used. The decrease in target resolution is determined by:

$$\Delta RES = \Delta P \cdot \phi_s \qquad (D-13)$$

Where:

ΔP = Difference in number of pulses above the noise level at the integrator input and output.

Figures D-6b through D-10 show a decrease in target angular resolution due to use of the feedback integrator of 1.2 to 1.5 degrees. For aircraft at a range of 60 nautical miles, this would result in a decrease in angular resolution of 1.5 nautical miles.

In order to determine the effect of the integrator input limit level settings on the probability of target detection, the integrator output pulse train distribution must be best fitted to a Chi-square distribution by determining the degrees of freedom of the Chi-square distribution which best fit the integrator output pulse train. The probability of target detection was determined for the integrator input limit level set at 2.0 volts (Figure D-6b), and for the integrator input limit level set at 0.34 volts (Figure D-10). The mean peak signal-to-noise ratio for the pulse train shown in Figure D-6b was 20.35 dB, and the pulse train distribution best fitted a Chi-square distribution with four degrees of freedom. The mean peak signal-to-noise ratio for the pulse train shown in Figure D-10 was 18.48 dB, and the pulse train distribution best fitted a Chi-square distribution with

TABLE D-2

TARGET AZIMUTH SHIFT CAUSED BY FEEDBACK INTEGRATION

Figure Reference	Signal-to-Noise Ratio (DB)	Input Limiter Limit (Volts)	Center Pulse Position Relative to Unintegrated Pulse (ΔCp)	Target Azimuth Shift (Degrees)
Figure D-3b	3	2.0	8	0.600
Figure D-4b	5	2.0	10	0.750
Figure D-5b	10	2.0	12	0.900
Figure D-6b	15	2.0	13	0.975
Figure D-7	15	1.00	13	0.975
Figure D-8	15	0.7	13	0.975
Figure D-9	15	.50	12	0.900
Figure D-10	15	.34	12	0.900

two degrees of freedom. For a Swerling Case III target and probability of false alarm of 10^{-6}, the probability of target detection for the integrator output pulse trains shown in Figures D-6b and D-10 was determined using probability of detection curves given by Meyer and Mayher (1973) and making appropriate adjustments for the different degrees of freedom. The probability of target detection was determined to be .9998 and .9995 for the integrator output pulse trains shown in Figures D-6b and D-10, respectively. The high probability of detection for the two target return pulse trains shown in Figures D-6b and D-10 is due to the high mean signal-to-noise ratio of the pulse trains, and the number of pulses at the integrator output (approximately 35 pulses above 1.25 volts). Therefore, the probability of target detection does not change significantly by varying the integrator input limit level from 2.0 volts to .34 volts.

Also, measurements were made on the ASR-8 radar using observers to determine the PPI Minimum Discernible Signal (MDS) level as a function of integrator input limit level settings. The measurements showed the desired target PPI MDS level was independent of the integrator (enhancer) limit level adjust switch settings greater than five. This was due to the fact that the integrated (enhanced) target PPI MDS level was -104 dBm (peak signal-to-noise approximately 5.0 dB) which produced a SNR approximately equal to the integrator input limit level setting five. With the integrator limit level adjust switch set at five, the integrator suppressed non-synchronous interference for both the normal and MTI channel. Therefore, the PPI MDS measurements made on the ASR-8 indicate that asynchronous interference can be suppressed by the feedback integrator without a significant change in the radar PPI MDS level.

Interference

The following is a discussion of the feedback integrator signal processing properties to asynchronous normal and MTI channel interference. To analyze the signal processing properties of a feedback integrator, a careful investigation of the Pulse Repetition Frequency (PRF) relationship of the interfering and desired signal must be made. If the interfering signal PRF is different from the desired signal, the recirculated interference pulses will not arrive back at the input to the integrator coincidentally with the next pulse in the interfering train, and integration of successive pulses will not occur. However, for certain PRF's, partial integration can occur.

If the relationship in the following equation holds, partial integration will occur:

$$\pm (PRF_{INT}) = n (PRF_{DSR}) \qquad \text{(D-14)}$$

Where:

PRF_{INT} = PRF of the interfering radar

PRF_{DSR} = Design PRF of the receiver

r and s are integers

The integer, r, indicates minimum number of times an interfering pulse must circulate through the integrator before it will coincide with another interference pulse.

Generally, a more thorough investigation than the application of Equation D-14 is required to determine if partial integration will occur. This is due to the fact that all aeronautical radionavigation radars in the 2.7 to 2.9 GHz band operate in a staggered PRF mode to suppress blind speeds in the radar MTI channel. For radars operating in the stagger mode, both the interfering and desired signal stagger pulse train must be investigated. Aeronautical radionavigation radars in the 2.7 to 2.9 GHz band have two, three, four, and six stagger modes. Figures D-14 and D-15 show the six stagger modes of the ASR-7 (AN/GPN-12) and the four stagger modes of the ASR-8 (AN/GPN-20), respectively. An examination of these figures indicates that partial integration of an interfering signal is very unlikely. Also, most aeronautical radiolocations radars in the 2.7 to 2.9 GHz band have several PRF modes which are not integral multiples of each other. Therefore, it is very unlikely that partial integration of an interfering signal will occur between aeronautical radionavigation radars in the 2.7 to 2.9 GHz band. The height finding radars in the 2.7 to 2.9 GHz band have a PRF of 250 to 400, and could potentially cause partial integration interference.

Figures D-16 through D-18 show the simulated response of a feedback integrator to a single interfering pulse for normal channel asynchronous interference. The first interfering pulse at the integrator output is slightly greater than the integrator input limit level setting (V_{IL}) due to the addition of noise, and each recirculated pulse has an amplitude of K times the preceding pulse. Figure D-18 shows that an input limit level setting of 0.34 volts will suppress asynchronous normal channel interference. For comparison purposes, Figures D-19 through D-21 show a measured ASR-8 normal channel feedback integrator (enhancer) output signal response to asynchronous interference for integrator input limiter switch settings of 63, 15, and 7, respectively. Figure D-21 shows that for an integrator input limiter switch setting of 7, asynchronous normal channel interference will be suppressed to a one volt peak noise level, and will not be visible on the PPI display.

Figure D-22 shows a simulated normal channel radar unintegrated output for three interference sources (ASR-5, INR = 10 dB; ASR-8, INR = 15 dB; and AN/FPS, INR = 20 dB), and a desired target signal-to-noise ratio of 15 dB. Figure D-23 shows for the same interference condition the radar output after feedback integration for an input limit level setting of 0.34 volts. The asynchronous interference has been suppressed (compare Figure D-23 with D-10) by the feedback integrator.

Figure D-14. ASR-7 Six Stagger Sequence

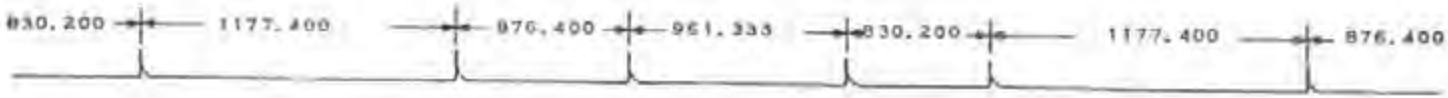

Figure D-15. ASR-8 Four Stagger Sequence

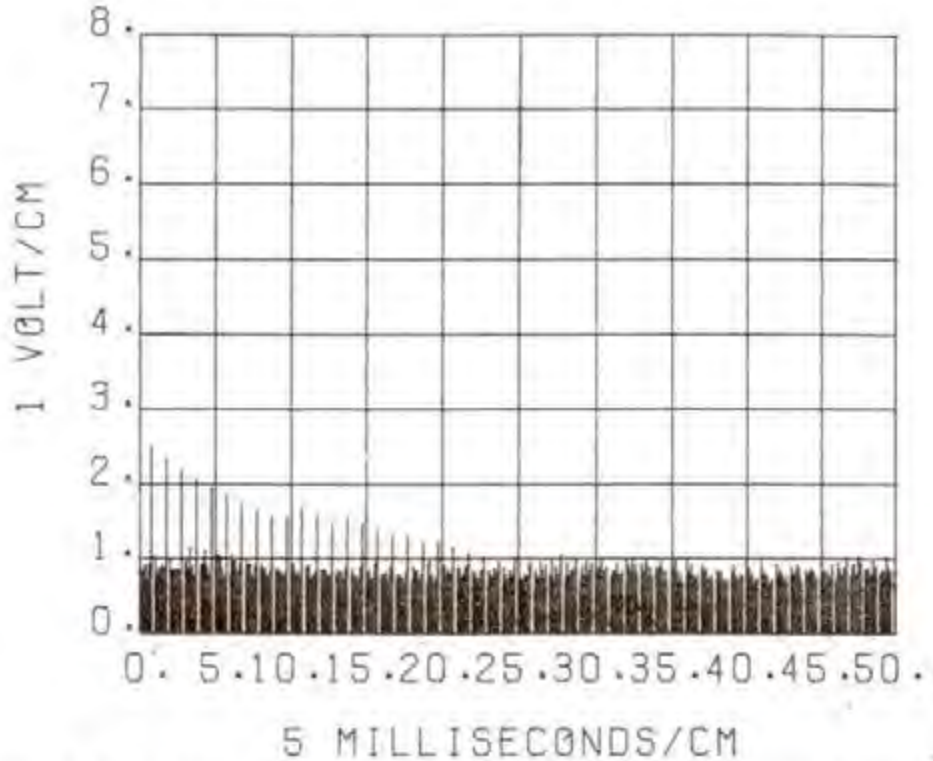

Figure D-16. Simulated Feedback Integrator Output for Asynchronous Normal Channel Interference (V_L = 2.0, INR = 30 dB)

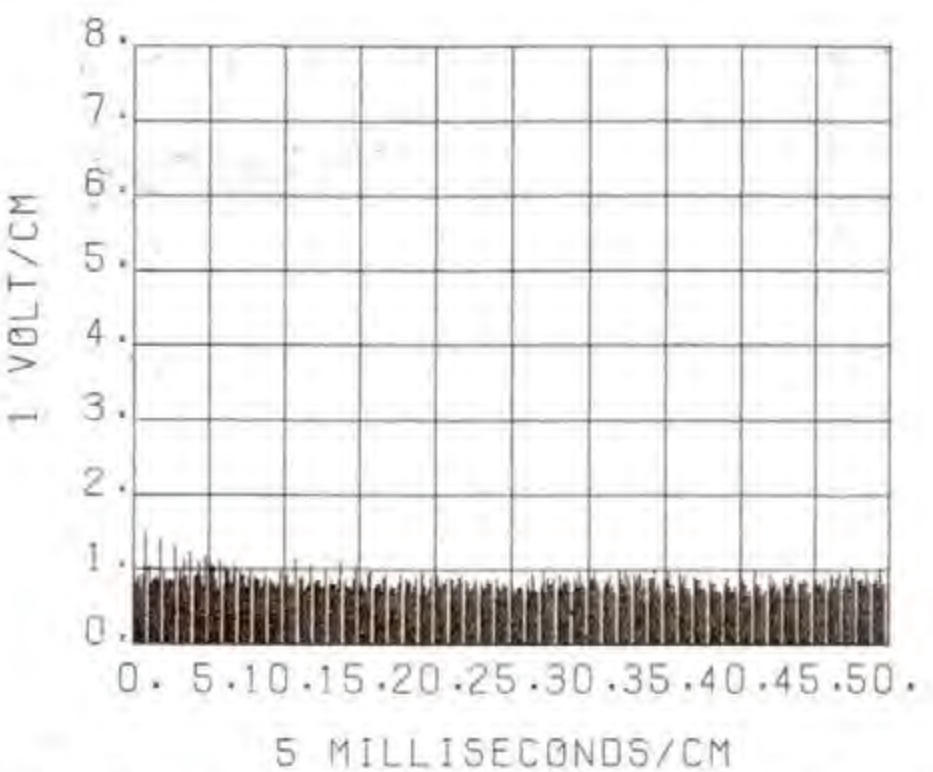

Figure D-17. Simulated Feedback Integrator Output for Asynchronous Normal Channel Interference (V_L = 1.0, INR = 30 dB)

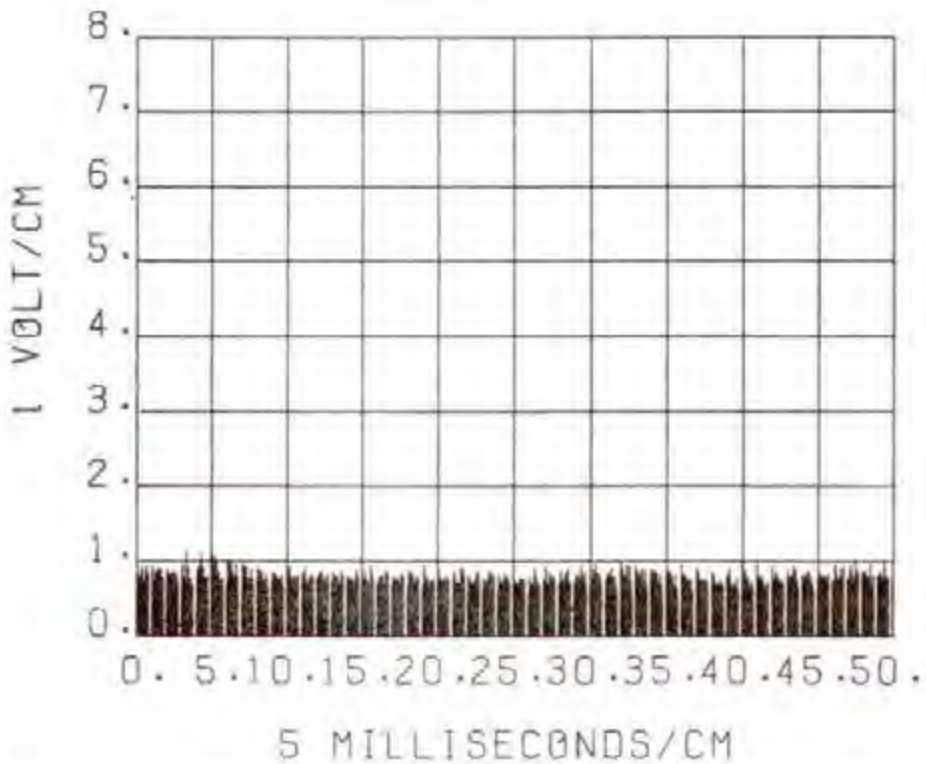

Figure D-18. Simulated Feedback Integrator Output for Asynchronous Normal Channel Interference (V_L = 0.34, INR = 30 dB)

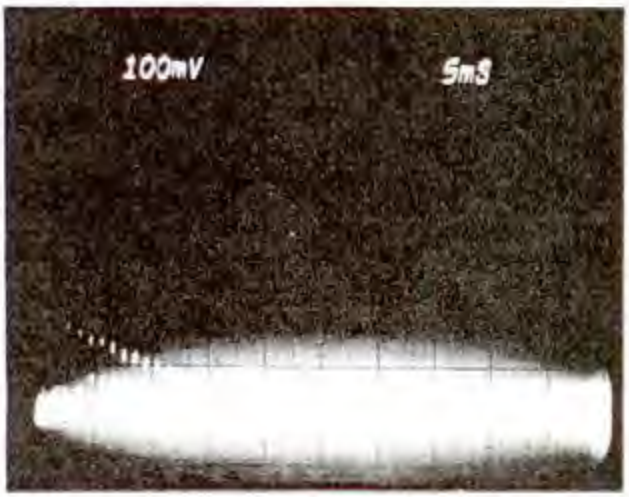

Figure D-19. Measured ASR-8 Integrator Output for Asynchronous Normal Channel Interference

Limit Adjust = 63
I = -80 dBm

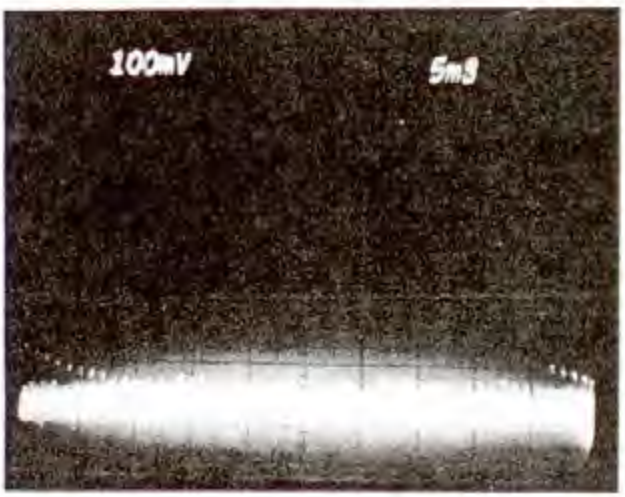

Figure D-20. Measured ASR-8 Integrator Output for Asynchronous Normal Channel Interference

Limit Adjust = 15
I = -80 dBm

Figure D-21. Measured ASR-8 Integrator Output for Asynchronous Normal Channel Interference

Limit Adjust = 7
I = -80 dBm

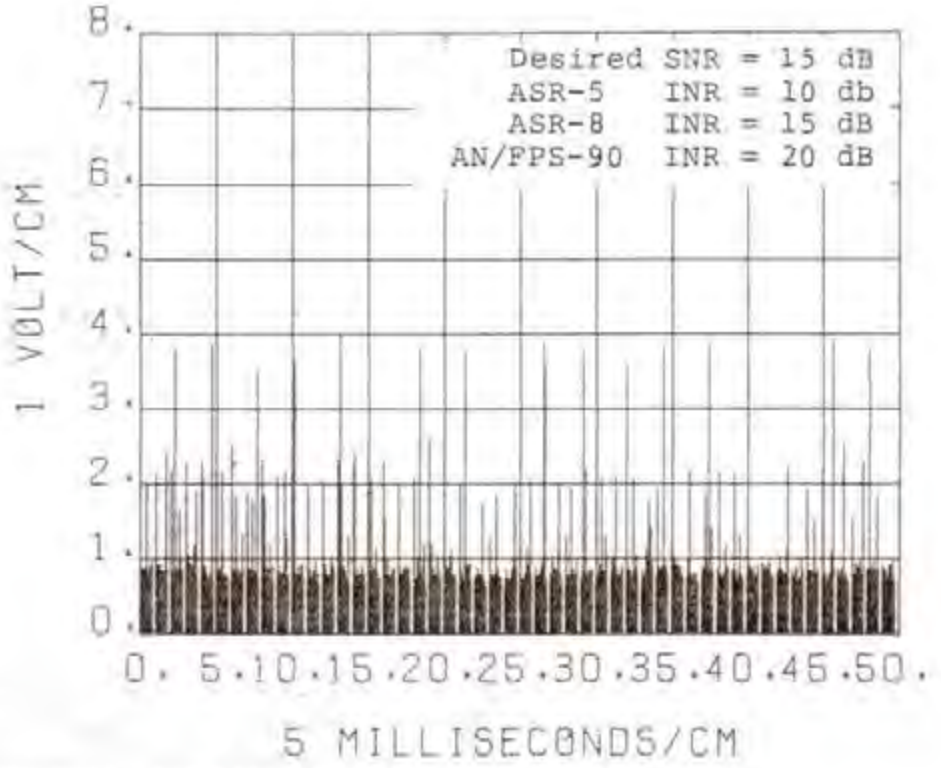

Figure D-22. Simulated Normal Channel Unintegrated Radar Output with Interference

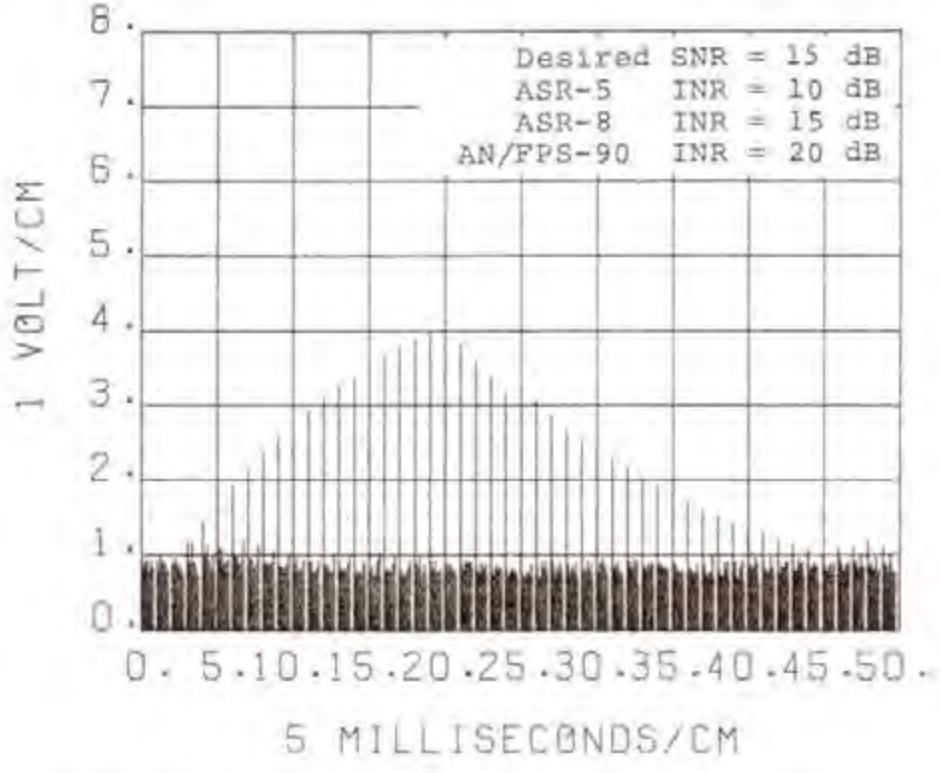

Figure D-23. Simulated Normal Channel Integrated Radar Output with Interference

Figures D-24 through D-26 show the simulated response of a feedback integrator to a single interfering pulse for MTI channel asynchronous interference. The MTI channel is simulated for a double stage canceller without feedback (1 and 2 CASC mode). As mentioned in Appendix C, for asynchronous interference a double stage MTI canceller will cause three synchronous pulses at the MTI canceller output for each asynchronous interfering pulse. Thus, asynchronous MTI channel interference will be enhanced by the feedback integrator unless the integrator input limit level is properly adjusted. This MTI channel asynchronous integration effect is shown in Figures D-24 through D-26. These figures show a three pulse integration, and then a pulse train decay of K times the previous pulse. For a radar operating in a single stage MTI canceller mode, only two pulses would be integrated. If the radar is operating in a MTI mode where canceller feedback is used for velocity response shaping, several pulses will be integrated for each asynchronous interfering pulse. Figure D-26 shows that for asynchronous interference in a double stage MTI canceller channel, a feedback integrator input limit level (V_L) setting of .34 volts will suppress the asynchronous interference level at the integrator output to 1.0 volts. In order to suppress the interference to the 1.0 volt level, additional subtraction (0.5 volts for the MTI channel as compared to 0.3 volts for the normal channel) was required at the integrator input. This additional subtraction reduces the noise level below the standard one volt level. A discussion of the additional circuitry prior to the feedback integrator is given in Appendix E.

Figures D-27 through D-29 show for comparison with the simulated integrator model (Figures D-24 through D-26) measured ASR-8 MTI channel integrator (enhancer) output signal response to asynchronous interference for integrator input limit switch settings of 63, 15, and 5, respectively. Figures D-27 and D-28 show the enhancement of the asynchronous interference by the integrator due to the three pulse synchronous response of the MTI double canceller circuitry. Figure D-29 shows that for an integrator (enhancer) limiter switch setting of 5, asynchronous MTI channel interference will be suppressed to the one volt peak noise level, and thus will not be visible on the PPI display. It should also be noted that the MTI channel required a limiter switch setting of 5 to suppress the asynchronous interference as compared to a limiter switch setting of 7 to suppress normal channel asynchronous interference. This is to be expected because of the synchronous pulse output response of the MTI channel to asynchronous interference. Also a comparison of Figure D-19 with Figure D-27 shows that the feedback integrator will enhance the MTI channel interference if the feedback integrator is not adjusted properly.

Figure D-30 shows a simulated single channel MTI canceller radar unintegrated output for three interfering sources (ASR-5,INR = 10 dB; ASR-8, INR = 15 dB; and AN/FPS-90, INR = 20 dB), and a desired target signal-to-noise ratio (SNR) of 20 dB. As discussed previously the asynchronous MTI channel interference can be enhanced if the feedback enhancer is not adjusted properly. Figure D-31 shows a simulated output of a

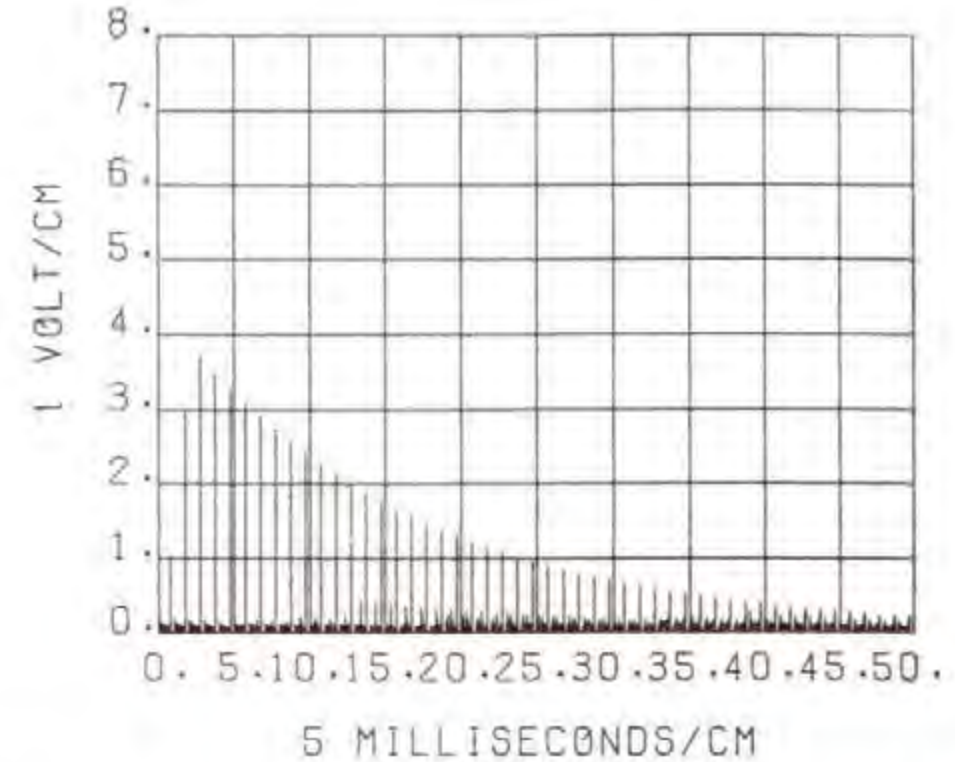

Figure D-24. Simulated Feedback Integrator Output for Asynchronous MTI Channel Interference (V_L = 2.0, INR = 30 dB)

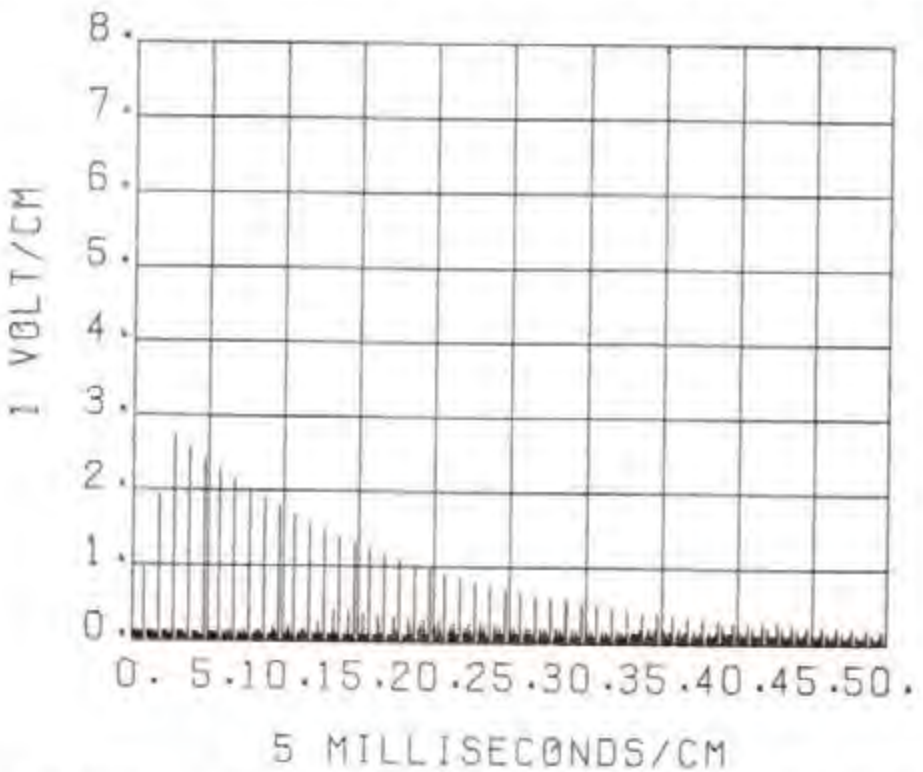

Figure D-25. Simulated Feedback Integrator Output for Asynchronous MTI Channel Interference (V_L = 1.0, INR = 30 dB)

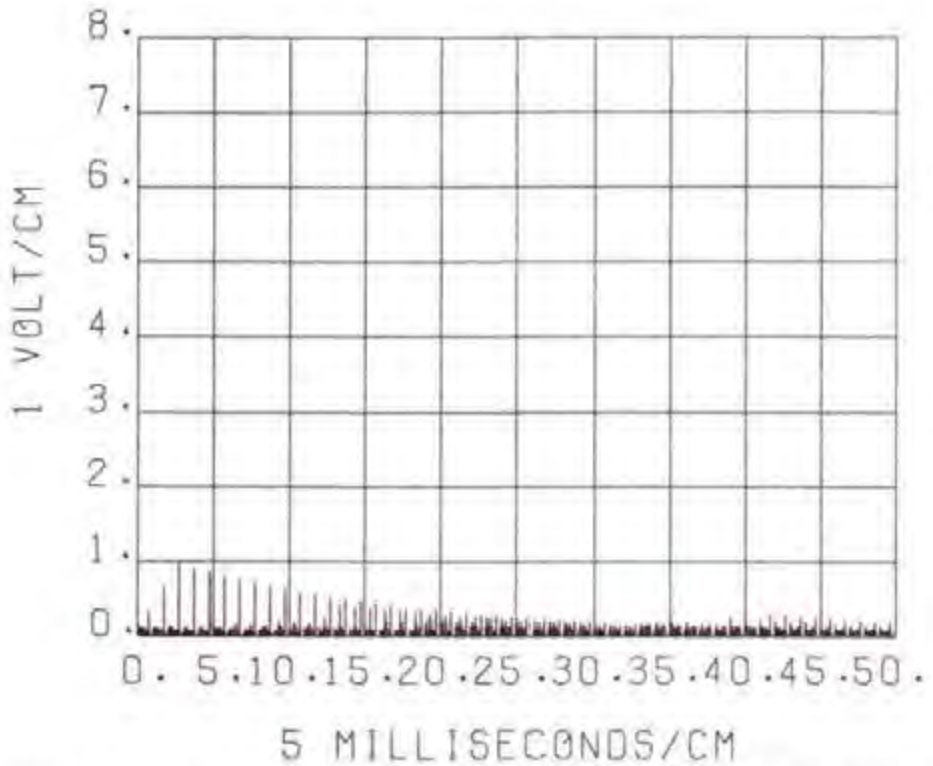

Figure D-26. Simulated Feedback Integrator Output for Asynchronous MTI Channel Interference (V_L= 0.34, INR 30.0 dB)

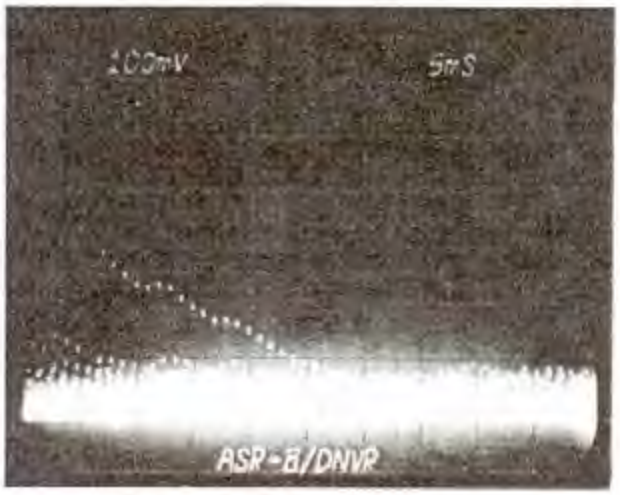

Figure D-27. Measured ASR-8 Integrator Output for Asynchronous MTI Channel Interference

Limit Adjust = 63
I = -80 dBm

Figure D-28. Measured ASR-8 Integrator Output for Asynchronous MTI Channel Interference

Limit Adjust = 15
I = -80 dBm

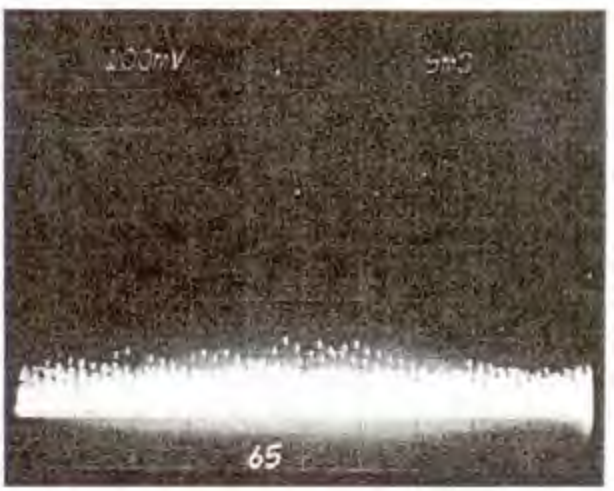

Figure D-29. Measured ASR-8 Integrator Output for Asynchronous MTI Channel Interference

Limit Adjust = 5
I = -80 dBm

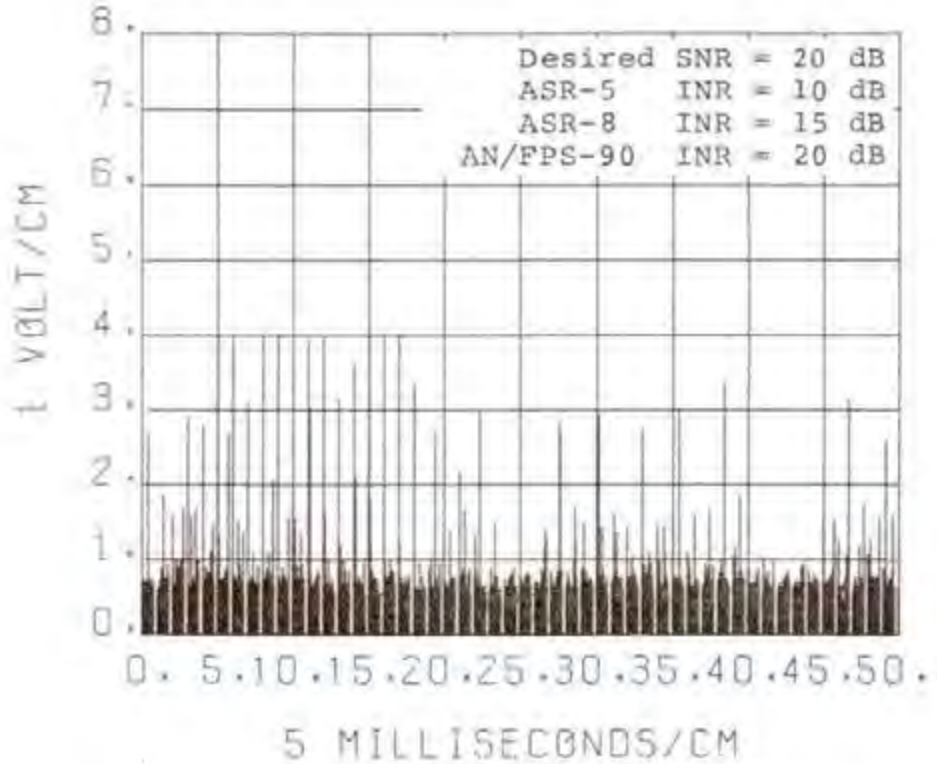

Figure D-30. Simulated MTI Channel (mode 1 & 2 CASC) Unintegrated Radar Output with Interference

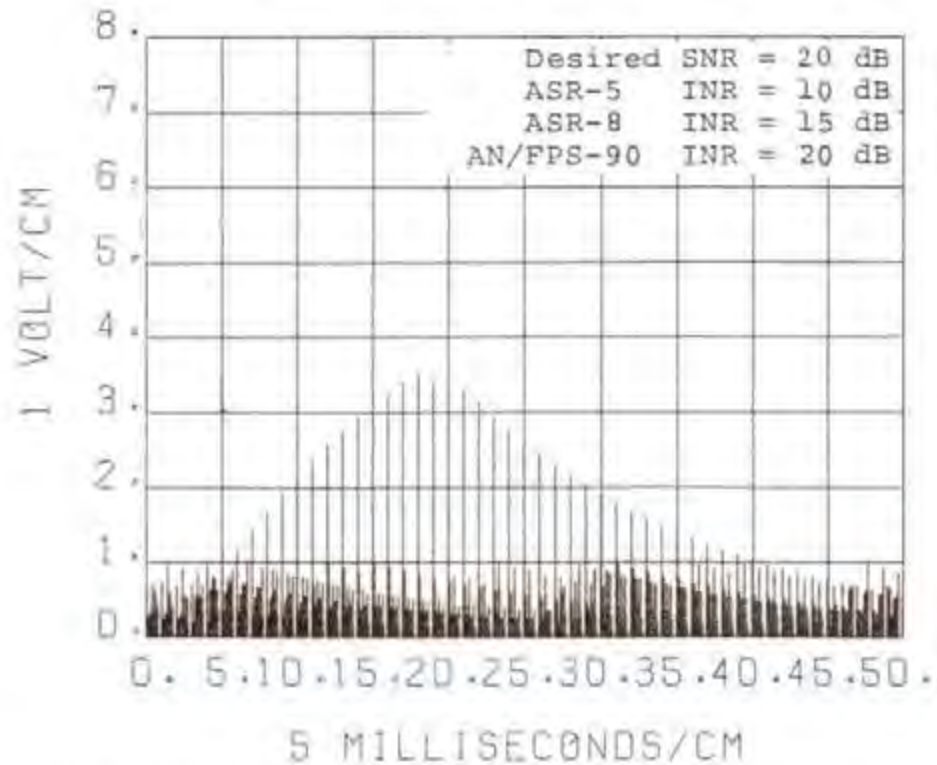

Figure D-31. Simulated MTI Channel (mode 1 & 2 CASC) Integrated Radar Output with Interference

feedback integrator for the feedback integrator input limit level adjusted at .34 volts for the same interference condition shown in Figure D-30. The asynchronous interference has been suppressed by the feedback integrator.

In summary, the simulation of the feedback integrator has shown that asynchronous interference can be suppressed by a feedback integrator if adjusted properly. Measurements made on the Stapleton Airport ASR-8 radar in Denver, Colorado, also showed that on-tune interference levels of 50 dB above the receiver noise level (approximately -60 dBm) could be suppressed in both the normal and MTI channels so that they did not appear on the PPI display. The ASR-8 radar has a feedback integrator (enhancer) and dual channel (Inphase and Quadrature) MTI channel processing. The measured change in target detection sensitivity in suppressing the asynchronous interference was found to be 1 dB or less. Also given that the feedback integrator is going to be used, the trade-offs in target azimuth shift, angular resolution and target detection sensitivity to suppress asynchronous interference are minimal.

BINARY INTEGRATOR

The ASR-7 and AN/GPN-12 radars are made by the same manufacturer, and the enhancer used in the two radars are electronically identical. The integrator (enhancer) used in the two radars can be represented by the block diagram shown in Figure D-32. The binary integrator consists of a threshold detector or comparator, binary counter (adder/subcontractor circuit), a five bit shift register memory, and a digital-to-analog (D/A) converter. Each PRF period is divided into range bins of .625 μs. If a pulse of a target return pulse train exceeds the comparator threshold level, the enhancer stores a one level digital signal in the shift register memory for that range bin. If the successive pulses of the target return pulse train continue above the comparator threshold in the given range bin, the binary counter will add one level to the stored digital signal in the shift register memory in each PRF period until a maximum integrator level of 31 is reached. If in any PRF period the signal fails to exceed the comparator threshold, the binary counter subtracts one from the stored integrator state in the given range bin until a digital signal level of zero is reached. The subtraction provides the target return pulse train signal decay required after the antenna beam has passed the target, and also enables the suppression of asynchronous interfering signals. The voltage amplitude at the enhancer D/A converter output is determined by the binary counter level (0 to 31) for the particular range bin times .125 volts. Therefore, for a binary counter level of 31, the maximum enhancer output voltage would be 3.875 volts (31 x .125).

FAA Integrator Modification

The following is a discussion on the modification the FAA made to the ASR-7 integrator (enhancer) to improve the desired signal probability of detection, target azimuth shift, and angular resolution loss caused by the conventional integrator used in the ASR-7 radar.

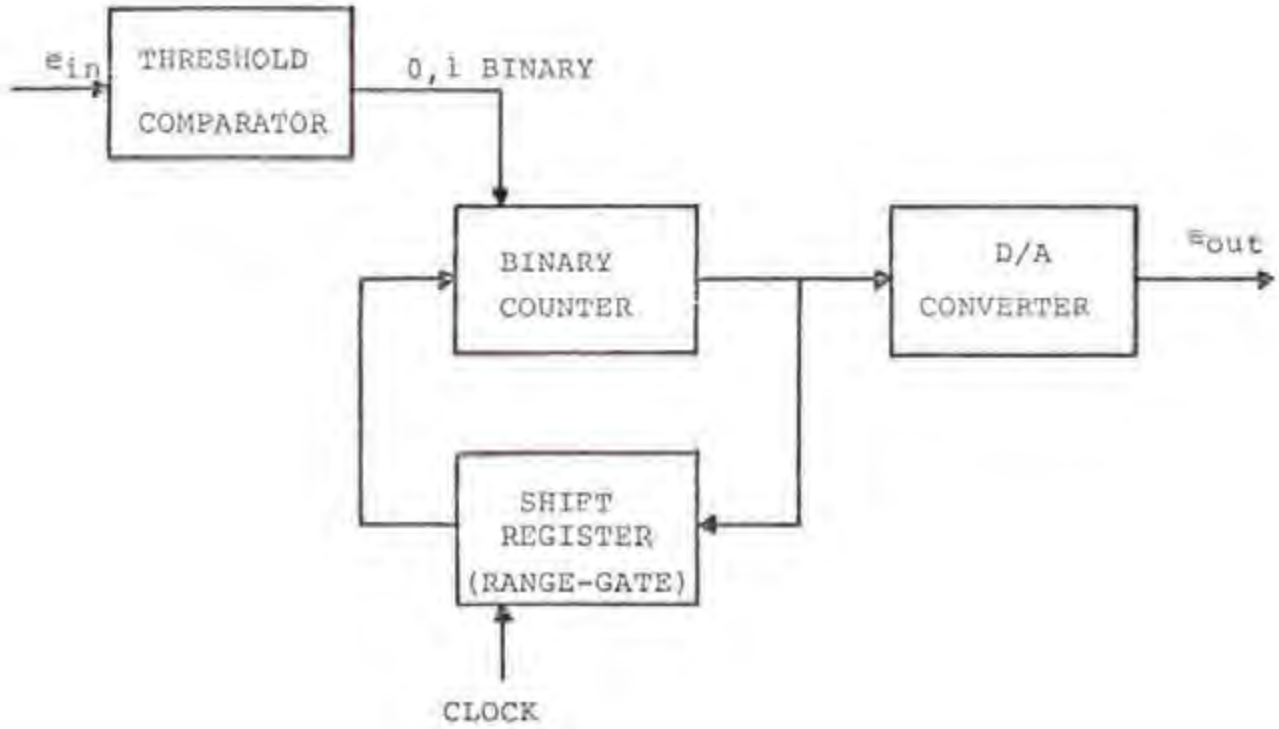

Figure D-32 ASR-7 (AN/GPN-12) Binary Integrator Block Diagram

The FAA made modifications to the manufacturer's integrator (enhancer) printed circuit board due to deficiencies that were observed on the ASR-7 video enhancer at operational field sites. Deficiencies that were observed were: (1) loss of weak targets due to design of the enhancer integrator, and (2) excessive azimuth shift of the target (NAFEC Letter Report, FAA-MA-76-39-LR, 1976).

Figure D-33 shows a block diagram of the FAA modified video enhancer. The major modification made by the FAA is the replacement of the binary counter (IC's) with a programmable read-only-memory (PROM) logic. The PROMS permit the bypassing of some of the intermediate levels (E_j = 0 to 31), depending on the PROM programming. Figure D-34 shows the FAA standard hit/miss characteristic curve which is programmed into the PROMS. The figure shows that the enhancer state is a nonlinear function of the target hits above the comparator threshold level. It only takes four hits to get to level 8 (one volt noise level), and six hits to get to level 31 (3.875 volts). This results in a strong target enhancement with only a few hits. The primary advantage of the PROM enhancer is that, due to its programmable feature, it permits a radar site flexibility in selecting a hit-count sequence based on the radar sites environment (interference and clutter). Similarly, the miss-count sequence can be precisely controlled to minimize target azimuth shift and maximize angular resolution. In this way, the video enhancer performance can be optimized to give improved performance in a variety of environmental conditions.

The following discussion will center on the particular signal processing characteristics of the conventional integrator deployed in the ASR-7 and AN/GPN-12 and the modified ASR-7 integrator to noise, desired target return pulse train, and asynchronous interference.

Noise

The noise amplitude distribution at the normal or dual MTI channel integrator (enhancer) input is Rayleigh distributed, and the noise amplitude distribution at a single MTI channel integrator input is one-sided Gaussian distributed. The noise amplitude distributions at the normal or dual MTI channel output can be expressed as:

$$p(v) = \frac{v}{\sigma^2} e^{-v^2/2\sigma^2}; \quad 0 \leq v \leq +\infty \qquad \text{(D-15)}$$

where the rms noise level is $\sqrt{2}\sigma$. The noise amplitude distribution at the output of a single channel MTI canceller after rectification can be expressed as:

$$p(v) = \frac{2}{\sqrt{2\pi}\sigma} e^{-v^2/2\sigma^2}; \quad 0 \leq v \leq +\infty \qquad \text{(D-16)}$$

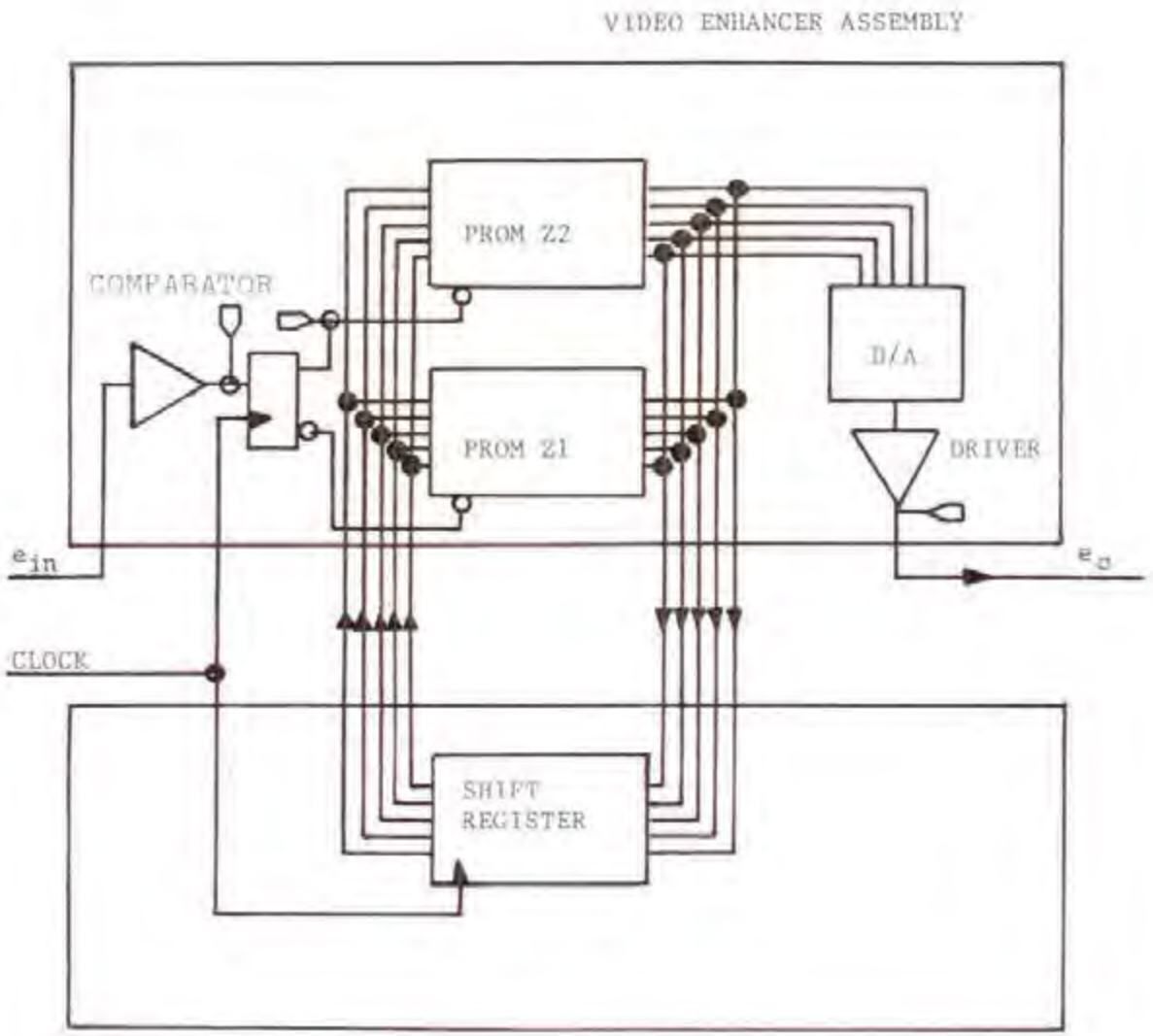

Figure D-33 FAA Modified ASR-7 Enhancer Block Diagram

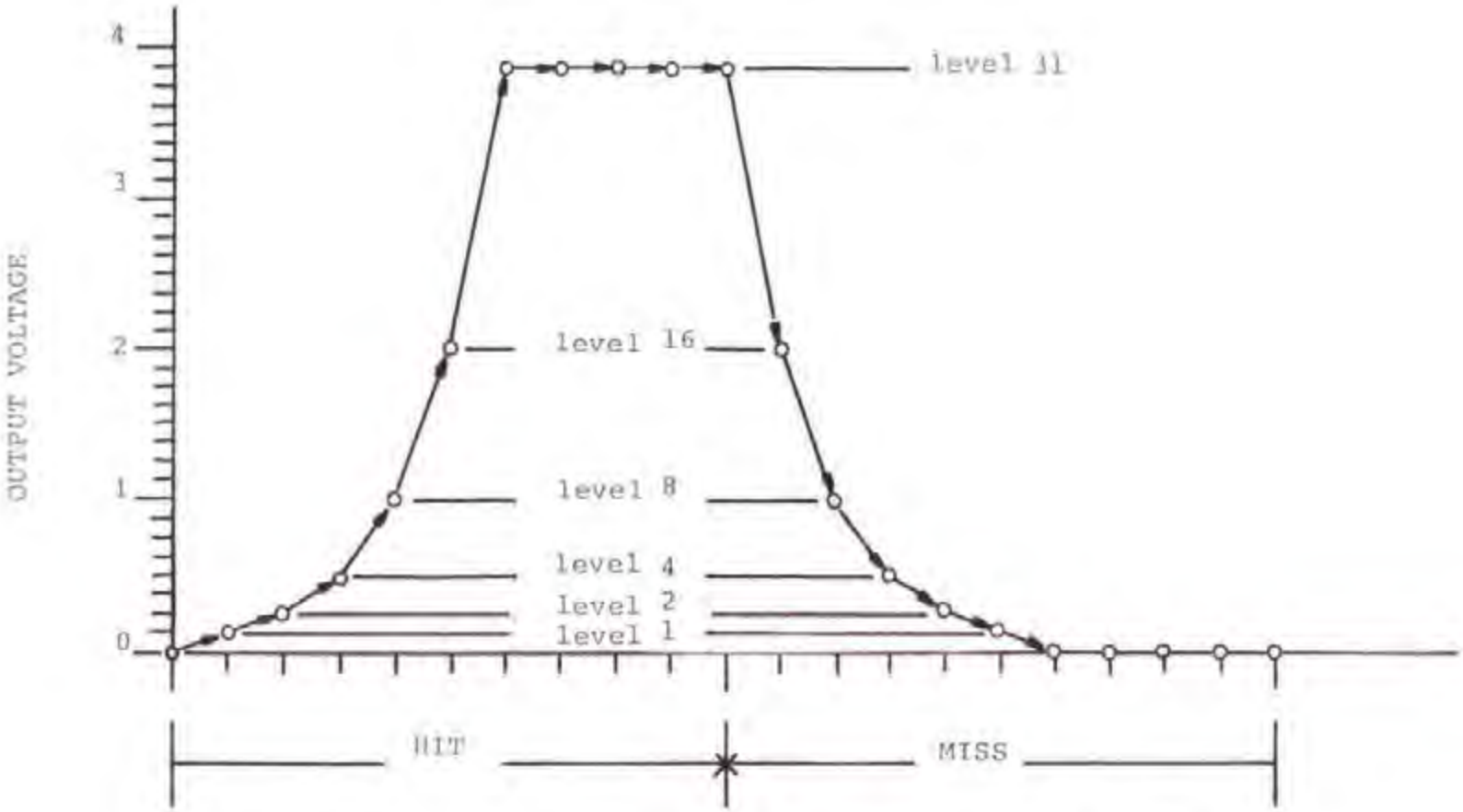

Figure D-34. Hit/Miss Characteristic Curve for FAA Modified ASR-7 Enhancer

where the rms noise level is σ.

The probability of noise causing the threshold comparator to put out a binary one in a range bin, P_{N1}, can be found for the normal and MTI channels by integrating Equations D-15 and D-16 from the threshold voltage level, T, to plus infinity. Figure D-35 shows the probability of noise causing a binary one, P_{N1}, at the threshold comparator output as a function of the threshold comparator threshold-to-rms noise ratio in dB for the normal and MTI channels.

The probability of the receiver noise causing the binary counter in the integrator to reach state E_j can be modeled by a one-dimentional random walk with reflecting barriers where levels 0 and 31 are the reflecting barriers. That is, the first and last rows of the Markov chain transition matrix are defined by (P_{N0}, P_{N1}, 0, ...) and (0, ..., 0, P_{N0}, P_{N1}). Since the noise is continually summed in the binary integrator the number of steps (k) in the random walk is infinite. It can be shown that a one-dimentional random walk with reflecting barriers model for an infinite number of steps is identical to a truncated single channel queue. The arrival rate, λ, and the departure rate, μ, of the queuing system is given by:

$$\lambda = \frac{P_{N1}}{\Delta T} \qquad \text{(D-17)}$$

$$\mu = \frac{1-P_{N1}}{\Delta T} = \frac{P_{N0}}{\Delta T} \qquad \text{(D-18)}$$

Where:

P_{N0} = Probability of the noise causing a 0 at threshold comparator output

P_{N1} = Probability of the noise causing a 1 at threshold comparator output

ΔT = Period of the radar range bin

$1/\lambda$ = False alarm time

The probability that the binary counter is in state, E_j, at epoch $t + \Delta T$ can be expressed as (Suaty, 1968):

$$P_j(t+\Delta T) = P_j(t)[1 - \lambda\Delta T - \mu\Delta T] + P_{j-1}(t)\,\lambda\Delta T + P_{j+1}(t)\,\mu\Delta T \qquad \text{(D-19)}$$

It can be shown that the probability of the binary counter being in any state, E_j (from the difference equation solution) due to noise P_{nj}, can be expressed as:

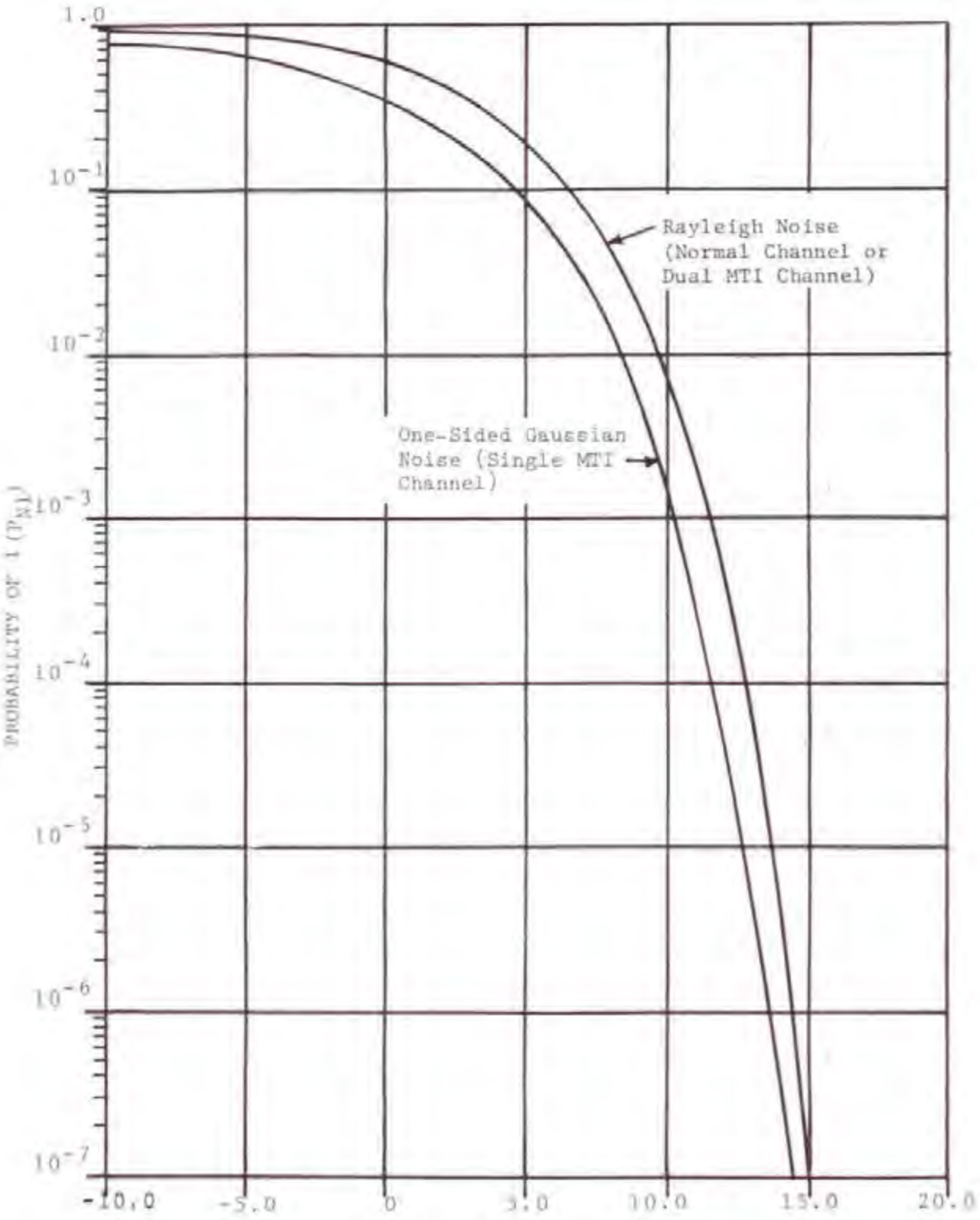

Figure D-35. Probability of Noise Causing a Binary 1 at the Threshold Comparator Output

$$P_{nj} = \lim_{t \to \infty} P_j(t) \qquad \text{(D-20a)}$$

$$= \frac{(\lambda/\mu)^{j-1}}{\sum_{j=1}^{\rho} (\lambda/\mu)^{j-1}} = \frac{(P_{N1}/P_{N0})^{j-1}}{\sum_{j=1}^{\rho} (P_{N1}/P_{N0})^{j-1}} \qquad \text{(D-20b)}$$

Where:

ρ = Number of states (function of counter level sequence)

The values for P_{N1} as a function of the threshold-to-rms noise ratio are obtained from Figure D-35 for the various channels, and $P_{N0} = 1-P_{N1}$. It should also be noted that the integrator output noise amplitude distribution is independent of the noise amplitude distribution at the input to the integrator. Since the integrator output noise distribution is independent of the noise amplitude distribution at the input of the integrator, an analytical expression for the integrator noise gain can not be expressed. However, the integrator output rms noise level can be expressed as:

$$N_{Io} = \sqrt{\sum_{j=1}^{\rho} [0.125(j-1)P_{nj}]^2} \qquad \text{(D-21)}$$

The rms noise level at the integrator output is a function of the threshold comparator threshold level setting. Normally the threshold comparator threshold level is adjusted to produce a peak noise level at the integrator outputs of one volt. Therefore, the binary counter level should not exceed counter level 8 (8 x .125 = 1.0 volts) with a probability of .0001 for a probability of false alarm of 10^{-4}. That is:

$$\sum_{j=1}^{c} P_{nj} \geq .9999 \qquad \text{(D-22)}$$

where:

c = State corresponding to counter level 8

TABLE D-3 shows the probability of the binary counter reaching each state due to noise, P_{nj}, and the cumulative probability of P_{nj} for comparator threshold settings with a probability of binary one, P_{N1}, of 10^{-2}, 10^{-1}, and .2625.

TABLE D-3

PROBABILITY OF NOISE CAUSING THE INTEGRATOR TO BE IN STATE E_j

State E_j	Counter Level	$P_{NI} = 10^{-2}$		$P_{NI} = 10^{-1}$		$P_{NI} = .2625$	
		P_{nj}	ΣP_{nj}	P_{nj}	ΣP_{nj}	P_{nj}	ΣP_{nj}
1	0	.989898990+000	.989898990+000	.888888891+000	.888888891+000	.644067805+000	.644067805+000
2	1	.999897957-002	.999997970+000	.907654306-001	.987654321+000	.229244467+000	.873312273+000
3	2	.100999792-003	.999998969+000	.109719165-001	.998628258+000	.815954864-001	.954907759+000
4	3	.102019991-005	.999999990+000	.121932626-002	.999847584+000	.290424606-001	.983950220+000
5	4	.103050495-007	.100000000+001	.135480693-003	.999983065+000	.103371467-001	.994207366+000
6	5	.104091408-009	.100000000+001	.150534101-004	.999998118+000	.367932332-002	.997966690+000
7	6	.105142835-011	.100000000+001	.167260189-005	.999999791+000	.130958963-002	.999276279+000
8	7	.106204802-013	.100000000+001	.185844562-006	.999999977+000	.466125110-003	.999742405+000
9	8	.107277657-015	.100000000+001	.206493955-007	.999999997+000	.165908933-003	.999908313+000
10	9	.108361269-017	.100000000+001	.229437723-008	.100000000+001	.590523308-004	.999967366+000
11	10	.109455826-019	.100000000+001	.254930799-009	.100000000+001	.210186257-004	.999988384+000
12	11	.110561439-021	.100000000+001	.283256438-010	.100000000+001	.748120557-005	.999995866+000
13	12	.111678219-023	.100000000+001	.314729370-011	.100000000+001	.266280192-005	.999998528+000
14	13	.112806281-025	.100000000+001	.349699294-012	.100000000+001	.947776931-006	.999999476+000
15	14	.113945737-027	.100000000+001	.388554765-013	.100000000+001	.337344323-006	.999999814+000
16	15	.115096702-029	.100000000+001	.431727509-014	.100000000+001	.120071705-006	.999999934+000
17	16	.116259294-031	.100000000+001	.479697223-015	.100000000+001	.427373656-007	.999999976+000
18	17	.117433629-033	.100000000+001	.532996905-016	.100000000+001	.152116115-007	.999999992+000
19	18	.118619826-035	.100000000+001	.592218773-017	.100000000+001	.541438225-008	.999999997+000
20	19	.119818004-037	.100000000+001	.658020847-018	.100000000+001	.192712448-008	.999999999+000
21	20	.121028285-039	.100000000+001	.731134262-019	.100000000+001	.685925647-009	.100000000+001
22	21	.122250792-041	.100000000+001	.812371388-020	.100000000+001	.244143021-009	.100000000+001
23	22	.123485647-043	.100000000+001	.902634859-021	.100000000+001	.868983613-010	.100000000+001
24	23	.124732975-045	.100000000+001	.100292760-021	.100000000+001	.309299244-010	.100000000+001
25	24	.125992903-047	.100000000+001	.111436398-022	.100000000+001	.110089559-010	.100000000+001
26	25	.127265557-049	.100000000+001	.123818218-023	.100000000+001	.391844183-011	.100000000+001
27	26	.128551066-051	.100000000+001	.137575796-024	.100000000+001	.139469960-011	.100000000+001
28	27	.129849560-053	.100000000+001	.152861993-025	.100000000+001	.496418490-012	.100000000+001
29	28	.131161170-055	.100000000+001	.169846655-026	.100000000+001	.176691323-012	.100000000+001
30	29	.132486020-057	.100000000+001	.188718503-027	.100000000+001	.628901303-013	.100000000+001
31	30	.133824269-059	.100000000+001	.209687221-028	.100000000+001	.223846221-013	.100000000+001
32	31	.135176028-061	.100000000+001	.232985797-029	.100000000+001	.796740767-014	.100000000+001

The table shows that for a probability of a binary one due to noise of .2625, Equation D-22 is satisfied. That is, the peak noise level will be approximately one volt if the threshold comparator is set for P_{N1} = .2625. Therefore, using Figure D-35, the threshold comparator threshold-to-rms noise (T/N) ratio should be set at 1.5 dB for the MTI channel and 4.25 dB for the normal channel.

TABLE D-4 shows the probability of the binary counter reaching each state due to noise, P_{nj}, and the cumulative probability of P_{nj} for the FAA modified integrator and P_{N1} of 10^{-2}, 10^{-1}, and .135. The table shows that a threshold comparator setting of P_{N1} = .135 will limit the peak noise level to approximately one volt. That is, Equation D-22 is satisfied for a P_{N1} of .135. Again, using Figure D-35, the threshold comparator T/N ratio should be set for the FAA modified integrator at 3.2 dB for the MTI channel and 6.0 db for the normal channel.

TABLE D-5 shows the probability of the binary counter reaching each state due to noise, P_{nj}, and the cumulative probability of P_{nj} for a computer simulation of the enhancer hardware (see Appendix E). The simulated run was for a threshold comparator setting of P_{N1} = .2625 (same as in TABLE D-3). Only one thousand noise samples were taken. Therefore, the probability of being in each state, P_{nj}, will only be accurate for $P_{nj} \geq .005$. TABLE D-5 compares favorably with TABLE D-3, thus validating Equation D-20b.

Desired Signal

For a nonfluctuating target (Marcum's Case 0), the probability of the desired signal exceeding the threshold comparator level (P_{S1} probability for a binary one in a range bin) for the normal channel has a Rice (1954) PDF (also known as the Modified Rayleigh and Q-function).

$$P_{S1} = \int_{T}^{\infty} \frac{v e^{\frac{-(v^2+A^2)}{2\sigma^2}}}{\sigma^2} I_0\left(\frac{vA}{\sigma^2}\right) dv \qquad (D-23)$$

where:

I_0 ( ) = Modified Bessel function of the first kind of order zero

A = Peak signal-amplitude, in volts

σ = rms noise level, in volts

T = Threshold comparator threshold level, in volts

The integrand of Equation D-23 is the signal-plus-noise amplitude distribution at the threshold comparator input for the normal or dual MTI channel (see Figure 3-10). Figure D-36 shows the probability of the desired signal-plus-noise exceeding the threshold comparator level (P_{S1}, probability

TABLE D-4

PROBABILITY OF NOISE CAUSING THE MODIFIED FAA INTEGRATOR TO BE IN STATE E_j

State E_j	Counter Level	$P_{N1} = 10^{-2}$	
		P_{nj}	ΣP_{nj}
1	0	.989898990+000	.989898990+000
2	1	.999897957-002	.999897970+000
3	2	.100999792-003	.999998969+000
4	4	.102019991-005	.999999990+000
5	8	.103050495-007	.100000000+001
6	16	.104091408-009	.100000000+001
7	31	.105142835-011	.100000000+001

State E_j	Counter Level	$P_{N1} = 10^{-1}$	
		P_{nj}	ΣP_{nj}
1	0	.888889077+000	.888889077+000
2	1	.987654512-001	.987654528+000
3	2	.109739388-001	.998628467+000
4	4	.121932652-002	.999847793+000
5	8	.135480722-003	.999983274+000
6	16	.150534132-004	.999998327+000
7	31	.167260144-005	.100000000+001

State E_j	Counter Level	$P_{N1} = .135$	
		P_{nj}	ΣP_{nj}
1	0	.843932543+000	.843932543+000
2	1	.131712012+000	.975644555+000
3	2	.205562096-001	.996200765+000
4	4	.320819449-002	.999408959+000
5	8	.500700862-003	.999909660+000
6	16	.781440635-004	.999987804+000
7	31	.121958940-004	.100000000+001

TABLE D-5

PROBABILITY OF NOISE CAUSING THE INTEGRATOR TO BE IN STATE E_j (SIMULATED)

State E_j	Counter Level	$P_{N1} = .3625$	
		P_{nj}	EP_{nj}
1	0	.632103689+000	.632103689+000
2	1	.235294118+000	.867397807+000
3	2	.867397807-001	.954137587+000
4	3	.329012961-001	.987038883+000
5	4	.109670987-001	.998005982+000
6	5	.199401795-002	.100000000+001
7	6	.000000000	.100000000+001
8	7	.000000000	.100000000+001
9	8	.000000000	.100000000+001
10	9	.000000000	.100000000+001
11	10	.000000000	.100000000+001
12	11	.000000000	.100000000+001
13	12	.000000000	.100000000+001
14	13	.000000000	.100000000+001
15	14	.000000000	.100000000+001
16	15	.000000000	.100000000+001
17	16	.000000000	.100000000+001
18	17	.000000000	.100000000+001
19	18	.000000000	.100000000+001
20	19	.000000000	.100000000+001
21	20	.000000000	.100000000+001
22	21	.000000000	.100000000+001
23	22	.000000000	.100000000+001
24	23	.000000000	.100000000+001
25	24	.000000000	.100000000+001
26	25	.000000000	.100000000+001
27	26	.000000000	.100000000+001
28	27	.000000000	.100000000+001
29	28	.000000000	.100000000+001
30	29	.000000000	.100000000+001
31	30	.000000000	.100000000+001
32	31	.000000000	.100000000+001

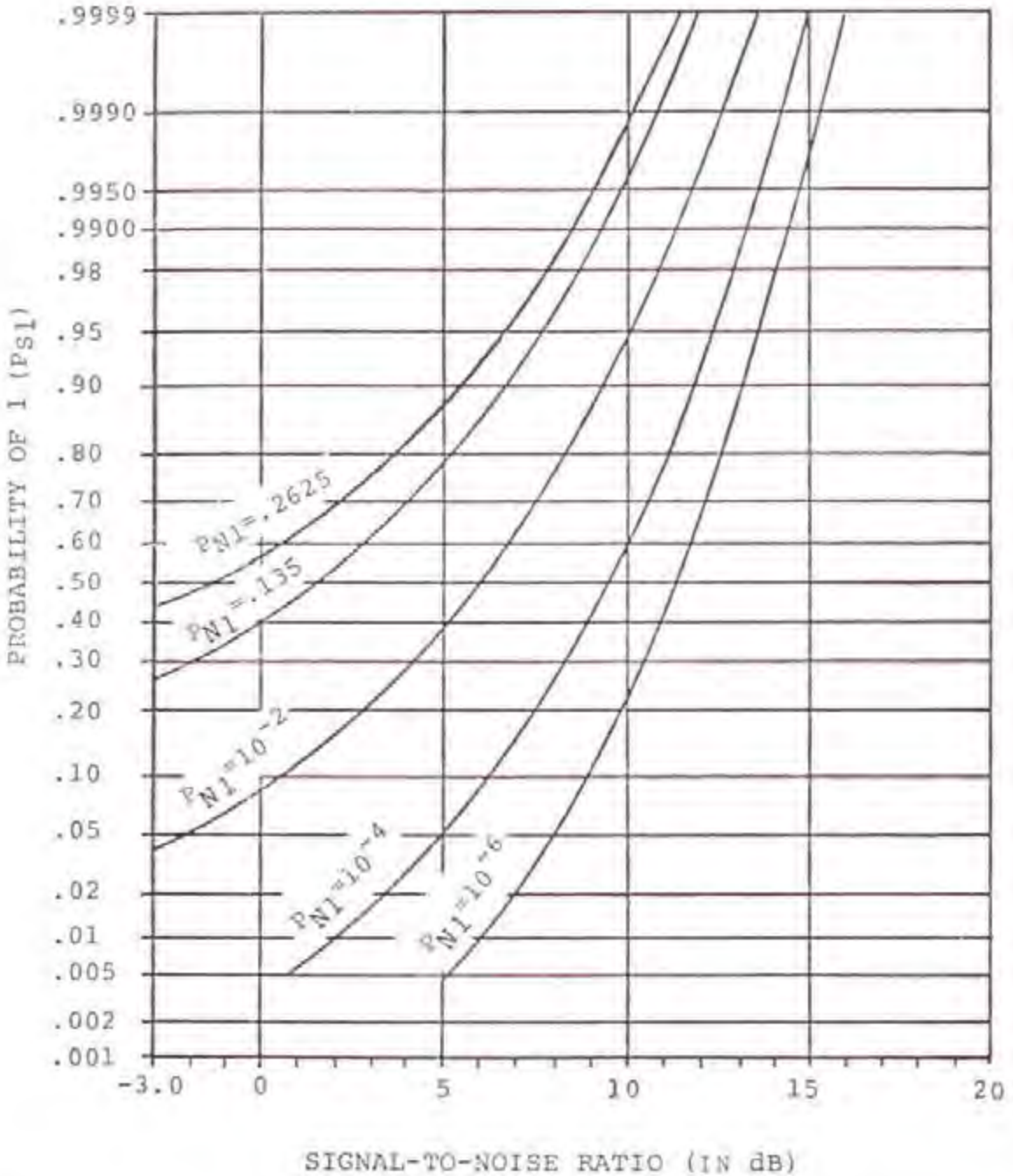

Figure D-36. Probability of 1 at the Threshold Comparator Output as a Function of the Signal-to-Noise Ratio at the threshold Comparator Input for the Normal Channel.

of a binary one in a range bin). The probability of exceeding the threshold comparator level, P_{S1}, is shown as a function of the signal-to-noise ratio (SNR) and probability of the noise causing the threshold comparator to put out a binary one in a range bin, P_{N1}. The curves were obtained by simulating the signal-plus-noise distribution at the normal channel output. The simulation is discussed in Appendix E.

For a nonfluctuating target (Marcum's Case 0), the probability of the desired signal exceeding the threshold comparator level (P_{S1}, probability of a binary one in a range bin) for a single channel MTI canceller when averaged over all doppler frequencies can be approximated by (See Equation C-41):

$$P_{S1} = \int_{T}^{\infty} \frac{2}{\sqrt{2\pi(\sigma^2+A^2/2)}} e^{\frac{-v^2}{2(\sigma^2+A^2/2)}} dv \qquad \text{(D-24)}$$

The integrand of Equation D-24 is the signal-plus-noise distribution at the threshold comparator input for a single channel MTI canceller (see Figure 3-35). Figure D-37 shows the probability of the desired signal-plus-noise exceeding the threshold comparator level (P_{S1}, probability of a binary one in a range bin). The probability of exceeding the threshold comparator level, P_{S1}, is shown as a function of the signal-to-noise ratio (SNR) and probability of the noise causing a binary one in a range bin, P_{N1}. The curves were obtained by simulating the signal-plus-noise distribution at the single channel MTI canceller output. The simulation is discussed in Appendix E.

A comparison of Figures D-36 and D-37 shows that for signal-to-noise ratios (SNR's) greater than zero dB the probability of the signal-plus-noise exceeding the threshold comparator level (P_{S1}, probability of a binary one in a range bin) is greater for the normal channel than for the single MTI channel. This would be expected when comparing the signal-plus-noise amplitude distributions at the integrator threshold comparator input. (See Figure 3-10 for the normal channel and Figure 3-35 for the single MTI channel).

The probability of a desired target return pulse train of 20 pulses causing the binary integrator to be be in state E_j can be determined by using a one-dimensional random walk with reflecting barriers model where levels 0 and 31 are the reflecting barriers. That is, the first and last rows of the Markov chain transition matrix are defined by (P_{S0}, P_{S1}, 0 , ...) and (0,...0, P_{S0}, P_{S1}). The term P_{S0} is defined as the probability of the desired signal not exceeding the threshold comparator level (P_{S0}, probability of a binary zero in a range bin), and P_{S1} is defined as the probability of the desired signal exceeding the threshold comparator level (P_{S1}, probability of a binary one in a range bin). The actual probability of the desired pulse train causing the binary integrator to be in state E_j for a given signal-to-noise ratio is given by:

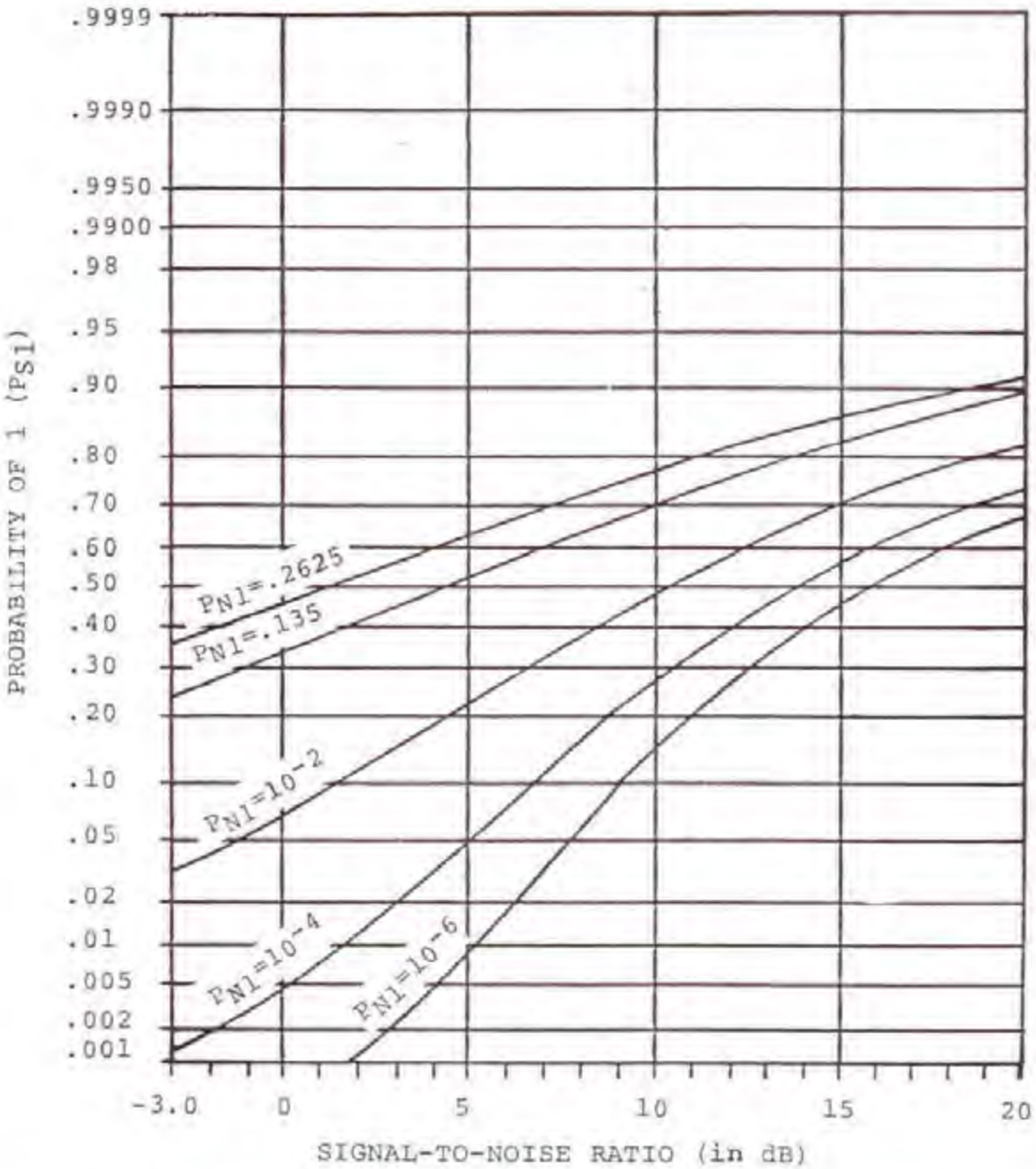

Figure D-37. Probability of 1 at the Threshold Comparator Output as a Function of the Signal-to-Noise Ratio at the Threshold Comparator Input for a Single Channel MTI Canceller

$$P_{sj} = \frac{\sum_{k=1}^{N} P_{ij}^{(k)}}{\sum_{j=1}^{p} \sum_{k=1}^{N} P_{ij}^{(k)}} \qquad \text{(D-25a)}$$

where:

$$P_{ij}^{(k)} = \frac{(p/q)^{-1}}{(p/q)^{p}-1}\left(\frac{p}{q}\right)^{j-1} + \frac{2p}{p}\sum_{r=1}^{p-1} \frac{x_i^{(r)} y_j^{(r)} \left[2\sqrt{pq}\cos \pi r/p\right]^k}{1 - 2\sqrt{pq}\cos \pi r/p} \qquad \text{(D-25b)}$$

and

$$x_i^{(r)} = \left(\frac{q}{p}\right)^{i/2} \sin \frac{\pi r i}{p} - \left(\frac{q}{p}\right)^{(i+1)/2} \sin \frac{\pi r (i-1)}{p} \qquad \text{(D-25c)}$$

$$y_j^{(r)} = \left(\frac{p}{q}\right)^{j/2} \sin \frac{\pi r j}{p} - \left(\frac{p}{q}\right)^{(j-1)/2} \sin \frac{\pi r (j-1)}{p} . \qquad \text{(D-32d)}$$

p = Number of states (function of counter level sequence)

$q = P_{S0}$ = Probability of 0 at threshold comparator output

$p = P_{S1}$ = Probability of 1 at threshold comparator output

N = Number of desired signal pulses in target return pulse train

The values for P_{S1} as a function of signal-to-noise ratio are obtained from Figure D-36 for the normal channel and Figure D-37 for the single MTI channel, and $P_{S0} = 1 - P_{S1}$. The term $P_{ij}^{(k)}$ is defined as the probability of a transition from state E_i to state E_j in exactly k steps. In other words, $P_{ij}^{(k)}$ is the conditional probability of entering state E_j at the kth step given the initial state is E_i. Equation D-25b was obtained from Feller (1968).

TABLE D-6 shows the probability of the FAA modified integrator being in state E_j for a desired target return pulse train of 20 pulses, given that the initial state, E_i, was state 1. The table shows the probability of the

TABLE D-6

PROBABILITY OF DESIRED SIGNAL TARGET RETURN PULSE TRAIN OF 20 PULSES CAUSING THE FAA MODIFIED INTEGRATOR TO BE IN STATE E_j

State E_j	Counter Level	$P_{S1} = .600$	
		P_{sj}	ΣP_{sj}
1	0	.147409993+000	.147409993+000
2	1	.177353622+000	.324763614+000
3	2	.156627014+000	.481390628+000
4	4	.136325570+000	.617716198+000
5	8	.122056103+000	.739772301+000
6	16	.118857942+000	.858630243+000
7	31	.141369757+000	.100000000+001

State E_j	Counter Level	$P_{S1} = .800$	
		P_{sj}	ΣP_{sj}
1	0	.333096427-001	.333096427-001
2	1	.833176873-001	.116627330+000
3	2	.836663318-001	.200293662+000
4	4	.859261801-001	.286219842+000
5	8	.984266549-001	.384646497+000
6	16	.160277434+000	.544923930+000
7	31	.455076070+000	.100000000+001

State E_j	Counter Level	$P_{S1} = .995$	
		P_{sj}	ΣP_{sj}
1	0	.505040409-003	.505040409-003
2	1	.505040408-001	.510090813-001
3	2	.505040413-001	.101513123+000
4	4	.505041066-001	.152017229+000
5	8	.505190671-001	.202536296+000
6	16	.537338534-001	.256270150+000
7	31	.743729850+000	.100000000+001

desired signal being in state E_j as a function of the probability of the desired signal exceeding the threshold comparator level (P_{S1}) of .6, .8, and .995. The initial state, E_j, of 1 was chosen since for a probability of the noise exceeding the threshold comparator level (P_{N1}) of .135 the integrator is in state 1 with a probability of .8439 (see TABLE D-4).

The signal processing of the ASR-7 binary integrator was simulated to investigate the tradeoffs to the desired signal in suppressing asynchronous interference. Both the normal and single MTI channel signal processing was simulated. A detailed discussion of the simulation model is given in Appendix E. A simulated ASR-7 enhancer output for a desired target return pulse train of 20 pulses without noise present is shown in Figures D-38 and D-39 for the conventional ASR-7 enhancer and the FAA modified ASR-7 enhancer respectively. A comparison of Figures D-38 and D-39 shows that the FAA Modified ASR-7 enhancer provides a significant improvement in signal enhancement, target azimuth shift, and angular resolution.

Figures D-40 through D-43 show simulated radar performance of the FAA modified enhancer for the normal channel as a function of the signal-to-noise ratio (SNR). The desired target return pulse train consists of 20 pulses. Each figure shows the simulated radar output with the enhancer off (unintegrated) and enhancer on (integrated). Figure D-40, SNR = 3 dB; and Figure D-41, SNR = 5 dB; show that with the enhancer off the desired signal is down in the noise. However, when the enhancer is on the signal is pulled out of the noise by the binary enhancer. This should be expected since the probability of the desired signal exceeding the threshold comparator level, P_{S1}, is greater than the probability of the noise exceeding the threshold comparator level, P_{N1} = .135, for SNR's of 3 and 5 dB (see Figure D-36).

Figures D-44 through D-46 show simulated radar performance of the FAA modified enhancer for the single MTI channel (mode 1 and 2 CASC) as a function of the signal-to-noise ratio (SNR) with the enhancer off (unintegrated) and on (integrated). A comparison of Figures D-40 with D-44 and D-42 with D-45 (same SNR for normal and MTI channels) shows that the signal enhancement is greater for the normal channel than for the MTI channel. This should be expected since the probability of the desired signal exceeding the threshold comparator level, P_{S1}, is greater for the normal channel than for the single MTI channel for a given SNR. (Compare Figures D-36 and D-37.)

The target azimuth shift due to integration is given by Equation D-12. Using Figure D-39 and Equation D-12, the FAA modified binary enhancer causes a target azimuth shift of approximately .179 degrees. The feedback integrator caused a target azimuth shift of approximately .900 degrees. Therefore, the FAA modified binary enhancer results in a significant improvement in target azimuth shift over the feedback integrator.

The property of the radar to distinguish between targets is called resolution. Using Figure D-39 and Equation D-13, the use of the FAA modified binary enhancer does not cause any loss in target angular resolution. It was

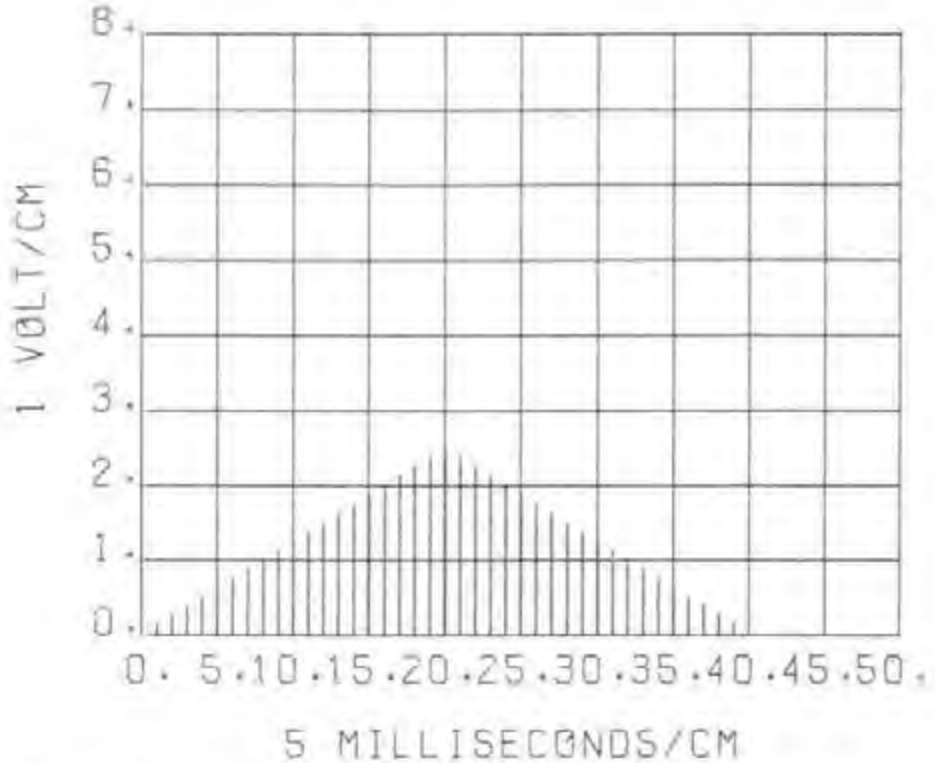

Figure D-38. Simulated Binary Integrator Output for Target Return Pulse Train (ASR-7, AN/GPN-12)

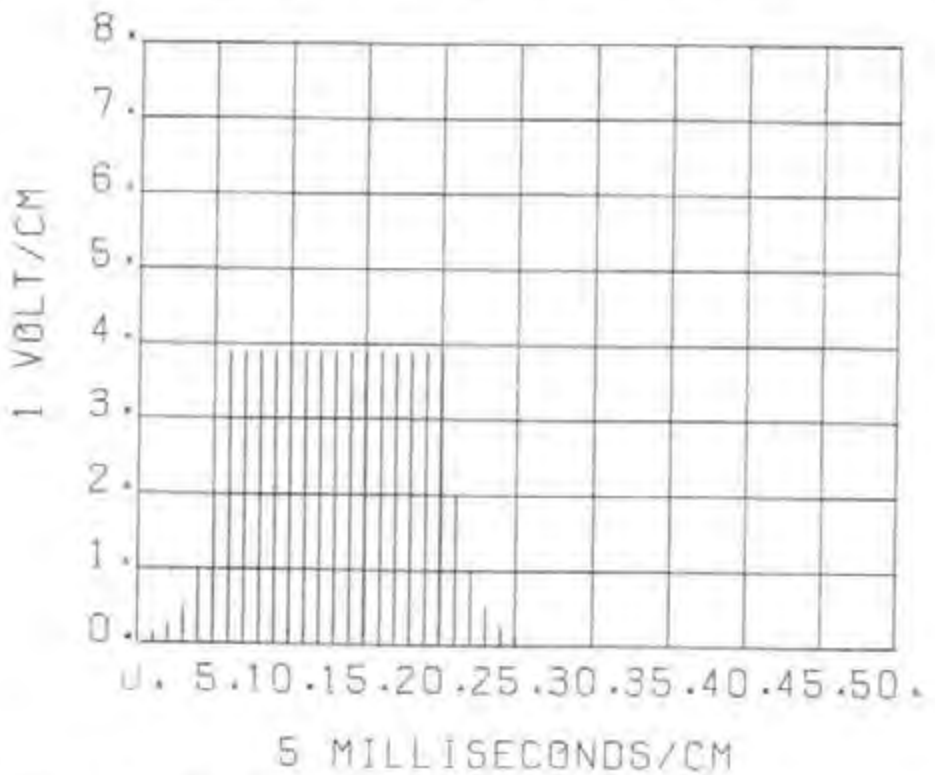

Figure D-39. Simulated FAA Modified Binary Integrator Output for Target Return Pulse Train (ASR-7)

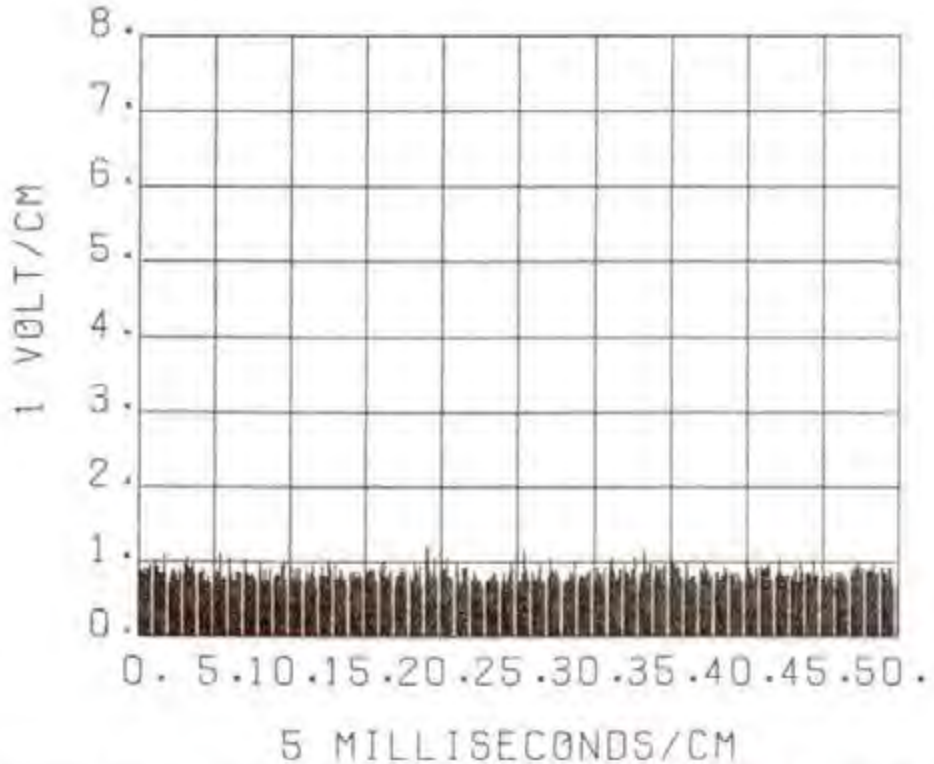

Figure D-40a. Simulated Normal Channel Unintegrated Target Return Pulse Train for a SNR = 3dB

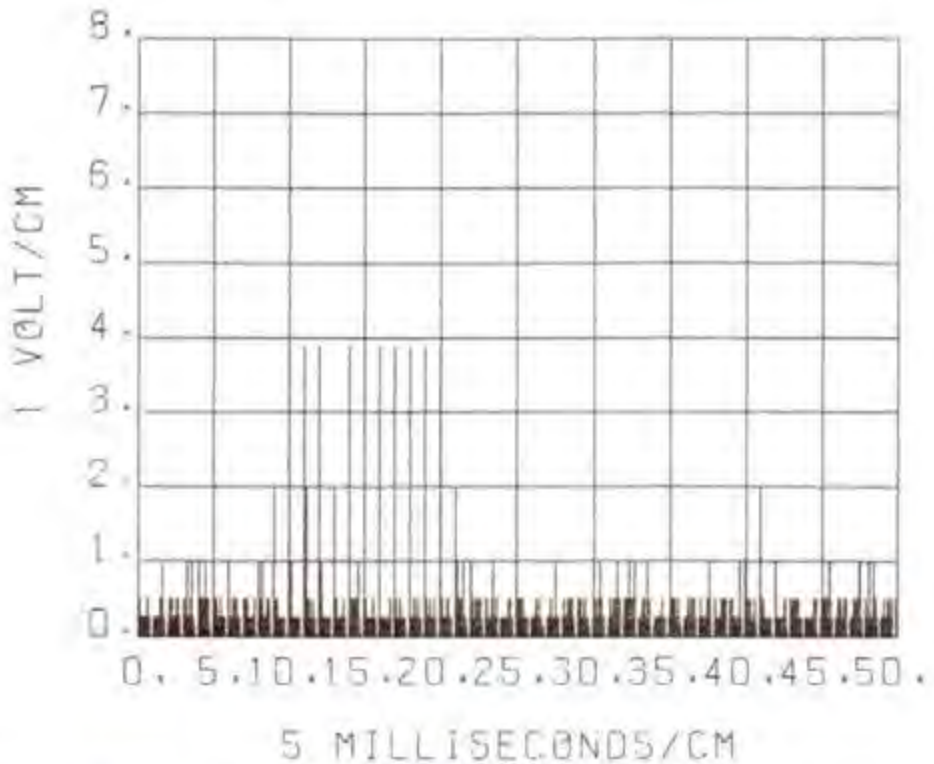

Figure D-40b. Simulated Normal Channel Integrated Target Return Pulse Train for a SNR = 3dB

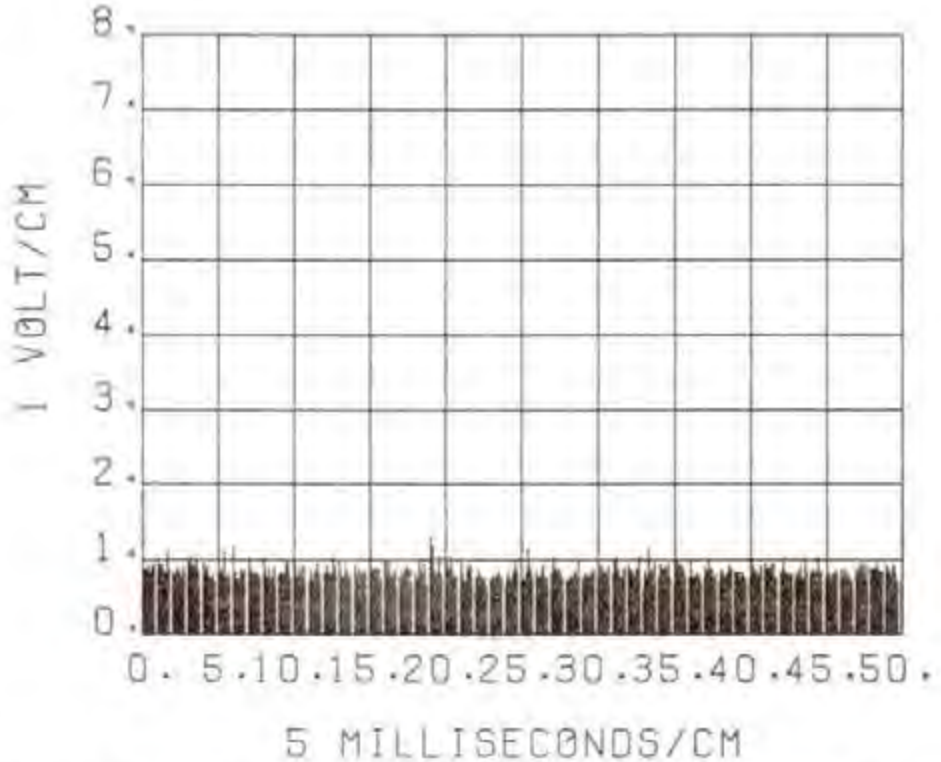

Figure D-41a. Simulated Normal Channel Unintegrated Target Return Pulse Train for a SNR = 5dB

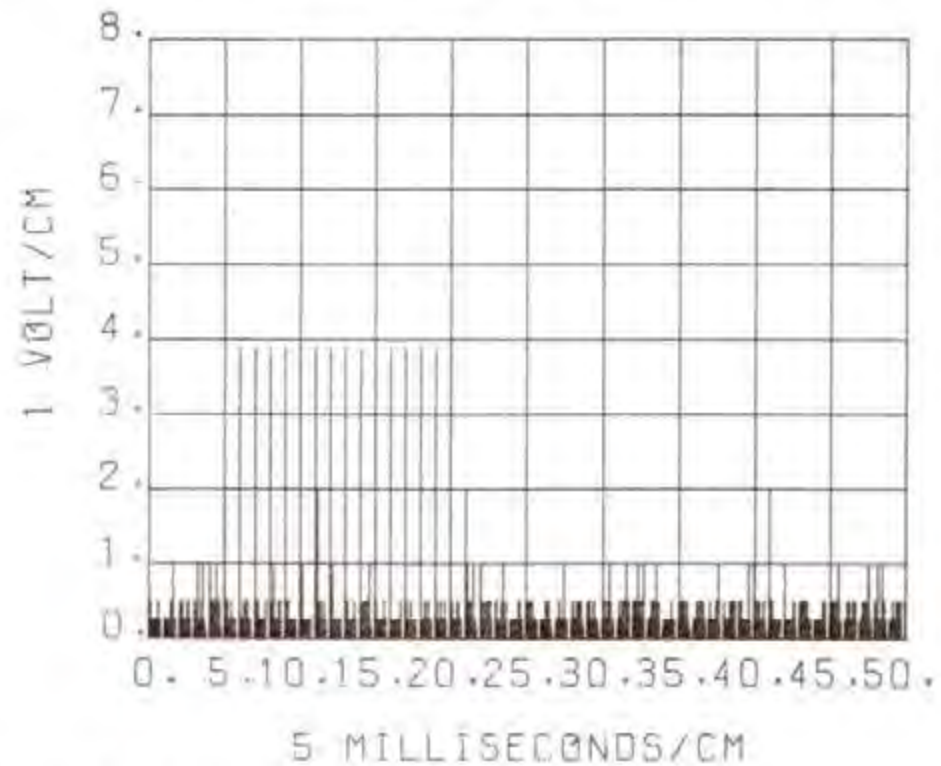

Figure D-41b. Simulated Normal Channel Integrated Target Return Pulse Train for a SNR = 5dB

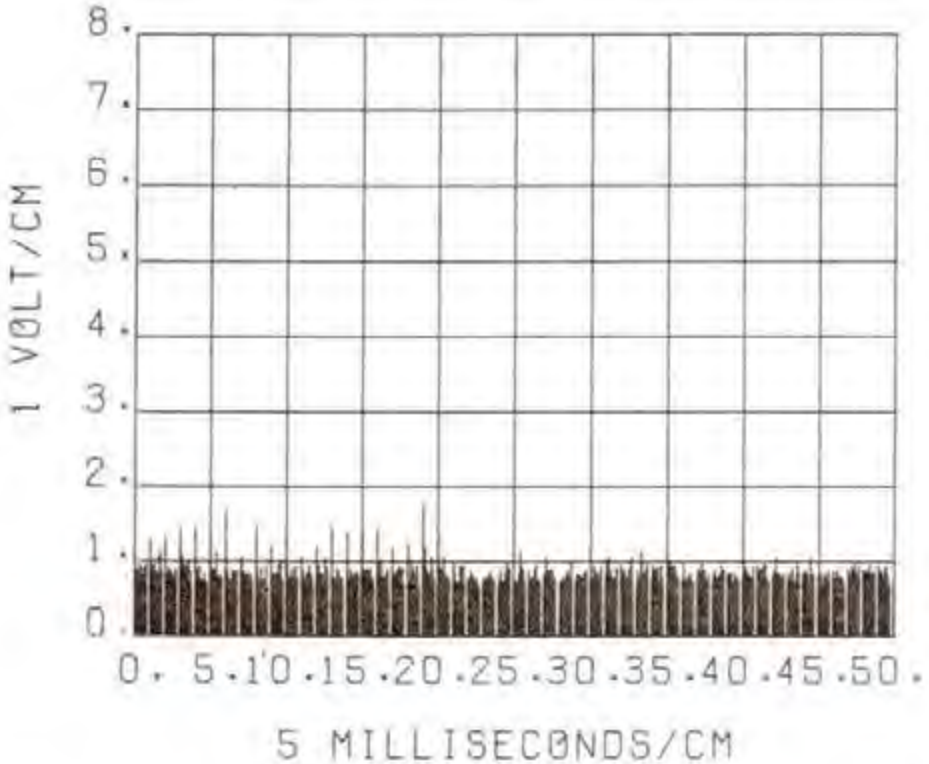

Figure D-42a. Simulated Normal Channel Unintegrated Target Return Pulse Train for a SNR = 10dB

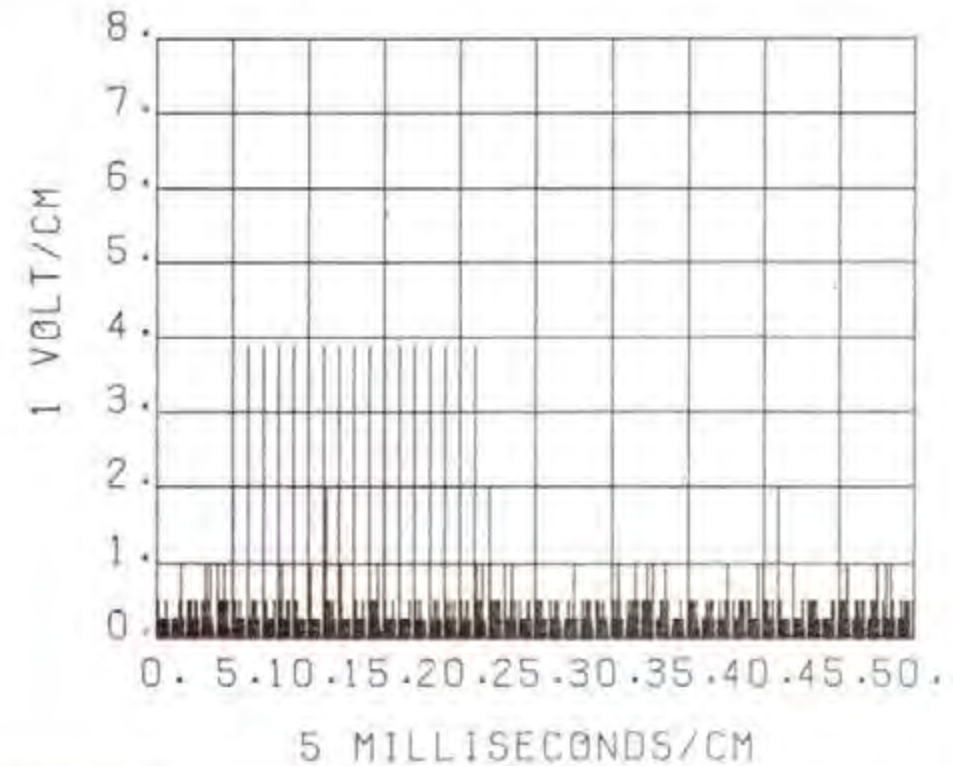

Figure D-42b. Simulated Normal Channel Integrated Target Return Pulse Train for a SNR = 10dB

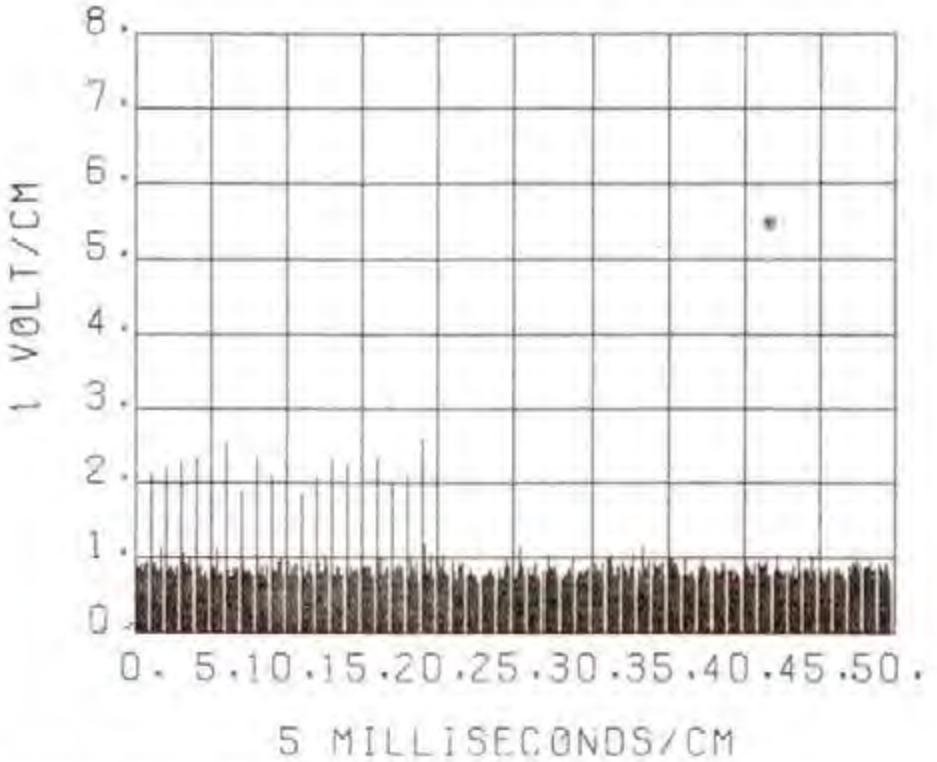

Figure D-43a. Simulated Normal Channel Unintegrated Target Return Pulse Train for a SNR = 15dB

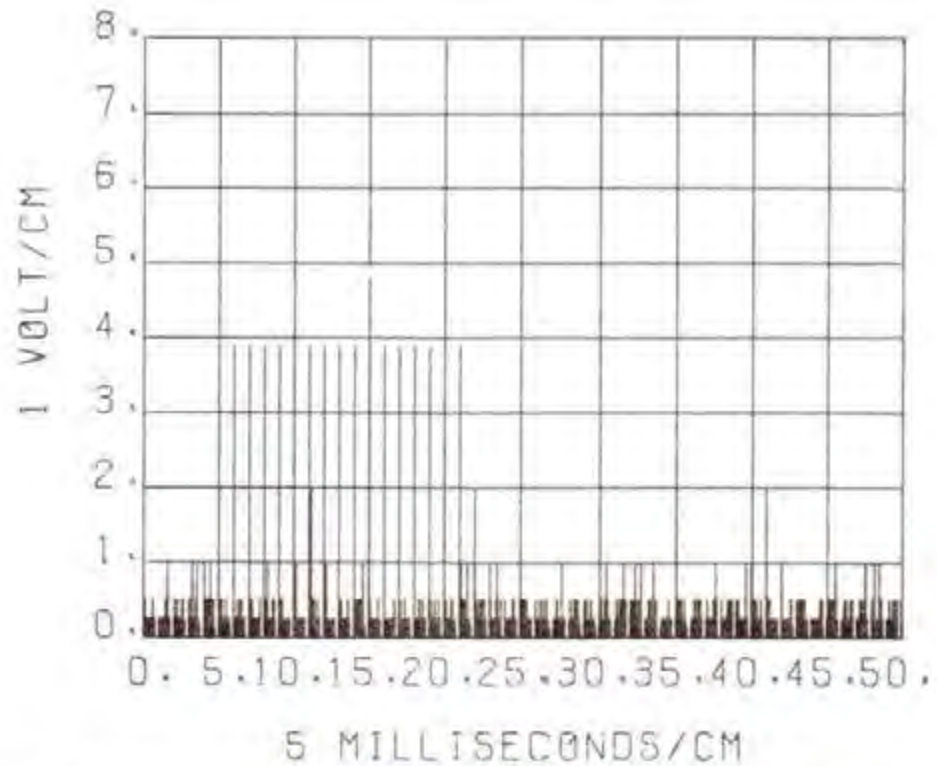

Figure D-43b. Simulated Normal Channel Integrated Target Return Pulse Train for a SNR = 15dB

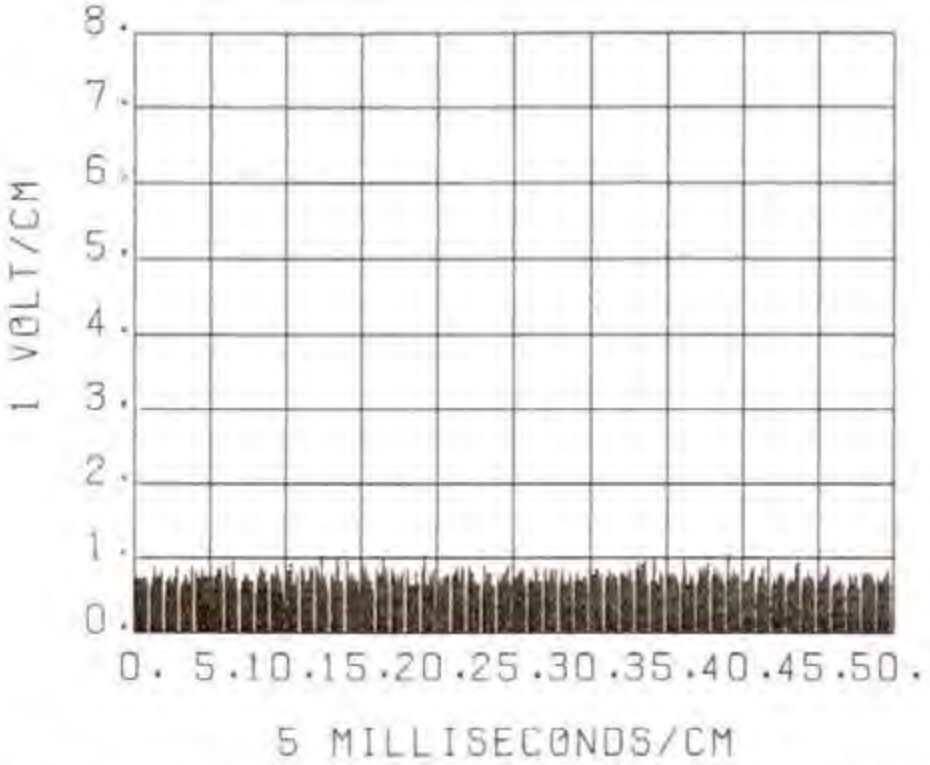

Figure D-44a. Simulated MTI Channel (Mode 1 & 2 CASC) Unintegrated Target Return Pulse Train for a SNR = 3dB

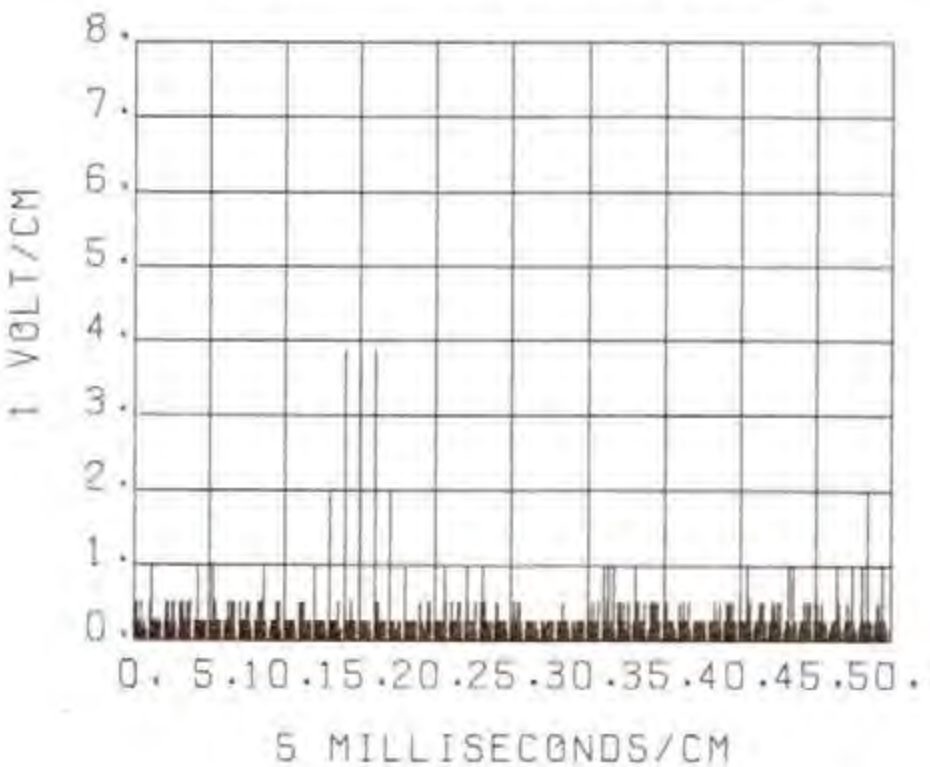

Figure D-44b. Simulated MTI Channel (Mode 1 & 2 CASC) Integrated Target Return Pulse Train for a SNR = 3dB

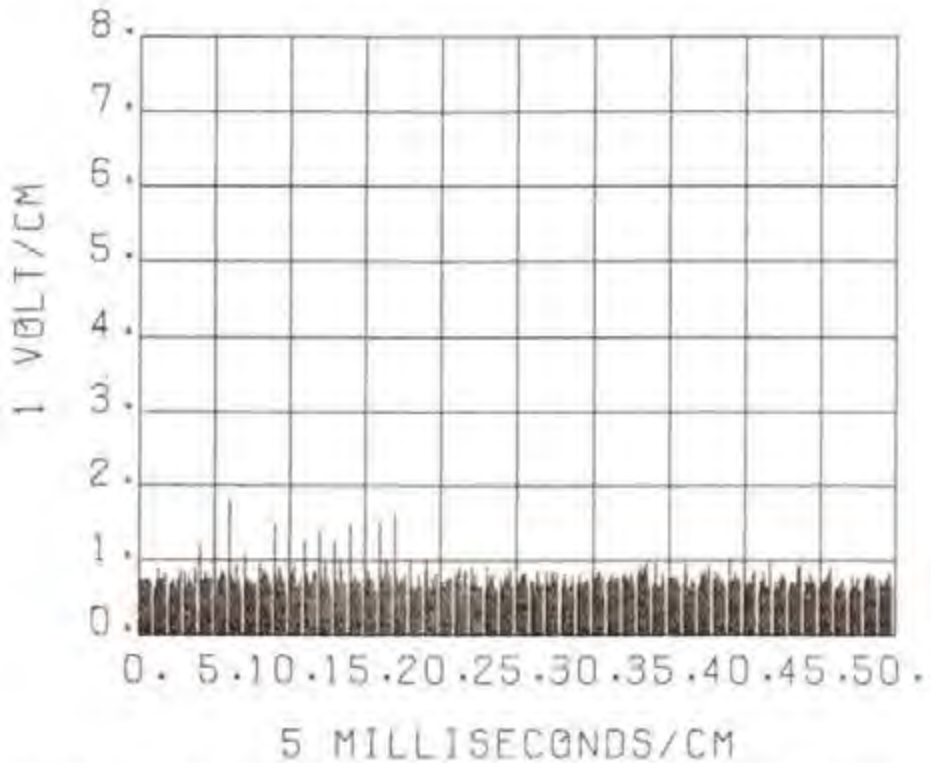

Figure D-45a, Simulated MTI Channel (Mode 1 & 2 CASC) Unintegrated Target Return Pulse Train for a SNR = 10dB

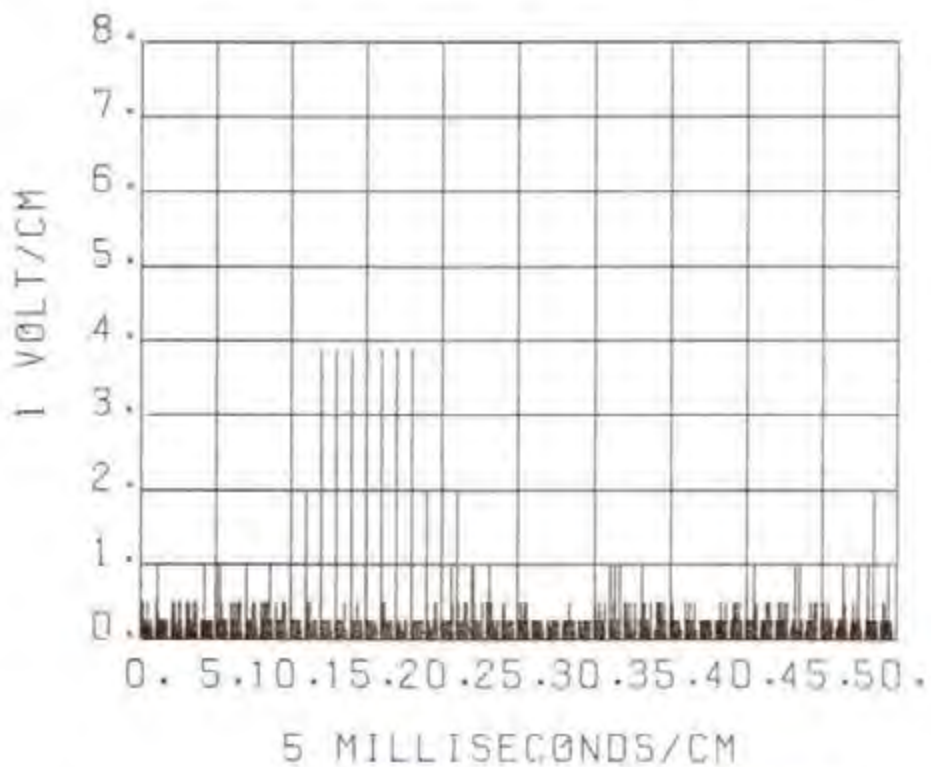

Figure D-45b. Simulated MTI Channel (Mode 1 & 2 CASC) Integrated Target Return Pulse Train for a SNR = 10dB

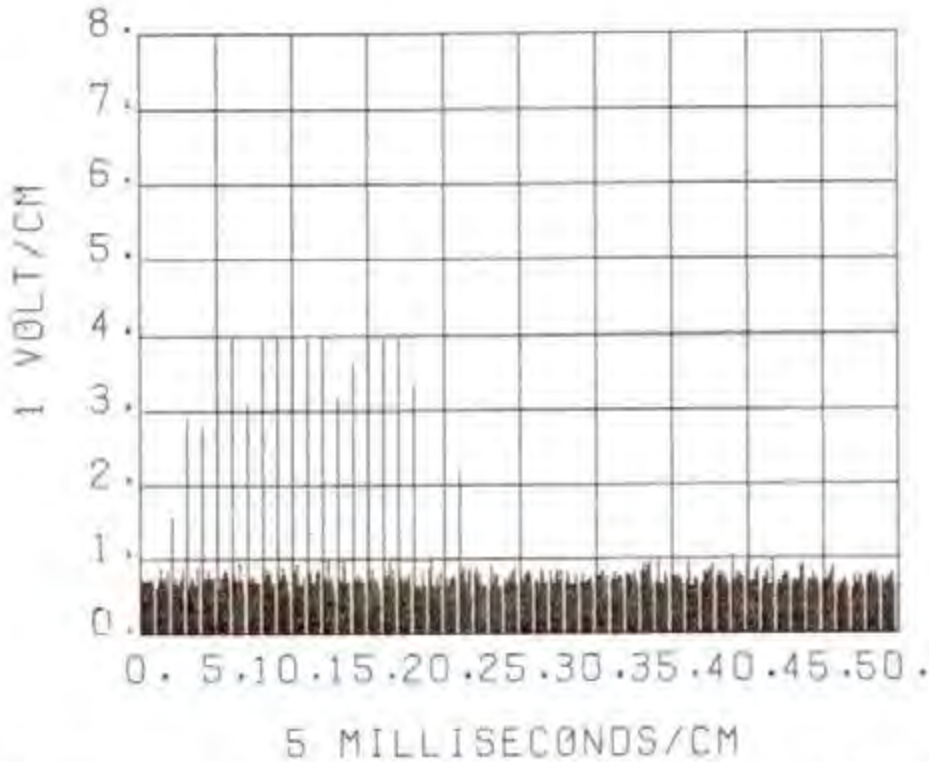

Figure D-46a. Simulated MTI Channel (Mode 1 & 2 CASC) Unintegrated Target Return Pulse Train for a SNR = 20dB

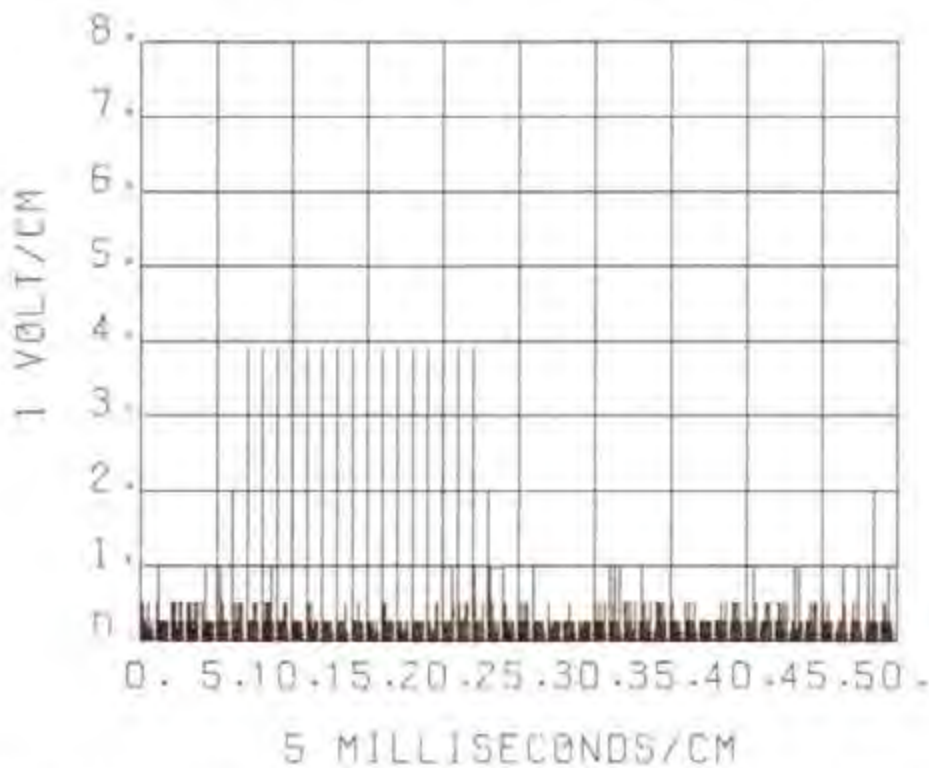

Figure D-46b. Simulated MTI Channel (Mode 1 & 2 CASC) Integrated Target Return Pulse Train for a SNR = 20dB

previously shown that the feedback integrator caused between 1.2 and 1.5 degrees loss in angular resolution.

Interference

The capability of the binary integrator in the ASR-7 to suppress asynchronous interference was also investigated using the radar simulation model (see Appendix E). Three interfering radar sources were simulated: ASR-5, ASR-8, and the AN/FPS-90. Figures E-3 through E-5 in Appendix E show the respective time waveforms simulated for each of the radar interfering sources.

For the normal radar channel, the probability of the interference, P_{ij}, appearing above the one volt peak noise level (enhancer state 8) can be expressed as:

$$P_{ij} = P_{n8} \cdot P_{I1} \cdot (1-e^{-\nu(\tau+RB_S)}) \qquad (D-26)$$

where:

P_{n8} = Probability of the noise causing the enhancer to be in level 8

P_{I1} = Probability of the interference exceeding the threshold comparator level setting

ν = Interfering pulse arrival rate, in pulses per second

τ = Interfering signal pulse width, in seconds

RB_S = Radar quantizer range bin sample time, in seconds

The probability of the noise causing the enhancer to be in level 8 is a function of the enhancer threshold comparator level setting, and the hit/miss sequence programmed in the enhancer. For the FAA modified enhancer and a probability of the noise exceeding the threshold comparator level (P_{N1}) of .135, the probability of the noise causing the enhancer to be in level 8 is .0005 (see TABLE D-4). For an ASR-8 interfering source (ν = 1040, τ = 0.6 μ sec, RB_S = .166 μ sec), the probability of the interference causing the enhancer to exceed level 8 (one volt level) is 3.98×10^{-7} assuming $P_{I1} = 1$. The value of P_{I1} is a function of the interference-to-noise ratio at the enhancer input and can be obtained using Figure D-36. Figure D-47a shows a simulated normal channel radar unintegrated output for three interference sources (ASR-5, INR = 10 dB; ASR-8, INR = 15 dB; and AN/FPS-90, INR = 20 dB), and a desired target signal-to-noise ratio of 15 dB. Figure D-47b shows for the same interference condition the radar output after integration. The asynchronous interference has been suppressed (compare Figure D-43b with D-47b).

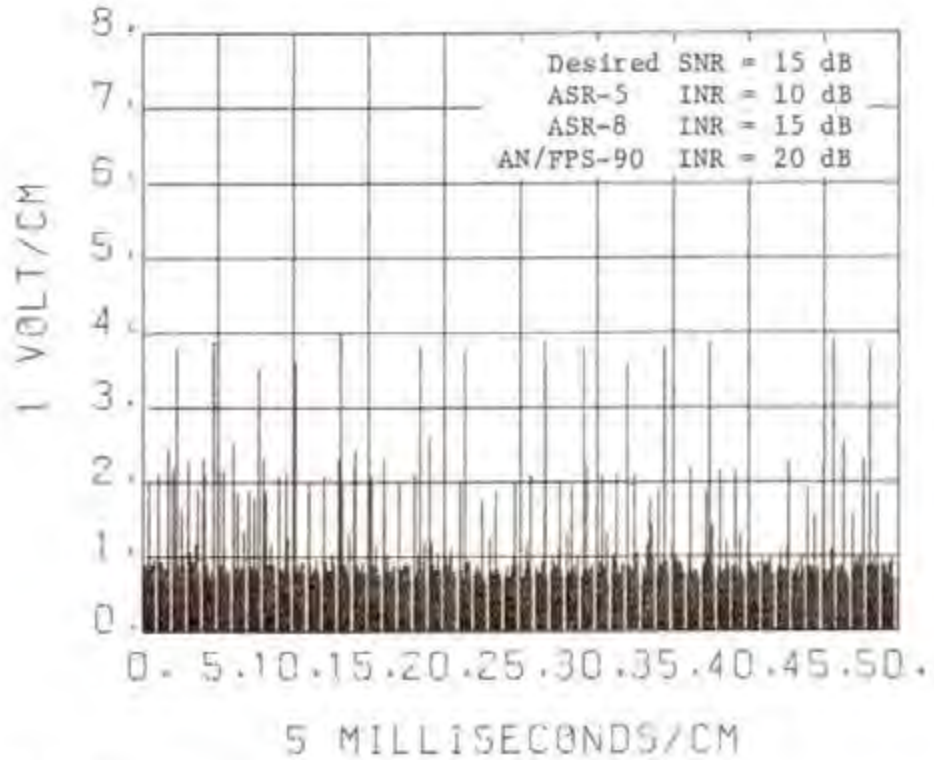

Figure D-47a. Simulated Normal Channel Unintegrated Radar Output with Interference

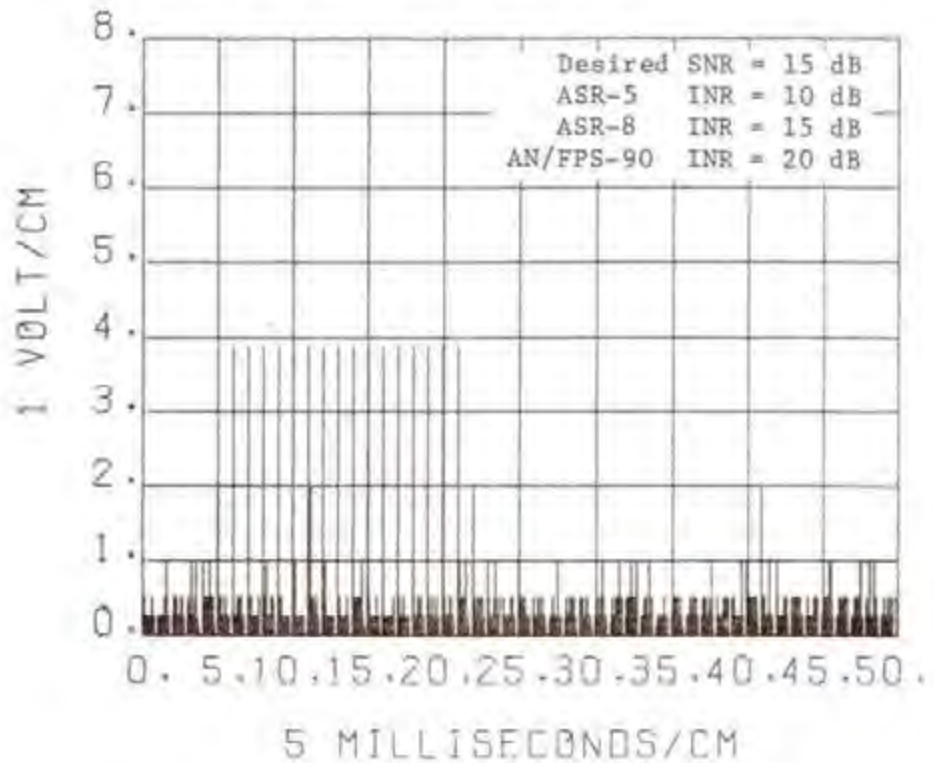

Figure D-47b. Simulated Normal Channel Integrated Radar Output with Interference

For the MTI channel, the analytical expression for the probability of the interference, P_{ij}, appearing above the one volt noise level (enhancer level 8) becomes complex. This is due to the fact that the MTI canceller transfer properties to asynchronous interference results in several synchronous interfering pulses at the MTI canceller output. (See Figures C-16 through C-20.) To assess the probability of the interference causing the enhancer to exceed level 8, all the combination of ways of exceeding level 8 must be considered along with the varying INR of the synchronous interfering pulses at the canceller output. Because of this, the best way of analyzing the capability of the enhancer to suppress asynchronous interference in the radar MTI channel is by simulation. Figure D-48a shows a simulated MTI channel radar unintegrated output for three interfering sources (ASR-5, INR = 10 dB; ASR-8, INR = 15 dB; and AN/FPS-90, INR = 20 dB), and a desired target signal-to-noise ratio (SNR) of 20 dB. Figure D-48b shows for the same interference condition the radar output after integration. The asynchronous interference has been suppressed (compare Figures D-46b with Figure D-48b).

In summary, the FAA modified binary enhancer has the capability of suppressing asynchronous interference with very little trade-offs in target azimuth shift, target angular resolution and desired target probability of detection. Asynchronous interference can be suppressed by the FAA modified enhancer by either adjusting the threshold comparator level setting, or by programming a hit/miss state sequence that will suppress the interference. Thus the FAA modified ASR-7 enhancer can be adjusted to optimize the radar desired signal performance in a variety of environmental conditions.

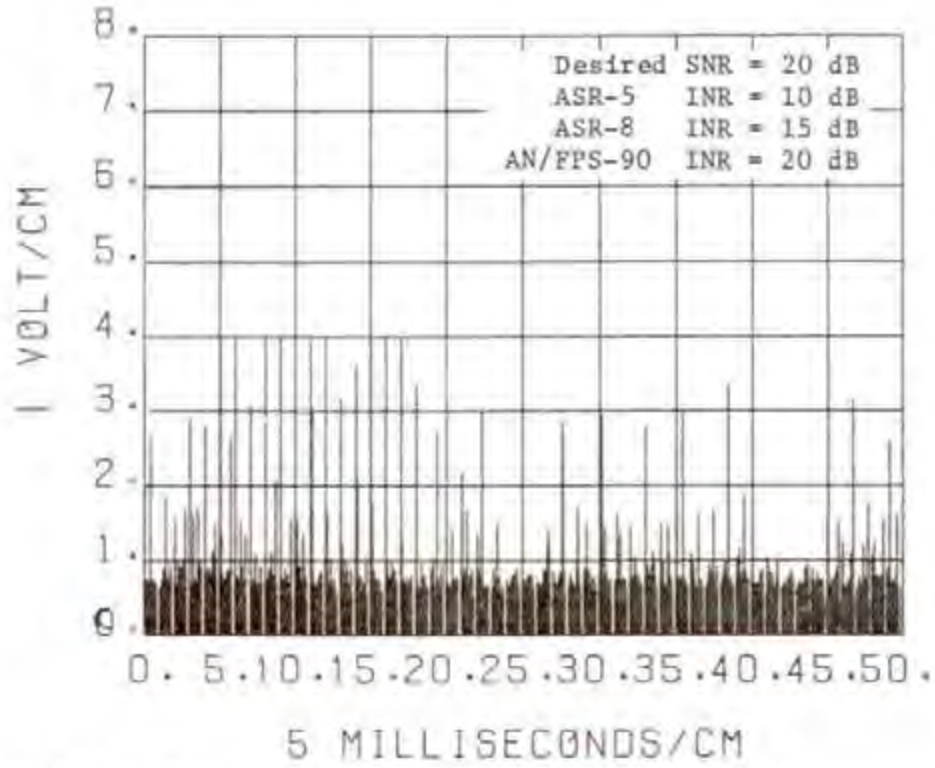

Figure D-48a. Simulated MTI Channel (mode 1 & 2 CASC)
Unintegrated Radar Output with Interference

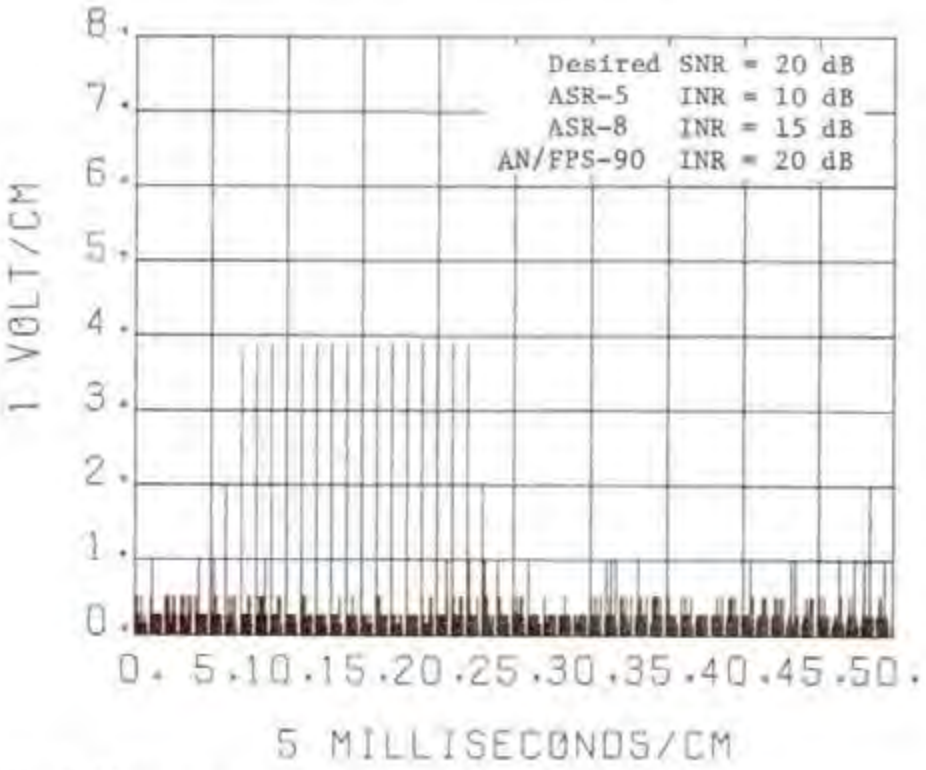

Figure D-48b. Simulated MTI Channel (mode 1 & 2 CASC)
Integrated Radar Output with Interference

APPENDIX E

RADAR SIMULATION

INTRODUCTION

This appendix discusses the techniques used to simulate the primary radar performance so that trade-off investigations could be made as a function of radar signal processing characteristics in the presence of a parametric range of noise, desired signal, and asynchronous interfering signal conditions. The primary radar simulated was the ASR-7. Only the normal and Moving Target Indicator (MTI) channels of the radar were simulated. The portion of the ASR-7 radar simulated was the processor unit (i.e., normal channel envelope detector output and MTI channel phase detector output to the radar output).

In addition, for study of the properties of the feedback enhancer, the simulation provides the capability to use a feedback enhancer in place of the ASR-7 binary enhancer. It should be noted however, that the ASR-7 does not have a feedback enhancer.

PROCESSOR UNIT DESCRIPTION

A detailed description of the primary radar processor unit is given in Section 3. Figure E-1 shows a block diagram of the ASR-7 processor unit hardware which was simulated. The portion of the processor unit normal channel simulated was the normal channel enhancer functional switch, enhancer and alignment hardware. The portion of the processor unit MTI channel simulated was the MTI cancellers, enhancer functional switch, enhancer, and alignment hardware. The simulation model has the capability of displaying the processor unit output in the unenhanced and enhanced modes of both the normal and MTI channels on either an oscilloscope or Plan Position Indicator (PPI) display.

In order to reduce the simulation model computer run time and for analytical simplicity, the conventional analog-to-digital (A/D) and digital-to-analog (D/A) converters at the processor unit input and output respectively were not simulated. However, the received signal amplitudes were simulated in time by dividing the radar receive period after each transmitted pulse into 1200 range bins .625 microseconds long corresponding to the actual A/D and D/A converter hardware of the ASR-7. Since the quantization noise caused by A/D converters is small compared to the inherent receiver noise, not simulating the A/D and D/A converters will not result in unrealistic simulation of the ASR-7 processor unit.

The clock timing for the range bins and desired signal characteristics are shown in Figure E-2. The ASR-7 system clock timing and desired signal

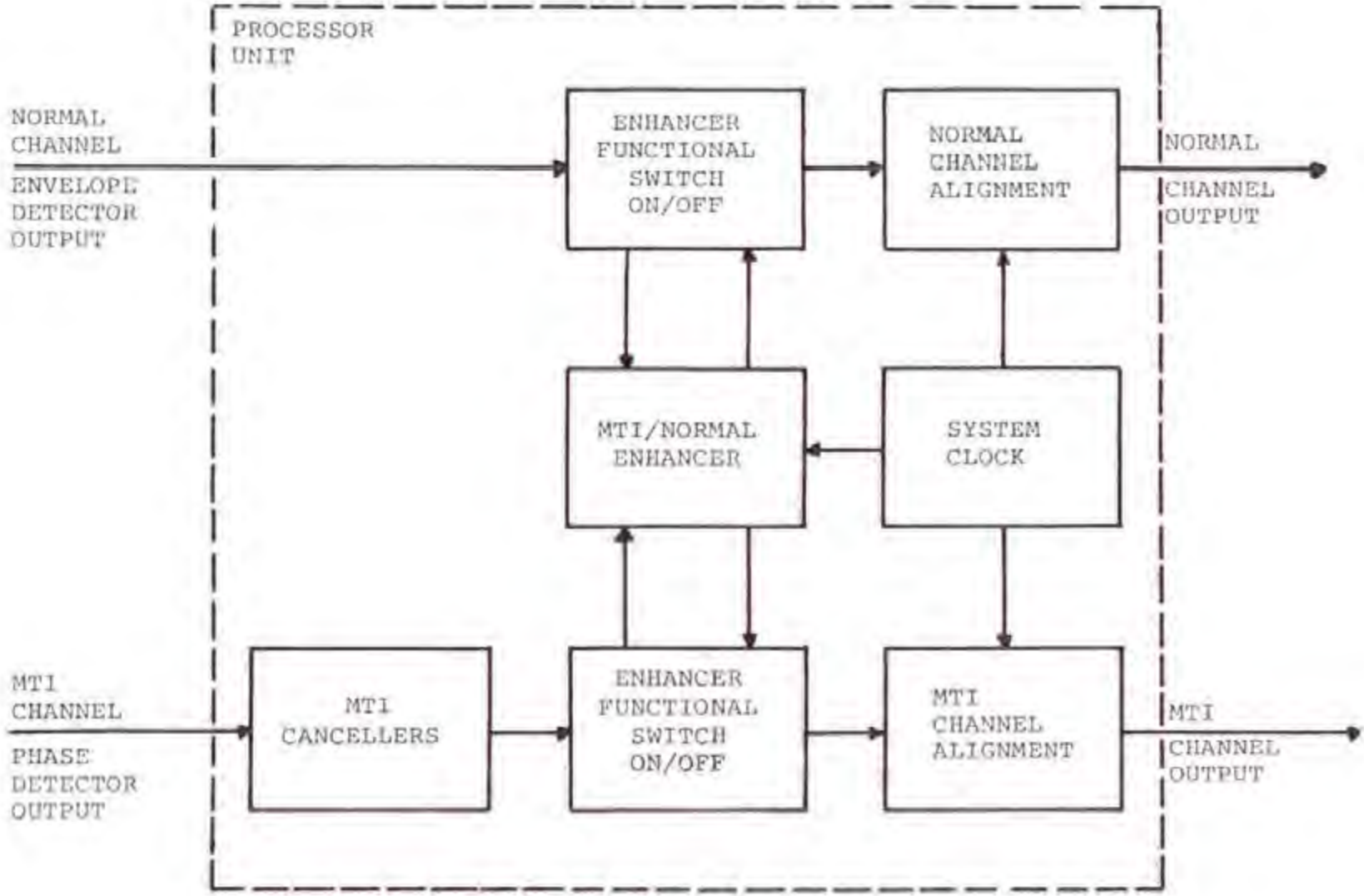

Figure E-1. Block Diagram of Simulated ASR-7 Processor Unit

PW = 0.833 μsec

PPF = 1002 Average (6-Pulse Stagger)

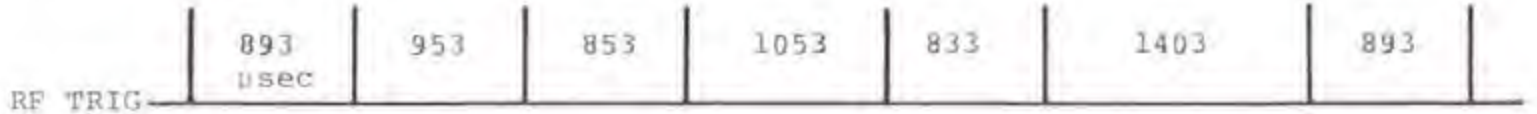

Figure E-2. Clock Timing and Desired Signal Characteristics for ASR-7 Radar

characteristics were simulated for the radar operating in the six-stagger mode which has an average Pulse-Repetition-Frequency (PRF) of 1002 Pulses-Per-Second (PPS). The clock timing also controls the video realignment (destaggering to an average PRF of 1002) at the processor output for Plan Position Indicator (PPI) display. Using the nominal ASR-7 characteristics, the degrees of antenna scan per pulse (ϕ_s) is given by:

$$\phi_s = \frac{6 \cdot RPM}{PRF} = \frac{6 \cdot 12}{1002} = 0.07185628874°/pulse \qquad (E-1)$$

where:

RPM = Antenna scan rate, in rpm (12 for ASR-7)

PRF = Radar pulse repetition frequency, in PPS (1002 for ASR-7)

The number of Azimuth Change Pulses (ACP) per antenna scan for the ASR-7 is:

$$ACP = \frac{360°}{\phi_s} = 5010 \qquad (E-2)$$

Therefore, in summary the simulation of the ASR-7 processor unit was done by:

a. Dividing the receive period after each pulse into 1200 range bins .625 microseconds long,

b. each range bin is approximately 0.0718 degrees wide, and

c. there are 5010 azimuth change pulses (ACPs) per antenna scan.

DESIRED SIGNAL

Figure E-2 shows the pulse width and PRF stagger sequence of the ASR-7 desired signal. The radar simulation model has the capability of simulating a single desired target at any specified range and bearing. The received desired signal pulse train (number of pulses from a target (N)) consists of 20 pulses determined by:

$$N = \frac{PRF \cdot BW}{6 \cdot RPM} = \frac{(1002)(1.5)}{(6)(12)} = 20 \qquad (E-3)$$

where:

PRF = Radar pulse repetition frequency, in PPS (1002 for ASR-7)

BW = Antenna 3 dB beamwidth, in degrees (1.5 degrees for ASR-7)

RPM = Antenna scan rate, in rpm (12 for ASR-7)

The range bin in which the target is located (TRB) was calculated by:

$$TRB = \frac{TR}{RTT \cdot RBT} \qquad (E-4)$$

where:

TRB = Target range bin location, between 1 and 1200

TR = Target range, in nautical miles

RTT = Round-trip time, equals .081 nautical miles per microsecond

RBT = Range bin time, equals .625 microseconds per range bin

The target location (bearing) in Azimuth Change Pulses (ACP) was calculated by:

$$TACP = \frac{TB \cdot PRF}{6 \cdot RPM} \qquad (E-5)$$

where:

TACP = Target azimuth change pulse, between 1 and 5010

TB = Target bearing, in degrees

PRF = Radar pulse repetition frequency, in PPS (1002 for ASR-7)

RPM = Antenna scan rate, in rpm (12 for ASR-7)

The desired signal voltage amplitude in each range bin as a function of the desired signal signal-to-noise ratio (S/N) is discussed later in the normal and MTI channel simulation sections.

INTERFERING SIGNALS

Three types of interfering radar signals were simulated: ASR-5, ASR-8, and AN/FPS-90. The radar simulation model has the capability of having any combination of the three interfering sources present. Figures E-3 through E-5 show the signal timing characteristics of the ASR-5, ASR-8, and AN/FPS-90 interfering radars used in the simulation model. The interfering signal voltage amplitude in each range bin as a function of the interference-to-noise ratio (I/N) is discussed later in the normal and MTI channel simulation sections.

NOISE

In range bins where there was no desired signal or interfering signal the radar inherent noise level was simulated. The simulation of the noise amplitude in each range bin is discussed in the normal and MTI channel simulation sections.

NORMAL CHANNEL SIMULATION

The following is a discussion of the techniques used to simulate the noise, desired signal, and interfering signal levels in the normal channel, and the processor unit hardware in the normal channel.

Noise Distribution

The voltage amplitude distribution of the noise at the normal channel envelope detector output is Rayleigh distributed. The Rayleigh distributed voltage amplitude characteristics of the noise were simulated by letting

$$n_{edo}(t) = \sigma\sqrt{-2 \ln U} \qquad \text{(E-6)}$$

where:

σ = RMS noise level at detector input, in volts

U = Random number uniformly distributed between 0 and 1.0

For each range bin in which noise only is present, a noise voltage amplitude using Equation E-6 was simulated by randomly selecting values between 0 and 1.0 for U.

Signal-Plus-Noise Distribution

The signal-plus-noise voltage amplitude distribution at the envelope detector output has a Rice distribution (also called the Marcum "Q" function). The amplitude characteristics of the signal-plus-noise for the

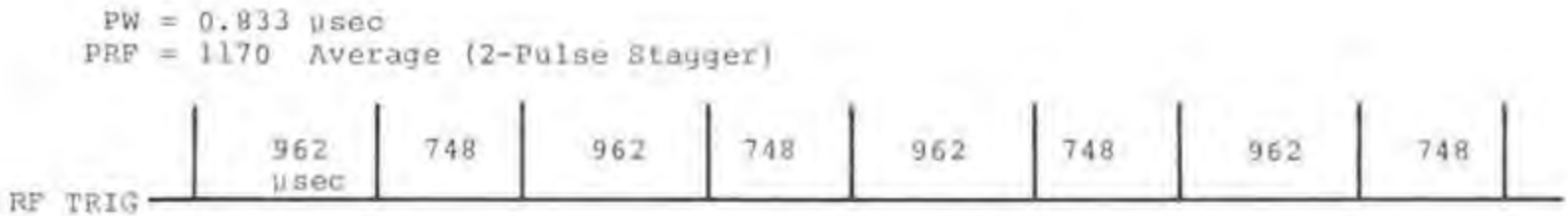

Figure E-3. ASR-5 Interfering Signal Characteristics

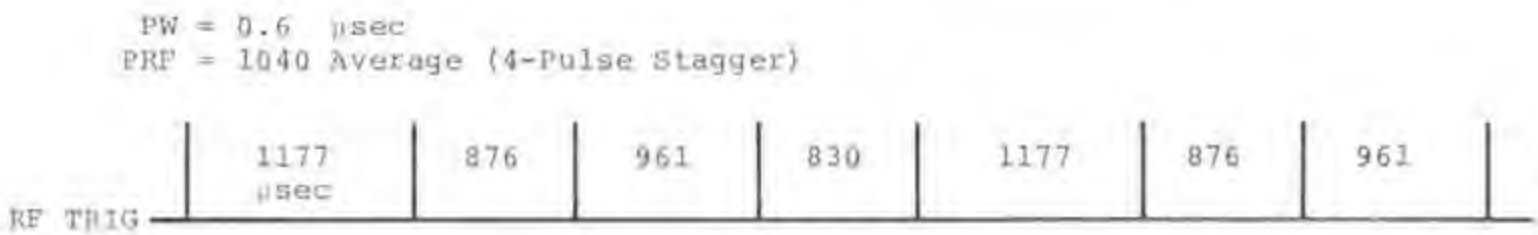

Figure E-4. ASR-8 Interfering Signal Characteristics

Figure E-5. AN/FPS-90 Interfering Signal Characteristics

desired and interfering signals were simulated by:

$$(S+N)_{edo}(t) = \sqrt{X^2+Y^2} \qquad (E-7)$$

where:

$X = R \cos(2\pi V) + A$

$Y = R \sin(2\pi V)$

$R = \sigma\sqrt{-2 \ln U}$

σ = RMS noise level at envelope detector input, in volts

A = Peak-signal level at envelope detector input, in volts

U and V = Random numbers between 0 and 1.0

For the case where "A" equals zero (no signal present), Equation E-7 is equivalent to Equation E-6. Equation E-7 was used to simulate the signal-plus-noise voltage amplitude for both the desired pulse train and interfering signal. The timing of the desired and undesired signals were programmed using List Processing Techniques. For each range bin in which a desired or interfering pulse is present, a signal-plus-noise voltage amplitude using Equation E-7 was simulated by randomly selecting values between 0 and 1.0 for U and V. Figure E-6 shows the simulated signal-plus-noise voltage amplitude distribution as a function of the signal-to-noise ratio (S/N) in dB generated using Equation E-7. The RMS noise voltage level (σ) was set at .25 volts. This corresponds to a one volt peak noise level generally set at the radar receiver output.

Normal Channel Enhancer

The ASR-7 enhancer hardware which was simulated is shown in Figure E-7. The enhancer is basically a digital circuit with an adjustable threshold detector as a simple A/D converter. The enhancer circuit consists of the threshold detector, the digital adder/subtracter circuits, a full range shift register storage, and a D/A converter. If an echo signal exceeding the set threshold level exists in any given range bin, the enhancer stores a one level digital signal in its shift register memory. If the signal continues above the threshold in the given range bin, the enhancer will increase the level stored in each PRF period until a maximum amplitude of 31 is reached. If in any PRF period the signal fails to exceed the threshold level, the enhancer subtracts from the stored level in that particular range bin. The clock timing for the shift register was simulated for the ASR-7 six-stagger mode (see Figure E-2).

A detailed discussion of the signal processing properties of the ASR-7 enhancer is given in Appendix D.

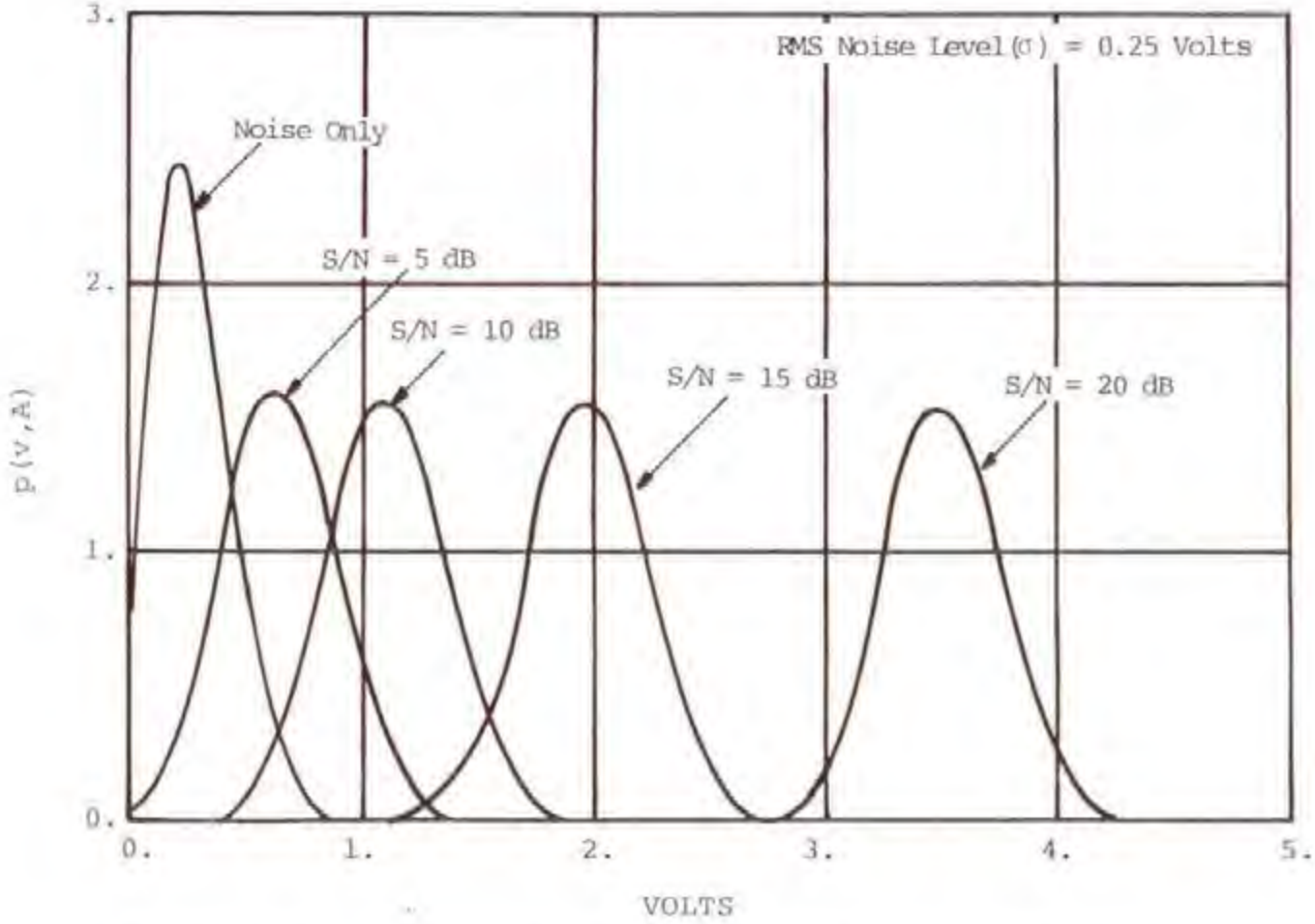

Figure E-6. Probability Density Function for Noise Only and for Signal-Plus-Noise at the Normal Channel Envelope Detector Output.

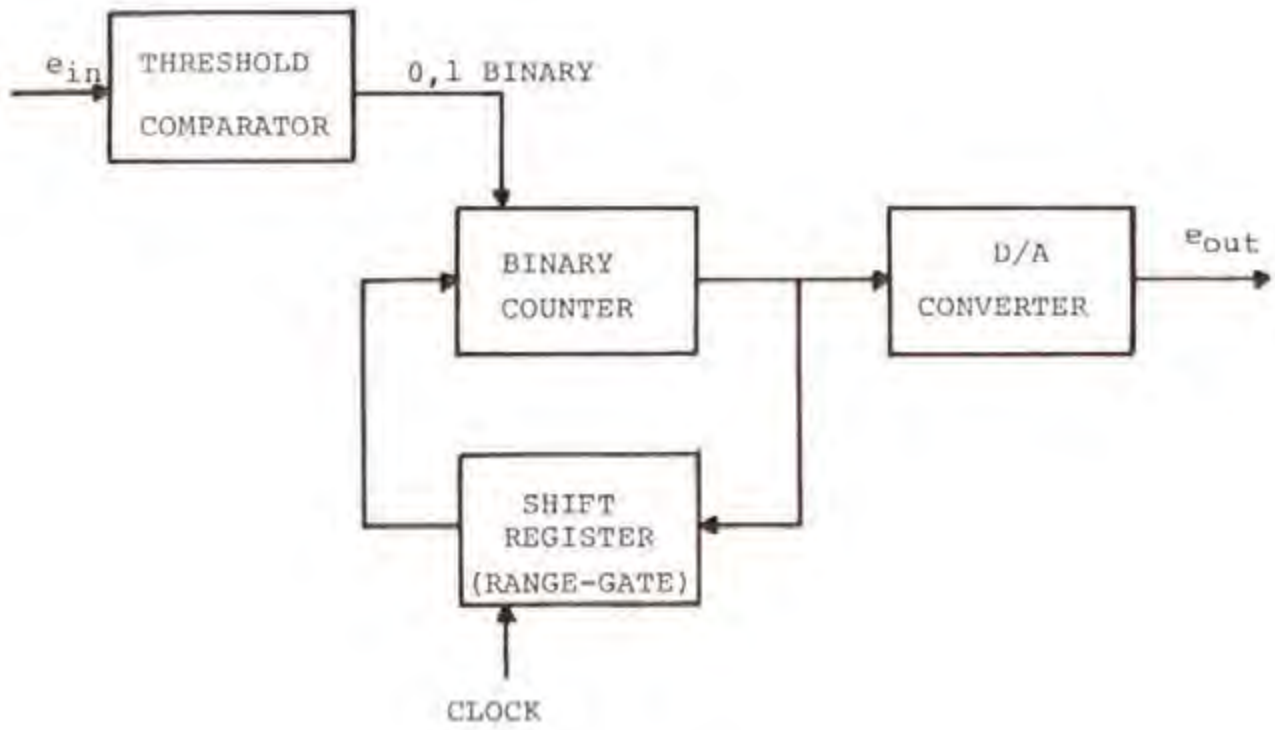

Figure E-7. ASR-7 (AN/GPN-12) Binary Integrator Block Diagram

Normal Channel Alignment

The normal channel alignment circuits provide the delay required during STAGGER PRF operation to insure that a specific range bin in each PRF receive period occurs at the average PRF of 1002. The STAGGER PRF operation and clock timing which was simulated is shown in Figure E-2. The stagger video occurs with the PRF periods of 893 microseconds, 953 microseconds, 853 microseconds, 1053 microseconds, 833 microseconds, and 1403 microseconds. To align these with the average period of 998 microseconds, clock timing from the RF trigger is used to control the alignment circuit delay selection.

MTI CHANNEL SIMULATION

The following is a discussion of the techniques used to simulate the noise, desired signal, and interfering signal in the MTI channel, and the processor unit hardware in the MTI channel.

Noise Distribution

The voltage amplitude distribution of the noise at the phase detector output is Gaussian distributed. The Gaussian distributed voltage amplitude characteristics of the noise were simulated by letting:

$$n_{pdo}(t) = R \cos 2\pi V \qquad \text{(E-8)}$$

where:

$$R = \sigma\sqrt{-2 \ln U}$$

σ = RMS noise level at phase detector input, in volts

U and V = Random numbers uniformly distributed between 0 and 1.0

For each range bin in which noise only is present, a noise voltage amplitude using Equation E-8 was simulated by randomly selecting values between 0 and 1.0 for U and V.

Signal-Plus-Noise Distribution

The signal-plus-noise voltage amplitude distribution at the phase detector output was simulated by:

$$(S+N)_{pdo}(t) = R \cos 2\pi V + A \cos 2\pi W \qquad \text{(E-9)}$$

where:

A = Peak-signal level at phase detector input, in volts

V and W = Random numbers uniformly distributed between 0 and 1.0

For the case where "A" equals zero (no signal present), Equation E-9 is equivalent to Equation E-8. Equation E-9 was used to simulate the signal-plus-noise voltage amplitude for both the desired pulse train and interfering signal. The timing of the desired and undesired signals were programmed using List Processing Techniques. For each range bin in which a desired or interfering pulse is present, a signal-plus-noise voltage amplitude using Equation E-9 was simulated by randomly selecting values between 0 and 1.0 for U, V, and W. Figure E-8 shows the simulated signal-plus-noise voltage amplitude distribution as a function of the signal-to-noise ratio (S/N) in dB generated using Equation E-9. The rms noise voltage level was set at .25 volts.

MTI Cancellers

The MTI double stage canceller hardware in the ASR-7 radar was simulated. It was necessary to simulate the ASR-7 MTI canceller hardware in order to investigate the performance of the ASR-7 enhancer in the presence of asynchronous interference since the impulse response of a double stage MTI canceller with feedback will produce several synchronous pulses. A detailed discussion of the signal transfer properties of a double stage MTI canceller to asynchronous interference is discussed in Appendix C. The following is a discussion of the simulation of the ASR-7 double stage MTI canceller.

The ASR-7 digital canceller consists of two identical delay line type cancellers in cascade, with switch selectable feedback. Figure E-9 shows the canonical form of the ASR-7 MTI canceller which was simulated. The figure shows the transfer function coefficients which represent the ASR-7 hardware. The feedforward coefficients (a_i) are $a_0 = 1/2$, $a_1 = -1$, and $a_2 = 1/2$. The feedback coefficients (b_i) for the various canceller modes are:

CANC 2 :	$b_1 = 0$:	$b_2 = 0$
25 dB SCV:	$b_1 = 1\frac{1}{4}$:	$b_2 = -\frac{1}{4}$
30 dB SCV:	$b_1 = \frac{1}{2}$:	$b_2 = -\frac{1}{4}$
35 dB SCV:	$b_1 = \frac{3}{8}$:	$b_2 = -\frac{1}{4}$
40 dB SCV:	$b_1 = \frac{1}{4}$:	$b_2 = -\frac{1}{4}$

A digital word from each range bin is fed into the canceller. If this range bin contains only clutter, the canceller output will be virtually zero. If it contains a moving target the difference amplitude will represent a sample taken from the doppler cycle. The storage element in each canceller consists of eight parallel shift register chains 1200 range bins long. The digital words are clocked in parallel down the 1200 shift-register bins at a 1.6 MHz rate. The timing for the delays in the MTI canceller were simulated for the ASR-7 six-stagger mode shown in Figure E-2. List Processing Techniques were

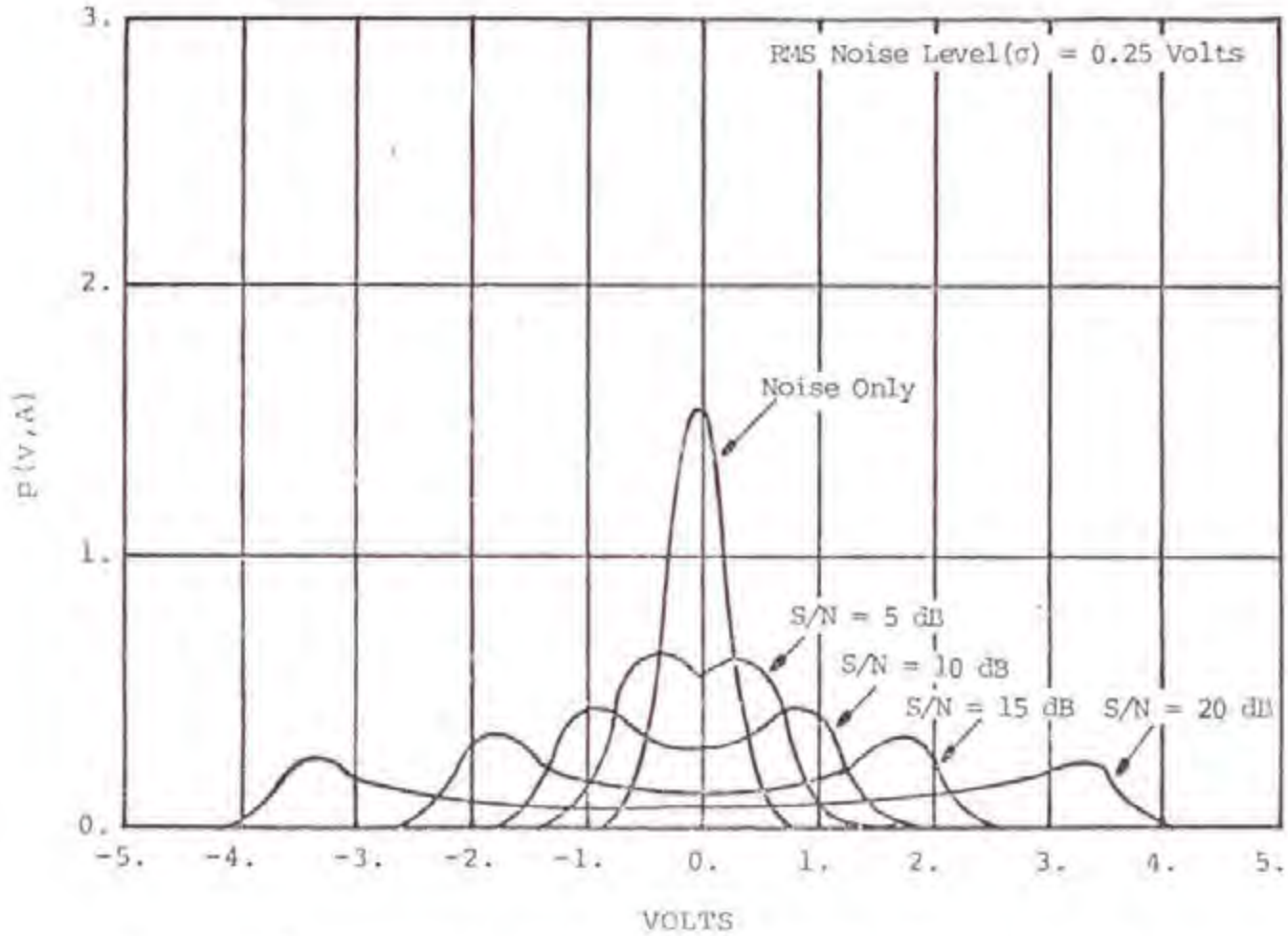

Figure E-8. Probability Density Function for Noise Only and for Signal-Plus-Noise at the MTI Phase Detector Output.

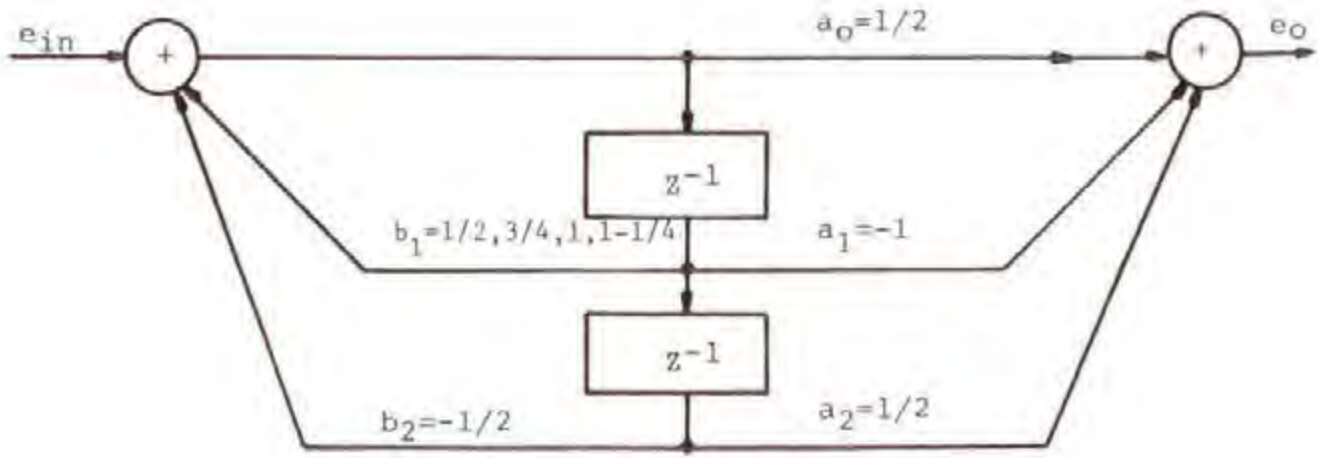

Figure E-9. Canonical Form of Simulated ASR-7 MTI Canceller

used in programming the timing of the ASR-7 six-stagger sequence.

Appendix C contains a detailed discussion of the signal processing properties of the MTI cancellers.

MTI Channel Enhancer

The MTI channel enhancer circuitry is identical to the normal channel enhancer. The simulation of the enhancer was discussed in the normal channel simulation section.

MTI Channel Alignment

The MTI channel alignment circuitry is identical to the normal channel alignment circuitry. The simulation of the alignment circuitry was discussed in the normal channel simulation section.

FEEDBACK ENHANCER

As mentioned at the beginning of this appendix, a feedback enhancer capability was added to the simulation. Figure E-10 shows the feedback enhancer model used in the simulation. The first three blocks: the attenuator, subtractor and bottom clipper are ,strictly speaking, not part of the ASR-8 enhancer circuit board (which it attempts to model). However, these functions are effectively found in other circuits, and it was found necessary to include them to achieve realistic results. Appendix D has a detailed discussion of the feedback integrator.

OUTPUT DISPLAY

Two radar output displays were simulated: the radar output oscilloscope display, and the radar output PPI display. The radar simulation model has the capability of displaying both the normal and MTI channels in the unenhanced and enhanced modes. Appendix D contains oscilloscope display outputs as a function of a parametric range of noise, desired signal, and asynchronous interfering conditions. Also, the trade-offs of the desired signal properties in utilizing an enhancer to suppress interfering signals are discussed in Appendix D. Figure E-11 is 45 degrees of a simulated PPI display of interference.

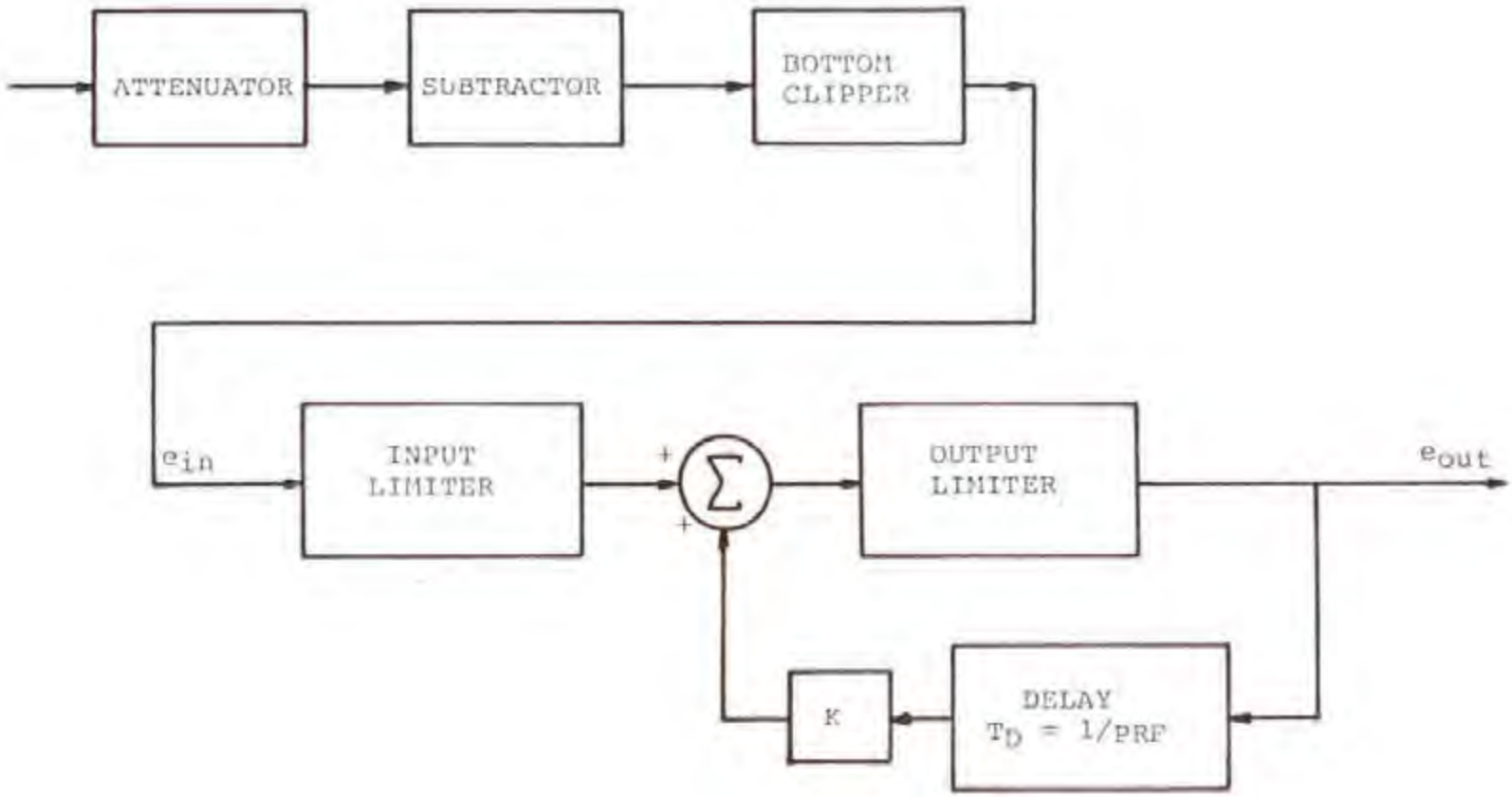

Figure E-10. Feedback Integrator Block Diagram

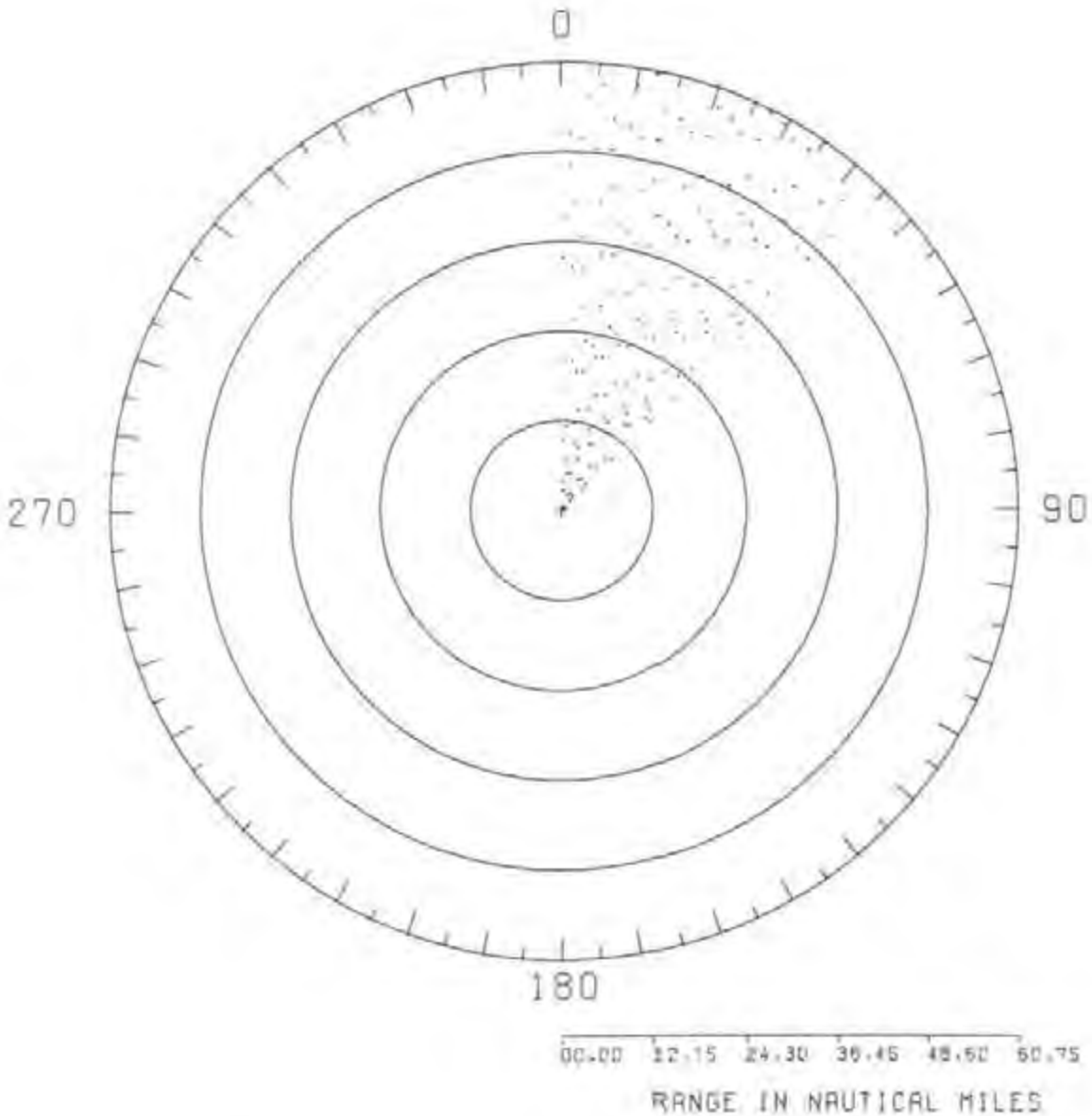

Figure E-11. Simulated PPI Display of Interference

APPENDIX F

INTRODUCTION

This Appendix includes derivations of the equations, and a description of the computer programs used to analyze the impact of radar pulse interference on ARTS-IIIA/RDAS performance. The first section derives the equation used to evaluate the effect of interference on target and false target hit probabilites. The derivation of equations used to compute clutter hit, target hit, and noise hit probability are also included in the first section. The second section describes computer programs that were written to compute the probability of false alarm and target detection.

DERIVATION OF EQUATIONS

Effect of Interference on Hit Probability

The following is a derivation of the equation that gives the probability of a hit (logical 1) at the rank order detection process (includes the rank quantizer and hit processor shown in Figure 4-4) output when interference is present. The derived equation is a general equation that can be used to determine the effect of interference on the probability of a hit (logical 1) when noise, desired signal or clutter are in the range bin of interest. The effect of interference on the probability of a hit when noise, desired signal, or clutter is present in the range bin of interest is a function of the probability of a hit (logical 1) when noise only is present (P_{nl}), probability of a hit when noise and desired signal only are present (P_{sl}), and the probability of a hit when noise and clutter only are present (P_{cl}), respectively. For purposes of deriving a general equation for all of the above conditions, a general term (P_l) will be used to represent a hit for P_{nl}, P_{sl}, and P_{cl}. The equations for P_{nl}, P_{sl}, and P_{cl} will then be derived later. The derivations are described for a rank quantizer threshold 24 to minimize verbiage. However, the results are applicable to any rank quantizer threshold.

The rank order detection processing technique employed in the Radar Data Acquisition Subsystem (RDAS) involves comparing the voltage level in the range bin of interest with that in 24 other adjacent range bins. A logical 1 or hit is generated if the voltage level in the range bin of interest exceeds a particular number (rank quantizer threshold) of the adjacent comparison range bins. If it is assumed that no interfering pulses fall in the comparison range bins and, the level of the interfering pulses is always greater than the voltage level in the comparison range bins, a hit will be generated every time an interference pulse falls in the range bin of interest. Let A represent the event in which one or more interfering pulses fall in the range bin of interest. A hit can also be generated without the presence of interference if the voltage level due to signal-plus-noise, noise only, or clutter exceeds the voltage level in the comparison range bins. Let B represent the event in which a hit is generated when no interference is

present. The probability of a hit being generated with interference or without interference is given by (Davenport, 1958):

$$P(A \cup B) = P(A) + P(B) - P(A \cap B) \qquad (F\text{-}1)$$

where $A \cup B$ represents the event in which A or B occurs and $A \cap B$ represents the event in which both A and B occur. Since events A and B are independent of each other, Equation F-1 can be written in the form:

$$P(A \cup B) = P(A) + P(B) - P(A)P(B) \qquad (F\text{-}2)$$

The generation of a hit (logical 1) can be inhibited if a strong interfering pulse falls in one or more of the rank quantizer comparison range bins, because the voltage level in the range bin of interest will then not exceed all the comparison range bin voltage levels. The following derivations assume that all the interfering pulses are the same level, and as previously stated, greater than the noise, clutter, or target voltage level. These assumptions imply that an interfering pulse falling in the rank quantizer range bin of interest will not generate a hit if one or more of the interfering pulses simultaneously fall into the rank quantizer comparison range bins. Let C represent the event of an interfering pulse falling into one or more of the comparison range bins, and P(C) the probability of that event occurring. A hit can only occur if event A or B occurs and no interfering pulses fall in the comparison range bins. Since Equation F-2 gives the probability of A or B occurring and 1-P(C) the probability of an interfering pulse not falling in the comparison range bins, the probability of a hit occurring with interference present is given by:

$$P_{I1} = [P(A) + P(B) - P(A)P(B)][1-P(C)] \qquad (F\text{-}3)$$

The product of Equation F-2 and [1-P(C)] is used in Equation F-3 because event C can be considered independent of events A and B. This is possible because the interfering pulses arrive randomly in time and the no interference voltage level is assumed to be insignificant compared with the level of the interfering pulses.

Equation F-3 defines the probability of a hit due to asynchronous interference for the ARTS-IIIA/RDAS connected to the victim radar normal channel. This equation will be expanded for the case in which the ARTS-IIIA/RDAS is connected to the radar MTI channel. Approximately three synchronous interfering pulses are generated by the MTI canceller circuits for each asynchronous interference pulse at its input. This affects the probability of interfering pulses falling in a given rank quantizer range bin. An interfering pulse falling in the rank quantizer range bin of

interest could be due to an asynchronous interfering pulse at the input of the MTI falling in the range bin of interest on the present ACP (event A_1), previous ACP (event A_2), or two ACPs before (event A_3). Therefore, the probability of an interfering pulse falling in the rank quantizer range bin of interest is given by:

$$P(A_1 \cup A_2 \cup A_3) = P(A_1) + P(A_2) + P(A_3) - P(A_1 \cap A_2) - P(A_1 \cap A_3) - P(A_2 \cap A_3) + P(A_1 \cap A_2 \cap A_3) \qquad (F\text{-}4)$$

Since the probability of an asynchronous interfering pulse falling in a particular range bin is the same for all ACPs, and independent of each other, Equation F-4 can be written in the form:

$$P(A_1 \cup A_2 \cup A_3) = 3P(A) - 3[P(A)]^2 + [P(A)]^3 \qquad (F\text{-}5)$$

Equation F-5 can be closely approximated by $3P(A)$ since $P(A) < 10^{-4}$ and the product terms are small compared to $3P(A)$.

Based on the assumptions in this analysis, it is required that no interfering pulses fall in the rank quantizer comparison range bins for a hit to be generated. In order for this to occur with the ARTS-IIIA/RDAS connected to the MTI channel, it is necessary that interfering pulses do not fall in these range bins at the MTI circuit input for three consecutive ACPs. It was previously shown that $1-P(C)$ is the probability of an interfering pulse not falling in the comparison range bins, where $P(C)$ is the probability of interfering pulses falling in the comparison range bins. Therefore, the probability of interfering pulses not falling in the comparison range bin for three consecutive ACPs is $[1-P(C)]^3$. Substituting $[1-P(C)]^3$ for $[1-P(C)]$ and $3P(A)$ for $P(A)$ in Equation F-3 gives:

$$P_{I1} = [3P(A) + P(B) - 3P(A)P(B)]\ [1-P(C)]^3 \qquad (F\text{-}6)$$

Equations F-3 and F-6 can be represented by one general equation

$$P_{I1} = [N\,P(A) + P(B) - N\,P(A)\,P(B)]\ [1-P(C)]^N \qquad (F\text{-}7)$$

where N is set equal to 1 for the ARTS-IIIA/RDAS connected to the radar normal channel and set equal to 3 if connected to the MTI channel.

The random arrival of asynchronous interfering pulses in time can be described by a Poisson probability distribution (Davenport, 1958).

Therefore, the probability of an interfering pulse overlapping the sample time of the range bin of interest is given by:

$$P(A) = 1-e^{-x_1 v} \qquad \text{(F-8)}$$

where:

X_1 = Time interval that an interfering radar pulse can overlap the sample time of the rank quantizer range bin of interest, seconds

v = Interfering pulse arrival rate, pulses/second

The probability of an interfering pulse overlapping the sample time of one or more comparison range bins is given by:

$$P(C) = 1-e^{-x_2 v} \qquad \text{(F-9)}$$

where:

X_2 = Time interval that an interfering radar pulse can overlap one or more of the rank quantizer comparison range bins sample times, seconds

Substituting Equations F-8 and F-9 into Equation F-7 and letting the probability of a hit without interference, P(B), equal P_1 gives:

$$P_{11} = [N(1-e^{-x_1 v})+P_1-N(1-e^{-x_1 v})P_1][1-(1-e^{-x_2 v})]^N \qquad \text{(F-10)}$$

Algebraic simplification of this equation gives the basic equation that was used in the analysis:

$$P_{11} = [N(1-P_1)(1-e^{-x_1 v}) + P_1]e^{-Nx_2 v} \qquad \text{(F-11)}$$

Some justification for the assumption that the interfering pulses are greater than the target return pulses at the ASR-7 radar MTI circuit output needs to be presented, since the amplitude of a given interfering pulse out of the ASR-7 MTI circuit can be zero depending on its phase angle relative to the COHO reference signal. For example, the MTI phase detection in the ASR-7 radar will give a zero output voltage if the difference in phase between the interfering pulse and the coherent oscillator signal is 90 degrees (see Appendix C). The simulation of interfering radar effects on the ASR-7 radar

(see Appendix E) involved obtaining pulse amplitude statistics at the MTI circuit output. A modified cumulative distribution of these statistics are shown in Figure F-1 for various signal-to-noise ratios (SNR's). The vertical axis gives the percentage of time that the horizontal axis signal-plus-noise voltage level is exceeded. The curves are applicable to either randomly arriving constant amplitude interfering or target return pulses since the simulations assumed no phase correlation between pulses. The curves in Figure F-1 indicate that if the interfering pulse levels are much greater than the target return pulses at the input of the MTI circuits, there is a high probability that this condition will also exist at the MTI circuit outputs (ARTS-IIIA/RDAS input). For example, assume that the interference-to-noise ratio (INR=20 dB) is 10 dB greater than the signal-to-noise ratio (SNR=10 dB). For this case, Figure F-1 indicates the interference-plus-noise level would exceed 1.5 volts at the MTI output 60 percent of the time while the signal-plus-noise level would exceed this level only 2 percent of the time. This example indicates that it is reasonable to make the worst-case assumption that the interfering pulses are greater than the target return pulses at the ARTS-IIIA/RDAS input when connected to the ASR-7 MTI channel. This worst-case assumption is even more reasonable for the ASR-8 radar dual channel MTI since it employs quadrature phase detectors. A single non-zero amplitude pulse at the dual channel MTI input, regardless of its phase, will not be zero amplitude at its output.

Probability of False Target Hit

This subsection derives the equation for probability of a false target hit due to noise without the presence of interference. A false target hit is defined as the generation of a target hit (logical 1) when no target is present. A hit is generated for these conditions if the noise level in the rank quantizer range bin of interest is greater than RQT of the J comparison range bins. This rank order detection process results in a constant false target hit probability if the rank quantizer range bin sample outputs V_1, V_2, ..., V_j, V_{j+1} are independent and identically distributed. These statistical conditions are assumed for the following derivations. Let F define the cumulative distribution,

$F(v) = P(V<v)$, where V represents rank quantizer comparison range bin samples. In J independent noise samples V_i, i=1,....J, from the J rank quantizer comparison range bins, the probability that exactly RQT (rank quantizer threshold) will be less than the J+1 sample (sample from rank quantizer range bin of interest) is given by:

$$\binom{J}{RQT} [F(v)]^{RQT} [1-F(v)]^{J-RQT} \qquad (F-12)$$

The value of v in this equation represents the noise voltage level in the range bin of interest. The binomial coefficient in Equation F-12 takes into

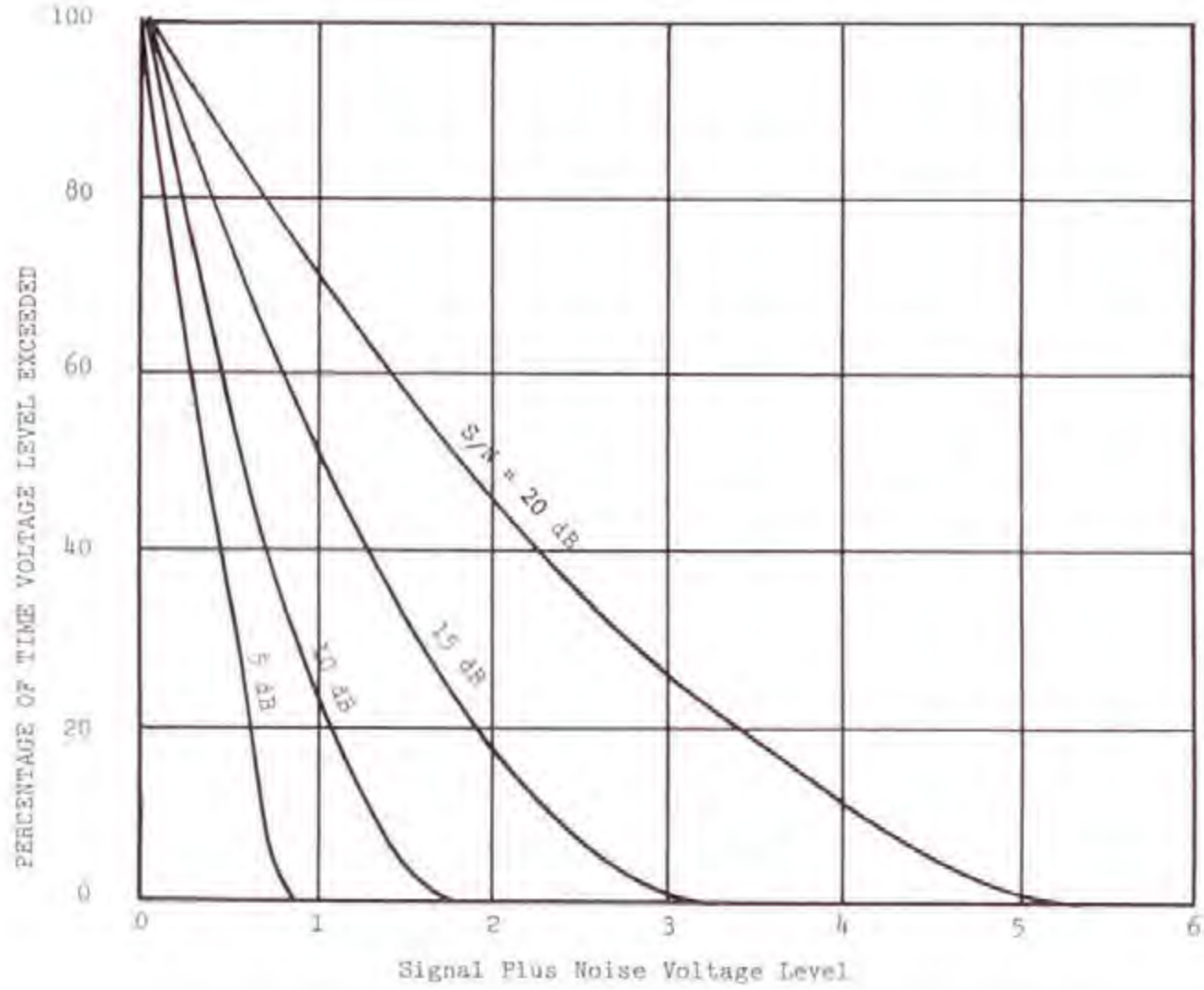

Figure F-1. Modified Cumulative Distribution of Signal-Plus-Noise at ASR-7 Radar MTI Channel Output for Various Signal-to-Noise Voltage Ratios

account the different combinations of RQT out of J things. The probability that the sample in the rank quantizer range bin of interest is greater than RQT of J comparison range bins is given by:

$$\sum_{K=RQT}^{J} \binom{J}{K} [F(v)]^K [1-F(v)]^{J-K} \qquad (F-13)$$

The value v can be considered sample values drawn from the rank quantizer range bin of interest. If it is assumed that this sample space has a cumulative distribution F(v), taking the expected value of the Equation F-13 gives the probability (P_{n1}) that a sample from the rank quantizer range bin of interest will exceed RQT of the rank quantizer comparison range bin sample levels:

$$P_{n1} = \int_0^1 \sum_{K=RQT} \binom{J}{K} [F(v)]^K [1-F(v)]^{J-K} d[F(v)]$$

$$= \sum_{K=RQT}^{J} \int_0^1 \binom{J}{K} [F(v)]^K [1-F(v)]^{J-K} d[F(v)] \qquad (F-14)$$

This equation gives the probability of a false target hit occurring due to only noise. A general term in Equation F-14 is:

$$\int_0^1 \binom{J}{K} [F(v)]^K [1-F(v)]^{J-K} d[F(v)] \qquad (F-15)$$

Substituting the dummy variable u for F(v) and evaluation of F-15 by repeated integration by parts gives:

$$\int_0^1 \binom{J}{K} u^K (1-u)^{J-K} du = \frac{1}{J+1} \qquad (F-16)$$

Substituting Equation F-16 for each term in Equation F-14 gives:

$$P_{n1} = \sum_{K=RQT}^{J} \frac{1}{J+1} = \frac{J+1-RQT}{J+1} \qquad (F-17)$$

This equation indicates that the probability of a false target hit due to noise is independent of the noise distribution F(v) and only a function of hardware parameters. It should, however, be reiterated that the equation is only valid when range bin noise samples are independent and identically distributed. The equation would only give approximate false hit values for correlated clutter.

Probability of Target Hit

This subsection derives the equation for probability of target hit without interference present. A target hit is defined as the generation of a target hit (logical 1) when a target is present. The derivation considers the target signal present in the rank quantizer range bin of interest and no target signal present in the rank quantizer comparison range bins. Assume that the samples from the comparison range bins are independent and identically distributed with a cumulative distribution function $F(v) = P(V<v)$. The probability of the target signal-plus-noise level in the range bin of interest being greater than the level in RQT of the J comparison range bins is therefore given by:

$$\sum_{K=RQT}^{J} \binom{J}{K} [F(v)]^K [1-F(v)]^{J-K} \qquad (F-18)$$

The value v in this equation represents the signal-plus-noise voltage level in the range bin of interest. Assume that the target-plus-noise-signal level v in the rank quantizer range bin of interest has a cumulative distribution function $G(v) = P_{s+n}(V<v)$. The signal-plus-noise level v can be considered as sample values from probability space with cumulative distribution function G(v). If it is assumed that these samples (target return pulses) are from an identical target distribution and independent, the expected values of Equation F-18 can be taken to obtain the probability of a hit occuring when the target is present:

$$P_{sl}(J,RQT) = \int_0^1 \sum_{K=RQT}^{J} \binom{J}{K} [F(v)]^K [1-F(v)]^{J-K} d[G(v)] \qquad (F-19)$$

After substituting the appropriate cumulative distribution for signal-plus-noise G(v) and noise F(v), Equation F-19 was used in the analysis to compute the target hit probability. It should be pointed out that the assumption of pulse-to-pulse independence in deriving Equation F-19 implies that the equation will only give estimated values when the target return pulse are correlated in amplitude.

COMPUTER PROGRAM DESCRIPTIONS

Probability of False Alarm Program

This subsection describes a computer program written for the analysis to compute probability of false alarm. The previous sections derived equations for computing the probability of false target hits with and without interference. These false target hits were related to the probability of false alarm from curves generated by the false alarm probability program.

The target detection stage of the (see Figure 4-2) ARTS-IIIA/RDAS maintains a record of the target hits and misses in azimuth for a given range bin. When the consecutive misses in the record equals or exceeds a miss count threshold (3 or 4), the accumulated sum of the target hits in the record is compared with a hit count threshold. If the hit count equals or exceeds the hit count threshold, a target is declared. The record of hits and misses is initialized when the first hit occurs and continues for 30 ACPs. The record is extended beyond the 30th ACP if the hit count threshold at this ACP is satisfied, but the miss count threshold is not.

Because the record azimuth window can vary in length, a mathematical expression describing the hit processing becomes intractable. A straightforward method of calculating the false alarm probability is to employ a Monte Carlo simulation. However, the false alarm probabilities have approximate values of 10^{-6} and would require more than one million repetitions in the simulation to evaluate. Consequently, the computation time on even modern computers would become excessive. For this reason, and to avoid questions of statistical confidence, a deterministic approach was taken to compute the probability of false alarm. A computer program was written which employs a combination of simulation and analytical methods. The technique basically involves identifying all possible combinations of hit and miss sequences which satisfy the target declaration criteria and computing the probability of each occurring. The type of calculations performed by the computer program can be described mathematically by:

$$PFA = \sum_{L=(HCT+MCT)}^{30} \sum_{i=1}^{2^L} f(i) \cdot P_1^{HC_i} (1-P_1)^{MC_i} \qquad (F\text{-}20)$$

where:

PFA = Probability of false alarm

P_1 = Probability of false target hit occurring

HC_i = Hit count (sum of hits) for i th hit/miss sequence combination and record length L

MC_i = Miss count (sum of misses) for i th hit/miss sequence combination and record length L

HCT = Hit count threshold required to be satisfied for target declaration

MCT = Miss count threshold required to be satisfied for target declaration

L= Record length or window width in ACPs

and

$$f(i) = \begin{cases} 1 & \text{target declaration criteria satisfied} \\ 0 & \text{target declaration criteria not satisfied} \end{cases} \qquad \text{(F-21)}$$

The "i" in the above equation signifies a particular hit/miss sequence combination. A computer subroutine algorithm sets f(i) equal to 1 if the particular hit/miss sequence combination satisfies the target declaration criteria and zero otherwise. The upper index of the inner summation indicates that 2^L hit/miss sequence combinations were examined for a given record length (azimuth window) to determine if the target declaration criteria had been met. The probability of each sequence occurring, which satisfies the target declaration criteria, was computed and summed. The outer summation is taken to add the false alarm probabilities for all possible record lengths up to the system maximum (without extension) of 30 ACPs. The lower limit of the summation (HCT + MCT) gives the minimum record length (azimuth window) in which the target declaration criteria can be satisfied. It should be pointed out that Equation F-20 implies that the probability of a noise hit occurring on a given ACP is independent of it occurring on any other ACP. Therefore, the results of the simulation are not applicable to correlated clutter.

The actual implementation of Equation F-20 in the computer program took a slightly different form to save computer time:

$$PFA = \sum_{L=(HCT+MCT)}^{24} \sum_{i=1}^{2^L-2-MCT} f(i) \cdot P_1^{HC_i+2} (1-P_1)^{MC_i+MCT} \qquad \text{(F-22)}$$

This form of the equation reduced the number of binary (hit/miss) sequences that had to be generated and tested for compliance with the target declaration criteria. It takes advantage of the fact that every binary sequence that satisfies the target declaration criteria begins with a hit and ends with a hit plus MCT consecutive misses. For example, with a MCT of 3 the binary sequence takes the form (1.....1000). Therefore only the hit

(1) and miss (0) combinations between the first and last 1 need to be considered. To further save computer time, the program was written to generate false alarm versus record length curves for record lengths up to 24 ACPs. These curves were then used to extrapolate the probability of false alarm for record lengths up to 30 ACPs. The error in the final extrapolated probability of false alarm value due to extrapolation is estimated to be less than 2 percent. This error is small because the contribution to the false alarm probability calculation was relatively small for record lengths greater than 24.

As previously stated, the record of hits and misses are extended by the RDAS beyond 30 ACPs if on the 30th ACP the hit count threshold has been satisfied, but the miss count threshold has not. The contribution of record lengths greater than 30 ACPs to the system probability of false alarm was computed and found to be insignificant.

The sequence of program operations to compute the probability of false alarm is outlined below:

(1) For a given record length (azimuth window), generate all possible hit/miss sequence combinations.

(2) Test each hit/miss sequence combination to determine which satisfy the target declaration criteria.

(3) For each identified hit/miss sequence combination that satisfies the target declaration criteria compute the probability of it occurring using the known probabilities of individual hits or misses occurring.

(4) Add the probabilities computed for each hit/miss sequence combinations occurring that satisfy the target declaration criteria.

(5) Perform the above operations for each record length (azimuth window) up to 24 ACPs.

(6) Generate a curve of false alarm probability versus record length.

Probability of Target Detection Program

This subsection describes a computer program that was written to compute probability of target detection. The program generated curves that were used in the analysis to relate probability of target hit to probability of target detection.

Basically, the computer program uses the Monte Carlo technique to simulate target hit and miss sequences and then counts the number of hit/miss sequence cases which satisfy the target declaration criteria. The percentage of hit/miss sequence cases that satisfy the target detection criteria was

computed to obtain the predicted target detection probability. A total of 30 ACPs were considered in each simulated sequence of hits and misses. The first five and last five ACPs of the sequence considered only the presence of noise in the range bin while the middle 20 ACPs in the sequence considered the target to be present. It was assumed in the simulation that the target was present for 20 ACPs because this is the typical number of return pulses received by an ASR-7 or ASR-8 radar from an aircraft target. This is evident from evaluation of Equation 3-21 for typical ASR-7 and ASR-8 radar parameter combinations. Noise only ACPs, before and after the target, were included in the simulation because noise in these range bins affect the probability of the target being detected. In particular, the noise in the range bins (ACPs) before the target increases the probability of the hit count threshold being satisfied, and noise in the range bin following the end of the target decrease the probability of the miss count threshold being satisfied. A number of test simulations were conducted to determine how many range bins should be included before and after the target range bins. The test simulations indicated that including five noise only range bins before and after the target range bins provides a good trade-off between computer time and predicted detection probability accuracy. It is estimated that including only five range bins before and after the target range bins, instead of an infinite number, introduces less than 1 percent error in the predicted target detection probability.

The Monte Carlo simulation of the hit/miss sequence is described mathematically by the function:

$$f_j(U) = \begin{cases} 1 & \text{for } U \leq P_1 \\ 0 & \text{for } U > P_1 \end{cases} \qquad \text{(F-23)}$$

where:

j = The particular ACP index number which can range from 1 to 30,

U = Random number uniformly distributed between 0 and 1.0

P_1 = The probabillity of a hit (logical 1) occurring.

The value of P_1 in Equation F-22 depends on the particular ACP and if noise only or signal-plus-noise is considered present in the range bin corresponding to a particular ACP. The value of P_1 for the first five and last five ACPs (j = 1-5 and 26-30) in each simulated hit/miss sequence corresponds to the probability of a target hit occurring due to only noise and was computed from Equation 4-5. A noise hit probability of 0.08 was used for a rank quantizer threshold setting of 23, and a noise hit probability of 0.04 for a rank quantizer threshold of 24. The value of P_1 in Equation F-23

for the middle 20 ACPs (j = 6-25) in each simulated hit/miss sequence represents the probability of a hit occurring due to the presence of an aircraft target. The simulation considered the probability of a hit occurring on a given ACP to be independent of the probability of it occurring on any other ACP. In other words, the simulation does not consider the possibility of pulse-to-pulse correlation of the target or clutter return pulses. In addition, the computed detection probabilities are for one antenna rotation and do not include the improved detection characteristics that can result from antenna scan-to-scan target tracking.

As stated previously, the program was used to generate target detection probability versus target hit probability curves (see Figures 4-27, 4-28 and 4-29). Each curve corresponds to a particular combination of detection parameter settings (rank quantizer threshold, hit count threshold, and miss count threshold). Each point on the curve was determined from ten thousand repeated hit/miss sequence simulations. Other points on the curves were obtained by performing these simulations with different target hit probability P_1 values substituted in Equation F-23. However, the value of P_1 in Equation F-23 for noise only ACPs was held constant for all points on a given curve.

It should be pointed out that the simulations did not include the effect of interference on the noise hit probabilities corresponding to the range bins not occupied by the target. This drastically reduced the number of curves and computer time required for the target detection calculations. Neglecting the interference effects on noise hit probabilities did not significantly affect the computed detection probability values. This fact is evident from the detection probability curves in Figures 4-27 and 4-28. The curves in Figure 4-27 are for a rank quantizer threshold of 23 or equivalently (see Equation 4-5) a noise hit probability of 0.04, and the curves in Figure 4-28 for a noise hit probability of 0.08. Comparison of corresponding curves in Figures 4-27 and 4-28 for the same hit and miss count thresholds indicates a 0.04 change in noise hit probability does not change the predicted detection probability by more than 0.02. It was shown in the false alarm portion of the analysis (see TABLES 4-3 and 4-5) that continual interference from three radars does not change the noise hit probability by more than 0.006. This indicates that the effect of interference on noise hit probability is small enough to be neglected in the detection probability calculation.

APPENDIX G

SYSTEM CHARACTERISTICS

INTRODUCTION

This appendix contains a conpendium of system characteristics of radars in the 2.7 to 2.9 GHz band.

TABLE G-1

ASR-5 SYSTEM CHARACTERISTICS*

ANTENNA CHARACTERISTICS

A.	Type:	Shaped beam, cosecant squared in elevation from half power point to +30 degrees
B.	Gain:	34 dB
C.	Beamwidth: elevation: 5 degrees azimuth: 1.5 degrees	
D.	Polarization:	Linear, vertical, or circular; remotely selectable
E.	Antenna Rotation Rate:	13 or 15 RPM

TRANSMITTER CHARACTERISTICS

A.	Output Tube:	Magnetron (5586, DX276 or QK1643)
B.	Frequency:	Tunable 2.7 to 2.9 GHz
C.	Peak Power:	400 - 500 kW
D.	Pulsewidth:	.833 microsecond
E.	PRF:	Selectable 900 to 1200 PPS (2-pulse stagger on or off)

RECEIVER CHARACTERISTICS

A. System Noise Figure: 4 dB maximum

B. Receiver Bandwidth:

Normal IF:	2.7 MHz
MTI IF:	5.0 MHz
Normal Video:	2.0 MHz
MTI Video:	2.0 MHz

C. Minimum Discernible Signal (MDS):

Normal Receiver:	-109 dBm
MTI Receiver:	-107 dBm

D. Scope Range (NM): 60 nautical miles

*Also applicable to ASR-4, ASR-6, and AN/FPN-47

TABLE G-2

ASR-7 SYSTEM CHARACTERISTICS*

ANTENNA CHARACTERISTICS

A.	Type:	Shaped beam, cosecant squared in elevation from upper half power point to +30 degrees
B.	Gain:	34 dB
C.	Beamwidth:	
	elevation: 5 degrees azimuth: 1.5 degrees	
D.	Polarization:	Linear, vertical, or circular; remotely selectable
E.	Antenna Rotation Rate:	15 RPM

TRANSMITTER CHARACTERISTICS

A.	Output Tube:	Magnetron (DX276, 8798)
B.	Frequency:	2.7 to 2.9 GHz
C.	Peak Power:	425 kW
D.	Pulsewidth:	0.833 microsecond
E.	PRF:	6-pulse stagger with 1002 PPS average, or fixed (selectable from 713 - 1200 PPS)

RECEIVER CHARACTERISTICS

A.	System Noise Figure:	4.75 dB
B.	Receiver Bandwidth:	
	Normal IF: 2.7 MHz MTI IF: 5.0 MHz	
C.	Minimum Discernible Signal (MDS):	
	Normal Receiver: -108 dBm Log Receiver: -106 dBm MTI Receiver: -106 dBm Log MTI Receiver: -104 dBm	
D.	Scope Range (NM):	60 nautical miles

*Also applicable to AN/GPN-12

TABLE G-3

ASR-8 SYSTEM CHARACTERISTICS

ANTENNA CHARACTERISTICS

A. Type: Shaped Beam, cosecant squared in elevation from half power point to +30 degrees

B. Gain: 33.5 dB Normal Beam
32.5 dB Passive Beam

C. Beamwidth:

elevation: 4.8 degrees
azimuth: 1.35 degrees

D. Polarization: Linear verticle or circuler, remotely selectable

E. Antenna Rotation Rate: 12.5 RPM

TRANSMITTER CHARACTERISTICS

A. Output Tube: Klystron (VA-87E)

B. Frequency: Tunable 2.7 to 2.9 Hz

C. Peak Power: 1.4 MW

D. Pulsewidth: 0.6 microsecond

E. PRF: 4-pulse stagger with 1040 average, or fixed (selectable from 700 - 1200 PPS)

RECEIVER CHARACTERISTICS

A. System Noise Figure: 4.0 dB maximum

B. Receiver Bandwidth:

Normal IF: 1.2 MHz
MTI IF: 5.0 MHz
Log IF: 1.2 MHz
MTI Video: 585 kHz

C. Minimum Discernible Signal (MDS):

Normal Receiver: -110 dBm
Log Receiver: -109 dBm
MTI Receiver: -108 dBm

D. Scope Range (NM): 60 nautical miles

TABLE G-4

WSR-57 SYSTEM CHARACTERISTICS

ANTENNA CHARACTERISTICS

A.	Type:	Parabolic disk (12 ft. diameter)
B.	Gain:	38 dB
C.	Beamwidth:	2.2 degrees
D.	Polarization:	Linear, horizontal
E.	Antenna Rotation Rate:	0 to 5 RPM -5 to +45 degrees elevation

TRANSMITTER CHARACTERISTICS

A.	Output Tube:	Magnetron (QK729-733)
B.	Frequency:	Tunable 2.7 to 2.9 GHz
C.	Peak Power:	500 kW
D.	Pulsewidth:	0.5 microsecond (short pulse) 4.0 microseconds (long pulse)
E.	PRF:	658 PPS (short pulse) 164 PPS (long pulse)

RECEIVER CHARACTERISTICS

A.	System Noise Figure:	4.0 dB
B.	Receiver IF Bandwidth:	4.5 MHz for short pulse and 0.75 MHz for long pulse
C.	Minimum Discernible Signal (MDS):	
		-100 dBm (short pulse) -108 dBm (long pulse)
D.	Scope Range (NM):	250 nautical miles

TABLE G-5

WSR-74S SYSTEM CHARACTERISTICS

ANTENNA CHARACTERISTICS

A.	Type:	Parabolic Disk (12 ft. diameter)
B.	Gain:	38 dB
C.	Beamwidth:	2.2 degrees maximum
D.	Polarization:	Linear, horizontal
E.	Antenna Rotation Rate:	0 to 5 RPM -5 to +45 degrees elevation

TRANSMITTER CHARACTERISTICS

A.	Output Tube:	Coaxial Magnetron
B.	Frequency:	2.7 to 2.9 GHz
C.	Peak Power:	565 kW
D.	Pulsewidth:	1 microsecond (short pulse) 4 microseconds (long pulse)
E.	PRF:	545 PPS on short pulse 164 PPS on long pulse

RECEIVER CHARACTERISTICS

A.	System Noise Figure:	
B.	Receiver IF Bandwidth:	Not less than 1.5 MHz for short pulse and .375 MHz for long pulse
C.	Minimum Discernible Signal (MDS):	
D.	Scope Range (NM):	50, 125, and 250 nautical miles

TABLE G-6

AN/FPS-6 SYSTEM PARAMETERS*

ANTENNA CHARACTERISTICS

A.	Type:	Shaped beam, fan beam in azimuth
B.	Gain:	39 dB
C.	Beamwidth:	
	vertical: 0.85 degree horizontal: 3.2 degrees	
D.	Polarization:	
E.	Antenna Rotation Rate:	7.5 RPM, 20-30 CPM

TRANSMITTER CHARACTERISTICS

A.	Output Tube:	Magnetron (QK327A) or Coaxial Magnetron (VSM-1143)
B.	Frequency:	Tunable 2.7 to 2.9 GHHz
C.	Peak Power:	5.0 MW
D.	Pulsewidth:	2.0 microseconds
E.	PRF:	250 to 400 PPS

RECEIVER CHARACTERISTICS

A.	System Noise Figure:	8.0 dB
B.	Receiver Bandwidth:	800 kHz
C.	Minimum Discernible Signal (MDS):	
	Normal: -106 dBm	
D.	Scope Range (NM):	200 nautical miles

*Also applicable to AN/FPS-90

TABLE G-7

AN/GPN-20 SYSTEM CHARACTERISTICS

ANTENNA CHARACTERISTICS

A.	Type:	Shaped beam, cosecant squared in elevation from half power point to +30 degrees
B.	Gain:	33.5 dB Normal beam 32.5 dB Passive beam
C.	Beamwidth:	
	elevation: 4.8 degrees azimuth: 1.35 degrees	
D.	Polarization:	Vertical or circular (LH)
E.	Antenna Rotation Rate:	12 or 15 RPM

TRANSMITTER CHARACTERISTICS

A.	Output Tube:	Magnetron (8798), diplex filtered
B.	Frequency:	Tunable 2.7 to 2.9 GHz
C.	Peak Power:	500 kW
D.	Pulsewidth:	0.833 microsecond
E.	PRF:	Staggered with 1040 average (selectable from 849 - 1204 PPS)

RECEIVER CHARACTERISTICS

A.	System Noise Figure:	4 dB
B.	Receiver Bandwidth:	
	Normal IF: 1.2 MHz MTI IF: 5.0 MHz Log IF: 1.2 MHz MTI Video: 585 kHz	
C.	Minimum Discernible Signal (MDS): Normal Receiver: -110 dBm Log Receiver: -109 dBm MTI Receiver: -108 dBm	
D.	Scope Range (NM):	60 nautical miles

TABLE G-3

AN/CPN-4 SYSTEM CHARACTERISTICS

ANTENNA CHARACTERISTICS

A.	Type:	Shaped beam, cosecant squared in elevation from half power point to +30 degrees
B.	Gain:	31 dB
C.	Beamwidth:	
	elevation: 3.6 degrees azimuth: 2.2 degrees	
D.	Polarization:	Horizontal or circular, remotely selectable
E.	Antenna Rotation Rate:	20 ± 2 RPM

TRANSMITTER CHARACTERISTICS

A.	Output Tube:	Magnetron (5586)
B.	Frequency:	Tunable 2780 to 2820 MHz
C.	Peak Power:	600 kW
D.	Pulsewidth:	0.5 microsecond
E.	PRF:	1500 PPS

RECEIVER CHARACTERISTICS

A.	System Noise Figure:	4.0 dB
B.	Receiver Bandwidth:	
	Normal IF: 2.25 MHz MTI IF: 4.5 MHz	
C.	Minimum Discernible Signal (MDS):	
	Normal: -106 dBm MTI: -104 dBm	
D.	Scope Range (NM):	30 nautical miles

TABLE G-9

AN/MPN-13 SYSTEM CHARACTERISTICS*

ANTENNA CHARACTERISTICS

A.	Type:	Shaped beam, cosecant squared in elevation from half power point to +30 degrees
B.	Gain:	36 dB
C.	Beamwidth:	
	elevation: 3.6 degrees azimuth: 2.2 degrees	
D.	Polarization:	Horizontal or circular, remotely selectable
E.	Antenna Rotation Rate:	15 RPM

TRANSMITTER CHARACTERISTICS

A.	Output Tube:	Magnatron (8798)
B.	Frequency:	Tunable 2780 to 2820 MHz
C.	Peak Power:	750 kW
D.	Pulsewidth:	0.7 microsecond
E.	PRF:	1100 PPS (3-pulse stagger on or off)

RECEIVER CHARACTERISTICS

A.	System Noise Figure:	4.0 dB
B.	Receiver Bandwidth:	
	Normal: 2.25 MHz MTI: 4.5 MHz	
C.	Minimum Discernible Signal (MDS):	
	Normal: -106 dBm MTI: -104 dB,	
D.	Scope Range (NM):	30 nautical miles

*Also applicable to AN/MPN-14 and AN/MPN-15

TABLE G-10

AN-TPN-24 SYSTEM CHARACTERISTICS

ANTENNA CHARACTERISTICS

A.	Type:	Shaped beam, cosecant squared in elevation from half power point to +30 degrees
B.	Gain:	33.6 dB
C.	Beamwidth:	
	elevation: 6 degrees azimuth: 1.55 degrees	
D.	Polarization:	Vertical or circular
E.	Antenna Rotation Rate:	15 RPM

TRANSMITTER CHARACTERISTICS

A.	Output Tube:	Magnetron (8798), diplex filtered
B.	Frequency:	Tunable 2.7 to 2.9 GHz
C.	Peak Power:	450 kW
D.	Pulsewidth:	1.0 microseconds
E.	PRF:	12 staggered (1050 Hz average)

RECEIVER CHARACTERISTICS

A.	System Noise Figure:	2.5 dB
B.	Receiver Bandwidth:	
	Normal: 1.0 MHz	
C.	Minimum Discernible Signal (MDS):	
	Normal: -112 dBm for 6 dB S/N	
D.	Scope Range (NM):	60 nautical miles

APPENDIX H

REFERENCES

Atlantic Research Corporation (December, 1974), "Degradation to Search Radar PPI Performance in an Electromagnetic Environment."

Davenport, Wilbur B. Jr. and William L. Root (1958), Random Signals and Noise , McGraw-Hill Book Co.

Dillard, George M., and Charles E. Antoniak (September, 1970), "A Practical Distribution-Free Detection Procedure for Multiple Range-Bin Radars", IEEE Transactions on Aerospace and Electronic Systems , Volume AES-6, No. 5.

Feller, William (1968), An Introduction to Probability Theory and its Applications, Volume I, Third Edition, John Wiley and Sons, Inc.

Fleck, R. (March, 1967), "Procedures for Computing Separation Criteria and Off-Frequency Rejection in Electromagnetic Compatibility Problems", ECAC, ESD-TR-67-5.

Gannaway, R. (October, 1965), "Signal-to-Noise Ratio in Receivers Using Linear or Square-Low Envelope Detectors", Proceeding of the IEEE, pp. 1645 - 1646.

Hinkle, R. and R. Mayner (April, 1975), "Spectrum Resource Assessment in the 2.7- 2.9 GHz Band, Phase I - Background and Study Definition," Report No. 1/73 - P1.

Hinkle, R.; R. Pratt; and R. Matheson (August, 1976), "Spectrum Resource Assessment in the 2.7 to 2.9 GHz Band, Phase II: Measurement and Model Validation (Report No. 1)," OT Report 76-97.

Letter Report (June 11, 1976), Video Ennancer Modification, FAA-NA-76-39.

Maluzzo, Michael A. (July, 1972), "Analysis of Factors Affecting Electromagnetic Compatibility of Radars Operating in the 2700 to 2900 MHz Band", FAA Report No. FAA-RD-71-91.

Meyer, Daniel P. and Herbert A. Mayer (1973), Radar Target Detection, Academic Press.

Meyers, R. (August, 1971), "A Receiver Waveform Simulation (RWS) Model", ECAC, ESD-TR-71-099.

Nathanson, F. E. and P. J. Luke (January, 1972), "Loss From Approximations to Square-Law Detectors in Quadrature Systems with Postdetection Integration", IEEE Transactions on Aerospace and Electronic Systems.

Nathanson, Fred E. (1969), Radar Design Principles , McGraw-Hill Book Co.

Natrella, Mary Gibson (1963), Experimental Statistics , Handbook 91, U.S. Department of Commerce, National Bureau of Standards.

Newhouse, Paul D. (May, 1969), "Peak Output Power in Victim Receivers", ECAC Radar Analysis Bulletin No. 2.

Ng, Harold J. (October, 1977), "Table of Error Probability and Error Function", Office of Telecommunications, U.S. Department of Commerce, TN-77-5.

Paupolis, A. (1965), Probability, Random Variables, and Stochastic Processes, McGraw-Hill Book Co.

Rice, S. O. (1954), "Mathematical Analysis of Random Noise", in Selected Papers on Noise and Stochastic Processes, N. Wax, Ed. New York.

Saaty, Thomas L. (1961), Elements of Queueing Theory , McGraw-Hill Book Co.

Seely, Samuel (1956), Electron-Tube Circuitry , McGraw Hill Book Co.

Skolnik, M. I. (1962), Introduction to Radar System , McGraw-Hill Co.

Skolnik, M. I. (1970), Radar Handbook , McGraw-Hill Book Co.

Summary Minutes First OTP Meeting on 2700-2900 MHz Spectrum Resource and Allocation Provision, 27 October 1972.

Summary Minutes Second OTP Meeting on 2700-2900 MHz Spectrum Resource and Allocation Provision, 13 December 1972.

Trunk, G. V. (July, 1970), "Detection Results for Scanning Radars Employing Feedback Integration", IEEE Transactions on Aerospace and Electronic Systems , Volume AES-6 No. 4.

Trunk, G. V. (July, 1972), "Comparison of the Collapsing Losses in Linear and Square-Law Detectors", Proc. IEEE, Volume 60, No. 6, pp. 743-744.

Trunk, G. V. (April, 1977) "MTI Noise Integration Loss" NRL Report 8132.

Uffi, Domenick J. (December, 1969), "Test and Evaluate Dual Diversity for Airport Surveillance Radars (ASR)", Report No. NA-69-50 (RD-69-56).

White, D.R.J., (1972), "Electromagnetic Interference Handbook," Vol. 5.